Ion-Ion Association in Electrolyte Solutions: A Theoretical Investigation

Naseri Boroujeni, Saman

Publication date:
2023

Document Version
Publisher's PDF, also known as Version of record

Doctor of Philosophy
Doctoral thesis in Chemical Engineering

DTU Chemical Engineering
Department of Chemical and Biochemical Engineering

Ion-Ion Association in Electrolyte Solutions: A Theoretical Investigation

Author: Saman Naseri Boroujeni

DTU

Supervisor: Prof. Georgios M. Kontogeorgis
Co-supervisors: Dr. Bjørn Maribo-Mogensen & Ass. Prof. Xiaodong Liang

Center for Energy Resources and Engineering
Department of Chemical and Biochemical Engineering
Technical University of Denmark
Søltofts Plads
Building 229
2800 Kongens Lyngby, Denmark

To my wife Yasaman

And

To my parents Reza and Nasrin

چه دانستم که این سودا مرا زین سان کند مجنون
دلم را دوزخی سازد دو چشمم را کند جیحون

چه دانستم که سیلابی مرا ناگاه برباید
چو کشتی‌ام در اندازد میان قلزم پرخون

زند موجی بر آن کشتی که تخته تخته بشکافد
که هر تخته فروریزد ز گردش‌های گوناگون

نهنگی هم برآرد سر خورد آن آب دریارا
چنان دریای بی‌پایان شود بی‌آب چون هامون

شکافد نیز آن هامون نهنگ بحر فرسارا
کشد در قعر ناگاهان به دست قهر چون قارون

چو این تبدیل‌ها آمد نه هامون ماند و نه دریا
چه دانم من دگر چون شد که چون غرق است در بی‌چون

چه دانم‌های بسیار است لیکن من نمی‌دانم
که خوردم از دهان بندی در آن دریا کفی افیون

مولوی (Rumi)

1207-1278

Preface

This thesis is submitted in partial fulfillment of the requirements for the Ph.D. degree at Technical University of Denmark, DTU. Research was carried out from December 2020 to November 2023 in the department of chemical and biochemical engineering at DTU, under the supervision of Professor Georgios M. Kontogeorgis, Associate Professor Xiaodong Liang, and Dr. Bjørn Maribo-Mogensen. The Ph.D. program was funded by the European Research Council and the chemical and biochemical engineering department at DTU.

I am immensely thankful to my supervisors for their support, which has been the cornerstone of my project. Their consistent encouragement to explore creative concepts and question existing models has been essential to the success of this study. Attending international conferences, a benefit made possible by their backing, has given me invaluable chances to connect with others and partake in enlightening conversations with specialists in the area.

I am deeply thankful to Professor Gillespie, Professor Valiskó, and Professor Boda for generously sharing the results of their Monte Carlo simulations, which significantly enriched the depth of my work.

My gratitude extends to my office-mate, Gcinisizwe, and an exceptional group of colleagues, Julia, Daria, Aswin, Rasmus, Nefeli, Fufang, Martin, Randi, Andre, Gabriel, Maryam, and Evangelos. Your commitment, teamwork, and steadfast backing have changed our workplace into a center of brilliance. Each one of you, through project collaboration and words of encouragement, has played an indispensable role in the success of our collective efforts.

A special thank you goes to Bjørn, Jon, Christos, Sari, Rasmus, Niels, Martin, Darren, and Diego at Hafnium Labs for their exceptional hospitality during my external stay. Their warmth and generosity not only made my time with the company productive but also turned it into an enjoyable and enriching experience. I extend my gratitude to Hafnium Labs as a whole for fostering an environment that facilitated my learning and effective contribution.

My sincerest gratitude goes out to my friends Mohammad, Aref, Hossein, Mahtab, Amirali, Ashkan, Akbar, Lavin, Matin, Mahya, Omid, Amin, Maryam, Mina, and Bahman for their support throughout my Ph.D. experience. Your encouragement, understanding, and lasting friendship have been of great value, particularly during the most difficult times of my research.

My deepest appreciation is reserved for my parents, Reza and Nasrin, for their guidance and unconditional love that has shaped me into the person I am today. I am truly thankful for the warmth and kindness bestowed upon me by my brother, Soheil, and his wife, Zahra. A special thank you to the source of our joy, their delightful daughter, Kajal, whose laughter and innocence bring immense joy to our family. I am also thankful to my father, mother, and brother-in-law, Abdoreza, Leila, and Soroush, for their consistent encouragement and support.

And to my beloved wife, Yasaman, your unwavering love and support have been my anchor through every challenge and triumph. Your presence is my greatest blessing, and I am forever grateful for the warmth and strength you bring to my life.

Kongens Lyngby, 30$^{\text{th}}$ November 2023

Saman Naseri Boroujeni

Abstract

This doctoral dissertation explores the concept of ion-ion association within electrolyte solutions, with the aim of enhancing existing methods for predicting the properties of such solutions. This study follows two distinct paths that eventually come together to form a unified framework. Initially, an emphasis is placed on investigating the electrical conductivity, a key transport property significantly affected by ion pair formation in electrolyte solutions. Within this research, theoretical works dedicated to predicting electrical conductivity are identified from the existing literature. Through a comparative study, their strengths and weaknesses are elucidated. Subsequently, two novel models, one for single-salt and another for multi-salt electrolytes, are developed to predict the electrical conductivity of electrolyte solutions under the assumption of complete dissociation. These models are constructed based on the Ebeling hierarchy of Smoluchowski dynamics and Debye-Hückel-Onsager theory. Rigorous evaluations are conducted by comparing the predictions of the models with experimental data. The findings affirm that the developed models exhibit high accuracy and reliability under conditions where the assumption of complete dissociation holds.

In the second line of research, the issue of ion pairing in electrolyte solutions is approached from a thermodynamic perspective. This research, similar to the first, begins with a thorough examination of the equations of state for charged hard sphere fluids. This investigation involves comparing the predictions of four distinct equations of state, which consider ion pairing and serve as the foundation for other models, with numerical solutions to the Poisson-Boltzmann equations, Monte Carlo simulations, and experimental data.

Subsequently, a novel equation of state named Binding Debye-Hückel for charged hard sphere fluids is developed. This model draws on the Debye-Hückel theory, Kirkwood theory, Wertheim theory, and the reference cavity approximation. To validate the BiDH model, its predictions are compared with Monte Carlo simulations documented in the existing literature. The validation specifically focuses on evaluating the mean ionic activity coefficient, the individual activity coefficient, and the osmotic coefficient. Through meticulous evaluations, the study demonstrates the accuracy and reliability of the BiDH model.

In the final research phase, the models previously established and verified for electrical conductivity, which did not consider the impact of ion pairing, are combined with the Binding Debye-Hückel model designed to account for ion pairing effects. Initially, an effort is made to predict the properties, particularly electrical conductivity, of diverse electrolyte solutions where ion pairing may play a significant role. This includes aqueous electrolyte solutions, mixed-solvent electrolyte solutions, and ionic liquid-co-solvent systems, all under the assumption of an implicit solvent model.

Subsequently, a novel electrolyte equation of state termed Binding eSAFT-VR-Mie is formulated. Following this, a new unified framework for the development and validation of models for electrolyte solutions is introduced. This unified approach is applied to predict the properties of aqueous electrolyte solutions across a spectrum of affinity for forming ion pairs, ranging from slightly or non-associative to highly associative electrolyte solutions. The study provides evidence of the effectiveness and reliability of this unified framework.

Resume

Denne phDafhandling udforsker konceptet ion-ion-associering inden for elektrolytopløsninger med det formål at forbedre eksisterende metoder til at forudsige egenskaberne af sådanne opløsninger. Denne afhandling følger to forskellige spor, der til sidst samles for at danne en forenet ramme. Indledningsvist lægges der vægt på undersøgelsen af elektrisk ledningsevne, en nøgletransportegenskab, der påvirkes betydeligt af dannelse af ionpar i elektrolytopløsninger. Inden for denne forskning identificeres teoretiske værker, der er dedikeret til at forudsige elektrisk ledningsevne, fra den eksisterende litteratur. Gennem en sammenlignende undersøgelse afklares deres styrker og svagheder. Derefter udvikles to nye modeller, en for enkeltsalt og en anden for multisalt-elektrolytter, til at forudsige den elektriske ledningsevne af elektrolytopløsninger under antagelsen om fuldstændig dissociation. Disse modeller er konstrueret baseret på Ebeling-hierarkiet af Smoluchowski-dynamik og Debye-Hückel-Onsager-teori. Der udføres strenge evalueringer ved at sammenligne modellernes forudsigelser med eksperimentelle data. Resultaterne bekræfter, at de udviklede modeller udviser høj nøjagtighed og pålidelighed under forhold, hvor antagelsen om fuldstændig dissociation gælder.

I den anden forskningslinje behandles problemet med ionparbinding i elektrolytopløsninger fra en termodynamisk synsvinkel. Denne forskning, ligesom den første, begynder med en grundig undersøgelse af ligningerne for tilstandsændringer for opladede hårde kuglefluider. Denne undersøgelse omfatter sammenligning af forudsigelser fra fire forskellige ligninger for tilstandsændringer, der medregner ionpardannelse og tjener som grundlag for sammenligning med andre modeller, med numeriske løsninger til Poisson-Boltzmann-ligninger, Monte Carlo-simulationer og eksperimentelle data.

Derefter udvikles en ny model kaldet Binding Debye-Hückel for opladede hårde kuglefluider. Denne model bygger på Debye-Hückel teorien, Kirkwood teorien, Wertheim teorien og RCA. For at validere BiDH-modellen sammenlignes dens forudsigelser med Monte Carlo-simulationer dokumenteret i den eksisterende litteratur. Valideringen fokuserer specifikt på vurdering af den gennemsnitlige ioniske aktivitetskoefficient, den individuelle aktivitetskoefficient og den osmotiske koefficient. Gennem omhyggelige evalueringer demonstrerer undersøgelsen nøjagtigheden og pålideligheden af BiDH-modellen.

I den sidste forskningsfase kombineres modellerne, der tidligere er etableret og verificeret for elektrisk ledningsevne, uden at tage hensyn til virkningen af ionparbinding, med Binding Debye-Hückel-modellen designet til at tage hensyn til virkningen af ionparbinding. Indledningsvis forsøges det at forudsige egenskaberne, især elektrisk ledningsevne, af forskellige elektrolytopløsninger, hvor ionparbinding kan spille en betydelig rolle. Dette inkluderer vandige elektrolytopløsninger, opløsningsmiddelblandede elektrolytopløsninger og ioniske væske-coopløsningsstoffer, alle under antagelse af en implicit opløsningsmiddelmodel.

Derefter formuleres en ny tilstandsligning for elektrolyter kaldet Binding eSAFT-VR-Mie. Efter dette introduceres en ny forenet ramme for udvikling og validering af modeller for elektrolytopløsninger. Denne forenede tilgang anvendes til at forudsige egenskaberne af vandige elektrolytopløsninger på tværs af et spektrum af tilbøjelighed til at danne ionpar, der spænder fra lidt eller ikke-associerende til meget associerende elektrolytopløsninger. Undersøgelsen præsenterer bevis for effektiviteten og pålideligheden af denne forenede ramme.

Contents

List of Figures

List of Tables

Abbreviations

AAD	Average absolute deviation
AARD	Average absolute relative deviation
AGCMC	Adaptive grand canonical Monte Carlo
AN	Acetonitrile
AMSA	Associative mean spherical approximation
BBGKY	Bogoliubov Born Green Kirkwood Yvon
BD	Brownian dynamics
BiDH	Binding Debye-Hückel
BiMSA	Binding mean spherical approximation
BMM	Breil-Michelsen-Mollerup
CHS	Charged hard sphere
CIP	Contact ion pairs
CPA	Cubic plus association
CS	Carnahan-Starling
DH	Debye-Hückel
DHO	Debye-Hückel-Onsager
DHOLL	Debye-Hückel-Onsager limiting law
DHOEE	Debye-Hückel-Onsager extended equation
DHOSiS	Debye-Hückel-Onsager smaller-ion shell
DI	Dipole ion
DRS	Dielectric relaxation spectroscopy
EoS	Equation of state
GCMC	Grand canonical Monte Carlo
HC	High concentration
HS	Hard sphere
FO	Fuoss-Onsager
IGCMC	Iterative grand canonical Monte Carlo
IIAC	Individual ionic activity coefficient

IL	Ionic liquid
LC	Low concentration
MAL	Mass action law
MC	Monte Carlo
MC	Medium concentration
MD	Molecular dynamic
MIAC	Mean ionic activity coefficient
MSA	Mean spherical approximation
NIST	National institute of standards and technology
NRTL	Nonrandom two-liquid
PB	Poisson Boltzmann
QV	Quint and Viallard
RCA	Reference cavity approximation
RDH	Restricted Debye-Hückel
RDF	Radial distribution function
RPM	Restricted primitive model
RSP	Relative static permittivity
SAFT	Statistical associating fluid theory
SAFT-VR	Statistical associating fluid theory for variable range interactions
SDH	Symmetrical Debye-Hückel
PC-SAFT	Perturbed-chain statistical associating fluid theory
PPC-SAFT	Polar perturbed-chain statistical associating fluid theory
SIP	Solvent separated ion pairs
SSIP	Solvent-shared ion pairs
UNIQUAC	Universal quasichemical
UPM	Unrestricted primitive model
WOZ	Wertheim-Ornstein-Zernike

List of Symbols

Physics Constants

ε_0	Vacuum Permittivity	$8.854187 \times 10^{-12}\,\mathrm{F\,m^{-1}}$
e	Elementary charge	$1.60217646 \times 10^{-19}\,\mathrm{C}$
F	Faraday constant	$96485.3365\,\mathrm{C\,mol^{-1}}$
k_B	Boltzmann constant	$1.3806503 \times 10^{-23}\,\mathrm{J\,K^{-1}}$
N_A	Avogadro's constant	$6.0221415 \times 10^{23}\,\mathrm{mol^{-1}}$
R	Ideal gas constant	$8.314472\,\mathrm{J\,K^{-1}\,mol}$

Greek Symbols

α	Fraction of unbound ions	
α_0	Electronic polarizability	$\mathrm{m^3}$
$\bar{\rho}$	Number density of components	$\mathrm{m^{-3}}$
$\bar{\sigma}$	Average diameter	m
β	Association volume	
β	k_BT	J
β_n	Cumulative formation constant of the complex	
χ	Specific conductivity	$\mathrm{S\,m^{-1}}$
$\delta k/k$	Relaxation effect	
$\delta v/v^0$	Electrophoretic effect	
ΔV	Electric potential	V
Δ	Association strength	$\mathrm{m^3}$
δ	Dipole moment	$\mathrm{C\,m}$
ϵ	Potential energy of interaction	J
ϵ	$4\pi\varepsilon_0\varepsilon_r$	
η	Viscosity	$\mathrm{Pa\,s}$
γ	Activity coefficient	
γ^*	Asymmetrical rational activity coefficient	
Γ^{-1}	MSA screening length	m
$\gamma_\pm$	Mean ionic activity coefficient	

$\hat{\varphi}$	Fugacity coefficient	
$\hat{\varphi}^{\infty}$	Fugacity coefficient at the infinitely diluted solution	
κ	Association volume	
κ	Inverse Debye length	m^{-1}
κ'	Inverse Debye length after ion-ion association	m^{-1}
Λ	Molar conductivity	$\mathrm{S\,m^2\,s^{-1}}$
λ	Ionic conductivity	$\mathrm{S\,m^2\,mol^{-1}}$
λ^0	Ionic conductivity at infinite dilution	$\mathrm{S\,m^2\,mol^{-1}}$
λ_a	Attractive exponent in the Mie potential	
λ_r	Repulsive exponent in the Mie potential	
μ	Chemical Potential	$\mathrm{J\,mol^{-1}}$
μ	Relative ionic strength	
ν	Stoichiometry coefficients of ion i	
ω	Absolute mobility	$\mathrm{s\,kg^{-1}}$
ω	Stoichiometric coefficient	
ϕ	Osmotic coefficient	
ψ	Electric potential	V
ρ	Density	$\mathrm{kg\,m^{-3}}$
ρ	Total number density	m^{-3}
ρ^*	$\rho\sigma^3$	
σ	Ionic diameter	m
σ	Segment size parameter	m
σ^B	Born diameter	m
$\tilde{\rho}$	Number density of free ions	m^{-3}
ε_r	Relative static permittivity	
ϱ	Number density of species after association	m^{-3}

Other Symbols

$\bar{N}$	Total number of components	
$\tilde{a}$	Reduced Helmholtz free energy	
A	Area	m^2
A	Helmholtz free energy	J
a	Activity	

b	Co-volume parameter	$\mathrm{m^3\,mol^{-1}}$
C	Characteristic measure of a Mie potential	
C	Number of species	
c	Concentration	$\mathrm{mol\,m^{-3}}$
D	Diffusion coefficient	$\mathrm{m^2\,s^{-1}}$
E	External electric field	$\mathrm{N\,C^{-1}}$
F	Mayer function	
G	Conductance	S
G	Gibbs free energy	J
g	Radial distribution function	
h	Pair correlation function	
I	Association Kernel	
I	Ionic strength	$\mathrm{mol\,m^{-3}}$
I	Ionization potential	eV
i	Total ion current density	$\mathrm{m^{-2}\,s}$
J	Ionic flux	$\mathrm{mol\,m^{-2}\,s}$
K°	Association constant at infinite dilution	$\mathrm{m^3}$
$K^{A_iB_j}$	Association volume	$\mathrm{m^3}$
l	Length	m
l_B	Bjerrum length	m
M	Molecular weight	$\mathrm{kg\,mol^{-1}}$
M	Number of types of cations	
m	Mass	kg
m	Molality	$\mathrm{mol\,kg^{-1}}$
N	Number of components	
N	Number of types of anions	
n	Moles of components	mol
P	Area	Pa
R	Resistance	Ω
S	Number of association sites in each molecule	
T	Temperature	K
t	Time	s

t	Transference number	
T^*	$k_B T/\epsilon$	
u	Intermolecular potential	J
V	Volume	m^3
v	Velocity	$\mathrm{m\,s}^{-1}$
W	potential of the mean force	J
w	Mass	kg
x	Mole fraction	
x	$\kappa\sigma$	
x'	$\kappa'\sigma$	
X^{A_i}	Fraction sites of type A that are not bonded to any other sites	
y	Cavity function	
Z	Compressibility factor	
Z	Valence type	

Subscripts

$+-$	Between cation and anion
$+$	Cation
$-$	Anion
$\pm$	Entire electrolyte
i	Component i
ij	Between components i and j
j	Component j
k	Component k
m	Component m
n	Component n
E	Electrolyte
eff	Effective
ion	Ions
ip	Ion pairs
w	water

Superscripts

0	Equilibrium

0	Reference state
1	Non-equilibrium
$*$	Reduced
∞	Infinite dilution
A_iB_j	Between the site A of the molecule i and the site B of molecule j
ASSOC	Association term
BiMSA	Binding mean spherical approximation
BORN	Born term
c	Molarity scale
CHAIN	Chain term
conv	Conventional
CS	Carnahan-Starling
d	Drift
DH	Debye-Hückel term
ELE	Electrostatic contribution
ele	Electrophoretic
eq	Equivalent
ext	External
GCMC	Grand canonical Monte Carlo
HS	Hard sphere term
IDEAL	Ideal term
int	Internal
m	Molality scale
MAL	Mass action law term
Mie	Mie fluid
MONO	Monomer term
MSA	Mean spherical approximation
r	residual
ref	Reference
rel	Relaxation
s	Solvent
sat	Saturation

SDH Symmetrical Debye-Hückel

sol Solvation

Vectors and Tensors

$\bar{\mathbf{T}}$ Hydrodynamic interaction tensor

$\mathbf{E}$ Electric field vector

$\mathbf{F}$ Force

$\mathbf{J}$ Flux vector

$\mathbf{P}$ Momentum coordinate vector

$\mathbf{r}$ Spatial coordinate vector

$\mathbf{v}$ Velocity vector

Part I

Bringing to the Context

CHAPTER 1

Introduction

Electrolyte solutions, whether in liquid or gel form, consist of ions that are typically generated when salts, acids, or bases dissolve in solvents such as water. These solutions are of significant importance for a wide array of chemical, biological, and industrial applications.

In the realm of electrochemistry, electrolyte solutions are indispensable components in various processes, encompassing corrosion, batteries, supercapacitors, and fuel cells. Their influence extends even further into sectors such as the oil and gas industry. Here, hydrocarbon compounds coalesce with brine solutions, often concentrated electrolyte solutions sourced from oil reservoirs, and undergo processing within separation and refinery facilities. Changes in system conditions, such as pressure or temperature fluctuations, can lead to the formation of scales in critical areas such as pipelines, wells, or heat exchangers. The emergence of these scales detrimentally impacts the overall performance of these facilities, necessitating preventive measures.

Moreover, electrolyte solutions play a pivotal role in addressing environmental concerns, particularly in the removal of CO_2 from streams through absorption techniques. By leveraging the properties of electrolyte solutions, these techniques contribute to the mitigation of carbon dioxide emissions, showcasing the versatile and indispensable nature of electrolytes in addressing both industrial and environmental challenges.

Beyond their prominent roles in electrochemical processes and industrial applications, electrolyte solutions find diverse and critical applications in other fields such as biology, geology, and biotechnology.

In all the mentioned applications of electrolyte solutions, it is required that the thermodynamic, transport, or physical properties of the system are calculated using a robust, accurate, and fast property prediction tool.

In these applications, electrolyte solutions are usually very complex, containing multiple ions and solvents with the possibility of reaction between species, formation of complexes, and phase separation. Therefore, the development of prediction tools for the properties of electrolyte solutions is essential from both engineering and scientific perspectives.

Tools and methods for predicting the properties of electrolyte solutions lag behind those for non-electrolyte systems, both in terms of thermodynamic and transport properties. In a recent review on the future of applied thermodynamics, de Hemptinne et al. [1] pointed out:

> *"While all the above indicate areas where future developments toward better predictive models are needed, there are three fields which require particular attention: electrolytes, polymers, and systems containing complex multifunctional compounds."*

A similar sentiment is echoed in the work of Gupta et al. [2] in their review of the property prediction needs of the chemical industry. They highlighted the following:

> *"Development of electrolyte models has attracted the attention of numerous researchers since the seminal work of Debye and Hückel almost a century ago. Still, it is fair to state that the overall maturity and robustness of electrolyte models still lag behind those of non-electrolyte models."*

From these statements, as well as other similar observations [3], it is evident that property predictions of electrolyte solutions demand special attention. While the detailed reasons for

the lag in development of thermodynamic and transport property models for electrolyte solutions, compared with those for nonelectrolyte systems, are beyond the scope of this study, one potential explanation might be the coexistence of long-range and short-range interactions in these solutions.

In this chapter, the literature on the property prediction methods for electrolyte solutions with a focus on thermodynamic and transport properties is briefly analyzed to find the knowledge gap. Based on this evaluation, the action to fill the gap is proposed, and actions taken in the subsequent chapters according to this proposal are explained.

1.1 Thermodynamic Properties

The unique behavior of electrolyte solutions has led researchers to categorize modeling approaches into electrostatic and non-electrostatic components. For example, in excess Gibbs free energy models (often termed activity coefficient models), G^{ex} is presented as a combination of short-range (or non-electrostatic or physical) and long-range (or electrostatic) contributions. This approach is mirrored in Helmholtz free energy models or equations of state. In these models, just like in the activity coefficient models, the Helmholtz free energy is partitioned into non-electrostatic and electrostatic contributions.

For the electrostatic contributions to either the Helmholtz free energy or the excess Gibbs free energy, models typically stem from two primary theories: Debye-Hückel (DH) [4] and mean spherical approximation (MSA) [5, 6].

Models that address ion-ion interactions and are based on the DH theory include, but are not limited to, the Pitzer-Debye-Hückel [7], Extended Debye-Hückel, and Full Debye-Hückel [4, 8, 9]. On the other hand, models derived from the MSA theory encompass implicit MSA [5, 6], explicit MSA [10], non-primitive MSA [11–18], Binding MSA (BiMSA) [19, 20], and Associative MSA (AMSA) [21–29].

In activity coefficient models, the non-electrostatic contributions to the excess Gibbs free energy include the NRTL [30–32], extended UNIQUAC [33–36], and COSMO-RS [37, 38] models.

For the non-electrostatic contributions of Helmholtz free energy models, typical choices are cubic equations of state (as reviewed by Kontogeorgis et al. [39]), CPA [40] (which led to eCPA [39, 41–53]), PC-SAFT [54, 55] (and its electrolyte extension ePC-SAFT [56–63]), SAFT-VR [64, 65] (and its variant SAFT-VRE [66, 67]), SAFT-VR-Mie [68] (along with eSAFT-VR-Mie [69–75]), and PPC-SAFT (subsequently, ePPC-SAFT [76, 77]).

The literature on electrolyte thermodynamics is abundant, yet there are still many unresolved issues. Resolving these issues would be beneficial in improving the accuracy of property prediction methods. Maribo-Mogensen [41] and Olsen [78] in their Ph.D. thesis and Kontogeorgis et al. [39] in a recent review paper raised a few questions/challenges regarding the thermodynamic modeling of electrolyte solutions. Some of these questions are summarized here and further questions are also added.

The questions related to the theory of electrolyte thermodynamics are as follows.

- What theory should be employed to calculate the ion-ion interactions? Should it be primitive or non-primitive? Should it be based on the DH or the MSA theories?
- What is the significance of the interactions between ions and solvents? Should these be taken into account explicitly or implicitly?
- What is the significance of ion-ion association? Can it be modeled using either a chemical or a statistical mechanics approach?
- What type of relative static permittivity (RSP) should be taken into consideration when constructing electrostatic models? Should the solvent or the solution be used?

What model should be employed to calculate the RSP? Is kinetic depolarization a factor that needs to be taken into account? Is it necessary to explicitly factor in ion solvation?

- What type of model should be used for the non-electrostatic component? Should it be an Excess Gibbs free energy model or a residual Helmholtz free energy model? Will the selection of the non-electrostatic model have an effect on the results of property predictions?

The questions related to the development of electrolyte thermodynamic models are as follows.

- What parameters should be used in the parameter estimation procedure?
- What experimental data should be used in parameter estimation?
- What is the sensitivity of the properties to the model parameters?
- What is the performance of models in the region where experimental data are not used for parameter estimation? How predictive are the models?
- Are the parameters transferable?

The answers to these questions are challenging, yet vital, in model development for the thermodynamic properties of electrolyte solutions. Some of these questions are attempted to be answered by Marib-Mogensen [79], Olsen [78], and Kontogeorgis et al. [9, 39].

From these studies, the following conclusions can be drawn:

- The selection of the non-electrostatic component in equations of state for electrolytes may not be particularly significant, especially when compared to other elements of constructing a model for electrolyte systems.
- When the circumstances are comparable, it is hard to pick one of the DH and MSA equations over the other, as they both appear to be equally effective for electrolyte solutions.
- The discussion surrounding the importance of the RSP in the equations of state for electrolytes has been intense. The question of whether to employ a constant value for the solvent or opt for a concentration-dependent value, aligning with experimental data, remains unresolved. Both approaches have their merits and find usage in various literature on electrolyte models.
- The question of whether it is permissible to introduce a composition-dependent RSP after deriving the electrostatic contribution to Helmholtz energy, when the derivation was initially based on the assumption of a constant RSP, is still unresolved. Even though disregarding the assumption in the derivation may not be thermodynamically inconsistent, it is unclear if it is physically correct.
- In the parameter estimation, the main properties are mean ionic activity coefficient (MIAC), osmotic coefficient, and density.
- The choice of the sets of parameters in the parameter estimation procedure depends mainly on the choice of the non-electrostatic contribution to the electrolyte EoS. An ion-specific parameter estimation is more preferable compared with a salt-specific parameter estimation. Parameters are usually a size parameter (diameter of ions) and one or more energy parameters. It seems that the current models are far from a fully predictive approach since the prediction of properties such as density without adjusting the size parameter is almost impossible.

- High temperature systems, highly concentrated solutions, mixed solvent electrolyte solutions, and liquid-liquid equilibrium have shown to be challenging in modeling. A combination of ion-ion association and ion-solvent interactions are vital for capturing the physics in these conditions or systems.

Upon reviewing the literature on electrolyte thermodynamics, it is evident that the consensus within the community leans toward either the DH theory or the MSA theory for modeling long-range electrostatic interactions in their comprehensive forms. In recent years, much of the research has focused on exploring various combinations of parameters, objective functions, and RSP models to refine predictions, primarily with models originating from the eCPA [42], ePPC-SAFT [76], and eSAFT-VR-Mie [70] equations of state.

While these efforts have certainly deepened our understanding of the thermodynamics of electrolyte solutions, the outcomes remain somewhat ambiguous. For example, the decision on whether to use a composition-dependent or independent model for the RSP remains an unresolved issue. Moreover, many equations of state have demonstrated that a composition-dependent RSP, which diminishes marginally with increased salt concentration, can effectively model the thermodynamic properties of both aqueous and non-aqueous electrolyte solutions. The use of a concentration-dependent RSP is in accordance with thermodynamic principles. However, any arbitrary determination of its variation with salt concentration necessitates justification. Such arbitrary choices concerning RSP functions relative to concentration also prompts the question: Are we indeed modulating the electrostatic interactions by altering the medium's RSP?

Another avenue for refining models of electrolyte solutions involves incorporating previously ignored effects in both the electrostatic and non-electrostatic parts. One such overlooked effect is ion pairing. Marcus [80] noted:

> *"Ion pairing describes the (partial) association of oppositely charged ions in electrolyte solutions to form distinct chemical species called ion pairs."*

From references such as [80, 81], it is evident that ion pairs exist in the solutions. In the realm of electrolyte thermodynamics, only a few studies have taken ion pair formation into account. These studies either address ion pairing through a chemical approach, positing an equilibrium reaction between ions and ion pairs [57, 62, 82], or introduce association sites to ions, treating ion pairing in a manner akin to hydrogen-bond-forming molecules [76, 77].

The drawback of the first method lies in the need to determine the ion pair parameters either through assumptions or parameter fitting. Additionally, the dipolar nature of ion pairs is often overlooked. In contrast, the second approach models ion pair formation, which stems from long-range electrostatic interactions, using a short-range square-well potential, making it a departure from the actual system's reality. Furthermore, defining multiple sites for each ion can lead to the formation of ion networks, which, at least for simple electrolytes, have not been observed.

From a different perspective, advanced theories have been developed in the literature to implicitly factor in ion pairing within long-range electrostatic interactions. MSA theory has a rich literature that includes BiMSA [20] and AMSA [21–29]. Within the DH framework, no model has developed that implicitly accounts for the ion-ion association. However, it seems that a model that incorporates the ion-ion association in a manner similar to the BiMSA theory is required to be developed on the basis of the DH theory.

In summary, considerable effort has been put into advancing the accuracy and reliability of electrolyte thermodynamic models, primarily through enhancements in parameter estimation procedures. In these works, the physics used for the electrostatic contribution to the free energy of the system remains unchanged, relying on either the DH or MSA theories. While these contributions have enriched our understanding, particularly in the realm of parameter estimation, the ultimate objective of developing an accurate and reliable model for the

thermodynamic properties of electrolyte solutions remains elusive. It may now be the time to consider revising the models, such as substituting the ion-ion segments of the equations of state with their binding or associative counterparts, to potentially achieve a more accurate and robust representation.

1.2 Transport Properties

The transport properties of electrolyte solutions include, but are not limited to, electrical conductivity, self-diffusion, mutual diffusion, viscosity, and transference number. From a theoretical point of view, these properties are non-equilibrium dynamics of ions when an external or internal force is exerted on the ions. In the case of electrical conductivity, an external electric field is applied to the system that causes the movement of ions. For diffusion, the drifting force is the chemical potential gradient while for viscosity, it is the velocity gradient.

The prediction of the transport properties of electrolyte solutions is challenging because of the combination of the long-range electrostatic forces and non-equilibrium dynamics. Since the methodology introduced by Onsager and Fuoss [83] for non-equilibrium processes in electrolyte solutions, many models have been developed for the prediction of these properties [84].

One of the challenges of transport properties is that, unlike thermodynamic properties, it is not possible to develop generic models. For example, when an EoS is developed for electrolyte solutions, all thermodynamic properties can be calculated with the mean of the first- and second-order derivatives of the residual Helmholtz free energy. However, when a model for electrical conductivity is developed, it cannot be used with some conversion methods for the viscosity. As a result, it is not possible to study all transport properties together. In this work, we focus on electrical conductivity because of its importance in industrial applications and its sensitivity to ion pairing.

Regarding electrical conductivity, the following questions and challenges should be addressed:

- What type of model should be used to represent the electrical conductivity of electrolyte solutions: primitive or non-primitive?
- What theory should be employed in the construction of the model: MSA or DH?
- Which model accurately predicts the electrical conductivity of the electrolyte solutions? What are the limitations? Where and why do the models fail?
- What is the impact of ion-solvent interactions?
- What is the effect of ion-ion association?
- What is the current state of research regarding multi-component electrolyte solutions in general?

Unfortunately, the answers to many of these questions are not yet available from studies in the literature. However, it can be pointed out that:

- The DH theory has not been used to model the electrical conductivity of electrolyte solutions for over three decades.
- It is thought that DH-based models are only suitable for solutions with very low concentrations, while MSA-based models can be used for systems with higher concentrations.

- The accuracy of the models developed in the literature has not been systematically assessed.
- It is not clear what is the effect of ion-solvent interactions on the prediction of electrical conductivity.
- Most of the models developed in the literature are for a special case where the solution contains a single type of cation and anion. There are very few models for multi-component systems.
- Among all the models in the literature, only a few of them consider the size asymmetry of the ions.

Exploring electrolyte solutions calls attention to a critical gap in our understanding of their electrical conductivity. To bridge this knowledge void, a meticulous examination of major models from the literature is imperative. It is essential to recognize and address the restrictions that are present in these current models, turning these difficulties into chances for creativity. Addressing the gap requires the development of novel models that account for ion size asymmetry in both single- and multi-salt systems, rooted in the DH theory. By addressing this gap in knowledge, we can make significant advancements and gain a better understanding of how electrolytes behave.

1.3 Objectives and Research Design

As mentioned above, the models for the prediction of the properties of electrolyte solutions are not capable of satisfying industrial needs. As a result, further efforts are required to enhance the models in a more predictive and accurate direction. It has been mentioned that there are many questions regarding the prediction of both the thermodynamic and transport properties of electrolyte solutions. Therefore, further efforts are required to arrive at a fundamental understanding of electrolyte thermodynamics by answering these questions.

The main objective of this study is to increase the understanding of the concept of ion-ion association from two angles; thermodynamics and electrical conductivity, and then, if possible, to provide a new generation of useful and physically sound models for electrolyte solutions.

The minor objective of the Ph.D. thesis related to the main aim of the work can be divided into three parts. The first part focuses on the goals of the project related to the electrical conductivity of electrolyte solutions. The second part focuses on the targets of the projects related to the thermodynamic modeling of the associative electrolyte solution in which ion-ion association is active in them. The last part of the thesis focuses on the target of the project related to the unified and simultaneous investigation of the ion-ion association from both thermodynamic modeling and electrical conductivity.

The targets of the first part (encapsulated in Part II of the Ph.D. thesis) are:

- Recognition of the main model developed in the literature for the electrical conductivity of electrolyte solutions.
- Evaluation of the performance of the models developed in the literature to find their strengths and weaknesses.
- Exploring the effect of possible enhancement of electrical conductivity models by using a composition-dependent RSP and viscosity.
- Outlining a robust and rigorous method for the derivation of an electrical conductivity model based on the dynamic of ions in the solution.

- Development of an electrical conductivity model that is accurate, robust, and general.

The targets of the second part (encapsulated in Part III of the Ph.D. thesis) are the following:

- Finding major works in the literature on the incorporation of the ion-ion association in electrostatic interactions in the electrolyte solution.
- Performing an evaluation to find the weaknesses and strengths of the models.
- Fill the knowledge gap by developing an EoS for charged hard-sphere fluids that accounts for the ion-ion association based on the DH theory.

The targets of the last part (encapsulated in Part IV of the Ph.D. thesis) are:

- Combining the models for electrical conductivity and EoS for the associative electrolyte solution to enhance the prediction of the electrical conductivity in an implicit solvent model.
- Developing an electrolyte EoS that considers the formation of ion pairs in the solution.
- Introducing a unified framework for the investigation of ion-ion association in electrolyte solutions.
- Evaluating the unified framework in a predictive manner to find the limitations and strengths of the models.

To achieve the primary objectives and associated targets of the Ph.D. project, a methodical approach has been employed for parts II and III. These parts cover a step-by-step process. First, we conduct a thorough review of the literature focusing on either electrical conductivity or the thermodynamic modeling of ion-ion associations. Subsequently, we identify and implement existing models based on their distinctiveness. A systematic and equitable comparison will then be made between the model predictions and either the experimental data or the numerical simulation results. This comparative analysis aims to determine the strengths and weaknesses of the models and to identify any knowledge gaps. If necessary, efforts will be made to devise new models to address these gaps. Finally, the newly developed models will undergo extensive and systematic evaluation and validation to ensure their suitability for future application.

In part IV, an integration of models developed in the preceding sections, along with models from the existing literature, will be executed. This integrated approach aims to investigate the thermodynamic properties and electrical conductivity of associative electrolyte solutions. This investigation encompasses a spectrum of systems, including associative aqueous solutions, mixed-solvent systems, ionic liquid co-solvent systems, and aqueous solutions that form ion complexes. The objective is to simultaneously explore and analyze these diverse situations to obtain a comprehensive understanding of the subject matter.

1.4 Structure of the Thesis

This Ph.D. thesis is organized into four parts (Figure 1.1), encompassing a total of nine chapters. The second part is specifically focused on the electrical conductivity of electrolyte solutions under the assumption of full dissociation. This part comprises four detailed chapters, which dive into various aspects of the electrical conductivity phenomenon.

Moving on to the third part, the thesis shifts its focus to the concept of ion-ion association. Within this section, two chapters are dedicated to exploring and understanding the ion-ion association, providing a comprehensive examination of this aspect of the research.

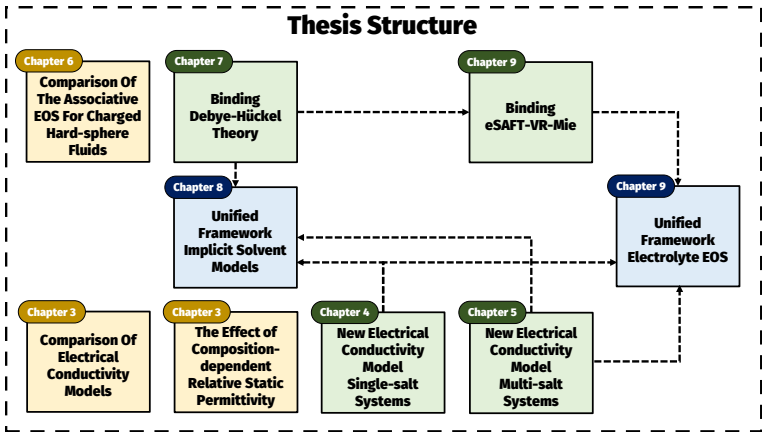

Figure 1.1. The structure of the Ph.D. thesis.

The final part of the thesis is dedicated to a unified investigation of the thermodynamic properties and electrical conductivity. This part integrates the models developed in both Parts II and III, facilitating a cohesive exploration of the subject matter. Each chapter within this part contributes to the unified understanding of thermodynamic properties and electrical conductivity, drawing on the insights gained from the preceding sections.

This doctoral dissertation is composed of the following chapters, each of which examines a distinct topic:

- **Chapter 2: Modeling of Electrical Conductivity**
  - Physical background of the electrical conductance process.
  - Literature review of the electrical conductance process in electrolyte solutions.
  - Introduction of the Ebeling hierarchy of the Smoluchowski dynamic for the movement of ions.
  - Introduction to the Fuoss-Onsager (FO) continuity equation.
  - Presentation of the equations for the derivation of new electrical conductivity models by inputting an equilibrium pair correlation function for both single-salt and multi-salt systems.
- **Chapter 3: Practical Investigation of Electrical Conductivity Models**
  - Presentation of the models developed in the literature for the electrical conductivity of single-salt systems.
  - Presentation of the compiled database of experimental data for the electrical conductivity of aqueous electrolyte solutions.
  - Comparison of the predictions of six electrical conductivity models developed in the literature with each other and with the experimental data.
  - Extension of the model by using a composition-dependent RSP and viscosity.
- **Chapter 4: New Model for Electrical Conductivity of Electrolyte Solutions; Single-Salt Systems**
  - Derivation of a new model based on the methodology explained in Chapter 2 for single-salt electrolyte solutions.

  - Extensive evaluation of the developed model by comparing its predictions with experimental data at various conditions and systems.
  - Comparison of the predictions of the developed model with the predictions of the models presented in Chapter 3.

- **Chapter 5: New Model for the Electrical Conductivity of Electrolyte Solutions; Mixed-Salt Systems**
  - Derivation of a new model based on the methodology explained in Chapter 2 for multi-salt electrolyte solutions.
  - Validating the accuracy of the model by comparing its predictions with various ternary salt-salt-water systems.
  - Discussion of the limitations of the developed model and possible remedies.

- **Chapter 6: Thermodynamic Modeling of Ion-Ion Association**
  - Presentation of a literature review on the thermodynamic modeling of ion-ion association in electrolyte solutions.
  - Performing a systematic investigation of four equations of state for charged hard-sphere fluids by comparing their predictions with numerical simulations and experimental data.
  - Validating the structural properties predicted by the models with the help of electrical conductivity models and data.

- **Chapter 7: Binding Debye-Hückel Theory**
  - Developing a new EoS for charged hard-sphere fluids that accounts for ion-ion association based on the reference cavity approximation, DH theory, Kirkwood theory, and Wertheim theory.
  - Validating the developed EoS by comparing the predicted mean ionic activity coefficient, individual activity coefficient, and osmotic coefficient with those of Monte Carlo simulations in a predictive manner.
  - Investigation of the importance of the ion-ion associations.
  - Investigation of the importance of cavity function.
  - Comparison of the BiDH and BiMSA models.

- **Chapter 8: Implicit Solvent Investigation**
  - Concurrent investigation of mean ionic activity coefficient and electrical conductivity of aqueous 2:2 sulfates.
  - Electrical conductivity of mixed solvent systems and ionic liquid-co-solvent systems using the BiDH theory and the single-salt electrical conductivity model.
  - Electrical conductivity of electrolytes forming ion complexes using the multi-salt electrical conductivity model.

- **Chapter 9: Binding eSAFT-VR-Mie**
  - Development of the Binding eSAFT-VR-Mie EoS.
  - Introduction of a unified framework for the simultaneous investigation of thermodynamic properties and electrical conductivity.
  - Presenting the evidence of ion-ion association for aqueous electrolyte solutions.

- Prediction of the liquid density, mean ionic activity coefficient, osmotic coefficient, and molar conductivity of three aqueous electrolyte solutions.
- Discussion of the effect of considering the ion-ion association in the prediction of electrolyte solutions.
- Discussion of the importance of the standard state association constant and Onsager's bookkeeping rule.

Part II

Electrical Conductivity

CHAPTER 2

Modeling of the Electrical Conductivity

The conductance of electrolyte solutions has been a long-standing yet complex topic in physical chemistry. Because of its importance in fields like electrochemistry, biophysics, chemical engineering, and biochemistry, it has received consistent research attention over the past hundred years. Chapter 1 explored the critical nature of this property. It emphasized its significance in both the formulation of electrolyte equations of state and its essential role in batteries and energy storage devices.

In this chapter, the electrical conductance process in electrolyte solutions will be explored from different distinct angles. First, the physical background of the electrical conductance process will be elucidated and the specific, molar, and equivalent conductivity will be defined. From a modeling perspective, the variation of electrical conductivity with salt concentration will be examined, and the concepts of relaxation and hydrodynamic effects will be elaborated upon. Various theoretical modeling strategies for the investigation of the electrical conductance process will be discussed. Notably, due to their significance in subsequent chapters, the continuity equation approaches will be extensively covered. Lastly, the equations necessary to develop a new electrical conductivity model based on the continuity approach will be presented.

2.1 Physical Background

When subjected to an external electric field, previously stationary ions in an electrolyte solution begin to migrate toward electrodes with opposite charges. Figure 2.1 depicts the macroscopic perspective of this ionic drift under the influence of an electric field. The phenomenon in which ions are driven by an external force leading to their movement or drift towards either the cathode or anode is termed the conductance process.

The steady-state (time-independent) flux of ions in the conductance process can be related to the external electric field as:

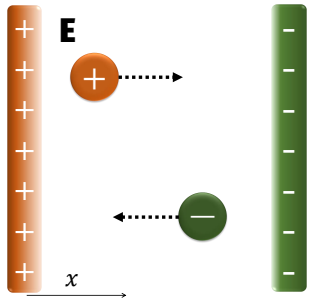

Figure 2.1. Independent migration or drift of ions.

$$J = A + BE + CE^2 + \cdots \tag{2.1}$$

In Eq. 2.1, J represents the ionic flux, defined as the quantity of moles of ions passing through a unit area every second, while E denotes the external electric field, which is a scalar quantity. For scenarios where the external electric field is minimal, which encompasses nearly all experimental electrical conductivity measurements, terms beyond the linear can be disregarded. Moreover, in the absence of an electric field, the ionic flux is zero. Hence, A in Eq. 2.1 must equate to zero. As a result, the ionic flux can be expressed as:

$$J = BE \tag{2.2}$$

The amount of charge that passes through a unit area per second is represented by the total current density of the ion (or charge flux), denoted by i. It can be linked to the ionic flux and on the basis of Eq. 2.2, to the external electric field, as illustrated in Eq. 2.3:

$$i = JZF = ZFBE \tag{2.3}$$

In the given equation, Z represents the valence of the ions and (F) represents the Faraday constant. The conductivity (or specific conductivity) can subsequently be defined as:

$$\chi \equiv ZBF \tag{2.4}$$

Consequently, the total current density i can be associated with the electric field as presented in Eq. 2.5:

$$E = \frac{i}{\chi} \tag{2.5}$$

Given that the electric field is defined by the electric potential per unit of length ($E = \frac{\Delta V}{l}$), and the total current is represented by iA, where A is the area of crossing, Eq. 2.5 corresponds to Ohm's law:

$$R = \frac{1}{G} = \frac{l}{\chi A} \tag{2.6}$$

In Eq. 2.6, R and G denote the resistance and conductance of the electrolyte solution, respectively. The conductivity of electrolyte solutions, when normalized by the salt concentration, was characterized by the German physicist Friedrich W. G. Kohlrausch [85]. He introduced the concept of molar conductivity as follows.

$$\Lambda \equiv \frac{\chi}{c_E} \tag{2.7}$$

As highlighted by Laidler and Meiser [85], the molar conductivity of electrolyte solutions can be conceptualized as the conductance offered by one mole of an electrolyte in a cell that has a surface area of $1\,m^2$ and a length of $1\,m$.

Within the literature surrounding the conductance process, there is another term frequently mentioned known as equivalent conductivity. This refers to the conductivity of a solution containing $1 g-eq$ of solute. However, Laidler and Meiser [85] noted that IUPAC recommends against using equivalent conductivity due to its inherent ambiguity. They instead propose to use the molar conductivity of $\frac{1}{\nu_i \mid Z_i \mid}$ moles of solute. Consequently, equivalent conductivity can be defined as:

$$\Lambda(\frac{1}{\nu_i \mid Z_i \mid} M_{\nu_+} A_{\nu_-}) = \frac{\chi}{\nu_i \mid Z_i \mid c_E} = \frac{\Lambda}{\nu_i \mid Z_i \mid}, i = + \, or \, - \tag{2.8}$$

The aforementioned properties were established with the aim of deriving a universal attribute for each salt in the conductance process within electrolyte solutions. Conductivity was introduced to account for the effects of geometry. Molar conductivity serves to standardize the effects of concentration, and equivalent conductivity was conceived to normalize the effects of charge concentration. Following this standardization, it was anticipated that the equivalent conductivity of electrolytes would depend solely on the type of electrolyte, regardless of salt concentration or ion valence type. Contrary to this expectation, experiments showed that the equivalent conductivity of electrolyte solutions decreases as the salt concentration increases. The origin of this behavior in electrolyte solutions stirred debate in the closing decades of the 19th century and the initial decades of the 20th century, which is elaborated upon in the section detailing the Historical Background of electrical conductivity.

However, following the foundational contributions of Debye, Hückel, and Onsager between 1923 and 1927 [4, 86–88], it is widely accepted that the conductivity of electrolyte solutions stems from three distinct components: ideal, hydrodynamic (also known as the electrophortic effect) and electrostatic (also known as the relaxation effect).

2.1.1 Ideal Contribution

The ideal contribution to ionic conductivity, also called *independent migration of ions or drift of ions*, arises from the mobility of ions when they are not pulled or pushed by other ions in the conductance process. In other words, the ideal contribution to ionic conductivity is the ionic conductivity at infinite dilution, denoted as λ_i^0.

Figure 2.1 shows a diagram that represents the ideal contribution to ionic conductivity. This figure illustrates that ions are driven by an external electric field (E), which causes them to migrate or drift toward electrodes with opposite charges. In the context of the ideal contribution to ionic conductivity, it is believed that the ions move freely, unaffected by the other ions in the solution. This scenario is typical when the solution is infinitely diluted, ensuring that there are no specific ion-ion interactions in the ideal contribution.

In a stationary state where there is neither an external electric field nor a concentration gradient in the solution, the ions move randomly, but their average displacement remains zero. However, when an external electric field is applied to the solution, one direction (aligned with the electric field) becomes more preferable to the ion movement than other directions. Under such circumstances, the average ion displacement is no longer zero.

If an ion were entirely isolated, for instance, in a vacuum, it would continue to accelerate until it hit the electrode. But in an electrolytic solution, the ion quickly encounters another ion or solvent molecule in its path, causing a disruption in its speed and trajectory. The ion's movement is not seamless; it is as though the medium resists the ion's movement. Consequently, the ion stops, resumes, and follows. However, the external electric field provides the ion with a specific direction (towards the oppositely charged electrode), so even with its erratic movement, the ion gradually makes its way towards this electrode. Thus, the movement of an ion is biased in a specific direction.

The mean of the velocity component of an ion derived from the external force is essentially the multiplication of the acceleration caused by this force and the average interval between collisions. Therefore, the terminal drift velocity v_i^d is defined as Eq. 2.9:

$$v_i^d = \frac{\mathbf{F}_i^{ext}}{m_i}\tau_i \tag{2.9}$$

In Eq. 2.9, the terms $\mathbf{F}_i^{ext}$, m_i, and τ_i represent the force exerted on the ion by the external electric field, the mass of the ion, and the average time interval between successive collisions of the ion, respectively. Following this, the absolute mobility of the ions is defined as:

$$\omega_i \equiv \frac{\tau_i}{m_i} \equiv \frac{v_i^d}{\mathbf{F}_i^{ext}} \tag{2.10}$$

According to Bockris et al. [89] in Section 4.4.4 of their book, the overall current density can be correlated to the conventional ion mobility defined as $\omega_i^{conv} = \omega_i e Z_i$. This relationship is expressed in Eq. 2.11:

$$i = \sum_{j=1}^{C} i_j = \sum_{j=1}^{C} e Z_j \rho_j \omega_j^{conv} E \tag{2.11}$$

In Eq. 2.11, ρ_j signifies the density of the number of ions. Z_i and e represent the ionic valence and the elementary charge, respectively. Combining equations 2.5 and 2.11, the specific conductivity of the electrolyte solution can be obtained as Eq. 2.12:

$$\chi = \frac{i}{E} = \sum_{j=1}^{C} e Z_j \rho_j \omega_j^{conv} \tag{2.12}$$

Eq. 2.12 illustrates the ideal contribution to the solution's specific conductivity. The central component of this equation is either the conventional mobility or the absolute mobility of ions.

The absolute mobility of the ions quantifies the drift velocity resulting from the external force $\mathbf{F}^{ext}$. In Eq. 2.9, it is proposed that the terminal drift velocity of the ions is determined solely by the interactions between the ion and the solvent. To put it another way, the influence of electrostatic interactions is set aside. This supposition is accurate predominantly when the solution is infinitely diluted. In such circumstances, the absolute mobility of ions, referred to as ω_i, can be associated with the diffusion coefficient and ionic conductivity using the Einstein equation and the definition of specific conductivity, as referenced in [89, 90]:

$$\omega_i = \frac{D_i^0}{k_B T} = \frac{N_A \lambda_i^0}{F^2 |Z_i|} \tag{2.13}$$

In the prediction of the conductivity of electrolyte solutions, it is often more practical to utilize the ionic conductivity or diffusion coefficient at infinite dilution, rather than the absolute or conventional mobility. In summary, the ideal contribution to the specific conductivity can be expressed as Eq. 2.14:

$$\chi^{ideal} = \frac{e^2}{k_B T} \sum_{j=1}^{C} \rho_j D_j^0 Z_j^2 = \frac{1}{N_A} \sum_{j=1}^{C} \rho_j \mid Z_j \mid \lambda_j^0 \tag{2.14}$$

2.1.2 Hydrodynamic Contribution

The hydrodynamic, often referred to as the electrophoretic, correction to the ideal conductivity is a consequence of ions moving simultaneously towards their oppositely charged electrodes. To gain a clearer understanding of this correction or effect, it is beneficial to consider the ionic cloud or atmosphere model proposed by Debye and Hückel [4, 86]. In this conceptualization, Debye and Hückel pictured a central ion (irrespective of its charge) positioned at the origin of a spherical coordinate, encircled by a cloud of oppositely charged ions (with fewer ions of the same charge present). This representation of electrolyte solutions, in the absence of an external electric field, is illustrated in Figure 2.2.

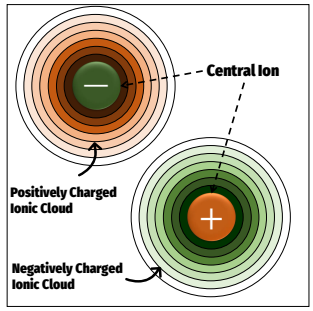

Figure 2.2. The ionic atmosphere in a stationary state.

A distinctive feature of this ionic cloud is its perfect sphericity. Thus, as described by Debye and Hückel, both the electric potential and local number density of ions depend solely on the distance from the center of the central ion. This conceptualization has been extensively discussed by Bockris et al. [89]. It is vital to recognize that, given that this ionic cloud primarily comprises oppositely charged ions, it represents a charged sphere with a charge opposite to that of the central ion. The radius of this sphere is equivalent to the inverse of the Debye length (κ).

Imagine that an external electric field is applied to the solution. Under this influence, the central ion is driven towards the electrode with the opposite charge. Concurrently, the ions within the ionic cloud are propelled either toward the cathode or the anode on the basis of their individual charges. For simplicity, let us consider there is a central ion with an encompassing ionic cloud bearing the opposite charge (overlooking the fact that the ionic cloud comprises individual ions). When an external electric field is introduced, the central ion moves, let us say, in the positive direction of the x-axis, as depicted in Figure 2.3. Being oppositely charged, the ionic cloud is also affected by the external electric field, propelling it in the negative direction of the x-axis. Because the central ion is intrinsically part of the ionic cloud, this motion exerts a counteracting push on the central ion, opposing its initial movement, which in turn decreases its velocity.

This hindrance to the movement of the ions during the conductance process diminishes their velocity, and consequently, the ionic conductivity compared to the ideal velocity or conductivity. Given that the size of the ionic cloud is similar to that of a colloid particle, this phenomenon is termed electrophoretic, drawing parallels with the electrophoresis observed in colloidal systems.

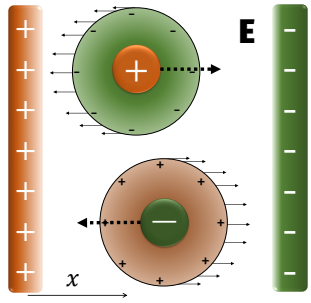

Figure 2.3. A schematic of the hydrodynamic contribution to the electrical conductivity.

2.1.3 Electrostatic Contribution

When subjected to an electric field, the ion distribution function becomes skewed and loses its symmetry. Consequently, the likelihood of locating an ion around the central one is not solely dependent on distance, but also varies with direction. In such scenarios, an asymmetric distribution function is required. This added complexity makes the theoretical exploration of electrical conductivity more challenging [89].

A more direct approach to managing an ellipsoid-shaped ionic cloud (as shown in Figure 2.5) is to start by assuming a symmetric ionic atmosphere and then introduce a slight perturbation. Picture, for a moment, a perfectly spherical ionic cloud encircling a stationary central ion. Now, envision an external force that displaces this central ion along the x-axis. In response, the ionic cloud repositions itself in alignment with the central ion's new location. The electric field created by this ongoing adjustment, or relaxation, of the cloud trailing the ion and gathering ahead of it is referred to as the relaxation field [89, 90].

One immediate outcome of the relaxation phenomenon is that the charge center of the ionic cloud (which bears a charge opposite to that of the central ion) lags behind the central ion during this process. As a result, it applies a force counter to the direction of the external electric field. This leads to a decrease in the ionic velocity and, subsequently, the ionic conductivity [89, 90].

This force reduces the velocity or conductivity of ions compared to the ideal case. The electrical force that arises due to the asymmetry of the ionic cloud, which is made simpler by the relaxation depiction, is referred to as the relaxation contribution to the electrical conductivity of electrolyte solutions.

2.2 Historical Background

In 1923, Peter J. Debye and Erich Hückel authored two pivotal papers that laid the foundation for the contemporary theory of electrolyte solutions [4, 86]. In their initial paper titled *"On the Theory of Electrolytes I. Freezing Point Depression and Related Phenomena"*, they addressed the inconsistencies present in the Arrhenius and van't Hoff theories concerning the osmotic and activity coefficients of strong electrolytes.

In their subsequent paper [86] titled *"On the Theory of Electrolytes. II Limiting Law for Electric Conductivity"*, Debye and Hückel discussed the process of electrical conductance in electrolyte solutions. Contrary to their first paper, here they confined their analysis to infinitely diluted solutions regarding electrical conductivity, emphasizing that:

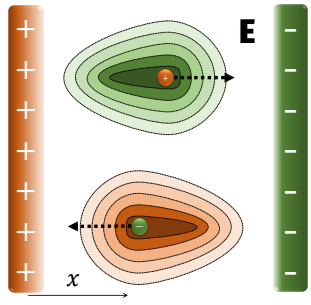

Figure 2.4. The egg-shaped ionic atmosphere in the conductance process.

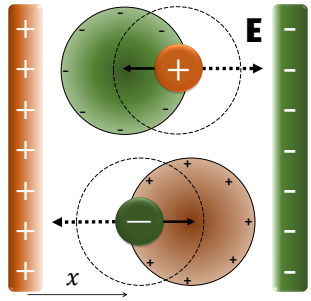

Figure 2.5. A schematic for the relaxation or electrostatic contribution to the electrical conductivity.

> *"Since even the limiting case of low concentrations needs a lengthy discussion, we have limited ourselves, in the following, consistently to this case, and have not attempted to generalize the formulas in order to make them applicable to higher concentrations."*

They introduced a limiting law concerning molar conductivity. Their model suggested that the molar conductivity could have a linear relationship with the square root of the salt concentration. Nonetheless, their model could not accurately predict the slope of this linear decrease when compared to the experimental findings of Kohlrausch.

Born in Oslo on 27 November 1903, Lars Onsager was a mere 22 years old when he approached Peter Debye in his Zürich office to highlight the inaccuracies in their theory regarding electrical conductivity [91]. In subsequent years, specifically 1926 and 1927, Onsager published two papers [87, 88] titled *On the theory of electrolytes. I* and *On the theory of electrolytes. II*. Through these publications, he modified the theory developed by Debye and Hückel on the limiting law of electrical conductivity.

Lars Onsager's monumental work on electrolytes encompasses approximately one-third of his entire body of work and stands out for its depth, clarity, and innovation. As a brilliant chemical engineer, he postulated what is now known as the fourth law of thermodynamics or the Onsager reciprocal relations even before earning his Ph.D. The respected physicists in the domain of electrolyte theory, Werner Ebeling and Jean-Claude Justice [91], have encapsulated Onsager's significant contributions in this realm.

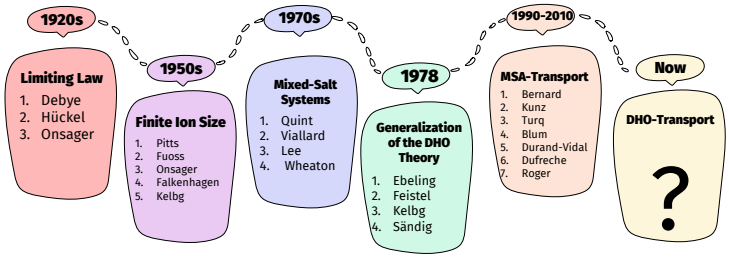

Figure 2.6. Historical background of electrical conductance process. Graphic is from Slidesgo and Freepik.

In 1932, Onsager, in collaboration with his student Raymond Fuoss, published a paper titled *Irreversible processes in electrolytes. diffusion, conductance, and viscous flow in arbitrary mixtures of strong electrolytes* [83]. Ebeling and Justice remarked on this work, as cited in [91], calling it *"the most comprehensive work published so far on irreversible processes in electrolytes"*. This paper was a foundational work for the theory of electrical conduction in electrolyte solutions and is considered the basis for any theoretical investigation of electrical conductivity.

In the seminal works of Debye and Hückel [86], Onsager [87, 88], and the collaborative effort of Onsager and Fuoss [83], ions were conceptualized as point charges. As a result, only the limiting law could be determined from these theories. Advancing this field in 1953, Pitts [92] modified the theory on conductance and viscous flow in electrolyte solutions. He assumed that all ions in the solution possess a definitive size, equivalent to distance of the closest approach. Through this framework, Pitts was able to enhance the applicability of the electrical conductivity model by accounting for ions with finite size. However, when addressing viscosity, he did not bring any alterations to the findings previously presented by Falkenhagen et al. [93].

Following Pitts' contribution [92], there were substantial advances in the field by researchers such as Fuoss and Onsager [94–100], Falkenhagen et al. [101, 102], Quint and Viallard [103–105], and Lee and Wheaton [106–108]. These scholars refined the limiting law for electrical conductivity by assuming a finite, yet consistent, size for all ions. Notably, among these extensive studies, the models presented by Quint and Viallard and Lee and Wheaton were particularly relevant to mixed electrolyte solutions.

It is important to emphasize that Onsager and Kim had earlier established the limiting law tailored for mixed electrolyte solutions [109]. Their groundbreaking research serves as the foundational framework for theoretical examinations concerning the electrical conductance process in multi-component systems.

A significant advancement in the theory of the conductance process came from the work of Ebeling, a student of Hans Falkenhagen, and his colleagues [110]. They expanded upon the Debye-Hückel-Onsager theory by using a hierarchy analogous to the BBGKY hierarchy. This pivotal paper laid the groundwork for subsequent models, encompassing not just electrical conductivity but also mutual and self-diffusion coefficients.

Bernard and his team [111] introduced a novel model for the electrical conductivity of electrolyte solutions, leveraging the MSA theory for the equilibrium segment of the pair correlation function. In the realm of electrical conductivity, this research is believed to be the pioneering effort that takes into account the size asymmetry of ions. Subsequently, the transport theory was thoroughly examined, leading to the emergence of the MSA-transport theory [112–117].

Subsequent to the advent of the MSA-transport theory, there have been limited studies, such as [118, 119], aimed at improving the prediction of electrical conductivity in electrolyte solutions. However, evaluations suggest that these models either lack accuracy compared to the MSA theory [120] or, at best, achieve similar precision [121].

This compilation of works is not comprehensive, but focuses on analytical theories of the electrical conductance process, aligning closely with the objectives of this thesis. In the subsequent section, we will delve into the modeling techniques used in the theoretical exploration of non-equilibrium thermodynamics and address related literature pertaining to molecular simulations.

2.3 Modeling Approaches

Dynamic processes in electrolyte solutions can be performed from various modeling approaches. Barthel et al., in their monograph [84], pointed out that the average time scale

of the processes can give us a good hint to choose between different modeling approaches. Then, they presented a guideline for modeling approaches based on the time scale of the processes. Figure 2.7 presents this guideline.

For extremely short processes, specifically when $t < \tau_1$, it is proposed that the spatial ($\mathbf{r}$) and momentum ($\mathbf{p}$) coordinates of both solutes and solvents be considered. The phase space in this context is directed by the Liouville equation, and the most suitable theoretical method to employ would be molecular dynamics (MD) simulation. This method aligns with the Born-Oppenheimer approach.

For time scales exceeding τ_1, it is pointed out that the solvent can be conceptualized as a *dynamic continuum*. This is because solvent fluctuations dissipate faster than those of ions. In such scenarios, the dynamics are solely represented by the spatial and momentum coordinates of the ions. Under these conditions, the Liouville equation simplifies to the Fokker-Planck equation. This Fokker-Planck stage, parallel to the Langevin dynamics, serves as the foundation for the Brownian dynamics (BD) simulation technique. Within this framework, the impact of the solvent is manifested through both a frictional force and a random force component. These forces intertwine with two additional force components, representing electrostatic interactions and the acceleration of ions resulting from collisions with solvent particles.

For duration where $t > \tau_2$, the ion velocities have settled and all particles reach their terminal velocities. As a result, there is no acceleration (or relaxation) observed. In this state, the frictional forces are precisely counteracted by the random forces and the forces resulting from ion-ion interactions. The system's progression in the phase space can then be approximated using the Smoluchowski equation.

An alternative approach transitions from the Fokker-Planck equation to classical hydrodynamic equations through a hierarchy reminiscent of Bogoliubov-Born-Green-Kirkwood-Yvon (BBGKY). The emergent description level parallels that provided by the Smoluchowski equation. At this juncture, the variables under consideration include time-dependent density correlation functions for two particles, along with the relative velocities of ions of types i and j. Beyond the Smoluchowski equation, the hydrodynamic continuity equations represent another optimal launching pad for theories on this plane.

2.4 Continuity Equation Approaches

2.4.1 Equation of Motion

Ebeling et al. [110] demonstrated that a hierarchy analogous to the BBGKY hierarchy (refer to Section 4.2.2 in ref. [84] for details) can be established for the Smoluchowski equation [84, 122]. For one-body densities, where $f_i = f_i(\mathbf{r})$, this is expressed as Eq. 2.15:

$$\frac{\partial f_i(\mathbf{r}_1, t)}{\partial t} + \nabla_1 \cdot \mathbf{J}_i(\mathbf{r}_1, t) = 0 \tag{2.15}$$

In the given equation, $\mathbf{J_i}$ represents the flux of ion i, which is defined as follows:

$$\mathbf{J}_i(\mathbf{r}_1, t) = f_i(\mathbf{r}_1, t)\mathbf{v}_i(\mathbf{r}_1, t) \tag{2.16}$$

And, $\mathbf{v}_i$ is the velocity vector:

$$\mathbf{v}_i(\mathbf{r}_1, t) = \mathbf{v}_i^s(\mathbf{r}_1, t) + \omega_i \mathbf{F}_i(\mathbf{r}_1, t) + \sum_{j=1}^{C} \int \bar{\mathbf{T}}_{ij}(\mathbf{r}_1, \mathbf{r}_2)\mathbf{F}_j^i(\mathbf{r}_1, \mathbf{r}_2) \frac{f_{ij}(\mathbf{r}_1, \mathbf{r}_2)}{f_i(\mathbf{r}_1)} d\mathbf{r}_2 \tag{2.17}$$

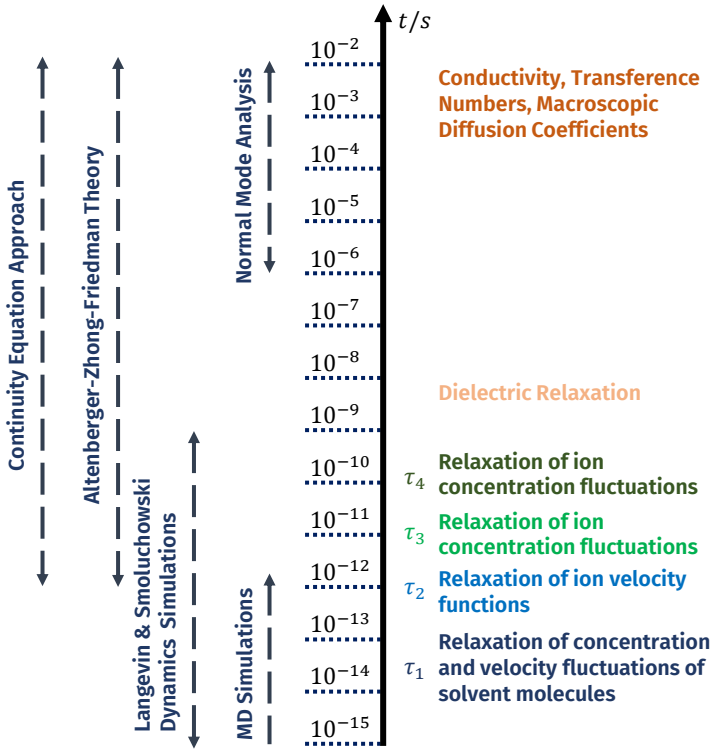

Figure 2.7. Time scales permitting a rough orientation on the typical dynamic properties of electrolyte solutions and the corresponding theoretical approaches (adapted from Barthel et al. [84]).

In the given equation, $\bar{\mathbf{T}}_{ij}$ represents the hydrodynamic interaction tensor between ions i and j, which can be identified as either the Rotne-Prager or the Oseen mobility tensors. Furthermore, $\mathbf{F}_i$ (as defined by Eq. 2.18) and $\mathbf{F}_j^i$ denote the average force on ion i and the average force on ion j situated at $\mathbf{r}_2$ when ion i is positioned at $\mathbf{r}_1$, respectively. f_{ij} describes the likelihood of locating ion i at $\mathbf{r}_1$ when ion j is at $\mathbf{r}_2$.

$$\mathbf{F}_i(\mathbf{r}_1) = \mathbf{F}_i^{ext}(\mathbf{r}_1) - k_B T \nabla_1 \ln f_i(\mathbf{r}_1) + \mathbf{F}_i^{int}(\mathbf{r}_1) \tag{2.18}$$

In Eq. 2.18, $\mathbf{F}_i^{ext}$ denotes the external force exerted on ion i. For the conductance process, this originates from the external electric field. Meanwhile, $\mathbf{F}_i^{int}$ signifies the internal force on ion i, which, in the context of conductance, corresponds to the relaxation force.

$$f_i(\mathbf{r}_1)\mathbf{F}_i^{int}(\mathbf{r}_1) = -\sum_{j=1}^{C} \int \nabla_1 \phi_{ij}(\mathbf{r}_1, \mathbf{r}_2) f_{ij}(\mathbf{r}_1, \mathbf{r}_2) d\mathbf{r}_2 \tag{2.19}$$

In Eq. 2.19, ϕ_{ij} is the potential between ion i and j. The mean force acting on ion j located at $\mathbf{r}_2$ when ion i is at $\mathbf{r}_2$ is given by Eq. 2.20:

$$\mathbf{F}_j^i(\mathbf{r}_1, \mathbf{r}_1) = -\mathbf{F}_i^{ext}(\mathbf{r}_1) - k_B T \nabla_2 \ln f_{ji}(\mathbf{r}_1, \mathbf{r}_1) + \mathbf{F}_{ji}^{int}(\mathbf{r}_1, \mathbf{r}_2) \tag{2.20}$$

The internal contribution to this force is written as follows:

$$\mathbf{F}_{ji}^{int}(\mathbf{r}_1,\mathbf{r}_2) = -\nabla_2\phi_{ji}(\mathbf{r}_1,\mathbf{r}_2) - \sum_{k=1}^{C}\int \nabla_1\phi_{ji}(\mathbf{r}_2,\mathbf{r}_3)\frac{f_{ijk}(\mathbf{r}_1,\mathbf{r}_2),\mathbf{r}_3)}{f_{ij}(\mathbf{r}_1,\mathbf{r}_2)} \tag{2.21}$$

The subsequent tier in the hierarchy of equations is represented by Eq. 2.22. This equation serves as the continuity equation for the two-particle densities, denoted as f_{ij}:

$$\frac{\partial f_{ij}(\mathbf{r}_1,\mathbf{r}_2,t)}{\partial t} + \nabla_1\cdot\mathbf{J}_i^j(\mathbf{r}_1,\mathbf{r}_2,t) + \nabla_2\cdot\mathbf{J}_j^i(\mathbf{r}_1,\mathbf{r}_2,t) = 0 \tag{2.22}$$

For a homogeneous system, under the condition that the external force remains constant, a condition applicable to the conductance process, the two and three body densities can be expressed as per Eq. 2.23 and Eq. 2.24, respectively:

$$f_{ij}(\mathbf{r}_1,\mathbf{r}_2) \simeq f_i(\mathbf{r}_1)f_j(\mathbf{r}_2)g_{ij}(\mathbf{r}_1,\mathbf{r}_2) \simeq \bar{f}_i(\mathbf{r}_1)\bar{f}_j(\mathbf{r}_2)g_{ij}(\mathbf{r}_1,\mathbf{r}_2) \tag{2.23}$$

$$\begin{aligned} f_{ijk}(\mathbf{r}_1,\mathbf{r}_2,\mathbf{r}_3) \simeq &\quad f_i(\mathbf{r}_1)f_j(\mathbf{r}_2)f_k(\mathbf{r}_3)g_{ijk}(\mathbf{r}_1,\mathbf{r}_2,\mathbf{r}_3) \\ \simeq &\quad \bar{f}_i(\mathbf{r}_1)\bar{f}_j(\mathbf{r}_2)\bar{f}_k(\mathbf{r}_3)g_{ijk}(\mathbf{r}_1,\mathbf{r}_2,\mathbf{r}_3) \end{aligned} \tag{2.24}$$

In equations 2.23 and 2.24, $\bar{f}_i$, g_{ij}, and g_{ijk} are the mean value of the two-body and three-body distribution functions f_i, respectively. The internal force is then given by Eq. 2.25:

$$\mathbf{F}_i^{int}(\mathbf{r}_1) = \mathbf{F}_i^{rel}(\mathbf{r}_1) = -\sum_{j=1}^{C}\bar{f}_j\int \nabla_1\phi_{ij}(\mathbf{r}_1,\mathbf{r}_2)g_{ij}(\mathbf{r}_1,\mathbf{r}_2)d\mathbf{r}_2 \tag{2.25}$$

From Eq. 2.17, the velocity equation can be obtained from the following equation:

$$\begin{aligned} \mathbf{v}_i(\mathbf{r}_1,t) = &\quad \mathbf{v}_i^s(\mathbf{r}_1,t) + \omega_i(\mathbf{F}_i^{ext}(\mathbf{r}_1,t) + \mathbf{F}_i^{rel}(\mathbf{r}_1,t)) + \\ &\sum_{j=1}^{C}\bar{f}_j\int \bar{\mathbf{T}}_{ij}(\mathbf{r}_1,\mathbf{r}_2)\mathbf{F}_j^i(\mathbf{r}_1,\mathbf{r}_2)g_{ij}(\mathbf{r}_1,\mathbf{r}_2)d\mathbf{r}_2 \end{aligned} \tag{2.26}$$

If the relaxation effects on hydrodynamics are disregarded, the hydrodynamic or electrostatic effects can be decoupled as follows:

$$\begin{aligned} &\sum_{j=1}^{C}\bar{f}_j\int \bar{\mathbf{T}}_{ij}(\mathbf{r}_1,\mathbf{r}_2)\mathbf{F}_j^i(\mathbf{r}_1,\mathbf{r}_2)g_{ij}(\mathbf{r}_1,\mathbf{r}_2)d\mathbf{r}_2 \approx \\ &\sum_{j=1}^{C}\bar{f}_j\int \bar{\mathbf{T}}_{ij}(\mathbf{r}_1,\mathbf{r}_2)\mathbf{F}_j(\mathbf{r}_1,\mathbf{r}_2)g_{ij}^0(\mathbf{r}_1,\mathbf{r}_2)d\mathbf{r}_2 \end{aligned} \tag{2.27}$$

Utilizing the Oseen tensor as outlined in Eq. 2.28, and substituting the average one-body density with the bulk density of ions ($\bar{f}_i = \rho_i$), we can refine Eq. 2.27 to an approximation represented by Eq. 2.29:

$$\bar{\mathbf{T}}_{ij} = \frac{1}{8\pi\eta\mathbf{r}_{ij}}(\bar{I}I + \frac{\mathbf{r}_{ij}\otimes\mathbf{r}_{ij}}{\mathbf{r}_{ij}^2}) \tag{2.28}$$

$$\sum_{j=1}^{C} \bar{f}_j \int \bar{\mathbf{T}}_{ij}(\mathbf{r}_1, \mathbf{r}_2)\mathbf{F}_j(\mathbf{r}_1, \mathbf{r}_2) g_{ij}^0(\mathbf{r}_1, \mathbf{r}_2) d\mathbf{r}_2$$
$$= \frac{2}{3\eta} \int_0^\infty \sum_{j=1}^{C} \rho_j r g_{ij}^0(r) dr (\mathbf{F}_j^{ext} + \mathbf{F}_j^{rel}) \tag{2.29}$$

The integral on the right-hand side of Eq. 2.29 fails to converge when $\sum_j \rho_j \mathbf{F}_j \neq 0$. If we overlook the solvent's hydrodynamic velocity, the right-hand side of Eq. 2.29 can be substituted with the expression in Eq. 2.30:

$$\frac{2}{3\eta} \int_0^\infty \sum_{j=1}^{C} \rho_j r h_{ij}^0(r) dr (\mathbf{F}_j^{ext} + \mathbf{F}_j^{rel}) \tag{2.30}$$

In the above expression, $h_{ij}^0 = g_{ij}^0 - 1$ represents the pair correlation function for ion j when it is near ion i. By substituting Eq. 2.30 into Eq. 2.26 and setting aside the solvent's hydrodynamic velocity ($\mathbf{v}_i^s$), we can formulate the equation for the velocity of the ion as shown in Eq. 2.31:

$$\mathbf{v}_i = \omega_i (\mathbf{F}_i^{ext} + \mathbf{F}_i^{rel}) + \frac{2}{3\eta} \int_0^\infty \sum_{j}^{C} \rho_j r h_{ij}^0 dr (\mathbf{F}_j^{ext} + \mathbf{F}_j^{rel}) \tag{2.31}$$

Eq. 2.31 serves as the foundational equation for many existing theories of electrical conductance. Nevertheless, the manner in which these equations are presented might vary across different sources.

2.4.2 Ideal Contribution

The ideal part of the electrical conductivity, discussed in Section 2.1.1, represents the motion of ions under the influence of an external electric field when unaffected by other ions. Under such circumstances, typically occurring at the infinite dilution limit, the velocity of the ion directly corresponds to the external electric force acting on the solution through the concept of *absolute mobility*.

$$\mathbf{v}_i^0 = \omega_i \mathbf{F}_i^{ext} \tag{2.32}$$

In Eq. 2.32, the term ω_i represents the absolute mobility of ions. This absolute mobility can be related to the diffusion coefficient at infinite dilution or the ionic conductivity at infinite dilution using the Nernst-Einstein equation (Eq. 2.13).

In the conductance process, the external electric force exerted on the ion can be expressed in terms of the external electric field, as depicted in Eq. 2.33:

$$\mathbf{F}_i^{ext} = eZ_i \mathbf{E} \tag{2.33}$$

Since we are interested only in the component of velocity in the x-direction perpendicular to the electrodes, we can drop the vector notation and use the scalar values. Hence:

$$v_i^0 = \omega_i F_i^{ext} = \omega_i e Z_i E = \frac{D_i^0}{k_B T}{}_i \, e Z_i E = \frac{N_A \lambda_i^0}{F^2 |Z_i|} e Z_i E \tag{2.34}$$

2.4.3 Hydrodynamic Contribution

As noted above, our focus is solely on the scalar value of ion velocities that align with the direction of the applied electric force, represented by the x direction in figures 2.1, 2.3, and 2.5. Consequently, we have eliminated the vector form from Eq. 2.31. Through straightforward calculations, we can express Eq. 2.31 as Eq. 2.35:

$$v_i = (v_i^0 + \delta v_i)(1 + \frac{F_i^{rel}}{F_i^{ext}}) \tag{2.35}$$

The term δv_i in Eq. 2.31 represents the adjustment of the velocity of the ions as they drift in response to the external electric field, factoring in hydrodynamic (or electrophoretic) effect. This correction can be derived from Eq. 2.36:

$$\delta v_i = \frac{2}{3\eta} \sum_j^C \rho_j e Z_j E \int_0^\infty r h_{ij}^0(r) dr \tag{2.36}$$

In Eq. 2.36, the term h_{ij}^0 denotes the equilibrium pair correlation function. To derive an equation accounting for the electrophoretic velocity adjustment of ions, one needs to specify the equilibrium pair correlation function between ions i and j. This particular equation plays a crucial role in Chapters 4 and 5, where new models for electrical conductivity are introduced. Additionally, it is worth noting that this equation has been formulated considering a mix of different types of ions. As such, it also accurately captures the electrophoretic effects in mixed-electrolyte solutions.

2.4.4 Relaxation Correction

The relaxation force that affects the central ion is detailed in Eq. 2.25. To compute this force, one necessitates a robust equation for the radial distribution function (RDF). This function varies on the basis of both distance and direction, given the asymmetry inherent in the ionic cloud. As highlighted in Section 2.1.3, following this methodology is not mathematically advantageous. An alternative avenue to ascertain the relaxation force acting on the central ion is through the FO continuity equation combined with the linear response theory.

The subsequent tier in the hierarchy introduced by Ebeling et al. [110] for the Smoluchowski equation, represented by Eq. 2.22, manifests as the FO continuity equation. This can be expressed as follows:

$$-\frac{\partial f_{ij}(\mathbf{r}, t)}{\partial t} = \nabla_1.(f_{ij}(\mathbf{r}, t)\mathbf{v}_{ij}) + \nabla_2.(f_{ji}(\mathbf{r}, t)\mathbf{v}_{ji}) \tag{2.37}$$

Within Eq. 2.37, the term $\mathbf{v}_{ij}$ symbolizes the velocity of the ion j located in the vicinity of ion i. In a steady state and by leveraging the assumptions from Eq. 2.23 pertaining to two-body densities, the FO continuity equation can be reformulated as presented in Eq. 2.38:

$$\nabla.(g_{ji}(\mathbf{r})\mathbf{v}_{ji}(\mathbf{r})) + \nabla.(g_{ij}(\mathbf{r})\mathbf{v}_{ij}(\mathbf{r})) = 0 \tag{2.38}$$

The velocity of ion j near ion i, denoted as $\mathbf{v}_{ji}$, can be correlated with the forces exerted on ion j when it is considered the central ion.

$$\mathbf{v}_{ji}(\mathbf{r}) = \mathbf{v}_i^s(\mathbf{r}) + \omega_i[\mathbf{F}_{ji}(\mathbf{r}) - k_B T \nabla \ln f_{ji}(\mathbf{r})] \tag{2.39}$$

The force acting on the ion i in the atmosphere of the ion j is given by Eq. 2.39:

$$\mathbf{F}_{ji} = \mathbf{F}_i^{ext} + \mathbf{F}_i^{int} - eZ_i\nabla\psi_j(\mathbf{r}) \tag{2.40}$$

In equations 2.39 and 2.40:

- $-k_BT\nabla \ln f_{ji}(\mathbf{r})$ represents the diffusion term influenced by Brownian motions.
- $\mathbf{F}_i^{ext}$ denotes the external force applied to ion i.
- $\mathbf{F}_i^{int}$ refers to the internal force on the ion i, which arises due to the uneven distribution of the ionic cloud.
- $-eZ_i\nabla\psi_j(\mathbf{r})$ signifies the force imposed by the ion j along with its surrounding atmosphere.

For ion j, the surrounding electric potential is presumed to be governed by the Poisson equation (Eq. 2.41).

$$\nabla^2\psi_j(\mathbf{r}) = \frac{4\pi}{\epsilon}\sum_{k=1}^{C}\rho_k eZ_k g_{jk}(\mathbf{r}) \tag{2.41}$$

Integrating equations 2.39 through 2.41 into Eq. 2.40 and preserving only the linear terms, the resulting expression becomes:

$$\begin{aligned} &k_BT(\omega_i+\omega_j)\nabla^2 g_{ji}(\mathbf{r}) + eZ_i\omega_i\nabla^2\psi_j(\mathbf{r}) \\ &-eZ_j\omega_j\nabla^2\psi_i(\mathbf{r}) = (\omega_i\mathbf{F}_i^{ext} - \omega_j\mathbf{F}_j^{ext})\cdot\nabla g_{ji}(\mathbf{r}) \end{aligned} \tag{2.42}$$

The challenge can be addressed by assuming a first-order perturbation in the ionic cloud when subjected to an external electric field. Consequently, expressions for the electric potential, pair correlation function, and RDF can be articulated as depicted in equations 2.43, 2.44, and 2.45, in the order:

$$\psi_i(\mathbf{r}) = \psi_i^0(\mathbf{r}) + \psi_i^1(\mathbf{r}) \tag{2.43}$$

$$h_{ij}(\mathbf{r}) = h_{ij}^0(\mathbf{r}) + h_{ij}^1(\mathbf{r}) \tag{2.44}$$

$$g_{ij}(\mathbf{r}) = g_{ij}^0(\mathbf{r}) + g_{ij}^1(\mathbf{r}) \tag{2.45}$$

In the aforementioned equations, the superscript 0 signifies the contributions from equilibrium or steady-state conditions to the electric potential, the pair correlation function and the RDF. Conversely, the superscript 1 indicates the contributions arising from the first-order perturbation under non-equilibrium conditions to these functions. The perturbed potential, pair correlation function, and RDF adhere to the symmetry conditions defined as follows:

$$g_{ij}^1(-\mathbf{r}) = -g_{ij}^1(\mathbf{r}) \tag{2.46}$$

$$h_{ij}^1(-\mathbf{r}) = -h_{ij}^1(\mathbf{r}) \tag{2.47}$$

$$\psi_i^1(-\mathbf{r}) = -\psi_i^1(\mathbf{r}) \tag{2.48}$$

By substituting equations 2.43 and 2.45 into Eq. 2.42, we obtain:

$$k_BT(\omega_i+\omega_j)\nabla^2 g_{ji}^1(\mathbf{r}) + eZ_i\omega_i\nabla^2\psi_j^1(\mathbf{r})$$
$$-eZ_j\omega_j\nabla^2\psi_i^1(\mathbf{r}) = (\omega_i\mathbf{F}_i^{ext} - \omega_j\mathbf{F}_j^{ext})\cdot\nabla g_{ji}^0(\mathbf{r}) \tag{2.49}$$

We can rearrange Eq. 2.49 to obtain a more streamlined expression as:

$$\nabla^2\nabla^2\psi_j^1(\mathbf{r}) \quad -\frac{4\pi}{\epsilon k_BT}\sum_{i=1}^{C}\frac{\rho_i e^2 Z_i^2\omega_i}{\omega_j+\omega_i}\nabla^2\psi_j^1(\mathbf{r}) - \frac{4\pi}{\epsilon k_BT}\sum_{i=1}^{C}\frac{\rho_i e^2 Z_i Z_j\omega_i}{\omega_j+\omega_i}\nabla^2\psi_i^1(\mathbf{r})$$
$$= -\frac{4\pi}{\epsilon k_BT}\sum_{i=1}^{C}\rho_i e Z_i\frac{\omega_i\mathbf{F}_i^{ext} - \omega_j\mathbf{F}_j^{ext}}{\omega_j+\omega_i}\cdot\nabla g_{ji}^0(\mathbf{r}) \tag{2.50}$$

In this equation, κ is the inverse Debye length defined as:

$$\kappa^2 \equiv \frac{4\pi e^2}{\epsilon k_BT}\sum_{j=1}^{C}\rho_j Z_j^2 \tag{2.51}$$

In addition, μ_i is the relative ionic strength defined as:

$$\mu_i \equiv \frac{\rho_i e^2 Z_i^2}{\sum_{j=1}^{C}\rho_j e^2 Z_j^2} \tag{2.52}$$

The mean mobility is also defined as Eq. 2.53:

$$\bar{\omega} \equiv \sum_{j=1}^{C}\mu_j\omega_j \tag{2.53}$$

The limiting transference number of the ion i is also defined as:

$$t_i \equiv \frac{\mu_i\omega_i}{\bar{\omega}} \tag{2.54}$$

The equation represented by Eq. 2.49 can be reformulated in a more streamlined manner, as depicted in Eq. 2.55.

$$\sum_{i=1}^{C}(\nabla^2\delta_{ji} - \kappa^2 a_{ji})\nabla^2\left(\frac{\psi_i^1(\mathbf{r})}{eZ_i}\right) = -\frac{\kappa^2}{eZ_j}\sum_{i=1}^{C}\frac{\mu_i}{eZ_i}\frac{\omega_i\mathbf{F}_i^{ext} - \omega_j\mathbf{F}_j^{ext}}{\omega_i+\omega_j}\cdot\nabla g_{ji}^0(\mathbf{r}) \tag{2.55}$$

Within this equation, a_{ji} represents the elements of a matrix A, as defined in Eq. 2.56. Furthermore, δ_{ji} signifies the Kronecker delta.

$$a_{ji} \equiv \delta_{ji}\sum_{k=1}^{C}\frac{\bar{\omega}}{\omega_j+\omega_k} + \frac{\bar{\omega}t_i}{\omega_j+\omega_i} \tag{2.56}$$

Eq. 2.55 represents a system of ordinary differential equations that need to be solved to determine the perturbed portion of the electric potential (or the pair correlation function). Once this system is solved, the perturbed component of the pair correlation function can

be incorporated into Eq. 2.25, enabling the calculation of relaxation-induced forces on the migrating ion.

In a single-salt system comprising one type of cation and anion, Bernard et al. [111] solved the system of ordinary differential equations by using Green's functions [123]. The resultant relaxation effect for such systems is depicted in Eq. 2.57:

$$\frac{\delta k_i}{k_i} = -\Omega \int_{\sigma_{ij}}^{\infty} r h_{ij}^0(r) \exp(-\kappa_q r) dr \tag{2.57}$$

$$\Omega = \frac{\kappa_q^2}{3}\left[\frac{\sinh(\kappa_q \sigma_{ij})}{\kappa_q \sigma_{ij}} - \frac{\epsilon k_B T \kappa_q \sigma_{ij}^2}{e^2 Z_i Z_j}\left(\frac{\cosh(\kappa_q \sigma_{ij})}{\kappa_q \sigma_{ij}} - \frac{\sinh(\kappa_q \sigma_{ij})}{\kappa_q^2 \sigma_{ij}^2}\right)\right] \tag{2.58}$$

In Eq. 2.58, σ_{ij} is distance of the closest approach defined by Eq. 2.59:

$$\sigma_{ij} = \frac{\sigma_i + \sigma_j}{2} \tag{2.59}$$

In Eq. 2.58, κ_q is defined as Eq. 2.60:

$$\kappa_q^2 = \frac{4\pi}{\epsilon k_B T} \frac{\rho_i e Z_i \omega_i + \rho_j e Z_j \omega_j}{\omega_i + \omega_j} \tag{2.60}$$

In the context of a multi-salt electrolyte solution encompassing diverse types of cations and anions, Van Damme provided a solution to Eq. 2.49 [116], which was later expanded upon by Roger and colleagues [117] for size-asymmetry. The resulting equation detailing the relaxation effect for these complex systems is presented in Eq. 2.61.

$$\begin{aligned}\frac{\delta k_m}{k_m} \quad &= \frac{-\kappa^2 e Z_m}{3} \sum_{p=1}^{C} \zeta_m^p \sum_{j=1}^{C} \sum_{i=1}^{C} \frac{t_j \zeta_j^p \mu_j e (Z_i \omega_i - Z_j \omega_j)}{e^2 Z_i Z_j (\omega_i + \omega_j)} \\ &\frac{\sinh\left(\kappa \sqrt{q_p} \sigma_{ij}\right)}{\kappa \sqrt{q_p} \sigma_{ij}} \left[\int_{\sigma_{ij}}^{\infty} r \exp\left(-\kappa \sqrt{q_p} r\right) h_{ij}^0(r) dr\right]\end{aligned} \tag{2.61}$$

The parameters q_p and ζ_i^p are associated with the eigenvalues and the elements of the eigenvector, respectively, that emerge from resolving the set of differential equations (as detailed in equations 22-26 in the study by Van Damme [116]). These eigenvalues and eigenvectors are respectively outlined in equations 2.62 and 2.63.

$$q_p = \sum_{j=1}^{C} = \frac{\bar{\omega} t_j}{\omega_j + \delta_p} \tag{2.62}$$

$$\zeta_j^p = \frac{N_p \omega_j}{\omega_j^2 - \delta_p^2} \tag{2.63}$$

In the given equations, the term N_p is defined according to Eq. 2.64, while δ_p corresponds to a root of Eq. 2.65.

$$\frac{1}{N_p^2} = \sum_{j}^{C} \frac{t_j \omega_j^2}{(\omega_j^2 - \delta_p^2)^2} \tag{2.64}$$

$$-2\bar{\omega}\delta \sum_{j=1}^{C} \frac{t_i}{\omega_i^2 - \delta^2} = 0 \tag{2.65}$$

Just like the hydrodynamic effect, one must input the equilibrium pair correlation function into Eq. 2.61 to determine the relaxation force that affects the central ion. The selection of the equilibrium function is explored in Chapters 4 and 5, where two novel electrical conductivity models are introduced.

2.4.5 Conductivity Equation

Upon examination of both the relaxation and hydrodynamic effects, we can link the ionic conductivity of the ions to their velocity through the proportional relationship presented in Eq. 2.66:

$$\frac{\lambda_i}{\lambda_i^0} = \frac{v_i}{v_i^0} \tag{2.66}$$

Consequently, the solution's specific conductivity can be derived from Eq. 2.67:

$$\chi = \frac{e^2}{k_B T} \sum_{i=1}^{C} \rho_i D_i^0 Z_i^2 \left(1 + \frac{\delta v_i}{v_i^0}\right)\left(1 + \frac{\delta k_i}{k_i}\right) \tag{2.67}$$

Thus, both the molar and equivalent conductivity can be determined using equations 2.7 and 2.8, respectively.

2.5 Summary and Conclusions

In this chapter, the process of electrical conductance in electrolyte solutions was presented and the associated properties were defined. The physical factors contributing to the electrical conductivity of such solutions were briefly discussed, and models for its theoretical examination were reviewed.

Among the modeling approaches, the continuity methods were comprehensively detailed. The Ebeling hierarchy pertaining to the equation of motion for ions influenced by an external electric field was introduced. Moreover, an equation that accounts for the hydrodynamic (or electrophoretic) correction in comparison to the ideal behavior for the electrical conductivity was laid out. Additionally, the FO continuity equation was described, along with the equation addressing the electrostatic (or relaxation) correction compared to the ideal behavior for the electrical conductivity of both single-salt and multi-salt electrolyte solutions.

It was determined that, given the pair correlation function at a stationary state (the equilibrium pair correlation function) from an electrolyte theory, a novel electrical conductivity model can be formulated. The equilibrium pair correlation function derived from DH theory will be utilized in Chapters 4 and 5. On the basis of the equations presented in this chapter, new models for the electrical conductivity of electrolyte solutions will be devised.

Chapter Message

If the equilibrium pair correlation function is provided from an established theory, assumption, or numerical solution, the hydrodynamic and electrostatic contributions to the electrical conductivity can be conveniently evaluated. The choice of the equilibrium pair correlation function varies the final outcome.

CHAPTER 3

Practical Investigation of Electrical Conductivity Models

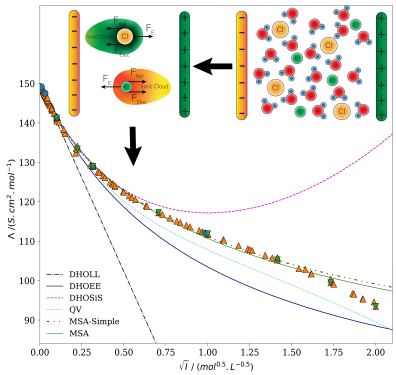

In Chapter 2, the electrical conductance process, its physical foundation, its historical evolution, and modeling techniques were briefly outlined. It was highlighted that, following the formulation of the limiting law by Debye and Hückel [86] and Onsager [87, 88], several models have been introduced in efforts to refine the limiting law.

Despite the development of numerous models for electrical conductivity, it remains unclear which models are optimal, especially across a broad spectrum of systems and conditions. Moreover, the applicability, accuracy, and reliability of these models are predominantly restricted to findings presented by their developers. Consequently, a comprehensive examination of these models for various electrolytes, spanning various concentrations and temperatures, is beneficial.

In this chapter, the predictive capabilities of six established electrical conductivity models are assessed over an extensive range of concentrations and temperatures. Aqueous solutions of various electrolytes (1:1, 1:2, 1:3, 1:4, 2:1, 2:2, 2:3, 2:4, 3:1, and 3:2) under low pressure conditions are specifically studied. The accuracy and reliability of these models are evaluated using experimental data for 126 electrolytes. Comparisons are made between model predictions and experimental data, even at high concentrations and temperatures. The precision of these models is further analyzed through error analysis. Lastly, the electrophoretic and relaxation components of the models are closely examined to provide a deeper understanding of their differences and to highlight their unique behaviors.

Furthermore, in this chapter, three new electrical conductivity models for single-salt solutions are introduced, drawing on the combination of hydrodynamic and electrostatic corrections previously established in the literature. Subsequently, the influence of ion-solvent interactions on the prediction of the electrical conductivity of aqueous solutions is explored by utilizing concentration-dependent RSP and viscosity.

The practical investigations presented in this chapter have previously been published in two papers in Industrial & Engineering Chemistry Research and Fluid Phase Equilibria.

- *Comparison of Models for the Prediction of the Electrical Conductivity of Electrolyte Solutions* [120] (Link).
- *On The Estimation of Equivalent Conductivity of Electrolyte Solutions: The Effect of relative static permittivity and Viscosity* [124] (Link).

3.1 Models

In this section, six notable electrical conductivity models from the current literature have been reviewed: DHOLL [83, 86–88, 125], DHOEE [90], DHOSiS [118], MSA [111, 112], MSA-Simple [113] and QV [103–105]. Additionally, three new models have been introduced that integrate relaxation effects, drawn from previous research [94, 101, 102], and the electrophoretic component from the DHOEE model. Although all these models are rooted in the continuity approach discussed in Chapter 2, the derivation techniques for each are varied. These differences are caused by variations in pair correlation functions, boundary conditions, or the methods used to address the FO continuity equation.

Beyond their initial derivations, these models have been reported in various ways by the authors. In this regard, a decision has been made to present all of these models in a uniform format to simplify their comparison. As a result, the electrical conductivity models are presented based on corrections to the ideal behavior as outlined in Eq. 3.1:

$$\lambda_i = \lambda_i^0 \left(1 + \frac{\delta v_i}{v_i^0}\right)\left(1 + \frac{\delta k}{k}\right) \tag{3.1}$$

Eq. 3.1 has been formulated based on the insights of Debye and Hückel. The decrease in ion mobility with concentration in the presence of an external electric field was attributed by the authors to both relaxation and electrophoretic effects. In this equation, $\left(\frac{\delta k}{k}\right)$ represents the reduction in mobility due to relaxation, and $\left(\frac{\delta v_i}{v_i^0}\right)$ indicates the decrease arising from electrophoretic effects. It is important to note that the expression $\left(\frac{\delta v_i}{v_i^0} \times \frac{\delta k}{k}\right)\lambda_i^0$ is excluded in the DHOLL, DHOEE, DHOSiS, and QV models. As a result, the ionic conductivity equation for these models has been shown in Eq. 3.2:

$$\lambda_i = \lambda_i^0 \left(1 + \frac{\delta v_i}{v_i^0} + \frac{\delta k}{k}\right) \tag{3.2}$$

As described in the previous chapter, the molar conductivity of electrolyte solutions denoted Λ which is the primary property investigated in this chapter is calculated from Eq. 3.3:

$$\Lambda = \sum_{i=+,-} \nu_i \left|Z_i\right| \lambda_i \tag{3.3}$$

In Eq. 3.3, ν_i and Z_i are defined as the stoichiometry and charge valence type of the ions, respectively. The connection between molar conductivity and equivalent conductivity for single-salt electrolyte solutions has been expressed as follows.

$$\Lambda = \nu_i \left|Z_i\right| \Lambda^{eq}, i = \{+ \; or - \} \tag{3.4}$$

Given that for a single-salt solution $\nu_+ \left|Z_+\right| = \nu_- \left|Z_-\right|$, the selection of either cation or anion for this conversion does not influence the outcome.

3.1.1 Debye-Hückel-Onsager Limiting Law (DHOLL) Model

The DHOLL model was originally formulated by Debye and Hückel [86] and subsequently refined by Onsager [87,88]. This model represents the first theoretical exploration of electrical conductivity that successfully demonstrated the linear decrease in the molar conductivity of electrolyte solutions with the square root of the salt concentration at infinite dilution. The version of the DHOLL model presented in this section is derived from Onsager's papers [87,88]. In his research, Onsager assumed the presence of a single type of cation and anion in a continuous solvent medium, each bearing point charges. The electrophoretic and relaxation effects of the DHOLL model are represented in equations 3.5 and 3.6, respectively.

$$\frac{\delta v_i}{v_i^0} = -\frac{F^2}{6\pi\eta N_A \lambda_i^0} |Z_i| \kappa \, , i = \{+ \, or \, -\} \tag{3.5}$$

$$\frac{\delta k}{k} = -\frac{|Z_+ Z_-| e^2}{12\pi\varepsilon_0\varepsilon_r k_B T} \frac{q}{1+\sqrt{q}} \kappa \tag{3.6}$$

$$q = \frac{|Z_+ Z_-|}{|Z_+| + |Z_-|} \frac{\lambda_+^0 + \lambda_-^0}{|Z_+| \lambda_-^0 + |Z_-| \lambda_+^0} \tag{3.7}$$

In the given equations, κ represents the inverse Debye length as defined in Eq. 2.51. The terms η and ε_r correspond to the viscosity and RSP of the solvent, respectively. Substituting equations 3.5 and 3.6 into Eq. 3.2, the ionic conductivity according to the DHOLL model can be expressed as shown in Eq. 3.8:

$$\lambda_i = \lambda_i^0 - \left[\frac{F^2}{6\pi\eta N_A} |Z_i| + \frac{|Z_+ Z_-| e^2}{12\pi\varepsilon_0\varepsilon_r k_B T} \frac{q}{1+\sqrt{q}} \lambda_i^0 \right] \kappa \, , i = \{+ \, or \, -\} \tag{3.8}$$

The equivalent conductivity for the DHOLL model can subsequently be derived by substituting Eq. 3.8 into Eq. 3.3:

$$\Lambda^{eq} = \lambda_+ + \lambda_- = \Lambda^0 - \left[\frac{F^2}{6\pi\eta N_A} (|Z_+| + |Z_-|) + \frac{|Z_+ Z_-| e^2}{12\pi\varepsilon_0\varepsilon_r k_B T} \frac{q}{1+\sqrt{q}} \Lambda^0 \right] \kappa \tag{3.9}$$

In Eq. 3.9, Λ^0 denotes the equivalent conductivity at infinite dilution.

3.1.2 Debye-Hückel-Onsager Extended Equation (DHOEE) Model

The DHOEE [90] stands as the counterpart in electrical conductivity models to the extended DH equation found in activity coefficient models. The relaxation component of this model was derived by Falkenhagen and his team [101], using the Eigen-Wicke distribution function [90]. This model takes into account a finite size for the ions, with the assumption that all ions possess the same diameter, termed distance of the closest approach ($\sigma_{+-} = 0.5(\sigma_+ + \sigma_-)$).

Furthermore, when considering the relaxation field, its exponential term was approximated using the first-order Taylor series expansion. In the process, the higher-order terms associated with $\kappa\sigma_{+-}$ are ignored. The electrophoretic and relaxation effects in the DHOEE model are expressed in equations 3.10 and 3.11, respectively.

$$\frac{\delta v_i}{v_i^0} = -\frac{F^2}{6\pi\eta N_A \lambda_i^0} |Z_i| \frac{\kappa}{1+\kappa\sigma_{+-}} \, , i = \{+ \, or \, -\} \tag{3.10}$$

$$\frac{\delta k}{k} = \frac{Z_+ Z_- e^2}{12\pi\varepsilon_0\varepsilon_r k_B T} \frac{q}{1-q} \frac{\kappa}{(1+\kappa\sigma_{+-})\,\kappa} \left[\exp(\kappa\sigma_{+-}(1-\sqrt{q})) - 1 \right] \tag{3.11}$$

The ionic conductivity of the DHOEE model can then be obtained from Eq. 3.12:

$$\lambda_i = \lambda_i^0 - \left[\frac{F^2}{6\pi\eta N_A}|Z_i| + \frac{|Z_+Z_-|\,e^2}{12\pi\varepsilon_0\varepsilon_r k_B T}\frac{q}{1+\sqrt{q}}\lambda_i^0\right]\frac{\kappa}{1+\kappa\sigma_{+-}}, i = \{+\,or\,-\} \tag{3.12}$$

The equivalent conductivity of this model is also obtained from Eq. 3.13:

$$\Lambda^{eq} = \Lambda^0 - \left[\frac{F^2}{6\pi\eta N_A}(|Z_+| + |Z_-|) + \frac{|Z_+Z_-|\,e^2}{12\pi\varepsilon_0\varepsilon_r k_B T}\frac{q}{1+\sqrt{q}}\Lambda^0\right]\frac{\kappa}{1+\kappa\sigma_{+-}} \tag{3.13}$$

3.1.3 Debye-Hückel-Onsager Smaller-ion Shell (DHOSiS) Model

The DHOSiS model was introduced more recently by Fraenkel, as mentioned in [118], with the objective of improving the DHOLL through the application of the so-called *smaller ion shell* theory, or SiS. Three pivotal modifications were made to the DHOLL by Fraenkel:

1. The ω value of the DHOLL model, which is denoted by $|Z_+Z_-|\frac{q}{1+\sqrt{q}}$ in Eq. 3.6, was multiplied to adapt it suitably for multi-valent electrolytes.
2. Taking into consideration the asymmetry in the size of the ions, he modified the representative size of the ionic atmosphere.
3. To counteract potential over-compensation from the second modification, he integrated an oversize offset factor.

The electrophoretic and relaxation components of the DHOSiS model are shown in equations 3.14 and 3.15, respectively.

$$\frac{\delta v_i}{v_i^0} = \frac{F^2}{6\pi\eta N_A\lambda_i^0}|Z_i|\,\omega^\dagger\Psi_i^*, i = \{+\,or\,-\} \tag{3.14}$$

$$\left(\frac{\delta k}{k}\right)_i = \frac{|Z_iZ_j|\,e^2}{12\pi\varepsilon_0\varepsilon_r k_B T}\frac{P^*q}{1+\sqrt{q}}\omega^\dagger\Psi_i^*, i = \{+\,or\,-\} \tag{3.15}$$

In the given equations, 3.14 and 3.15, the term P^* acts as the correction factor for the ω value found in the DHOLL model.

$$P^* = \begin{cases} \frac{|Z_-|}{\nu_-}t_+^0 + \frac{|Z_+|}{\nu_+}t_-^0 & \text{if} \quad |Z_+| \le |Z_-| \\ \frac{|Z_-|}{\nu_+}t_+^0 + \frac{|Z_+|}{\nu_-}t_-^0 & \text{if} \quad |Z_+| \ge |Z_-| \end{cases} \tag{3.16}$$

In Eq. 3.16, the terms t_+^0 and t_-^0 represent the transference numbers of the cation and the anion at infinite dilution, respectively. They are defined as the fraction of the ionic conductivity relative to the equivalent conductivity both at infinite dilution, given by the relation $t_i^0 = \lambda_i^0/\Lambda^0$.

In equations 3.14 and 3.15, adjustments made due to the size asymmetry of the ions in relation to the ionic cloud size, symbolized as Ψ_i^*, are outlined. These adjustments are further detailed in the equations 3.17 for cations and 3.18 for anions.

$$\Psi_+^* = \frac{-\kappa}{1+\kappa\sigma_{+-}}\left[1 - \frac{2\left(\exp(\kappa(\sigma_{+-}-\sigma_+)) - 1\right) - \kappa(\sigma_{+-}-\sigma_+)}{1+\kappa\sigma_+}\right] \tag{3.17}$$

$$\Psi_{-}^{*} = \frac{-\kappa}{1+\kappa\sigma_{+-}}\left[1+\frac{2\left(\exp(\kappa(\sigma_{-}-\sigma_{+-})\ )-1\right)-2\kappa(\sigma_{-}-\sigma_{+-})}{1+\kappa\sigma_{-}}\right] \tag{3.18}$$

The *oversize offset factor* symbolized as $\omega^{\dagger}$ is defined as Eq. 3.19:

$$\omega^{\dagger} = 1+\frac{\left(\lambda_{+}^{0}-\lambda_{-}^{0}\right)^{2}}{3\lambda_{+}^{0}\lambda_{-}^{0}}P^{*}q\kappa\sigma_{+-} \tag{3.19}$$

Finally, equations 3.20 and 3.21 represent the ionic and equivalent conductivity of the DHOSiS model, respectively.

$$\lambda_i = \lambda_i^0 + \left[\frac{F^2}{6\pi\eta N_A}|Z_i| + \frac{|Z_+Z_+|\,e^2}{12\pi\varepsilon_0\varepsilon_r k_B T}\frac{P^{*}q}{1+\sqrt{q}}\lambda_i^0\right]\omega^{\dagger}\Psi_i^{*}\ , i=\{+\ or\ -\} \tag{3.20}$$

$$\Lambda^{eq} = \Lambda^0 - \left[\frac{F^2}{6\pi\eta N_A}\sum_{i=+,-}|Z_i|\,\Psi_i^{*} + \frac{|Z_+Z_-|\,e^2}{12\pi\varepsilon_0\varepsilon_r k_B T}\frac{P^{*}q}{1+\sqrt{q}}\sum_{i=+,-}\lambda_i^0\Psi_i^{*}\right]\omega^{\dagger} \tag{3.21}$$

While the exact steps used to develop the DHOSiS model are unclear, it is evident that Fraenkel took a different route compared to other researchers. Most of the models investigated in this study, except for the DHOSiS model, were derived by solving the FO continuity equation [83, 87, 88] (or the generalized form reported by Ebeling et al. [110]) for the relaxation term. The output of this derivation procedure results in a salt-specific relaxation effect on the conductivity of ions. Onsager also discussed a salt-specific relaxation effect. Even in his Nobel Prize lecture, he pointed out that the relaxation field reducing the velocity of ions toward the oppositely charged electrode should be the same for the cation and the anion, or, in his words:

> *"The relaxation effect ought to reduce the mobilities of anion and cation in equal proportion. Much to my surprise, the results of Debye and Hückel did not satisfy that relation, nor the requirement that whenever an ion of type A is 10 A West of a B, there is a B 10 A East of that A."*

In conclusion, the DHOSiS model has an unspecified component, and without a clear derivation, it is impossible to further investigate what is missing.

3.1.4 DHO 1, 2, and 3 Models

As mentioned in the previous chapter, some efforts have been made for the extension of the relaxation field in the limiting law considering a finite size for ions. In almost all of these studies, it has been assumed that cation and anion share a similar size equivalent to distance of the closest approach. The derivation procedures of these models are more or less the same. But they differ in either the use of the equilibrium pair correlation function or in the choice of boundary conditions in the solution procedure of the FO continuity equation. Equations 3.22, 3.24 and 3.25 represent relaxation contributions to the reduction of ionic conductivity reported by Fuoss and Onsager [94], Falkenhagen et al. [101], and Falkenhagen and Kelbg [102], respectively.

$$\frac{\delta k}{k} = \frac{Z_+Z_-e^2}{12\pi\varepsilon_0\varepsilon_r k_B T}\left[\frac{1}{1+\sqrt{q}}\frac{1+0.5\kappa\sigma_{+-}\left(1+\sqrt{q}\right)\left[1-\left(1+\kappa\sigma_{+-}\right)/b\right]}{1+\kappa\sigma_{+-}\sqrt{q}+\kappa^2\sigma_{+-}^2 q/3}\right] \tag{3.22}$$

In Eq. 3.22, b is the ratio of the Bjerrum length (l_B) to distance of the closest approach defined as Eq. 3.23:

$$b = \frac{l_B}{\sigma_{+-}} = \frac{|Z_+ Z_-|\, e^2}{4\pi\varepsilon_0\varepsilon_r k_B T \sigma_{+-}} \tag{3.23}$$

$$\frac{\delta k}{k} = \frac{Z_+ Z_- e^2}{12\pi\varepsilon_0\varepsilon_r k_B T}\left[\frac{q}{1-q}\frac{\kappa}{\kappa\sigma_{+-}\left(1+\kappa\sigma_{+-}\right)}\left(\exp\left(\kappa\sigma_{+-}\left(1-\sqrt{q}\right)\right)-1\right)\right] \tag{3.24}$$

$$\frac{\delta k}{k} = \frac{Z_+ Z_- e^2}{12\pi\varepsilon_0\varepsilon_r k_B T}\left[\frac{q}{1+\sqrt{q}}\frac{\kappa}{\left(1+\kappa\sigma_{+-}\right)\left(1+\kappa\sigma_{+-}\sqrt{q}+\kappa^2\sigma_{+-}^2/6\right)}\right] \tag{3.25}$$

The ionic conductivity of the DHO 1-3 models can be calculated from equations 3.1 and 3.3 by replacing $\delta k/k$ from equations 3.22-3.25 , respectively. DHO1-3 models share the electrophoretic effect with the DHOEE model presented in Eq. 3.10.

3.1.5 Mean Spherical Approximation (MSA) Model

The model takes its foundation from the generalized derivation approach proposed by Ebeling et al. [110] (presented in Chapter 2) and integrates the MSA pair correlation function [5,6,84] for the equilibrium part. Furthermore, Bernard et al. [111] incorporated Poisson's equation to account for the non-equilibrium contribution of the overall potential. In addressing the inhomogeneous continuity equation, they utilized Green's function methodologies. An outstanding feature of this model is that it operates as an unrestricted primitive model (UPM), introducing a specific ion size parameter (the crystallographic ion size). In our study, we evaluate two iterations of MSA-based electrical conductivity models: the original [111] and its simplified counterpart [113].

Additionally, the MSA model underwent minor modifications primarily to simplify its implementation. Certain authors sought to provide an explicit formulation for the screening length parameter [126]. In contrast, others omitted specific expressions in the formulation (specifically $\Gamma^2\bar{\sigma}^2$ in equations B.17 and B.20) citing their negligible numerical significance [127]. The computational challenge of solving the implicit screening length equation is not particularly difficult, given that an appropriate method is employed. Without the second adjustment, the MSA model fails to accurately predict the equivalent conductivity at higher concentrations for certain electrolytes, like LaCl3 in aqueous solutions.

In this research, the original formulation [111] was chosen for several crucial reasons. First, our aim was to maintain a balanced comparison. Thus, contrasting a revised version of one model with the original iteration of another does not provide a fair comparison. Second, the minimal influence of an expression on results at low to medium concentrations does not justify its exclusion. Consequently, the MSA results showcased in this study follow the original formulation.

The electrophoretic and relaxation effects of the MSA model are defined in equations 3.26 and 3.27, respectively. The electrophoretic effect comprises two distinct contributions, whereas the relaxation effect encompasses three. Comprehensive equations detailing each individual contribution can be found in Appendix B.

$$\frac{\delta v_i}{v_i^0} = \frac{\delta {v_i}^1}{v_i^0} + \frac{\delta {v_i}^2}{v_i^0}\,, i = \{+\, or\, -\} \tag{3.26}$$

$$\frac{\delta k}{k} = \frac{\delta k_1^{Rel}}{k} + \frac{\delta k_2^{Rel}}{k} + \frac{\delta k_1^{Hyd}}{k} \tag{3.27}$$

The ionic and molar conductivity conductivity predicted by the MSA model can be obtained by substituting equations 3.26 and 3.27 into equations 3.1 and 3.3, respectively.

3.1.6 Mean Spherical Approximation Simple (MSA-Simple) Model

The MSA-Simple model [113] is the restricted primitive model (RPM) version of the MSA model that only considers the first approximation of the original model for relaxation and electrophoretic terms. Equations 3.28 and 3.29 present the electrophoretic and relaxation effects of the MSA-Simple model, respectively.

$$\frac{\delta v_i}{v_i^0} = -\frac{k_B T}{3\pi\eta D_i^0}\frac{\Gamma}{1+\Gamma\bar{\sigma}}\,, i = \{+\,or\,-\} \tag{3.28}$$

$$\frac{\delta k}{k} = \frac{1}{24\pi\varepsilon_0\varepsilon_r k_B T}\frac{\kappa_q^2 e^2 Z_+ Z_-}{\bar{\sigma}\left(1+\Gamma\bar{\sigma}\right)^2}\frac{\left(1-\exp(-2\kappa_q\bar{\sigma})\right)}{\left[\kappa_q^2+2\Gamma\kappa_q+2\Gamma^2\left(1-\exp(-\kappa_q\bar{\sigma})\right)\right]} \tag{3.29}$$

In equations 3.28 and 3.29, the simplified MSA screening parameter (Γ) is obtained from Eq. 3.30:

$$2\Gamma = \frac{\kappa}{(1+\Gamma\bar{\sigma})} \tag{3.30}$$

In addition, κ_q and $\bar{\sigma}$ are obtained from equations 3.31 and 3.32, respectively.

$$\kappa_q^2 = \frac{e^2}{\varepsilon_0\varepsilon_r k_B T}\frac{\rho_+ Z_+^2 D_+^0 + \rho_- Z_-^2 D_-^0}{D_+^0 + D_-^0} \tag{3.31}$$

In Eq. 3.31, the total number density of ions is denoted as ρ_i.

$$\bar{\sigma} = \frac{\sum_{i=+,-}\rho_i Z_i^2\sigma_i}{\sum_{i=+,-}\rho_i Z_i^2} \tag{3.32}$$

This model presents a unique advantage compared to other RPMs by introducing a specific equation for the salt-specific size parameter, represented as Eq. 3.32. For symmetrical electrolytes, this equation is reduced to $\bar{\sigma} = \sigma_{+-}$. But for asymmetrical electrolytes, more weight is placed on the ion with a higher valence. It should be noted that this equation was first derived by Blum [126]. He reported this by solving the implicit equation for the MSA screening parameter at the zero limit ($\lim_{\Gamma\to 0}\Gamma(\rho_i,\sigma_i,Z_i,T,\varepsilon_r)$).

3.1.7 Quint and Viallard (QV) Model

This model stands as an improvement over the models reported by Fuoss and Onsager [83,94–100,128]. One of its advancements is the inclusion of higher-order terms for both relaxation and electrophoretic effects. Moreover, diverging from the model developed by Fuoss and Onsager, the QV model [103–105] can be applied to multi-salt systems and asymmetrical electrolytes. The final formulation of the model, as presented by the authors, is depicted in Eq. 3.33:

$$\lambda_i = \lambda_i^0 - S_i^m I^{0.5} + E_i'^m I ln\left(I\right) + J_{1i}^m I - J_{2i}^m I^{1.5} + O\left(I^2\right) \tag{3.33}$$

In this equation, the terms S_i^m, $E_i'^m$, J_{1i}^m, and J_{2i}^m are complicated functions influenced by factors such as ionic conductivity at infinite dilution, ionic strength, distance of the closest approach, universal constants, and the valence type of ions.

In the derivation of Eq. 3.33, a dimensioned expression is encountered within the logarithm. This makes model programming complicated without explicit knowledge of the units. In this study, the QV model was reevaluated. The formulations of the relaxation and electrophoretic terms were handled separately before being integrated into Eq. 3.2. Eq. 3.34 represents the contribution from relaxation to the reduction of equivalent conductivity due to relaxation effects (a detailed formulation of these relaxation effects is given in equations B.29 and B.30 in Appendix B). Additionally, the contribution to the reduction of equivalent conductivity from electrophoretic effects is detailed in Eq. B.31 in Appendix B.

$$\frac{\delta k}{k} = \frac{\delta k_{1,2}}{k} + \frac{\delta k_2^P}{k} \tag{3.34}$$

3.2 Database

To provide a robust foundation for model validation, we meticulously assembled a comprehensive database. This extensive collection covers the molar conductivity of as many as 126 distinct aqueous electrolyte solutions. What makes our database particularly noteworthy is its broadness; it not only encompasses a wide range of electrolytes but also captures data at both high concentrations and elevated temperatures.

Data for our database have been obtained from a total of 23 distinct references, as specifically indicated in Figure 3.2. Among these, reference [129] stands out due to its unique nature. Instead of being just another original data source, it acts as a database of relatively old experimental measurements of the electrical conductivity. This reference consolidates experimental data related to the electrical conductivity of electrolyte solutions, drawing from a staggering 145 different resources.

To offer a visual overview and facilitate easier understanding, we have depicted summaries of this exhaustive database in two figures: Figures 3.1 and 3.2.

Figure 3.1 presents the number of data points in addition to the maximum salt concentration, where the temperature is 298.15 K for each electrolyte in the database. Figure 3.2 shows the number of references for each salt-water binary mixture, including individual sources extracted by us and sources used in reference [129].

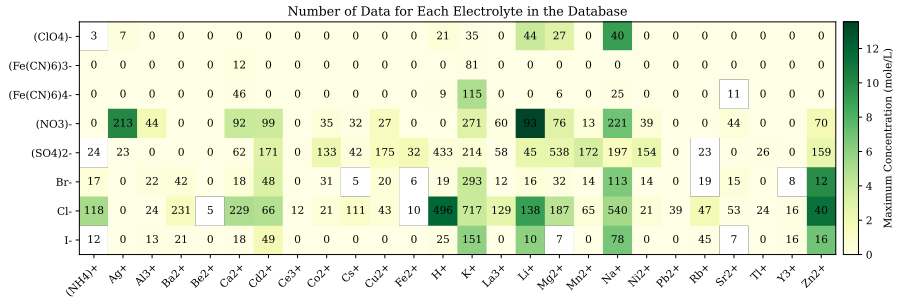

Figure 3.1. A summary of the number of data points and concentration range in the created database for 126 different electrolytes (the number on the figure shows the number of data points, and the color map shows the maximum concentration at 298.15 K in $mol \cdot L$) [129–150]. Reprinted with permission from ref. [120]. Copyright 2022 American Chemical Society.

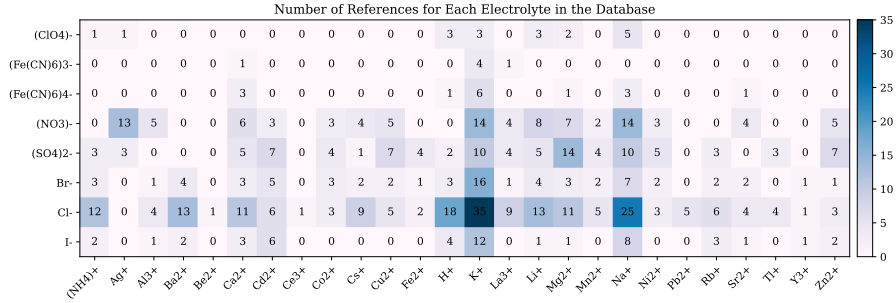

Figure 3.2. A summary of the number of references for each electrolyte in the database [129–150]. Reprinted with permission from ref. [120]. Copyright 2022 American Chemical Society.

3.3 Ions Properties

In models of electrical conductivity, ions are characterized by their size, charge, and absolute mobility at infinite dilution. Within these models, ions are conceived as ideal spherical particles possessing an ionic diameter. Absolute mobility of these ions, when the solution is infinitely diluted, is commonly expressed either as ionic conductivity at infinite dilution (represented as λ_i^0) or as the diffusion coefficient at infinite dilution (symbolized as D_i^0). The charge associated with the ions is indicated as an integer number multiple of the elementary charge (e), termed the ionic valence type, which is denoted as Z_i.

Except for the DHOLL model, all other models incorporate a salt- or ion-specific size parameter, denoted as σ_{+-} or σ_i. In the case of DHOEE, QV and other RPMs, this parameter is specific to the salt and is referred to as distance of the closest approach (σ_{+-}). On the other hand, for both versions of the MSA (full and simple) and the DHOSiS models, this parameter is ion-specific and is symbolized as σ_i.

The fundamental concept of this parameter is well-understood; however, disagreements arise when determining its exact value for use in electrical conductivity models. Fraenkel, in his works [151, 152], introduced an electric scale for the ionic diameter derived from equivalent conductivity data. Yet, in the DHOSiS model referenced in [118], he opted to use the ionic diameter calculated as a fit parameter based on the activity coefficient data (known as the activity scale) rather than the aforementioned electric scale. Onsager and Fuoss, in their studies [83, 94–100, 153], assumed that distance of the closest approach ought to be an adjustable parameter. Bernard and co-authors, in their paper [111], incorporated the crystallographic ionic diameter into their MSA-based model. Meanwhile, other scholars advocate for an effective concentration-dependent ionic radius, suggesting that its determination should be based on certain correlations, according to references [127, 154].

By adjusting the size parameter (σ_{+-} or σ_i), it is likely that the outcomes of the equivalent conductivity models can be enhanced. However, since this research does not focus on examining the capability of equivalent conductivity models to align with the experimental data using such adjustable parameters, we adopted the crystallographic ionic diameter for aqueous solutions, as reported by Marcus [155]. The diameters of the ions investigated in this study are listed in Table 3.1.

Another fundamental property when discussing equivalent conductivity is the equivalent conductivity at infinite dilution, represented as $\Lambda^0(T)$ or $\lambda_i^0(T)$. This property is an integral part of the ideal contribution to the specific conductivity outlined in Chapter 2 (see Eq. 2.34). Since electrical conductivity models are developed based on the correction to this ideal behavior, employing a precise value for this property is crucial for evaluating the

Table 3.1. The ionic conductivity at infinite dilution (λ_i^0) at 298.15 K in $S \cdot m^2 \cdot mol^{-1}$ and ionic diameter (σ_i) in m for ions studied in this work [155, 156].

Ion	$\lambda_i^0 \times 10^4$	$\sigma_i \times 10^{10}$	Ion	$\lambda_i^0 \times 10^4$	$\sigma_i \times 10^{10}$
$(NH_4)^+$	73.50	2.96	Mn^{2+}	53.50	1.66
Ag^+	61.90	2.30	Na^+	50.08	2.04
Al^{3+}	61.00	1.06	Ni^{2+}	49.60	1.38
Ba^{2+}	63.60	2.70	Pb^{2+}	71.00	2.38
Be^{2+}	45.00	0.90	Rb^+	77.80	2.98
Ca^{2+}	59.47	2.00	Sc^{3+}	64.70	1.50
Cd^{2+}	54.00	1.90	Sr^{2+}	59.40	2.50
Ce^{3+}	69.80	2.28	Tl^+	74.70	3.00
Co^{2+}	55.00	1.50	Y^{3+}	62.00	2.02
Cr^{3+}	67.00	2.28	Zn^{2+}	52.80	1.50
Cs^+	77.20	3.40	$(ClO_4)^-$	67.30	4.80
Cu^{2+}	53.60	1.46	$(Fe(CN)_6)^{3-}$	98.50	5.16
Fe^{2+}	54.00	1.56	$(Fe(CN)_6)^{4-}$	108.5	5.64
H^+	349.7	0.74	$(NO_3)^-$	71.42	3.58
K^+	73.48	2.76	$(SO_4)^{2-}$	80.00	4.60
La^{3+}	69.70	2.36	Br^-	78.10	3.92
Li^+	38.66	1.48	Cl^-	76.31	3.62
Mg^{2+}	53.00	1.44	I^-	76.80	4.40

models' accuracy.

Although the pivotal role of the equivalent conductivity at infinite dilution is widely recognized, only a handful of models can accurately estimate it. Most of these models are based on correlations or are semi-phenomenological in nature and depend, to a certain degree, on experimental data. In this study, drawing inspiration from Fraenkel's approach in references [151, 152], we aligned the ionic conductivity at infinite dilution experimental data with a combined expression, denoted as $\frac{(\varepsilon_r T)^2}{\eta}$. Additionally, we directly incorporated the experimental data at temperatures for which the ionic conductivity at infinite dilution measurements are available. Table 3.1 presents the ionic conductivity at infinite dilution for the ions investigated in this work at 298.15 K. The diffusion coefficient at infinite dilution used in the MSA and MSA-Simple models can also be calculated from the ionic conductivity at infinite dilution using the Nerst-Einstein equation (Eq. 2.13).

3.4 Water Properties

To predict equivalent conductivity, two properties of the solvent are essential: viscosity and RSP. In this study, we utilized either experimentally reported values or a correlation for both the viscosity and the RSP of water. The experimental values for viscosity and RSP can be found in Table 3.2.

Eq. 3.35 is the correlation used in this study for the temperature dependence of the water viscosity [157].

$$\ln\left(\frac{\eta}{\eta_0}\right) = a_1\left(\Delta T\right) + a_2\left(\Delta T\right)^2 + a_3\left(\Delta T\right)^3 + a_4\left(\Delta T\right)^4 + a_5\left(\Delta T\right)^5 \tag{3.35}$$

Table 3.2. The RSP and viscosity of water at various temperatures [129, 157].

Solvent	$T\,(K)$	ε_r	$\eta\,(Pa\cdot s)\times 10^3$
H_2O	273.15	87.82	1.791
	278.15	85.70	1.520
	283.15	84.05	1.307
	288.15	82.44	1.140
	293.15	80.23	1.002
	298.15	78.43	0.890
	303.15	76.65	0.797
	308.15	74.91	0.719
	313.15	73.21	0.653
	318.15	71.54	0.596
	323.15	69.91	0.547
	328.15	68.32	0.504
	343.15	63.74	0.405
	363.15	58.06	0.316
	373.15	55.38	0.283

In Eq. 3.35, the term ΔT is defined as $T - T_0$, where T_0 is 293.15 K. The viscosity of water at this reference temperature, represented as η_0, is 1.002 $mPa\cdot s$. The coefficients a_1 through a_5 in Eq. 3.35 are detailed in Table 3.3. This equation is applicable for temperatures ranging from 273.15 to 373.15 K.

The RSP of water is determined using Eq. 3.36, a semi-empirical equation presented by Mollerup and Michelsen [8].

$$\varepsilon_r\,(T) = \varepsilon_r\,(273.15K) + \frac{\beta_1}{2}\frac{N_A\delta^2}{\varepsilon_0 k_B M_W}\left(\frac{\rho(T)}{T} - \frac{999.84}{273.15}\right) \tag{3.36}$$

In the given equation, the coefficient β_1 is set to 3.31306 and $\varepsilon_r(273.15K)$ is 87.82. Moreover, the electric dipole moment of water, represented by δ, is 8.33e-30 $C\cdot m$. Additionally, M_W stands for the molecular weight of water. The density of water, $\rho(T)$, can be sourced from Eq. 3.37:

$$\rho\,(T) = 999.84 + 0.151782(T - 273.15) - 0.0450573(T - 273.15)^{1.55} \tag{3.37}$$

3.5 Comparative Study

In this section, we conduct a detailed comparison of the DHOLL, DHOEE, DHOSiS, MSA, MSA-Simple, and QV model predictions against each other and against experimental data. To ensure a fair comparison, we consistently apply the same parameters across all models. Initially, the effectiveness of the models will be evaluated starting from infinitely dilute solutions and extending to very high concentrations at a fixed temperature of 298.15 K (Section 3.5.1). Subsequently, the model predictions will be compared at different temperatures in section 3.5.2. A quantitative evaluation of these models will be presented in Section 3.5.3.

Table 3.3. The coefficients the water viscosity correlation.

a_1	a_2	a_3	a_4	a_5
-2.45e-2	1.86e-4	-1.71e-6	1.42e-8	-5.98e-11

Furthermore, an analysis concerning the reductions in equivalent conductivity stemming from hydrodynamic and relaxation effects will be discussed in Section 3.5.4.

3.5.1 Concentration Dependency

In this section, we examine the molar conductivity of ten distinct electrolytes (1:1, 1:2, 1:3, 1:4, 2:1, 2:2, 2:3, 2:4, 3:1, 3:2) at 298.15 K in water. The outcomes are graphed against the square root of the ionic strength. Given the wealth of experimental data available, this specific temperature was selected, allowing us to evaluate electrical conductivity models across a wider array of salts and concentration spectrum. The experimental data utilized in this section is sourced from a consolidated database, and all data is treated uniformly, irrespective of its origin.

The primary objective of this section is to assess the accuracy and reliability of the electrical conductivity models across an extensive concentration spectrum, using graphical analysis. Furthermore, the choice of ten electrolytes serves to demonstrate the capability of the models to predict the electrical conductivity of various types of electrolyte-water systems.

Figures 3.3 and 3.4 depict the molar conductivity of the ten selected electrolytes plotted against $\sqrt{I}$. For the KCl aqueous solution, the predictions of the models are more reliable than those for other electrolytes. Both the MSA and MSA-Simple models produce excellent predictions up to 1.5 $mol \cdot L^{-1}$, which is consistent with the observations in the literature [111, 113]. Similarly, the QV and DHOEE models align closely with the experimental data.

Moreover, it has been shown that there is a minimum in the predictions of the DHOSiS model at low to moderate concentrations. Subsequent to this minimum, the molar conductivity starts to rise with $\sqrt{I}$. This behavior, though varying in intensity, is identifiable across different electrolytes. It is worth noting that Fraenkel has previously presented the concentration range for the validity of this model, and the observed trends exceed those bounds [118].

Additionally, we have examined the experimental data for over 126 electrolytes at various temperatures. Interestingly, none of these electrolytes in the experimental data exhibited the pattern of increasing molar conductivity at elevated concentrations. As such, it can be asserted that the behavior exhibited by the DHOSiS model at medium to high concentrations is either nonphysical or certainly unusual. Apart from this anomaly, in most instances, the DHOSiS model offers fairly reliable predictions at low concentrations, specifically in the range $c = [0,\ 0.3]\ mol \cdot L$ which is denoted as LC.

For 1:2 electrolytes, as shown in Figure 3.3b, the predictions of the models are not particularly convincing. However, the DHOEE, MSA, and MSA-Simple models appear to be more accurate than the rest. When considering 1:3 electrolytes, the predictions of the DHOSiS model are significantly more reliable at LC. For both LC and medium concentrations (MC: $c = [0.3,\ 1]\ mol \cdot L^{-1}$), the DHOEE model provides acceptable results.

For the 2:2 sulfates, as depicted in Figure 3.3d, neither the MSA nor the MSA-Simple models provide satisfactory predictions, even at LC. From the experimental data for these electrolytes, we observed that the molar conductivity declines rapidly with $\sqrt{I}$ at LC. However, this decline becomes more gradual in MC and at high concentrations (HC: $c > 1\ mol \cdot L^{-1}$). Unfortunately, none of the models captured this trend accurately. Yet, at lower concentrations, both the QV and DHOSiS models could approximate the slope of the data more effectively than their counterparts.

Furthermore, 2:2 sulfates are recognized in the literature as associative electrolytes [84, 112, 113, 158]. For these electrolytes, Apelblat [159] was successful in predicting the conductivity in dilute solutions (up to 0.05 $mol \cdot L^{-1}$) utilizing the QV model, with Λ^0, K_A°, and σ_{+-} serving as fitting parameters. Similarly, Chhih et al. [113] managed to estimate the electrical conductivity of $ZnSO_4$ up to 1.0 $mol \cdot L^{-1}$ by employing the MSA-Simple model, using K_A° and σ_i as fitting parameters. In another study, Turq et al. [112] were able to

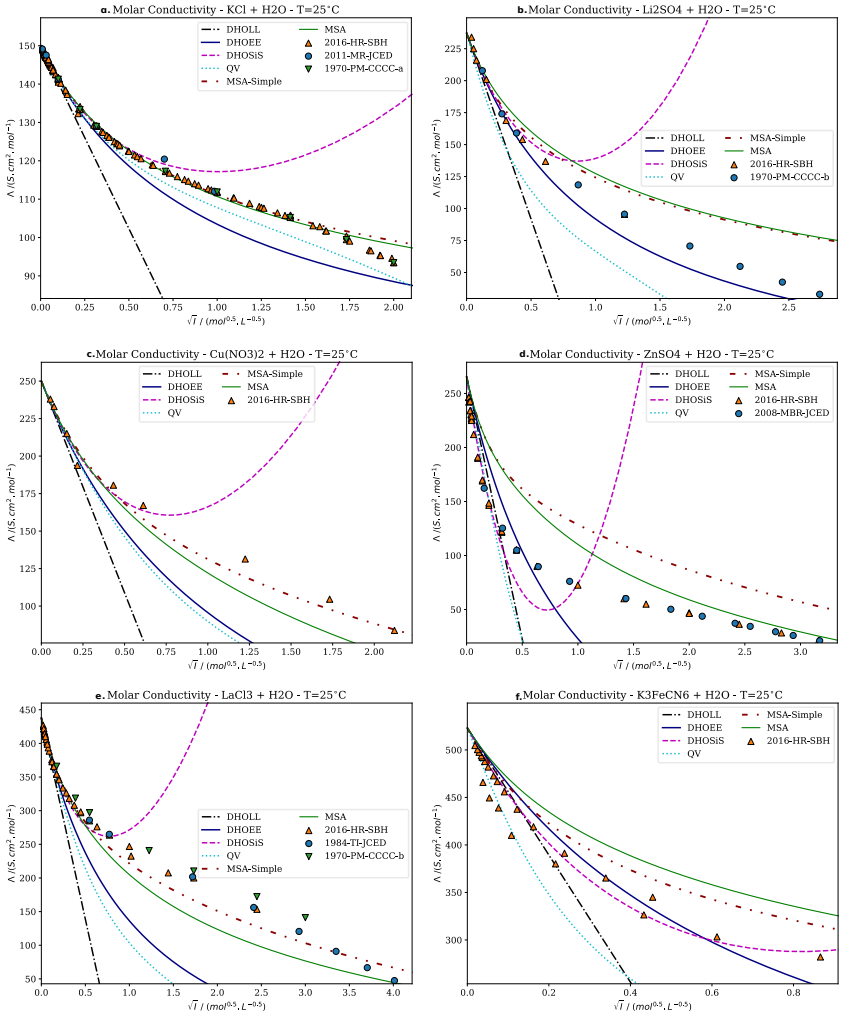

Figure 3.3. Molar conductivity (Λ) predictions at 298.15 K for various salts: (a) KCl (1:1), (b) Li_2SO_4 (1:2), (c) $Cu(NO_3)_2$ (2:1), (d) $ZnSO_4$ (2:2), (e) $LaCl_3$ (3:1), and (f) $K_3Fe(CN)_6$ (1:3) by the DHOLL, DHOEE, DHOSiS, MSA, MSA-Simple, and QV models, plotted against the square root of ionic strength ($\sqrt{I}$). Data points are sourced from the following references: 2016-HR-SBH [129], 1970-PM-CCCC-b [132], 1984-TI-JCED [141], and 2008-BMR-JCED [150]. Reprinted with permission from ref. [120]. Copyright 2022 American Chemical Society.

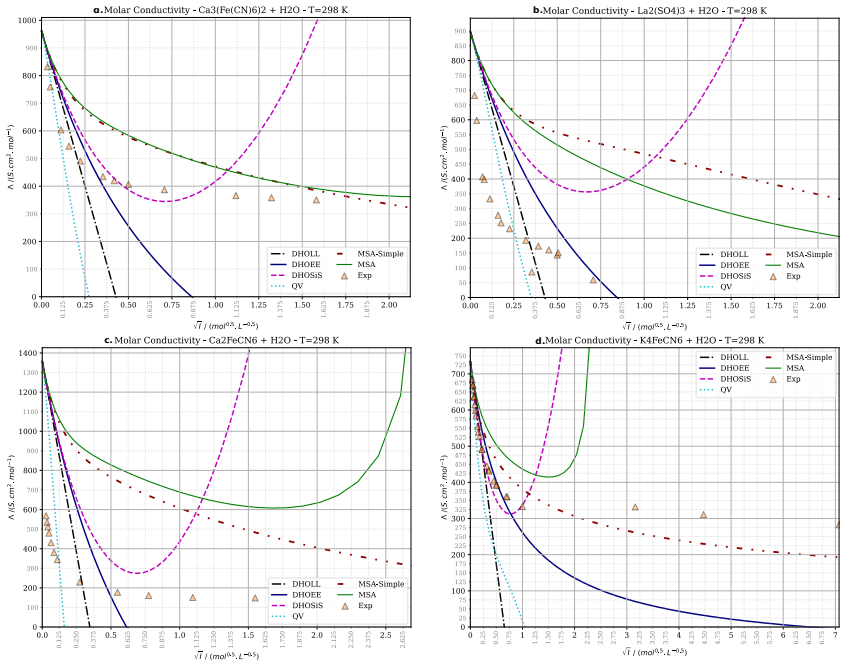

Figure 3.4. Predicted molar conductivity (Λ) at 298.15 K for various salts: (a) $Ca_3(Fe(CN)_6)_2$ (2:3), (b) $La_2(SO_4)_3$ (3:2), (c) $Ca_2Fe(CN)_6$ (2:4), and (d) $K_4Fe(CN)_6$ (1:4) using the DHOLL, DHOEE, DHOSiS, MSA, MSA-Simple, and QV models, plotted against the square root of ionic strength ($\sqrt{I}$). Data points are sourced from the reference [129]. Reprinted with permission from ref. [120]. Copyright 2022 American Chemical Society.

predict the equivalent conductivity of $MgSO_4$ up to 1.0 $mol \cdot L^{-1}$ with the MSA model, taking the (K_A°) and distance of the closest approach as fitting parameters.

In contrast, Anderko et al. [127] argued that by incorporating a concentration-dependent effective ionic radius, the predictive accuracy of the MSA model can be significantly improved, even for concentrations as high as 30 $mol \cdot kg^{-1}$. This applies to salts such as NaCl, KCl, NaBr, KBr, NaI, KI, $MgCl_2$, $AgNO_3$, NH_4NO_3, HNO_3, and HCl dissolved in water, and, importantly, this improvement was observed without considering ion pairing. However, it is worth mentioning that their approach introduces a six-parameter equation for the concentration-dependent ionic radius, which then necessitates fitting to the experimental electrical conductivity data.

Unlike the electrolytes depicted in Figure 3.3, the salts presented in Figure 3.4 have been examined less frequently in the context of electrical conductivity. However, by using data from our extensive database, we are equipped to assess the accuracy of the electrical conductivity models for these more uncommon electrolytes, namely 2:3, 3:2, 2:4, and 1:4. On a glance at Figure 3.4a, it is evident that the QV model offers an acceptable prediction of conductivity at LC. However, within the range of available data in the MC domain, all models' predictions are less accurate than expected. When examining 1:4 electrolytes, the DHOEE and DHOSiS models tend to produce more agreeable results at LC compared to their counterparts.

On the contrary, the predictive patterns of the MSA-Simple model outshine those of the other models. For 3:2 and 2:4 electrolytes, as illustrated in Figure 3.4b and c, the predictions of all the models deviate considerably from the experimental data, even in the LC range. Another significant observation is that for every salt depicted in this figure, experimental data demonstrates a swift decline with $\sqrt{I}$ at LC, but this decrease becomes more gradual as the concentrations approach the MC range.

In conclusion, for 2:4 and 1:4 electrolytes, both the MSA and DHOSiS curves exhibit a nonphysical trend where molar conductivity rises with $\sqrt{I}$. For certain electrolytes, such as $LaCl_3$, the predictions of the MSA model become indeterminate at HC. We delved into the MSA formulation to pinpoint the cause of this deviant behavior. Our analysis revealed that excluding the term $\Gamma^2\bar{\sigma}^2$ from equations B.17 and B.20 corrects the problem. Figure D.1 compares the results of three variations of the MSA model: the full MSA [111], the modified MSA [127], and the simple MSA [113] models. The sole distinction between the full MSA and the modified MSA is the absence of the term $\Gamma^2\bar{\sigma}^2$ in the latter.

As depicted in Figure D.1, the use of the modified MSA model addresses entirely the issue encountered with the full MSA model at HC. Conversely, at LC, the outcomes of the modified and full MSA are notably similar. It appears that at LC, it is permissible to leave out this expression since its numerical effect is insignificant. However, such a justification does not hold up at MC or HC.

3.5.2 Temperature Dependency

In this section, we examine the influence of temperature from two distinct angles. First, we graphically depict Λ against T at varying concentrations, accompanied by their respective experimental data for the DHOEE and MSA-Simple models (as shown in Figures 3.5 and 3.6). Subsequently, we illustrate the Λ vs. $\sqrt{I}$ on semi-log plots across different temperatures specifically for the DHOEE and MSA-Simple models, as presented in Figure 3.7.

Figures 3.5 and 3.6 show the temperature dependence of the predicted molar conductivity of aqueous solutions of $K_4Fe(CN)_6$ and $NaNO_3$, respectively. In these figures, graph (a) shows a comparison between the predictions of the MSA-Simple model and the experimental data, while graph (b) contrasts the predictions of the DHOEE model with the experimental findings.

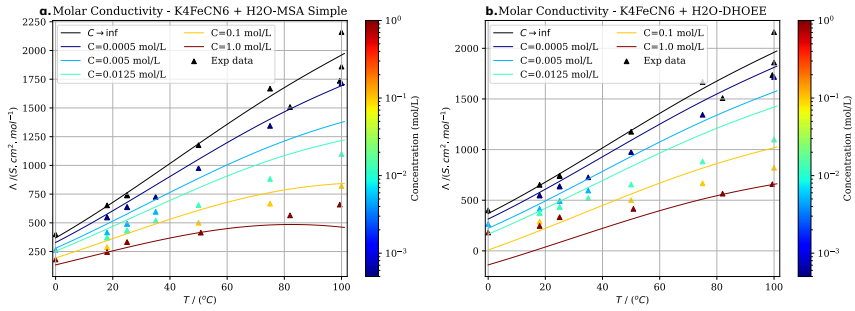

Figure 3.5. Predicted molar conductivity (Λ) of $K_4Fe(CN)_6$ using (a) MSA Simple and (b) DHOEE across various concentrations, plotted against temperatures up to 373.15 K. Data points are sourced from reference [129]. Reprinted with permission from ref. [120]. Copyright 2022 American Chemical Society.

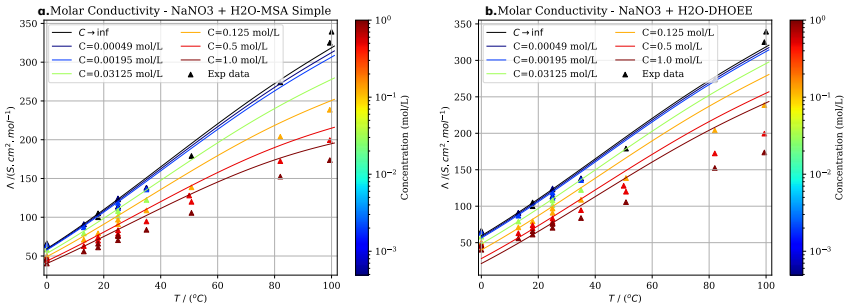

Figure 3.6. Predicted molar conductivity (Λ) of $NaNO_3$ using (a) MSA Simple and (b) DHOEE across various concentrations, plotted against temperatures up to 373.15 K. Data points are sourced from reference [129]. Reprinted with permission from ref. [120]. Copyright 2022 American Chemical Society.

When contrasting graphs (a) and (b) of Figures 3.5 and 3.6, it becomes evident that the predictions of the MSA-Simple model are more accurate than those of the DHOEE at lower temperatures. However, at elevated salt concentrations, neither model aligns well with the experimental data.

Upon examining Figure 3.7, a similar observation can be made about the MSA-Simple. When the predictions of the MSA-Simple model are accurate at a given temperature, such as the electrical conductivity of the $Ca(NO_3)_2$-Water system at 298.15 K (as seen in Figure 3.7c), they tend to be accurate at other temperatures as well. Furthermore, the MSA-Simple generally exhibits greater accuracy at lower temperatures, as evidenced in Figure 3.7d.

3.5.3 Quantitative Assessment of the Accuracy of the Models

In this section, the accuracy of the models is quantified using the absolute average deviation in percent (AAD %) as the error metric, as defined in Eq. 3.38. Given that the electrical conductivity models predict the decrease in equivalent conductivity from its infinite dilution value, we have opted for $\frac{\Lambda}{\Lambda^0}$ as the principal expression for this analysis.

$$AAD\ \% = \left[\frac{1}{N}\sum_{1}^{N}\left|\frac{\Lambda_{exp}}{\Lambda^0} - \frac{\Lambda_{pre}}{\Lambda^0}\right|\right] \times 100 \tag{3.38}$$

Electrolyte categorization in our analysis is based on its anion type and the charge of the cation (Z_{Cation}). This approach was taken because we observed that the experimental data exhibit a similar behavior when electrolytes are classified in this manner. Subsequently, the error associated with each electrical conductivity model was calculated for different concentration ranges, namely, LC, MC, and HC.

The graphical representation of our findings is included in Figure 3.8. These results illustrate the performance of different electrical conductivity models in six specific electrolyte categories, namely: MCl, MCl_2, MCl_3, MSO_4, $M(ClO_4)_2$, and MNO_3.

For electrolytes such as MCl, MCl_2, and MNO_3, the results are particularly revealing. Referring to Figure 3.8a, b, and f, it is apparent that, with the exception of the DHOLL model, other models exhibit decent predictions at LC and MC. However, it is worth noting that the errors associated with the predictions of MCl_2 and MNO_3 are generally higher

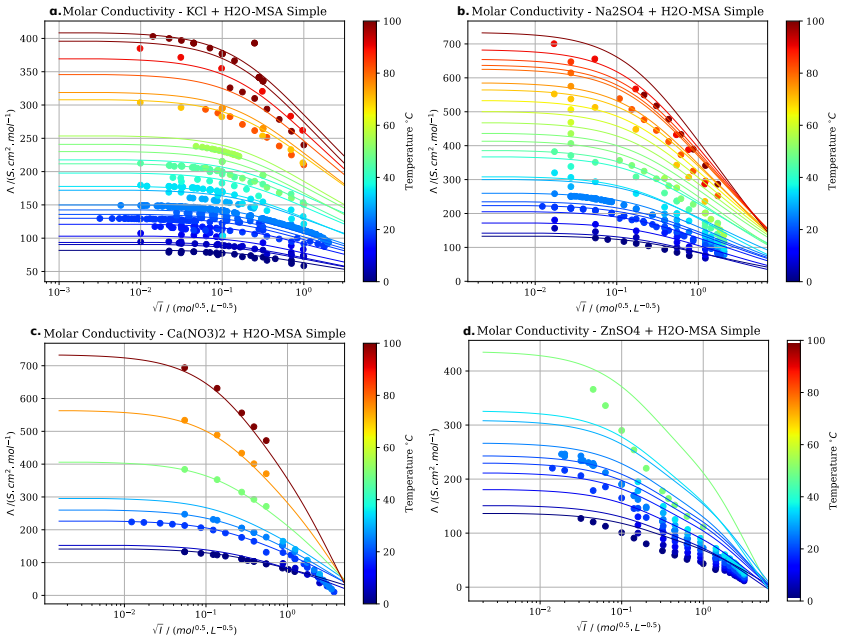

Figure 3.7. Predicted molar conductivity (Λ) of various salts using MSA Simple, plotted against the square root of ionic strength across different temperatures: (a) KCl, (b) Na_2SO_4, (c) $Ca(NO_3)_2$, and (d) $ZnSO_4$. Data points are sourced from references [129,131,133,134,141,150,160]. Reprinted with permission from ref. [120]. Copyright 2022 American Chemical Society.

compared to those of MCl. Furthermore, the predictions of the DHOSiS model show a significant increase in deviations when transitioning from LC and MC to HC.

For electrolytes MCl and MCl_2, the the DHOEE, MSA, MSA-Simple, DHOSiS, and QV models generally provide reasonable results up to MC. However, when considering MCl_3 as shown in Figure 3.8c, only the MSA and MSA-Simple models seem to produce relatively accurate predictions.

Turning our attention to 2:2 sulfates and 2:1 perchlorates, as shown in Figure 3.8d and e, the DHOSiS model stands out with excellent performance at LC. However, it is notable that the model deviations become substantially larger at higher concentrations. On the other hand, models like DHOEE, MSA, and MSA-Simple continue to display better predictive accuracy across the spectrum, even extending to HC when compared to the rest of the models.

It is essential to recognize the inherent limitations and uncertainties associated with the experimental data. Often, slight variations between predictions made by different electrical conductivity models may fall within the error bounds of the experimental data itself. As such, these minor discrepancies between models might not necessarily indicate a genuine difference in predictive capability, but could rather reflect the experimental uncertainty.

Given this context, for 1:1 electrolytes at LC, it is reasonable to consider predictions from the DHOEE, MSA, MSA-Simple, and DHOSiS models as essentially equivalent. Drawing definitive conclusions about the superiority of one model over another based on such slim margins could be misleading. It is always advisable to weigh the broader context and the

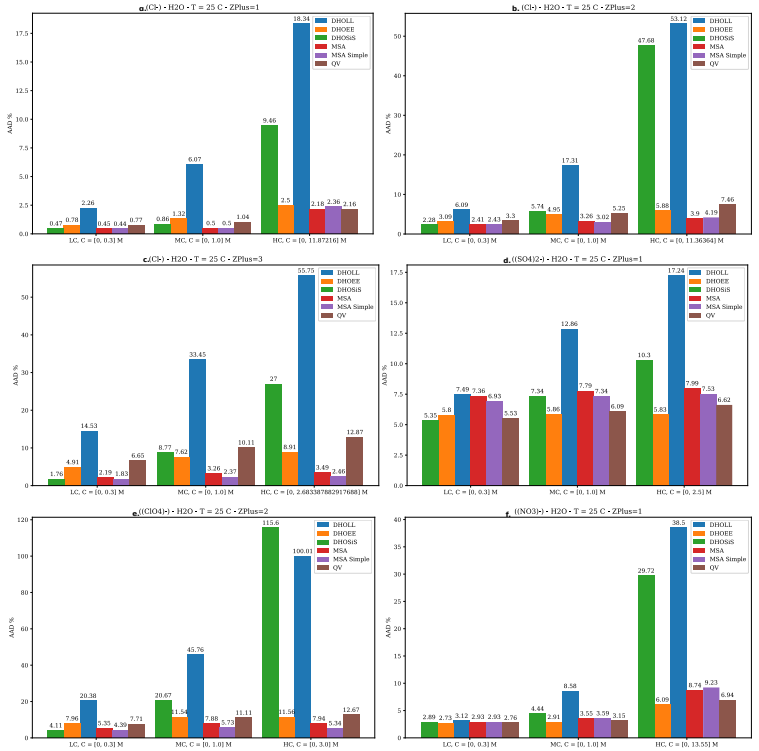

Figure 3.8. The average absolute deviation in percent (AAD%) of the DHOLL, DHOEE, DHOSiS, MSA, MSA-Simple, and QV models at low, medium, and high concentrations for (a) MCl, (b) MCl_2, (c) MCl_3, (d) MSO_4, (e) $M(ClO_4)_2$, and (f) MNO_3 aqueous solutions at 298.15 K is presented. Here, "M" represents the cation with varying valence types. Reprinted with permission from ref. [120]. Copyright 2022 American Chemical Society.

specifics of each application before selecting a model for practical use.

In summary, the DHOSiS model offers acceptable precision at LC. However, its precision decreases as concentrations increase, especially at MC and HC. Despite their straightforward design, both the DHOEE and MSA-Simple models deliver acceptable results in most situations, but they like other models face challenges with 2:2 sulfates. Moreover, a comparison between the MSA and MSA-Simple models reveals that MSA does not provide any significant advantages over its more streamlined counterpart. Thus, one can confidently opt for the simpler MSA version without sacrificing accuracy. Furthermore, even though the QV model incorporates higher-order terms from the FO continuity equation, Figure 3.8 highlights that its output is not considerably better than that of DHOEE.

To provide a complete view of the performance of the models, the arithmetic average of AAD% for various electrical conductivity models has been tabulated (refer to Table 3.4). To ensure fairness and prevent any bias due to electrolytes with a higher number of experimental data points, the arithmetic mean was employed. This ensures that every electrolyte, regardless of the number of data points but sharing the same valence type, has an equal influence on the values presented in Table 3.4.

Table 3.4 indicates that for 1:1 electrolytes, the performance of nearly all models is

Table 3.4. This table presents the mean of AAD% of the equivalent conductivity models for various electrolyte types at LC, MC, and HC. The experimental data points for the equivalent conductivity are sourced from references [129–150]. Reprinted with permission from ref. [120]. Copyright 2022 American Chemical Society.

Type	N_E	c^{max}		DHOLL	DHOEE	DHOSiS	MSA-Simple	MSA	QV
			LC	2.93	1.93	1.81	1.78	1.78	1.94
1:1	28	13.55	MC	6.89	2.37	2.40	1.92	1.95	2.20
			HC	19.9	3.57	12.9	3.93	3.73	3.50
			LC	15.0	7.45	7.59	9.68	11.0	8.95
1:2	6	2.5	MC	28.1	7.93	11.9	10.9	12.2	10.3
			HC	39.1	8.06	20.7	11.6	12.9	11.6
1:3	1	0.125	LC	29.2	11.5	8.33	12.6	16.9	24.1
			LC	72.2	40.6	43.3	48.5	58.1	69.2
1:4	3	5.0	MC	95.2	42.3	70.0	48.7	57.8	81.6
			HC	177	45.7	1149	49.2	57.5	132
			LC	25.1	13.0	10.3	10.2	10.5	13.6
2:1	34	11.36	MC	53.0	15.7	23.1	11.0	11.7	16.4
			HC	110	14.4	120	12.5	11.8	17.2
			LC	41.4	19.6	9.93	32.9	30.8	28.4
2:2	9	3.54	MC	123	28.7	49.7	33.5	28.0	51.7
			HC	220	36.6	202	32.5	25.2	73.6
2:3	1	0.17	LC	510	141	89.2	83.4	76.3	419
2:4	2	0.1	LC	483	248	254	316	321	608
			LC	50.7	20.9	8.27	9.66	11.82	26.7
3:1	10	2.68	MC	88.3	28.3	29.6	11.5	16.8	36.2
			HC	114	30.6	59.5	11.9	18.4	39.8
3:2	1	0.03	LC	169	150	197	258	244	173

reliable. For 2:1 electrolytes, the DHOEE, MSA, and MSA-Simple models emerge as the most consistent, while for 3:1 electrolytes, MSA and MSA-Simple appear to be the most accurate. However, for electrolyte types 1:4, 2:3, 2:4, and 3:2, none of the models offers satisfactory predictions even at LC. Furthermore, in both MC and HC, the predictions for 2:2 electrolytes generally diverge from the experimental results.

In closing, it is vital to recognize that electrical conductivity models are developed based on certain simplifying assumptions. The consequences of these assumptions define the concentration range within which the models can be reliably applied. For 1:1 electrolytes, the concentration limits of the DHOLL, DHOEE, DHOSiS, MSA, MSA-simple and QV models are 10^{-2}, 10^{-1}, 10^{-1}, 1, 1, and 10^{-1} $mol \cdot L^{-1}$, respectively. Furthermore, by adjusting the ion size parameter to the experimental electrical conductivity data and accounting for ion-ion associations using the mass action law, the concentration boundaries of these electrical conductivity models might be extended (see references [112, 113, 127, 130, 148–150] for a deeper dive). However, one should be cautious as there is a risk of over-fitting to the experimental data, leading to non-realistic values for parameters such as ionic diameter (for instance, negative ionic radii as highlighted in Table 3.10 of reference [89]) or the association constant. Therefore, when evaluating the performance of electrical conductivity models, it is crucial to factor in these concentration limits.

3.5.4 Evaluation of the Relaxation and Electrophoretic Terms

Previously, we highlighted that the electrical conductivity of electrolytes originates from two primary factors: the relaxation term and the electrophoretic term. Delving deeper into this topic, we now embark on a detailed examination of individual electrical conductivity models by evaluating how they account for the influences of both the relaxation and electrophoretic components. The insights into these evaluations are represented graphically in Figures 3.9 and D.2.

A closer look at the DHOLL formulation reveals a clear linear dependence of both the relaxation and electrophoretic terms on $\sqrt{I}$, evident through the factor of κ as depicted in Figure 3.9. Notably, the electrophoretic component of DHOLL is consistently lower than that of other models across all electrolytes. In the majority of electrolytes, the relaxation term is not as strong as those of its counterparts.

In contrast to DHOLL, the DHOEE model does not exhibit a straightforward linear relationship with $\sqrt{I}$ for either term. More specifically, when most salts are evaluated, the relaxation and electrophoretic terms of DHOEE present an upward curvature, as opposed to a linear trend.

The relaxation term of the QV model has a shape similar to that of an inverted S. At LC, it closely follows the DHOLL. As it moves to higher concentrations (MC), the decrease in $\frac{\delta k}{k}$ slows down before increasing again. The electrophoretic term of the QV model has a consistent pattern for both cations and anions, with most electrolytes having a minimum, though the exact spot of the minimum varies. This suggests that when exposed to an external electric force, the ions initially move quickly and then slow down as the concentration rises (not considering the opposing pull from the relaxation term). This complex behavior of the QV model is not obvious in the Λ vs. $\sqrt{I}$ graph, as it is masked by the contributions of the relaxation term.

The patterns observed in the MSA and MSA-Simple models are quite similar. In many cases, their relaxation and electrophoretic terms are closely aligned. Furthermore, the contribution of the relaxation term is less than that of the electrophoretic term. For all electrolytes studied, the relaxation term remains above -0.4, while the electrophoretic term can go below -1 in some cases. In some scenarios, the relaxation term of the MSA-Simple model reaches a minimum and then stabilizes. On the other hand, in certain situations, especially at higher concentrations, the relaxation term of the MSA model increases and eventually reaches a positive value, as shown in Figure D.2. It is important to note that a positive value for the relaxation term implies that the ionic cloud asymmetry is pushing the central ion in the direction of the external electric field, which is not physically accurate.

In Section 3.5.1, we highlighted the shortcomings of the predictions of the DHOSiS model

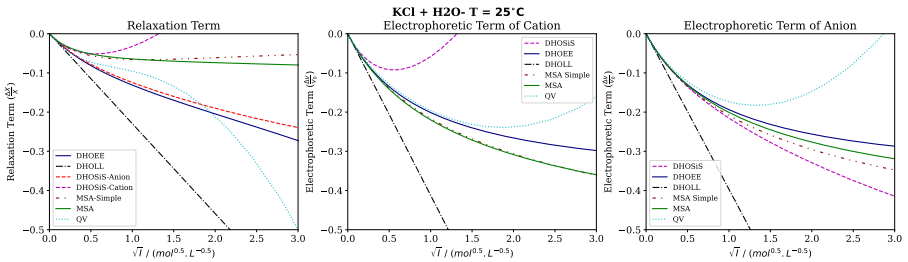

Figure 3.9. The relaxation and electrophoretic terms for KCl as predicted by the DHOLL, DHOEE, DHOSiS, MSA, MSA Simple, and QV models are plotted against the square root of the ionic strength at 298.15 K. Reprinted with permission from ref. [120]. Copyright 2022 American Chemical Society.

at medium to high concentrations, noting a nonphysical trend at such concentrations. Upon closer examination of the relaxation and electrophoretic terms, this peculiar behavior of the model becomes clearer. Both the relaxation and electrophoretic terms for the cations exhibit a minimum and then turn positive as we approach MC and HC. This behavior can be linked to a potentially inaccurate estimation of the ionic cloud size for cations (which are typically the smaller ions). This size appears to grow with increasing concentration beyond a certain threshold, which varies depending on the specific electrolyte.

Moreover, the relaxation term of the DHOSiS model is distinct in being ion-specific, in contrast to other models, including the MSA model, which is also a UPM. A closer examination of the mathematical framework used for the MSA model confirms that even when different sizes are assumed for anions and cations, the outcome is a salt-specific relaxation term. However, when the size of the ionic cloud (κ^{-1}) is replaced with an effective size (Ψ_i^*), the result is an ion-specific relaxation term, which calls for a proper justification. On the basis of this observation, one can infer that the ion-specific relaxation term may not be scientifically robust. Unless otherwise noted, the term for the positive ion certainly requires further refinement.

An additional observation regarding the DHOSiS model pertains to the derivation methodology of its mathematical formulations for the electrical conductivity. The derivation process is not explicitly elucidated in the original paper [118]. In particular, all other models have adopted a consistent methodology to derive the formulations for electrical conductivity (see Section 2.3).

However, in the case of the DHOSiS model, it is noted that three modifications were introduced to enhance the DHOLL, grounded on the "smaller ion shell" theory. As a result, in contrast to other models, it suggests that Fraenkel might not have directly derived the formulation by solving the FO continuity equation or by taking into account the motion of ions and their surrounding ionic cloud within a viscous environment.

It seems that the DHOSiS model was based on the DHOEE formulation, which represents an advancement over the DHOLL, essentially dividing the formula for equivalent conductivity by $1 + \kappa\sigma_{+-}$. However, the derivation process for DHOEE takes into account the ion movements in response to an external electric field within a viscous medium, while also addressing the hindering effect of the relaxation term through the solution of the FO continuity equation (details can be found in the references [90, 101, 120]). After dismissing the higher-order terms of κ in the relaxation and electrophoretic terms, DHOEE emerges. If a similar approach were applied without presuming identical ion sizes, an improved formula could emerge that elevates DHOEE from RPM to UPM (see Chapter 5). Nonetheless, the derivation route for DHOSiS, which clearly includes an ion-specific size parameter, remains ambiguous.

In addition to the derivation process, several key observations can be made about the DHOSiS model. Firstly, the model appears to exhibit nonphysical behaviors at MC and HC. This anomaly appears to be rooted in an nonphysical prediction of the radius of the ionic atmosphere surrounding the s ion, as depicted in Figure 3 of reference [118]. Fraenkel acknowledged this by highlighting the nonphysical nature of the "DH-SiS, s-ion" curve's minimum, but also emphasized that this lay beyond the concentration limit of both the DHO and DHO-SiS models. Notably, while the theory defines concentration boundaries for the DHOEE and MSA-Simple models, neither shows any nonphysical behaviors when they exceed these limits. In contrast, both Figure 3.3 and Table 3.4 suggest that their predictions remain relatively consistent for certain electrolytes even beyond their established concentration thresholds.

Third, Fraenkel employed ionic radii values that were fitted to activity coefficient data using the DHSiS model (activity scale) [118]. In the present study, we have chosen not to use these proposed ionic radii for two main reasons. First, the specific radii are not provided for all cations and anions, having been reported for only eleven cations and seven anions in [118]. Consequently, relying on the activity scale would make it impossible to predict the

electrical conductivity of numerous electrolytes. Secondly, the usage of activity coefficient experimental data in one model could skew the analysis and prevent an unbiased comparison.

3.6 Extension of the Models; The Effect of RSP and Viscosity

The influence of concentration-dependent RSP and viscosity on the predictions of equivalent conductivity models is examined. Both the full and simplified versions of the MSA models, as well as four equivalent conductivity models based on DHO (DHO1-3 and DHOEE), are used to predict the equivalent conductivity of nine 1:1 aqueous electrolyte solutions at 298.15 K. To explore the influence of RSP on the estimations of equivalent conductivity, three empirical RSP models are used in combination with the RSP of the solvent. Additionally, the effect of a concentration-dependent viscosity on the equivalent conductivity predictions is explored.

3.6.1 RSP Models

3.6.1.1 Breil-Michelsen-Mollerup (BMM) Model

Breil, Michelsen, and Mollerup [8] proposed an empirical model for the RSP of aqueous solutions, incorporating a correction factor for the pure water RSP (as described in Eq. 3.39). In this equation, $\varepsilon_r^{sat}(T)$ represents the RSP of water derived from Eq. 3.36. Here, c represents the salt concentration in $mol \cdot L^{-1}$, ν_i indicates the stoichiometric coefficient, Z_i denotes the charge valence type, and a_i is an ion-specific coefficient. The a_i coefficients for seven cations and four anions are detailed in Table 3.5.

$$\varepsilon_r(T,\ c) = \varepsilon_r^{sat}(T)\left[1 - \sum_i^{ions}\left(0.01 Z_i \nu_i c - \frac{Z_i \nu_i c a_i}{1 + 0.16 Z_i \nu_i c}\right)\right] \tag{3.39}$$

3.6.1.2 Polynomial Correlation

In this model, a polynomial equation, such as Eq. 3.40, is used to fit the RSP experimental data. Barthel et al. [84] provided the coefficients for Eq. 3.40 for various aqueous and non-aqueous solutions, as listed in Tables 7.6 and 7.7 of their book. The coefficients a_1-a_6 and the maximum salt concentrations for the aqueous solutions examined in this study are summarized in Table 3.6.

$$\varepsilon_r(T,c) = \varepsilon_w(T) + a_1 c^{\frac{1}{2}} + a_2 c + a_3 c^{\frac{3}{2}} + a_4 c^2 + a_5 c^{\frac{5}{2}} + a_6 c^3 \tag{3.40}$$

Table 3.5. The coefficients for the BMM model [8].

Cation	a_+	Anion	a_-
Li^+	0.1200	Cl^-	0.1173
Na^+	0.1062	Br^-	0.1348
K^+	0.0816	$(NO_3)^-$	0.1104
Cs^+	0.0650	$(SO_4)^{2-}$	0.0022
Mg_2^+	0.1155		
Ca_2^+	0.1097		
Ni_2^+	0.0553		

Table 3.6. The coefficients for Eq. 3.40 used in this work as reported by Barthel et al. [84].

Salt	a_1	a_2	a_3	a_4	a_5	c_{max}	
LiCl	0	-14.5	0	1.28	0	-0.0386	13.4
LiBr	0	-16.2	0	1.34	0	0	3.0
$LiNO_3$	0	-17.1	0	2.40	0	-0.15	6.0
NaCl	0	-13.8	0	0.98	0	0	4.0
$NaNO_3$	0	-13.3	0	1.25	0	0	4.0
KCl	0	-12.4	0	0.95	0	0	4.0
KBr	0	-12.8	0	0.83	0	0	3.0
KNO_3	0	-11.7	0	1.80	0	0	2.0
CsCl	0	-10.7	0	0.83	0	0	4.5
CsBr	0	-12.6	0	1.31	0	0	2.0

3.6.1.3 Simonin et al. Model

A linear correlation for the inversed RSP of aqueous solutions was developed by Simonin et al. [161–163] for various associative and non-associative electrolyte solutions. This model contrasts with other correlations since it has not been fitted to the RSP experimental data.

$$\varepsilon_r^{-1}(T,c) = \varepsilon_w^{-1}(T)\left[1 + \alpha_\varepsilon c\right] \tag{3.41}$$

Simonin et al. [161–163] employed the MSA [5, 6, 126] or BiMSA [20] implicit solvent models in a series of studies to estimate the osmotic coefficient of single-salt and multi-salt aqueous solutions. α_ε in Eq. 3.41, along with two parameters for a concentration-dependent cations radius and anions radius, as well as the association constant at infinite dilution (K_A°), was adjusted to match the osmotic coefficient data. Parameters for non-associative electrolyte solutions were tabulated in Tables 1 and 2 of ref. [161]. Adjusted parameters for associative electrolyte solutions are detailed in Tables 1, 2, and 3 of ref. [163]. The coefficients α_ε for the salt-water systems explored in this study are summarized in Table 3.7.

Table 3.7. The coefficients for the Simonin et al. [161–163] model (asterisk symbols mean that for these electrolytes ion pairing is considered).

Salt	a_ϵ	m_{max}
LiCl	15.450	19.2
LiBr	14.560	20.0
$LiNO_3$	14.390	10.0
NaCl	6.930	6.1
$NaNO_3$*	7.380	10.8
KCl	6.964	5.0
KBr	7.272	5.5
KNO_3*	10.800	3.5
CsCl	0.115	11.0
CsCl*	2.940	8.0
CsBr	2.327	5.0
CsBr*	4.110	5.0
$CsNO_3$*	10.200	1.5

3.6.2 Viscosity Correlation

A polynomial correlation introduced by Barthel et al. [164, 165] is utilized to estimate the viscosity of electrolyte solutions. The correlation for the viscosity of salt-water systems at 298.15 K is given by Eq. 3.42 [164, 165]. In this equation, $\eta_0(T)$ denotes the viscosity of the pure solvent, $\eta(T,\ c)$ represents the viscosity of the solution, A_i are the correlation coefficients and c is the molarity of the solution expressed in $mol \cdot L^{-1}$. The coefficients for this viscosity correlation, valid for binary salt-water systems at 298.15 K, are listed in Table 3.8 [164, 165]. A comparison between the reduced viscosity $(\frac{\eta}{\eta_0})$ as estimated by Eq. 3.42 and experimental values for salt-water systems at 298.15 K are illustrated in Figure D.4.

$$\ln\left(\frac{\eta(T,\ c)}{\eta_0(T)}\right) = A_1 c + A_2 c^2 + A_3 c^3 \tag{3.42}$$

3.6.3 Results

In this section, the influence of incorporating a concentration-dependent RSP and/or viscosity on the predictions of the electrical conductivity models, as described in Section 3.1, is examined. In the illustrations presented in this section, the integration of the electrical conductivity models, the RSP models, and the viscosity models is denoted by $\Lambda^A - \varepsilon_r^{(B)}(T,c) - \eta(T,c)$. The electrical conductivity model is represented by 'A', which can be MSA, MSA-Simple, DHOEE, or DHO1-3. The variable 'B' ranges from 1 to 4. The designations $\varepsilon^{(1)}(T)$, $\varepsilon^{(2)}(T,c)$, $\varepsilon^{(3)}(T,c)$, and $\varepsilon^{(4)}(T,c)$ are associated, respectively, with the solvent RSP, Eq. 3.40, Eq. 3.39, and Eq. 3.41. Furthermore, the viscosity of the solvent is indicated by $\eta(T)$, while the viscosity of the solution is indicated by $\eta(T,c)$.

In the initial part of this section, the influence of a concentration-dependent RSP on the predictions of the MSA model will be investigated for nine 1:1 aqueous solutions at 298.15 K. In the subsequent part, the impact of a composition-dependent RSP on the predictions of both the MSA-based and the DH-based models will be explored. In the final part, the combined effects of composition-dependent viscosity and RSP will be analyzed in relation to the predictions of the MSA-Simple and DHO3 models.

Table 3.8. The coefficients associated with the viscosity correlation, as given by Eq. 3.42, correspond to a system temperature of 298.15 K, where the value of $\eta_0(T)$ is 0.00089 $Pa \cdot s$. These coefficients have been sourced from the work of Barthel et al. [164, 165].

Salt	$A_1 \times 10^2$	$A_2 \times 10^3$	$A_3 \times 10^4$
LiCl	13.3	0.943	3.18
LiBr	11.4	-3.57	8.13
$LiNO_3$	9.64	4.90	2.01
NaCl	8.26	8.28	0.00
$NaNO_3$	4.55	18.1	-7.46
KCl	-7.21	4.84	4.06
KBr	-3.81	7.07	7.61
KNO_3	-4.63	24.4	-1.46
CsCl	-4.10	6.52	6.45
CsBr	-6.64	4.45	0.00

3.6.3.1 Effect of RSP

In this section, the effectiveness of the MSA model in predicting the electrical conductivity of non-associative or mildly associative electrolyte solutions using a concentration-dependent RSP is explored. The selection of the MSA model is based on two primary reasons. First, as evidenced in Section 3.5, this model stands out as the most precise or one of the top-tier models for predicting the electrical conductivity of aqueous electrolyte solutions. Second, from a derivation perspective, this model is among the most comprehensive, with possibility for extensions to multi-component systems.

For this purpose, as highlighted in Section 3.6.1, three empirical models are used. These include the BMM model [8], the polynomial correlation [84], and the model developed by Simonin et al. [161–163]. These are used to estimate $\varepsilon_r\,(c, T)$ for 1:1 electrolytes. Subsequently, the predictions of the MSA model, when integrated with these three $\varepsilon_r\,(c,\ T)$ formulations as well as the RSP of the solvent, are evaluated against experimental data.

To investigate the impact of $\varepsilon_r\,(c,\ T)$ on the predictions of electrical conductivity, nine 1:1 aqueous electrolyte solutions have been selected. The ion properties examined in this section are detailed in Table 3.1. These salt-water systems were primarily chosen on the premise that ion pairing has a minimal influence on the electrical conductivity in these mixtures. However, it is essential to highlight that, even in these electrolyte solutions, ion pairing can become significant at elevated concentrations. Moreover, for these mixtures, a range of sources provide the electrical conductivity experimental data. This availability allows for verification of the precision of the experimental data, enabling easy identification and exclusion of outliers from the assessment.

In Figure 3.10, the predictions made using the MSA model are shown. When the RSP is derived from pure water, the results are displayed with dashed-dot green curves. Curves arising from using Eq. 3.40, Eq. 3.39, and Eq. 3.41 are denoted by solid black, dashed red, and dotted blue curves, respectively. This figure presents the molar conductivity of compounds such as LiCl, $LiNO_3$, NaCl, $NaNO_3$, KCl, and KNO_3 at 298.15 k, plotted against the square root of their respective ionic strengths.

From figures 3.10 and D.5, it is evident that incorporating a composition-dependent RSP enhances the alignment of the predictions of the MSA model with experimental observations. Investigating further, three distinct patterns can be identified in these figures.

For clarity, we have introduced a term, c_{SD}, denoting the concentration threshold where deviations between the MSA model's predictions and experimental results begin to emerge. Essentially, the MSA model retains its predictive accuracy up to a concentration of $c_{SD}^{(RSP\ model)}$, with the superscript indicating the specific RSP model.

Examining compounds such as LiCl, $LiNO_3$, NaCl and LiBr (as seen in Figure 3.10a, b, c and also Figure D.5c), the observed sequence for c_{SD} is: $c_{SD}^{(1)}<c_{SD}^{(4)}<c_{SD}^{(2,3)}$.

For KNO_3 and $NaNO_3$ (depicted in Figure 3.10d and f), the sequence of c_{SD} reveals an equivalence: $c_{SD}^{(1)}=c_{SD}^{(4)}=c_{SD}^{(2,3)}$.

Lastly, in the case of KCl (illustrated in Figure 3.10e), the order of c_{SD} stands as: $c_{SD}^{(1)}<c_{SD}^{(2,3)}<c_{SD}^{(4)}$.

Furthermore, an in-depth term-by-term analysis for chlorides and nitrates, when using the MSA model, is illustrated in Figures 3.11 and D.6. Observing Figure 3.11, it becomes apparent that the impact of a concentration-dependent RSP on the relaxation terms for LiCl, NaCl, and KCl is strikingly similar. In contrast, when considering the electrophoretic terms of the cation, the effect is more pronounced as the ionic radius decreases. For example, in the LiCl-water system, a concentration-dependent RSP results in an electrophoretic term that falls below -1 for concentrations higher than 6 $mol \cdot L^{-1}$. This phenomenon, although not realistic, appears at a very high concentration (6 $mol \cdot L^{-1}$). At such concentrations, the basic assumptions made during the development of the MSA model, such as disregarding the structured nature of water, may no longer be valid.

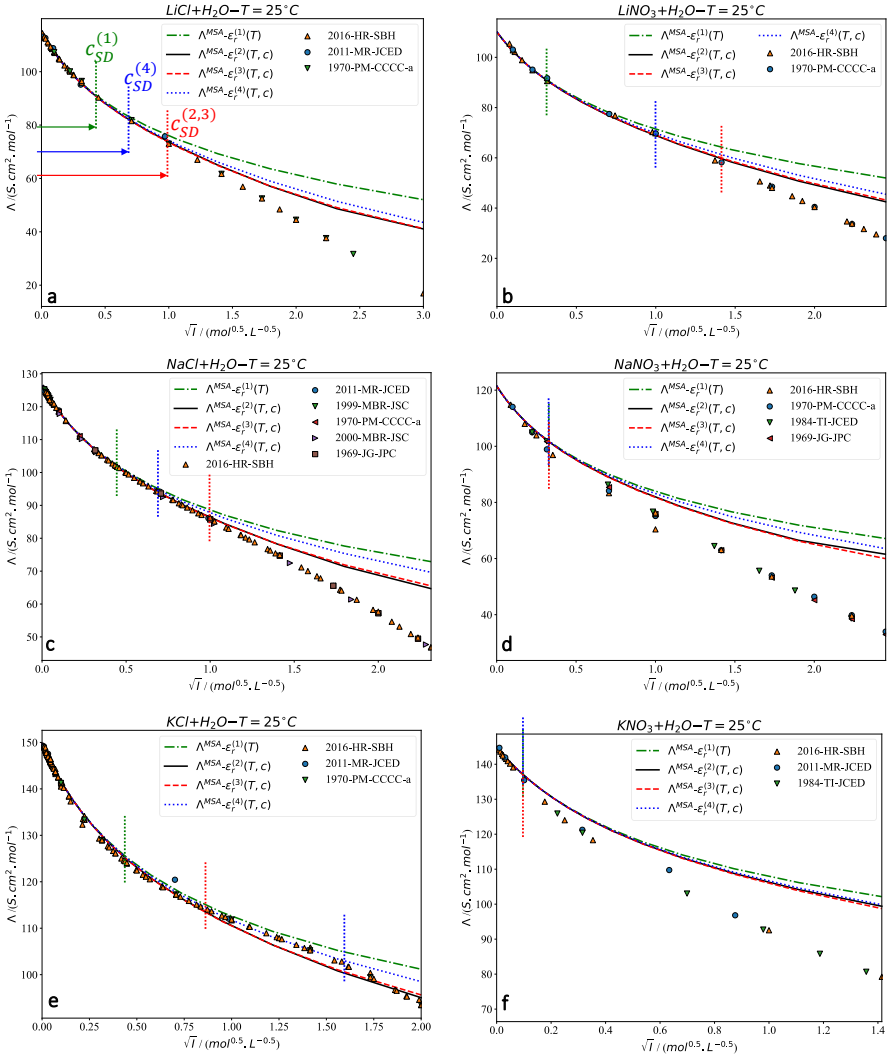

Figure 3.10. The influence of concentration-dependent RSP on the predictions made by the MSA model for various electrolytes at 298.15 K is explored. Electrolytes studied include (a) LiCl, (b) $LiNO_3$, (c) NaCl, (d) $NaNO_3$, (e) KCl, and (f) KNO_3. In these evaluations, c_{SD} represents the maximum concentration at which the MSA model reliably predicts electrical conductivity. For these predictions, various RSP models were utilized: a constant model, the Simonin et al. model [161–163], the polynomial correlation [84], and the BMM model [8]. Acronyms such as 2016-HR-SBH [129], 2011-MR-JCED [134], 1984-TI-JCED [141], 1999-MBR-JSC [149], 1970-PM-CCCC-a [131], 2000-MBR-JSC [148], and 1969-JG-JPC [166] denote the sources from which the data points were collected. Reprinted from ref. [124], Copyright 2023, with permission from Elsevier.

In conclusion, when examining the electrophoretic terms of Cl^- as depicted in Figure 3.11 and those of NO_3^- in Figure D.6, there is only a marginal variation upon incorporating a concentration-dependent RSP. Despite this minor alteration, it should be noted that the influence of a concentration-dependent RSP on the electrophoretic term of the anion increases as the radius of the cation decreases. The sequence of this effect is LiCl > NaCl > KCl. Despite the slight change, the impact of a concentration-dependent RSP on the electrophoretic term of the anion increases when the radius of the cation reduces (the effect is as follows LiCl>NaCl>KCl).

3.6.3.2 MSA vs. DHO-based Models

Barthel et al. [84] pointed out that:

> *"The modern theory of electrolyte solutions ... overcomes the drawbacks of the lcCM [low concentration chemical model] concerning its limited concentration range by integral equation ..."*

They also mentioned that

> *"... Accordingly, this approach [MSA] can be regarded as the natural extension of the low concentration chemical models up to concentrations of 1 mol $\cdot$ L^{-1} with the help of integral equation theories."*

The perspective on models derived from DHO theory is also evident in the empirical analysis of electrical conductivity data. In related studies [130, 148, 149, 167–169], a model akin to Eq. 3.33 is employed for dilute solutions, while the MSA-Simple model is favored for more concentrated solutions.

Upon a closer examination of the models developed since the theory was introduced by Debye and Hückel , it is evident that from 1950 to 1980, due to either a lack of motivation or constraints in computational capabilities, the electrical conductivity models were truncated to align with the concentration-dependent form proposed by Onsager and Fuoss [83]. These truncated equations are subsequently referred to as DHO-based models. Consequently, in terms of accuracy, these models cannot rival the more recently developed ones.

In this chapter, we integrate three relaxation models, those formulated by Fuoss and Onsager [94], Falkenhagen et al. [101], and Falkenhagen and Kelbg [102], with the electrophoretic term introduced by Robinson and Stokes [90]. This integration resulted in three new models, which are labeled DHO1-3. This section evaluates the comparative accuracy of these models against MSA-based models and the experimental data. Furthermore, the influence of incorporating a composition-dependent RSP on the predictions of these models is explored.

Figure 3.12 displays the predicted electrical conductivity of LiCl-water and $LiNO_3$-water systems at 298.15 K using the DHO1, DHO2 and DHO3 models. The predictions when the RSP is derived from pure water are represented by dashed-dot green curves. Predictions based on Eq. 3.40, Eq. 3.39, and Eq. 3.41 are illustrated by solid black, dashed red, and dotted blue curves, respectively.

From the data presented in Figure 3.12, several important observations can be made. Despite the widely held belief in the literature that theories based on DHO theory are primarily suitable for very dilute solutions, both the DHO1 and DHO3 models demonstrate impressive accuracy. Their performance appears to be comparable to that of the MSA and MSA-Simple models for the 1:1 electrolyte solutions under examination. Furthermore, the introduction of a composition-dependent RSP improves the predictive power of the DHO1 and DHO3 models. However, this enhancement is not consistent across all DHO-based models. Specifically, the accuracy of the DHO2 model appears to decrease when a

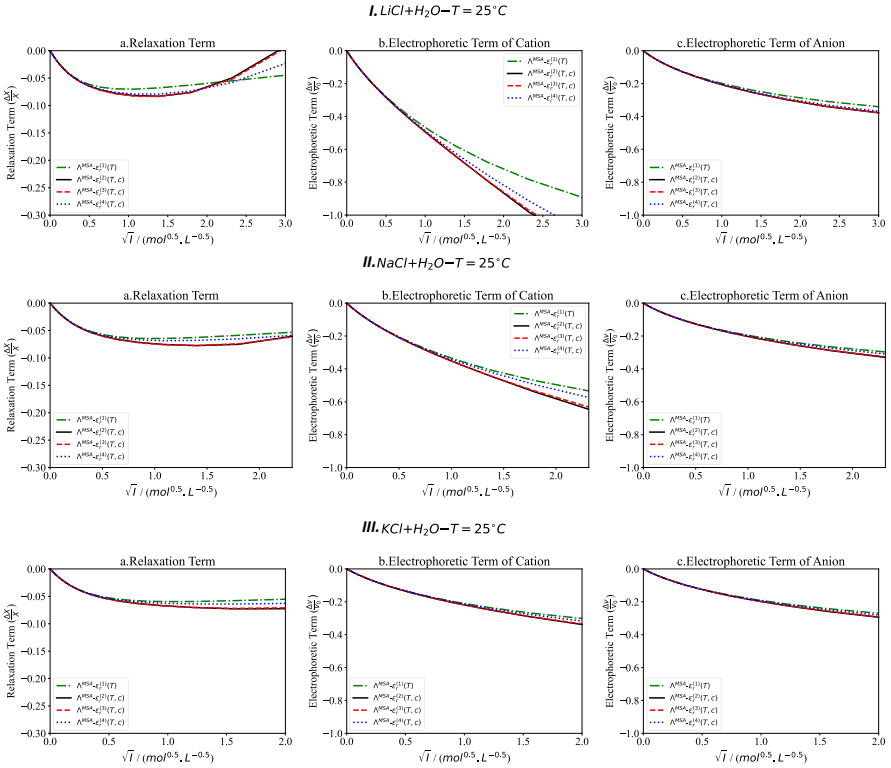

Figure 3.11. The influence of concentration-dependent RSP on the contributions to the relaxation and electrophoretic terms, as predicted by the MSA model, is investigated for aqueous solutions of (I) LiCl, (II) NaCl, and (III) KCl at 298.15 K. Reprinted from ref. [124], Copyright 2023, with permission from Elsevier.

composition-dependent RSP is used, which differs from the trends observed in the other models.

The predictions of the DHO1 and DHO3 models were compared with those of the MSA model. This comparison is crucial as it might challenge established views in the literature regarding the prediction of electrical conductivity. In Figure 3.13, the predictions of the DHO1, DHO3 and MSA models for aqueous solutions of 1:1 chlorides and nitrates at 298.15 K are presented.

From Figure 3.13, the following four key observations can be made. First, when considering the solvent RSP or solution RSP, the predictions of the DHO1, DHO3 and MSA models up to a concentration of 1 $mol \cdot L^{-1}$ are remarkably similar. Secondly, the predictions made by the DHO1 and DHO3 models are generally observed to be higher than those provided by the MSA model. Third, when a concentration-dependent RSP is utilized, a reduced discrepancy from the experimental data is seen across all models. Lastly, accurate predictions for the electrical conductivity of electrolyte solutions are given by the MSA model, the predictions by the DHO1 and DHO3 models are also noted to be accurate.

In summary, the DHO-based theory demonstrates accuracy and reliability comparable to those of the MSA-based theory in predicting electrical conductivity. Utilizing a compre-

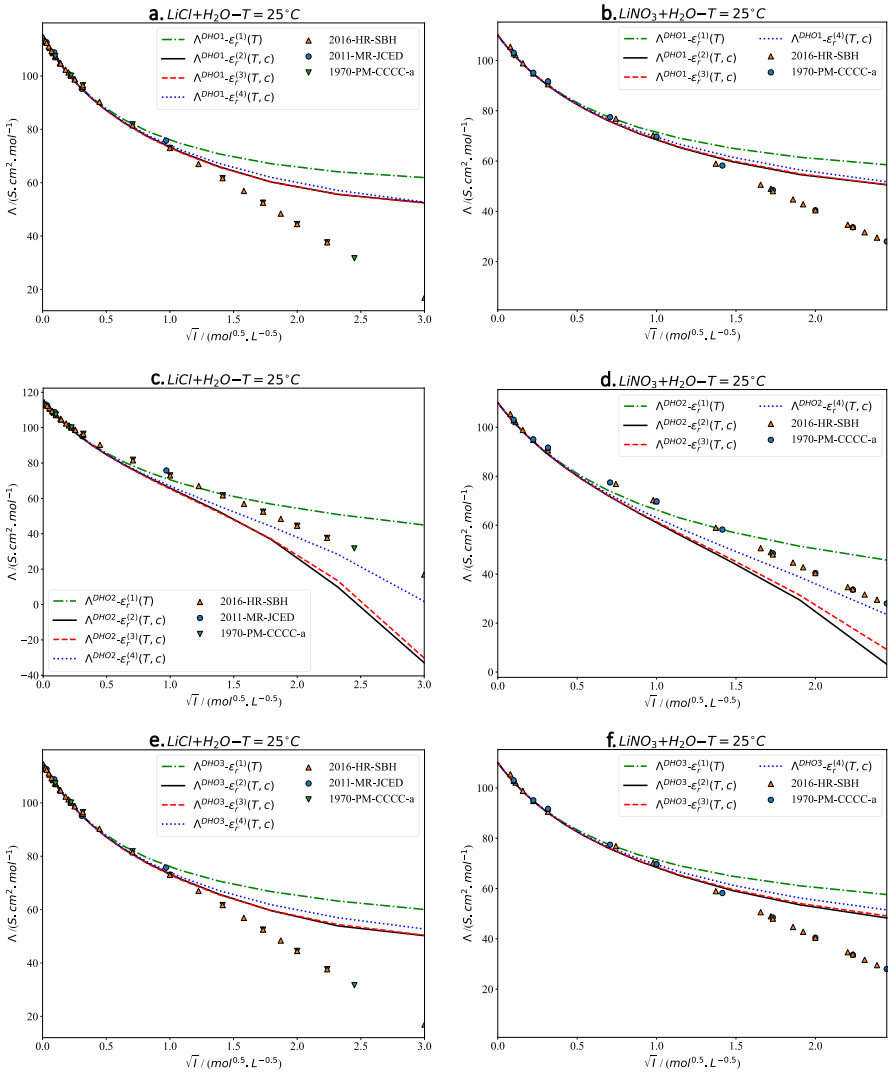

Figure 3.12. The influence of concentration-dependent RSP on the predictions of the DHO1, DHO2, and DHO3 models for LiCl and $LiNO_3$ aqueous solutions at 298.15 K is evaluated. These predictions are compared across using different RSP models: (1) constant RSP, (2) Barthel et al. [84], (3) BMM [8], and (4) Simonin et al. [161–163]. Acronyms follow those used in Figure 3.10. Reprinted from ref. [124], Copyright 2023, with permission from Elsevier.

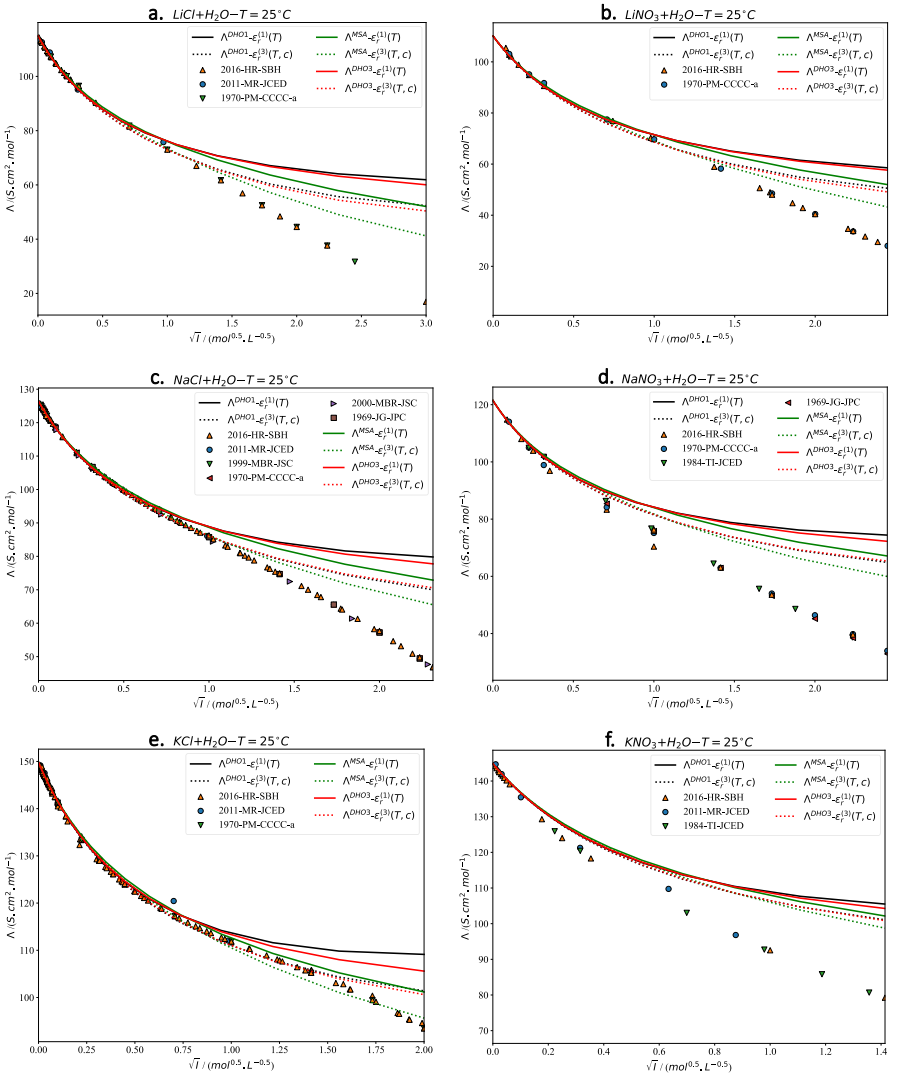

Figure 3.13. The predictions of DHO1, DHO3, and MSA are compared for (a) LiCl, (b) $LiNO_3$, (c) NaCl, (d) $NaNO_3$, (e) KCl, and (f) KNO_3 aqueous solutions at 298.15 K using RSP models 1 and 3. Acronyms follow those established in Figure 3.10. Reprinted from ref. [124], Copyright 2023, with permission from Elsevier.

hensive DHO approach, such as the DHO3 model highlighted in this chapter, allows precise predictions of electrical conductivity even at higher concentrations (up to 1 $mol \cdot L^{-1}$) for specific 1:1 electrolyte solutions.

3.6.3.3 Effect of Viscosity

Grüneisen [170] empirically noted that the reduced viscosity (η^*) of the electrolyte solutions exhibits a linear increase with the square root of concentration (Eq. 3.43). The elevation of η^* as the salt concentration increases has been attributed to ion-ion interactions by Falkenhagen et al. [171] and Onsager and Fuoss [83]. Independently, both parties derived the coefficient A using the DH theory in a methodology parallel to that used for equivalent conductivity.

$$\eta^* = \frac{\eta\,(T, c)}{\eta_0\,(T)} = 1 + Ac^{0.5} \tag{3.43}$$

Up to a concentration of 0.01 $mol \cdot L^{-1}$, Eq. 3.43 holds true. In 1929, Jones and Dole [172] suggested an empirical enhancement to the limiting law by introducing a Bc term (Eq. 3.44). Within this equation, the factor B is related to ion-solvent interactions. It assumes a positive value for structure-making ions and a negative one for structure-breaking ions [173].

$$\frac{\eta\,(T,\ c)}{\eta_0\,(T)} = 1 + Ac^{0.5} + Bc \tag{3.44}$$

In contrast to the conductance process, efforts to expand the limiting law of viscosity through the consideration of electrostatic ion-ion interactions did not yield successful results [92]. Therefore, it is inferred that the coefficient B is more related to ion-solvent interactions than ion-ion ones [173]. Furthering this, Ibuki and Nakahara [173] formulated a model to estimate the B coefficient using the Hubbard-Onsager dielectric friction theory [174–176]. Their predictions for the B values have been shown to align reasonably well with values derived from the experimental data.

Moreover, it is crucial to highlight that the foundational theories for both viscosity and electrical conductivity center around alterations in properties in relation to a reference system. For viscosity, this reference is the solvent, whereas for the electrical conductivity, it is the solution at infinite dilution. The ionic conductivity when at infinite dilution (λ_i^0) originates from ion mobilities in the development of electrical conductivity models, marking its position as the electrical conductivity reference system. In this context, the interactions between ions and solvents, without any other ion interference, are assessed. Therefore, in the electrical conductivity models, unlike the viscosity models, ion-solvent interactions have been, to some degree, implicitly taken into account.

From the existing literature, it is evident that there is a linkage between the theories governing electrical conductance and the viscous flow of electrolyte solutions. Yet, delving into this connection theoretically proves challenging given the intricacies of the theories involved. Instead of a direct theoretical exploration, one can assess the impact of concentration-dependent viscosity on the predictions of electrical conductivity models by contrasting them with experimental data.

Wishaw and Stokes [177] introduced an empirical adjustment to the Falkenhagen-Leist-Kelbg [101] equation by incorporating the relative viscosity ($\frac{\eta_0}{\eta}$) into the equivalent conductivity. They applied this model to the aqueous NH_4Cl solution at 298.15 K and found that it aligned well with the experimental findings. They opted for a solvated distance of the closest approach (4.35 Å) over the crystallographic distance of the closest approach (3.29 Å) in their computations. In a similar vein, Campbell and Kartzmark [178] utilized the Wishaw and Stokes [177] equation for a range of 1:1 aqueous nitrate solutions. Their results

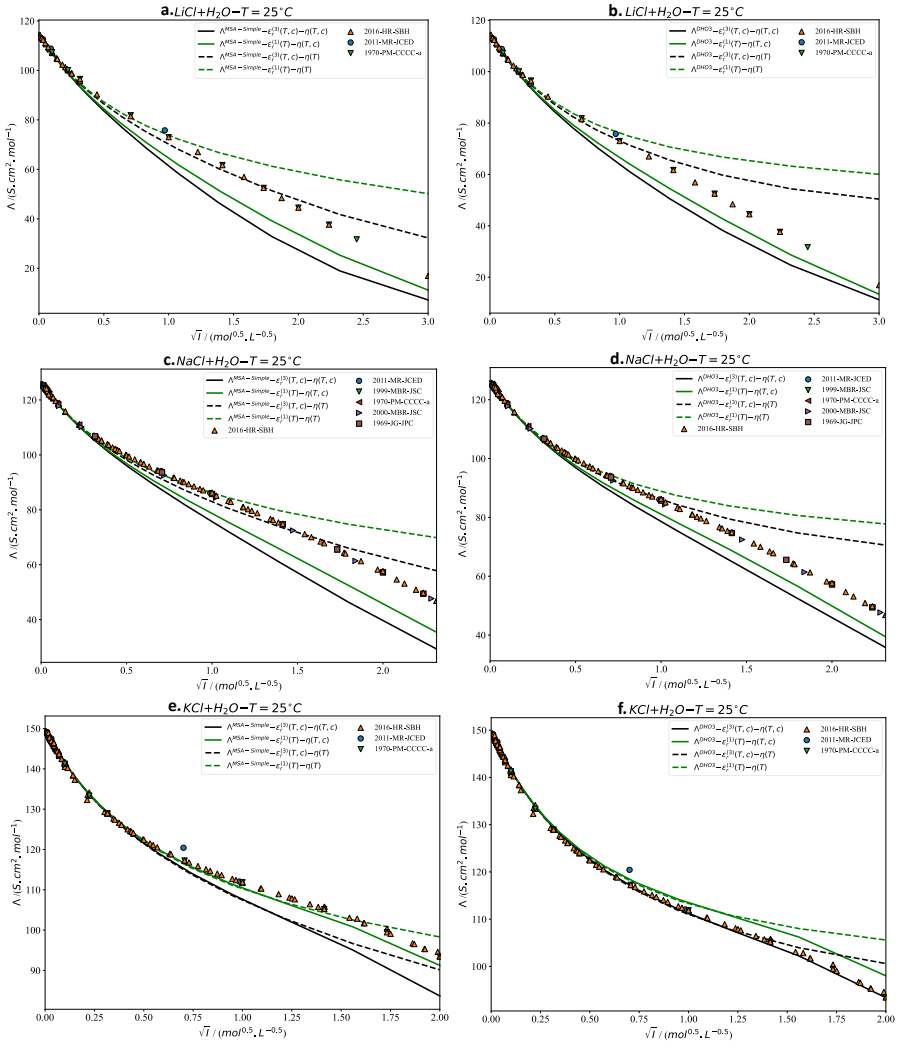

Figure 3.14. The influence of concentration-dependent viscosity and RSP on the predictions of the MSA-Simple and DHO3 models for LiCl, NaCl, and KCl in aqueous solutions at 298.15 K is examined. Acronyms adhere to those used in Figure 3.10. Reprinted from ref. [124], Copyright 2023, with permission from Elsevier.

exhibited an acceptable match with the experimental data. However, much like Wishaw and Stokes' approach [177], they also relied on the solvated distance of the closest approach for their calculations.

Monica et al. [179–181] further refined the equation of Wishaw and Stokes [177] by accounting for the solution's viscosity in the electrophoretic term. They investigated the electrical conductivity of several 1:1 aqueous solutions and noted a relatively accurate alignment between their theoretical predictions and their experimental results. However, during their research, they fine-tuned distance of the closest approach based on the experimental data for electrical conductivity. Similarly, Islam and co-authors [182] amended the Falkenhagen-Leist-Kelbg equation [90] to factor in a concentration-dependent RSP and viscosity. They incorporated the influence of this concentration-dependent viscosity on both the electrophoretic term and the ionic conductivity at infinite dilution. Their predictions for the electrical conductivity of aqueous solutions of LiCl, NaCl, NaBr, NaI, and KF demonstrated satisfactory agreement with the experimental results, although by making adjustments to distance of the closest approach.

In the this section, the influence of incorporating both concentration-dependent viscosity and RSP on the electrical conductivity predictions is examined. It should be highlighted that a concentration-dependent viscosity was integrated into both the relaxation and electrophoretic terms of the electrical conductivity models. Additionally, the impact of $\eta(T, c)$ on the ionic conductivity at infinite dilution (λ_i^0) was addressed by employing Waldens rule, wherein $\lambda_i^0 \eta$ is maintained as a constant.

Figures 3.14, D.7, and D.8 depict the molar conductivity of salt-water systems at 298.15 K using various methods. As observed in these figures, an increase in the viscosity of the solution with salt concentration (such as the NaCl-water system in Figure D.4) results in a reduced predicted electrical conductivity when the solution viscosity is employed, as opposed to using the viscosity of the solvent. On the contrary, for salts such as KNO_3, where the viscosity versus salt concentration curve exhibits a minimum, the utilization of the solution's viscosity leads to an elevated predicted electrical conductivity compared to when the solvent's viscosity is used.

3.7 Summary and Conclusions

This chapter provided a thorough and organized examination of the most recent advancements in modeling the electrical conductivity of electrolyte solutions.

Six electrical conductivity models from the existing literature, along with three novel models introduced in this chapter, were rigorously evaluated by comparing their predictions with the experimental data.

The summary of this analysis is as follows.

1. **DHOLL Model**:
    - Represents the limiting law of the electrical conductivity.
    - Effective mainly for predicting the slope of Λ against $\sqrt{c}$ in infinitely dilute solutions.
    - Lacks a size parameter.
    - Not recommended for electrical conductivity calculations at even low-concentration systems.
2. **DHOEE Model**:
    - An enhanced version of the DHOLL model that accounts for ion sizes.
    - Yields reliable results without generating nonphysical predictions.

- Given more precise DHO-based models, its use is not typically recommended.

3. **DHOSiS Model**:
   - Aims to expand DHO-based models to address size asymmetry.
   - Accurate for low-concentration solutions but exhibits unreliability in moderate concentrations.
4. **QV Model**:
   - Designed for multi-salt solutions while considering higher order effects.
   - Its accuracy does not stand out when compared to simpler models like DHOEE.
5. **DHO1 Model**:
   - Integrates the FO relaxation effect with the DHOEE electrostatic effect.
   - Competes in precision with the MSA-Simple and MSA models for 1:1 electrolyte solutions, but falls slightly short of the DHO3 model.
6. **DHO2 Model**:
   - Essentially the DHOEE model without truncating the exponential term.
   - Does not offer any significant accuracy advantage over the DHOEE model.
7. **DHO3 Model**:
   - Combines the Falkenhagen group's relaxation term with the DHOEE electrostatic term.
   - Exhibits impressive accuracy, on par with the MSA and MSA-Simple models.
   - This is the best version of the DHO theory in this chapter.
   - Stands out as the finest iteration of the DHO theory discussed in this chapter and has been chosen for subsequent discussions.
8. **MSA Model**:
   - The most complicated model designed for the electrical conductivity of electrolyte solutions.
   - Extremely accurate, particularly when ion-ion associations can be confidently excluded.
   - Its mathematical structure is more convoluted compared to other models.
   - Its multi-component extension has been further explored in the literature.
   - Chosen for further exploration in this research.
9. **MSA-Simple Model**:
   - A streamlined version of the MSA model that employs an average ionic diameter and omits higher order terms on relaxation and electrophoretic effects.
   - Offers accuracy close to the original MSA model in many scenarios.
   - Its widespread use in the literature for analyzing electrical conductivity data solidifies its relevance.
   - Also selected for continued exploration in this work.

Extension of models using concentration-dependent RSP and viscosity:

- Incorporating a concentration-dependent RSP slightly refines the predictions of electrical conductivity models.
- Incorporating both a concentration-dependent viscosity and RSP can sometimes enhance, but at other times deteriorate, the predictions of the electrical conductivity models.

Chapter Message

There is a clear need to evolve new models grounded in the DHO theory that accurately account for the size asymmetry of ions and are versatile enough to be expanded to multi-salt systems. Based on the evaluations presented in this chapter, the MSA, MSA-Simple and DHO3 models stand out and have been chosen for more in-depth exploration in subsequent chapters.

CHAPTER 4

New Model for the Electrical Conductivity of Electrolyte Solutions; Single-Salt Systems

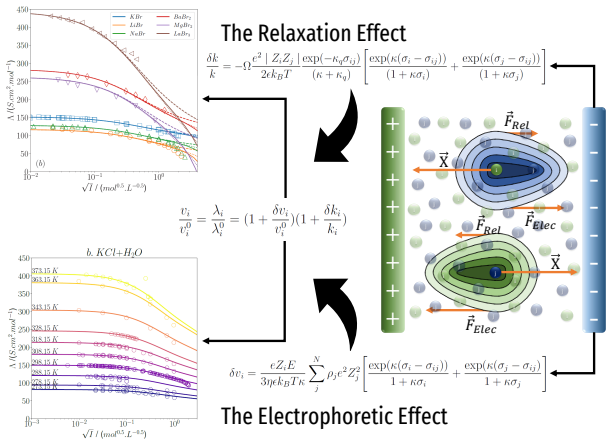

In Chapter 3, a comprehensive and systematic evaluation of different models from the literature, designed for predicting the electrical conductivity of electrolyte solutions, was carried out. From this assessment, three standout models were identified for deeper exploration: namely, the MSA model as introduced by Bernard et al. [111], the MSA-Simple model as introduced by Chhih et al. [113], and the DHO3 model as proposed by Naseri Boroujeni et al. [124].

In this chapter, a new electrical conductivity model based on the DHO theory is introduced. The goal is to address the existing gap in electrical conductivity models derived from the DHO theory that consider the size asymmetry of ions. Through this effort, not only the predictive capability of these models is enhanced, but a more comprehensive understanding of the behavior of electrolyte solutions is also provided.

In Section 2.4, the derivation of a new model for the electrical conductivity of electrolyte solutions was discussed, using the FO continuity equation and the hierarchy suggested by Ebeling et al. [110]. In this chapter, the focus shifts to employing Eq. 2.36 and Eq. 2.57. These equations are integrated with the pair correlation function introduced by Debye and Hückel, and the symmetrical pair correlation function proposed by Outhwaite [183], to develop a novel model.

Part of this chapter has already been published in the Journal of Physical Chemistry B.

- *New Electrical Conductivity Model for Electrolyte Solutions Based on the Debye-Hückel-Onsager Theory* [184] (Link).

4.1 Model Development

In this section, the equilibrium pair correlation functions, which will be utilized in this and the subsequent chapter for the development of a new electrical conductivity model, are introduced. Subsequently, based on the equations highlighted in section 2.3, the relaxation and electrophoretic corrections to the ideal contribution to the electrical conductivity are derived. Lastly, the equations pertaining to the ionic conductivity are provided.

4.1.1 Choice of the Pair Correlation Function

As highlighted in Chapter 2, the pair correlation function (h_{ij}) comprises two parts: the equilibrium (h^0_{ij}) and the non-equilibrium (h^1_{ij}) parts. The perturbed, or non-equilibrium part of the pair correlation function, is determined by solving the FO continuity equation (Eq. 2.55). On the other hand, the definition for the stationary, or equilibrium segment of the pair correlation function must be explicitly provided. In this section, the choice of the equilibrium pair correlation function is examined.

The equilibrium pair correlation function between two ions is described in past literature via methods such as the DH theory, integral equations, and simulation techniques, which include the numerical solution to the Poisson-Boltzmann (PB) equation or Monte Carlo (MC) simulations. Among these methodologies for deriving the equilibrium pair correlation function, only the DH and MSA theories offer an analytical solution, rendering them preferable for this research. Consequently, in this investigation, the pair correlation function deduced from the DH theory is adopted. In the subsequent discussion, the RDF derived from the DH theory, the MSA theory, the numerical solution of the PB equation, and MC simulations is compared.

Inherently, the equilibrium pair correlation function, denoted by $h^0_{ij}(r)$, is intertwined with the equilibrium RDF and the equilibrium electrical potential, symbolized as $\psi^0_i(r)$. This connection is shown in Eq. 4.1.

$$h^0_{ij}(r) = g^0_{ij}(r) - 1 = \exp\left[(\frac{-eZ_j\psi^0_i(r)}{k_BT})\right] - 1 \simeq -\frac{eZ_j\psi^0_i(r)}{k_BT} \tag{4.1}$$

Debye and Hückel [4] effectively derived a solution from the linearized version of the PB equation. This led to the articulation of the electric potential, presented in Eq. 4.2:

$$\psi^0_i(r) = \frac{eZ_i}{\epsilon}\frac{\exp(\kappa\sigma_i)}{1+\kappa\sigma_i}\frac{\exp(-\kappa r)}{r} \tag{4.2}$$

In the mentioned equation, the expression $\kappa = \sqrt{\frac{4\pi e^2}{\epsilon k_B T}\sum_j \rho_j Z_j^2}$ is referred to as the inverse Debye length. By utilizing equations 4.1 and 4.2, the pair correlation function stemming from the DH theory can be determined, proving pivotal for the derivation of relaxation and electrophoretic effects. This correlation is demonstrated in Eq. 4.3:

$$rh^0_{ij}(r) \simeq -\frac{e^2Z_iZ_j}{\epsilon k_BT}\frac{\exp(\kappa\sigma_i)}{1+\kappa\sigma_i}\exp(-\kappa r) \tag{4.3}$$

Upon examining Eq. 4.3, it is evident that the equilibrium pair correlation function deduced from the DH theory is not symmetrical (as indicated in Eq. 4.4), revealing a discrepancy. Nonetheless, as highlighted by Outhwaite [183], the noted asymmetry arises from the inherent nature of the PB equation and is not a byproduct of the linearization technique utilized by Debye and Hückel.

$$rh_{ij}^{0}(r) \neq rh_{ji}^{0}(r) \tag{4.4}$$

To address this discrepancy, two potential solutions are suggested. The initial solution advocates for averaging the ion sizes, which results in a RPM. On the other hand, Outhwaite [183] suggests averaging the RDFs to ensure symmetry in the equilibrium pair correlation function. Given the aim of this research to formulate a model that takes into account the size asymmetry of ions, the first approach is seemed less suitable. Thus, the latter method is employed, which not only considers ion size asymmetry in the model but also effectively amends the inconsistency observed in the DH pair correlation function.

The pair correlation function, symmetrized by taking the average of the RDF ($g_{ij}(r) = h_{ij}(r) + 1$) between ion i and ion j as recommended by Outhwaite [183], is illustrated in Eq. 4.5:

$$g_{ij}^{0}(r) = g_{ji}^{0}(r) = H(r - \sigma_{ij}) \exp\left[- \frac{eZ_i\psi_j^{0}(r) + eZ_j\psi_i^{0}(r)}{2k_BT} \right] \tag{4.5}$$

In this expression, $H(r - \sigma_{ij})$ denotes the Heaviside step function. Using this expression, the pair correlation function can be formulated as shown in Eq. 4.6:

$$rh_{ij}^{0}(r) = rh_{ji}^{0}(r) = -\frac{e^2 Z_i Z_j}{2\epsilon k_B T} \left[\frac{\exp(\kappa(\sigma_i - r))}{1 + \kappa\sigma_i} + \frac{\exp(\kappa(\sigma_j - r))}{1 + \kappa\sigma_j} \right] \tag{4.6}$$

The RPM version of the DH pair correlation function, which is used to derive the electrophoretic and relaxation effects in the RPM formulation of this electrical conductivity model, is expressed as:

$$rh_{ij}^{0}(r) = rh_{ji}^{0}(r) = -\frac{e^2 Z_i Z_j}{\epsilon k_B T} \frac{\exp(\kappa\sigma_{ij})}{1 + \kappa\sigma_{ij}} \exp(-\kappa r) \tag{4.7}$$

In the given equation, $\sigma_{ij} = 0.5(\sigma_i + \sigma_j)$ denotes distance of the closest approach between ions.

Before moving forward with equations for the electrophoretic and relaxation effects, it is crucial to evaluate the accuracy of the equilibrium pair correlation functions. Initially, the equilibrium RDF ($g_{+-}^{0} = 1 + h_{ij}^{0}$) is compared with both the MSA theory and the MC simulations, as documented by Ambramo et al. [185]. Afterwards, the equilibrium RDFs at contact referenced in this research (specifically, DH (Eq. 4.1) and SDH (Eq. 4.5)) are compared with the numerical solution of the symmetrical PB equation according to Outhwaite [183], as well as the MSA theory and MC simulations outlined by Ambramo et al. [185].

Figure 4.1 displays the equilibrium RDF as determined by the DH theory (as referenced in Eq. 4.1) and the SDH approach (as mentioned in Eq. 4.5). These results are compared with the MSA theory and the MC simulations sourced from prior studies [185]. By analyzing Figure 4.1b, it is evident that at low salt concentrations ($c = 0.1\, mol \cdot L^{-1}$), there is a slight deviation in RDFs from DH, SDH, and MSA. Yet, these differ significantly from the MC simulations.

As depicted in Figure 4.1a, with higher salt concentrations ($c = 1.0\, mol \cdot L^{-1}$), a clear difference emerges between g_{+-}^{SDH}, g_{+-}^{DH}, and g_{-+}^{DH}. This distinction is further validated by Table 4.1 showcasing the equilibrium RDFs at contact. The table emphasizes that with increasing salt concentration, or when the ratio of ionic diameters diminishes, the gap between the DH and SDH RDFs widens.

Table 4.1 presents the contact equilibrium RDF obtained from the MSA theory, MC simulations, and numerical solutions of the symmetrical PB equation. From the data presented,

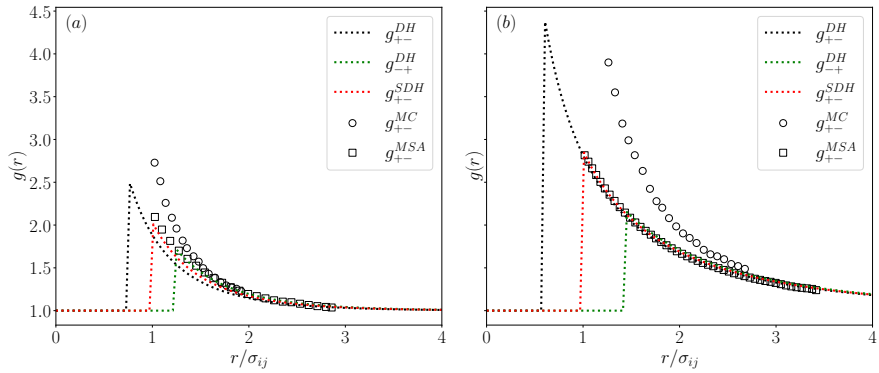

Figure 4.1. The RDFs derived from various approaches, including the DH theory (g_{+-}^{DH} and g_{-+}^{DH}), the symmetrical DH theory (g_{+-}^{SDH}), the MSA theory (g_{+-}^{MSA}), and MC simulations (g_{+-}^{MC}), are presented for 1:1 aqueous solutions. The conditions examined are: (a) $c = 1.0\, mol \cdot L^{-1}$ and size ratio $\varsigma = \sigma_-/\sigma_+ = 0.6$, and (b) $c = 0.1\, mol \cdot L^{-1}$ and size ratio $\varsigma = \sigma_-/\sigma_+ = 0.4$. Data for the MSA and MC simulations are taken from [185]. Reprinted with permission from ref. [184]. Copyright 2023 American Chemical Society.

Table 4.1. The equilibrium RDF derived from the DH theory (Eq. 4.1), compared with the SDH model (Eq. 4.5), is assessed alongside the numerical solution of the symmetrical PB equation [183], MC simulations [185], and the MSA theory [185] with a focus on the parameter $\varsigma = \sigma_-/\sigma_+$.

$c\,(mol \cdot L^{-1})$	ς	g_{+-}^{SPB}	g_{+-}^{MC}	g_{+-}^{MSA}	g_{+-}^{SDH}	g_{+-}^{DH}	g_{-+}^{DH}
0.100	0.8	3.82	3.80	2.37	2.357	2.340	2.373
0.100	0.6	4.73	4.85	2.58	2.579	2.543	2.614
0.100	0.4	6.23	6.20	2.86	2.870	2.814	2.927
0.425	0.8	2.79	2.95	2.12	2.046	2.004	2.088
0.425	0.6	3.35	3.55	2.30	2.246	2.152	2.339
0.425	0.4	4.26	4.50	2.54	2.519	2.363	2.674
1.000	0.8	2.29	2.50	2.00	1.846	1.782	1.911
1.000	0.6	2.67	2.90	2.13	2.029	1.882	2.177
1.000	0.4	3.29	3.45	2.33	2.289	2.034	2.544
1.968	0.8	1.96	2.40	1.96	1.696	1.610	1.781
1.968	0.6	2.23	2.65	2.05	1.867	1.667	2.066
1.968	0.4	2.66	3.00	2.19	2.122	1.765	2.478
1.968	0.1	4.06	4.65	2.59	2.800	2.083	3.516

it is evident that the analytical equilibrium RDFs - encompassing DH, SDH, and MSA - deviate from the outcomes of both the MC simulations and the numerical solution to the symmetrical PB equation.

On the other hand, the contact equilibrium RDFs of SDH and MSA exhibit significant similarities. In certain instances, g_{+-}^{SDH} matches more closely with the equilibrium RDF from the MC simulations and the numerical solutions of the symmetrical PB equation. In other instances, the equilibrium RDF from MSA is a better fit. From this comparison, it remains uncertain which equilibrium RDF holds a distinct edge over the others.

From this comparison, we determined three key insights. Firstly, at low salt concentrations or when the ratio of anion to cation diameter nears unity, the distinction between DH and SDH RDFs is insignificant. Secondly, the proximity of the MSA theory equilibrium RDF to simulations relative to the DH and SDH RDFs remains ambiguous. Thirdly, all analytical RDFs, encompassing DH, SDH, and MSA, showed significant deviations when compared to the MC simulations and the numerical solution to the symmetrical PB equation.

4.1.2 Relaxation Effect

As outlined in section 2.4, the relaxation correction to the ideal contribution of the electrical conductivity can be obtained from Eq. 2.57:

$$\frac{\delta k_i}{k_i} = -\Omega \int_{\sigma_{ij}}^{\infty} r h_{ij}^0(r) \exp\{(-\kappa_q r)\} dr \tag{2.57}$$

$$\Omega = \frac{\kappa_q^2}{3}\left[\frac{\sinh(\kappa_q \sigma_{ij})}{\kappa_q \sigma_{ij}} - \frac{\epsilon k_B T \kappa_q \sigma_{ij}^2}{e^2 Z_i Z_j}\left(\frac{\cosh(\kappa_q \sigma_{ij})}{\kappa_q \sigma_{ij}} - \frac{\sinh(\kappa_q \sigma_{ij})}{\kappa_q^2 \sigma_{ij}^2}\right)\right] \tag{2.58}$$

$$\kappa_q^2 = \frac{4\pi}{\epsilon k_B T} \frac{\rho_i e Z_i \omega_i + \rho_j e Z_j \omega_j}{\omega_i + \omega_j} \tag{2.60}$$

As illustrated in Eq. 2.57, the relaxation effect, represented as $\delta k_i/k_i$, is determined by evaluating the integral on the equation's right-hand side. This integration necessitates the equilibrium pair correlation function (h_{ij}^0). In our analysis, we employ three distinct pair correlation functions, previously discussed. These include the DH pair correlation function (as per Eq. 4.3), the Symmetrical Debye-Hückel (SDH) pair correlation function (from Eq. 4.5), and the Restricted Debye-Hückel (RDH) pair correlation function (outlined in Eq. 4.7).

By substituting $r h_{ij}^0(r)$ from equations 4.3, 4.5, and 4.7 into Eq. 2.57 and evaluating the integral, we can express the relaxation correction to the force exerted on the i-ion near the j-ion as equations 4.8, 4.9, and 4.10, respectively.

$$\frac{\delta k_i}{k_i} = -\Omega \frac{e^2 \mid Z_i Z_j \mid}{\epsilon k_B T} \frac{\exp\{(\kappa(\sigma_i - \sigma_{ij}))\} \exp\{(-\kappa_q \sigma_{ij})\}}{(\kappa + \kappa_q)(1 + \kappa \sigma_i)} \tag{4.8}$$

$$\frac{\delta k_i}{k_i} = \frac{\delta k_j}{k_j} = \frac{\delta k}{k} = -\Omega \frac{e^2 \mid Z_i Z_j \mid}{2\epsilon k_B T} \frac{\exp(-\kappa_q \sigma_{ij})}{(\kappa + \kappa_q)} \left[\frac{\exp(\kappa(\sigma_i - \sigma_{ij}))}{(1 + \kappa \sigma_i)} + \frac{\exp(\kappa(\sigma_j - \sigma_{ij}))}{(1 + \kappa \sigma_j)}\right] \tag{4.9}$$

$$\frac{\delta k_i}{k_i} = \frac{\delta k_j}{k_j} = \frac{\delta k}{k} = -\Omega \frac{e^2 \mid Z_i Z_j \mid}{\epsilon k_B T} \frac{\exp(-\kappa_q \sigma_{ij})}{(\kappa + \kappa_q)(1 + \kappa \sigma_{ij})} \tag{4.10}$$

4.1.3 Electrophoretic Effect

Similar to the relaxation effect, three different equations are employed to characterize the electrophoretic effect, using the DH, SDH, and RDH equilibrium pair correlation functions. For the derivation of equations accounting for the corrections due to hydrodynamic or electrophoretic effects on the ideal contribution to electrical conductivity, Eq. 2.36 is referenced. As detailed in section 2.4, this equation offers insights into the adjustments made to ion velocities because of hydrodynamic interactions.

$$\delta v_i = \frac{2}{3\eta} \sum_{j=1}^{C} \rho_j e Z_j E \int_0^\infty r h_{ij}^0(r) dr \tag{2.36}$$

By substituting $r h_{ij}^0(r)$ from Eq. 4.3 into Eq. 2.36 and evaluating the integral, Eq. 4.11 is obtained.

$$\delta v_i = -\frac{2}{3\eta} \frac{e Z_i E}{\epsilon k_B T} \frac{\sum_{j=1}^{C} \rho_j e^2 Z_j^2}{\kappa(1+\kappa\sigma_i)} = -\frac{e Z_i E}{6\pi\eta} \frac{\kappa}{(1+\kappa\sigma_i)} \tag{4.11}$$

Eq. 4.11 represents the modification in ion velocity attributable to electrophoretic effects when employing the DH equilibrium pair correlation function. By substituting from Eq. 4.5 into Eq. 2.36 and performing the integration, the velocity correction using the SDH equilibrium pair correlation function is achieved, as shown in Eq. 4.12.

$$\delta v_i = \frac{e Z_i E}{3\eta\epsilon k_B T \kappa} \sum_{j=1}^{C} \rho_j e^2 Z_j^2 \left[\frac{\exp(\kappa(\sigma_i - \sigma_{ij}))}{1+\kappa\sigma_i} + \frac{\exp(\kappa(\sigma_j - \sigma_{ij}))}{1+\kappa\sigma_j} \right] \tag{4.12}$$

Lastly, by incorporating the RDH equilibrium pair correlation function into the assessment of electrophoretic effects, a correction to the ion velocity can be determined. This is achieved by substituting Eq. 4.7 into Eq. 2.36. When integrated, this yields Eq. 4.13, as shown by Robinson and Stokes [90].

$$\delta v_i = -\frac{e Z_i E}{6\pi\eta} \frac{\kappa}{(1+\kappa\sigma_{ij})} \tag{4.13}$$

4.1.4 Ionic Conductivity Model

Given that the velocity of the i-ion in the solution is expressed as:

$$v_i = (v_i^0 + \delta v_i)(1 + \frac{\delta k_i}{k_i}) \tag{4.14}$$

The velocity v_i^0 represents the velocity of the i-ion unaffected by the presence of other ions when the system is subjected to an external electric field. In contrast, v_i denotes the velocity of the i-ion within the solution. The velocity of the i-ion without any interference from other ions (under the infinite dilution limit) can be correlated with the ionic absolute mobility (ω_i), the diffusion coefficient at infinite dilution (D_i^0), and the ionic conductivity at infinite dilution (λ_i^0), as follows:

$$v_i^0 = Z_i e \omega_i E = \frac{e Z_i D_i^0}{k_B T} E = \frac{e Z_i N_A \lambda_i^0}{F^2 |Z_i|} E \tag{4.15}$$

The proportion between the velocity of ions and their velocity at infinite dilution can be equated to the ratio of the ionic conductivity to its value at infinite dilution. Thus, by integrating equations 4.14 and 4.15, we obtain:

$$\frac{v_i}{v_i^0} = \frac{\lambda_i}{\lambda_i^0} = (1 + \frac{\delta v_i}{v_i^0})(1 + \frac{\delta k_i}{k_i}) \tag{4.16}$$

Integrating the equations for the relaxation and electrophoretic effects with Eq. 4.16 allows us to calculate the electrical conductivity of ions (λ_i). A summary of the equations for the relaxation and electrophoretic effects is provided in Table 4.2. The designated names of the models, which will be referenced later in the chapter, are also indicated.

The equations detailed in Table 4.2 alongside Eq. 4.16 represent the concluding formulations used for predicting the electrical conductivity of electrolyte solutions. In these formulations, values for Ω and κ_q are determined from equations 2.58 and 2.60, respectively. For deriving κ_q, the terms ω_i and ω_j are determined using Eq. 2.13. To estimate the electrical conductivity of a given solution, one needs the RSP ($\epsilon = 4\pi\varepsilon_0\varepsilon_r$) and viscosity ($\eta$) from the solvent(s), the ion's diameter (σ_i), its valence type (Z_i), its ionic conductivity at infinite dilution (λ_i^0), the temperature of the system (T) and salt concentration (c_E), as well as universal constants (N_A, F, e, and k_B).

After determining the ions' conductivity via Eq. 4.16 and the equations presented in Table 4.2, the solution's specific conductivity (χ) can be obtained via Eq. 4.17.

$$\chi = \frac{e^2}{k_B T}\left[\sum_{i=1}^{C} \rho_i D_i^0 Z_i^2 \left(1 + \frac{\delta v_i}{v_i^0}\right)\left(1 + \frac{\delta k_i}{k_i}\right)\right] \tag{4.17}$$

The molar conductivity of the solution (Λ) can be calculated from Eq. 2.7.

4.2 Results

In this section, we evaluate the developed models (Model 1-3 in Table 4.2) against the experimental data reported in the literature. For this evaluation, we compare the predicted

Table 4.2. The relaxation and electrophoretic models developed in this study and their corresponding names used in this work.

Model 1
$\frac{\delta v_i}{v_i^0} = -\zeta \frac{\kappa}{(1+\kappa\sigma_i)}$
$\frac{\delta k_i}{k_i} = -\Omega\theta \frac{\exp\left(\kappa(\sigma_i-\sigma_{ij})\right)\exp\left(-\kappa_q\sigma_{ij}\right)}{(\kappa+\kappa_q)(1+\kappa\sigma_i)}$
Model 2
$\frac{\delta v_i}{v_i^0} = -\zeta \frac{\kappa}{(1+\kappa\sigma_{ij})}$
$\frac{\delta k}{k} = -\Omega\theta \frac{\exp\left(-\kappa_q\sigma_{ij}\right)}{(\kappa+\kappa_q)(1+\kappa\sigma_{ij})}$
Model 3
$\frac{\delta v_i}{v_i^0} = -\frac{\zeta}{2\sum_j^N \rho_j Z_j^2} \sum_{j=1}^{C} \rho_j Z_j^2 \left[\frac{\exp\left(\kappa(\sigma_i-\sigma_{ij})\right)}{1+\kappa\sigma_i} + \frac{\exp\left(\kappa(\sigma_j-\sigma_{ij})\right)}{1+\kappa\sigma_j}\right]$
$\frac{\delta k}{k} = -\Omega\theta \frac{\exp\left(-\kappa_q\sigma_{ij}\right)}{2(\kappa+\kappa_q)} \left[\frac{\exp\left(\kappa(\sigma_i-\sigma_{ij})\right)}{(1+\kappa\sigma_i)} + \frac{\exp\left(\kappa(\sigma_j-\sigma_{ij})\right)}{(1+\kappa\sigma_j)}\right]$
$\zeta = \frac{F^2\lvert Z_i\rvert}{6\pi\eta N_A \lambda_i^0}$
$\theta = \frac{e^2\lvert Z_i Z_j\rvert}{\epsilon k_B T}$

electrical conductivity by Models 1-3 with the experimental data for binary salt-water solutions at temperatures from 273.15-373.15 K. In this evaluation, we do not adjust any parameters to the experimental data. For the ionic diameter, we use the reported crystallographic diameters in the literature by Marcus [155]. The ionic conductivity at infinite dilution has also been used from the reported values in the literature [129, 156]. Table 3.1 presents the ionic diameter and ionic conductivity at infinite dilution at 298.15 K for the ions used in this study.

The RSP and viscosity of the solvent (water in this section) has also been used from the values reported in the literature [157] as shown in Table 3.2.

4.2.1 Evaluation of Models 1-3 at 298.15 K

In this section, the accuracy of our proposed models for predicting the electrical conductivity of electrolyte solutions is assessed by contrasting the model predictions with the experimental data at 298.15 K. The performance of the models (Models 1-3) is examined against the experimental values from over 68 binary aqueous solutions comprising electrolytes of types 1:1, 2:1, 1:2, 2:2, 1:3, 3:1, 2:3, 3:2, 3:3, 1:4, and 2:4. The predictions for electrical conductivity are based on the ionic diameter and the ionic conductivity at infinite dilution, as detailed in Table 3.1. Importantly, no parameters are adjusted to fit the experimental data, meaning all calculations presented are strictly predictive.

From Figure 4.2, it is evident that the proposed models offer a reasonably satisfactory prediction for the molar conductivity of 1:1, 2:1, and 3:1 chloride and bromide aqueous solutions. However, there is noticeable divergence from the experimental data when the ionic strength approaches around 1 $mol \cdot L^{-1}$.

This figure illustrates a good correspondence between the predictions of the models and the experimental data for 1:1, 2:1, and 3:1 chloride and bromide aqueous solutions. Moreover, as the valence type of the cation decreases, the ionic strength threshold where the models' predictions begin to diverge from the experimental data appears to increase.

Unlike graphs (a) and (b) in Figure 4.2, graph (c) highlights the influence of the anion's valence type on the models' predictions. In this figure, all the electrolytes have potassium as the cation, while the anions are nitrate, sulfate, ferricyanide, and ferrocyanide. It is evident from the graph that the predictions of the models align well with the experimental results.

Additionally, as depicted in Figure 4.2 (d), the developed models efficiently predict the molar conductivity of 1:2 sulfate solutions. Nonetheless, mirroring the trends observed with bromide and chloride aqueous solutions in Figure 4.2 (a) and (b), the models' predictions diverge from the experimental results at elevated ionic strengths, particularly when exceeding 1 $mol \cdot L^{-1}$.

To understand the divergence of model predictions from experimental results at elevated ionic strengths, it is essential to revisit the underlying assumptions of the model. Initially, the models were developed on the notion that ions undergo complete dissociation in solutions. This inherently omits the potential presence and effects of ion pairs. Moreover, the solvent was perceived as a homogenous continuum, characterized by constant RSP and viscosity, thereby neglecting its structure. Furthermore, the strong electrostatic field surrounding the ions, which can lead to ions moving alongside their solvation shells, were overlooked due to our reliance on bare ionic diameters for electrical conductivity predictions.

In addition to the implications of ion pairing, overlooking ion-solvent interactions can also become more pronounced at elevated ionic concentrations. For instance, RSP of the NaCl-H_2O solution at 298.15 K decreases from 78.04 to 39.22 as the ionic strength of the solution rises from 0 to 4 $mol \cdot L^{-1}$. This alteration impacts various parameters, such as the pair correlation function, the electric potential around the central ion, and consequently, the relaxation and electrophoretic terms. Recent studies by us [124] (as discussed in Chapter 3) demonstrated that incorporating a concentration-dependent RSP can enhance the accuracy

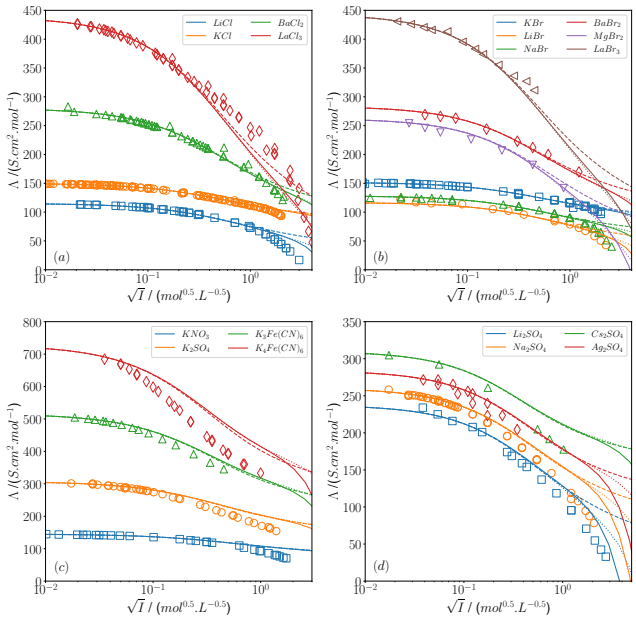

Figure 4.2. The molar conductivity (Λ) for various aqueous solutions at 298.15 K is plotted against the square root of ionic strength ($\sqrt{I}$). Specifically, we consider: (a) Solutions of LiCl, KCl, $BaCl_2$, and $LaCl_3$, (b) Solutions of LiBr, NaBr, KBr, $BaBr_2$, $MgBr_2$, and $LaBr_3$, (c) Solutions of KNO_3, K_2SO_4, $K_3Fe(CN)_6$, and $K_4Fe(CN)_6$, (d) Solutions of Li_2SO_4, Na_2SO_4, Cs_2SO_4, and Ag_2SO_4. In the plots, dotted lines represent results from Model 1, dashed lines showcase outcomes from Model 2, solid lines illustrate predictions by Model 3, while symbols indicate experimental data [129, 131, 132, 134, 141, 148, 149, 160, 166, 186]). Reprinted with permission from ref. [184]. Copyright 2023 American Chemical Society.

of electrical conductivity models at higher ionic strengths. Furthermore, they revealed that the influence of utilizing a concentration-dependent RSP becomes less pronounced for 1:1 electrolyte solutions when the ionic strength is below roughly 1 $mol \cdot L^{-1}$.

Additionally, beyond the previously noted insights, Figure 4.2 clearly shows that at lower ionic strengths, the difference in molar conductivity predictions by Models 1-3 is minimal. Yet, as the ionic strength increases, particularly in electrolytes where there is a notable size difference between cations and anions, like in Li_2SO_4, the predictions of Models 1-3 begin to diverge. A more detailed analysis of this phenomenon will be provided in Section 4.3.

4.2.2 Effect of Temperature

In this section, the focus is on assessing the accuracy of Model 3 across a range of temperatures. Model 3 was chosen for this evaluation because, unlike Model 1, it has a consistent

equilibrium pair correlation function and, in contrast to Model 2, it accounts for size dissimilarity between cations and anions. As highlighted in the previous section, there is not a significant discrepancy in the predictions of models 1-3. Hence, by concentrating solely on one model in this section, we can present the results in a more streamlined fashion.

Prior to exploring the predictions made by the model, it is vital to highlight the parameters within the model that are influenced by temperature. In Model 3, as outlined in Table 4.2, the ionic conductivity at infinite dilution, solvent viscosity, and solvent RSP are identified as parameters that vary with temperature. Furthermore, the system's temperature is explicitly incorporated into the equations, establishing it as a crucial component of the entire model.

As the temperature rises, the RSP and viscosity of the solvent typically decrease, while the ionic conductivity (or ionic mobility) tends to increase. For this investigation, we have referred to experimental measurements of water viscosity and RSP available in the literature, as detailed in Table 3.2.

The Walden's rule provides a general association between the ionic conductivity at infinite dilution and the viscosity of the solvent(s), formulated as $\lambda_i^0 \eta = constant$. Yet, as highlighted by Robinson and Stokes [90], the product of ionic conductivity and solvent viscosity does not consistently remain constant. A more precise empirical relationship is given by Smolyakov's equation [127], which links the natural logarithm of the Walden's product to a linear function of the inverse temperature: $\ln\left(\lambda_i^0 \eta\right) = A + B/T$. In our work, we either employ the ionic conductivity at infinite dilution values as reported in the literature [129] or we utilize Smolyakov's equation to calculate the temperature dependence of λ_i^0, as dictated by Table 4.3.

Figure 4.3a exhibit the performance of Model 3 in predicting the molar conductivity of aqueous sodium chloride solutions across a temperature range of 273.15-323.15 K. Within the figure, the solid lines represent the model's predictions, while the data points correspond to experimental measurements from the literature. Different colors are utilized to denote varying system temperatures. It is evident that Model 3 offers precise predictions for the molar conductivity of NaCl-H_2O solutions across the investigated temperature spectrum. This underscores the model's capability to account for temperature variations in electrical conductivity without necessitating any parameter adjustments to fit experimental data.

Figure 4.3b depicts the molar conductivity of aqueous potassium chloride solutions spanning temperatures from 273.15-373.15 K. Within this figure, the lines signify predictions derived from Model 3 (as referenced in Table 4.2), while the points indicate experimental data. Evidently, Model 3 efficiently predicts the molar conductivity of potassium chloride solutions, even at elevated temperatures, without the necessity to adjust any parameters to fit experimental data. It is worth highlighting that while the model's predictions closely align with experimental data for the majority of the temperature range, some divergence is evident at higher ionic strengths and elevated temperatures. Specifically, the model's predictions for 1 molar KCl-H_2O solutions closely match experimental data up to about 60 °C. Beyond this temperature, a minor discrepancy between the model's predictions and the

Table 4.3. The coefficients of the Smolyakov's equation (experimental data are from ref. [129, 130, 156]). Reprinted with permission from ref. [184]. Copyright 2023 American Chemical Society.

Ions	A	B
Na^+	-3.33	65.88
K^+	-3.49	231.57
Ba^+	-3.01	47.72
Cl^-	-3.41	216.57
$(SO_4)^{2-}$	-3.39	210.89

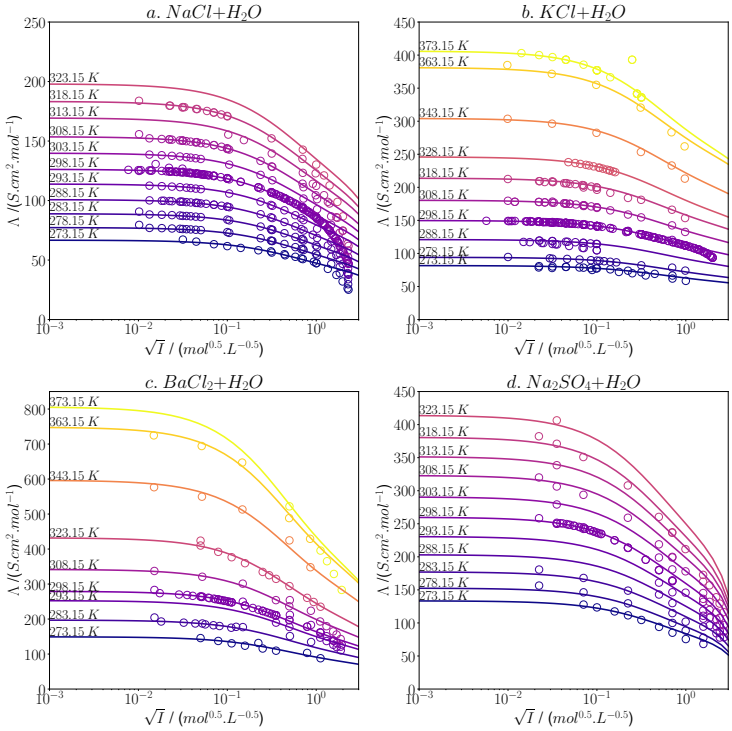

Figure 4.3. The molar conductivity (Λ) for aqueous solutions of (a) NaCl, (b) KCl, (c) $BaCl_2$, and (d) Na_2SO_4 is presented over a temperature range of 273.15 to 373.15 K. In these graphs, the lines represent Model 3 predictions, while the data points correspond to the experimental data [129,131,132,134,141,148,149,166,186]). Reprinted with permission from ref. [184]. Copyright 2023 American Chemical Society.

experimental data.

Figures 4.3c and d present the predictions of Model 3 for $BaCl_2$ and Na_2SO_4 aqueous solutions at temperatures range 273.15-373.15 K (it should be noted that there is only one experimental data point available for the Na_2SO_4 aqueous solution at 323.15 K). Similar to Figure 4.3a and b, the model predictions are in acceptable agreement with the experimental data at various temperatures. But, this agreement is less satisfactory compared to KCl and NaCl aqueous solutions.

4.3 Discussion

In section 4.2, the performance of the developed models (Models 1-3) was evaluated by contrasting their predictions against the experimental data. This examination was primarily focused on aqueous electrolyte solutions. Through our analysis, it was revealed that the molar conductivity of these mixtures, especially when the ionic strength is below 1 $mol \cdot L^{-1}$ and the ionic charges are relatively low, can be accurately predicted by the formulated models.

In this section, a thorough analysis of the predictions of the developed models is conducted. We compare the predictions from our models with those reported in existing literature, both qualitatively and quantitatively. To gain a more comprehensive understanding of the models' capabilities, we also compare ionic properties, such as the transference number, in addition to the solution properties.

4.3.1 Comparison With Other Models from the Literature

Figure 4.4 displays the predictions of Models 1-3 (detailed in Table 4.2) for four less commonly examined systems in the literature: $Na_4Fe(CN)_6$, $K_4Fe(CN)_6$, $Ca_3(Fe(CN)_6)_2$, and $LaFe(CN)_6$ aqueous solutions at 298.15 K. Within this figure, the predictions from the newly developed models (Models 1-3) are compared against the MSA [111], MSA-Simple [113], and DHO3 [124] models from existing literature (those that have been selected for further investigation in Chapter 3), as well as against the experimental data. Additionally, parameters listed in Table 3.1 serve as the foundation for predicting the molar conductivity across all models.

In the Appendix, Figures D.11 through D.17 further compare the models formulated in this research with those from existing literature. It is pertinent to mention that the models selected for this comparison are among the most reliable ones from the literature, recognized for their accuracy across a wide spectrum of salt concentrations and temperatures. Models that demonstrated less precision, as identified in Chapter 3, have been excluded from this comparative analysis due to previously raised concerns regarding their unreliability and precision.

As shown in Figure 4.4a and b, the predictions of Models 1-3 developed in this research, alongside the MSA-Simple model, are more accurate than those of the MSA and DHO3 models. On the other hand, for the $Ca_3(Fe(CN)_6)_2$ and $LaFe(CN)_6$ aqueous solutions, all models tend to overestimate the molar conductivity, as demonstrated in Figure 4.4c and d. From Figure D.11, it becomes clear that for 1:1 aqueous solutions, especially when the sizes of the cation and anion are closely matched, the molar conductivity predictions of all models converge closely.

From Figures D.12 and D.13, it is evident that Models 1-3, in conjunction with the MSA, MSA-Simple, and DHO3 models, provide a reasonably accurate prediction for the molar conductivity of earth metal chlorides and bromides (such as Ba, Mg, and Ca). In contrast, a significant divergence from the experimental data is observed for transition metal solutions like Cd and Co chlorides, bromides, and iodides. This deviation can probably be attributed to the tendency of these metals to form ion complexes.

As observed in Figure D.16, all models consistently over-predict the molar conductivity for 2:2 sulfates. Given that the ions in these salts are recognized for their ion pair formation tendencies, it offers a credible reason for the deviation of all models from the experimental results. A more detailed examination of this phenomenon will be provided in Chapters 8 and 9.

Figure 4.5 illustrates the electrophoretic and relaxation effects for salt-water solutions as predicted by Models 1-3, compared with those of the MSA model [111], the MSA-Simple model [113], and the DHO3 model [124]. These effects correspond to the molar conductivities showcased in Figure 4.4.

From the qualitative analysis conducted, it becomes apparent that the models based on the DHO theory, as formulated in this chapter, yield comparable, if not superior, results to those grounded in the MSA theory. When observing Figures 4.4 and D.11-D.17, it is clear that our formulated models (Models 1-3) align with or even exceed the predictive capabilities of the MSA and MSA-Simple models. Such observations challenge earlier claims suggesting that a DHO-based model is predominantly applicable for salt concentrations

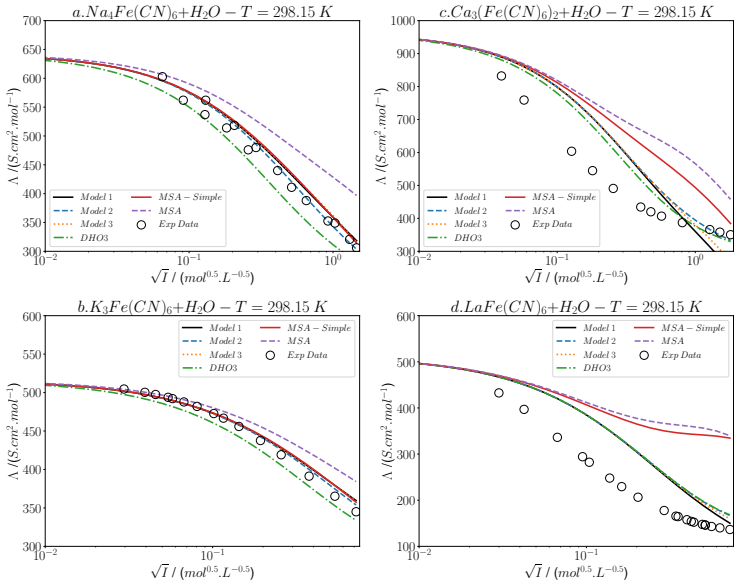

Figure 4.4. The molar conductivity predictions at 298.15 K for (a) $Na_4Fe(CN)_6$, (b) $K_4Fe(CN)_6$, (c) $Ca_3(Fe(CN)_6)_2$, and (d) $LaFe(CN)_6$ aqueous solutions by Models 1-3 are compared with those from the MSA model [111], the MSA-Simple model [113], and the DHO3 model [124]. Additionally, experimental data from the literature [129] are presented alongside for reference. Reprinted with permission from ref. [184]. Copyright 2023 American Chemical Society.

below 0.1 $mol \cdot L^{-1}$ [84]. Given the debate this raises, a deeper dive through quantitative analysis is essential and will be addressed in the following section.

4.3.2 Evaluation of the Performance of the Developed Models

In section 4.3.1, the potential reasons for the discrepancies between model predictions and experimental data at elevated ionic strengths were examined. Drawing from the underlying assumptions of the model, it was concluded that the model's evaluation is most pertinent for scenarios where the ionic strength is approximately less than 1 $mol \cdot L^{-1}$. Consequently, this section is dedicated to the assessment of the developed models under conditions where the ionic strength is below this threshold, aligning more closely with the model's foundational assumptions.

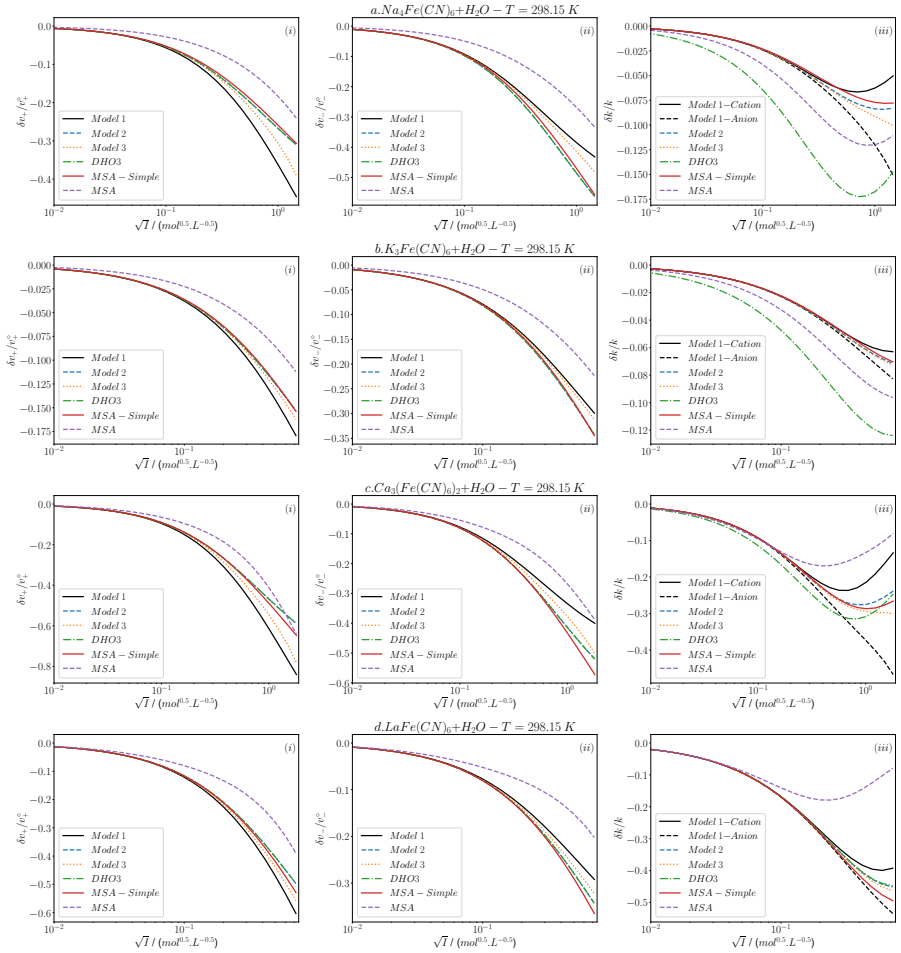

Figure 4.5. The predictions for the electrophoretic effects shown in graphs (i) and (ii), as well as the relaxation effect depicted in graph (iii), for (a) $Na_4Fe(CN)_6$, (b) $K_4Fe(CN)_6$, (c) $Ca_3(Fe(CN)_6)_2$, and (d) $LaFe(CN)_6$ aqueous solutions at 298.15 K by Models 1-3 are compared with those from the MSA model [111], the MSA-Simple model [113], and the DHO3 model [124]. Reprinted with permission from ref. [184]. Copyright 2023 American Chemical Society.

Table 4.4. The percentage of relative absolute average deviation (AARD%) for the predicted electrical conductivity by the models presented in this study (specifically, Models 1-3 as listed in Table 4.2), as well as the MSA [111], MSA-Simple [113], and DHO3 [124] models, is evaluated. This evaluation covers a range of aqueous electrolyte solutions with the following stoichiometries: 1:1, 2:1, 3:1, 1:2, 2:2, 3:2, 1:3, 1:4, and 2:4 at a temperature of 298.15 K. The experimental data for this analysis have been sourced from the subsequent references [129–132, 134, 141, 149, 160, 186]). Reprinted with permission from ref. [184]. Copyright 2023 American Chemical Society.

Salt	AARD%						N_d
	Model 1	Model 2	Model 3	MSA	MSA-Simple	DHO3	
$AgNO_3$	2.28	2.32	2.29	2.39	2.19	2.37	12
CsCl	0.61	0.61	0.61	0.57	0.66	0.58	11
HCl	0.39	0.39	0.37	0.39	0.39	0.39	78
KBr	0.38	0.36	0.37	0.41	0.60	0.30	39
KCl	0.26	0.27	0.26	0.40	0.26	0.32	141
KI	1.13	1.03	1.11	1.23	1.54	0.81	13
KNO_3	3.44	3.45	3.44	3.61	3.26	3.54	24
LiBr	2.59	2.05	2.38	2.01	2.21	2.05	10
LiCl	0.53	0.56	0.51	0.47	0.42	0.59	39
$LiClO_4$	1.26	0.74	1.12	0.81	0.92	0.68	14
$LiNO_3$	0.78	0.90	0.72	0.88	0.61	0.94	15
NaBr	1.12	1.05	1.05	0.84	1.10	1.08	20
NaCl	0.40	0.47	0.42	0.59	0.31	0.51	120
$NaClO_4$	1.26	1.59	1.33	1.52	1.31	1.69	22
NaI	0.78	0.61	0.72	0.58	0.74	0.56	50
$NaNO_3$	4.75	5.12	4.89	5.55	4.57	5.31	20
NH_4Cl	1.43	1.43	1.43	1.50	1.27	1.51	19
RbCl	0.99	0.99	0.99	0.99	0.91	1.03	8
$BaBr_2$	1.26	1.12	1.24	1.07	1.13	1.26	7
$BaCl_2$	1.10	1.02	1.08	1.39	1.28	1.50	47
$Ca(NO_3)_2$	0.85	0.38	0.76	1.38	0.64	1.28	9
$CaBr_2$	3.07	2.76	3.01	2.75	2.81	3.04	7
$CaCl_2$	1.39	1.17	1.35	0.87	1.15	1.22	64
$CdCl_2$	46.81	48.69	47.18	50.44	48.92	50.33	9
CdI_2	112.88	118.91	114.09	119.10	116.51	121.62	9
$Co(NO_3)_2$	4.14	3.58	4.05	2.92	3.45	3.46	6
$CoCl_2$	5.06	4.91	5.02	5.03	5.04	5.36	15
$Cu(NO_3)_2$	3.38	2.73	3.28	2.15	2.57	2.37	6
$CuBr_2$	3.54	2.91	3.44	2.55	2.86	2.39	7
$CuCl_2$	1.60	0.82	1.47	0.55	0.55	0.53	6
$Mg(ClO_4)_2$	7.98	5.46	7.57	6.08	6.40	4.47	15
$Mg(NO_3)_2$	5.24	4.46	5.11	3.88	4.24	3.96	25
$MgBr_2$	2.48	3.77	2.73	4.16	3.71	4.61	7
$MgCl_2$	2.14	1.53	2.02	1.15	1.46	1.22	33
$Mn(NO_3)_2$	9.29	10.03	9.40	10.91	10.41	11.05	6
$MnCl_2$	2.84	2.87	2.84	3.09	3.02	3.41	24
$Ni(NO_3)_2$	5.07	4.37	4.95	3.78	4.20	3.89	6
$NiCl_2$	2.92	2.72	2.88	2.57	2.72	2.74	15
$Sr(NO_3)_2$	1.81	2.08	1.84	3.03	2.48	2.79	7
$SrBr_2$	1.75	1.53	1.71	1.53	1.59	1.78	6
$Zn(NO_3)_2$	5.48	4.46	5.29	3.85	4.41	4.05	11
$Al(NO_3)_3$	7.99	5.75	7.62	4.08	4.68	5.18	7
$AlBr_3$	11.25	8.06	10.70	6.32	7.27	6.68	10

Table 4.4. (Continued.)

Salt	AARD%						N_d
	Model 1	Model 2	Model 3	MSA	MSA-Simple	DHO3	
$La(NO_3)_3$	9.01	7.50	8.80	6.79	6.19	6.51	6
$LaBr_3$	1.80	1.55	1.78	0.93	1.31	1.44	12
$LaCl_3$	3.31	2.70	3.22	1.34	2.13	2.40	41
Ag_2SO_4	2.40	2.29	2.41	3.50	2.53	2.06	12
H_2SO_4	9.97	9.84	9.84	10.16	10.20	8.83	11
K_2SO_4	2.72	2.55	2.72	4.10	2.73	1.53	32
Li_2SO_4	2.39	2.22	2.66	5.90	3.19	2.08	10
Na_2SO_4	1.59	1.40	1.66	3.64	1.83	0.98	40
$CdSO_4$	39.02	41.67	40.18	55.72	51.00	41.89	17
$CoSO_4$	20.85	23.61	22.09	34.89	31.47	23.74	27
$CuSO_4$	29.21	31.74	30.27	43.86	40.29	31.87	32
$FeSO_4$	28.75	31.92	30.07	43.32	39.89	32.10	15
$MgSO_4$	15.48	17.04	16.14	24.70	22.45	17.11	51
$MnSO_4$	30.75	33.74	32.04	47.56	43.24	33.93	26
$NiSO_4$	21.63	24.66	22.96	36.27	32.91	24.79	27
$ZnSO_4$	21.84	23.95	22.74	33.47	30.63	24.06	29
$La_2(SO_4)_3$	175.14	179.67	176.53	238.75	232.14	188.17	15
K_3FeCN_6	2.33	1.98	2.35	4.66	2.39	1.09	15
$Ca_3(Fe(CN)_6)_2$	19.19	20.33	20.18	39.60	32.51	15.42	9
$LaFeCN_6$	30.46	33.63	32.30	98.29	91.75	33.87	20
H_4FeCN_6	41.33	39.84	40.82	43.37	42.14	30.53	6
K_4FeCN_6	9.21	7.71	9.26	15.72	8.84	2.87	20
Na_4FeCN_6	3.41	1.98	3.64	10.68	3.78	5.72	12
Ca_2FeCN_6	172.10	175.92	175.65	230.94	203.70	155.90	10
Mg_2FeCN_6	67.70	68.57	69.33	104.81	89.38	50.69	6
Average	15.25	15.56	15.50	20.77	19.05	14.91	

*The value provided below the name of the models represent their corresponding AARD%
*In electrolytes that have been underlined, the ionic strength is less than 1 $mol \cdot L^{-1}$

Table 4.4 presents the relative average deviation (expressed in percentage) as given by Eq. 4.18. This deviation corresponds to the predictions made by models formulated in this study, as well as the MSA [111], MSA-Simple [113], and DHO3 [124] models which have been previously established in the literature. The evaluations consider aqueous electrolyte solutions with stoichiometries of 1:1, 2:1, 3:1, 1:2, 2:2, 3:2, 1:4, and 2:4, all observed at 298.15 K.

In the table, the predictions of molar conductivity from the models are compared to experimental data from 70 different binary salt-water solutions. The number of data points and the highest ionic strength for each solution are also included for clarity. Most of the solutions have a maximum ionic strength of 1 $mol \cdot L^{-1}$. However, some electrolytes have a lower maximum ionic strength, which is either due to solubility restrictions or the lack of experimental observations.

$$AARD\% = \frac{1}{N_d} \sum_{s=1}^{N_d} \left(\frac{\mid \Lambda_s^{exp} - \Lambda_s^{pre} \mid}{\Lambda_s^{exp}} \right) \times 100 \tag{4.18}$$

To begin with, Table 4.4 clearly illustrates the discrepancies between each model's predictions and actual experimental values for different electrolyte solutions. It is evident from

Table 4.5. The average of the percentage of relative absolute average deviation (AARD%) for the electrical conductivity predictions from the models presented in this study, namely Models 1-3, as well as the MSA [111], MSA-Simple [113], and DHO3 [124] models, is evaluated. This assessment encompasses a variety of aqueous electrolyte solutions with stoichiometries of 1:1, 2:1, 3:1, 1:2, 2:2, 3:2, 1:3, 1:4, and 2:4, all at 298.15 K and with an ionic strength less than or equal to 1 $mol \cdot L^{-1}$. The experimental data utilized for this analysis are sourced from the subsequent references [129–132, 134, 141, 149, 160, 186]). Reprinted with permission from ref. [184]. Copyright 2023 American Chemical Society.

Type	$\overline{AARD\%}$					
	Model 1	Model 2	Model 3	MSA	MSA-Simple	DHO3
+1:-1	1.5	1.4	1.4	1.4	1.3	1.4
+2:-1	14.7	14.7	14.7	14.7	14.5	14.9
+3:-1	5.8	4.6	5.7	3.7	4.1	4.1
+1:-2	5.5	5.3	5.5	7.2	5.6	4.3
+2:-2	25.9	28.5	27.1	40.0	36.5	28.7
+1:-3	2.3	2.0	2.4	4.7	2.4	1.1
+2:-3	19.2	20.3	20.2	39.6	32.5	15.4
+3:-3	30.5	33.6	32.3	98.3	91.8	33.9
+1:-4	18.0	16.5	17.9	23.3	18.3	13.0
+2:-4	119.9	122.2	122.5	167.9	146.5	103.3

this data that no single model consistently outperforms others across all electrolyte categories. Notably, 1:1 chlorides, bromides, perchlorates, and iodides generally display a lower AARD% across all models compared to other electrolytes. To illustrate, while the AARD% for NaCl remains below 1% for all models, the same metric exceeds 4.5% for $NaNO_3$. This suggests that a model's accuracy is intimately linked to the specific ions present in the solution. Additionally, the models' performance varies significantly based on the electrolyte's valence; 1:1 electrolytes tend to have AARD% values that are lower than those of 2:1 and other high valence electrolytes.

The accuracy of each model is apparent when examined in the context of specific electrolyte solutions. As demonstrated in Table 4.4, the AARD% for 1:1 chlorides, bromides (with the exception of LiBr), perchlorates, and iodides, as well as lithium nitrate aqueous solutions at 298.15 K, registers below 2 percent across all models, inclusive of those from the literature. This indicates an acceptable alignment with experimental data for these specific electrolytes. Notably, the difference in AARD% between Models 1 and 2 for these solutions is marginal. Given the inherent uncertainties in experimental data, minor variations, particularly those manifesting in the first or second decimals of the AARD%, do not necessarily signify a model's superior accuracy or lack thereof.

For aqueous solutions of sodium and potassium nitrate, the agreement between model predictions and experimental data is not as close as seen for most 1:1 electrolyte solutions. The higher AARD% for $NaNO_3$ and KNO_3 solutions might be due to ion pairing in these systems, as suggested in existing literature [187].

From Table 4.4, it is evident that the AARD% for 2:1 aqueous solutions is greater than that for 1:1 electrolyte solutions. Particularly, the model predictions for cadmium chloride and iodide solutions exhibit significant errors, amounting to 46% and 113%, respectively. For these solutions, the effects go beyond just strong ion pairing; there is also documentation of ion triplets and higher aggregate formations [127, 188]. Except for $CdCl_2$ and CdI_2, the model-predicted molar conductivities generally align satisfactorily with experimental data. Furthermore, for a majority of the 2:1 electrolytes, Models 1 and 2 tend to outperform the

other models in terms of AARD%.

In evaluating the AARD% of the models introduced in this study against the MSA model for 3:1 electrolytes, the MSA model tends to align more closely with the experimental data. Conversely, for 1:2 sulfates, 1:3 ferricyanides, and 1:4 ferrocyanides, this study's models, along with the DHO3 model, demonstrate better accuracy than both the MSA and MSA-Simple models. Notably, for 2:2 sulfates, where ion pairing is important [189–194], there is a considerable divergence between model predictions and experimental data. When examining 2:3 and 2:4 electrolyte solutions, none of the models offer precise predictions.

Table 4.4 is indeed information-dense, making direct interpretation challenging. To streamline understanding, it is more practical to consider the models' performance via the average AARD% specific to each electrolyte category rather than individual electrolytes. In Table 4.5, we have compiled the mean AARD% for distinct electrolyte types. Here, both our study's models and those from the literature are grouped according to the valence characteristics of their cations and anions.

From Table 4.5, it is evident that the predictions from the models we developed are least accurate for 2:2, 3:3, and 2:4 aqueous solutions. Conversely, these models demonstrate their highest accuracy for 1:1, 3:1, 1:2, and 1:3 electrolyte aqueous solutions.

Additionally, when comparing the performance of our newly developed models with those from existing literature, we see that our models align with the accuracy of the MSA, MSA-Simple, and DHO3 models. This insight is significant, considering the distinct theoretical differences between these models. The MSA and MSA-Simple models utilize the MSA pair correlation function for stationary contributions to the correlation function, and the MSA model does not overlook the higher order contributions (T_1 and T_2) to the FO continuity equation. On the other hand, the DHO3 model's relaxation effect adopts the Eigen-Wicke [101, 102] equation, diverging from the Boltzmann distribution function. This comparison not only highlights the adaptability of various modeling approaches but also challenges the commonly held belief that the MSA theory offers a more precise depiction of the physics inherent in electrolyte solutions.

It is worth noting that models such as Model 1-3, DHO3, and MSA-Simple, which truncate the higher-order terms in the continuity equation (T1 and T2 as per Eq. 22 in ref. [111]), exhibit a level of accuracy similar to the MSA model, which includes these terms. This suggests that excluding these terms does not significantly impact predictions related to molar conductivity. This aligns with a previous observation by Bernard et al. [111], who pointed out that the second and hydrodynamic contributions arising from T1 and T2 are relatively minor compared to the first-order term. Figure 4.6 further supports this statement, demonstrating that higher-order contributions to the relaxation ($\delta k^2/k$ and $\delta k^{Hyd}/k$) and electrophoretic ($\delta v_i^2/v_i^\circ$) effects are much smaller in magnitude compared to their first-order counterparts. Consequently, the decision to truncate these terms when assessing the relaxation effect in this study appears to be well-founded.

4.3.3 Effect of Ionic Properties

The developed electrical conductivity models, as outlined in the equations presented in Table 4.2, are primarily based on three key components: the ionic conductivity at infinite dilution, the relaxation effect, and the electrophoretic effect. The ionic conductivity at infinite dilution reflects the mobility of ions in the absence of other ions and is influenced by ion-solvent interactions, a complex aspect beyond the scope of this study. Typically, this property is determined by extrapolating electrical conductivity data to zero concentration. However, there exist a few models capable of estimating the ionic conductivity (or mobility) at infinite dilution [127, 152, 195].

In this section, an investigation is conducted into the impact of ionic properties, including valence type and diameter, on the relaxation and electrophoretic effects in the conduction

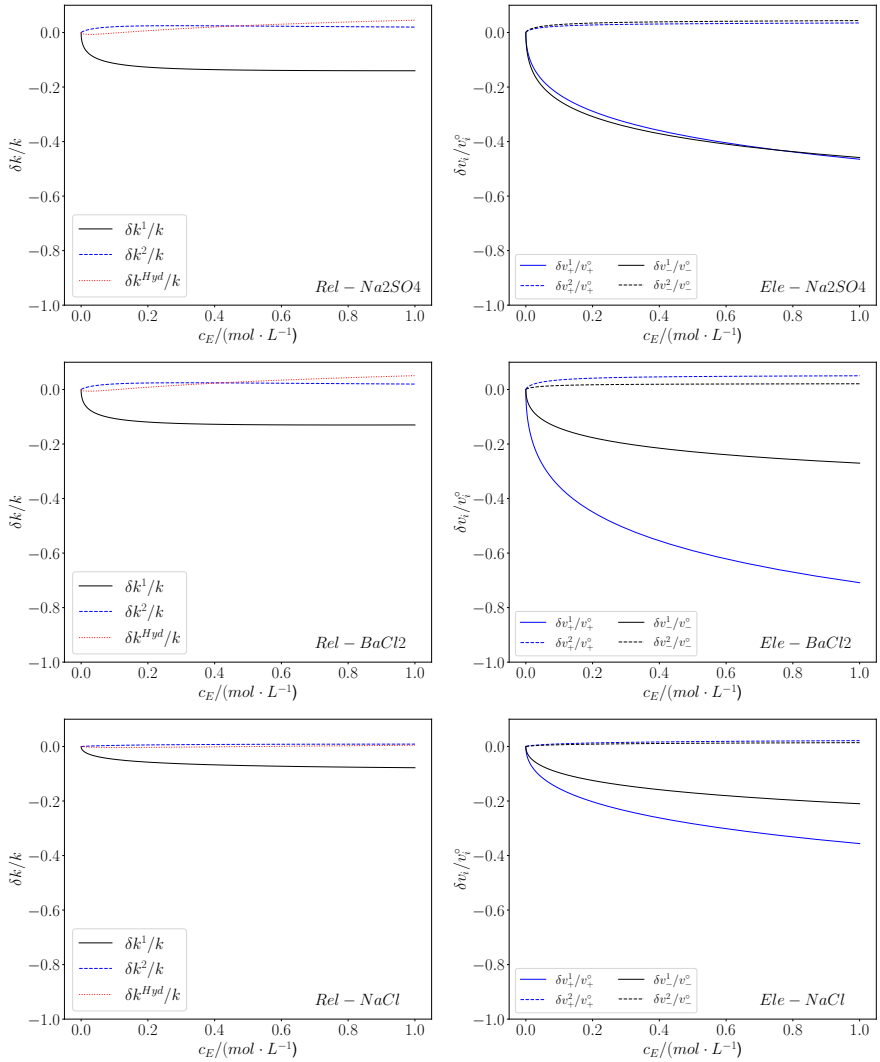

Figure 4.6. The influence of higher order terms on the relaxation and electrophoretic effects from the MSA model. Reprinted with permission from ref. [184]. Copyright 2023 American Chemical Society.

process. To achieve this, nine different electrolyte solutions are selected: NaCl, $BaCl_2$, $LaCl_3$, Li_2SO_4, $MgSO_4$, $La_2(SO_4)_3$, $K_3Fe(CN)_6$, $Ca_3(Fe(CN)_6)_2$, and $LaFe(CN)_6$, all studied at a temperature of 298.15 K.

The ionic conductivity equation allows for the interpretation of two corrections to the ionic conductivity at infinite dilution. This section focuses on the analysis of how ionic properties impact these corrections. Figure 4.7 illustrates these corrections in the context of nine electrolyte solutions, all at a solution ionic strength of one $mol \cdot L^{-1}$ and a system temperature of 298.15 K. The arrangement of electrolytes in this figure is based on their valence type.

The figure illustrates that the electrophoretic effect $(1 + \frac{\delta v_i}{v_i^0})$ plays a dominant role in contributing to the ionic conductivity for cations in all the electrolyte solutions. In contrast, for anions, the difference between the electrophoretic and relaxation contributions is less pronounced, and in some cases, the relaxation effect surpasses the electrophoretic one. Moreover, the relaxation correction tends to be more substantial for cations compared to anions, whereas the electrophoretic correction is generally smaller for cations than for anions.

The electrical conductance process's sensitivity to ionic properties can also be explored through the transference number (t_i), which reveals the individual ions' contributions to electrical conductivity in the solution. The transference number of ions in the solution can be defined as shown in Eq. 4.19. This property is typically experimentally determined using methods such as the moving boundary method, cell measurements, and others [90].

$$t_i = \frac{\lambda_i}{\sum_j (\lambda_j)} \tag{4.19}$$

Figure 4.8 illustrates the transference numbers for aqueous solutions of hydrochloric acid, sodium chloride, potassium chloride, barium chloride, calcium chloride, and lanthanum chloride at 298.15 K as a function of the square root of ionic strength. The solid lines represent Model 3 predictions, while the dotted lines represent MSA model predictions. Experimental data points from the literature are also included for reference.

The change in the transference number of cations with the ionic strength depends on their transference number at infinite dilution (t_+^0). When t_+^0 is around 0.5, as seen in KCl

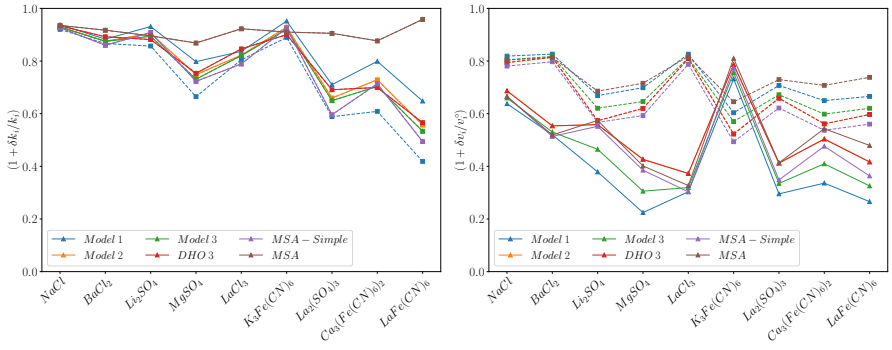

Figure 4.7. The contributions to the ionic conductivity have been predicted by Model 1-3, MSA, MSA-Simple, and DHO3 models for aqueous solutions of NaCl, $BaCl_2$, $LaCl_3$, Li_2SO_4, $MgSO_4$, La_2SO_4, $K_3Fe(CN)_6$, $Ca_3(Fe(CN)_6)_2$, and $LaFe(CN)_6$ at a temperature of 298.15 K and an ionic strength of 1 $mol \cdot L^{-1}$. Reprinted with permission from ref. [184]. Copyright 2023 American Chemical Society.

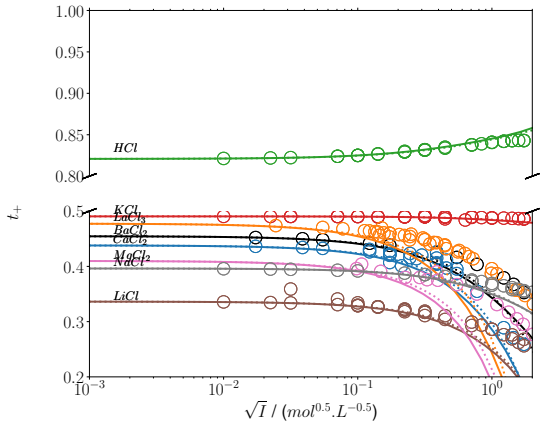

Figure 4.8. The transference numbers of the cation (t_+) for aqueous solutions of hydrochloric acid (HCl), lithium chloride (LiCl), sodium chloride (NaCl), potassium chloride (KCl), barium chloride ($BaCl_2$), calcium chloride ($CaCl_2$), magnesium chloride ($MgCl_2$), and lanthanum chloride ($LaCl_3$) at 298.15 K are depicted. The solid lines represent predictions from Model 3, while the dotted lines represent predictions from the MSA model. Experimental data points from the literature [129,196–199] are also included for comparison. Reprinted with permission from ref. [120]. Copyright 2023 American Chemical Society.

aqueous solutions, the transference number remains relatively constant with variations in ionic strength, as illustrated in Figure 4.8. However, when t_+^0 exceeds 0.5, as observed in HCl aqueous solutions, the transference number of the cation increases as the ionic strength rises, as shown in Figure 4.8. Conversely, when the transference number of the cation at infinite dilution is less than 0.5, it decreases with increasing ionic strength, as demonstrated in Figure 4.8 for NaCl.

In addition to the variation in transference numbers with ionic strength, it is important to note that the primary contribution to the electrical conductivity in sodium and potassium chloride solutions comes from the anion. However, in the case of hydrochloric acid, the predominant contribution is from the hydrogen ion, which has a relatively high transference number of around 0.8. Robinson and Stokes [90] have suggested that hydrogen ions (H^+ or H_3O^+) in the solution may be involved in a unique mechanism due to their exceptionally high ionic mobility. They proposed that this unusual behavior could be explained by a phenomenon known as *'proton jump'*, in which protons move from one water molecule to another during the conduction process.

Furthermore, Figure 4.8 illustrates that the predictions made by Model 3 are in reasonable agreement with the experimental measurements. Notably, for aqueous solutions of HCl, NaCl, and KCl, the agreement is particularly better when compared to other solutions.

4.4 Summary and Conclusions

In this chapter, three novel models have been introduced for the calculation of electrical conductivity in unassociated single-salt electrolyte solutions. These models have been based on the DHO theory, which addresses relaxation effects. They have been differentiated by assumptions regarding ion sizes, with two models considering varying ion sizes and the

third assuming identical ion sizes. Electrophoretic effects have been calculated in these models using Stokes' law and the forces acting on the ionic cloud, assuming that the ionic cloud remains undisturbed by external electric fields. The derivation of these models has incorporated three equilibrium RDFs associated with the DH theory.

An evaluation was conducted to assess the accuracy of the equilibrium RDFs by comparing them to MC simulations, numerical solutions to the symmetrical PB equation, and the MSA theory. The findings showed a close agreement with the MSA theory but a deviation from the results of the MC simulations and numerical solutions to the symmetrical PB equation. Among the developed models, Model 3 was chosen as the final model due to its consistent equilibrium RDF and its capability to account for different ion sizes.

A comparative analysis was conducted to assess the accuracy of the developed models in comparison to models from the literature and experimental data. The results demonstrated that the developed models performed well in terms of accuracy, both quantitatively and qualitatively. They showed good agreement with experimental data under specific conditions, although this agreement was not consistent across all systems. In several cases, the models tended to overestimate molar conductivity at higher ionic strengths, and the onset of this deviation varied depending on the specific salt.

Chapter Message

In this chapter, a new model was developed to predict the electrical conductivity of single-salt electrolyte solutions. Its accuracy has been assessed through comparisons with the experimental data and other existing models. This model offers a DHO equivalent to the MSA model for electrical conductivity, providing researchers with a valuable tool for their work.

CHAPTER 5

New Model for the Electrical Conductivity of Electrolyte Solutions; Mixed-Salt Systems

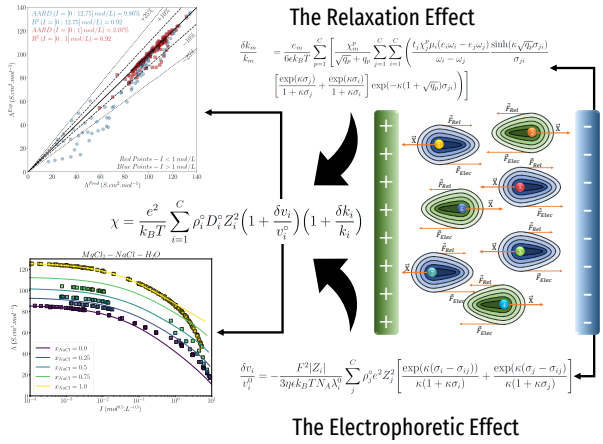

In Chapter 4, a new electrical conductivity model was developed based on Ebeling hierarchy of the Smoluchowski equation, FO continuity equation, and DH theory for a system containing single types of cation and anion. The developed model was extensively assessed by comparing its predictions with the experimental data and with other models developed in the literature. In this chapter, we extend the electrical conductivity model for multi-component systems containing arbitrary types of cations and anions. The content of this chapter has been previously submitted for publication.

- *A Novel Model for Predicting the Electrical Conductivity of Multi-salt Electrolyte Solutions [200].*

5.1 Model Development

In a homogeneous solvent with a constant permittivity ($\epsilon = 4\pi\varepsilon_0\varepsilon_r$) and viscosity ($\eta$), a solution of electrolytes comprising C types of ions, each characterized by unique ionic diameters (σ_i), is examined. It is assumed that all ions are perfectly spherical in shape, and the formation of ion pairs is disregarded. Furthermore, it is assumed that the motion of all ions is considered based on their bare ionic diameter.

In Chapter 2, it is emphasized that the electrical conductivity of electrolyte solutions, as proposed by Debye and Hückel [86], deviates from ideal behavior due to the influences of relaxation and electrophoretic forces. Therefore, as suggested by Onsager and Kim [109]

and subsequently employed by Durand-Vidal et al. [201], van Damme et al. [116], and Roger et al. [117], the calculation of the specific conductivity (χ) of the solution can be carried out using Eq. 2.67.

$$\chi = \frac{e^2}{k_B T} \sum_{i=1}^{C} \rho_i D_i^0 Z_i^2 \left(1 + \frac{\delta v_i}{v_i^0}\right)\left(1 + \frac{\delta k_i}{k_i}\right) \tag{2.67}$$

In Eq. 2.67, C is the representation of the number of types of ions in the solution. ρ_i, D_i^0, and Z_i represent the number density, the diffusion coefficient at infinite dilution, and the valence type of the ion i, respectively. The terms $\delta v_i/v_i^0$ and $\delta k_i/k_i$ indicate the electrophoretic and relaxation corrections for ion i, respectively. Additionally, k_B and T denote the Boltzmann constant and the temperature of the system.

5.1.1 Relaxation Effect

In Chapter 2, the ultimate equation (Eq. 5.1), previously provided by Roger et al. [117] to obtain the relaxation correction of the ionic conductivity, was presented. It has been noted that, akin to single-salt systems, the computation of the relaxation field necessitates only the input of the equilibrium pair correlation function.

$$\begin{aligned}\frac{\delta k_m}{k_m} \quad &= \frac{-\kappa^2 e Z_m}{3} \sum_{p=1}^{C} \zeta_m^p \sum_{j=1}^{C} \sum_{i=1}^{C} \frac{t_j \zeta_j^p \mu_j e (Z_i \omega_i - Z_j \omega_j)}{e^2 Z_i Z_j (\omega_i + \omega_j)} \\ &\frac{\sinh\left(\kappa\sqrt{q_p}\sigma_{ij}\right)}{\kappa\sqrt{q_p}\sigma_{ij}} \left[\int_{\sigma_{ij}}^{\infty} r \exp\left(-\kappa\sqrt{q_p} r\right) h_{ij}^0(r) dr\right]\end{aligned} \tag{5.1}$$

In Eq. 5.1, κ is the inverse Debye length, as defined by Eq. 2.51, where $\epsilon = 4\pi\epsilon_0\epsilon_r$ represents the dielectric constant of the medium. Furthermore, t_j and μ_j stand for the transport number at an infinite dilution (Eq. 2.54) and the relative ionic strength (Eq. 2.52), respectively.

$$\kappa = \sqrt{\frac{4\pi e^2}{\epsilon k_B T} \sum_{j=1}^{C} \rho_j Z_j^2} \tag{2.51}$$

$$t_i = \frac{\mu_i \omega_i}{\bar{\omega}} \tag{2.54}$$

In Eq. 2.54, ω_i and $\bar{\omega}$ represent the individual and average absolute mobility of the ion i, respectively. Individual mobility of an ion can be determined through the ionic conductivity (λ_i^0) and the diffusion coefficient at infinite dilution (D_i^0), as outlined in Eq. 2.13. Likewise, the mean mobility of the ions can be computed utilizing Eq. 2.53.

$$\mu_i = \frac{\rho_i e^2 Z_i}{\sum_{j=1}^{C} \rho_j e^2 Z_j} \tag{2.52}$$

$$\omega_i = \frac{D_i^0}{k_B T} = \frac{N_A \lambda_i^0}{F^2 |Z_i|} \tag{2.13}$$

$$\bar{\omega} = \sum_{j=1}^{C} \mu_j \omega_j \tag{2.53}$$

The values q_p and ζ_i^p represent the eigenvalues and components of the eigenvector obtained in solving the set of differential equations (equations 22-26 in ref. [116]). Expressions for eigenvalues and eigenvectors are provided in equations 2.62 and 2.63, respectively.

$$q_p = \sum_{j=1}^{C} = \frac{\bar{\omega} t_j}{\omega_j + \alpha_p} \tag{2.62}$$

$$\zeta_j^p = \frac{N_p \omega_j}{\omega_j^2 - \delta_p^2} \tag{2.63}$$

The quantity N_p is determined by Eq. 2.64, and δ_p is one of the roots of Eq. 2.65.

$$\frac{1}{N_p^2} = \sum_{j=1}^{C} \frac{t_j \omega_j^2}{(\omega_j^2 - \delta_p^2)^2} \tag{2.64}$$

$$-2\bar{\omega}\alpha \sum_{j=1}^{C} \frac{t_i}{\omega_i^2 - \delta^2} = 0 \tag{2.65}$$

Van Damme et al. [116] suggested, in agreement with Onsager and Kim [109], that the roots of Eq. 5.2 should be arranged in the following order:

$$0 = \delta_1^2 < \omega_1^2 < \delta_2^2 < \omega_2^2 < \cdots < \delta_C^2 < \omega_C^2 \tag{5.2}$$

This particular order facilitates the solution of Eq. 5.2 for δ_p using root bracketing, interval bisection, and inverse quadratic interpolation methods. In this work, the Brent algorithm [202], implemented in the SciPy library, was employed to solve this nonlinear equation.

In Eq. 5.1, σ_{ij} is distance of the closest approach defined by Eq. 2.59. And, the stationary pair correlation function is denoted by h_{ij}^0.

$$\sigma_{ij} = \frac{\sigma_i + \sigma_j}{2} \tag{2.59}$$

To determine the relaxation effect on the ion m, it is necessary to supply the pair correlation function in the stationary state to Eq. 5.1. Following this, the integration process is carried out. In the investigations conducted by van Damme et al. [116] and Roger et al. [117], the pair correlation function from the MSA theory is utilized, as outlined in Eq. 14 of ref. [117].

In this chapter, similar to our earlier exploration of single-salt solutions (Chapter 4), we employ DH theory to calculate the pair correlation function in the stationary state. Eq. 4.5 presents the formula for the pair correlation function and the RDF at the stationary state, derived from the SDH model [184].

$$h_{ij}^0(r) = g_{ij}^0(r) - 1 = H(r - \sigma_{ij}) \exp\left[- \frac{eZ_i\psi_j^0(r) + eZ_j\psi_i^0(r)}{2k_BT} \right] - 1 \tag{5.3}$$

In Eq. 5.3, $H(r - \sigma_{ij})$ denotes the Heaviside step function. Furthermore, the electric potential (ψ_i^0) is determined by solving the linearized PB equation, as proposed by Debye and Hückel [4, 86], represented by Eq. 4.2.

$$\psi_i^0(r) = \frac{eZ_i}{\epsilon} \frac{\exp(\kappa\sigma_i)}{1 + \kappa\sigma_i} \frac{\exp(-\kappa r)}{r} \tag{4.2}$$

Combining equations 5.3 and 4.2, it gives:

$$rh_{ij}^{0}(r) = rh_{ji}^{0}(r) = -\frac{e^2 Z_i Z_j}{2\epsilon k_B T}\left[\frac{\exp(\kappa(\sigma_i - r))}{1+\kappa\sigma_i} + \frac{\exp(\kappa(\sigma_j - r))}{1+\kappa\sigma_j}\right] \tag{4.5}$$

The integral in Eq. 5.1 can be calculated by replacing $rh_{ij}^{0}(r)$ with the expression in Eq. 4.5.

$$\begin{aligned} I \quad &= -\int_{\sigma_{ij}}^{\infty} r\exp\left(-\kappa\sqrt{q_p}\sigma_{ij}\right)h_{ij}^{0}(r)dr \\ &= -\frac{e^2 Z_i Z_j}{2\epsilon k_B T}\left[\frac{\exp(\kappa\sigma_j)}{1+\kappa\sigma_j} + \frac{\exp(\kappa\sigma_i)}{1+\kappa\sigma_i}\right]\frac{\exp\left(-\kappa(1+\sqrt{q_p})\sigma_{ij}\right)}{\kappa(1+\sqrt{q_p})} \end{aligned} \tag{5.4}$$

By inserting Eq. 5.4 into Eq. 5.1, we can calculate the relaxation correction term as shown in Eq. 5.5:

$$\begin{aligned} \frac{\delta k_m}{k_m} \quad = \frac{e_m}{6\epsilon k_B T}\sum_{p=1}^{C}\Bigg[\frac{\chi_m^p}{\sqrt{q_p}+q_p}\sum_{j=1}^{C}\sum_{i=1}^{C}\Bigg(\frac{t_j\chi_j^p\mu_i(e_i\omega_i - e_j\omega_j)}{\omega_i-\omega_j}\frac{\sinh\left(\kappa\sqrt{q_p}\sigma_{ji}\right)}{\sigma_{ji}} \\ \left[\frac{\exp(\kappa\sigma_j)}{1+\kappa\sigma_j} + \frac{\exp(\kappa\sigma_i)}{1+\kappa\sigma_i}\right]\exp\left(-\kappa(1+\sqrt{q_p})\sigma_{ji}\right)\Bigg)\Bigg] \end{aligned} \tag{5.5}$$

5.1.2 Electrophoretic Effect

In Chapter 4, in contrast to the relaxation effect where we assumed the existence of only a single type of cation and anion in the solution for the derivation of the single-salt case, the electrophoretic term is derived for a multi-component mixture of ions. Therefore, the electrophoretic correction to the specific conductivity does not require an extension for mixed electrolytes.

In this section, we present the results of the previously derived electrophoretic term. Eq. 4.12 presents the correction term to the hydrodynamic velocity resulting from electrophoretic forces acting on ion i. Here, E represents the external electric field applied to the solution, and η denotes the viscosity of the solvent(s).

$$\delta v_i = \frac{eZ_i E}{3\eta\epsilon k_B T}\sum_{j=1}^{C}\rho_j e^2 Z_j^2\left[\frac{\exp(\kappa(\sigma_i - \sigma_{ij}))}{\kappa(1+\kappa\sigma_i)} + \frac{\exp(\kappa(\sigma_j - \sigma_{ij}))}{\kappa(1+\kappa\sigma_j)}\right] \tag{4.12}$$

The specific conductivity can be determined by using Eq. 2.67, which requires an electrophoretic correction. This correction is given by Eq. 5.6.

$$\frac{\delta v_i}{v_i^0} = -\frac{F^2|Z_i|}{3\eta\epsilon k_B T N_A \lambda_i^0}\sum_{j=1}^{C}\rho_j e^2 Z_j^2\left[\frac{\exp(\kappa(\sigma_i - \sigma_{ij}))}{\kappa(1+\kappa\sigma_i)} + \frac{\exp(\kappa(\sigma_j - \sigma_{ij}))}{\kappa(1+\kappa\sigma_j)}\right] \tag{5.6}$$

The equation includes the Faraday constant, symbolized by F, and Avogadro's number, denoted by N_A.

5.2 Results

In this section, we evaluate the accuracy of the developed model by comparing its predictions against the experimental data available in the literature. Our assessment focuses on the predicted electrical conductivity, determined through equations 2.67, 5.5, and 5.6, and its alignment with corresponding experimental data for ternary mixed salt-water solutions. The temperature range considered for this comparison ranges from 273.15 to 298.15 K. It is crucial to emphasize that no adjustments are made to the model parameters during this evaluation. The ionic diameter values are extracted from the study by Marcus [155], which provides crystallographic diameters reported in the literature. Furthermore, the ionic conductivity at infinite dilution is sourced from previously reported values [129, 156]. Table 3.1 details the ionic diameter and ionic conductivity at 298.15 K for the ions used in this research. The RSP and viscosity of the solvent are obtained from values previously reported in the literature [84, 157].

The model predictions are compared with the experimental data by contrasting either the specific conductivity (χ) or the molar conductivity (Λ), which is expressed in Eq. 5.7. It should be noted that the definition of the molar conductivity for multi-component systems is different than that of single-salt systems.

$$\Lambda = \frac{\chi}{I} \tag{5.7}$$

The ionic strength of the solution, denoted by I, is given by Eq. 5.8. This equation assumes that all electrolytes are completely dissociated.

$$I = \frac{1}{2}\sum_{i=1}^{C} c_i Z_i^2 \tag{5.8}$$

The molar concentration of the ions in the solution is represented by c_i in Eq. 5.8. Furthermore, the mole fraction of salts in the ternary systems, excluding solvent, is denoted by x_1 and is expressed as:

$$x_1 = \frac{c_{1,+} Z_{1,+}}{c_{1,+} Z_{1,+} + c_{2,+} Z_{2,+}} \tag{5.9}$$

Eq. 5.9 shows the relative molar concentration of cations of salt 1 and salt 2. $c_{1,+}$ and $c_{2,+}$ are the molar concentrations of the cations from salt 1 and salt 2, respectively, and $Z_{1,+}$ and $Z_{2,+}$ are the ion valance types of the cations from salt 1 and 2, respectively.

Figure 5.1 depicts the molar conductivity of three ternary mixed salt-water systems at 298.15 K. In all these systems, the cations are K^+ and Na^+, while the anions for the first, second and third systems are Cl^-, Br^- and I^-, respectively. The lines in Figure 5.1 represent the model predictions for the molar conductivity, utilizing equations 2.67, 5.5, 5.6, and 5.7, while the points correspond to the experimental data. Notably, the concentrations of salt 1 and salt 2 are the same in these systems.

Figure 5.1 offers an opportunity to evaluate the influence of the anion on the performance of the developed model. As shown in the figure, the model effectively predicts the molar conductivity of the solutions in all three systems when the ionic strength is below 1 $mol \cdot L^{-1}$. However, at higher ionic strengths, it becomes apparent that the model tends to overestimate the molar conductivity of the solutions.

Figure 5.2 presents a comparison between the model predictions and experimental data for three solutions of HCl-salt-water systems. In the cases of HCl-NaCl-H_2O and HCl-KCl-H_2O solutions, the hydrochloric acid concentration is kept constant at 0.0978 $mol \cdot L^{-1}$ across varying ionic strengths. Similarly, for HCl-LiCl-H_2O solutions, the concentration of HCl is also consistent at 0.0974 $mol \cdot L^{-1}$.

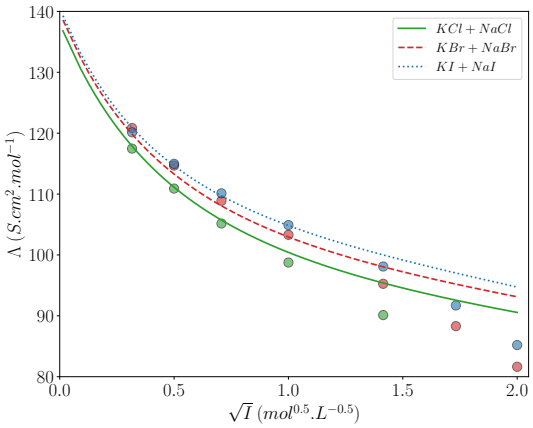

Figure 5.1. This figure presents the molar conductivity (Λ) of KCl-NaCl-H_2O (green lines and points), KBr-NaBr-H_2O (red lines and points), and KI-NaI-H_2O (blue lines and points) solutions at 298.15 K predicted by the new model compared with the experimental measurements reported in the literature [203]. In this figure, lines represent the model predictions while symbols are experimental data. Reprinted with permission from ref. [200]. Copyright 2023 American Chemical Society.

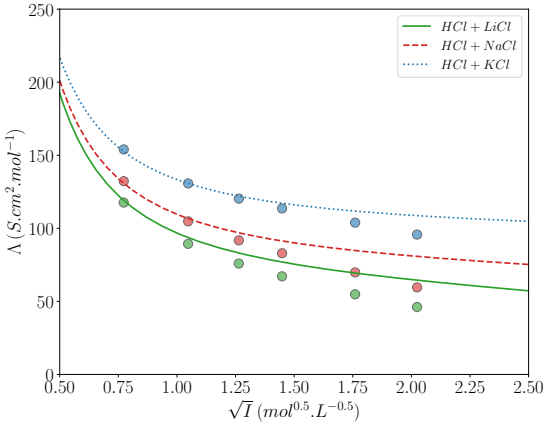

Figure 5.2. The molar conductivity (Λ) of HCl-LiCl-H_2O (green lines and points), HCl-NaCl-H_2O (red lines and points), and HCl-KCl-H_2O (blue lines and points) solutions at 298.15 K predicted by the new model compared with the experimental data reported in the literature [204]. In this figure, lines represent model predictions while symbols are experimental data. Reprinted with permission from ref. [200]. Copyright 2023 American Chemical Society.

Upon comparing the lines representing the predictions of the model with the experimental data points, it becomes evident that the model performs well and accurately predicts the molar conductivity when the ionic strength is below 1 $mol \cdot L^{-1}$. However, as the ionic strength increases, the model predictions start to deviate from the experimental data. Notably, the model tends to overpredict the molar conductivity. This discrepancy suggests that there might be an additional factor or effect missing from the model that accelerates the decrease in molar conductivity with increasing ionic strength. Further investigation is required, as will be presented in the Discussion section, to identify and incorporate this missing factor into the model to enhance its accuracy at higher ionic strengths.

Figure 5.3 illustrates the comparison between theoretical predictions and experimental data for a ternary system of KCl-NaCl-H_2O at 298.15 K. The molar conductivity is plotted against the solvent-free mole fraction of KCl, as defined in Eq. 5.9. The various colors in the figure represent solutions with varying ionic strengths, ranging from 0.1 to 4 $mol \cdot L^{-1}$.

From Figure 5.3, it is apparent that the developed model accurately predicts the molar conductivity of solutions for all values of x_{KCl} when the ionic strength is less than or equal to 1 $mol \cdot L^{-1}$. However, at higher ionic strengths, a significant deviation is observed between the predictions of the model and the experimental data, regardless of the value of x_{KCl}.

Figure 5.4 depicts a different scenario compared to Figures 5.1 to 5.3 in two aspects. Firstly, one of the salts present in the solution is a 2:2 electrolyte, indicating a different ionic charge density. Second, the performance of the model is evaluated at various temperatures, allowing an assessment of its temperature dependence.

Figure 5.4 illustrates the molar conductivity of two aqueous solutions containing NaCl. In the first case, denoted by solid lines and square points, $CaSO_4$ serves as the second salt. In the second case, $MgSO_4$ acts as the second electrolyte, marked by dashed lines and circular points. In particular, in the $MgSO_4$-NaCl-H_2O system, x_{MgSO_4} is 0.0574, while in the $CaSO_4$-NaCl-H_2O system, x_{CaSO_4} is 0.0233.

Observing Figure 5.4, it is evident that the model predictions closely align with the experimental measurements, indicating a good agreement. However, it is crucial to note that

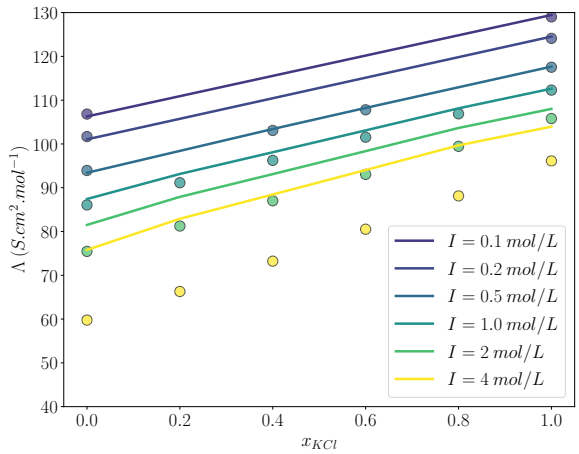

Figure 5.3. This figure presents the molar conductivity (Λ) of KCl-NaCl-H_2O at 298.15 K where x_{KCl} varies from 0 to 1 at various solution's ionic strengths (lines are model predictions and points are experimental data from ref. [203]). Reprinted with permission from ref. [200]. Copyright 2023 American Chemical Society.

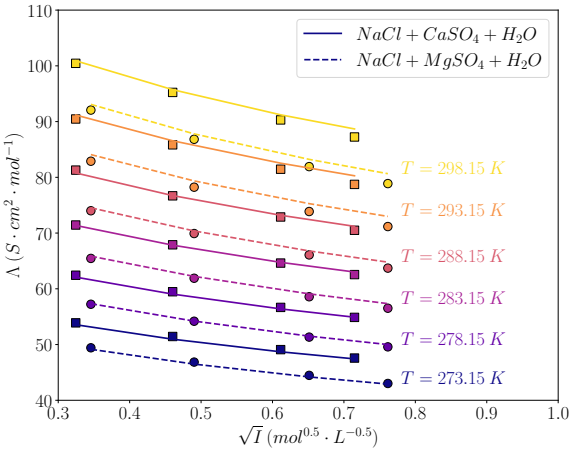

Figure 5.4. This figure presents the molar conductivity (Λ) of $MgSO_4$-NaCl-H_2O (dashed lines and square points), and $CaSO_4$-NaCl-H_2O (solid lines and circle points) solutions at various temperature varies from 0 to 298.15 K (experimental data from reference [205,206]). In this figure, lines represent model predictions while symbols are experimental data. Reprinted with permission from ref. [200]. Copyright 2023 American Chemical Society.

this agreement is observed for ionic strengths below 1 $mol \cdot L^{-1}$ and at low concentrations of the 2:2 sulfate salt. Consequently, the model performance for higher ionic strengths or elevated concentrations of the 2:2 sulfate salt may necessitate further investigation.

In Figure 5.5, the molar conductivity of $MgCl_2$ and $BaCl_2$-NaCl-H_2O solutions at 298.15 K is compared between theory and experiment. The colors represent the solvent-free mole fraction of NaCl, ranging from 0 to 1. The solid lines represent the model predictions, while the points depict the experimental data. It is clear from the figure that the model predictions align closely with the experimental data for both ternary systems up to an ionic strength of 1 $mol \cdot L^{-1}$.

The model exhibits outstanding predictive accuracy for the electrical conductivity of ternary systems involving 3 or 4 ions and a solvent. Although the alignment between theory and experiments has been established for specific systems, it is crucial to evaluate the performance of the model across a broader spectrum of systems. To achieve this, we have assembled an extensive database encompassing measured electrical conductivity data for 24 ternary systems. Table 5.1 offers an overview of this database, including the corresponding references. This compilation helps us in evaluating and validating the accuracy of the model across diverse ternary systems.

Figure 5.6 shows the comparison between the predicted molar conductivity obtained from the developed model and the experimental measurements reported in the literature for all ternary mixed salt-water solutions compiled in Table 5.1. The solid line in Figure 5.6 represents the line of the perfect fit, signifying perfect agreement between the model predictions and the experimental data. The dashed and dotted lines indicate the accuracy of the model with 10% and 25% deviation, respectively, providing a visual evaluation of the performance of the model. It should be noted that the molar conductivity values for solutions with an ionic strength of 1 $mol \cdot L^{-1}$ or less are shown in red, while more concentrated solutions are represented by blue points.

Observing Figure 5.6, it is clear that the majority of the points are closely aligned with

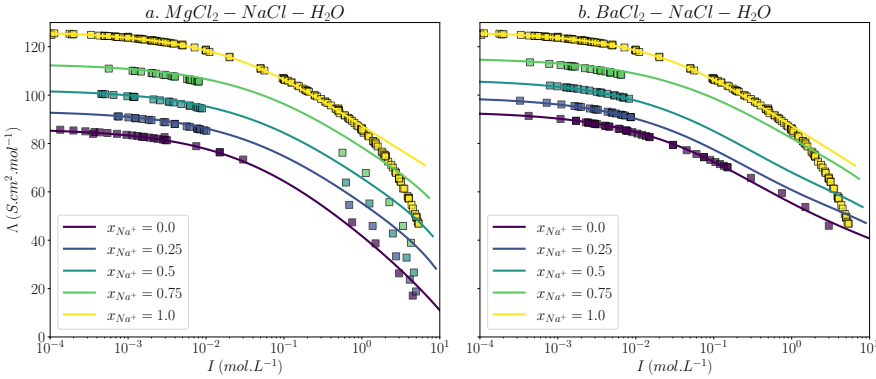

Figure 5.5. This figure presents the molar conductivity (Λ) of (a)$MgCl_2$-NaCl-H_2O and (b)$BaCl_2$-NaCl-H_2O solutions at 298.15 K depicted versus the ionic strength (I) where x_{NaCl} varies from 0 to 1 (experimental data are from reference [148,149,207,208]). In this figure, lines are model predictions while symbols represent experimental data. Reprinted with permission from ref. [200]. Copyright 2023 American Chemical Society.

Table 5.1. This table provides a summary of the database used to evaluate the new model, displaying the maximum ionic strength (I) and the number of data points (N_d) for each mixed salt aqueous solution. (a. Stearn et al. [203], b. Suhrmann et al. [204], c. Rysselberghe et al. [209], d. Bianchi et al. [208, 210], e. Bianchi et al. [207], f. Bremner et al. [206], g. Hammet al. [205]).

System	Max(I) $mol \cdot L^{-1}$	N_d	Ref.	System	Max(I) $mol \cdot L^{-1}$	N_d	Ref.
KCl +NaCl	4	18	a	KI +NaCl	1	3	c
HCl +KCl	4.1	6	b	KNO_3 +NaCl	1	5	c
HCl +LiCl	4.1	6	b	KBr +NaBr	4	21	a
HCl +NaCl	4.1	6	b	NaCl +$NaNO_3$	1	5	c
KI +LiCl	1	3	c	$MgCl_2$ +NaCl	4.95	75	d
KBr +HCl	4.1	6	b	$MgSO_4$ +NaCl	0.58	4	f
HCl +KI	4.10	4	b	$CaSO_4$ +NaCl	0.51	4	g
HCl +$MgCl_2$	6.1	5	b	LiCl +$MgCl_2$	12.75	10	c
KCl +KI	1	3	c	$LiNO_3$ +$NaNO_3$	5	3	c
KCl +KNO_3	1	5	c	$Mg(NO_3)_2$ +$LiNO_3$	4.13	3	c
KCl +NaI	1	3	c	KI +NaI	4	21	q
KCl +$NaNO_3$	1	5	c	$BaCl_2$ +NaCl	0.01	61	e

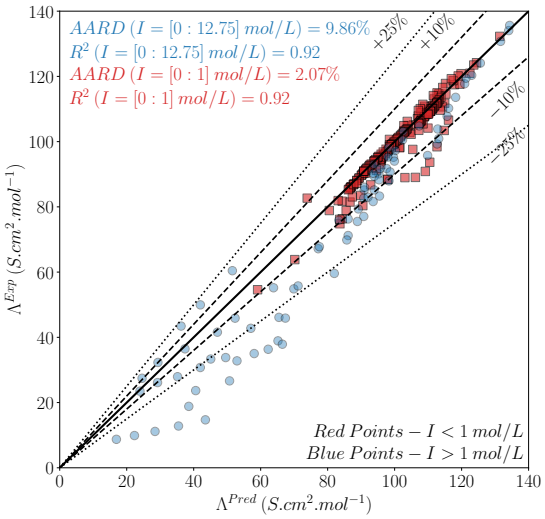

Figure 5.6. This figure presents the predicted vs. observed plot of the molar conductivity of mixed salt-water ternary solutions at 298.15 K (experimental data are from reference [203–209, 211, 212]). Line in this figure is the line of the perfect fit. Reprinted with permission from ref. [200]. Copyright 2023 American Chemical Society.

the line of the perfect fit, signifying acceptable accuracy of the developed model. However, for solutions with an ionic strength greater than 1 $mol \cdot L^{-1}$, the agreement between theory and experiment is not as satisfactory. To quantitatively analyze the performance of the model, two metrics have been considered.

Initially, the absolute average relative deviation (AARD%), as defined in Eq. 4.18, has been computed. For solutions with an ionic strength less than or equal to 1 $mol \cdot L^{-1}$, the AARD% is determined to be 2.1%. This means that on average the model predictions deviate from the experimental data by approximately 2.1%.

$$AARD\% = \frac{100}{N_d} \sum_{i=1}^{N_d} \frac{\mid \Lambda_i^{pre} - \Lambda_i^{exp} \mid}{\Lambda_i^{exp}} \tag{4.18}$$

Second, the coefficient of determination (R^2) has been calculated to evaluate the goodness of fit between the prediction of the model and the experimental data (equations 5.10-5.12). The R^2 values for solutions with an ionic strength less than or equal to 1 $mol \cdot L^{-1}$ are 0.92, indicating a strong correlation between the model predictions and the experimental data.

$$R^2 = 1 - \frac{RSS}{TSS} \tag{5.10}$$

$$RSS = \sum_{i}^{N_d} (\Lambda_i^{exp} - \Lambda_i^{pre})^2 \tag{5.11}$$

$$TSS = \sum_{i}^{N_d} \left(\Lambda_i^{exp} - \bar{\Lambda}^{exp}\right)^2 \tag{5.12}$$

However, when considering all solutions within the range of ionic strength from 0 to 12.75 $mol \cdot L^{-1}$, the AARD% increases to 9.9%, indicating a higher level of deviation between the model predictions and the experimental data. However, the R^2 value remains consistent at 0.92, which indicates a sustained correlation between the predictions of the model and the experimental data.

In summary, the developed model presents satisfactory accuracy for solutions with an ionic strength of 1 $mol \cdot L^{-1}$ or less. However, its performance decreases for more concentrated solutions, as evidenced by the higher AARD% and the reduced agreement with the experimental data.

5.3 Discussion

In the results section, the performance of the newly developed model was assessed by comparing its predictions of molar conductivity or specific conductivity with experimental data for simple electrolyte solutions. From the analysis of Figures 5.1 to 5.6, it is apparent that the newly developed model can accurately predict the electrical conductivity of ternary mixed salt-water solutions when the ionic strength is less than 1 $mol \cdot L^{-1}$. Importantly, this accuracy was achieved without the need to adjust the ionic diameter to match the experimental data, unlike the existing models reported in the literature [116, 117, 201].

Indeed, the observed discrepancy between model predictions and experimental data, particularly in the regime of ionic strengths exceeding 1 $mol \cdot L^{-1}$, is not unique to the developed model. It has also been observed in other models reported in the literature for both single-salt and mixed electrolyte systems [111, 113, 115, 120, 201, 213].

This observation indicates that accurately predicting the molar conductivity at high ionic strengths poses a challenging task, and there may be additional factors or phenomena that are not fully considered in existing models. These unaccounted factors could contribute to accelerating the reduction of molar conductivity as the ionic strength increases. To address this discrepancy and enhance the accuracy of modeling electrolyte solutions, further research and refinement of the models are essential. This involves considering additional factors or phenomena that influence conductivity behavior at high ionic strengths. However, potential sources of error and the corresponding strategies to mitigate deviations from experimental measurements are discussed here.

The difference between the predictions of the model and the experimental data may be due to assumptions made during the development of the model. It is therefore essential to review these assumptions and assess their effect on the accuracy of the predicted electrical conductivity.

First, in developing the model, the assumption was made that the solvent is a continuum medium where ions move. However, in reality, the solvent has a structure. Two main effects have been overlooked by neglecting the solvent's structure. First, because of the high electrostatic field around the ions, solvent molecules align with this field, causing ions to typically move in the solution with their solvating molecules around them. Second, electrorestriction of solvent molecules around ions leads to dielectric saturation and a decrease in relative permittivity. At lower ionic strengths, the impact of dielectric saturation is less pronounced, allowing the model to accurately predict the conductivity of solutions when $I \leq 1\, mol \cdot L^{-1}$. However, at higher ionic strengths, the impact of the reduction of the RSP on electrical conductivity may become more significant.

To address the issue of neglecting ion movement with their solvation shells, the model has incorporated effective ionic radii instead of crystallographic ionic radii. In essence, these effective ionic radii are composition-dependent. Typically, the use of effective ionic radii involves adjusting the model predictions to align with the experimental data. This adjustment may introduce a more correlative rather than predictive nature to the model.

On the other hand, the impact of dielectric saturation can be readily considered by incorporating a composition-dependent relative permittivity. Research by Naseri Boroujeni et al. [124] (Chapter 3) has shown that the use of a concentration-dependent relative permittivity leads to an improved agreement between theory and experiment for both MSA-based and DHO-based models.

Another assumption made in model development is the complete dissociation of the electrolytes in solutions, neglecting the presence of ion pairs or higher aggregates. However, it has been established that this assumption becomes invalid under conditions of high salt concentrations, elevated temperatures, and low solvent permittivity. Studies indicate that accounting for the formation of ion pairs in electrolyte solutions requires adjustments to electrical conductivity models [113, 148, 214, 215]. Despite this, critics may argue that the attribution of the ion-ion association as an explanation is merely an attempt to rationalize the limitations of the developed model. Therefore, a more comprehensive investigation into this assumption is valuable for gaining a deeper understanding.

Additionally, apart from the solvent effect discussed above, it should be noted that the developed model tends to overestimate molar conductivity in most systems, as evident in Figure 5.6 where most data points fall below the line of the perfect fit. This overestimation of molar conductivity has also been observed in previous studies using models such as MSA [111], MSA-Simple [113], and DHO3 [124]. These models exhibit a similar pattern of overestimating molar conductivity for electrolyte solutions at ionic strengths exceeding 1 $mol \cdot L^{-1}$. The reason behind this overestimation could be attributed to the inclusion of ions that, in real solutions, do not significantly contribute to electrical conductivity due to ion pairing.

In conclusion, validating or refuting the presence of ion pairs in electrolyte solutions poses a formidable challenge. However, several observations indirectly support the idea of ion pair formation [80, 81]. Furthermore, the formation of ion pairs provides a plausible explanation for the inconsistencies observed between the models and the experimental data. Therefore, it is important to improve the existing model by integrating the concept of ion pair formation, as it holds substantial significance in comprehending and resolving the observed discrepancies.

Eq. 5.13 presents the specific conductivity of a system comprising charged hard spheres, where the formation of ion pairs is allowed. In this equation, α_i represents the fraction of unbound ions, while M and N denote the number of cations and anions types in the solution. Furthermore, ρ_{ij} and D^0_{ij} represent the number density and diffusion coefficient at an infinite dilution limit of ion pairs, respectively. The charge of the ion pairs is expressed as $Z_{ij} = Z_i + Z_j$. The electrophoretic and relaxation effects of the ion pairs, computed from equations 5.6 and 5.5, are denoted as $\delta v_{ij}/v^{\circ}_{ij}$ and $\delta k_{ij}/k_{ij}$, respectively.

$$\begin{aligned}\chi \quad &= \frac{e^2}{k_B T}\left[\sum_{i=1}^{C}\rho_i\alpha_i D_i^0 Z_i^2\left(1+\frac{\delta v_i}{v_i^0}\right)\left(1+\frac{\delta k_i}{k_i}\right)+\right.\\ &\left.\sum_{i=1}^{M}\sum_{j=1}^{N}\tilde{\rho}_{ij}D_{ij}^0 Z_{ij}^2\left(1+\frac{\delta v_{ij}}{v_{ij}^0}\right)\left(1+\frac{\delta k_{ij}}{k_{ij}}\right)\right]\end{aligned} \tag{5.13}$$

For a precise determination of the specific conductivity in solutions containing associative electrolytes, it is essential to consider the proportion of unbound ions and the number density

of ion pairs. Thus, in this investigation, the developed model needs to be integrated with a thermodynamic model that incorporates the formation of ion pairs. Notably, promising models explored and developed by Naseri Boroujeni et al. [214] address this specific aspect.

Furthermore, the calculation of the electrophoretic and relaxation effects of charged ion pairs presents certain challenges, such as the conversion of a dumbbell-shaped ion pair into a spherical charged particle, and the ionic conductivity of ion pairs at infinite dilution. These complexities need to be thoroughly examined.

Finally, it could be contended that the deviation from experimental measurements stems from the utilization of the pair correlation function from the DH theory, either due to the nonphysical behavior of the Boltzmann distribution or the linearization of the PB equation.

It is crucial to highlight that in the case of electrolyte solutions where all species (ions) exhibit comparable sizes, as elucidated by Robinson and Stokes [90], the local concentration of neighboring ions around the central ion never attains a nonphysical value. Consequently, attributing the deviation from experimental measurements to the use of the pair correlation function derived from the DH theory may not be valid in such cases.

Furthermore, even if we accept the notion that the pair correlation function utilized in the DH theory might lack accuracy and contribute to the deviation from the experimental data, it is pertinent to acknowledge that employing more sophisticated pair correlation functions, such as those derived from the MSA theory, still leads to deviations from experimental measurements at comparable ionic strengths. This implies that the challenge may not stem solely from the accuracy of the pair correlation function but could be influenced by other factors or phenomena not encompassed by the existing theories.

5.4 Summary and Conclusions

In this chapter, a novel model was formulated to predict the electrical conductivity of mixed electrolyte solutions. This model seeks to correct the ideal behavior of ionic conductivity, taking into account relaxation and electrophoretic effects. The DH theory has been employed to account for the relaxation effect in solving the FO continuity equation. Furthermore, the electrophoretic correction, initially devised for single-salt solutions, was used for the mixed electrolyte solutions, given its original formulation for a mixture of an arbitrary number of charged species.

The effectiveness of the model has been extensively assessed through a meticulous comparison between its predictions and experimental data for 24 ternary mixed salt-water solutions. This evaluation includes the utilization of crystallographic ionic radii and reported ionic conductivity values at infinite dilution. The findings indicate an acceptable agreement between the predictions of the model and the experimental data for solutions with an ionic strength below 1 $mol \cdot L^{-1}$. However, at higher ionic strengths, the model exhibits a tendency to overestimate the molar conductivity of aqueous solutions.

Potential causes of the observed deviation between model predictions and experimental measurements have been explored. The hypothesis suggests that overlooking the solvent structure and ion pair formation may contribute to the observed discrepancies, particularly at high ionic strengths. To address this, it is proposed that the formation of ion pairs should be considered, especially in solutions with high ionic strengths. Additionally, incorporating a composition-dependent relative permittivity could be beneficial in capturing the solvent's structural effects.

Chapter Message

In this chapter, a novel model was formulated to predict the electrical conductivity of mixed electrolyte solutions. This introduces a physics-based, user-friendly model for accurately predicting electrical conductivity, particularly applicable to investigating systems where ion pairs are charged species and systems forming charged complexes.

Part III

Ion-Ion Association in Electrolyte Solutions

CHAPTER 6

Thermodynamic Modeling of Ion-Ion Association

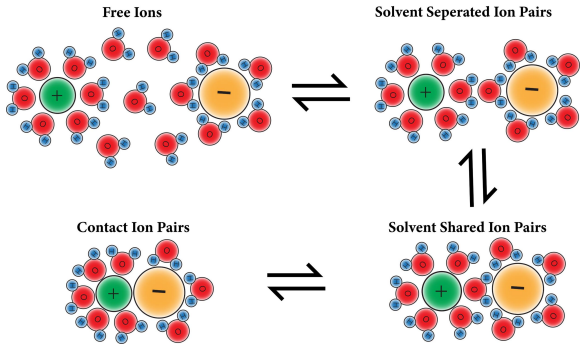

The previous part of this thesis was dedicated to the electrical conductivity of electrolyte solutions. A systematic investigation was conducted on the accuracy and robustness of the models developed in the literature. Furthermore, two new models for the electrical conductivity of single- and multi-salt electrolyte solutions were developed and extensively validated against the experimental data.

It has been shown that the models developed in this work and those from the literature start to deviate from the experimental data chiefly at elevated salt concentrations. Then, it has been speculated that one of the reasons for this discrepancy is the full dissociation assumption in the model development.

In this chapter and in the following chapter of this thesis, the concept of ion-ion association is studied from a thermodynamic point of view. Particularly, in this chapter, the thermodynamic models developed in the literature are reviewed, and a comprehensive investigation is performed to evaluate their accuracy and robustness.

Part of this chapter has already been published in the Journal of Molecular Liquids:

- *Mean ionic activity coefficient of associative electrolyte solutions: A comparison study [214]* (Link).

6.1 Literature Review

Bjerrum, in 1926, introduced the concept of ion-ion association in electrolyte solutions [216]. This work was, in its time, insightful and, yet, controversial. It was only three years after the seminal work of Debye and Hückel [4] that a theory that assumes full dissociation fits better to the experimental observations compared to the electrolyte theory of Arrhenius.

At this time, Bjerrum brought the attention of the scientific community to the fact that neither the full dissociation assumption in the Debye and Hückel theory nor the speculation of Arrhenius completely captures the reality of solutions. Reality is something in between.

Since the work of Bjerrum, many efforts have been made to shed light on the concept of ion-ion association. The concept of ion-ion association has been well reviewed by Kraus [217], Szwarc [218], Marcus and Hefter [80], and van der Vegt et al. [81]. Because of its importance, it has also been extensively investigated in monographs and books on electrolyte solutions. The works of Robinson and Stokes [90], Barthel et al. [84], and Harned and Owen [219] are examples among them.

Looking at the literature on ion-ion association, it seems very extensive and at the same time very confusing. For a better understanding, the work dedicated to the concept of ion pairing can be categorized into the statistical mechanics or thermodynamic treatment of the ion-ion association, the experimental treatment of the ion-ion association, and recently the ion-ion association from molecular simulations.

The second and third categories have been extensively reviewed by Marcus and Hefter [80] and van der Vegt et al. [81]. To gain a better comprehension of these techniques, the reader can refer to the sources mentioned and the references within them.

The reviewed paper and the references therein are valuable sources for the investigation of ion-ion association, mainly from a structural point of view. However, we examine the concept of the ion-ion association from the property prediction angle. Therefore, the thermodynamic and statistical mechanics approaches dedicated to the concept of ion-ion association are more valuable to us. Hence, it is valuable to review the approaches and models that have been introduced for the incorporation of ion pairing in electrolyte thermodynamics.

The approaches that have been used to account for ion pairing can be categorized into chemical approaches and statistical mechanics approaches (see Figure 6.1). In chemical approaches, the ideal gas reference of the system will be changed by changing the species present in the solution. In this approach, it has been assumed that there are free ions and ion pairs as species in the solution. On the other hand, in the statistical mechanic approaches, the ideal gas reference of the system is intact. The species in the solution are ions (and neutral compounds in non-primitive models). The ion pairs are not independent species. In these approaches, the effect of ion pairing is taken into account by adding an association term (sometimes called a mass action law (MAL)) to the free energy of the system.

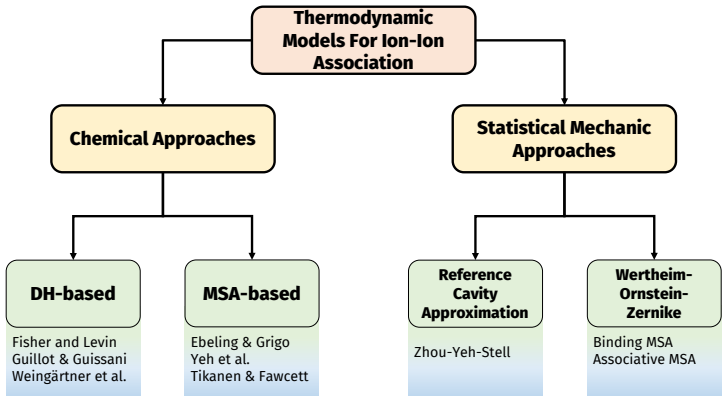

Figure 6.1. Thermodynamic modeling of associative electrolyte solutions.

6.1.1 Chemical Approaches

In the chemical approaches, the ideal gas reference state of the system is altered by defining a pseudo-system in which species are free ions and ion pairs. The distribution of species, then, is obtained by solving the MAL equations. Most of the studies dedicated to the concept of ion pairing stem from these approaches.

For the theoretical investigation of ion-ion association especially from the thermodynamic point of view, it can be seen that a brief review is required. These approaches, as outlined in Figure 6.1, are either DH-based or MSA-based.

Ebeling and Grigo [220–223] introduced a new method following the work of Bjerrum to account for ion pairing in a RPM fluid. Their model consists of the Carnahan-Starling [224] EoS for the hard-sphere (HS) contribution and the MSA model for the electrostatic contributions. They studied the phase transition and the osmotic coefficient [220], electrical conductivity [221], and the RDF [222, 223] of the associative electrolyte solution using this model. They named this model MSA-MAL (mean spherical approximation-mass action law).

In this model, they assumed that the ion-ion association does not affect the hard sphere contribution. Furthermore, they assumed that the activity coefficient of the ion pairs is equal to one. In addition, only electrostatic contributions to the activity coefficient were considered in the MAL. Yeh et al. [225] modified the Ebeling and Grigo model by accounting for the ion dipole interactions between free ions and ion pairs. As a result, the activity coefficient of ion pairs is no longer one.

Tikanen and Fawcett [226–229] employed a model similar to the Ebeling and Grigo model to estimate the MIAC of the real electrolyte solutions. Their model is different from the Ebeling and Grigo model in a way that it accounts for the size asymmetry of the ions, the RSP is composition-dependent, and the hard sphere is from Mansoori et al. [230, 231].

Fisher and Levin [232–234] studied the phase transition in RPM fluids in electrolyte solutions by modifying the Bjerrum approach for ion pairing. They introduced dipole-ion (DI) interactions into their EoS with a methodology similar to the Kirkwood model [235].

Guillot and Guissani [236] perform an extensive investigation of the phase transition in RPM fluids. They extended the approach of Fisher and Levin by modifying the HS contribution to the Helmholtz free energy. Furthermore, they extended the model by accounting for the variation of the RSP of the system resulting from the presence of ion pairs which are dipolar species. They also tried to extend MSA-based equations by accounting for DI interactions and also variation of the RSP due to the formation of dipolar ion pairs.

Thermodynamic modeling of the ion-ion association in a chemical approach has also been studied by Weiss and Schröer using DH theory [237]. They extended the model developed by Fisher and Levin by accounting for the variation of the RSP of the system owing to the formation of dipolar ion pairs. In this work, they focused on the phase transition in RPM fluids similar to Fisher and Levin and Guillot and Guissani.

The developed equations of state have been used mainly for the phase transition and criticality for RPM fluids. For a comprehensive review on this subject, the reader can refer to the review papers by Weingärtner and Schröer [238] and Schröer [239]. From a thermodynamic point of view, it does not matter whether a model is developed for property prediction or phase transition in model fluids. However, the mentioned equations of state have not been used and studied in a practical manner.

6.1.2 Statistical Mechanics Approaches

Another class of approaches that has been used in the literature for the thermodynamic modeling of associative electrolyte solutions are statistical mechanic approaches. In these approaches, the ideal gas reference state is the same as that for non-associative electrolyte solutions. The species present in the solution are also the same as those for thermodynamic

models for non-associative electrolytes. There is an additional term in the free energy of the system that represents the association.

The energy contribution to the total free energy of the system as a result of the ion-ion association is the result of Wertheim theory. This contribution is only a function of the fraction of free ions in the solution. The models based on this approach differ from each other in the way in which they calculate the fraction of free ions. There are two approaches to calculate the fraction of free ions: the reference cavity approximation (RCA) or solving the Wertheim-Ornstein-Zernike (WOZ) equation.

Stell and his co-workers [240–245] introduced the concept of RCA. Then, they introduced three equations of state (PMSA1-3) based on the RCA and MSA theory for RPM fluids. They then used these three models to predict the critical point of these fluids and compared them with the MC simulations and other models.

The concept of RCA is quite simple and is based on the fact that the cavity function defined as $y_{+-} = g_{+-}(r)\exp(\beta u_{+-}(r))$ can be approximated as the cavity function in the non-association limit. This approach will be extensively discussed in Chapter 7. Then, the fraction of free ions can be calculated from a MAL equation, and correspondingly the free energy of the system and other thermodynamic properties will be calculated on the basis of that.

Another approach for the calculation of the fraction of unbound ions is based on incorporation saturation effects in the Ornstein-Zernike equation. BiMSA [19,20] and AMSA [21–29] originate from this approach.

6.2 Practical Investigation of Associative Thermodynamic Models

The models formulated for associative electrolyte solutions can be examined either through a theoretical approaches or a practical one. Previous research often used the theoretical method, comparing ionic fluid criticalities as predicted by these models to those from molecular simulations. Yet, apart from the BiMSA [20] and Ebling and Grigo [220–223, 231] models, we believe that to the best of our knowledge no other equations of state have been practically analyzed against the experimental data. Moreover, it remains unclear which among the developed models is superior to the others.

As a result, this chapter focuses on evaluating the thermodynamic models for associative electrolyte solutions from the literature using a practical perspective. We have chosen four implicit solvent models for this purpose: the Ebeling-Grigo [220–223, 231], Zhou-Yeh-Stell [240, 242–245], Fisher-Levin-Guillot-Guissani [233, 234, 236], and Bernard-Blum [19, 20] models. We then assess and compare these equations of state methodically and impartially.

Firstly, the models' predictions were evaluated by comparing them to the numerical solutions of the PB equation and MC simulations. Next, the direct predictions of the models were compared to the experimental data for four 2:2 salt-water mixtures at 298.15 K. The HS diameter and the average distance between ion pairs were then fine-tuned based on the MIAC from the experimental data. In the final step, the computed fraction of free ions was verified by contrasting the predicted electrical conductivity, using either the DHO- or MSA-based theories, with the experimental data.

In this section, the RPMs used for examining ion-pairing are discussed. An analysis is conducted on a classical system consisting of N cations and N anions, both represented as charged hard spheres (CHS) in a continuous solvent medium with a constant RSP (ε_r). For this system, the overall number density is denoted by $\rho_0 = N/V$. The electrolyte solution is considered symmetrical, defined by $Z_+ = -Z_- = Z$. Furthermore, it is posited that both the cations and anions in the solution possess an identical ionic diameter (σ).

6.2.1 Chemical Approaches

Initially, it is assumed that the salt(s) completely dissociate in the solution, as represented by Eq. 6.1. In this equation, Z_i denotes the valence of the ion, while ν_i signifies the stoichiometric coefficient where i can be either positive (+) or negative (−).

$$C_{\nu_+}^{Z_+} A_{\nu_-}^{Z_-} \rightarrow \nu_+ C^{Z_+} + \nu_- A^{Z_-} \tag{6.1}$$

For this electrolyte, the chemical potential can be written as Eq. 6.2 (Eq. 1.37 in ref. [84]):

$$\mu_E(P,T) = \mu_E^{\infty(c)}(P,T) + \nu RT \ln((c_\pm/c^*)\gamma_\pm^c) \tag{6.2}$$

In the given equation, the sum of stoichiometric coefficients is represented by $\nu = \nu_+ + \nu_-$. Here, R stands for the ideal gas constant, and T indicates the temperature measured in Kelvin. The term $\mu_E^{\infty(c)}$ signifies the chemical potential of the electrolyte at the reference state of infinite dilution, expressed in molarity scale. The expression for $c_\pm$ is given by $(\nu_+^{\nu_+}\nu_-^{\nu_-})^{(1/\nu)}c_E$, and c^* is defined as $1\ mol \cdot L^{-1}$. The coefficient $\gamma_\pm^c$ refers to the MIAC, presented in the molarity scale.

Subsequently, it is postulated that free ions maintain an equilibrium with ion pairs or more complex aggregates, as indicated by the chemical equilibrium reaction in Eq. 6.3.

$$\omega_+ C^{Z_+} + \omega_- A^{Z_-} \rightleftharpoons \left[C_{\omega_+} A_{\omega_-}\right]^{Z_+ + Z_-} \tag{6.3}$$

In Eq. 6.3, the stoichiometric coefficients for the equilibrium reaction are represented by ω_+ and ω_-. The ion aggregates, denoted as $[C_{\omega_+} A_{\omega_-}]^{Z_+ + Z_-}$, are referred to by the superscript $+-$ when deriving the activity coefficient of the electrolyte and the MAL.

Based on the equilibrium reaction equation, Eq. 6.4 can be formulated. In this equation, μ'_{+-}, μ'_+, and μ'_- respectively represent the chemical potential of ion pair, free cation, and free anion.

$$\mu'_{+-}\,(P,\ T) - \omega_+ \mu'_+\,(P,\ T) - \omega_- \mu'_-\,(P,\ T) = 0 \tag{6.4}$$

In Eq. 6.5, the concentration of both free ions and ion pairs is presented, introducing α as an auxiliary parameter. Here, c_E denotes the concentration of the electrolyte, expressed in $mol \cdot L^{-1}$. When considering ion pairs, α signifies the proportion of free ions. However, in the context of ion aggregates, α represents the association degree.

$$c_+ = \alpha\nu_+ c_E,\ c_- = \left[1 - (1-\alpha)\,\frac{\nu_+}{\nu_-}\frac{\omega_-}{\omega_+}\right]\nu_- c_E,\ c_{+-} = (1-\alpha)\,\frac{\nu_+}{\omega_+}c_E \tag{6.5}$$

The chemical potential of the electrolyte is derived from the chemical potentials of the free ions and ion pairs as follows:

$$\mu_E = \alpha\nu_+\mu'_+ + \left[1 - (1-\alpha)\frac{\nu_+}{\nu_-}\frac{\omega_-}{\omega_+}\right]\nu_-\mu'_- + (1-\alpha)\nu + \omega_+\mu'_{+-} \tag{6.6}$$

Combining Eq. 6.4 with Eq. 6.6, it gives:

$$\mu_E = \nu_+\mu'_+ + \nu_-\mu'_- \tag{6.7}$$

Subsequently, the definition of the chemical potential of a component within a mixture is applied as detailed in Eq. 6.8:

$$\mu'_i = \mu_i^{\infty(c)} + RT\ln\left(a_i^{(c)}\right) = \mu_i^{\infty(c)} + RT\ln\left(\frac{c_i}{c^*}\gamma_i^c\right) \tag{6.8}$$

By substituting Eq. 6.8 into Eq. 6.7 (while dropping the dependencies on P and T for the sake of brevity), the result is:

$$\mu_E = [\nu_+\mu_+^{\infty(c)} + \nu_-\mu_-^{\infty(c)}] \; + RT\ln[(\frac{c_+}{c^*}\gamma_+^c)^{\nu_+}(\frac{c_-}{c^*}\gamma_-^c)^{\nu_-}] \tag{6.9}$$

By setting μ_E from Eq. 6.9 equal to μ_E from Eq. 6.2, we obtain:

$$[\nu_+\mu_+^{\infty(c)} + \nu_-\mu_-^{\infty(c)}] \; + RT\ln[(\frac{c_+}{c^*}\gamma_+^c)^{\nu_+}(\frac{c_-}{c^*}\gamma_-^c)^{\nu_-}] = \mu_E^{\infty(c)} + \nu RT\ln((c_\pm/c^*)\gamma_\pm^c) \tag{6.10}$$

Given the assumption that $\mu_E^{\infty(c)} = \nu_+\mu_+^{\infty(c)} + \nu_-\mu_-^{\infty(c)}$, the expression for the MIAC of the electrolyte becomes:

$$\gamma_\pm^c = \frac{c^*}{c_\pm}\left[\left(\frac{c_+}{c^*}\gamma_+^c\right)^{\nu_+}\left(\frac{c_-}{c^*}\gamma_-^c\right)^{\nu_-}\right]^{1/\nu} \tag{6.11}$$

By omitting c^* from Eq. 6.11 and applying the definition of $c_\pm = (\nu_+^{\nu_+}\nu_-^{\nu_-})^{(1/\nu)}c_E$, the resulting equation is:

$$\gamma_\pm^c = \frac{1}{c_E}\left[\frac{(c_+\gamma_+^c)^{\nu_+}\,(c_-\gamma_-^c)^{\nu_-}}{(\nu_+{}^{\nu_+}\nu_-{}^{\nu_-})}\right]^{1/\nu} \tag{6.12}$$

Replacing c_+ and c_- from Eq. 6.5 in Eq. 6.12, it gives:

$$(\gamma_\pm^c)^\nu = \alpha^{\nu_+}\left[1-(1-\alpha)\,\frac{\nu_+}{\nu_-}\frac{\omega_-}{\omega_+}\right]^{\nu_-}\left(\gamma_\pm'^c\right)^\nu \tag{6.13}$$

If we assume a symmetrical electrolyte solution ($\nu_+ = \nu_- = 1$) and only consider ion pairs ($\omega_+ = \omega_- = 1$), then:

$$\gamma_\pm^c = \alpha\gamma_\pm'^c \tag{6.14}$$

6.2.1.1 Ebeling and Grigo (EG) Approach

Ebeling and Grigo [220–222] explored a classical system composed of charged hard spheres, building upon the Bjerrum method of ion pairing [216]. They postulated a chemical equilibrium between free ions and ion pairs, as shown in Eq. 6.3. Using the equilibrium reaction equation (Eq. 6.4), the concentration of free ions and ion pairs in the solution was determined. For the CHS system, an EoS was formulated. Eq. 6.15 encapsulates the EoS introduced by EG for charged hard spheres. To address the hard sphere component, the CS equation was employed [224]. For the interaction between ions, the MSA model was utilized.

$$\frac{\beta}{N}A^r = \frac{\beta}{N}\left(A^{CS} + A^{MSA}\right) \tag{6.15}$$

During the formulation of this EoS, it was posited that ion pairing does not influence the hard sphere components. As a result, A^{CS}, P^{CS}, and $\ln\gamma_i^{CS}$ were incorporated under the assumption of complete dissociation in the solution, as shown in equations 6.16, C.2, and C.3, respectively. It is pertinent to highlight that the packing factor (η) is determined using the total number density prior to the association, represented by (ρ_0).

$$\frac{\beta A^{CS}}{N} = \frac{\eta\,(4-3\eta)}{(1-\eta)^2} \tag{6.16}$$

$$\eta = \frac{\pi \rho_0 \sigma^3}{6} \tag{6.17}$$

Conversely, the number densities of free ions were incorporated in the original MSA formulation to address ion pairing. The representations for A^{MSA}, P^{MSA}, and $\ln \gamma_i^{MSA}$ are provided in equations 6.18, C.10, and C.11, where the variable x' is used in lieu of x in the formulation.

$$\frac{\beta A^{MSA}}{N} = -\frac{1}{12\pi\rho_0\sigma^3}\left[2 + 6x' - 3x'^2 - 2\left(1 + 2x'\right)^{3/2}\right] \tag{6.18}$$

$$x' = \kappa'\sigma = \sqrt{\frac{\alpha\rho_0 \left(Ze\right)^2}{k_B T \varepsilon_0 \varepsilon_r}}\sigma \tag{6.19}$$

The assumption was made that ion pairs in the solution behave ideally, leading to $\gamma_{+-}^c = 1$. Moreover, only the electrostatic component from the MSA model was utilized in both the MAL and the computation of the free ions' fraction. Consequently, the MAL can be distilled down to the form presented in Eq. 6.20.

$$\frac{2\left(1-\alpha\right)}{\rho_0 \alpha^2} = K_{+-}^{\circ}\left[\gamma_{\pm}^{\prime MSA}\right]^2 \tag{6.20}$$

After solving this non-linear problem for the fraction of free ions (α), the thermodynamic properties such as $\gamma_{\pm}^c$, ϕ, and A^r can be calculated.

6.2.1.2 Fisher-Levin-Guillot-Guissani (FLGG) Approach

In a series of publications, Fisher and Levin (FL) developed an implicit EoS for ionic fluids, drawing on the Bjerrum treatment and the EG model [232–234]. Guillot and Guissani later modified this model by integrating the hard sphere component [236]. In our analysis, we refer to the implicit EoS introduced by FL and modified by GG as the Fisher-Levin-Guillot-Guissani methodology (FLGG). This methodology employs a revised version of the CS model to describe HS interactions. The DH model is deployed for ion-ion interactions. Additionally, the influence of dipolar ion pairs is acknowledged through dipole-ion (DI) interactions, a concept pioneered by Fisher and Levin [232–234]. Furthermore, a chemical approach is adopted to determine the fraction of free ions.

$$\frac{\beta}{N}A^r = \frac{\beta}{N}\left(A^{HS} + A^{DH} + A^{DI}\right) \tag{6.21}$$

$$\frac{2\left(1-\alpha\right)}{\rho_0 \alpha^2} = K_{+-}^{\circ}\ \frac{\gamma_+\gamma_-}{\gamma_{+-}} \tag{6.22}$$

Within the given formulations, A^{HS} and P^{HS} are derived using the modified CS model, as specified in equations 6.23 and C.20, respectively. For a detailed explanation of σ_m, one can consult with ref. [236] or Appendix C.

$$\frac{\beta A^{HS}}{N} = \left(1+\alpha\right)\rho_0 \frac{\eta_m\left(4-3\eta_m\right)}{2\left(1-\eta_m\right)^2} \tag{6.23}$$

$$\eta_m = \frac{1}{12}\pi\left(1+\alpha\right)\rho_0\sigma_m^3 \tag{6.24}$$

The DH components contributing to the residual Helmholtz free energy, activity coefficient, and pressure are denoted by equations 6.25, C.24, and C.25, respectively. Within

these equations, the value of x' is determined by accounting for the number density of the free ions, as elucidated in Eq. 6.19.

$$\frac{\beta A^{DH}}{N} = -\frac{1}{4\pi\rho_0\sigma^3}\left[\ln\left(1+x'\right) - x' + \frac{x'^2}{2}\right] \tag{6.25}$$

The contributions of the DI to the residual Helmholtz free energy are represented by equations 6.26 and 6.27. Within these equations, the term x_{eff} is defined as $\kappa'\sigma_{eff}$, where $\sigma_{eff} = (\sigma+\sigma_{ip})/2$. Fisher and Levin [232–234] have proposed that the diameter of the dipolar hard spheres, denoted by σ_{ip}, is equivalent to 1.314σ. Consequently, σ_{eff} is calculated to be 1.162σ.

$$\frac{\beta A^{DI}}{N} = -\frac{e^2Z^2}{8\pi\varepsilon_0\varepsilon_r k_B T\sigma}(1-\alpha)\left(\frac{\sigma}{\sigma_{eff}}\right)^3 x_{eff}^2\omega\left(x_{eff}\right) \tag{6.26}$$

$$\omega\left(x_{eff}\right) = \frac{3}{x_{eff}^4}\left[ln\left(1+x_{eff}+\frac{1}{3}x_{eff}^2\right) - x_{eff} + \frac{1}{6}x_{eff}^2\right] \tag{6.27}$$

The equations for the pressure and activity coefficient are presented in Appendix C.

6.2.2 Statistical Mechanics Approaches

6.2.2.1 Zhou, Yeh, and Stell (ZYS) Approach

In a succession of publications, Zhou et al. [240–245] introduced an implicit solvent model grounded on the RCA. Within this framework, both the Helmholtz free energy and the pressure are calculated from equations 6.30 and C.31. These equations were originally formulated for equimolar dimerization by Wertheim [246–251].

$$\frac{\beta}{N}A^r = \frac{\beta}{N}\left(A^{CS} + A^{MSA} + A^{MAL}\right) \tag{6.28}$$

In these equations, A^{CS} is the same as Eq. 6.16.

Within the mentioned equations, the term $y_{+-}^{ref} = \gamma_+\gamma_-/\gamma_{+-}$ signifies the cavity function between cations and anions in a completely dissociated reference state. By merging this cavity function with the MAL, one can calculate the fraction of free ions as follows:

$$\frac{2(1-\alpha)}{\rho_0\alpha^2} = y_{+-}^{ref}K_{+-}^{\circ} \tag{6.29}$$

ZYS incorporated the MSA model for interactions between ions and utilized the CS model to account for the hard sphere interactions in the solution. Additionally, through a thermodynamic cycle, they derived the activity coefficient for dipolar ion pairs in a state where there is no association ($\alpha = 1$). As a result, they developed an EoS for implicit solvent models, as depicted in equations 6.28-6.34.

$$\frac{\beta A^{MSA}}{N} = -\frac{1}{12\pi\rho_0\sigma^3}\left[2+6x+3x^2-2\left(1+2x\right)^{3/2}\right] \tag{6.30}$$

$$\frac{\beta A^{MAL}}{N} = \frac{1-\alpha}{2} + \ln\left(\alpha\right) \tag{6.31}$$

The fraction of unassociated ions is determined using Eq. 6.32, which represents the analytical solution to the MAL equation.

$$1-\alpha=\frac{1+\rho_0 K^{\circ}_{+-} y^{ref}_{+-}-\sqrt{1+2\rho_0 K^{\circ}_{+-} y^{ref}_{+-}}}{\rho_0 K^{\circ}_{+-} y^{ref}_{+-}} \tag{6.32}$$

In Eq. 6.32, the reference cavity function (y^{ref}_{+-}) is calculated as Eq. 6.33:

$$y^{ref}_{+-}=\frac{2-\eta}{2\left(1-\eta\right)^3}\exp\left(-\frac{2z^2\lambda}{\sigma}\left[\frac{0.5x^2-x-1+\sqrt{1+2x}}{x^2}\right]\right) \tag{6.33}$$

$$\lambda=\frac{e^2}{4\pi\varepsilon_0\varepsilon_r k_B T} \tag{6.34}$$

It should be noted that x in Eq. 6.30 is different from x' in Eq. 11. The former is calculated by using the total number density of ions ($x=\kappa\sigma=\sqrt{\frac{\rho_0(Ze)^2}{k_B T\varepsilon_0\varepsilon_r}}\sigma$). In contrast, the latter is calculated using the number density of free ions. In addition, the fraction of free ions (α) can be calculated analytically in this EoS. The equations for pressure and activity coefficient are presented in Appendix C.

6.2.2.2 Binding Mean Spherical Approximation (BiMSA) Approach

Bernard and Blum [19, 20] formulated a thermodynamic model for a mixture of CHS using the Wertheim framework. They addressed a neutral system comprising a varying number of components and resolved the WOZ equation specifically for pairing scenarios. For an equimolar CHS system, the Helmholtz free energy in the BiMSA model can be represented as per Eq. 6.35.

$$\frac{\beta}{N}A^r=\frac{\beta}{N}\left(A^{CS}+A^{BiMSA}+A^{MAL}\right) \tag{6.35}$$

In this formulation, the contribution from hard spheres using the CS model, denoted as A^{CS}, is presented in Eq. 6.16. The electrostatic component of the Helmholtz free energy is detailed in Eq. 6.36.

$$\frac{\beta A^{BiMSA}}{N}=-\frac{\beta e^2}{4\pi\varepsilon_0\varepsilon_r\rho_0}\frac{\Gamma^B}{1+\Gamma^B\sigma}\sum_k \rho_k Z_k^2+\frac{\left[\Gamma^B\right]^3}{3\pi\rho_0} \tag{6.36}$$

The dimerization or MAL contribution to the Helmholtz free energy is as follows:

$$\frac{\beta A^{MAL}}{N}=\ln\left(\alpha\right)+\frac{1-\alpha}{2} \tag{6.37}$$

In Eq. 6.36, Γ^B is the BiMSA screening parameter. It can be calculated by the simultaneous solution of transcendental and the MAL equations (equations 6.38 and 6.39):

$$4\left(1+\Gamma_B\sigma\right)^2=\left(\frac{\kappa}{\Gamma^B}\right)\frac{\alpha+\Gamma^B\sigma}{1+\Gamma^B\sigma} \tag{6.38}$$

$$\frac{2\left(1-\alpha\right)}{\rho_0\alpha^2}=K^{\circ}_{+-}\left[\left(\frac{1-0.5\eta}{\left(1-\eta\right)^3}\right)\exp\left(\frac{1}{\left(1+\Gamma^B\sigma\right)^2}\right)\right] \tag{6.39}$$

The equations for the pressure and activity coefficient are presented in Appendix C.

6.2.3 Ion Pairing at Infinite Dilution

Krienke et al. [252, 253] suggested that the association constant at infinite dilution can be calculated using either a structural or a thermodynamic approach. The structural approach, such as the Bjerrum model, begins with the pair correlation function ($g_{+-}(r)$) which is based on the interactions between opposite ions ($W^{\infty}_{+-}(r)$). The thermodynamic approach, such as the Ebeling model, derives the association constant from the comparison of the chemical and physical pictures. The structural approach can obtain $K^{\circ}_{+-}(T)$ from the MAL by removing the concentration-dependent part (Eq. 6.40) (see ref. [252] for more information).

$$K^{\circ}_{ij}(T) = 4\pi N_A \int_0^R r^2 \exp\big(-\beta W^{\infty}_{ij}(r)\big) dr \tag{6.40}$$

The potential of the mean force at an infinite dilution, denoted by $W^{\infty}_{+-}(r)$ in Eq. 6.40, is composed of a short-range component, $W^{\circ}_{+-}(r)$, and a long-range part, $W^{C}_{+-}(r)$. The short-range contribution is further divided into short-range interactions, $W^{Cor}_{+-}(r)$, and solvation effects, $W^{Solv}_{+-}(r)$. The long-range contribution is due to Coulombic interactions, as expressed in Eq. 6.43.

$$W^{\infty}_{ij}(r) = W^{\circ}_{ij}(r) + W^{C}_{ij}(r) \tag{6.41}$$

$$W^{\circ}_{ij}(r) = W^{cor}_{ij}(r) + W^{solv}_{ij}(r) \tag{6.42}$$

6.2.3.1 Bjerrum Approach

The Bjerrum model (Eq. 6.44) can be derived from Eq. 6.40 by assuming that $W^{solv}_{+-} = 0$ and setting the upper limit of the integral as q. Bjerrum [216] proposed that all oppositely charged ions with a separation distance between σ_{+-} and q should be considered as ion pairs. However, it has been noted in the literature that the selection of the upper limit is arbitrary. Furthermore, the lower limit does not necessarily have to be the contact distance between ion pairs.

$$W^{\infty}_{ij} = \begin{cases} 0 & \text{if} \quad r < \sigma_{ij} \\ \frac{Z_i Z_j e^2}{4\pi\varepsilon_0\varepsilon_r r} & \text{if} \quad r \geq \sigma_{ij} \end{cases} \tag{6.43}$$

$$K^{\circ}_{ij}(T) = \begin{cases} 0 & \text{if} \quad l_{ij} < \sigma_{ij} \\ 4\pi N_A \int_{\sigma_{ij}}^{l_{ij}} r^2 \exp\big(\frac{2q}{r}\big) dr & \text{if} \quad l_{ij} > \sigma_{ij} \end{cases} \tag{6.44}$$

$$q = \frac{l^B_{ij}}{2} = \frac{e^2 \mid Z_i Z_j \mid}{8\pi\varepsilon_0\varepsilon_r k_B T} \tag{6.45}$$

6.2.3.2 Low Concentration Chemical Model (lcCM)

Equation 6.46 is an adaptation of the Bjerrum model that takes into account solvation interactions, assuming an average contribution of $W^{Solv}_{+-} = W^{*}_{ij}$ for distances between σ_{+-} and R. The upper limit of the integral in this model is $R = \sigma_{+-} + n\sigma_s$, where n is the number of solvent molecules between ion pairs [254].

$$K^{\circ}_{ij}(T) = 4\pi N_A \exp\big(-\beta W^{*}_{ij}\big) \int_{\sigma_{ij}}^{l_{ij}} r^2 exp(\frac{2q}{r}) dr \tag{6.46}$$

6.2.3.3 Ebeling Approach

Eq. 6.47 is the association constant formulated by Ebeling, which was obtained by comparing the osmotic coefficients derived from a physical picture and the chemical model [255].

$$K_{ij}^{\circ}(T) = 8\pi N_A \sigma_{ij}^3 \sum_{m\geq 2}^{\infty} \frac{(\frac{l_{ij}^B}{\sigma_{ij}})^{2m}}{(2m)!(2m-3)} \tag{6.47}$$

6.2.3.4 Barthel and Krienke Approach

Eq. 6.48 is the extension of the Ebeling model considering association at arbitrary distance [252, 253].

$$K_{ij}^{\circ}(T) = 8\pi \sum_i \sum_j \left[x_i x_j (l_{ij}^B)^3 B\Big(\frac{l_{ij}^B}{\sigma_{ij}}\Big) \right] \tag{6.48}$$

$B(x)$ is the Kirkwood function defined in Eq. 6.49:

$$B(x) = \sum_{k\geq 4}^{\infty} \frac{x^{k-3}}{k!(k-3)} \tag{6.49}$$

6.2.4 Comparison with simulations and Experiments

Our study aims to provide a comprehensive analysis of implicit solvent models designed to predict the thermodynamic properties of associative electrolyte solutions. We have selected four distinct models for our evaluation: EG, FLGG, BiMSA, and ZYS. As previously outlined, the EG and FLGG models are rooted in the chemical approach pioneered by Bjerrum. Conversely, BiMSA derives its principles from the solution of the WOZ equation [19, 20, 246–250]. ZYS, meanwhile, is grounded in the RCA methodology, an innovation by Stell and his team [27, 240–245].

To reiterate, our study revolves around two pivotal inquiries. Firstly, we are probing whether factoring in ion pairing offers a more accurate picture of the electrostatic interactions in electrolyte solutions. Secondly, we aim to determine if there exists a single ion-ion association model that stands out in terms of overall performance.

Our investigation is structured into two distinct segments. In the initial part, we compare the MIAC as predicted by the models against the numerical solutions of the PB equation and MC simulations. In the subsequent part, the models' predictions of MIAC are contrasted with the experimental data, specifically focusing on 2:2 aqueous sulfate solutions. When comparing the model predictions with the numerical solutions of the PB equation, our focus is on dilute solutions characterized by ionic strengths not exceeding 0.4 $mol \cdot L^{-1}$. Conversely, when comparing the model predictions with both the MC simulations and the experimental data, we turn our attention to more concentrated solutions, those with ionic strengths up to 10 $mol \cdot L^{-1}$.

6.2.4.1 Comparison with Simulations

To reiterate, the foundation of the Debye and Hückel model is rooted in the simplification of the PB equation, achieved through its linearization. This step was crucial as it permitted the derivation of an analytical solution to the otherwise complex equation. This simplification

is valid under the assumption that the potential energy of a central ion is much lower than the thermal energy, expressed mathematically as $eZ_j\psi_i(r) \ll k_BT$.

This linear approximation is effective in situations where ions are sparsely distributed, particularly in dilute solutions. In such conditions, the significant distances between the central ion and its neighbors ensure that electrostatic interactions are not overly intense, thus validating the use of the approximated model.

However, certain conditions leads to violation of this assumption. High concentration solutions, which naturally have a higher ionic density, invalidate the assumption due to the proximity of ions to one another. Similarly, electrolytes with ions bearing high valence increase the electrostatic interactions, making the linearization of the PB equation less accurate. Lastly, in systems with low dielectric constants, the interactions between charges are amplified, again posing challenges to the assumption of linearity.

Therefore, as a corrective measure to account for these scenarios where the foundational assumption of the Debye and Hückel model is violated, the Bjerrum approach of considering ion-ion associations becomes vital. In electrolyte solutions, especially those deviating from ideal dilute conditions, these associations play a pivotal role in dictating the overall behavior and thermodynamics of the system. They help correcting the shortcomings of the linearized PB equation, ensuring a more accurate representation of the ionic environment.

Modeling electrolyte solutions with ion pairing can help to overcome the restrictions of the linearized PB equation. By evaluating the electrostatic contributions of various models against the numerical solution of the non-linearized PB equation (represented by IPBE), we can assess:

1. **Model Validation:** If a model that factors in ion pairing aligns well with IPBE, it indicates the model has appropriately accounted for the PB equation's linear approximation constraints.

2. **Relevance of Ion Pairing:** Comparing models that neglect ion pairing (e.g., DH and MSA) with IPBE and ion-pairing models will help determine the importance of including ion pairing in such models.

Figure 6.2 depicts a comparison of the electrostatic contributions of the EG, BiMSA, ZYS, and FLGG models with the IPBE for electrolyte solutions of 1:1, 2:2, and 3:3 types. The figure also presents the electrostatic contributions derived from the DH and MSA theories (as per equations C.25 and C.35, respectively) under the assumption of complete dissociation in the solution. Additionally, the association constant at infinite dilution (K°_{+-}) is determined using the Bjerrum model (as described in Eq. 6.44). It is worth noting that no parameters were adjusted to fit the IPBE in these plots.

From the given data, it is evident that for 2:2 and 3:3 electrolytes, the DH and MSA theories tend to over-predict, while other models lean towards under-prediction concerning the electrostatic contribution to the MIAC. In contrast, for 1:1 electrolytes, the estimations from all models converge. Previous research by Malatesta [256] has highlighted the DH theory's tendency for overprediction. Similarly, Silva et al. [257] indicated that linearizing the

Table 6.1. The electrostatic contribution of the models (for the EG and the FLGG models $\ln\gamma^{MAL} = \ln\alpha$). Reprinted from ref. [214], Copyright 2023, with permission from Elsevier.

Model	Electrostatic contribution
EG	$\ln\gamma^{MSA} + \ln\gamma^{MAL}$
FLGG	$\ln\gamma^{DH} + \ln\gamma^{DI} + \ln\gamma^{MAL}$
BiMSA	$\ln\gamma^{BiMSA} + \ln\gamma^{MAL}$
ZYS	$\ln\gamma^{MSA} + \ln\gamma^{MAL}$

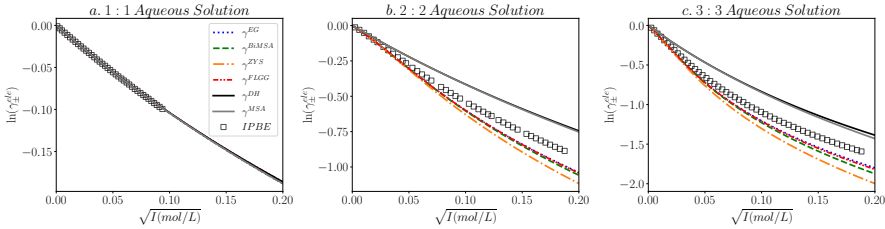

Figure 6.2. Comparison of the models' electrostatic contributions with the IPBE [256] for (a) 1:1 electrolytes with $\sigma = 4 \times 10^{-10}\,m$, (b) 2:2 electrolytes with $\sigma = 4 \times 10^{-10}\,m$, and (c) 3:3 electrolytes with $\sigma = 8 \times 10^{-10}\,m$, all calculated in aqueous solutions at 298.15 K. Reprinted from ref. [214], Copyright 2023, with permission from Elsevier.

PB equation leads to an overestimation of the MIAC. Nonetheless, the consistent underestimation observed in models that consider ion-ion association remains somewhat ambiguous. Given the uniformity of this underestimation across these associative models, the root cause might lie in a shared aspect: the association constant at infinite dilution, denoted as K°_{+-}.

Figure 6.3 demonstrates how the association constant influences the MIAC predictions within the FLGG model. The models K^{E}_{+-}, K^{B}_{+-}, and K^{BM}_{+-} are represented by Eq. 6.47, Eq. 6.44, and Eq. 6.44 (with ion pair distance set at $l_{+-} = 1.3\sigma$), respectively. The figure underscores that the choice of the reference state association constant model profoundly impacts the predicted MIAC by the FLGG model. Notably, for both 2:2 and 3:3 electrolyte solutions, employing the K^{BM}_{+-} model results in predictions that align closely with the IPBE values.

To address the discrepancy in using σ versus 1.3σ in Eq. 6.44, two crucial considerations are highlighted. Firstly, the initial presumption in Eq. 6.44 that solely contact ion pairs exist is contradicted by dielectric relaxation spectroscopy data [192], which shows the presence of various ion pair forms, namely contact ion pairs (CIP), solvent-shared ion pairs (SIP), and solvent-separated ion pairs (2SIP).

The second point is rooted in the fluid dynamics of the solution: the distance between ion pairs is not fixed but fluctuates, with its magnitude also being temperature-dependent.

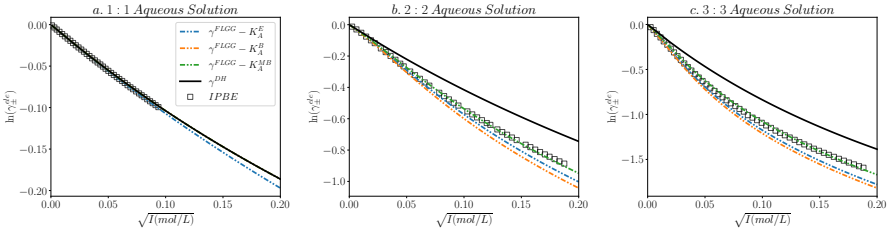

Figure 6.3. The electrostatic contribution of the FLGG model is notably influenced by the choice of infinite dilution association constant models. The figure highlights these effects across different σ values, specifically (a) $\sigma = 4 \times 10^{-10}\,m$, (b) $\sigma = 4 \times 10^{-10}\,m$, and (c) $\sigma = 8 \times 10^{-10}\,m$. Three models are compared: the Ebeling model (K^{E}_{+-}), the Bjerrum model (K^{B}_{+-}), and a modified Bjerrum model (K^{BM}_{+-}) for determining the association constant at infinite dilution. The IPBE data points, which serve as a reference, are sourced from Malatesta et al. [256]. Reprinted from ref. [214], Copyright 2023, with permission from Elsevier.

Thus, rather than assuming a static distance, it is more logical to adopt an average distance value, represented by $\langle r \rangle$. Levin and Fisher's study [233] posits that this average separation for ion pairs should not exceed 1.3σ (represented as $l_{+-}\langle r \rangle \leq 1.3\sigma$). Determining the precise average distance between ions at the macroscopic level is complex, which is why this study opts for the upper limit, 1.3σ, as an alternative for the ion pair separation distance. A more detailed adjustment of this parameter tailored to each model against MIAC experimental data at 298.15 K is presented in section 6.2.4.2.

In addition to IPBE, the predictions of the models can be compared with the MC simulations. Unlike comparison with the experimental data, the predictions of thermodynamic models can be compared with exactly the same systems without any concern about the impact of the solvent(s).

Figure 6.4 compares the predictions from various models with the MC simulations for two different 2:2 aqueous electrolyte solutions at 298.15 K. In Figure 6.4a, the designations L and VC represent MC simulations derived from references [258] and [259], respectively. Meanwhile, in Figure 6.4b, the labels MC-MI, MC-ES, and GCMC stand for canonical ensemble MC simulations employing the minimum image convention, canonical ensemble MC simulations using Ewald summation, and grand canonical MC simulations, respectively. Additionally, results from the DH and MSA theories have been incorporated with the hard sphere (HS) contribution derived from the CS equation (Eq. 6.16). This is done because MC simulations offer total MIAC, not just the electrostatic contribution. It is also noteworthy that in this figure, the modified Bjerrum model (K_{+-}^{BM}) has been employed as the association constant at infinite dilution across all models.

From Figure 6.4, it is evident that both HS+DH and HS+MSA models tend to overestimate the MIAC of charged spheres when compared with MC simulations. Conversely, the ZYS, BiMSA, FLGG, and EG models tend to predict values that are on the lower side. Notably, at diluted concentrations, the models which account for ion pairing ZYS, BiMSA, FLGG, and EG provide more accurate MIAC predictions than the HS+MSA and HS+DH models. However, as the concentration increases, the predictions from the HS+MSA, EG, and FLGG models align more closely with the results from MC simulations.

From the previous discussion, the contact distance between ion pairs is not necessarily the most accurate representation. To provide a more accurate description, we have introduced a modified distance between ion pairs. We define this distance as $l_{+-} = \theta \times \sigma$, where θ is a factor that can be adjusted to fit the predictions of MC simulations. The optimal values for θ are then used to determine the corresponding values of l_{+-} and K_{+-}° for each model. These

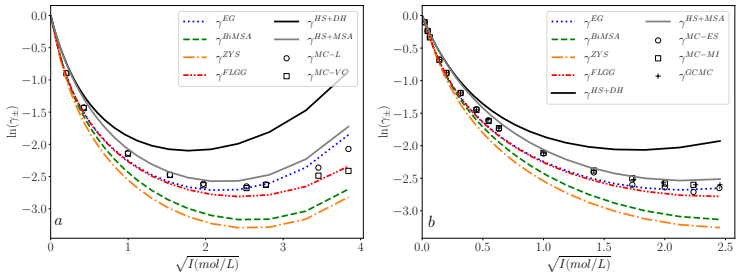

Figure 6.4. Comparison of the MIAC predicted by EG, FLGG, BiMSA, and ZYS models with the MC simulations for a 2:2 aqueous electrolyte solution at 298.15 when (a) $\sigma = 4.25 \times 10^{-10}$ m and (b) $\sigma = 4.2 \times 10^{-10}$ m (MC simulation data are used from ref. [260] for the graph (a) and from ref. [258, 259] for the graph (b)). Reprinted from ref. [214], Copyright 2023, with permission from Elsevier.

adjusted values, which better reflect the actual behavior of ions in solution, are presented in Table 6.2.

In Figure 6.5, the MIAC predictions made by various models are compared with MC simulations reported by Lamperski [258] in Figure 6.5a and by Gutiérrez-Valladares et al. [260] in Figure 6.5b, following the adjustments made to θ. This comparison elucidates that the models factoring in ion pairing yield an acceptable alignment with the experimental data. Nevertheless, it is worth noting that the predictions by EG and FLGG models are particularly more accurate, especially at lower concentrations. This suggests that these models, after adjustments, seem to have a superior accuracy in capturing the physics of the system.

Figure 6.6 displays the predicted fraction of free ions in the solution based on the models, plotted against the square root of ionic strength, both prior to and following the adjustment of θ. Within this figure, the black curves represent predictions using the K_{+-}^{BM} model. Meanwhile, the red curves employ the Bjerrum model, incorporating the l_{+-} values listed in Table 6.2 after their respective adjustments.

From the figure, it is evident that even though the MIAC predictions by the models (pre and post-adjustment of θ) are closely aligned, there is a notable difference in the predicted fractions of free ions. Moreover, the trends in the degree of dissociation (α) as predicted by the FLGG, ZYS, and BiMSA models align closely with one another but deviate from the trend indicated by the EG model.

The ZYS and BiMSA models predict notably lower fractions of ion pairs after adjusting θ when compared to the estimations of the FLGG and EG models. Regrettably, the literature does not offer any reported values for the fractions of free ions from MC simulations. As a result, it is challenging to comment further on the predicted fraction of free ions. Nevertheless, the predicted fraction of free ions greatly influences the prediction of the electrical conductivity of the electrolyte solutions [84, 120, 167]. Consequently, when ion pairing is a crucial factor, it is advisable to concurrently evaluate both the MIAC and electrical conductivity. Further elaboration on this matter will be provided in the subsequent section.

6.2.4.2 Comparison with the Experimental Data

In the preceding section, the predictions of the models were compared with outcomes from IPBE and MC simulations. It was demonstrated that a acceptable match between the

Table 6.2. This table presents the modifications in the distance between ion pairs and the corresponding association constant at infinite dilution, upon adjusting θ in the Bjerrum association constant model. Reprinted from ref. [214], Copyright 2023, with permission from Elsevier.

Model	l_{+-}	K_{+-}°	θ	l_{+-}	K_{+-}°	θ
	MC simulations from Gutiérrez-Valladares et al. [260]					
	Before adjustment			After adjustment		
EG	5.25	143.88	1.3	8.95	65.86	2.11
BiMSA	5.25	143.88	1.3	13.24	12.04	3.05
FLGG	5.25	143.88	1.3	7.99	81.12	1.85
ZYS	5.25	143.88	1.3	13.57	8.27	3.14
	MC simulations from Lamperski [258]					
	Before adjustment			After adjustment		
EG	5.46	145.37	1.3	6.18	120.11	1.47
BiMSA	5.46	145.37	1.3	12.81	16.72	3.05
FLGG	5.46	145.37	1.3	7.76	84.52	1.85
ZYS	5.46	145.37	1.3	13.19	12.36	3.14

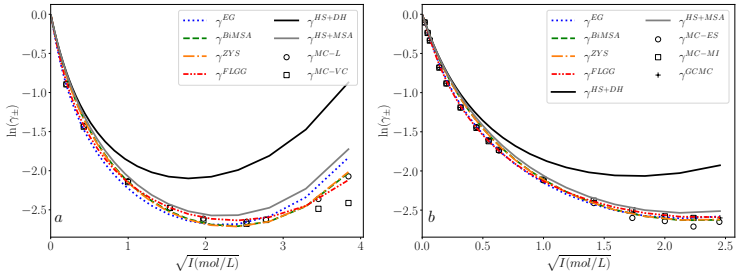

Figure 6.5. Similar to Figure 6.4, this figure contrasts the MIAC predictions by various models against MC simulations, but with the modification of θ in the Bjerrum association constant model. Reprinted from ref. [214], Copyright 2023, with permission from Elsevier.

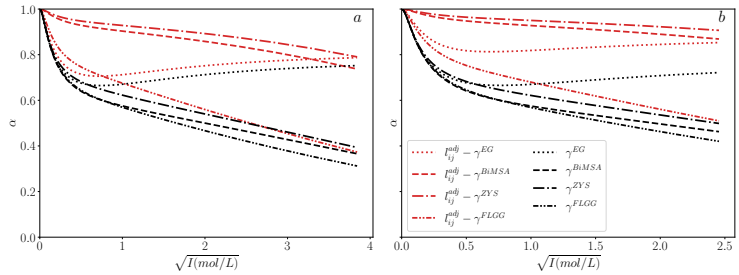

Figure 6.6. The graphs contrast the predicted fraction of free ions (α) from the EG, FLGG, BiMSA, and ZYS models for a 2:2 aqueous electrolyte solution at 298.15 K. This is depicted for cases (a) $\sigma = 4.2 \times 10^{-10}$ m and (b) $\sigma = 4.25 \times 10^{-10}$ m, both prior to and after the modification of θ. Reprinted from ref. [214], Copyright 2023, with permission from Elsevier.

models' predictions and the IPBE and MC simulations could be achieved by adjusting the time-averaged distance between ion pairs. However, the evolution of the fraction of free ions post-adjustment of l_{+-} was observed to be markedly distinct.

In this section, the predictions of the models in question will be assessed against the MIAC experimental data for four 2:2 aqueous sulfate solutions at 298.15 K. Subsequently, the ionic diameter and the time-averaged distance between ion pairs (l_{+-}) will be adjusted using the MIAC experimental data. The final step will involve the model parametrization being validated. This will be done by contrasting the electrical conductivity estimated by two model (either DHO-based or MSA-based) in conjunction with the models for associative electrolyte solutions introduced in sections 6.2.1 and 6.2.2 against experimental data.

It is noteworthy that the chosen systems exhibit pronounced ion-ion interactions in comparison to other forms of interactions, both electrostatic and non-electrostatic. As a result, the ion-solvent interactions, which were overlooked in the models explained in sections 6.2.1 and 6.2.2, exert a minimal influence on the solution's properties. This allows for the implicit solvent EoS, introduced in section 2, to be effectively employed in predicting the MIAC of these electrolytes.

In Table 3.1, the ionic diameters, ion valence types, and ionic conductivity at infinite dilution for ions at 298.15 K, which are utilized in the MIAC and electrical conductivity predictions of this section, are provided. The salt-specific diameters for $CdSO_4$, $CoSO_4$, $MgSO_4$, and $ZnSO_4$ are derived from the arithmetic average of the crystallographic ionic

radii as reported by Marcus [155] and tabulated in Table 3.1. Ionic conductivities at infinite dilution at 298.15 K are taken from values documented in the literature [120, 129].

Figure 6.7 presents a comparison between the model predictions and the MIAC experimental data for 2:2 aqueous electrolyte solutions at 298.15 K. In this representation, ionic diameters listed in Table 3 are applied across all models. The legends HS+DH and HS+MSA in the figure denote that MIAC is determined as the sum of hard sphere contributions and electrostatic inputs from the DH (Eq. 6.25) and MSA (Eq. 6.30) theories, respectively. In these two approaches, it is posited that the solution contains no ion pairs. Moreover, the K_{+-}^{BM} model is employed as the association constant at infinite dilution for all the models presented.

From the depicted figures, it is evident that the HS+DH and HS+MSA models tend to over-predict the MIAC for all systems at low to moderate ionic strengths. Yet, this discrepancy narrows with increasing ionic strength. A comparison between models that consider association (namely EG, FLGG, BiMSA, and ZYS) and those that do not (HS+DH and HS+MSA) at lower ionic strengths reveals that accounting for ion-pairing yields predictions that align more closely with the experimental data. Nevertheless, at higher ionic strengths, specifically at 1 $mol \cdot L^{-1}$, models both incorporating and disregarding ion pairing generally provide less accurate predictions for the MIAC of these electrolytes, with the exception of FLGG and EG for $CdSO_4$ and DH+HS for $MgSO_4$.

Among the models accounting for ion pairing, the EG and FLGG models yield predictions that align more closely with experimental data. Nonetheless, it is important to highlight that a consistent and precise match between theory and the experimental data is not observed across all systems. Interestingly, despite their differing theoretical foundations, the predictions from the EG and FLGG models are strikingly similar. While the EG model is rooted in the MSA theory, the FLGG model is derived from the DH theory. Furthermore, the EG model neglects the non-ideality of ion pairs in the solution and assumes that ion pairing does not influence hard sphere interactions.

6.2.5 Structural Properties; The Importance of Electrical Conductivity

As previously noted, once the distance between ion pairs is adjusted, the MIAC predictions from all models are in close agreement with each other and with the MC simulations. However, the models differ significantly in their predictions of the fraction of free ions (α). Therefore, it is essential to validate the predicted fraction of free ions with experimental data. Regrettably, direct measurements of the fraction of free ions (or ion speciation) are not feasible. Yet, the fraction of free ions can be indirectly validated using methods such as electrical conductivity [80, 81].

As detailed in Chapters 2-5, electrical conductivity is a transport property of electrolyte solutions, shedding light on ion movement under the influence of an external electric field. Given that ion pairs in symmetrical electrolytes are charge-neutral and do not contribute to the system's EC, this property serves as a valuable tool to examine ion pairing in electrolyte solutions.

Marcus and Hefter [80] outlined the pros and cons of examining ion pairing using electrical conductivity. A significant advantage is the high precision of electrical conductivity measurements, which can achieve a relative error of less than 0.02%. Moreover, electrical conductivity measurements are widely available for nearly all symmetrical electrolytes across various solvents. However, a notable drawback is that this approach is less relevant for asymmetrical electrolytes. In such cases, ion pairs are charged and thus contribute to the electrical conductivity.

As discussed in Chapter 3, the electrical conductivity of electrolyte solutions can be predicted using either the MSA or the DHO theory. Both theories have demonstrated the capability to predict the electrical conductivity of electrolyte solutions accurately when the

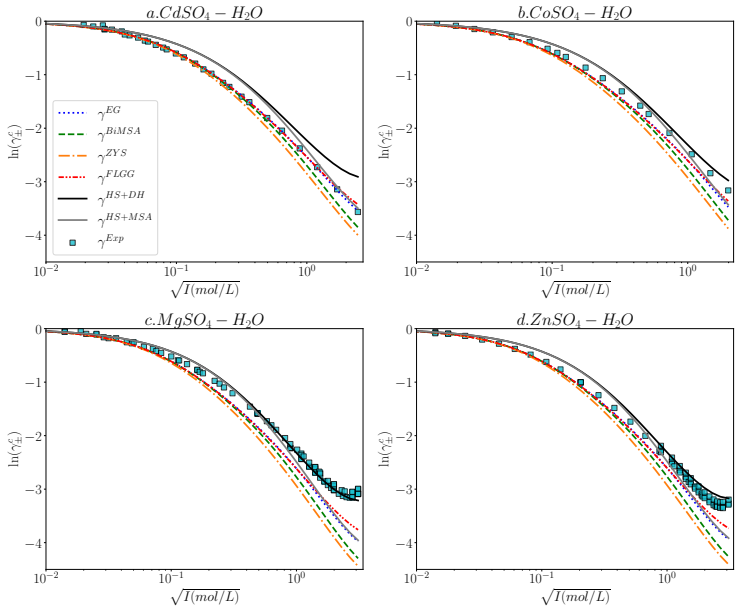

Figure 6.7. This figure compares the predicted MIAC of (a) $CdSO_4$, (b) $CoSO_4$, (c) $NgSO_4$, and (d) $ZnSO_4$ aqueous solutions at 298.15 K by the EG, BiMSA, ZYS, FLGG, HS+DH, and HS+MSA models. For these predictions, $l_{+-} = 1.3\sigma$ is applied in the Bjerrum association constant model. Experimental data are sourced from references [261–263]. Reprinted from ref. [214], Copyright 2023, with permission from Elsevier.

ion pairing is minimal. However, for systems like the 2:2 sulfate aqueous solutions, where ion pairing is significant [81, 189, 191–194, 264–267], the electrical conductivity models can be coupled with a thermodynamic model like EG, FLGG, BiMSA, or ZYS to address the partial dissociation.

In this section, as illustrated in Figure 6.8, we first adjust the values of σ and l_{+-} to match the MIAC experimental data at 298.15 K utilizing the EG, FLGG, ZYS, and BiMSA models. The Ebeling model serves as the foundation for the association constant at infinite dilution in this calibration process. Subsequently, leveraging the same parameters (σ and l_{+-}) and the fraction of free ions calculated from the MIAC models, we predict the electrical conductivity of the solutions using either DHO or MSA-based theories. Ultimately, the predicted electrical conductivity is compared with the experimental data as a validation step for the prediction of the fraction of free ions.

For estimating the electrical conductivity of solutions, two approaches are employed: an MSA-based method and a DHO-based one. In the MSA-based approach, we adopt the MSA-Simple model proposed by Chhih et al. [113]. Conversely, for the DHO-based approach, the DHO3 model formulated by Naseri Boroujeni et al. [124] is utilized. The specific and molar conductivities for both models can be derived from Eq. 2.67 and Eq. 6.50, respectively.

$$\chi = \frac{e^2}{k_B T} \sum_{i=1}^{C} \rho_i D_i^0 Z_i^2 \left(1 + \frac{\delta v_i}{v_i^0}\right)\left(1 + \frac{\delta k_i}{k_i}\right) \tag{2.67}$$

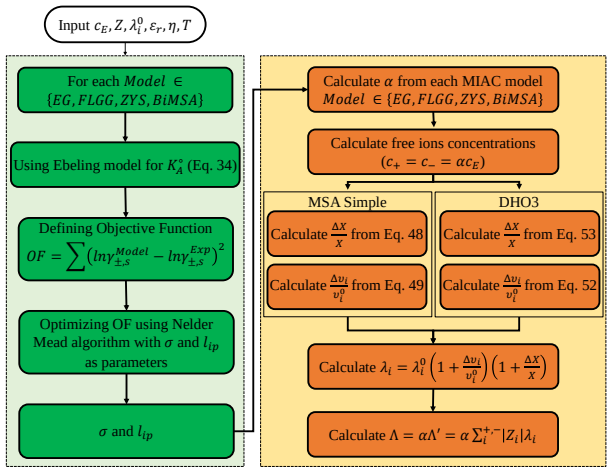

Figure 6.8. The approach used in this work to study concurrently the MIAC and the electrical conductivity of associative electrolyte solutions. Reprinted from ref. [214], Copyright 2023, with permission from Elsevier.

$$\Lambda = \frac{\chi}{c_E} \tag{6.50}$$

For the MSA-Simple model, equations 3.28 and 3.29 are used for the relaxation ($\delta k/k$) and the electrophoretic ($\delta v_i/v_i^0$) terms.

$$\frac{\delta v_i}{v_i^0} = -\frac{k_B T}{3\pi\eta D_i^0} \frac{\Gamma}{1+\Gamma\bar{\sigma}} \, , i = \{+ \, or \, -\} \tag{3.28}$$

$$\frac{\delta k}{k} = \frac{1}{24\pi\varepsilon_0\varepsilon_r k_B T} \frac{\kappa_q^2 e^2 Z_+ Z_-}{\bar{\sigma}\left(1+\Gamma\bar{\sigma}\right)^2} \frac{\left(1-\exp(-2\kappa_q\bar{\sigma})\right)}{\left[\kappa_q^2 + 2\Gamma\kappa_q + 2\Gamma^2\left(1-\exp(-\kappa_q\bar{\sigma})\right)\right]} \tag{3.29}$$

For the DHO3 model, equations 3.25 and 3.10 are used for the relaxation and the electrophoretic terms.

$$\frac{\delta k}{k} = \frac{Z_+ Z_- e^2}{12\pi\varepsilon_0\varepsilon_r k_B T} \left[\frac{q}{1+\sqrt{q}} \frac{\kappa}{\left(1+\kappa\sigma_{+-}\right)\left(1+\kappa\sigma_{+-}\sqrt{q}+\kappa^2\sigma_{+-}^2/6\right)}\right] \tag{3.25}$$

$$\frac{\delta v_i}{v_i^0} = -\frac{F^2}{6\pi\eta N_A \lambda_i^0} |Z_i| \frac{\kappa}{1+\kappa\sigma_{+-}} \, , i = \{+ \, or \, -\} \tag{3.10}$$

Additionally, the ionic conductivity at infinite dilution (λ_i^0) is taken from Table 3.1. In Eq. 3.28, the value for D_i^0 can be determined from the ionic conductivity at infinite dilution via the Nernst-Einstein equation, given as $D_i^0 = (k_B T N_A)/(F^2 \mid Z_i \mid)\lambda_i^0$.

In order to quantitatively evaluate the predictions from both MIAC and electrical conductivity models, we introduce the coefficient of determination (R^2) and the absolute average deviation in percentage (AAD%). These metrics are based on the comparison of predicted values to the experimental data. For R^2, it is derived using equations 6.51-6.53, where N_d denotes the number of experimental data points, y_i^{exp} represents the experimental data, y_i^{pre}

is the predicted value, and $\bar{y}^{exp}$ is the average of all experimental data. The formula for AAD% is given by Eq. 6.54.

$$R^2 = 1 - \frac{RSS}{TSS} \tag{6.51}$$

$$RSS = \sum_{i=1}^{N_d} (y_i^{exp} - y_i^{pre})^2 \tag{6.52}$$

$$TSS = \sum_{i=1}^{N_d} (y_i^{exp} - \bar{y}_i^{pre})^2 \tag{6.53}$$

$$AAD\% = \frac{1}{N_d} \sum_{i=1}^{N_d} \mid y_i^{exp} - \bar{y}_i^{pre} \mid \tag{6.54}$$

In the context of MIAC, errors are directly calculated using $\gamma_{\pm}^{exp}$ and $\gamma_{\pm}^{pre}$. However, for EC, to ensure a consistent comparison, both experimental data and predictions from the models are normalized by the molar conductivity at infinite dilution, denoted by Λ^0. As a result, for error calculations related to EC, $\Lambda_i^{exp}/\Lambda^0$ and $\Lambda_i^{pre}/\Lambda^0$ are employed.

Table 6.3 displays the parameters (σ and l_{+-}) that have been fine-tuned based on the MIAC experimental data using the EG, FLGG, ZYS, and BiMSA models. This table also presents the association constant at infinite dilution (K_{+-}°), the coefficients of determination (R^2), and the AAD% of these models when compared against both MIAC and electrical conductivity experimental data. Additionally, the table highlights the smallest AAD% and the largest R^2 values by underlining them.

In Figures 6.9 through 6.12, model predictions for MIAC, the fraction of free ions, molar conductivity as estimated by the MSA-Simple model, and molar conductivity based on the DHO3 model are presented. These predictions were generated using the EG, FLGG, ZYS, and BiMSA models for aqueous solutions of $MgSO_4$, $ZnSO_4$, $CoSO_4$, and $CdSO_4$ at a temperature of 298.15 K. Legends representing the specific model combinations for MIAC and electrical conductivity in these figures are detailed in Table 6.4. Experimental data points for both MIAC and electrical conductivity at ambient conditions are represented by cyan-colored squares.

From Figures 6.9-6.12 and Table 6.3, it is evident that all the MIAC models detailed in sections 6.2.1 and 6.2.2 offer accurate predictions for the MIAC of 2:2 sulfate solutions at ambient temperature. In terms of this property, the coefficients of determination for every solution and model exceed 0.95, and the AAD% values remain below 2%. This result is expected given that the ionic diameter (σ) and the distance between ion pairs (l_{+-}) were adjusted to fit the MIAC experimental data. It can be concluded that the models have the ability to be fitted to the experimental data.

Additionally, notable differences emerge in the predicted fractions of free ions among the models. The EG model, in particular, showcases a distinct trend where α initially declines with increasing ionic strength and then rises. In contrast, the other models demonstrate a consistent reduction in α with the rise in ionic strength. As depicted in graph b of Figures 6.9-6.12, for nearly all systems, the trend appears as: $\alpha^{ZYS} > \alpha^{BiMSA} > \alpha^{FLGG}$. Although it is highlighted earlier that no concrete conclusions can be drawn merely by comparing the MIAC or α estimated by the models elaborated in sections 6.2.1 and 6.2.2, it is undeniable that the varied predictions for the fractions of free ions by the MIAC models can substantially influence the molar conductivity predictions.

Observing graphs c and d in Figures 6.9-6.12, it is evident that when estimating the fractions of free ions by the FLGG model, the predicted electrical conductivity aligns most

Table 6.3. The parameters fine-tuned to the MIAC experimental data for each model are presented, along with the corresponding coefficient of determination and the absolute average deviation percentage for both MIAC and electrical conductivity predictions. Reprinted from ref. [214], Copyright 2023, with permission from Elsevier.

Model	σ	l_{+-}	K°_{+-} M^{-1}	R^2 $\gamma_{\pm}$	$AAD\%$ $\gamma_{\pm}$	R^2 MSAS	$AAD\%$ MSAS	R^2 DHO3	$AAD\%$ DHO3
Salt	$CdSO_4$								
EG	3.25	3.81	248.4	0.996	1.03	0.960	4.26	0.814	8.48
BiMSA	3.86	3.97	221.2	0.996	1.35	0.989	2.89	0.963	4.90
FLGG	3.25	3.76	257.1	0.996	1.02	0.994	1.52	0.966	3.63
ZYS	3.96	4.51	160.4	0.995	1.71	0.934	6.41	0.861	9.02
Salt	$CoSO_4$								
EG	3.49	4.65	150.0	0.997	0.89	0.982	3.09	0.923	5.60
BiMSA	4.04	4.88	135.2	0.997	1.16	0.992	2.25	0.974	3.78
FLGG	3.24	4.85	137.0	0.997	1.05	0.995	1.54	0.981	3.25
ZYS	4.12	5.92	95.1	0.995	1.53	0.958	5.26	0.917	7.20
Salt	$MgSO_4$								
EG	3.76	5.87	96.4	0.999	0.68	0.952	5.30	0.854	8.20
BiMSA	4.06	7.07	72.4	0.998	0.84	0.992	5.15	0.972	7.18
FLGG	3.70	5.06	125.9	0.999	0.68	0.995	1.59	0.978	3.12
ZYS	4.02	10.63	43.1	0.997	1.00	0.916	7.72	0.834	10.29
Salt	$ZnSO_4$								
EG	3.59	4.29	180.7	0.999	0.39	0.973	3.95	0.893	6.92
BiMSA	4.00	5.13	122.7	0.999	0.66	0.995	4.36	0.983	6.21
FLGG	3.57	4.13	198.7	1.000	0.40	0.996	1.33	0.986	2.57
ZYS	3.96	7.00	73.6	0.996	0.85	0.929	7.63	0.865	10.16

Table 6.4. The notation used in Figures 6.9-6.12 shows the employed models for the MIAC and the electrical conductivity. Reprinted from ref. [214], Copyright 2023, with permission from Elsevier.

	electrical conductivity Model	
	MSA-simple	DHO3
EG	$\Lambda^{MSAS} - \gamma^{EG}$	$\Lambda^{DHO3} - \gamma^{EG}$
FLGG	$\Lambda^{MSAS} - \gamma^{FLGG}$	$\Lambda^{DHO3} - \gamma^{FLGG}$
ZYS	$\Lambda^{MSAS} - \gamma^{ZYS}$	$\Lambda^{DHO3} - \gamma^{ZYS}$
BiMSA	$\Lambda^{MSAS} - \gamma^{BiMSA}$	$\Lambda^{DHO3} - \gamma^{BiMSA}$

closely with the experimental data for both MSA-Simple and DHO3 models. For solutions with low to medium ionic strength, the EG model provides the next best fit, whereas for solutions with high ionic strength, the BiMSA model emerges as the second-best fit. Notably, predictions of molar conductivity are least accurate when no ion-ion association is assumed in the solutions, irrespective of the chosen molar conductivity model. This interpretation is further supported quantitatively by Table 6.3. The data reveals that the highest R^2 values or the lowest AAD% values for molar conductivity predictions occur when the FLGG model estimates the fractions of free ions. This suggests that the FLGG model may offer a more accurate representation of the underlying physics compared to the other models.

To understand why the FLGG model provides a more accurate representation of the underlying physics compared to other models, it is essential to revisit the similarities and distinctions among these models. The primary variation between the FLGG and other models lies in the theory they employ for ion-ion interactions. Specifically, the FLGG model adopts the DH theory, while other models use the MSA theory. The FLGG model adopts a

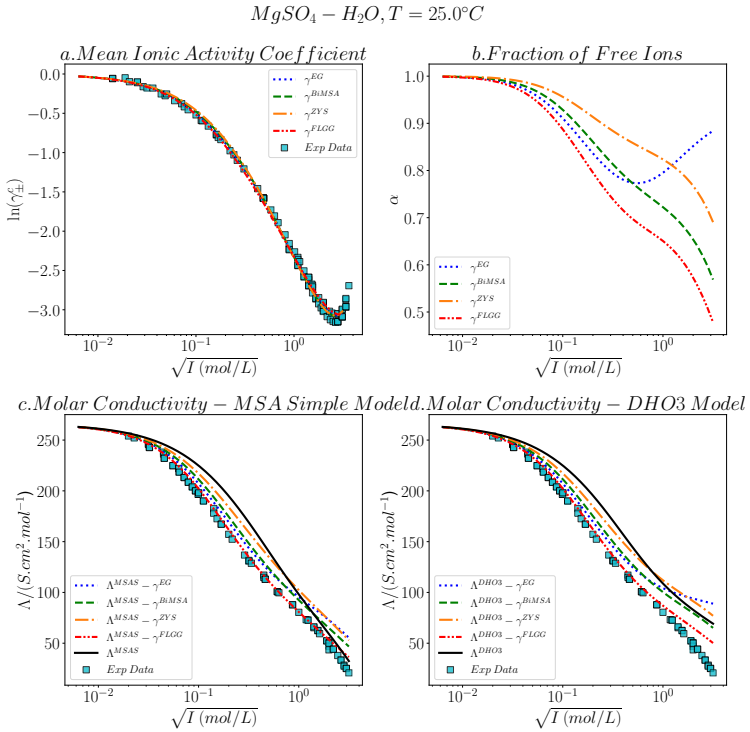

Figure 6.9. (a) MIAC, (b) fraction of free ions, (c) molar conductivity as predicted by the MSA-Simple model, and (d) molar conductivity as predicted by the DHO3 model for the $MgSO_4$-H_2O binary system at 298.15 K. The MIAC experimental data are sourced from ref. [261, 262], while the electrical conductivity experimental data are derived from ref. [129, 130]. Reprinted from ref. [214], Copyright 2023, with permission from Elsevier.

chemical approach, mirroring the EG model. Yet, the FLGG model acknowledges the non-ideality of ion pairs, distinguishing it from the EG model but aligning it with the ZYS model. Within the ZYS model, the assumption is that the cavity function can be approximated using the function at the non-association limit.

The discrepancies in molar conductivity predictions when using the fraction of free ions as predicted by the EG model can likely be linked to its assumption regarding ideal ion pairs in the solution ($\gamma_{+-} = 1$). While it is reasonable to consider ion pairs as ideal at lower ionic strengths, as suggested by certain studies [268], this assumption becomes invalid at higher ionic strengths. Given that ion pairs act as strong dipoles, they cannot be assumed to be ideal under such conditions. As a result, when the activity coefficient of ion pairs at elevated ionic strengths surpasses one, assuming ideal ion pairs can inadvertently lead to an overestimation of the fraction of free ions as ionic strength increases.

The less accurate predictions of the ZYS model might stem from the approximation used for the cavity function. Though this is a plausible explanation, it warrants a more comprehensive examination, which goes beyond the scope of this study. Lastly, while the predictions based on fractions of free ions calculated by the BiMSA model align fairly well with the electrical conductivity experimental data, they still do not match the accuracy

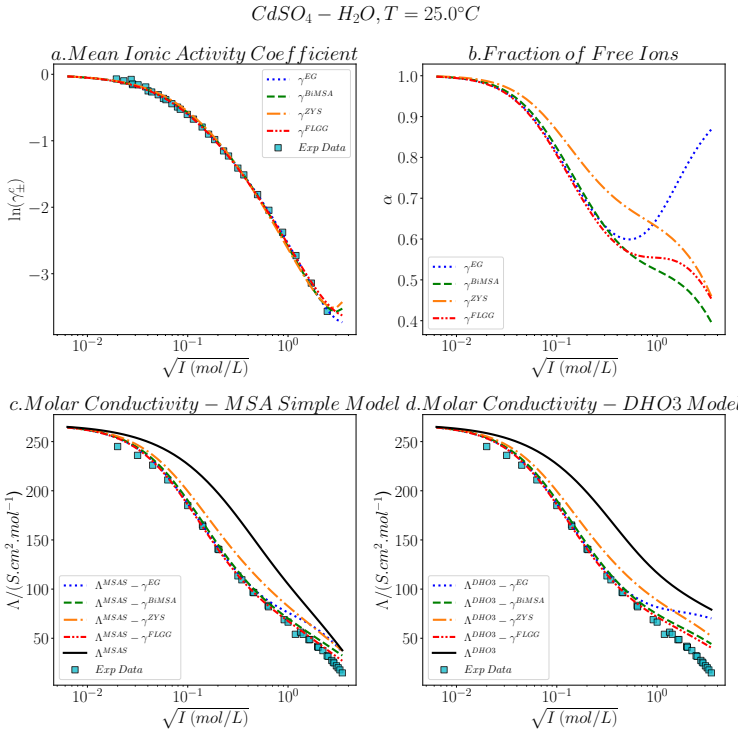

Figure 6.10. Similar to Figure 6.9, but for the $CdSO_4$-H_2O binary system at 298.15 K. The MIAC experimental data are sourced from ref. [261], while the electrical conductivity experimental data come from ref. [129]. Reprinted from ref. [214], Copyright 2023, with permission from Elsevier.

achieved by the FLGG model.

Furthermore, delving into the various contributions to the MIAC - specifically from electrostatic interactions, the MAL, HS, and, in the context of the FLGG model, DI contributions - might shed light on the exceptional precision of the FLGG model. Figures 6.13-6.16 depict the contributions from HS (illustrated by blue lines), electrostatic (denoted by black lines), MAL (represented by green lines), and DI interactions (highlighted by red lines) to the MIAC of $MgSO_4$, $CdSO_4$, $CoSO_4$, and $ZnSO_4$-H_2O solutions at 298.15 K, as predicted by the FLGG, EG, ZYS, and BiMSA models.

From the depicted figure, it is evident that the primary contribution to the MIAC across all models stems from electrostatic interactions. Following that, contributions from the MAL and HS contributions rank as the second and third most significant, respectively. For the FLGG model, the DI interactions offer a relatively minor negative contribution to the MIAC.

The FLGG model exhibits the least negative contribution from electrostatic interactions, while the ZYS model (at low ionic strengths) and the EG model (at high ionic strengths) show the most pronounced negative contributions. When considering the MAL, the BiMSA model contributes the least, while the EG model stands out with the most significant contribution. In terms of HS contributions to the MIAC, the order is ZYS > BiMSA > EG > FLGG.

In the FLGG model, the negative contributions to the MIAC arise from ion-ion, DI, and MAL contributions. In contrast, for the other models, these negative contributions

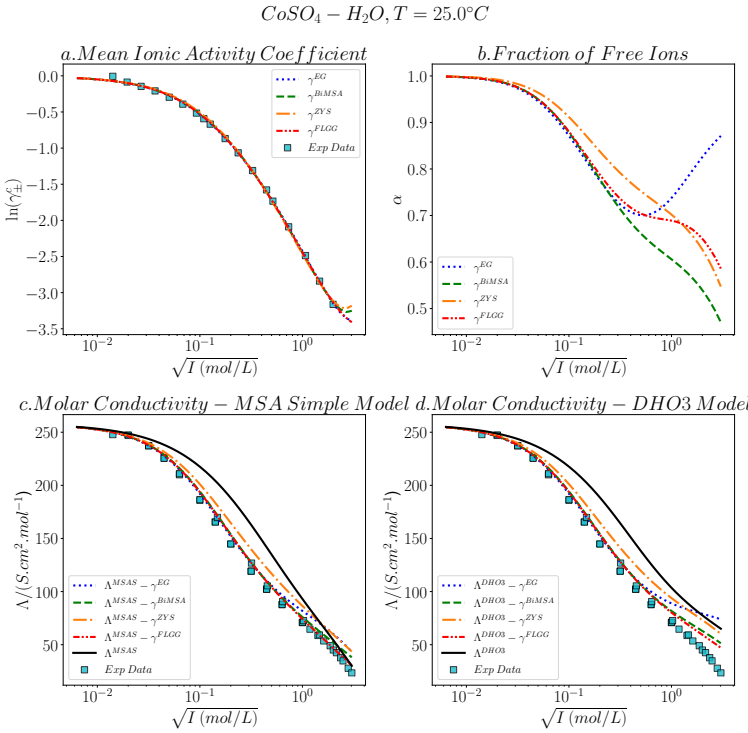

Figure 6.11. Similar to Figure 6.9, but for the $CoSO_4$-H_2O binary system at 298.15 K. The MIAC experimental data are sourced from ref. [261], while the electrical conductivity experimental data come from ref. [129, 213]. Reprinted from ref. [214], Copyright 2023, with permission from Elsevier.

stem solely from ion-ion and MAL contributions. During the model's fitting to the MIAC experimental data, parameters are fine-tuned (via the optimization algorithm) such that the sum of these negative effects, combined with the positive influence of HS interactions, aligns closely (within a certain tolerance) to the experimental data. As a result, a stronger negative contribution from ion-ion interactions necessitates a lesser negative input from the MAL, yielding a larger fraction of free ions. Given that the fraction of free ions plays a pivotal role in predicting molar conductivity, a reduced fraction results in more significant deviations from experimental conductivity data. Therefore, achieving a harmonious balance between the contributions of ion-ion interactions and the MAL is crucial for an accurate representation of the free ion fraction. The illustrations in Figures 6.9-6.12 indicate that the FLGG model adeptly maintains this balance.

Figure 6.17a displays the molar conductivity predictions of the MSA-Simple model with fractions of free ions derived from the FLGG model across different temperatures. Meanwhile, Figure 6.17b illustrates the MIAC as predicted by the FLGG model over a range of temperatures. Within this illustration, experimental data points are denoted by colored squares, with the shade of the markers and lines representing the temperature of the system, corresponding to the color bar situated to the figure's right. Across all temperatures, the parameters outlined in Table 6.3 are employed for both MIAC and molar conductivity predictions. Ionic conductivities at infinite dilution are also adopted from literature values [130].

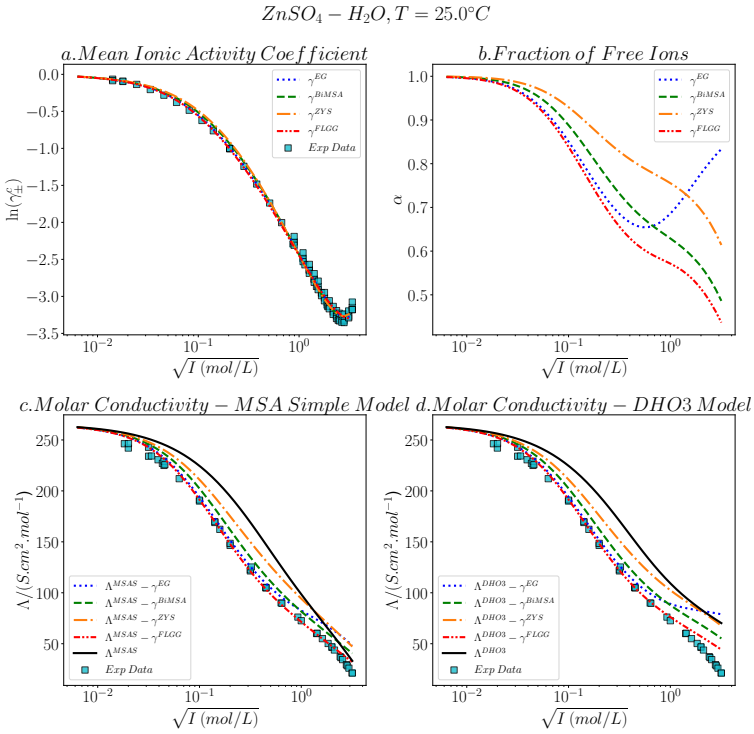

Figure 6.12. Similar to Figure 6.9, but for the $ZnSO_4$-H_2O binary system at 298.15 K. The MIAC experimental data are sourced from ref. [262], while the electrical conductivity experimental data come from ref. [129, 213]. Reprinted from ref. [214], Copyright 2023, with permission from Elsevier.

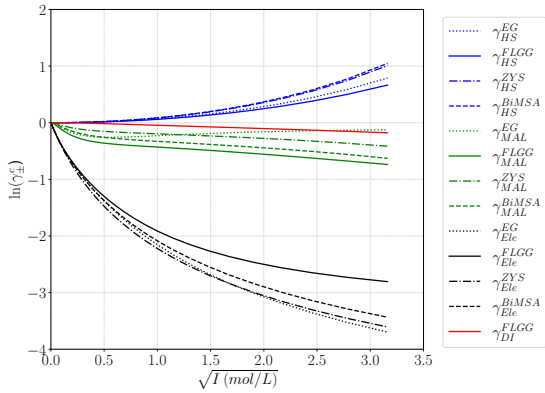

Figure 6.13. Predicted contributions to the activity coefficient of the $MgSO_4$ aqueous solution at 298.15 K by the FLGG, EG, ZYS, and BiMSA models. Reprinted from ref. [214], Copyright 2023, with permission from Elsevier.

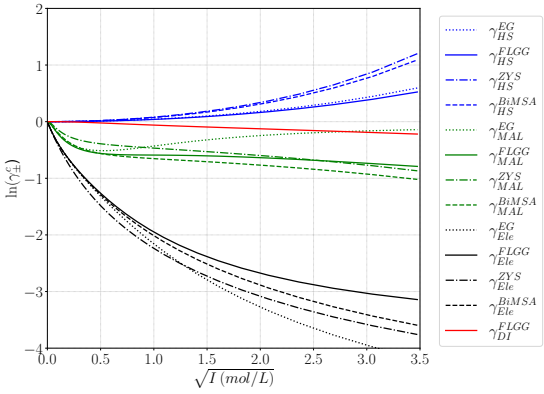

Figure 6.14. Predicted contributions to the activity coefficient of the $CdSO_4$ aqueous solution at 298.15 K by the FLGG, EG, ZYS, and BiMSA models. Reprinted from ref. [214], Copyright 2023, with permission from Elsevier.

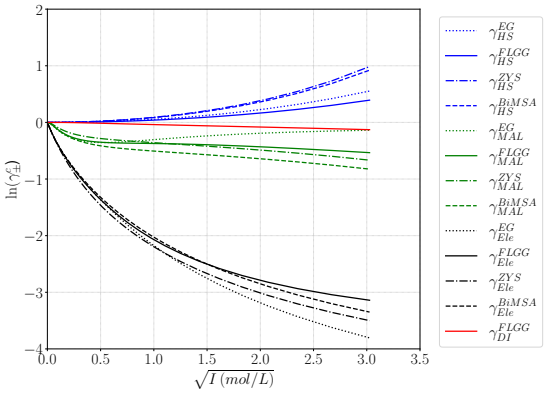

Figure 6.15. Predicted contributions to the activity coefficient of the $CoSO_4$ aqueous solution at 298.15 K by the FLGG, EG, ZYS, and BiMSA models. Reprinted from ref. [214], Copyright 2023, with permission from Elsevier.

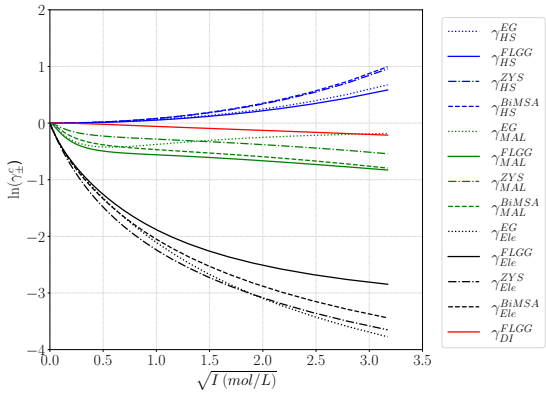

Figure 6.16. Predicted contributions to the activity coefficient of the $ZnSO_4$ aqueous solution at 298.15 K by the FLGG, EG, ZYS, and BiMSA models. Reprinted from ref. [214], Copyright 2023, with permission from Elsevier.

Observing the figure, it is evident that an impressive alignment between theory and experiment is observed across diverse temperatures for both MIAC and molar conductivity, when utilizing the MSA-Simple and FLGG models.

6.3 Summary and Conclusions

In this chapter, we conducted a comprehensive assessment of four implicit solvent models for associative and two for non-associative electrolyte solutions. Our focus was on the MIAC and molar conductivity of these solutions. The models for associative electrolyte solutions we examined were the EG, FLGG, ZYS, and BiMSA models. The EG and FLGG

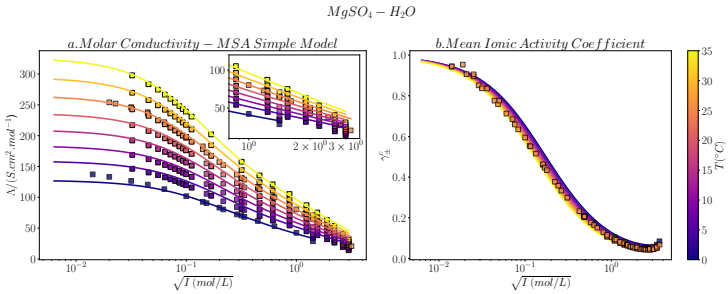

Figure 6.17. (a) The molar conductivity and (b) the MIAC for $MgSO_4$-H_2O solutions across different temperatures, as predicted by the MSA-Simple and FLGG models. These predictions are compared against the experimental data (depicted as colored squares). The predictions utilize parameters from Table 3.1. The experimental data for MIAC are sourced from references [261, 262, 269], and the electrical conductivity experimental data comes from references [129, 130]. Reprinted from ref. [214], Copyright 2023, with permission from Elsevier.

models use a chemical approach, ZYS is based on the RCA, and BiMSA is derived from the WOZ equation. The non-ion-pairing models combine the hard sphere component with the electrostatic contributions from DH (labeled HS+DH) and MSA (labeled HS+MSA) theories.

This research aimed to answer two main questions: Is the addition of ion pairing in modeling electrolyte solutions essential for a more accurate prediction of the MIAC? And which of the associative equations of state is the most effective? To answer these, we compared the predicted MIAC from the models with the IPBE, the MC simulations, and the experimental data.

We observed that the predictions of the models that did not take into account ion pairing were more accurate than those that did when compared to the IPBE. Interestingly, when the contact separation distance of ion pairs in the Bjerrum model was replaced with an extended average value, the electrostatic contribution predicted by the FLGG model was in agreement with the IPBE. When compared to the MC simulations, the MIAC predictions from FLGG, EG, and HS+MSA were similar to the MC simulations of a 2:2 electrolyte solution. By adjusting the average ion pair distance to fit the MC simulations, we found that while all models could be adjusted to match the MIAC from the MC simulations, the fraction of free ions they predicted varied.

We investigated the effect of high-valence electrolytes on ion pairing in aqueous solutions, examining four 2:2 electrolyte solutions. The results showed that the FLGG, EG, and HS+MSA models were more accurate in predicting the experimental data than other models for 2:2 electrolytes.

We adjusted the hard sphere diameter and ion pair separation distance to fit the MIAC experimental data for 2:2 aqueous solutions at 298.15 K. We then calculated the molar conductivity of these solutions, based on the fraction of free ions from MIAC models and two electrical conductivity models. Qualitative and quantitative evaluations showed that the electrical conductivity predictions were in better agreement with the experimental data when the free ion fractions were estimated using the FLGG model. This implies that the FLGG model more accurately captures the physics of associative electrolyte solutions than the other models.

Chapter Message

This chapter has concluded that the FLGG model, which includes ion pairing, is the most accurate in predicting MIAC for electrolyte solutions. This conclusion was only achievable through the validation of the fraction of unbound ions using electrical conductivity.

CHAPTER 7

Binding Debye-Hückel Theory

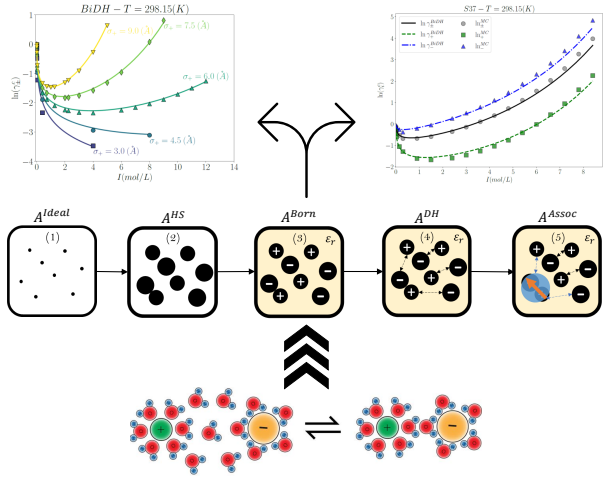

In the literature, two theories are mainly used to describe long-range ion-ion interactions in electrolyte equations of state. These theories, DH [4] and MSA [5, 6], assume that the solvent is a continuous medium and the ions are charged spheres. It is also assumed that electrolytes completely dissociate in the solution. However, research has demonstrated that this assumption is not always valid, depending on the electrolyte, solvent, and conditions [80, 81, 148, 189, 192, 194, 264].

To address the limitations of assuming complete dissociation in electrolyte solutions, a more realistic approach has been adopted. Rather than assuming instantaneous full dissociation, it is now accepted that electrolytes completely dissociate when they are dissolved in the liquid. Following this initial dissociation, ions with opposite charges exhibit a propensity to form ion pairs or even higher aggregates in the solution.

As described in Chapter 6, the consideration of ion-ion association can be approached through two main methods: the chemical approach, and the statistical mechanics approach.

The chemical approach [220–222, 225–229, 232–234, 237, 270] considers ion pairs as distinct species in the solution. This approach modifies the thermodynamic reference, so that only the free ions contribute to electrostatic interactions. Subsequently, the MAL equation is solved numerically to calculate the chemical potential and the associated properties of the electrolyte solutions.

The second approach is based on Wertheim's formulation [246–251] for the saturation effects in the Ornstein-Zernike equations. BiMSA [19, 20] and AMSA [21–29] are derived from this approach.

BiMSA-EXP, an adaptation of BiMSA, has been widely used to estimate the thermodynamic properties of real electrolyte solutions. Simonin and his colleagues have employed the BiMSA in a number of studies to analyze aqueous solutions with a concentration-dependent RSP and cation diameter [163, 188, 271–279].

Wertheim's formulation, which incorporates saturation effects within the Ornstein-Zernike equation, has been extended to include ion-ion associations beyond dimerization. However, this is not the focus of the current investigation. Those interested in further exploring this topic are encouraged to consult the references [23, 280–284] and related literature.

Stell and his colleagues [240,241,243,245] proposed a method to incorporate the MAL into the statistical mechanics treatment of ionic mixtures. This method involves approximating the cavity function with the reference cavity function in the non-association limit, and then computing the residual Helmholtz free energy due to ion-ion association based on Wertheim's results [242, 250, 285].

Subsequent research [242, 244] has demonstrated the potential of this approach to create an EoS for RPMs based on the MSA theory.

The literature in the field of ion-ion association has mainly focused on the MSA theory. Various models have been used to analyze different aspects of ion-ion association in electrolyte solutions. Nevertheless, recent studies have shown that the DH theory is just as effective as the MSA theory [9, 50, 73, 79], but is simpler to apply and derive. To take full advantage of the DH theory, more advanced models that include ion-ion association must be developed.

In this chapter, we explore the development of an EoS for a dimerizing charged hard sphere fluids. We employ the RCA proposed by Stell and colleagues [240, 241, 245] which incorporates the DH theory [4] to describe ion-ion interactions and the Kirkwood theory [235] to account for ion-dipole interactions. Additionally, we utilize Wertheim's result [242, 250, 285] to consider the contribution of association to the free energy.

We evaluate the performance of the developed EoS by comparing its predictions to MC simulations reported in the literature. We focus on the mean ionic activity, individual ionic activity, and osmotic coefficients, which are all essential for understanding the thermodynamic behavior and properties of the system.

Part of this chapter has already been published in the Journal of Chemical Physics:

- *Binding Debye-Hückel Theory for Associative e Electrolyte Solutions [286]* (Link).

7.1 Model Development

It is assumed that the mixture consists of M different cations and N different anions, all in a solvent that maintains a constant RSP (ε_r). The ions discussed in this research are distinguished by their individual diameters (σ_i) and their specific charge (Z_i). Moreover, the solvent(s) is characterized by the RSP.

The number density of ions and ion pairs after association are represented by $\tilde{\rho}_m$, $\tilde{\rho}_n$, and $\tilde{\rho}_{mn}$ in this chapter. The total number density of ions, which include both free ions and those in pairs, are denoted as ρ_m and ρ_n.

This section begins by introducing the RCA, which establishes a connection between the MAL and the ratio of activity coefficients when no association occurs. A method is then presented for calculating the fraction of unassociated ions (α_i) for a system with M types of cation and N types of anion, through the application of a specific equation for the RCA. It is then demonstrated that, in a particular case where only one type of cation and anion is present, the fraction of free ions can be determined analytically. Subsequently, the Bjerrum model [216] for the association constant at infinite dilution is discussed. Finally, the EoS is introduced, which includes the components contributing to the Helmholtz free energy.

7.1.1 Reference Cavity Approximation

The RCA developed by Stell and colleagues [27, 240, 242–245] is a theoretical foundation for understanding ion-ion association in electrolyte solutions. This approach is illustrated in Figure 7.1 with a thermodynamic cycle for the association of two ions, m and n, in both vacuum and fluid media. ΔG_2 and ΔG_4 represent the reversible work required to bring the two ions from an infinite distance to a separation of r in a vacuum and a fluid, respectively. ΔG_1 is the solvation free energy of the ion pair, and ΔG_3 is the sum of the solvation free energies of the individual ions.

The solvation free energy for a single ion pair (ΔG_1) is obtained from a thermodynamic cycle, as shown in Eq. 7.1.

$$\Delta G_1 = \Delta G_4 + \Delta G_3 - \Delta G_2 = \mu^r_{mn} \tag{7.1}$$

The residual chemical potential of the ion pair mn is represented by μ^r_{mn}. Stell and Zhou [241] showed that values for ΔG_2 and ΔG_4 can be obtained from equations 7.2 and 7.3, which are given below:

$$\Delta G_2 = u_{mn}(r) = \frac{Z_m Z_n e^2}{4\pi\varepsilon_0 r} \tag{7.2}$$

$$\Delta G_4 = -\frac{1}{\beta}\ln(g_{mn}(r)) \tag{7.3}$$

The total free energy change associated with the transfer of ions m and n from a vacuum to a fluid is calculated by summing the individual free energy changes.

$$\Delta G_3 = \mu^r_m + \mu^r_n \tag{7.4}$$

In these equations, $u_{mn}(r)$ denotes the pair potential, and $g_{mn}(r)$ represents the RDF between cation m and anion n. Additionally, the term β is defined as $1/k_B T$. The residual chemical potentials for ion m and ion n are indicated as μ^r_m and μ^r_n respectively.

The equation defining the cavity function that describes the interaction between ions m and n is provided as Eq. 7.5:

$$y_{mn}(r) \equiv g_{mn}(r)\exp(\beta u_{mn}(r)) \tag{7.5}$$

Substituting equations 7.2-7.4 into Eq. 7.1 and integrating Eq. 7.5, the resulting expression is as follows:

$$\ln(y_{mn}(r)) = \beta[\mu^r_m + \mu^r_n - \mu^r_{mn}(r)] \tag{7.6}$$

It is crucial to note that equations 7.1-7.6 directly mirror equations 2.2-6 as presented in ref. [241].

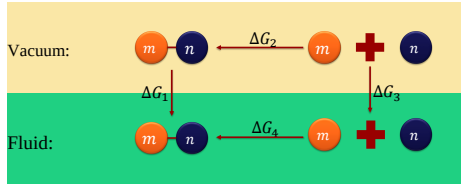

Figure 7.1. This figure presents a thermodynamic cycle for ion-ion association [240, 241, 243, 245]. Reproduced from ref. [286], with the permission of AIP Publishing.

Assuming a chemical equilibrium between ions m and n and the ion pair mn, this is represented as shown in Eq. 7.7:

$$m + n \rightleftharpoons mn \tag{7.7}$$

Applying the definition of the chemical potential as provided in Eq. 7.8, where $\mu_i^{id}(\boldsymbol{\rho}, T) = \mu_i^{\circ}(T) + \frac{1}{\beta}\ln(\rho_i)$ denotes the ideal gas chemical potential, and μ_i^r represents the residual chemical potential:

$$\mu_i(\boldsymbol{\rho}, T) \equiv \mu_i^{id}(\boldsymbol{\rho}, T) + \mu_i^r(\boldsymbol{\rho}, T) \tag{7.8}$$

And the chemical equilibrium equation (Eq. 7.9):

$$\sum_i \omega_i \mu_i = 0 \tag{7.9}$$

The association constant between ions m and n can be derived from Eq. 7.10.

$$K_{mn}(\boldsymbol{\rho}, T) = \frac{\tilde{\rho}_{mn}}{\tilde{\rho}_m \tilde{\rho}_n} = K_{mn}^{\circ}(T) y_{mn}(\boldsymbol{\rho}, T) \tag{7.10}$$

In Eq. 7.10, $K_{mn}^{\circ}(T)$ denotes the association constant at infinite dilution, and ω_i represents the stoichiometric coefficients.

Stell and colleagues [240] expanded upon Eq. 7.10 by including terms associated with the number density of ion pairs, as depicted in Eq. 7.11:

$$\frac{K_{mn}}{K_{mn}^{\circ}} = y_{mn} = \left(y_{mn}\right)_{\tilde{\rho}_{mn}=0} + \left(\frac{\partial y_{mn}}{\partial \tilde{\rho}_{mn}}\right)_{\tilde{\rho}_{mn}=0} \tilde{\rho}_{mn} + \cdots \tag{7.11}$$

They showed that the zeroth-order approximation of Eq. 7.11 is almost accurate when the association occurs at the surface of the repulsive core of the interactive potentials.

$$K_{mn} = \frac{\tilde{\rho}_{mn}}{\tilde{\rho}_m \tilde{\rho}_n} = K_{mn}^{\circ} y_{mn}^{ref} \tag{7.12}$$

Eq. 7.12 suggests that the cavity function for two free ions in the presence of both free ions and ion pairs can be accurately approximated by the cavity function for free ions when disregarding associations.

Zhou and Stell explored the accuracy of the assumption in their paper [243]. They discovered that the association within the repulsive core of ions can lead to an overestimation of the association extent, resulting in a higher calculated number density of ion pairs. However, they also confirmed that if the association occurs at the surface of the ions' repulsive core, the assumption is accurate within a reasonable margin of error. For further information, please refer to Figures 5 and 7 in their study [243].

Therefore, this assumption is generally reliable for ion-ion associations where the ions do not share electrons. In cases where ion complexes form that are not easily distinguishable from simple associations, one should be careful. It is possible that the assumption may overestimate the degree of association.

7.1.2 Equation of State

In this section, we employ Wertheim's two-density theory of association to construct a novel model that accommodates electrostatic interactions arising from ion-ion association. The formulation begins by considering mixtures with multiple cation and anion types. We then simplify the approach for single-salt electrolyte solutions, featuring only one type of

cation and anion, to illustrate the theoretical robustness and practical feasibility of our model. Subsequently, we delve into the Bjerrum approach, outlining the calculation of the association constant in a reference state. The section culminates in an exploration of the contributions to the Helmholtz free energy.

7.1.2.1 General Case

In our model, we examine a mixture containing various types of cations (M) and anions (N) within a continuous solvent medium. We assume that each ion possesses a single association site, excluding the formation of aggregates other than ion pairs. As a result, each cation-anion pair can potentially form an ion pair within the solution. To address this dimerization aspect, we adopt the Wertheim two-density framework (ρ_m and $\tilde{\rho}_m$). Here, ρ_m denotes the total number density of ions, while $\tilde{\rho}_m$ represents the number density of unbound ions. Additionally, ions are characterized by their diameter (σ_m) and valence (Z_m), and the solvent is defined by its RSP (ε_r). The number density of ion pairs composed of cation m and anion n is denoted by $\tilde{\rho}_{mn}$. The relationship among the total, unbound, and ion pair number densities is expressed in Eq. 7.13:

$$\rho_m = \tilde{\rho}_m + \sum_{l=1}^{N} \tilde{\rho}_{ml} \tag{7.13}$$

α_m is the fraction of unbound ions (free ions) defined as Eq. 7.14:

$$\alpha_m = \frac{\tilde{\rho}_m}{\rho_m} = 1 - \sum_{l=1}^{N} \frac{\tilde{\rho}_{ml}}{\rho_m} \tag{7.14}$$

By rearranging Eq. 7.12 and substituting in the unbound number densities from Eq. 7.14, the following result is obtained:

$$\tilde{\rho}_{mn} = K^{\circ}_{mn} y^{ref}_{mn} \left[\rho_m - \sum_{l=1}^{N} \tilde{\rho}_{ml}\right] \left[\rho_n - \sum_{l=1}^{M} \tilde{\rho}_{ln}\right] \tag{7.15}$$

Therefore, once the reference cavity function is established, the number density of ion pairs can be calculated by solving Eq. 7.15. The RCA can be determined by using equations 7.5 and 7.6, which are explained in section 7.1.1. For the cavity function affected by HS interactions, where the pair potential for a hard sphere fluid is zero ($u_{mn} = 0$), it is clear from Eq. 7.5 that it is equivalent to the RDF. The RDF at contact for a hard sphere fluid can be obtained from (Eq. 7.16).

$$g^{HS}_{mn}(\sigma_{mn}) = \frac{1}{1-\zeta_3} + \frac{2\sigma_m\sigma_n}{\sigma_{mn}} \frac{3\zeta_2}{(1-\zeta_3)^2} + (\frac{2\sigma_m\sigma_n}{\sigma_{mn}})^2 \frac{2\zeta_2^2}{(1-\zeta_3)^3} \tag{7.16}$$

In this equation, σ_{mn} is the distance of the closest approach defined as Eq. 7.17.

$$\sigma_{mn} = \frac{\sigma_m + \sigma_n}{2} \tag{7.17}$$

$$\zeta_l = \frac{\pi}{6} \sum_j \rho_j \sigma_j^l \ , l = \{0, 1, 2, 3\} \tag{7.18}$$

In the case that $l = 3$, ζ_l gives the packing factor.

In order to incorporate the electrostatic contributions within the reference cavity function, Eq. 7.6 is used. This equation requires the inclusion of the residual chemical potential due to both ion-ion and ion-dipole interactions in the non-association limit. In our analysis, we apply the DH theory to characterize ion-ion interactions and the Kirkwood theory to address ion-dipole interactions (for detailed derivations, please refer to the works cited [4,8,9,79,235]).

In the given context, it is posited that the DH theory for ion-ion interactions is encapsulated within a continuum medium of a solvent. Here, the equations designated by 7.19 through 7.21 elucidate this theory. Within these equations, the symbol A^{DH} is assigned to the residual Helmholtz energy that arises due to interactions among ions, and the variables N and ρ_{tot} signify the total ion count and the total ion number density, respectively.

$$\frac{\beta A^{DH}}{N} = -\frac{\sum_j \rho_j Z_j^2 \chi_j}{4\pi\rho_{tot}\sum_j \rho_j Z_j^2} \tag{7.19}$$

$$\chi_j = \frac{1}{\sigma_j^3}\left(\ln(1+\kappa\sigma_j) - \kappa\sigma_j + 0.5(\kappa\sigma_j)^2\right) \tag{7.20}$$

In this equation, κ is the inverse Debye length defined as Eq. 7.21.

$$\kappa^2 = \frac{e^2}{\varepsilon_0\varepsilon_r k_B T}\sum_{k=1}^{C}\rho_k Z_k^2 \tag{7.21}$$

It is worth noting that the DH expression for the residual Helmholtz free energy is a perturbation to the Helmholtz free energy of a HS fluid. Therefore, equations 7.19 and 7.21 make use of the ion density prior to association. The effect of ion-ion association is then taken into account by adding the residual Helmholtz free energy due to the ion-ion association to the Helmholtz free energy of the system.

The derivative of the residual Helmholtz free energy with respect to the mole number yields the residual chemical potential, as demonstrated in Eq. 7.22.

$$\frac{\mu_k^{DH}}{RT} = \frac{\sum_j \rho_j Z_j^2 \chi_j}{4\pi(\rho_{tot}\sum_j \rho_j Z_j^2)^2} Z_k^2 - \frac{Z_k^2}{4\pi\rho_{tot}\sum_j \rho_j Z_j^2}\left(\chi_k + \frac{\kappa}{2}\frac{\sum_j \rho_j Z_j^2 \xi_j}{\sum_j \rho_j Z_j^2}\right) \tag{7.22}$$

The derivative of the auxiliary function χ_i with respect to the inverse Debye length (κ) is denoted by ξ_j.

$$\xi_j = \frac{1}{\sigma_j^2}\left(\frac{1}{1+\kappa\sigma_j} + \kappa\sigma_j + 1\right) \tag{7.23}$$

Eq. 7.24 expresses the residual Helmholtz free energy that results from the interactions between dipolar ion pairs and ions in a solvent continuum medium, which was first proposed by Kirkwood [8, 235].

$$\frac{\beta A^{DI}}{N} = -\frac{3\sum_j \rho_j \delta_j^2 \beta_j \theta_j}{4\pi e^2 \rho_{tot}\sum_j \rho_j Z_j^2} \tag{7.24}$$

The dipole moments of the components in the solution are represented by δ_j, while β_j and θ_j are parameters that are specified in equations 7.25 and 7.26, respectively.

$$\beta_j = \left(\frac{\varepsilon_0\varepsilon_r}{2\varepsilon_0\varepsilon_r + \varepsilon_{in,j}}\right)^2 \tag{7.25}$$

In this equation, the permittivity of the ion j inside the core is represented by $\varepsilon_{in,j}$. We assume that the value of $\varepsilon_{in,j}$ is between 0 and $\varepsilon_0\varepsilon_r$, which implies that β_j is between $\frac{1}{9}$ and $\frac{1}{4}$.

$$\theta_j = \frac{1}{\sigma_j^5}(-4\kappa\sigma_j + (\kappa\sigma_j)^2 + 2\ln\left(1 + \kappa\sigma_j + 0.5(\kappa\sigma_j)^2\right) - 4\tan^{-1}(\kappa\sigma_j + 1) - \pi)) \tag{7.26}$$

The residual contribution to the chemical potential arising from ion-dipole interactions, as explained by the Kirkwood theory, can be determined by calculating the mole number derivatives of Eq. 7.24, as depicted in Eq. 7.27.

$$\frac{\mu_k^{DI}}{RT} = \frac{3\sum_j \rho_j\delta_j^2\beta_j\theta_j}{4\pi e^2}Z_k^2 - \frac{3}{4\pi e^2\sum_j \rho_j Z_j^2}\left(\delta_k^2\beta_k\theta_k + \frac{\kappa Z_k^2}{2}\frac{\sum_j \rho_j\delta_j^2\beta_j\tau_j}{\sum_j \rho_j Z_j^2}\right) \tag{7.27}$$

The derivative of θ_j with respect to the inverse Debye length is denoted by τ_j, as expressed in Eq. 7.28.

$$\tau_j = \frac{1}{\sigma_j^4}\left(\frac{(\kappa\sigma_j)^3}{1 + \kappa\sigma_j + 0.5(\kappa\sigma_j)^2}\right) \tag{7.28}$$

We need to calculate the residual chemical potential of ions in the non-association limit for the electrostatic contribution to the RCA. To do this, we use the equations 7.22 and 7.27 to calculate μ_m^r and μ_n^r. The residual chemical potential of the ion pairs in the non-association limit (μ_{mn}^r) is then calculated from these equations. The contribution of DH to the residual chemical potential of ion pairs (μ_{mn}^{DH}) is calculated using $Z_{mn} = Z_m + Z_n$ and χ_{mn} (where σ_{mn} is used instead of σ_k) instead of Z_k and χ_k in equation 7.22.

We can calculate the residual chemical potential in the absence of association considering an imaginary system with M types of cations, N types of anions, and $M \times N$ pairs of ions. In this system, the dipole moments of both cations and anions are set to zero ($\delta_m = 0$ and $\delta_n = 0$), and the number density of ion pairs (ρ_{mn}) is also set to zero. By taking the limit of Eq. 7.27 as $\tilde{\rho}_{mn}$ approaches zero, we can determine the contribution of ion-dipole interactions to the residual chemical potential. This can be done by using Eq. 7.29.

$$\left[\frac{\mu_{mn}^{DI}}{RT}\right]_{\tilde{\rho}_{mn}\to 0} = -\frac{3\delta_{mn}^2\beta_{mn}\theta_{mn}}{4\pi e^2\sum_j \rho_j Z_j^2} \tag{7.29}$$

The reference cavity function can be determined using Eq. 7.30, which is shown below:

$$\ln\left(y_{mn}^{ref}\right) = \beta\left[\mu_m^{ELE} + \mu_n^{ELE} - \mu_{mn}^{ELE}\right]_{\rho_{mn}\to 0} + \ln\left(g_{mn}^{HS}(\sigma_{mn})\right) \tag{7.30}$$

In Eq. 7.30, μ_m^{ELE} and μ_n^{ELE} are the chemical potentials due to electrostatic interactions, which are contributions from the DH theory (Eq. 7.22). Additionally, μ_{mn}^{ELE} is the chemical potential due to electrostatic interactions (both ion-ion and ion-dipole interactions) for the ion pairs mn when the number density of the ion pairs approaches zero. For a symmetric electrolyte, $\mu_{mn}^{ELE} = \mu_{mn}^{DI}$ and can be obtained from Eq. 7.29. For asymmetric electrolytes, $\mu_{mn}^{ELE} = \mu_{mn}^{DI} + \mu_{mn}^{DH}$ with $Z_{mn} = Z_m + Z_n$ and $\sigma_{mn} = 0.5(\sigma_m + \sigma_n)$.

Using Eq. 7.30 in Eq. 7.15, the number density of bonded ions ($\tilde{\rho}_{mn}$) and the proportion of free ions (α_i) can be calculated.

7.1.2.2 Single-salt System

In the special case where there is only one type of cation and anion in the solution, Eq. 7.15 can be solved analytically. This section provides an analytical solution to Eq. 7.15. The superscripts + and − are used to denote the cation and anion, respectively. Consequently, Eq. 7.15 can be simplified to Eq. 7.31, as follows:

$$\tilde{\rho}_{+-} = K^{\circ}_{+-} y^{ref}_{+-} [\rho_{+} - \tilde{\rho}_{+-}][\rho_{-} - \tilde{\rho}_{+-}] \tag{7.31}$$

$$\Delta_{+-} = K^{\circ}_{+-} y^{ref}_{+-} \tag{7.32}$$

We can determine the number density of ion pairs ($\tilde{\rho}_{+-}$) by solving the quadratic equation and using Eq. 7.32 to define Δ_{+-}. The result is given in Eq. 7.33.

$$\tilde{\rho}_{+-} = \frac{2\Delta_{+-}\rho_{+}\rho_{-}}{1 + \Delta_{+-}\rho_{tot} + \sqrt{1 + 2\Delta_{+-}\rho_{tot} + (\Delta_{+-}(\rho_{+} - \rho_{-}))^2}} \tag{7.33}$$

The fraction of free cations and anions can be determined using Eq. 7.34.

$$\alpha_{+} = 1 - \frac{\tilde{\rho}_{+-}}{\rho_{+}}, \alpha_{-} = 1 - \frac{\tilde{\rho}_{+-}}{\rho_{-}} \tag{7.34}$$

7.1.2.3 Association Constant at Infinite Dilution

Krienke and Barthel [252, 253] demonstrated that the association constant in the reference state can be linked to the potential of the mean force at infinite dilution (W°_{mn}), as expressed in Eq. 7.35:

$$K^{\circ}_{mn}(T) = 4\pi N_A \int_0^R r^2 \exp(-\beta W^{\circ}_{mn}) dr \tag{7.35}$$

$$W^{\circ}_{mn} = \begin{cases} \infty & \text{if} \quad r < \sigma_{mn} \\ \frac{Z_m Z_n e^2}{4\pi\varepsilon_0\varepsilon_r r} & \text{if} \quad r \geq \sigma_{mn} \end{cases} \tag{7.36}$$

If we take into account only the Coloumbic interactions for the potential of mean force (Eq. 7.36) as proposed by Bjerrum [216], Eq. 7.35 can be simplified to Eq. 7.37.

$$K^{\circ}_{mn}(T) = \begin{cases} 0 & \text{if} \quad l_{mn} < \sigma_{mn} \\ 4\pi N_A \int_{\sigma_{mn}}^{l_{mn}} r^2 \exp\left(\frac{2q}{r}\right) dr & \text{if} \quad l_{mn} > \sigma_{mn} \end{cases} \tag{7.37}$$

$$q = \frac{l_B}{2} = \frac{e^2 \mid Z_m Z_n \mid}{8\pi\varepsilon_0\varepsilon_r k_B T} \tag{7.38}$$

In his 1926 paper, Bjerrum evaluated the probability that an ion m is at a certain distance r from ion n. If Z_m and Z_n have the same sign, the probability increases with r. On the other hand, if they have opposite signs, there is a minimum at half of the Bjerrum length, l_B. He suggested that ions with opposite charges that are less than $l_B/2$ apart should be considered associated pairs. Nevertheless, he noted that this distinction between free and associated ions is somewhat arbitrary.

7.1.2.4 Contributions to the Helmholtz Free Energy

In the previous section, we discussed the reference cavity function used in our study (Eq.7.30), as well as methods for calculating the number density of free ions in a general situation (Eq. 7.15) and a particular single salt case (equations 7.33 and 7.34). This section will focus on the EoS, emphasizing the contributions to the Helmholtz free energy.

A schematic of the components that make up the Helmholtz free energy is shown in Figure 7.2. This diagram begins with the ideal gas, whose Helmholtz free energy contribution is given by Eq. 7.39 as outlined in ref. [68].

$$\frac{\beta A^{Ideal}}{N} = \left(\sum_j x_i \ln \rho_i \Lambda_i^3 \right) - 1 \tag{7.39}$$

The proportion of ion i relative to the total number of ions is represented by $x_i = N_i/N$, and the thermal de Broglie volume for ion i is indicated by Λ_i^3.

The following part of the Helmholtz free energy is due to the hard sphere contribution. We followed the HS contribution as described by Boublik [287] and Mansoori et al. [230], as outlined below:

$$\frac{\beta A^{HS}}{N} = \frac{1}{\zeta_0} \left[\frac{3\zeta_1\zeta_2}{1-\zeta_3} + \frac{\zeta_2^3}{\zeta_3(1-\zeta_3)^2} + \left(\frac{\zeta_2^3}{\zeta_3^2} - \zeta_0 \right) \ln(1-\zeta_3) \right] \tag{7.40}$$

The Helmholtz free energy has a third component, which is the solvation free energy of ions when they are moved from a vacuum to a solvent. To calculate this, we used the Born equation [288], as demonstrated in Eq. 7.41.

$$\frac{\beta A^{Born}}{N} = \frac{\beta e^2}{8\pi\varepsilon_0\rho_{tot}} \sum_i \frac{\rho_i Z_i^2}{\sigma_i} \left(\frac{1}{\varepsilon_r} - 1 \right) \tag{7.41}$$

It is worth noting that the diameter of the ions used in Eq. 7.41 can be different from the hard sphere diameter of the ions [42]. Generally, the Born equation of the equations of state for electrolyte solutions employs a different diameter, referred to as the Born diameter.

The fourth factor that contributes to the Helmholtz free energy is derived from the electrostatic interactions between ions. As mentioned above, the DH theory is used to take

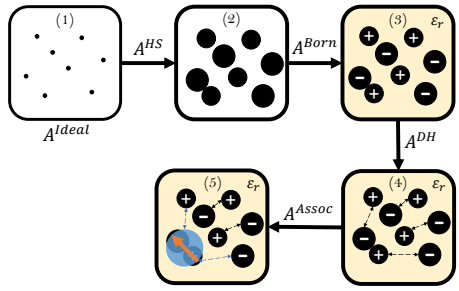

Figure 7.2. A schematic representation of the components of the Helmholtz free energy used in the BiDH theory is shown. These components are the ideal gas contribution (Eq. 7.39), the hard sphere contribution (Eq. 7.40), the solvation free energy based on the Born model (Eq. 7.41), the ion-ion interactions from the DH theory (Eq. 7.19), and the ion-ion association from the Wertheim theory (Eq. 7.42). Reproduced from ref. [286], with the permission of AIP Publishing.

these ion-ion interactions into account. The Helmholtz free energy contribution of the DH theory due to these interactions is shown in Eq. 7.19.

The last part of the Helmholtz free energy is derived from the ion-ion association, as shown in (5) of Figure 7.2. After calculating the proportion of free ions using the solutions from equations 7.15 and 7.30 or equations 7.33 and 7.34, the contribution of ion-ion association can be obtained based on the results of Wertheim's theory [250]. This has been further explored by Zhou et al. [244] and Chapman et al. [285], as demonstrated below.

$$\frac{\beta A^{Assoc}}{N} = -\sum_i \frac{\rho_i}{\rho_{tot}} \left[\ln(\alpha_i) + \frac{1-\alpha_i}{2} \right] \tag{7.42}$$

The Helmholtz free energy of the charged HS system can be determined by utilizing Eq. 7.43:

$$\frac{\beta(A - A^{Ideal})}{N} = \frac{\beta A^r}{N} = \frac{\beta}{N}(A^{HS} + A^{DH} + A^{Assoc} + A^{Born}) \tag{7.43}$$

It is important to note that the total number density of ions (ρ_i) is included in all the equations mentioned above. The use of this metric in equations 7.22 and 7.29 is due to the approximation of the cavity function by its non-association limit counterpart. Therefore, when calculating the cavity function as shown in Eq. 7.30, it is essential to use the total number density of ions.

The utilization of the total number density of ions for ion-ion interactions, as shown by A^{DH} in Eq. 7.43, is made clear when observing Figure 7.2. This figure demonstrates that the ion-ion association is seen as a free energy perturbation in comparison to the non-association baseline (transitioning from (4) to (5)). This method, which is different from the chemical approach found in the literature [220–222, 225, 228, 229, 232–234, 236], keeps the ideal gas reference of the system unchanged. Thus, until the last step, the system only consists of ions. The formation of ion pairs is only taken into account during the final stage, indicating its effect on the free energy of the system.

The residual Helmholtz free energy can be used to calculate other thermodynamic properties of the system. This is done by taking the derivatives of the residual Helmholtz free energy, as shown in Eq. 7.43, in accordance with the instructions given by Mollerup and Michelsen [8].

7.2 Model Validation

This research concentrates on the formation of a novel EoS for a charged hard-sphere fluid that takes into account the ion-ion association. The EoS was created by combining the DH theory with the RCA and Wertheim's theory. In the preceding section, the residual Helmholtz free energy for a system of charged hard spheres was discussed.

This section aims to evaluate the predictive power of the constructed model. It is important to note that the model disregards the structure of the solvent. Therefore, when the model's predictions are compared with the experimental data, extra attention must be paid to ion-solvent interactions, making the validation of the model more complex. Nevertheless, it is still beneficial to compare the model predictions with molecular simulations, as this enables an exact comparison of the same system without any concerns about parameters or neglected physics of the system.

This section examines the accuracy of the BiDH model by comparing its predictions of mean ionic activity, individual ionic activity, and osmotic coefficients with those from the MC simulations of charged hard-sphere fluids.

We have taken steps to reduce the risk of bias and improve the strength of theory validation through MC simulations. To do this, we have used data from a variety of sources, including the simulations mentioned in Table 7.1. By utilizing MC simulations from multiple sources, we can evaluate the accuracy of the theoretical model in different contexts, which can demonstrate the generalizability and usefulness of the models beyond certain situations.

We evaluated the performance of our model by collecting a database of MC simulations from the literature. These simulations were for aqueous solutions with single salt and assumed the solvent was a continuous medium with constant RSP. The database included simulations for 1:1, 2:1, 3:1 and 2:2 electrolytes and had a total of 1,172 MIAC, 1,667 IIAC and 1,396 osmotic coefficient data points.

Table 7.1 summarizes the ionic diameter, the ionic valence type, and the system names associated with them. The systems are divided into four categories based on the starting letter of their names, and their respective references are provided. Systems beginning with "S" are from ref. [289] and have a RSP of 78.308. These include MIAC, IIAC, and the osmotic coefficient. Systems starting with "G" are sourced from ref. [260] and have a RSP of 78.5. They comprise the MIAC and the osmotic coefficient. Systems beginning with "L" are obtained from ref. [258] and have a RSP of 78.55. They consist of MIAC and IIAC. Systems starting with "V" are referenced in [290] and have a RSP ranging from 20 to 120. These also include MIAC and IIAC. All the mentioned systems are at a temperature of 298.15 K.

It should be mentioned that Lamperski [258], Abbas et al. [289], Gutiérrez-Valladares et al. [260], and Gillespie et al. [290] have adopted various methodologies, such as the inverse grand canonical Monte Carlo (IGCMC), the approach proposed by Svensson and Woodward [291], canonical and grand canonical MC simulations based on the standard Metropolis sampling algorithm [292], and adaptive grand canonical Monte Carlo (A-GCMC) [293], respectively.

Table 7.1. This table summarize the systems and their associated table name, ionic diameter, and ion valence type. The AAD% of MIAC was predicted by the BiDH and HS+DH models. The tables beginning with the letters S, G, L and V are MC simulations from the references [289], [260], [258], and [290], respectively.

	σ_-	σ_+	$AAD\%$ $\ln\gamma_\pm^{BiDH}$	$AAD\%$ $\ln\gamma_\pm^{DH}$		σ_-	σ_+	$AAD\%$ $\ln\gamma_\pm^{BiDH}$	$AAD\%$ $\ln\gamma_\pm^{DH}$
$Z_+ = +1$, $Z_- = -1$									
S1	4.14	4.14	1.62	8.43	S68	3.94	2.68	1.57	6.41
S2	3.62	4.40	3.42	9.61	S69	3.70	3.70	1.06	3.46
S3	4.32	4.32	4.14	9.35	S70	4.30	2.98	1.17	4.26
S4	3.92	4.50	4.32	9.90	S71	3.91	3.91	0.77	1.96
S5	4.64	4.64	2.63	8.52	S72	4.20	3.40	1.05	4.48
S6	4.40	4.64	7.53	10.41	S73	2.24	2.24	2.82	5.08
S7	4.34	4.34	1.14	8.64	S74	2.66	1.80	2.75	5.21
S8	4.80	3.70	4.80	9.90	S75	3.08	1.38	1.84	4.15
S9	3.98	3.98	1.09	5.41	S76	0.30	4.00	6.19	4.95
S10	3.58	4.20	0.87	6.09	S77	3.47	3.47	1.45	6.23
S11	3.98	3.98	1.48	7.53	S78	2.66	4.10	1.40	6.46
S12	3.62	4.20	2.57	9.67	S79	4.50	2.04	1.11	5.62
S13	4.12	4.12	1.70	8.99	S80	3.46	3.36	1.51	6.74
S14	3.92	4.10	3.36	9.66	S81	3.76	3.76	1.21	8.47
S15	4.66	4.66	2.71	8.60	S82	2.66	4.60	1.06	6.70
S16	4.40	4.50	6.70	10.23	S83	4.50	2.76	1.10	6.78
S17	4.52	4.52	2.62	7.58	S84	4.58	2.68	1.08	6.71
S18	4.80	4.00	7.07	10.51	S85	4.40	4.40	0.72	2.92
S19	3.96	3.96	1.14	5.41	S86	5.00	3.40	0.64	4.79
S20	3.58	4.20	0.87	6.09	S87	3.82	4.20	1.38	8.19

Table 7.1. (Continued.)

	σ_-	σ_+	$AAD\%$ $\ln\gamma_\pm^{BiDH}$	$AAD\%$ $\ln\gamma_\pm^{DH}$		σ_-	σ_+	$AAD\%$ $\ln\gamma_\pm^{BiDH}$	$AAD\%$ $\ln\gamma_\pm^{DH}$
S21	3.50	3.50	1.72	7.30	S88	4.12	4.30	4.13	10.12
S22	3.62	3.36	1.38	6.43	S89	4.24	4.80	5.10	10.22
S23	3.68	3.68	0.75	5.67	S90	5.00	3.50	1.53	7.15
S24	3.92	3.36	1.13	6.44	S91	3.82	4.00	1.35	7.44
S25	3.96	3.96	1.14	5.41	S92	4.12	3.90	1.94	8.89
S26	4.40	3.36	1.30	6.88	S93	4.60	4.30	1.40	6.41
S27	3.60	3.60	1.19	6.97	S94	5.00	3.80	4.55	9.41
S28	4.80	2.04	1.25	7.11	S95	2.88	1.58	2.21	4.36
S29	2.84	2.84	2.15	4.34	S96	3.82	3.16	1.34	4.41
S30	3.58	2.04	2.20	4.72	S97	4.12	3.16	1.15	4.47
S31	3.26	3.26	2.01	6.74	S98	4.20	2.44	1.38	4.81
S32	3.62	2.70	1.69	5.48	S99	3.70	3.56	2.53	11.50
S33	3.30	3.30	1.71	6.57	G1	4.25	4.25	0.29	2.24
S34	3.92	2.68	1.57	5.99	G2	3.62	5.43	0.27	2.28
S35	3.70	3.70	1.39	7.67	L1	4.25	4.25	5.04	10.01
S36	4.40	2.68	1.15	6.21	L5	3.00	4.25	1.26	8.81
S61	2.87	2.87	1.16	2.23	V1	3.00	1.50	1.23	2.57
S62	2.66	3.08	1.17	2.24	V2	3.00	3.00	1.34	3.59
S63	3.70	2.04	0.96	2.02	V3	3.00	4.50	2.72	6.43
S64	2.38	3.36	1.10	2.17	V4	3.00	6.00	2.57	5.19
S65	3.38	3.38	1.29	3.31	V5	3.00	7.50	2.95	4.35
S66	2.66	3.96	1.59	6.42	V6	3.00	9.00	3.04	3.41
S67	3.86	2.76	1.60	6.45					
$Z_+ = +2$, $Z_- = -1$									
S37	4.98	4.98	8.23	27.98	S52	4.40	5.94	6.14	19.99
S38	3.62	5.90	10.42	25.92	S53	5.16	5.16	4.82	21.23
S39	5.16	5.16	4.82	21.23	S54	4.80	5.30	7.22	22.39
S40	3.92	6.20	8.84	22.28	S55	4.00	4.00	3.83	16.54
S41	5.40	5.40	9.25	21.77	S56	3.58	4.30	3.13	20.03
S42	4.40	6.18	11.18	23.44	S100	3.82	5.70	3.96	18.50
S43	5.50	5.50	8.14	20.21	S101	4.12	6.00	6.43	20.83
S44	4.80	6.00	12.22	23.37	S102	4.60	5.98	7.77	21.41
S45	4.60	4.60	3.27	18.39	L3	4.20	4.20	3.38	21.34
S46	3.58	5.90	10.05	25.97	V13	3.00	1.50	2.39	3.24
S47	4.76	4.76	3.54	19.63	V14	3.00	3.00	3.22	12.96
S48	3.62	5.48	4.68	21.71	V15	3.00	4.50	2.03	15.20
S49	5.12	5.12	5.08	19.96	V16	3.00	6.00	6.01	15.34
S50	3.92	5.80	6.73	22.48	V17	3.00	7.50	4.60	9.96
S51	5.30	5.30	5.49	21.67	V18	3.00	9.00	2.65	7.38
$Z_+ = +3$, $Z_- = -1$									
S57	5.10	5.10	3.62	32.85	V19	3.00	1.50	13.58	12.65
S58	3.62	7.20	18.84	39.77	V20	3.00	3.00	8.04	24.71
S59	4.80	4.80	3.14	30.38	V21	3.00	4.50	6.12	18.43
S60	3.62	6.40	11.10	29.94	V22	3.00	6.00	7.39	19.02
S103	3.82	7.00	15.25	42.54	V23	3.00	7.50	6.10	14.94
S104	3.82	6.20	13.22	39.24	V24	3.00	9.00	10.04	17.75
L4	4.20	4.20	6.62	32.10					
$Z_+ = +2$, $Z_- = -2$									
G3	4.25	4.25	8.98	26.43	V9	3.00	4.50	6.79	22.29

Table 7.1. (Continued.)

	σ_-	σ_+	$AAD\%$ $\ln\gamma_\pm^{BiDH}$	$AAD\%$ $\ln\gamma_\pm^{DH}$		σ_-	σ_+	$AAD\%$ $\ln\gamma_\pm^{BiDH}$	$AAD\%$ $\ln\gamma_\pm^{DH}$
L2	4.20	4.20	8.97	58.46	V10	3.00	6.00	5.03	40.42
V7	3.00	1.50	33.8	58.57	V11	3.00	7.50	4.08	28.48
V8	3.00	3.00	13.37	23.96	V12	3.00	9.00	2.39	17.15

7.2.1 Mean Ionic Activity Coefficient

Figures 7.3-7.6 provide a comprehensive comparison between the MIAC of various electrolytes, as predicted by the BiDH model, and the corresponding results obtained through MC simulations. This comparison allows us to evaluate the accuracy and reliability of the BiDH model, as well as to identify any discrepancies or shortcomings of the model. The figures show that the predictions of the BiDH model are represented by the lines, while the data points are the results of the MC simulations.

The BiDH model is shown in Figure 7.3 to predict MIAC compared to the MC simulations reported by Lamperski et al. [258]. The specifications of the charged hard spheres investigated in this figure are outlined in Table 7.1. The RSP of the solvent for systems L2-L4 is 78.55 and for systems L1 and L5 is 78.65. It is noteworthy that the IGCMC technique is employed to calculate the MIAC and IIAC.

Compared to the MC simulations of Abbas et al. [289], Figure 7.4 shows the BiDH predictions. The Metropolis algorithm is employed by Abbas et al. [289] in the canonical ensemble for their MC simulations, while the Widom insertion method is used for the activity coefficients. For all systems beginning with letter S (including those in Figure 7.4), the RSP of the solvent is the RSP of water at 298.15 K.

The figures demonstrate that the BiDH predictions are consistent with the MC simulations. It should be noted that L1 and S4, L2, S42, S46, and L3, and S103, S104, and L4 are 1:1, 2:2, 2:1, and 3:1 electrolyte solutions, respectively.

Figures 7.5 and 7.6 illustrate the effect of ionic diameter on the accuracy of the MIAC prediction by the BiDH model. In the 1:1 electrolyte system, the diameter of the cation ranges from 3 to 9 (Å) while the diameter of the anion remains at 3 (Å). For the 2:2 electrolyte system, the RSP is 78.45 and the temperature is 298.15 K. The comparison between the BiDH model and the MC simulations reported by Gillespie et al. [290] is presented in both figures.

It is evident that BiDH theory is capable of predicting the MIAC of electrolyte solutions over a broad range of ionic size asymmetry, with the ratio of $\frac{\sigma_+}{\sigma_-}$ ranging from 1 to 3.

The MIAC predictions of the BiDH model are compared to the MC simulations summarized in Table 7.1 in Figure 7.7. Points in orange, green, red, and purple represent 1:1, 2:1, 2:2 and 3:1 electrolytes, respectively. The circle, triangle, square, and diamond points signify systems beginning with the letters S, L, G, and V, respectively. The R^2 and absolute average deviation in percent ($AAD\%$) are also displayed in this figure.

The predicted MIAC results of the BiDH model are in close agreement with the MC simulations in a wide range of $\ln\gamma_\pm$ values, from -4 to +4. It is remarkable that the model's accuracy is consistent regardless of the asymmetry of the ionic charges and ionic diameter.

7.2.2 Individual Ionic Activity Coefficient

In this section, we evaluate the ability of the BiDH model to predict the IIAC of charged hard sphere fluids by comparing it to MC simulations from the literature. Figures 7.8 and 7.9 show the activity coefficients of cations (green line and points), anions (blue line and points) and salts (black line and points) for systems S37 [289] and V21 [290], respectively.

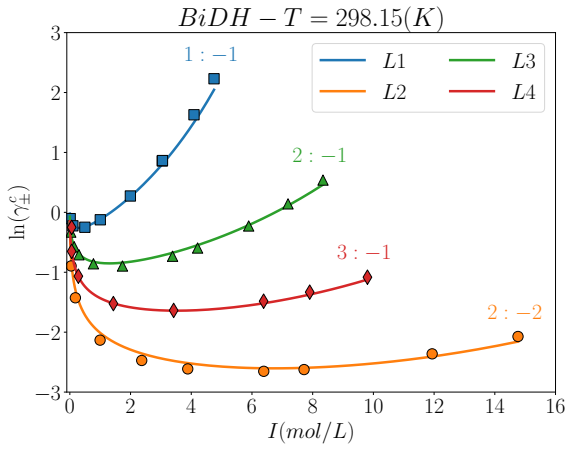

Figure 7.3. This Figure shows the BiDH model predictions of the MIAC ($\ln \gamma_{\pm}^{c}$) for systems L1-L4, which are summarized in Table 7.1, and these predictions are compared to the MC simulations from ref. [258] (represented by symbols). Reproduced from ref. [286], with the permission of AIP Publishing.

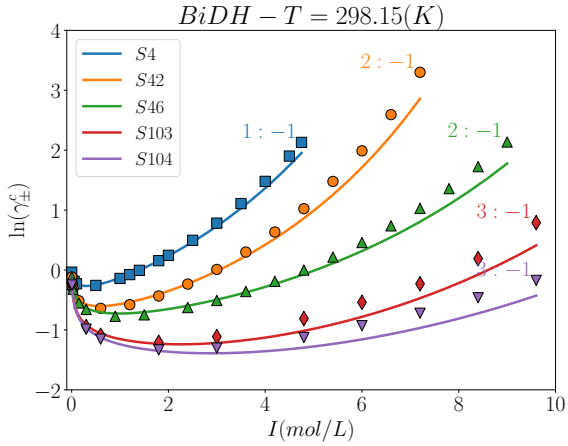

Figure 7.4. The BiDH model (solid lines) was used to predict the MIAC ($\ln \gamma_{\pm}^{c}$) for systems S4, S42, S46, S103, and S104, which are summarized in Table 7.1. These predictions were then compared to the MC simulations (symbols) from ref. [289]. Reproduced from ref. [286], with the permission of AIP Publishing.

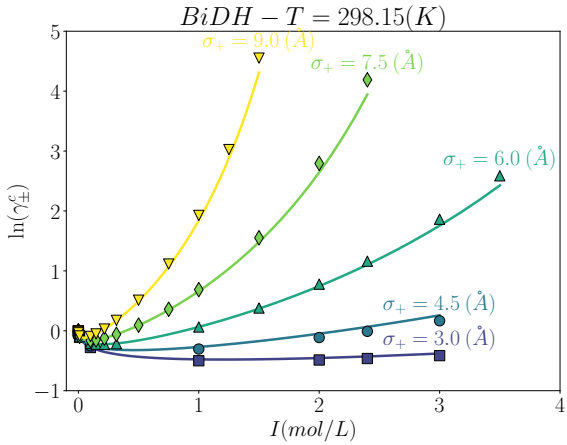

Figure 7.5. This figure presents the MIAC ($\ln \gamma_\pm^c$) predictions of the BiDH model for 1:1 electrolytes with different cation's diameters (shown next to the lines) which is compared with the MC simulations (symbols) from ref. [290]. Reproduced from ref. [286], with the permission of AIP Publishing.

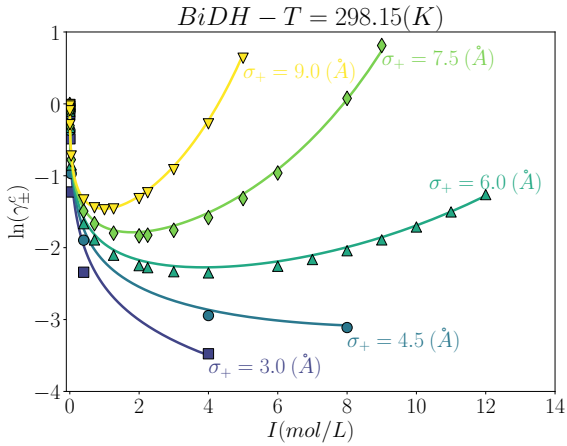

Figure 7.6. This figure presents the MIAC ($\ln \gamma_\pm^c$) predictions of the BiDH model for 2:2 electrolytes with different cation's diameters (shown next to the lines) which is compared with the MC simulations (symbols) from ref. [290]. Reproduced from ref. [286], with the permission of AIP Publishing.

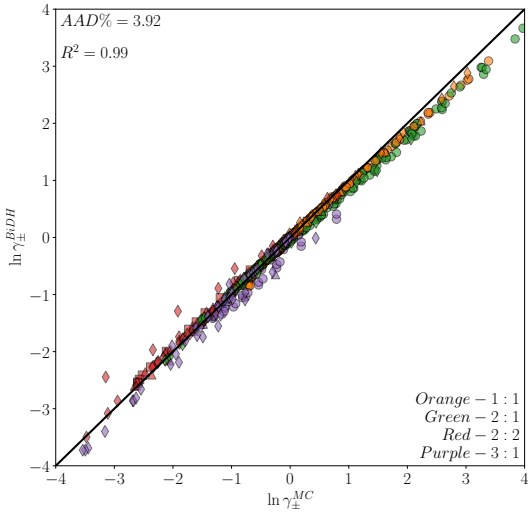

Figure 7.7. The predicted MIAC ($\ln \gamma_{\pm}^{BiDH}$) by the BiDH model is compared to the MIAC from MC simulations [258, 260, 289, 290] ($\ln \gamma_{\pm}^{MC}$), with the solid black line representing the perfect fit. Reproduced from ref. [286], with the permission of AIP Publishing.

Figures D.18-D.28 presents the IIAC for other systems summarized in Table 7.1. The BiDH model's predictions are also included, and they are compared to the MC simulations. It is clear from these figures that the predictions of the BiDH model are in good agreement with the MC simulations.

Figure 7.10 offers a detailed comparison between the IIAC predicted by the BiDH model and the MC simulations for all the systems in Table 7.1. The BiDH model is seen to be fairly accurate in predicting the IIAC, for highly asymmetric ions in size. Nevertheless, its performance is slightly less impressive for the IIAC, with $R_+^2 = 0.97$ and $R_-^2 = 0.93$, compared to the MIAC with $R^2 = 0.99$.

The adjustment to the DH theory for ion-ion association that was made in this research has been successful, even in difficult cases where the ions have very high charges or are of very different sizes. Classical ion-ion interaction theories, such as the MSA theory [5, 6], have had difficulty with these types of situation, as demonstrated by Gillespie et al. [290]. However, the new versions of the MSA theory have been found to be accurate for both IIAC, as reported by Høye and Gillespie [294], and MIAC in these scenarios [290].

7.3 Discussion

In the previous section, we provided an overview of the results of the comparison of the predictions of the BiDH model with the MC simulations. The findings showed that the BiDH model is accurate in predicting the MIAC and IIAC of various charged hard sphere fluids. In this section, we will look more closely at the evaluation of the BiDH model. We will start by addressing the question of whether it is necessary to consider the ion-ion

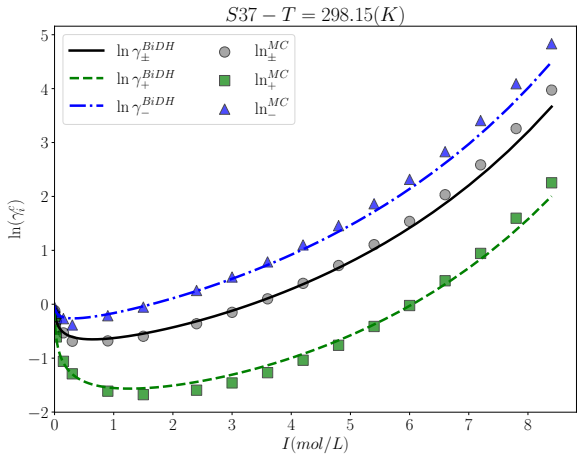

Figure 7.8. This figure presents the predicted IIAC by the BiDH model (lines) ($\ln \gamma_i^c$) for system S37 (a 2:1 electrolyte with $\sigma_- = 4.98 \times 10^{-10}\, m$ and $\sigma_+ = 4.98 \times 10^{-10}\, m$ from ref. [289], which was then compared to the MC simulations (symbols). Reproduced from ref. [286], with the permission of AIP Publishing.

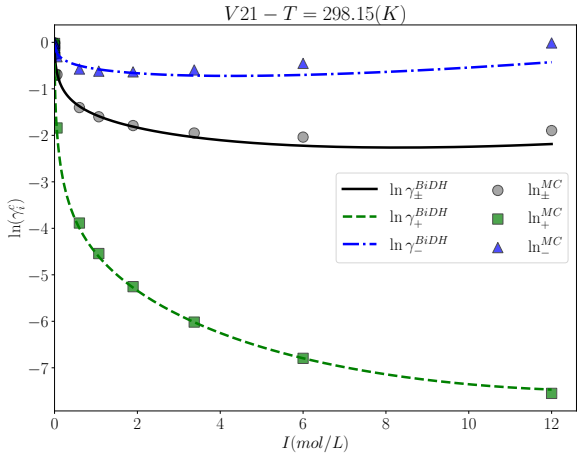

Figure 7.9. This figure presents the predicted IIAC by the BiDH model (lines) ($\ln \gamma_i^c$) for simulation V21 (a 3:1 electrolyte with $\sigma_- = 3 \times 10^{-10}\, m$ and $\sigma_+ = 4.5 \times 10^{-10}\, m$) from ref. [290], which was then compared to the MC simulations (symbols). Reproduced from ref. [286], with the permission of AIP Publishing.

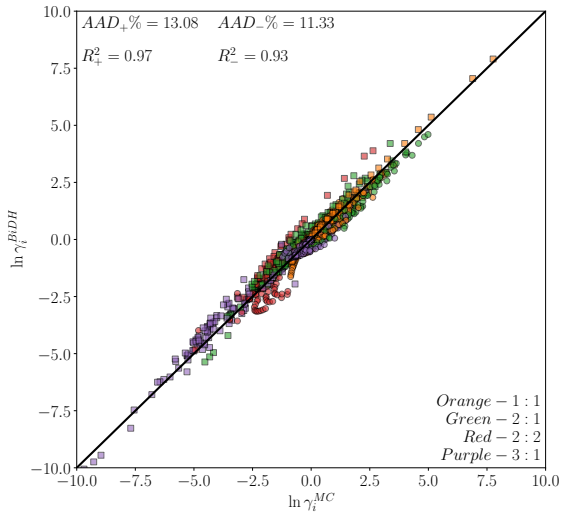

Figure 7.10. The predicted IIAC by the BiDH model ($\ln \gamma_i^{BiDH}$ with $i = +\ or\ -$) is compared to the IIAC from MC simulations [258, 260, 289, 290] ($\ln \gamma_i^{MC}$) with the solid black line representing the perfect fit. Reproduced from ref. [286], with the permission of AIP Publishing.

association for predicting the thermodynamic properties of electrolyte solutions. Then, we will emphasize the importance of using a physically meaningful cavity function to take into account the ion-ion association. Lastly, we discuss the significance of ion-dipole interactions in cavity function and their effect on the structural properties of associative electrolytes, such as the proportion of unbound ions.

7.3.1 Importance of Ion-Ion Association

Previous research [42, 59, 69, 70] has shown that the thermodynamic properties of electrolyte solutions, even those containing electrolytes with a high probability of ion-ion association, can be roughly estimated by assuming complete dissociation of electrolytes. This raises the question of the importance of ion-ion association in determining the common properties of electrolyte solutions, such as MIAC. Therefore, in this section, we compare the predictions of the BiDH model, which takes into account ion-ion association, with those of the DH theory, which disregards ion-ion association.

The comparison of the predicted MIAC, osmotic coefficient, and IIAC using BiDH (solid lines), HS + DH (dashed lines) and MC simulations (points) is shown in Figures 7.11-7.12. The parameters used for these predictions are listed in Table 7.1. The only difference between the BiDH theory (Eq. 7.43) and the HS+DH model is the way the ion-ion association is treated in the Helmholtz free energy. The BiDH theory takes into account ion-ion association, leading to a contribution A^{Assoc} in the free energy and thus affecting other properties. On the other hand, the HS+DH model assumes that all ions in the solution exist as free ions, resulting in no contribution to the free energy or other thermodynamic properties due to ion-ion association.

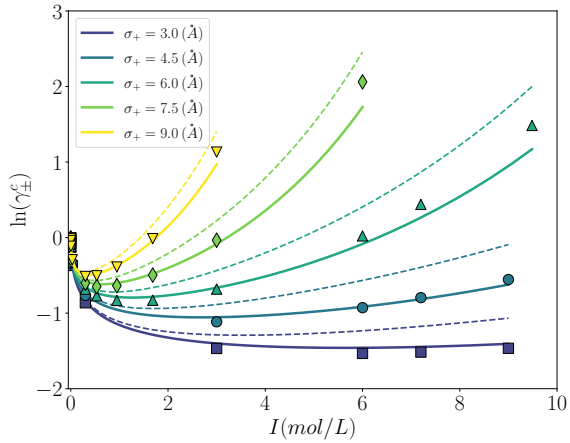

Figure 7.11. The BiDH model (solid lines) and the HS + DH model (dashed lines) were used to predict the MIAC ($\ln\gamma^c_\pm$) for systems V14-18 (2:1 electrolytes where $\sigma_- = 3\times10^{-10}\,m$ and σ_+ are 3, 4.5, 6, 7.5, and 9 $\times10^{-10}\,m$, respectively). These predictions were compared to the results of MC simulations (symbols) from ref. [290]. Reproduced from ref. [286], with the permission of AIP Publishing.

The comparison between the BiDH model and the MC simulations in Figures 7.11, 7.12, and 7.13 reveals a better agreement for the former. Table 7.1 provides quantitative evidence to support this observation, with the $AAD\%$ of MIAC produced by the BiDH model being consistently lower than the MIAC predicted by the HS+DH model. It is clear that the BiDH model improves the predictions of the DH theory by incorporating ion-ion association. However, it is worth noting that the HS+DH model can also achieve a satisfactory agreement with the MC simulations by adjusting the ionic diameters employed in the predictions. The main issue here is how to justify the modification of the ionic diameter, given that in MC simulations there are no solvent molecules, and thus no solvated ionic diameter exists.

This research is not focused on determining which thermodynamic model is the most effective in predicting properties such as MIAC, IIAC, and osmotic coefficient. Instead, we are exploring whether the ion-ion association should be taken into account when modeling electrolyte solutions. To this end, we developed an EoS tailored for charged hard sphere systems, which includes modifications to the DH theory. Our findings demonstrate that this new EoS is more accurate in predicting the MIAC, IIAC and osmotic coefficient for these systems (see Figures 7.11-7.13). To determine which thermodynamic model is the most accurate in predicting the MIAC, IIAC, and osmotic coefficient in electrolyte solutions, a comprehensive comparison of various models cited in the literature (such as those in [20, 214, 220–222, 232–234, 236, 242, 290, 294–296] and associated references) is necessary. However, this comparison, which should include both simulation data and the experimental data, is beyond the scope of our current study.

7.3.2 Cavity Function

The BiDH theory is based on the cavity function, which is essential to calculate the proportion of unbound ions by using the ratio of activity coefficients for reactants and products. This section looks at the comparison between the cavity function used in the BiDH model

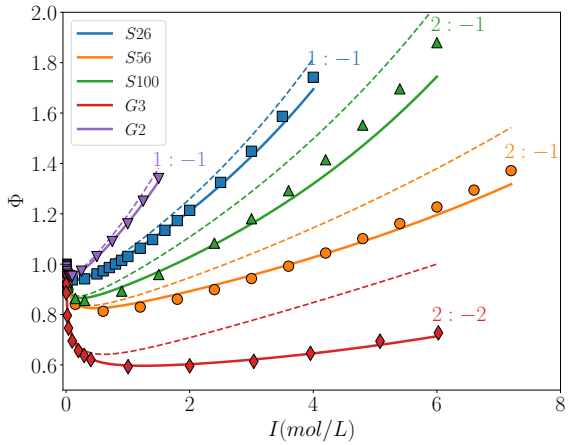

Figure 7.12. The BiDH model (solid lines) and the HS + DH model (dashed lines) were used to predict the osmotic coefficient (ϕ) for the systems S26, S56, S100, G3, and G2, which are presented in Table 7.1 from ref. [260,289]. The predictions were then compared to the MC simulations (symbols). Reproduced from ref. [286], with the permission of AIP Publishing.

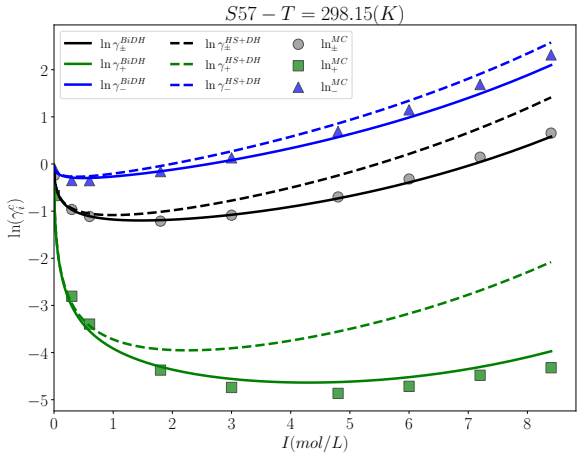

Figure 7.13. This figure shows the comparison of the predicted IIAC ($\ln \gamma_i^c$) by the BiDH model (solid lines) with the predicted IIAC by the HS + DH model (dashed lines) and MC simulations [289] (symbols) that is conducted for system S57, where $Z_+ = 3$, $Z_- = -1$, $\sigma_+ = 5.1 \times 10^{-10}\ m$, and $\sigma_+ = 5.1 \times 10^{-10}\ m$. Reproduced from ref. [286], with the permission of AIP Publishing.

and the BiMSA model. Additionally, we explore the importance of ion-dipole interactions in cavity function, emphasizing their role in accurately depicting the structural poperties of electrolyte solutions. When the cavity function is compared with and without ion-dipole interactions, we can gain an understanding of their influence on the predicted results. Lastly, we address why the definition of a single association site in the SAFT framework for ions and treating the ion-ion association as hydrogen bonding may not reflect the true physical behavior of electrolyte systems, stressing the need for a more precise method to capture the ion-ion association and its effects on thermodynamic properties.

7.3.2.1 Cavity Function from the BiMSA Theory

Bernard and Blum [19, 20] combined Wertheim's version of the Ornstein-Zernike equation with the MAL to create the BiMSA model. Although the exact derivation and results of BiMSA, particularly BiMSA-EXP, are beyond the scope of this study, a closer look reveals that an exponential approximation was used to represent the contact probabilities as the closure equation. This approximation led to the formulation of a cavity function expressed in Eq. 7.44:

$$y_{mn}^{BiMSA} = g_{mn}^{HS} \exp\left[-\frac{\lambda\left(Z'_m Z'_n - Z_m Z_n\right)}{\sigma_{mn}}\right] \tag{7.44}$$

This equation yields Z'_m and λ, which are determined by equations 7.45 and 7.46 (as shown in the following).

$$Z'_m = \frac{Z_m - \eta^B \sigma_m^2}{1 + \Gamma^B \sigma_m} \tag{7.45}$$

$$\lambda = \frac{\beta e^2}{4\pi\varepsilon_0\varepsilon_r} \tag{7.46}$$

$$\frac{\left[\Gamma^B\right]^2}{\pi\lambda} = \sum_i \rho_i z_i'^2 + \sum_{m,n} Z'_m Z'_n \frac{\tilde{\rho}_{mn}}{\sigma_{mn}} \tag{7.47}$$

$$\eta^B = \frac{\pi}{2\Delta\Omega}\left[\sum_i \frac{\rho_i \sigma_i Z_i}{u_i} + \sum_{m,n} \frac{\sigma_m^2 Z_n}{u_m u_n} \frac{\tilde{\rho}_{mn}}{\sigma_{mn}}\right] \tag{7.48}$$

$$\Delta = 1 - \zeta_3 \tag{7.49}$$

$$\Omega = 1 + \frac{\pi}{2\Delta}\left[\sum_i \frac{\rho_i \sigma_i^3}{u_i} + \sum_{m,n} \frac{\sigma_m^2 \sigma_n^2}{u_m u_n} \frac{\tilde{\rho}_{mn}}{\sigma_{mn}}\right] \tag{7.50}$$

$$u_i = 1 + \Gamma^B \sigma_i \tag{7.51}$$

The BiMSA parameters, denoted as Γ^B and η^B, are determined through calculations based on equations 7.47-7.49. The number density of bonded ions, represented as $\tilde{\rho}_{mn}$, is affected by the cavity function and the number density of other bonded ions, as described in Eq. 7.15. This leads to a system of nonlinear equations, including equations 7.15, 7.47, and 7.48, which must be solved numerically. In this study, the number density of ion pairs ($\tilde{\rho}_{mn}$) and the BiMSA screening parameter are the primary unknown variables, with η^B as the secondary unknown variable. An initial guess of $\Gamma_0^B = \kappa/2$ and $\tilde{\rho}_{mn} = 0$ is used to

numerically solve the system of $M \times N$ MAL equations (Eq. 7.15) along with Eq. 7.47. After the determination of the BiMSA parameters, the cavity function of the BiMSA can be calculated using Eq. 7.44.

7.3.2.2 Cavity Function from SAFT

The remarkable success of thermodynamic perturbation theory in modeling hydrogen bonding has led to the exploration of whether the same approach can be used to study ion-ion association in electrolyte solutions using SAFT-type models. In SAFT-type equations of state, the molecular association resulting from hydrogen bonding is usually represented by the inclusion of electron-donor or acceptor sites on the molecules. The interactions between these sites are then described by a square-well potential, which is characterized by two parameters: the association energy ($\epsilon^{A_iB_j}$ or well depth) and the association volume ($\kappa^{A_iB_j}$ or $\beta^{A_iB_j}$, also known as well width). The fraction of molecules not bonded at site A (X^{A_i}) is then calculated using Eq. 7.52, where $\Delta^{A_iB_j}$ stands for the association strength (equations 7.53 and 7.54).

$$X^{A_i} = \frac{1}{1 + N_A \sum_j \sum_{B_i} \rho_j X^{B_j} \Delta^{A_iB_j}} \tag{7.52}$$

From SAFT [285], we have the following:

$$\Delta^{A_iB_j} = \sigma_{ij}^3 \kappa^{A_iB_j} g_{ij}^{HS} \left[\exp\left(\beta\epsilon^{A_iB_j}\right) - 1\right] \tag{7.53}$$

In this equation, g_{ij}^{HS} is the RDF of the hard sphere at contact and $\sigma_{ij} = 0.5(\sigma_i + \sigma_j)$. From CPA [40], we have:

$$\Delta^{A_iB_j} = b_{ij}\beta^{A_iB_j} g_{ij}^{HS} \left[\exp\left(\beta\epsilon^{A_iB_j}\right) - 1\right] \tag{7.54}$$

The co-volume parameter b_{ij} is related to the diameter of ions [42]. Assuming that each ion has a single association site, the fraction of components not bound at site A (X^{A_i}) can be simplified to the fraction of unbound components (α_i), as shown in Eq. 7.55:

$$X^{A_i} = \frac{\tilde{\rho}_i}{\rho_i} = \alpha_i \tag{7.55}$$

The symbols Δ_{ij}, β_{ij}, and κ_{ij} can be used to denote the strength, volume, and energy of the association between components, respectively. The fraction of unbound ions can then be determined using Eq. 7.56:

$$\alpha_i = \frac{1}{1 + N_A \sum_j \rho_j \alpha_j \Delta_{ij}} \tag{7.56}$$

When looking at a fluid made up of only charged hard spheres, with or without a dispersion term, and assuming that the sphere diameters remain constant regardless of temperature, certain simplifications can be made. In this case, the number of segments (m_i) is equal to 1, and the diameter of each component is represented by σ_i. This means that the only density-dependent factor that affects the association strength in SAFT-type models is g_{ij}^{HS}, which is the RDF of hard spheres. Therefore, the composition-dependent cavity function in SAFT-type equations of state is equivalent to the RDF of hard spheres.

$$y_{ij}^{SAFT} = g_{ij}^{HS} \tag{7.57}$$

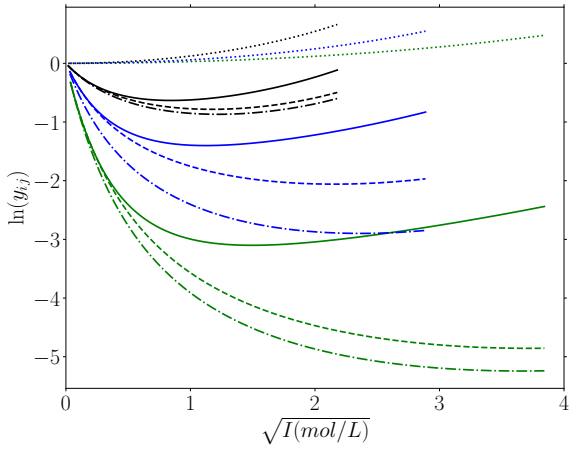

Figure 7.14. The cavity function ($\ln y_{ij}$) of the BiDH model (represented by solid lines), the BiDH model without the ion-dipole term (dashed lines), the BiMSA model (dashed-dotted lines), and SAFT-type models (dotted lines) for 1:1 (black lines), 2:1 (blue lines), and 3:1 (green lines) are shown. Reproduced from ref. [286], with the permission of AIP Publishing.

7.3.2.3 Cavity Function Assuming Ion Pairs Are Not Dipolar

In the method section, we applied Kirkwood theory [235], which was originally developed for zwitterions, to consider ion-dipole interactions in the zero-density limit of ion pairs. If we assume that the ion pairs are not dipolar, the cavity function and the fraction of unbound ions will be different. We also demonstrated the cavity function we developed without the ion-dipole term ($\mu_{mn}^{DI} = 0$ in Eq. 7.30). Figure 7.14 shows the cavity function predicted by BiDH (Eq. 7.30), BiDH without ion-dipole term (Eq. 7.30 when $\mu_{mn}^{DI} = 0$), BiMSA (Eq. 7.44), and SAFT-type EoS (Eq. 7.57) in relation to the ionic strength for the systems L1-L3 listed in Table 7.1.

Our aim in this comparison is to evaluate the cavity function we used in this study, based on the RCA approach by Stell et al. [240], against the cavity function derived from the WOZ equation reported by Bernard et al. [20] (Eq. 7.44). This will help us determine if the approximations made by Stell and his team are accurate. Additionally, we present the cavity function from our model that does not take into account ion-dipole interactions, since the BiMSA model also disregards them. Therefore, a more suitable comparison would be between the cavity functions of the BiDH without the ion-dipole term and the BiMSA models.

As demonstrated in Figure 7.14, the cavity functions of BiDH, BiDH without the ion-dipole term, and BiMSA are similar and have a similar slope at very low ionic strengths, indicating their consistent behavior at infinite dilution. However, as the ionic strength increases, these three cavity functions start to differ from each other. Notably, the cavity function of BiDH without the ion-dipole term follows a trend similar to that of BiMSA, displaying close qualitative agreement between the two. In contrast, the cavity function of BiDH has a distinct trend at higher ionic strengths, diverging from the other two models.

Figure 7.14 reveals why introducing association sites to ions within the SAFT equations of state, to account for ion-ion association, may be flawed. The figure shows that the cavity function of the SAFT-type EoS has a distinct pattern compared to the other models. In

particular, the logarithm of the cavity function is consistently positive and remains close to zero.

This comparison yields two main insights. First, the cavity function used in SAFT-type EoS may not be adequate to accurately represent the ion-ion association, as it does not take into account the electrostatic nature of the association. This implies that further considerations are necessary to consider the electrostatic contributions to the cavity function. Second, the approach proposed by Stell et al. to approximating the cavity function appears to be accurate, as demonstrated by the agreement between the BiDH and BiMSA models. This confirms the validity of their methodology and its capability in predicting the cavity function in electrolyte solutions.

7.3.3 Effect of RSP

This section seeks to evaluate the ability of the BiDH model to predict the MIAC of electrolytes in systems with a lower RSP. Previously, the systems studied had a RSP close to that of pure water, around 78.5. Here, we expand our research to encompass systems with lower RSP. This will enable us to investigate the model's performance under conditions where electrostatic interactions between ions are expected to be more powerful.

At a temperature of 298.15 K and with the anion diameter fixed at 3 Å, Figure 7.15 shows the logarithm of the MIAC plotted against the cation diameter for 1:1 electrolyte systems with different RSP values of the solvent.

The BiDH model is capable of accurately predicting MIAC for electrolytes with solvent RSP values of 48, 78.5, and 120, as demonstrated in Figure 7.15. However, when the RSP of the solvent is 20, a slight divergence from the MC simulations is observed. This discrepancy can be attributed to the fact that the upper limit of the Bjerrum association constant equation at the reference state depends only on the ionic diameter and not on the solvent

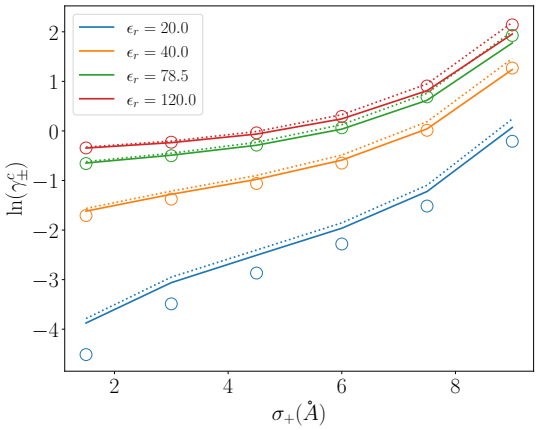

Figure 7.15. The BiDH theory was used to predict the effect of RSP on 1:1 electrolytes with an anion diameter of 3×10^{-10} m, an ionic strength of 1 $mol \cdot L$, and a temperature of 298.15 K (solid lines). The results were compared to those from the HS+DH model (dotted lines) and MC simulations reported by Gillespie et al. [290] (points). Reproduced from ref. [286], with the permission of AIP Publishing.

properties. Consequently, the equation underestimates the association constant at infinite dilution, leading to a over-prediction of MIAC.

It is essential to emphasize that the upper limit of the Bjerrum model (l_{mn} in equation 7.37) marks a cutoff point beyond which oppositely charged ions are not taken into account as ion pairs. Logically, this cut-off distance should depend on the temperature, solvent(s) properties, and ions. Nevertheless, to the best of our knowledge, no methods have been proposed to predict this cut-off distance apart from half of the Bjerrum length, which is also an arbitrary selection. It could be adjusted to the experimental data in cases where real systems are being studied or simulated, as in the context of this study. However, such an adjustment could lead to the formation of a semi-empirical model rather than a predictive one. Therefore, in this study, we continue to use a global parameter (θ) that links the distance of the closest approach to this cutoff distance.

BiDH has been shown to be effective in situations where the RSP is much lower than that of water. This implies that it is suitable for practical applications where the permittivity of the solvent decreases as the salt concentration increases. This theory could be particularly useful in the II component of the II+IW theory, as discussed in the comprehensive review by Valiskó and Boda [295], thus eliminating the need for computationally expensive GCMC simulations or less accurate analytical methods such as the DH theory or the traditional MSA theory.

7.3.4 Structural Properties

The preceding sections have thoroughly examined the macroscopic thermodynamic properties that are usually evaluated. Furthermore, the BiDH theory provides insight into the structural properties of the solution, such as the proportion of unbound ions (α_i). Examining this feature in more detail is essential since it is the basis of the constructed model and of great importance.

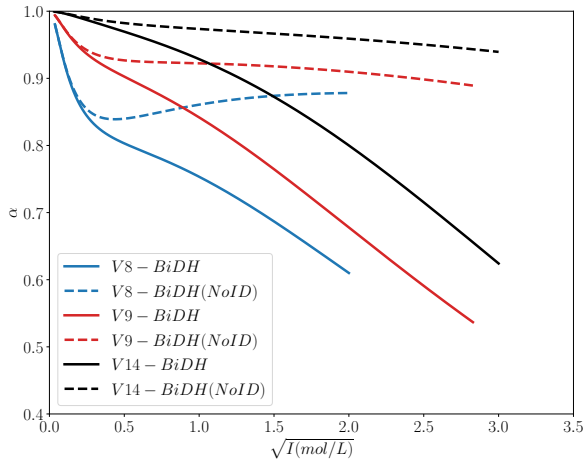

Figure 7.16. This figure presents the predictions of the BiDH theory for the proportion of free ions (α) for systems V8, V9, and V14 (shown in Table 7.1) with (solid lines) and without (dashed lines) taking into account ion-dipole interactions. Reproduced from ref. [286], with the permission of AIP Publishing.

The graph in Figure 7.16 shows the correlation between the proportion of unbound ions and the ionic strength for systems V8, V9 and V14. Solid lines indicate the estimated fraction of unbound ions when ion-dipole interactions are taken into account in the cavity function, while dashed lines indicate predictions without taking into account ion-dipole interactions.

The figure illustrates the substantial effect of including ion-dipole interactions in the cavity function on the fraction of unbounded ions. Without these interactions, the fraction of unbound ions initially decreases with increasing ionic strength but then increases slightly or remains constant at higher ionic strengths. This behavior was previously reported by Naseri Boroujeni et al. [214] for the Ebeling-Grigo model (see Chapter 6), which assumes ideal ion pairs with an activity coefficient of one.

The accuracy of the predicted fraction of unbound ions cannot be accurately determined without taking into account the structural properties of ionic fluids. As Naseri Boroujeni et al. [214] have pointed out, the validation of the developed model necessitates the inclusion of molar conductivity, which is essential for assessing structural properties. To validate the predicted fraction of free ions, it is necessary to incorporate the BiDH theory into a comprehensive EoS such as CPA [40], PC-SAFT [54], or SAFT-VR-Mie [68] that takes into account non-electrostatic interactions. Subsequently, thermodynamic properties such as MIAC, osmotic coefficient, and density should be evaluated for real electrolyte solutions. Finally, structural properties, including the fraction of unbound ions, should be linked to an electrical conductivity model (such as models mentioned in these references [120, 124]), allowing a comparison between the predicted molar conductivity and the experimental data. This investigation will be presented in the last part of this thesis.

7.3.5 BiDH vs. BiMSA

In this section, a formal comparison analysis of two equations of state for charged hard-sphere systems, BiDH and BiMSA, is performed. For this analysis, three properties of charged hard-sphere fluids are studied, MICA, osmotic coefficient, and fraction of unbound ions. In the first part, the effect of the size of the ions on the predictions of these properties is evaluated. In the second part, the effect of the charge of ions present in the solutions on the predictions of the models is analyzed. Lastly, in the third part, the effect of the RSP of the system on the predictions of the models is studied. The objective of this study is to assess the sensitivity of the models on major parameters in order to deepen our understanding for the integration of the mentioned models in an electrolyte EoS.

It should be noted that in this comparison analysis, all parameters and properties are exactly the same for both models. The Bjerrum model is used for the association constant at infinite dilution and the upper limit of the Bjerrum integral is set to $1.07\sigma_{+-}$.

7.3.5.1 Sensitivity to Size Asymmetry

In this section, MIAC, osmotic coefficient, and the fraction of free ions of a 2:2 electrolyte solution in which the RSP of the solvent is fixed at 80 is predicted by BiDH and BiMSA. For the calculation of the properties mentioned, the diameter of the anion is fixed at 3 Å while the diameter of the cation varies from 0.5 to 10 Å. The salt concentration also varies from 0.25 to 2 $mol \cdot L^{-1}$.

Figure 7.17 presents the effect of the variation of the cation diameter on the prediction of MIAC, osmotic coefficient, and free ion fraction by the BiDH and BiMSA models. As can be seen from this figure, the predictions of the BiDH and BiMSA models for the MIAC and the osmotic coefficient are very close to each other, disregarding the ratio of cation to anion diameter or salt concentration. However, as is evident from graphs c and d in Figure 7.17, the fraction of free ions predicted by the BiDH and BiMSA models are both quantitatively different.

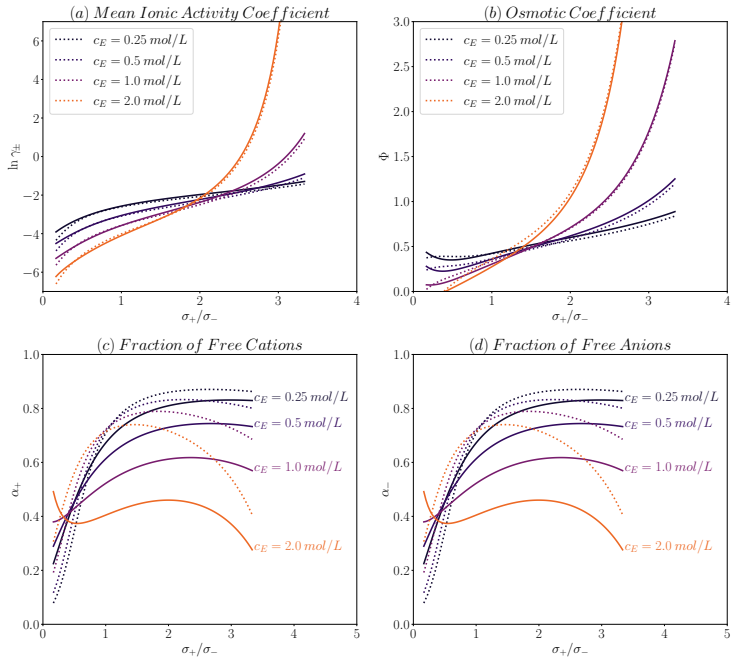

Figure 7.17. This figure compares the predictions of the BiDH and BiMSA model for electrolyte solutions where $Z_- = -2$, $Z_+ = +2$, $\sigma_- = 3 \times 10^{-10}\ m$, $\varepsilon_r = 80$ and the salt concentration is 0.25, 0.5, 1.0, 2.0 $mol \cdot L^{-1}$ corresponding to the colors. Solid lines are predictions from the BiDH model, while dotted lines are predictions from the BiMSA model.

From this sensitivity analysis, it can be implied that varying the diameter of ions, as it is usually an adjusting parameter, affects almost similarly the predictions of MIAC and the osmotic coefficient, which are usually the properties used in parameter estimation. However, the impact of varying the ionic diameter on the fraction of free ions is very different. The question is whether it is possible to verify which fraction of free ions better describe the physics of the system, and whether this question can be answered unless other properties are considered.

7.3.5.2 Sensitivity to Ion Charges Asymmetry

In this section, the effect of charge of the ions on the MIAC, osmotic coefficient, and fraction of free ions predicted by the BiDH and BiMSA models is discussed. Figure 7.18 presents the predictions of the properties mentioned for nine electrolyte solutions in which the charge of the cations varies from 1 to 3 and the charge of the anions varies from -1 to -3.

As is evident from Figure 7.18, the predictions of MIAC and osmotic coefficient by the BiDH and BiMSA models are very close to each other while the fractions of free ions are very different. Charges of the ions are not adjusting parameters in the electrolyte equations of state or other models. However, it should be noted that the fraction of free ions predicted by the BiDH model is lower than the fraction of free ions predicted by the BiMSA model.

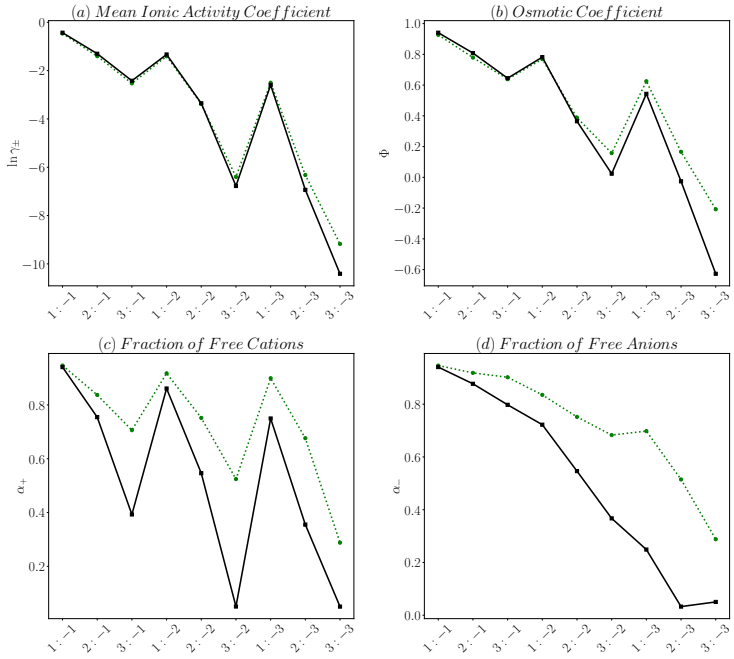

Figure 7.18. This figure compares the predictions of the BiDH and BiMSA model for electrolyte solutions where $\sigma_- = 3.5$, $\sigma_+ = 3$, $c_E = 1\, mol \cdot L^{-1}$ and the RSP of the solvent is 80. Solid lines are predictions from the BiDH model, while dotted lines are predictions from the BiMSA model.

7.3.5.3 Sensitivity to RSP

In this section, the sensitivity of the predictions of the models to the variation of the RSP is studied. Figure 7.19 shows the predictions and the corresponding specification of the electrolyte. As can be seen from this figure, the predicted MIAC and osmotic coefficient by the BiDH and BiMSA models are very close to each other, while the fraction of free ions is very different.

From this sensitivity analysis, a very important conclusion can be drawn. Both BiDH and BiMSA models provide similar results when macroscopic properties such as MIAC and the osmotic coefficient are compared. However, the fractions of free ions predicted by the models are both quantitatively and qualitatively different.

7.4 Summary and Conclusions

This study focused on the development of a new EoS for a charged hard sphere fluid that incorporates ion-ion association. The EoS was developed using the DH theory along with the RCA and Wertheim's theory. The predictive accuracy of the developed model was assessed by comparing its predictions with various MC simulations reported in the literature for charged hard-sphere fluids. The assessment focused on the MIAC, IIAC, and osmotic coefficient obtained by the model, compared with values reported in MC simulations.

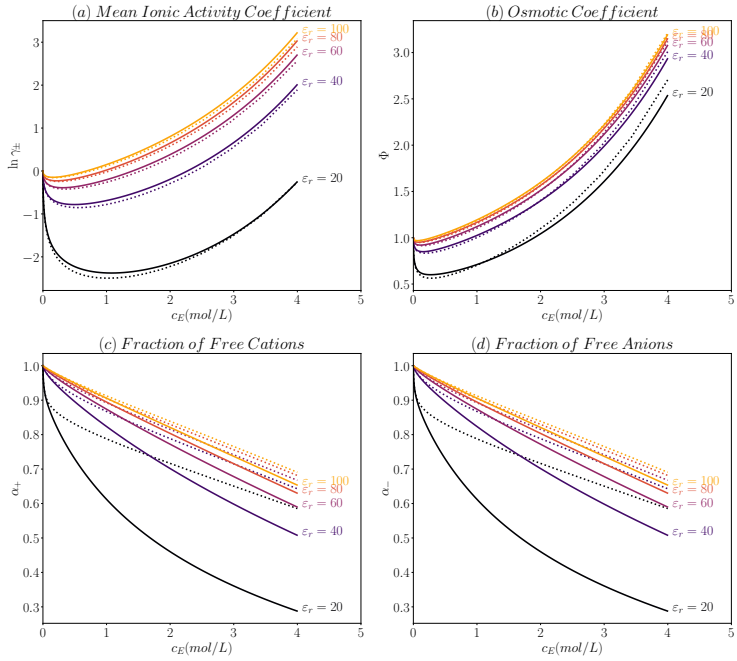

Figure 7.19. This figure compares the predictions of the BiDH and BiMSA model for electrolyte solutions where $Z_- = -1$, $Z_+ = +1$, $\sigma_- = 6 \times 10^{-10}\ m$, $\sigma_+ = 3 \times 10^{-10}\ m$ and the RSP of the solvent is 100, 80, 60, 40 and 20 corresponding to the colors. Solid lines are predictions from the BiDH model, while dotted lines are predictions from the BiMSA model.

The comparisons between the model predictions and the MC simulations revealed a good agreement for the MIAC, IIAC, and osmotic coefficients. The predictions showed consistency across different electrolyte systems, including 1:1, 2:1, 3:1, and 2:2 electrolytes, with varying ionic diameters.

The importance of considering ion-ion association was highlighted by comparing the predictions of the developed model with the DH theory, which neglects ion-ion association. The results demonstrated that incorporating ion-ion association in the model improved its accuracy in predicting thermodynamic properties of electrolyte solutions, such as the MIAC and IIAC.

The significance of the cavity function in the model was discussed, comparing it with the cavity function from the BiMSA theory. The incorporation of ion-dipole interactions within the cavity function was found to be crucial in accurately representing the structural properties of electrolyte solutions. Furthermore, the limitations of solely defining an association site in the SAFT framework were emphasized, highlighting the need for a more precise approach in capturing ion-ion association and its effects on thermodynamic properties.

Overall, the developed EoS showed promising predictive capabilities for charged hard sphere fluids with ion-ion association. The comparisons with MC simulations provided validation and demonstrated the accuracy and generalizability of the model across different electrolyte systems.

Chapter Message

The main conclusion of this research is the successful formulation of a new EoS for charged hard sphere fluids that includes ion-ion association, which has been shown to be more accurate than the DH theory. This was confirmed through extensive comparisons with MC simulations for a variety of electrolyte systems.

Part IV

The Unified Framework

CHAPTER 8
Implicit Solvent Investigation

In Chapter 6, it has been shown that to investigate the effect of ion-ion association in electrolyte solutions, a concurrent investigation of thermodynamic properties and electrical conductivity is required.

In chapter 7, a new EoS has been developed for charged hard-sphere fluids where ion pairing is taken into account. In chapters 4 and 5, two models (single- and multi-salt) for the electrical conductivity of unassociated electrolyte solutions were developed.

In this chapter, the developed EoS and electrical conductivity models will be combined to produce a unified investigation of the property predictions of associative electrolyte solutions. In this chapter, unlike in the following chapter, the structure of the solvent is ignored. Therefore, a unified investigation will be performed considering an implicit solvent model. In the first part of the investigation, the BiDH theory (presented in chapter 7) and the single-salt electrical conductivity model (presented in chapter 4) will be combined to predict the molar conductivity and MIAC of three integral systems. These systems are 2:2 aqueous sulfates, sodium chloride-water-1,4-dioxane system, and ionic liquid-co-solvent solutions.

In the second part, the effectiveness of the electrical conductivity model developed for mixed electrolyte solutions in chapter 5 will be used to predict the electrical conductivity of electrolyte solution that forms ion complexes.

Part of this chapter has already been published or submitted for publication in the following papers.

- *New electrical conductivity model for electrolyte solutions based on Debye-Hückel-Onsager theory [184].*
- *A Novel Model for Predicting the Electrical Conductivity of Multi-salt Electrolyte Solutions [200].*

8.1 Ion Pairing and Conductivity

In Chapter 4, a meticulous assessment of the newly developed electrical conductivity model was carried out, comparing its with other models documented in the literature. Tables 4.4 and 4.5 illustrate that as the charge of ions increases, the accuracy of both the developed model and the existing models decreases. This analysis also reveals a consistent tendency of the developed models to overestimate conductivity when compared to experimental data. Consequently, the root cause of this discrepancy must be sought in an assumption made during the model derivation, leading to the overestimation of conductivity. The hypothesis that ion pairs are responsible for the inconsistency was first suggested by Fuoss and Kraus [297] and has been supported by subsequent research [80, 84].

In Chapter 7, a new EoS for associative electrolyte solutions named BiDH was developed. The capability of the EoS was assessed by comparing its predictions with the MC simulations.

In this chapter, the BiDH model is combined with the developed electrical conductivity model for the prediction of associative electrolyte solutions assuming implicitly the influence of the solvent(s).

Eq. 8.1 present the specific conductivity of associative electrolyte solutions for a symmetrical ($Z_+ = -Z_-$) single-salt electrolyte solution.

$$\chi = \frac{e^2}{k_B T}\left[\sum_{i=1}^{+,-} \rho_i \alpha_i D_i^0 Z_i^2 \left(1 + \frac{\delta v_i}{v_i^0}\right)\left(1 + \frac{\delta k_i}{k_i}\right)\right] \tag{8.1}$$

In Eq. 8.1, α_i is the fraction of unbound ions. To compute this fraction, the BiDH EoS is used. Since in this section a special case of ion pairing for symmetrical single-salt electrolyte solutions is considered, equations 7.33-7.38 are used for the calculation of the fraction of unbound ions. Within these equations, the association constant at infinite dilution must be computed using the Bjerrum model (Eq. 7.35). In this equation, the upper limit of the integral, signifying a cutoff distance beyond which oppositely charged ions are regarded as ion pairs, remains unknown. To the best of our knowledge, there is no definitive predictive method to estimate this upper limit.

Moreover, this upper limit is inherently dependent on factors such as system temperature, salt concentration, ions, and solvent(s). We have illustrated that the upper limit of the Bjerrum integral can be linked to the distance of the closest approach through a simple scalar factor, represented as $l_{mn} = \theta\sigma_{mn}$ [286]. It has been demonstrated that θ can be considered a global parameter dependent on the solvent(s) but not influenced by salt concentration, ions, or system temperature.

To avoid rendering the model estimations empirical, a decision has been made to employ a temperature- and ion-independent factor. This choice is motivated by a commitment to uphold the predictive nature of the model, avoiding the introduction of unnecessary complexity or potential biases.

To compute relaxation and electrophoretic effects, the variable κ should be replaced by $\kappa' = \sqrt{\frac{4\pi e^2}{\epsilon k_B T} \sum_j \alpha_j \rho_j Z_j^2}$ in the equations 4.10 and 4.13.

The molar conductivity of the solution (Λ) can be calculated with Eq. 8.2 in which c is the salt concentration of the solution assuming full dissociation.

$$\Lambda = \frac{\chi}{c} \tag{8.2}$$

In this section, an exploration of three systems is undertaken where the prediction of molar conductivity may be significantly influenced by ion pairing. Following the approach described in Chapters 7 and 4, a predictive examination is performed without making any adjustments to fit the experimental data. Therefore, the van der Waals diameter (or, in the case of simple electrolytes, the crystallographic ionic diameter) provided in Table 3.1 is used for the calculations. The ionic conductivities at infinite dilution, along with the permittivity and viscosity of the solvent, are derived from values reported in the existing literature and are detailed in Tables 3.1 and 3.2.

To demonstrate the effectiveness of this approach, three specific systems have been selected for investigation, where ion-ion association has been shown to be highly significant. These systems comprise the aqueous solution of 2:2 sulfates, ionic liquid-co-solvent solutions, and mixed solvent electrolyte solutions. The choice of these systems is intended to assess the model's capabilities and validate our method in diverse scenarios where the impact of ion pairing is substantial.

8.1.1 Aqueous Solutions

Figure 8.1 shows the molar conductivity of aqueous magnesium sulfate solutions at different temperatures. The dashed lines in this figure represent the molar conductivity predicted by Model 3 (as detailed in Chapter 4), disregarding the influence of the ion pairing. In contrast, the solid lines show the predicted molar conductivity, taking into account the impact of ion pairing, utilizing the BiDH model in conjunction with Model 3.

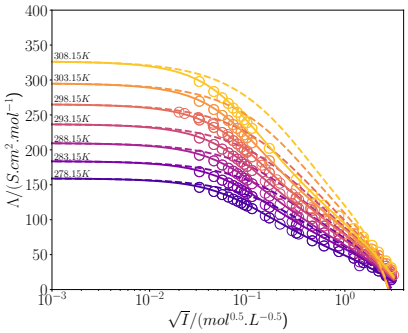

Figure 8.1. This figure present the molar conductivity of $MgSO_4$ aqueous solutions predicted by the Model 3 where ion pairing is (solid lines) and is not (dashed lines) considered (symbols are experimental data from ref. [130]). Reprinted with permission from ref. [120]. Copyright 2023 American Chemical Society.

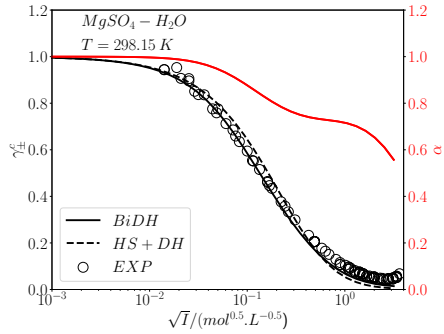

Figure 8.2. The MIAC ($\gamma_{\pm}^{c}$) of $MgSO_4$ aqueous solution at 298.15 is predicted by the BiDH model (solid line) and by the HS+DH model (dashed lines). symbols represent experimental data from ref. [130]. Red solid line represents the fraction of unbound ions predicted by the BiDH model. Reprinted with permission from ref. [120]. Copyright 2023 American Chemical Society.

To predict the fraction of unbound ions (α_i) as mandated by Eq. 8.1, equations 7.33-7.38 are used. In the computation of the reference cavity function and molar conductivity, it is assumed that the RSP is not concentration-dependent and is equivalent to the permittivity of the solvent. Furthermore, the upper limit of the Bjerrum integral (Eq. 7.35) is specified as $l_{+-} = 1.15\sigma_{+-}$.

Figure 8.1 clearly illustrates that the correction of Model 3 to incorporate the influence of the ion-ion association has significantly improved the accuracy of the predicted molar conductivity of the solution. This improvement is also evident in other 2:2 sulfates, as elaborated in Appendix D (Figures D.29-D.32).

8.1.2 Mixed-solvent systems

The second system explored in this section to assess the impact of ion-ion association is the solution of NaCl-water-1,4-dioxane. This system is particularly intriguing due to the significant variation in the dielectric constant of the solvent (in an implicit solvent model), ranging from 51 to 13 as the salt-free mole fraction of 1,4-dioxane increases from 0.1104 to 0.4002. Consequently, the influence of reducing the permittivity of the solvent(s) can be investigated in this system.

Figure 8.3 illustrates the molar conductivity of the NaCl-Water-1,4-dioxane system at different temperatures and salt-free mole fractions of 1,4-dioxane. As in Figure 8.1, the solid lines represent the predicted molar conductivity with Model 3, considering the effect of ion-ion association, while the dashed lines depict the predicted molar conductivity with Model 3 assuming full dissociation.

Calculating the molar conductivity involves utilizing the RSP and viscosity, as tabulated in Table 8.1. The ionic diameters of sodium and chloride are extracted from the values provided in Table 3.1. Additionally, the ionic conductivity at infinite dilution for both cation and anion is obtained from the existing literature and is detailed in Table 8.1. Furthermore, the scalar factor for the upper limit of the Bjerrum model (θ) is set to 1.13, 1.13, 1.08, and 1.008, corresponding to salt-free mole fractions of 1,4-dioxane of 0.1104, 0.2, 0.2979, and 0.4002, respectively.

Similar to the observations in Figure 8.1, Figure 8.3 underscores that considering the ion-ion association in the calculation of molar conductivity markedly improves the predictions made by Model 3. Additionally, this figure highlights that the accounting of the ion pairing becomes increasingly crucial as the salt-free mole fraction of 1,4-dioxane increases. This aligns with our expectation because we hypothesized that in systems with a lower RSP of the solvent(s), ion pairing would exhibit more noticeable activity.

Table 8.1. The RSP and viscosity of the water-1,4-dioxane mixed solvent, along with the ionic conductivity at infinite dilution of the cation and anion, are provided. These values are reported for varying no-salt mole fraction of 1,4-dioxane (x_D), ranging from 0.1104 to 0.4002 [148, 149].

				T (K)			
x_D	278.15	283.15	288.15	293.15	298.15	303.15	308.15
				ε_r			
0.1104	51.846	50.519	49.031	47.688	46.387	45.154	43.937
0.2000	35.395	34.370	33.322	32.421	31.425	30.596	29.730
0.2979	23.801	23.098	22.420	21.768	21.135	20.527	19.940
0.4002	16.038	15.579	15.133	14.727	14.304	13.915	13.531
				$\eta \times 10^3\ (Pa \cdot s)$			
0.1104	3.0727	2.6029	2.2280	1.9303	1.6848	1.4869	1.3243
0.2000	3.5632	3.0271	2.5966	2.2438	1.9652	1.7310	1.5332
0.2979	3.4398	2.9458	2.5465	2.2197	1.9507	1.7267	1.5377
0.4002	3.0605	2.6475	2.3106	2.0304	1.7993	1.6034	1.4373
				$\lambda_+^0 \times 10^4\ (S \cdot m^2 \cdot mol^{-1})$			
0.1104	15.37	18.04	20.95	24.08	27.44	31.00	34.77
0.2000	12.35	14.49	16.83	19.35	22.07	24.97	28.05
0.2979	10.99	12.83	14.77	16.90	19.18	21.61	24.19
0.4002	9.950	11.49	13.17	14.97	16.90	18.94	21.10
				$\lambda_-^0 \times 10^4\ (S \cdot m^2 \cdot mol^{-1})$			
0.1104	22.37	26.07	30.04	34.29	38.77	43.48	48.41
0.2000	17.59	20.49	23.62	26.97	30.54	34.28	38.23
0.2979	15.30	17.74	20.27	23.00	25.93	29.00	32.22
0.4002	13.51	15.5	17.64	19.90	22.30	24.80	27.42

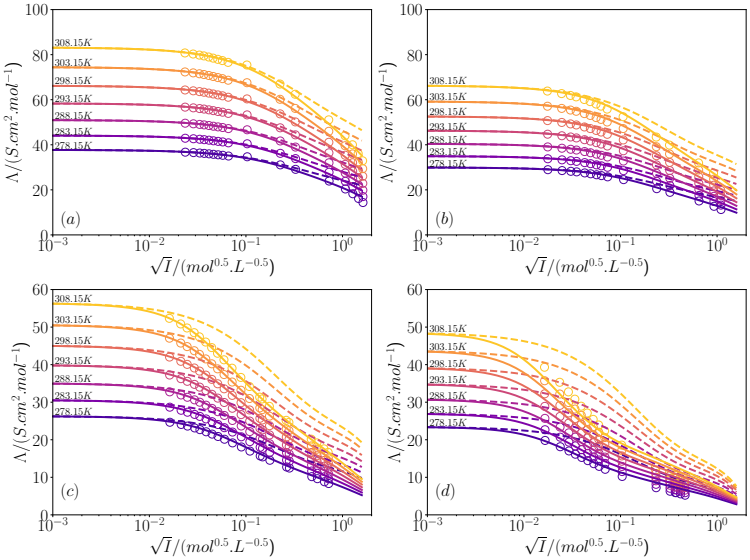

Figure 8.3. This figure present the molar conductivity of NaCl-water-1,4-dioxane ternary mixtures predicted by Model 3, considering ion pairing (solid lines) and not considering ion pairing (dashed lines). The salt-free mole fractions of 1,4-dioxane are (a) 0.1104, (b) 0.2, (c) 0.2979, and (d) 0.4002. Symbols in the plot represent experimental data from ref. [148,149]. Reprinted with permission from ref. [120]. Copyright 2023 American Chemical Society.

8.1.3 Ionic Liquid Co-solvent Systems

In this section, we assess the predictive capability of Model 3 by comparing its predictions with the experimental data of imidazolium ionic liquid (IL) co-solvent systems. In the initial example shown in Figure 8.4, water serves as the co-solvent, while in Figure 8.5, acetonitrile (AN) is the chosen co-solvent.

In these figures, akin to Figures 8.1 and 8.3, solid lines represent the predicted molar conductivity, incorporating the influence of ion-ion association, while dashed lines signify the molar conductivity assumed under full dissociation. To account for the effect of ion pairing, Eq. 8.1 is employed for calculating the specific conductivity, and the fraction of unbound ions is derived from equations 7.33-7.38.

For these calculations, we have assumed that ionic liquids are spherical entities, with their van der Waals diameter as reported by Beichel et al. [298], and as tabulated in Table 8.2. The ionic conductivity at infinite dilution for these ILs is also taken from the existing literature and is detailed in Table 8.2. Furthermore, the scalar factor for the upper limit of the Bjerrum model (θ) is set to 1.45 for aqueous solutions and 1.457 for IL-AN solutions.

It is important to note that in the molar conductivity calculation procedure, the assumption is made that the RSP remains constant and is equal to the RSP of the co-solvent. Additionally, given that the valence type of the IL is equal to one, ion pairs do not contribute to the specific conductivity. As a result, there is no need to calculate the relaxation and electrophoretic effects of ion pairs.

Figure 8.4 illustrates the molar conductivity of aqueous solutions of 1-Hexyl-3-methylimidazolium chloride at temperatures ranging from 293.15 to 313.15 K. As evident in this figure, akin to systems with simple salt aqueous solutions, assuming full dissociation leads to an overestima-

Table 8.2. The ionic conductivity at infinite dilution (λ_i^0) in $S \cdot m^2 \cdot mol^{-1}$ and ionic diameter (σ_i) in m for the studied ionic liquids in this work are sourced from references [298, 299].

T (K)	Ion	$\lambda_i^0 \times 10^4$	$\sigma_i \times 10^{10}$
	Co-solvent:	Water	
293.15	$[C_6MIM]^+$	24.90	6.91
298.15	$[C_6MIM]^+$	30.91	6.91
303.15	$[C_6MIM]^+$	34.35	6.91
308.15	$[C_6MIM]^+$	38.30	6.91
313.15	$[C_6MIM]^+$	40.65	6.91
	Co-solvent:	AN	
298.15	$[C_2MIM]^+$	83.00	5.94
298.15	$[C_4MIM]^+$	75.00	6.47
298.15	$[C_6MIM]^+$	67.25	6.91
298.15	$[BF_4]^-$	115.4	4.57

tion of the prediction of the molar conductivity. In contrast, considering the effect of ion-ion association brings about a substantial enhancement in the accuracy of molar conductivity predictions.

Figure 8.5 shows the correlation between the predicted molar conductivity of Model 3 and the experimental data for three IL-AN solutions. These solutions include the following ionic liquids: 1-Ethyl-3-methylimidazolium tetrafluoroborate ([C_2MIM][BF_4]), 1-Butyl-3-methylimidazolium tetrafluoroborate ([C_4MIM][BF_4]), and 1-Hexyl-3-methylimidazolium tetrafluoroborate ([C_6MIM][BF_4]). The figure illustrates the molar conductivity of binary IL-co-solvent systems across a range from very dilute solutions to the pure IL system.

As shown in Figure 8.5, unlike simple electrolyte solutions, the molar conductivity decreases from near 200 $S \cdot cm^2 \cdot mol^{-1}$ at infinite dilution to near zero when the mole fraction of the IL is equal to 1. Therefore, these systems, along with other ionic liquid-co-solvent

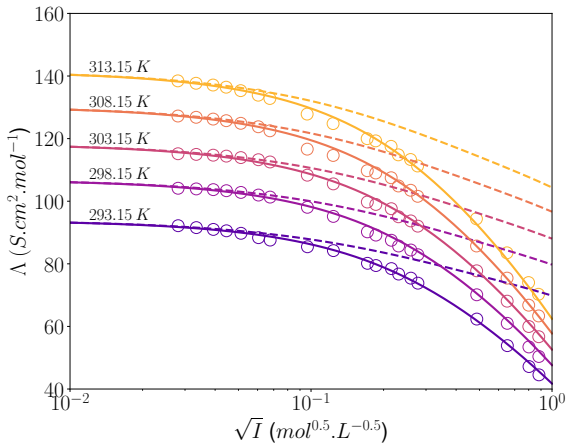

Figure 8.4. This figure presents the molar conductivity (Λ) of [C_6MIM]Cl aqueous solutions predicted by Model 3, where ion pairing is considered (solid lines), and is not considered (dashed lines). Symbols in the plot represent experimental data from ref. [299]. Reprinted with permission from ref. [120]. Copyright 2023 American Chemical Society.

systems, represent a special case due to mutual solubility.

Figure 8.5 illustrates that the predicted molar conductivity, assuming full dissociation, significantly deviates from the experimental data. This outcome was anticipated, given the high activity of ion-ion association in IL-co-solvent solutions.

As is evident from Figure 8.5, taking into account the ion-ion association leads to a substantial improvement in the prediction of molar conductivity by Model 3. This figure demonstrates that even when the mole fraction of the IL is equal to 1, a more accurate prediction is achieved.

It is important to note that expecting the model to accurately predict the molar conductivity of this system across the entire range from pure AN to pure IL is unrealistic because of two factors. Firstly, in IL-co-solvent systems, ion-ion association may lead to the formation of higher aggregates, a consideration that is omitted here. Second, and more significantly, the implicit solvent picture of the systems breaks down at a very high content of ionic liquids, resulting in observed deviations. Therefore, the variation of the RSP should be taken into account in the evaluation of molar conductivity. Examining these two assumptions goes beyond the scope of this chapter.

8.2 Conductivity of Systems Forming Ion Complexes

In Chapter 4, it has been shown that all models developed by us or from the existing literature fail to predict the molar conductivity of certain aqueous electrolyte solutions. It has been speculated that in these solutions, ions form not only ion pairs but also ion complexes. However, as mentioned in Chapter 5, for these systems where the number of types of conducting species is greater than two, the models mentioned in Chapter 4 cannot be used. In Chapter 5, a new model for the electrical conductivity of multi-component systems was developed. In this section, the model developed in Chapter 5 is used to predict the molar conductivity of electrolyte solutions that form ion complexes.

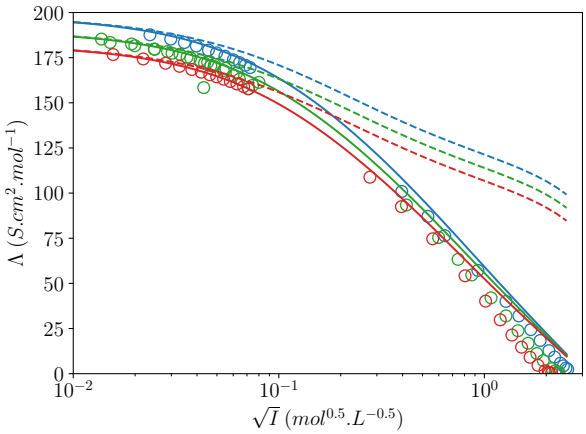

Figure 8.5. This figure presents the molar conductivity (Λ) of [C_2MIM][BF_4]-AN (blue lines and symbols), [C_4MIM][BF_4]-AN (green lines and symbols), and [C_6MIM][BF_4]-AN (red lines and symbols) systems at 298.15 K predicted by Model 3, considering ion pairing (solid lines) and not considering ion pairing (dashed lines). Symbols in the plot represent experimental data from ref. [300, 301]. Reprinted with permission from ref. [120]. Copyright 2023 American Chemical Society.

In this section, two distinct systems known to form ion complexes are explored. The first involves aqueous solutions of cadmium halide, characterized by halide ions such as Br^-, Cl^-, and I^-. The second set comprises ternary solutions that combine cadmium halide, potassium halide, and water.

In the context of the mentioned systems, the first step involves assessing the concentrations of both ions and ion complexes. This is accomplished by applying the methodology described by Simonin [302].

For electrolytes that demonstrate complexation, we posit that cadmium cations form n ion complexes with the X^- anion, as defined by Eq. 8.3:

$$Cd^{2+} + nX^- \rightleftharpoons CdX_n^{2-n} \tag{8.3}$$

For reactions in equilibrium, the corresponding equilibrium equation can be formulated as presented in Eq. 8.4:

$$\beta_n = \frac{\gamma_n^c}{\gamma_+^c(\gamma_-^c)^n}\frac{c_n}{c_+(c_-)^n} \tag{8.4}$$

In Eq. 8.4, β_n, γ_n^c, c_n represent the cumulative formation constant of the complex, the activity coefficient and the concentration, all on the molarity scale, for the complex of ions consisting of n anions. γ_+^c, γ_-^c, c_+, and c_- denote the activity coefficient of cadmium, anion, and the concentration of cadmium and anion on the molarity scale, respectively.

In addressing this speciation problem, n reaction equilibrium equations (Eq. 8.4), along with two equations for the conservation of Cd^{2+} and X^-, need to be solved numerically. These calculations require determining the activity coefficients of the components which, in turn, depend on the concentrations of the respective components. To estimate these activity coefficients, we applied the MSA model [5, 6].

The calculations mentioned above were performed using the freely available CHEAQS Next software [303, 304]. Comprehensive computational procedures are described in references [302, 305].

As indicated in the literature [302] with respect to cadmium halides, the maximum number of anions in the complex, denoted n, is set to 4. The cumulative complex formation constant was obtained from the NIST database [306]. The logarithmic values of these constants, used in this study, are outlined in Table 8.3 corresponding to the equilibrium reactions 1-4.

To calculate the activity coefficients and specific conductivity, the diameter of the species is also crucial. We used the equation proposed by Simonin [302] to determine the diameter of the ion complexes. This equation is outlined in Eq. 8.5:

$$\sigma_n^3 = \frac{p}{p+n}(\sigma_+^3 - b_+^3) + b_+^3 + n\sigma_-^3 \tag{8.5}$$

In Eq. 8.5, b_+ denotes the bare cation diameter, and $n + p$ represents the coordination number of the cation. Within this context, n anions and p water molecules are associated with the cation. Diameters of ion complexes, computed using Eq. 8.5 and denoted as σ_i,

Table 8.3. The cumulative complex formation constant (β_n as defined in Eq. 8.4) of cadmium halide electrolytes is sourced from the NIST database [306] and the CHEAQS Next software [303, 304].

Salt	$\log_{10}(\beta_1)$	$\log_{10}(\beta_2)$	$\log_{10}(\beta_3)$	$\log_{10}(\beta_4)$
$CdBr_2$	2.150	3.000	3.000	2.900
$CdCl_2$	1.980	2.600	2.002	1.470
CdI_2	2.280	3.920	5.000	6.000

Table 8.4. This table includes the ionic conductivity at infinite dilution (λ_i^0) at 298.15 K, ionic diameters using the Marcus diameter and Eq. (σ_i^M), and ionic diameters from ref. [302] (σ_i) for the ion complexes studied in this work.

Ion Complex	$\lambda_i^0 \times 10^4\ (S \cdot m^2 \cdot mol^{-1})$	$\sigma_i^M \times 10^{10}\ (m)$	$\sigma_i \times 10^{10}\ (m)$
Cd^{2+}	53.00	1.900	5.590
$[CdBr]^+$	26.16	4.063	5.800
$[CdBr_3]^-$	25.54	5.724	5.810
$[CdBr_4]^{2-}$	50.50	6.281	5.880
Br^-	78.10	3.920	3.390
$[CdCl]^+$	26.14	3.787	5.751
$[CdCl_3]^-$	25.48	4.668	5.237
$[CdCl_4]^{2-}$	50.33	5.304	5.422
Cl^-	76.31	3.620	3.620
$[CdI]^+$	26.15	4.515	6.010
$[CdI_3]^-$	25.49	6.402	6.390
$[CdI_4]^{2-}$	50.38	7.031	6.620
I^-	76.8	4.400	4.320

are presented in Table 8.4. This table also includes the diameters for cadmium and halides as sourced from ref. [302].

Anderko et al. [127] have introduced an alternative methodology for determining the diameter of ion complexes, represented in Eq. 8.6. Within this approach, the computed diameters of ion complexes are designated as σ_i^M. It is essential to note that the tabulated ion diameters refer to the bare ionic diameter, using values reported by Marcus [155]. For the scope of this study, we exclusively utilize σ_i^M in the calculations related to electrical conductivity.

$$\sigma_n^3 = \sigma_+^3 + n\sigma_-^3 \tag{8.6}$$

To predict electrical conductivity, it is essential to determine the ionic conductivity at infinite dilution (λ_i^0) for ion complexes. In this chapter, we utilize the method proposed and validated by Anderko et al. [127] to calculate the λ_i^0 of these ion complexes, as presented in Eq. 8.7:

$$(\lambda_n^0)^3 = \frac{\mid Z_n \mid}{\left[\left(\frac{\mid Z_+ \mid}{\lambda_+^0}\right)^3 + n\left(\frac{\mid Z_- \mid}{\lambda_-^0}\right)^3\right]^{1/3}} \tag{8.7}$$

Table 8.4 provides details on the ionic conductivities of the ion complexes, as well as the ions used to predict electrical conductivity.

In this study, three distinct approaches are employed to predict the electrical conductivity of electrolyte solutions that form ion complexes, as outlined in Table 8.5. In Scheme 1, we determine the concentration of ion complexes as previously described and utilize the corresponding ionic diameter (σ_i from Table 8.4) for conductivity predictions, the same diameter used as in the calculation of the activity coefficient. In Scheme 2, we operate under the assumption that no ion complexes form. As a result, we compute electrical conductivity analogous to the methods for simple electrolytes discussed earlier. Scheme 3 mirrors Scheme 1 in approach but distinguishes itself by using the ionic diameters of bare ions (σ_i^M from Table 8.4) for conductivity predictions, while still using σ_i from Table 8.4 for calculation of activity coefficients.

Table 8.5. This table outlines the schemes employed in this study for calculating the electrical conductivity of electrolyte solutions that form ion complexes.

Scheme	Ion complex formation	Ionic diameter	Figure 8.6	Table 8.5
1	Yes	σ_i in Table 8.4	Solid lines	Λ_1
2	No	σ_i in Table 3.1	Dashed lines	Λ_2
3	Yes	σ_i^M in Table 8.4	Dotted lines	Λ_3

Figure 8.6 illustrates the molar conductivity (Λ) and species concentration (c_i) of CdX_2 aqueous solutions at 298.15 K, following the schemes outlined in Table 8.5. More specifically, graphs a, c, and e of the figure show the molar conductivity, while graphs b, d, and f show the species concentrations.

The observations depicted in Figure 8.6 can be analyzed from two perspectives. First, one can compare the molar conductivity predicted by Schemes 1-3 with the experimental data for each electrolyte solution. Subsequently, the concentration distribution of various species within each CdX_2-water system can be examined.

As shown in Figure 8.6 (particularly in graphs a, c and e), the molar conductivity predicted by the model developed in this study aligns closely with the experimental data when employing Schemes 1 or 3. In contrast, in line with observations from Chapter 4, the assumption of complete dissociation according to Scheme 2 results in a significant overestimation of the molar conductivity.

Upon closer inspection of the concentrations of species, it becomes evident that the concentrations of simple ions (Cd^{2+}, Br^-, Cl^-, I^-) deviate significantly from their stoichiometric values. Consequently, for these systems, the assumption of full dissociation is notably erroneous. As demonstrated in this figure and confirmed by prior studies, electrical conductivity models based on this assumption fail to accurately predict the molar conductivity.

It is crucial to emphasize that the molar conductivity presented in Figure 8.6 is a direct prediction without any parameter adjustments made to align with the experimental data. Furthermore, no adjustments were made during species concentration calculations; all properties and parameters were derived directly from the literature. To our knowledge, only the ionic diameter of the cation was adjusted to fit the osmotic coefficient experimental data by Simonin [302], which means that no empirical modifications were incorporated into the calculations of the molar conductivity. Given the accurate predictions shown in Figure 8.6, this confirms that our model developed effectively predicts the molar conductivity for systems comprising more than two charged species.

Table 8.6 presents the predictions of the molar conductivity of the model developed using Schemes 1-3 for the three CdX_2-KX-H_2O systems at 298.15 K, with X representing Br, Cl, or I. It is apparent from the table that the predictions using Schemes 1 and 3 align reasonably well with the experimental data. On the contrary, the predictions made with Scheme 2 deviate significantly from the observed measurements.

In the systems highlighted in Table 8.6, the agreement between model predictions (using Schemes 1 and 3) and experimental data for CdI_2-KI aqueous solutions, particularly at elevated concentrations of KI, is notably lacking. It is important to note that, unlike KBr and KCl, the NIST database suggests that KI forms ion complexes with $\log_{10}(\beta_1) = -0.4$. This assumption, at high potassium iodide concentrations, implies that a significant portion of potassium ions exists as neutral KI(aq) species. For instance, with $c_{KI} = 4\, mol.L^{-1}$ and $c_{CdI_2} = 0.5 mol.L^{-1}$, nearly 44% of potassium ions are found as neutral KI(aq) species. Consequently, the predicted molar conductivity considerably underestimates the experimental readings at high concentrations of KI, in contrast to the outcomes for CdI_2 aqueous solutions (as seen in Figure 8.6) and $CdBr_2$-KBr and $CdCl_2$-KCl aqueous solutions (as detailed in Table 8.6).

From the data obtained in this study, it remains not conclusive whether the postulated

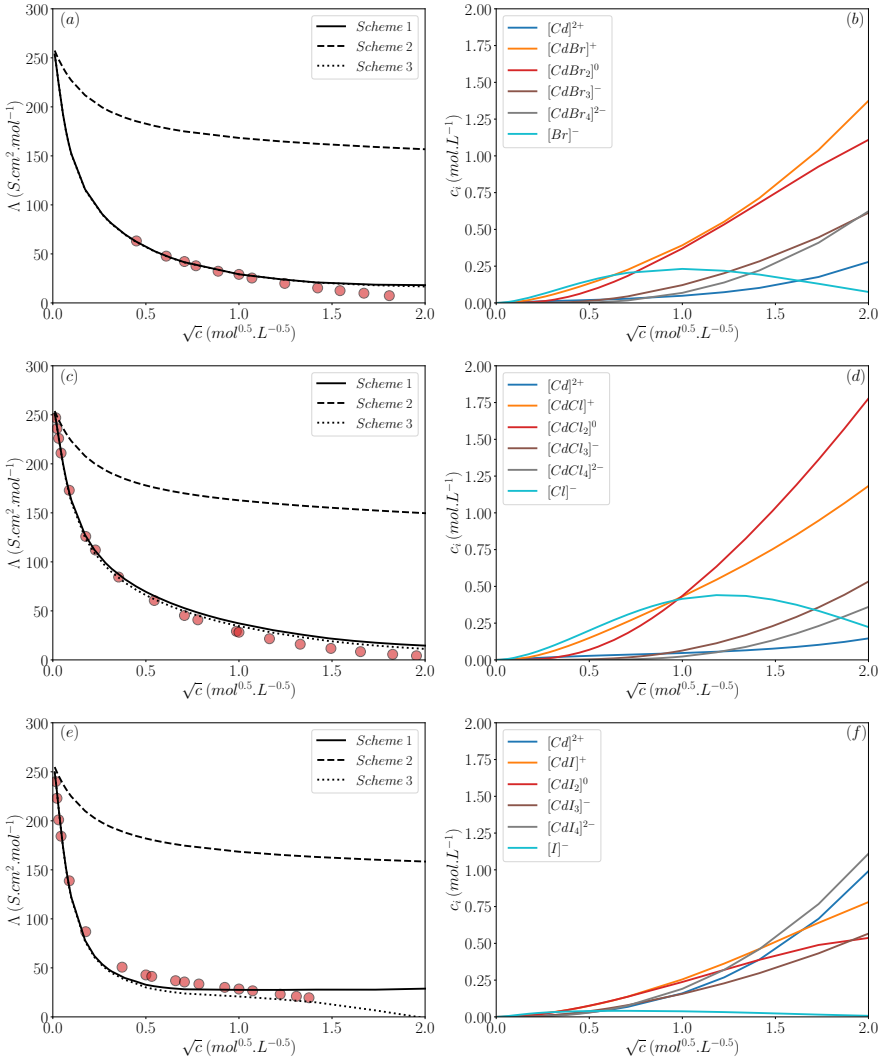

Figure 8.6. This figure illustrates the molar conductivity (Λ) predicted by the developed model in Chapter 5 according to the schemes summarized in Table 8.5 and the concentration distribution (c_i) estimated using the CHEAQS Next software of (a) and (b) $CdBr_2$, (c) and (d) $CdCl_2$, and (e) and (f) CdI_2 aqueous solutions at 298.15 K (symbols are experimental data from ref. [211, 307]). Reprinted with permission from ref. [200]. Copyright 2023 American Chemical Society.

Table 8.6. This table displays the molar conductivity predicted by the model, taking into account the formation of ion complexes with the diameter from ref. [302] (Λ_1) and the Marcus diameter (Λ_3), compared to the experimental data (Λ^{exp}). It also includes the molar conductivity predicted assuming full dissociation (Λ_2) for CdX_2-KX aqueous solutions at 298.15 K. (The experimental data is from ref. [211]). Reprinted with permission from ref. [200]. Copyright 2023 American Chemical Society.

c_{CdX2}	c_{KX}	Λ^{exp}	Λ_1	Λ_2	Λ_3
X=Br^-					
0.167	0.667	65.314	62.982	87.705	64.864
0.250	0.500	47.440	46.464	78.349	47.485
0.333	0.333	34.545	33.286	70.261	33.596
0.333	1.333	58.290	54.937	82.822	57.532
0.417	0.167	23.972	22.653	63.221	22.414
0.500	1.000	40.456	38.744	73.823	40.250
0.667	0.667	26.659	26.995	66.148	27.560
0.833	0.333	18.335	17.287	59.581	17.078
X=Cl^-					
0.040	0.830	99.411	98.429	104.254	100.350
0.080	0.670	84.802	85.660	97.292	86.991
0.130	0.500	69.225	69.732	88.207	70.370
0.170	0.330	56.417	55.139	79.617	55.133
0.170	1.670	79.321	79.358	92.528	81.846
0.210	0.170	42.713	39.982	70.322	39.386
0.330	1.330	58.625	60.237	82.371	61.856
0.500	1.000	41.316	44.372	73.338	45.180
0.670	0.670	27.810	31.630	65.727	31.727
0.830	0.330	17.387	21.234	59.277	20.744
X=I^-					
0.100	0.100	35.575	31.094	77.390	31.091
0.100	1.000	88.677	69.412	98.840	71.226
0.200	1.000	69.869	53.351	89.958	55.037
0.300	0.300	28.975	25.168	72.150	25.335
0.500	0.100	15.263	13.006	61.391	11.986
0.500	0.200	18.424	15.580	63.914	14.801
0.500	0.300	21.300	18.217	66.114	17.777
0.500	0.500	26.490	23.124	69.748	23.326
0.500	0.800	33.378	27.689	73.803	28.636
0.500	1.000	37.676	30.482	75.846	31.818
0.500	1.500	48.043	35.631	79.451	37.399
0.500	2.000	55.329	37.674	81.677	39.566
0.500	3.000	63.160	37.300	83.916	39.217
0.500	4.000	65.451	35.111	84.606	36.959
0.800	0.800	23.891	21.385	67.275	21.515
1.000	1.000	22.503	20.095	65.895	20.137

formation of ion complexes for potassium iodide is mistaken or if the value of β_1 is erroneous. A more detailed examination of both the thermodynamic and transport properties of these systems is warranted. However, it is pertinent to highlight a distinct anomaly observed for the CdI_2-KI aqueous solutions, especially at elevated potassium iodide concentrations: the predicted molar conductivity substantially deviates from the experimental values, skewing considerably lower.

8.3 Summary and Conclusions

In this chapter, the models developed in the previous parts of this thesis were combined to predict the molar conductivity and MIAC of the associative electrolyte solution simultaneously where the solvent is treated as a continuum medium.

The successful integration of ion pairing into the prediction of electrical conductivity for associative electrolyte solutions has been demonstrated. We examined three pivotal systems, which include 2:2 aqueous sulfates, NaCl-water-1,4-dioxane, and ionic liquid-co-solvent systems. Across all these systems, the integration of the BiDH EoS introduced in Chapter 7 and the electrical conductivity model established in Chapter 4 consistently led to a modification in the predicted electrical conductivity.

The ability of the model developed in Chapter 5 to predict the electrical conductivity of electrolytes that form ion complexes has been rigorously evaluated. Results reveal that the model predictions, when considering ion complex formation, align very closely with the experimental data for such systems. This underscores the reliability and robustness of our model, even when applied to more complicated systems.

Chapter Message

Whether the systems form ion pairs or ion complexes, the combination of the BiDH EoS and the electrical conductivity models (single- and multi-salt) has shown to be accurate and reliable.

CHAPTER 9

Binding eSAFT-VR-Mie

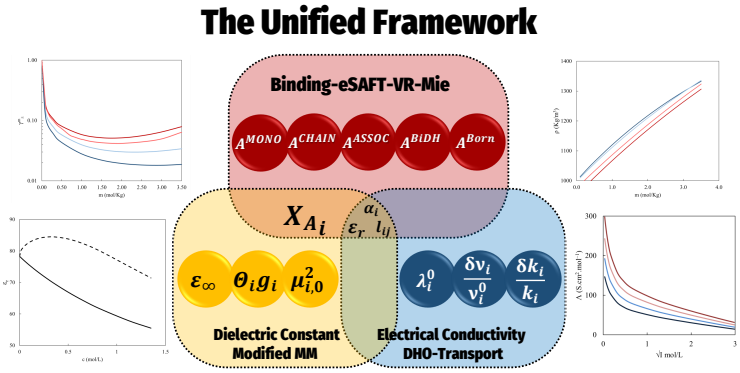

In this chapter, we introduce a novel EoS termed Binding eSAFT-VR-Mie. The non-electrostatic component of this EoS is derived from the SAFT-VR-Mie model, as formulated by Lafitte et al. [68]. This base model was later modified in the association part by Dufal et al. [308]. To address the electrostatic component, we employ the BiDH theory [286], as explained in Chapter 7, in conjunction with the Born equation [288] to handle ion solvation.

In order to investigate ion pairing in electrolyte solutions, we recommend a unified framework anchored on the concurrent examination of thermodynamic properties and electrical conductivity. Utilizing this proposed electrolyte EoS along with the unified framework, we set forth predictions for the properties of three binary salt-water systems at 298.15 K. Consequent discussions will shed light on the implications of integrating the ion-ion association into property calculations, the significance of the chosen reference state, the selection of relative permittivity, and potential avenues for refinement.

This chapter brings together models from earlier chapters as well as additional ones from the existing literature to conduct a comprehensive exploration of property predictions in electrolyte solutions. To enhance readability, certain equations from the preceding chapters are reiterated here. The aim is to make this chapter of the Ph.D. thesis self-contained, eliminating the need for readers to be familiar with topics covered in the preceding chapter before delving into this one.

In Section 9.1, we introduce the Binding eSAFT-VR-Mie, describing its framework alongside the replication of the electrical conductivity models developed in Chapters 4 and 5. Within this section, we also elaborate on our methods for calculating the thermodynamic properties and molar conductivity, and unveil our unified framework. Following this, Section 9.2 provides our predictive results for liquid density, MIAC, osmotic coefficient, and molar conductivity for three binary salt-water systems. The fraction of unbound ions is highlighted, and a deep dive into the specific contributions to the activity coefficient of ions is provided. In the subsequent Section 9.3, we discuss the implications of incorporating the ion-ion association in predicting the properties of electrolyte solutions. We reflect on the importance of the reference-state association constant, drawing from Onsager's bookkeeping rule, while

suggesting potential model enhancements. The chapter concludes in Section 9.4, where we summarize the primary insights and conclusions derived from our theoretical exploration.

9.1 Methods

In this chapter, we consider a system comprising C components. Among these, C_{ion} are charged cations and anions, while the remaining components are neutral compounds. We permit the formation of ion pairs between oppositely charged ions, but we neglect the emergence of larger aggregates such as ion triplets. Long-range interactions are captured through implicit solvent methodologies, which incorporate the RSP of the solvent or solvents into the equations, termed "electrostatic contributions." For this purpose, we employ the recently developed BiDH model [286] (as explained in Chapter 7). Meanwhile, the molecular interactions, termed "non-electrostatic contributions," are described using the SAFT-VR-Mie EoS [68, 308].

For the system under consideration, the specific properties corresponding to the canonical ensemble (denoted as NVT) include the number of species, represented as N_i (which includes both ions and molecules), the volume of the system, indicated as V and the temperature, symbolized as T. Throughout the chapter, we utilize the mole number (n_i), mole fraction (x_i), number density (ρ_i), and concentration (c_i) in line with the relationship given in Eq. 9.1.

$$x_i = \frac{N_i}{\bar{N}},\ \rho_i = \frac{N_i}{V},\ n_i = \frac{N_i}{N_A},\ c_i = \frac{N_i}{N_A V} \tag{9.1}$$

In Eq. 9.1, N_A is the Avogadro number.

$$\bar{N} = \sum_{j=1}^{C} N_j,\ \bar{\rho} = \sum_{j=1}^{C} \rho_j \tag{9.2}$$

Furthermore, we employ molality, a specific concentration measure tailored for electrolyte solutions. Molality is defined as the number of moles of solute per kilogram of solvent.

$$m_i = \frac{n_i}{\sum_j w_j},\ j \in solvents \tag{9.3}$$

In Eq. 9.3, w_i is the mass of solvent molecules.

9.1.1 Equation of State

In this research, the EoS is articulated through contributions to the reduced residual Helmholtz free energy, as described in Eq. 9.4:

$$\tilde{a}^r \equiv \frac{A^r}{N k_B T} \equiv \frac{A - A^{IDEAL}}{N k_B T} \tag{9.4}$$

The contributions of the reduced residual Helmholtz free energy are expressed in Eq. 9.5. Among these contributions, the non-electrostatic elements of the EoS are represented by $\tilde{a}^{MONO}$, $\tilde{a}^{CHAIN}$, and $\tilde{a}^{ASSOC}$ [68]. The solvation effect on the reduced residual Helmholtz free energy, when ions transition from a vacuum environment to a fluid medium, is captured by $\tilde{a}^{BORN}$ [288]. Furthermore, the BiDH theory [286] provides insight into ion-ion interactions, which are denoted by $\tilde{a}^{DH}$ and $\tilde{a}^{MAL}$ in the equation. These components collectively provide a comprehensive view of the interactions within the system being studied.

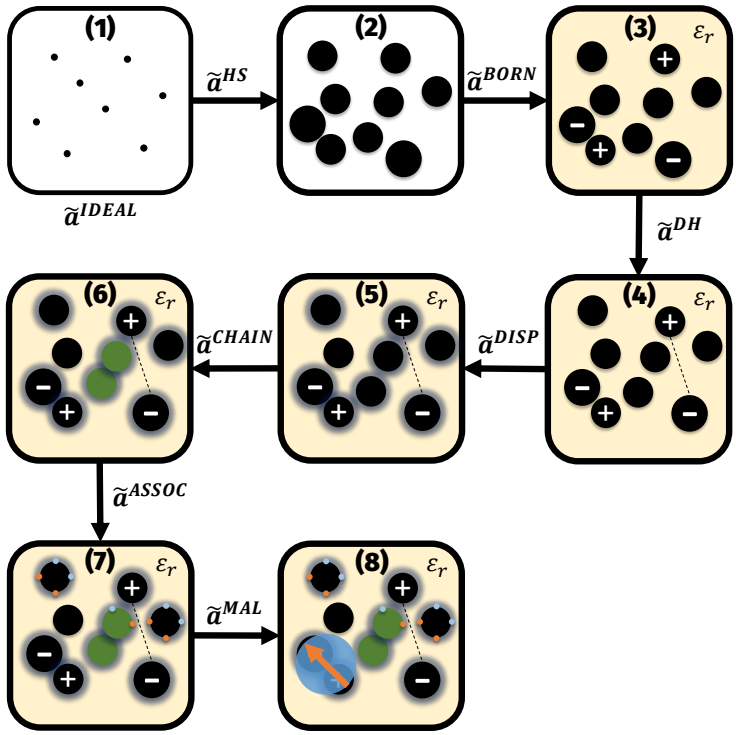

Figure 9.1. This figure show a schematic representation of the Binding eSAFT-VR-Mie. (1) is the ideal gas contribution, (2) is the hard sphere contribution, (3) is the solvation free energy based on the Born model, (4) is the ion-ion interactions from the DH theory, (5) is the contribution due to short-range dispersion interactions, (6) is the due to the formation of chain, (7) is the contribution due to hydrogen bonding, and (8) is ion-ion association from the BiDH theory.

$$\tilde{a}^{r} = \tilde{a}^{MONO} + \tilde{a}^{CHAIN} + \tilde{a}^{ASSOC} + \tilde{a}^{BORN} + \tilde{a}^{DH} + \tilde{a}^{MAL} \tag{9.5}$$

9.1.2 SAFT-VR-Mie

The SAFT-VR-Mie EoS offers a molecular perspective on the thermodynamics of fluids, linking the Helmholtz free energy to the temperature, volume, and composition of a given system. Within this framework, the basic constituents of the fluid, be the molecules or ions, are visualized as chains comprised of interconnected, homonuclear spherical segments. The interactions between these segments are dictated by a spherically symmetric Mie potential (Eq. 9.6), which captures the essence of both attractive and repulsive forces between particles. For systems where hydrogen bonding is significant, the model incorporates off-center square-well sites on these chains, ensuring an accurate portrayal of the attractive forces resulting from such bonding. In this EoS, each entity is composed of m_i of these segments, with their mutual interactions encapsulated by the nuances of the Mie potential. This configuration

allows SAFT-VR-Mie to model a wide range of molecular interactions, catering to the diverse nature of fluids.

$$u_{ij}^{Mie}(r) = C_{ij}\epsilon_{ij}\left[\left(\frac{\sigma_{ij}}{r_{ij}}\right)^{\lambda_{r,ij}} - \left(\frac{\sigma_{ij}}{r_{ij}}\right)^{\lambda_{a,ij}}\right] \tag{9.6}$$

$$C_{ij} = \frac{\lambda_{r,ij}}{\lambda_{r,ij} - \lambda_{a,ij}}\left(\frac{\lambda_{r,ij}}{\lambda_{a,ij}}\right)^{\frac{\lambda_{a,ij}}{\lambda_{r,ij}-\lambda_{a,ij}}} \tag{9.7}$$

Within Eq. 9.6, σ_{ij} represents the diameter of the segment, ϵ_{ij} corresponds to the maximum energy of interaction between the segments, while $\lambda_{r,ij}$ and $\lambda_{a,ij}$ represent the repulsive and attractive exponents, respectively. Eq. 9.8 presents the contributions to the reduced residual Helmholtz free energy of the SAFT-VR-Mie EoS:

$$\tilde{a}^{SAFT-VR-Mie} = \tilde{a}^{MONO} + \tilde{a}^{CHAIN} + \tilde{a}^{ASSOC} \tag{9.8}$$

The contribution to the reduced Helmholtz free energy from monomer interactions through a Mie potential in a mixture can be represented by Eq. 9.9:

$$\tilde{a}^{MONO} = \left(\sum_{i=1}^{C} x_i m_i\right)\left(\tilde{a}^{HS} + \beta\tilde{a}^1 + \beta^2\tilde{a}^2 + \beta^3\tilde{a}^3\right) \tag{9.9}$$

The equation incorporates several components. The term $\tilde{a}^{HS}$ denotes the reduced Helmholtz free energy of a reference hard sphere system, derived from the EoS by Boublik [287] and Mansoori et al. [230]. The terms $\tilde{a}^1$, $\tilde{a}^2$, and $\tilde{a}^3$ represent the first-, second-, and third-order perturbations of the hard sphere reference fluid, respectively. These perturbations stem from the high temperature perturbation theory formulated by Barker and Henderson [309, 310].

For brevity, the specific equations for the hard sphere reference fluid and the associated perturbation terms are omitted in this context. For a comprehensive understanding and detailed mathematical formulations, the readers are referred to the primary source by Lafitte et al. [68].

The contribution to Helmholtz free energy from the formation of molecular chains within the Mie segment fluid is rooted in the Wertheim TPT1 theory [246–251]. This theory draws inspiration from a model that characterizes association at an infinite association strength, as detailed in ref. [285]. This model presents a representation of spherical segments that are tangentially bonded. Notably, the model is concise in its representation; its contribution is determined exclusively by the RDF of the segments at their contact separation.

$$\tilde{a}^{CHAIN} = -\sum_{i=1}^{C} x_i(m_i^{seg} - 1)\ln g_{ii}^{Mie}(\sigma_{ii}) \tag{9.10}$$

In Eq. 9.10, the term g_{ii}^{Mie} signifies the RDF of the monomeric Mie fluid evaluated at the contact separation distance, σ_{ii} [68].

In the SAFT framework, association interactions arise from a collection of off-center attractive sites, usually characterized using spherically symmetric square-well potentials. A key feature of this association description is the restriction that only two segments can participate in each interaction, and each segment pair can only engage in a single interaction. These association sites come into play within a limited range, which is approximately the size of the segments, and they impart directional forces due to their off-centered placement.

The component of the Helmholtz free energy attributed to association, represented as $\tilde{a}^{ASSOC}$, has its roots in Wertheim's TPT1 theory [246–251]. A succinct representation of this contribution can be articulated as [311, 312]:

$$\tilde{a}^{ASSOC} = \sum_{i=1}^{C} x_i \sum_{A_i}^{S} \left(\ln X^{A_i} - 0.5 X^{A_i} + 0.5 \right) \tag{9.11}$$

In Eq. 9.11, X^{A_i} is the fraction sites of type A that are not bonded to any other sites. In addition, S is the number of association sites in each molecule. X^{A_i} is calculated from Eq. 9.12:

$$\frac{1}{X^{A_i}} = 1 + \sum_{j=1}^{C} \rho_j \sum_{B_j}^{S} (X^{B_j} \Delta^{A_i B_j}) \tag{9.12}$$

In Eq. 9.12, $\Delta^{A_i B_j}$ signifies the bond strength between the site A of the molecule i and the site B of the molecule j. This can be correlated with the volume of association ($K^{A_i B_j}$), the Mayer function corresponding to the bonding interactions ($F^{A_i B_j}$), and the termed association kernel ($I(T^*, \rho^*, \lambda_r)$), as depicted in Eq. 9.13:

$$\Delta^{A_i B_j} = F^{A_i B_j} K^{A_i B_j} I(T^*, \rho^*, \lambda_r) \tag{9.13}$$

In Eq. 9.14, the Mayer function is derived, where $\epsilon^{A_i B_j}$ represents the energy associated with the interaction between the site A of molecule i and the site B of molecule j.

$$F^{A_i B_j} = \exp\left(-\frac{\epsilon^{A_i B_j}}{k_B T} \right) \tag{9.14}$$

In this work, the Mie kernel, as introduced by Dufal et al. [308], is employed and is described by Eq. 9.15:

$$I(T^*, \rho^*, \lambda_r) = \sum_{i=0}^{i+j \leq 10} \sum_{j=0} a_{ij}(\lambda_r) (\rho^*)^i (T^*)^j \tag{9.15}$$

For the details on the definitions ρ^* and T^*, as well as the coefficients a_{ij}, readers are referred to ref. [308]. To maintain conciseness, these details are omitted here.

9.1.3 BiDH Theory

In Section 9.1.2, the non-electrostatic components of the reduced Helmholtz free energy, as dictated by the SAFT-VR-Mie EoS, were discussed. The contributions arising from long-range ion-ion interactions are now examined, employing the recently developed BiDH model [286], as detailed in Chapter 7 for this purpose.

Details of the derivation and equations have been presented in Chapter 7. Here, some of the key information is reiterated, given that the intention is to present this work in a standalone chapter without the necessity to read other chapters.

In the development of the BiDH model, we made the assumption that the solvent behaves as a continuous medium with a relative permittivity that is independent of the concentration. The solution comprises C_{ions} types of cations and anions. Any given cation-anion pair has the potential to form an ion pair, described by the subsequent equilibrium equation:

$$Ca^{Z_+} + An^{Z_-} \rightleftharpoons [IP]^{Z_+ + Z_-} \tag{9.16}$$

The BiDH model is constructed upon a perturbation approach anchored to a reference state. Within this reference state, it is posited that the electrolytes undergo complete dissociation in the solution. Subsequently, the free energy of the system is adjusted to account for the formation of ion pairs.

The reference state, which assumes complete dissociation, is based on DH theory [4]. Eq. 9.17 shows the contribution of the DH theory to the reduced residual Helmholtz free energy of the system under this assumption:

$$\tilde{a}^{DH} = -\frac{\sum_{j=1}^{C_{ion}} x_j Z_j^2 \chi(\kappa\sigma_j)}{4\pi\rho \sum_i x_i Z_i^2} \tag{9.17}$$

In Eq. 9.17, κ is the inverse Debye length defined as Eq. 9.18:

$$\kappa^2 = \frac{4\pi e^2 N_A}{\epsilon k_B T} \sum_{i=1}^{C_{ion}} \rho_i Z_i^2 \tag{9.18}$$

Furthermore, $\chi(\kappa\sigma_j)$ is the auxiliary function of the DH model defined as Eq. 9.19:

$$\chi(\kappa\sigma_j) = \frac{1}{\sigma_j^3}\left(\ln(1+\kappa\sigma_j) - \kappa\sigma_j + 0.5(\kappa\sigma_j)^2\right) \tag{9.19}$$

In BiDH theory, the electrostatic contribution to the reduced residual Helmholtz free energy is corrected for the effect of the ion-ion association by adding the association contribution from Wertheim theory [246–251, 285, 311, 312]. To avoid an ambiguous notation of the contributions to the reduced residual Helmholtz free energy, instead of association (as used in the original work and also in Chapter 7), the contribution to $\tilde{a}^r$ due to ion-ion association is denoted as $\tilde{a}^{MAL}$.

The MAL contribution to $\tilde{a}^r$ due to ion-ion association is obtained from Eq. 9.20:

$$\tilde{a}^{MAL} = -\sum_{i=1}^{C_{ion}} x_i \left[\ln(\alpha_i) + \frac{1-\alpha_i}{2}\right] \tag{9.20}$$

In Eq. 9.20, α_i is the fraction of unbound ions (free ions) defined as:

$$\alpha_i = \frac{\tilde{\rho}_i}{\rho_i} \tag{9.21}$$

In Eq. 9.21, $\tilde{\rho}_i$ is the number density of the ions after association or the number density of free ions. ρ_i is the total number density of ions. In the BiDH theory, which allows only the formation of ion pairs, the fraction of unbound ions is calculated from the solution to Eq. 9.22:

$$\frac{1}{\alpha_i} = 1 + \sum_{j=1}^{C_{ion}} \rho_j \alpha_j \Delta_{ij} \tag{9.22}$$

Eq. 9.22 represents a more straightforward version of Eq. 9.12, wherein all the components involved in association possess a single association site. Nevertheless, it is important to note that in this equation, the association strength (Δ_{ij}) differs considerably from that attributed to hydrogen bonding.

In BiDH theory, the association strength between a cation-anion pair is calculated from Eq. 9.23:

$$\Delta_{ij} = K_{ij}^{\circ} y_{ij}^{ref} \tag{9.23}$$

This association strength is derived based on the RCA of Stell and his co-workers [240–244]. In the RCA, it has been assumed that the cavity function of an ion pair defined as $y_{ij}(r) \equiv g_{ij}(r)\exp(u_{ij}(r))$ can be approximated with the cavity function of two pairs of ions in the non-association limit (where the number density of ion pairs approaches zero).

In Eq. 9.23, K_{ij}° is the association constant at infinite dilution. It can be calculated using the Bjerrum model, as demonstrated in Eq. 9.24:

$$K_{ij}^{\circ} = 4\pi N_A \int_{\sigma_{ij}}^{l_{ij}} r^2 \exp\Big(\frac{2q_{ij}}{r}\Big) dr \tag{9.24}$$

In Eq. 9.24, the variable q_{ij} is defined according to Eq. 9.25. Furthermore, l_{ij} represents the upper boundary of the Bjerrum integral. The significance of this upper limit lies in the fact that ions positioned closer to the central ion than a distance of l_{ij} are considered to be part of ion pairs.

$$q_{ij} = \frac{e^2 \mid Z_i Z_j \mid}{8\pi\epsilon_0\epsilon_r k_B T} \tag{9.25}$$

Bjerrum, in his work [216], introduced the concept that ion pairs with a separation distance $r < q_{ij}$, where the ions possess opposite charges, should be considered as associated pairs. On the contrary, those ions positioned farther apart should be regarded as independent. His rationale for this criterion was based on the idea that, although somewhat arbitrary, it makes sense because the energy required to separate such ion pairs is at least twice the thermal energy. The choice of the upper limit of the Bjerrum integral will be further discussed in detail in subsequent sections of this chapter.

The reference cavity function, represented as y_{ij}^{ref}, is determined by the combination of two contributions: the electrostatic contribution, denoted as y_{ij}^{ELE} and the hard sphere contribution, denoted as g_{ij}^{HS}.

$$\ln\big(y_{ij}^{ref}\big) = \ln\big(y_{ij}^{ELE}\big) + \ln\big(g_{ij}^{HS}(\sigma_{ij})\big) \tag{9.26}$$

The hard sphere component of the reference cavity function, designated as g_{ij}^{HS}, is derived from the equations presented in the work of Boublik [287] and Mansoori et al. [230], as shown in Eq. 9.27.

$$g_{ij}^{HS}(\sigma_{ij}) = \frac{1}{1-\zeta_3} + \frac{2\sigma_i\sigma_j}{\sigma_{ij}}\frac{3\zeta_2}{(1-\zeta_3)^2} + (\frac{2\sigma_i\sigma_j}{\sigma_{ij}})^2\frac{2\zeta_2^2}{(1-\zeta_3)^3} \tag{9.27}$$

In this equation, σ_{ij} is the distance of the closest approach defined as:

$$\sigma_{ij} = \frac{\sigma_i + \sigma_j}{2} \tag{9.28}$$

$$\zeta_l = \frac{\pi}{6}\sum_{j=1}^{C} \rho_j \sigma_j^l \ , l = \{0,1,2,3\} \tag{9.29}$$

The electrostatic contribution to the reference cavity function is obtained from Eq. 9.30:

$$\ln\big(y_{ij}^{ELE}\big) = \frac{1}{k_B T}\Big[\mu_i^{DH} + \mu_j^{DH} - \big(\mu_{ij}^{DH}\big)_{\rho_{ij}\to 0} - \big(\mu_{ij}^{DI}\big)_{\rho_{ij}\to 0}\Big] \tag{9.30}$$

The equations for μ_i^{DH}, μ_{ij}^{DH}, and μ_{ij}^{DI} can be found in Chapter 7 or in ref. [286], and for the sake of conciseness, they will not be reiterated here. However, it is essential to emphasize that μ_{ij}^{DI} represents the contribution to the reference cavity function arising from ion-dipole interactions, as described in the Kirkwood model [8, 235].

9.1.4 Solvation Free Energy

The concept of solvation free energy is incorporated into the overall free energy of the system during the charging process. This component quantifies the energy required to transfer charged ions from the vacuum state to the fluid medium.

In this study, we employ the Born equation to describe the solvation of ions and Eq. 9.31 illustrates this particular contribution.

$$\tilde{a}^{BORN} = \frac{e^2}{4\pi\varepsilon_0 k_B T}\left(\frac{1}{\varepsilon_r} - 1\right)\sum_{i=1}^{C_{ion}} \frac{x_i Z_i^2}{\sigma_i^B} \tag{9.31}$$

In Eq. 9.31, the parameter σ_i^B corresponds to the Born diameter. There has been a significant debate on the physical interpretation of this radius. Some researchers associate it with σ_i from ion-ion interactions, as described in either the DH or MSA theories. On the other hand, others consider it as a distinct radius that represents the volume occupied by the ion within the solvent. In this study, we adopt the latter perspective, utilizing the Born diameter reported in the literature.

9.1.5 Electrical Conductivity

The electrical conductivity of electrolyte solutions can be determined using DHO-transport theory (models developed in Chapters 4 and 5) [184, 200] or MSA-transport theory [111, 114–117]. The details of these theories can be located in the existing literature. In this study, to maintain consistency with the thermodynamic model employed, we utilize the DHO-transport theory.

The derivation procedure and formulation of the electrical conductivity models, along with the validation of these models, were extensively presented in Chapters 4 and 5. In this section, a concise presentation of the models tailored for associative electrolyte solutions is provided.

The electrical conductivity models have been formulated under two primary assumptions: one for systems consisting of only two types of charged components, often referred to as the single-salt version, and the other for systems with arbitrary types of charged components. These models were developed with the premise that the solvent is a continuous medium, possessing a RSP and viscosity that do not vary with concentration. To simplify the presentation of these models, it is necessary to introduce a pseudo-system comprising C_{ion} ions and C_{ip} charged ion pairs. In total, this pseudo-system encompasses $\tilde{C} = C_{ion} + C_{ip}$ distinct types of charged species within the solution.

In the context of this pseudo-system, we define ϱ as the number density of all charged species present in the solution, encompassing both ions and ion pairs. As depicted in Eq. 9.32, C_{ion} elements of this vector represent the number density of free ions, denoted $\alpha_i\rho_i$. The remaining C_{ip} elements pertain to the number density of ion pairs. To simplify the formulation of equations, the number density of ion pairs has been transformed from a matrix representation into a vector format. Additionally, the number density of neutral ion pairs has been excluded from this vector.

$$\left\{\begin{array}{c}\alpha_1\rho_1\\ \alpha_2\rho_2\\ \alpha_3\rho_3\\ \vdots\\ \alpha_{C_{ion}}\rho_{C_{ion}}\end{array}\right\}\cup\left\{\begin{array}{ccccc}- & \tilde{\rho}_{12} & \tilde{\rho}_{13} & \cdots & \tilde{\rho}_{1C_{ion}}\\ - & - & \tilde{\rho}_{23} & \cdots & \tilde{\rho}_{2C_{ion}}\\ - & - & - & \cdots & \tilde{\rho}_{3C_{ion}}\\ \vdots & \cdots & & \ddots & \vdots\\ - & - & - & \cdots & -\end{array}\right\}\equiv\left\{\begin{array}{c}\alpha_1\rho_1\\ \vdots\\ \alpha_{C_{ion}}\rho_{C_{ion}}\\ \tilde{\rho}_{12}\\ \tilde{\rho}_{13}\\ \vdots\\ \tilde{\rho}_{(C_{ion}-1)C_{ion}}\end{array}\right\}\equiv\varrho \tag{9.32}$$

To predict electrical conductivity, in addition to the number density, information on the valence type (Z_i), diameter (σ_i), and ionic conductivity at infinite dilution (λ_i^0) of all charged species is required.

To compute the electrical conductivity of associative electrolyte solutions, it is necessary to establish a relationship between the parameters of the ion pairs and their constituent ions. The valence type of the ion pairs is characterized as $Z_{ij} = Z_i + Z_j$. The diameter of ion pairs is determined through a volumetric averaging process, which leads to the following mixing rule.

$$\bar{\sigma}_{ij}^3 = \sigma_i^3 + \sigma_j^3 \tag{9.33}$$

It is important to distinguish between the diameter of the ion pairs ($\bar{\sigma}_{ij}$) and the distance of the closest approach (σ_{ij}) as defined earlier. The ionic conductivity at infinite dilution of ion pairs is computed based on the ionic conductivity at infinite dilution of ions, as proposed by Anderko et al. [127], as shown in Eq. 9.34:

$$(\lambda_{ij}^0)^3 = \frac{\mid Z_i + Z_j \mid}{\left[\left(\frac{|Z_i|}{\lambda_i^0}\right)^3 + \left(\frac{|Z_j|}{\lambda_j^0}\right)^3\right]^{1/3}} \tag{9.34}$$

The specific conductivity of this system can be obtained from Eq. 9.35:

$$\chi = \frac{e^2}{k_B T}\left[\sum_{i=1}^{\bar{C}} \varrho_i D_i^0 Z_i^2 \left(1 + \frac{\delta v_i}{v_i^0}\right)\left(1 + \frac{\delta k_i}{k_i}\right)\right] \tag{9.35}$$

In Eq. 9.35, D_i^0 represents the diffusion coefficient of ions or ion pairs at infinite dilution. The diffusion coefficient at infinite dilution for an ion or ion pair can be related to its ionic conductivity at infinite dilution or absolute mobility using the Nernst-Einstein equation (Eq. 9.36). ϱ_i denotes the number density of charged species in the solution, which includes both ions and charged ion pairs. $\delta v_i/v_i^0$ corresponds to the hydrodynamic corrections applied to the specific conductivity of ions or ion pairs, while $\delta k_i/k_i^0$ represents the electrostatic corrections applied to the specific conductivity of ions or ion pairs.

$$\omega_i = \frac{D_i^0}{k_B T} = \frac{N_A \lambda_i^0}{F^2 |Z_i|} \tag{9.36}$$

Corrections for deviations from ideal behavior, stemming from hydrodynamic (or electrophoretic) and electrostatic (or relaxation) effects, should be incorporated from an electrical conductivity theory. In Chapters 4 and 5, we have introduced two innovative models for the electrical conductance of single-salt [184] and multi-salt [200] electrolyte solutions. In the former case, we assumed that there are only two types of charged components in the

solution that contribute to its electrical conductance. In the latter, we presented a model for a system containing arbitrary types of charged species.

In the context of ion-ion association, the single-salt model is suitable for binary salt-solvent solutions, where the salt is symmetrical. Consequently, the ion pair formed in such solutions is neutral and does not contribute to the electrical conductance of the solution. Figure 9.2a illustrates this scenario schematically.

In this situation, the number density of the components of the pseudo-system is:

$$\varrho = \begin{bmatrix} \alpha_+ \rho_+ \\ \alpha_- \rho_- \end{bmatrix} \tag{9.37}$$

As a result, the only conducting components in the system are free ions.

In all other scenarios, there are more than two types of conducting species present in the solution, and it is necessary to utilize the mixed-electrolyte version of the developed models. This situation arises either in binary salt-solvent systems with asymmetrical salts (as illustrated schematically in Figure 9.2b) or when there are more than two types of ions in the solution.

For instance, for a binary salt-solvent system in which the salt is asymmetrical, the number density of charged components is:

$$\varrho = \begin{bmatrix} \alpha_+ \rho_+ \\ \alpha_- \rho_- \\ \tilde{\rho}_{+-} \end{bmatrix} \tag{9.38}$$

The hydrodynamic correction to the ideal behavior of electrical conductivity in the general case, which applies to all situations involving arbitrary types of ions, is derived from Eq. 9.39:

$$\frac{\delta v_i}{v_i^0} = -\frac{F^2 \mid Z_i \mid}{3\eta\epsilon k_B T N_A \lambda_i^0} \sum_{j=1}^{\tilde{C}} \varrho_j e^2 Z_j^2 \left[\frac{\exp(\kappa'(\sigma_i - \sigma_{ij}))}{\kappa'(1+\kappa'\sigma_i)} + \frac{\exp(\kappa'(\sigma_j - \sigma_{ij}))}{\kappa'(1+\kappa'\sigma_j)} \right] \tag{9.39}$$

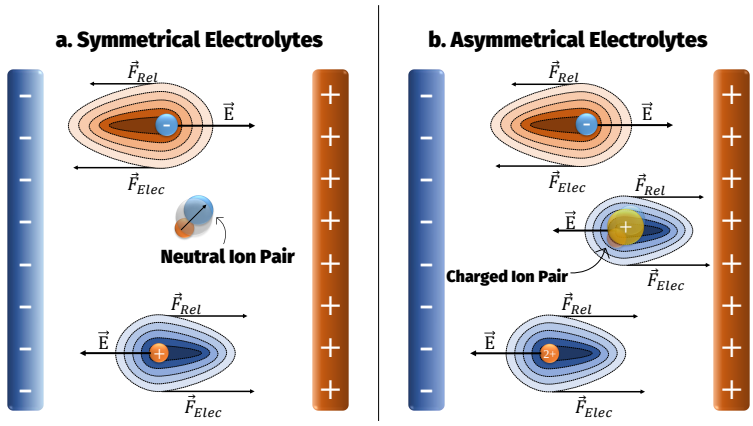

Figure 9.2. This figure presents the schematic of the electrical conductance process for a binary salt-solvent system where (a) the salt is symmetrical in which ion pairs does not contribute to the electrical conductivity and (b) the salt is asymmetrical in which ion pairs carry charge and contribute to the electrical conductivity.

In Eq. 9.39, κ' is the inverse Debye length after the ion-ion association defined as Eq. 9.40:

$$\kappa'^2 = \frac{4\pi e^2 N_A}{\epsilon k_B T} \sum_{i=1}^{\bar{C}} \varrho_i Z_i^2 \tag{9.40}$$

In the case of binary symmetrical electrolytes, as previously mentioned and shown in Figure 9.2a, the only conducting species in the solution are free cations and free anions. In this scenario, the electrostatic correction to the ideal behavior of the electrical conductance process can be determined using Eq. 9.41:

$$\frac{\delta k_+}{k_+} = \frac{\delta k_-}{k_-} = \frac{\delta k}{k} = -\Omega \frac{e^2 \mid Z_+ Z_- \mid}{2\epsilon k_B T} \frac{\exp(-\kappa_q \sigma_{+-})}{(\kappa' + \kappa_q)} \left[\frac{\exp(\kappa'(\sigma_+ - \sigma_{+-}))}{(1 + \kappa' \sigma_+)} + \frac{\exp(\kappa'(\sigma_- - \sigma_{+-}))}{(1 + \kappa' \sigma_-)} \right] \tag{9.41}$$

In Eq. 9.41, Ω and κ_q are defined as Eq. 9.42 and Eq. 9.43, respectively:

$$\Omega = \frac{\kappa_q^2}{3} \left[\frac{\sinh(\kappa_q \sigma_{+-})}{\kappa_q \sigma_{+-}} - \frac{\epsilon k_B T \kappa_q \sigma_{+-}^2}{e^2 Z_+ Z_-} \left(\frac{\cosh(\kappa_q \sigma_{+-})}{\kappa_q \sigma_{+-}} - \frac{\sinh(\kappa_q \sigma_{+-})}{\kappa_q^2 \sigma_{+-}^2} \right) \right] \tag{9.42}$$

$$\kappa_q^2 = \frac{4\pi}{\epsilon k_B T} \frac{\varrho_- e Z_- \omega_- + \varrho_- e Z_- \omega_-}{\omega_+ + \omega_-} \tag{9.43}$$

For electrolyte solutions containing more than two types of ions or for asymmetrical single-salt solutions, the electrostatic correction to the ideal behavior of electrical conductivity is obtained from Eq. 9.44:

$$\frac{\delta k_m}{k_m} = \frac{e Z_m}{6\epsilon k_B T} \sum_{p=1}^{\bar{C}} \left[\frac{\varsigma_m^p}{\sqrt{q_p} + q_p} \sum_{j=1}^{\bar{C}} \sum_{i=1}^{\bar{C}} \left(\frac{t_j \varsigma_j^p \mu_i (e Z_i \omega_i - e Z_j \omega_j)}{\omega_i - \omega_j} \frac{\sinh\left(\kappa' \sqrt{q_p} \sigma_{ji}\right)}{\sigma_{ji}} \left[\frac{\exp(\kappa' \sigma_j)}{1 + \kappa' \sigma_j} + \frac{\exp(\kappa' \sigma_i)}{1 + \kappa' \sigma_i} \right] \exp\left(-\kappa'(1 + \sqrt{q_p})\sigma_{ji}\right) \right) \right] \tag{9.44}$$

In this equation, κ' represents the inverse Debye length, as defined by Eq. 9.40, where $\epsilon = 4\pi\epsilon_0\epsilon_r$ denotes the dielectric constant of the medium. Furthermore, t_j and μ_j correspond to the transport number at infinite dilution (as given by Eq. 9.45) and the relative ionic strength (as defined in Eq. 9.46), respectively.

$$t_i = \frac{\mu_i \omega_i}{\bar{\omega}} \tag{9.45}$$

$$\mu_i = \frac{\varrho_i e^2 Z_i^2}{\sum_{j=1}^{\bar{C}} \varrho_j e^2 Z_j^2} \tag{9.46}$$

In Eq. 9.44, ω_i and $\bar{\omega}$ denote the absolute and average absolute mobility of the ion i, respectively. The absolute mobility of an ion can be determined on the basis of its ionic

conductivity (λ_i^0) and diffusion coefficient at infinite dilution (D_i^0), as shown in Eq. 9.36. Similarly, the average mobility of ions can be calculated using Eq. 9.47.

$$\bar{\omega} = \sum_{j=1}^{\tilde{C}} \mu_j \omega_j \tag{9.47}$$

The terms q_p and ζ_i^p correspond to the eigenvalues and components of the eigenvector obtained from the solution of a set of differential equations (equations 22-26 in ref. [116]). The eigenvalues and eigenvectors are determined by equations 9.48 and 9.49, respectively.

$$q_p = \sum_{j=1}^{\tilde{C}} = \frac{\bar{\omega} t_j}{\omega_j + \delta_p} \tag{9.48}$$

$$\varsigma_j^p = \frac{N_p \omega_j}{\omega_j^2 - \delta_p^2} \tag{9.49}$$

In these equations, the variable N_p is defined as per Eq. 9.50, and δ_p represents one of the roots of Eq. 9.51.

$$\frac{1}{N_p^2} = \sum_{j=1}^{\tilde{C}} \frac{t_j \omega_j^2}{(\omega_j^2 - \delta_p^2)^2} \tag{9.50}$$

$$-2\bar{\omega}\delta \sum_{j=1}^{\tilde{C}} \frac{t_i}{\omega_i^2 - \delta^2} = 0 \tag{9.51}$$

In accordance with the recommendations of Onsager and Kim [109], Van Damme et al. [116] proposed that the roots of Eq. 9.51 should follow the specified order:

$$0 = \delta_1^2 < \omega_1^2 < \delta_2^2 < \omega_2^2 < \cdots < \delta_{\tilde{C}}^2 < \omega_{\tilde{C}}^2 \tag{9.52}$$

This specific order streamlines the solution of Eq. 9.51 for δ_p enabling the use of root bracketing, interval bisection, and inverse quadratic interpolation techniques. In our research, we used the Brent algorithm [202], implemented in the SciPy library, to solve this nonlinear equation.

9.1.6 Thermodynamic and Transport Properties

The systems investigated in this study are binary salt-water systems. Consequently, to streamline the presentation of the equations, we introduce the thermodynamic and transport properties specific to these binary salt-water systems.

In this study, we focus on four properties of the electrolyte solutions: MIAC, osmotic coefficient, liquid density, and molar conductivity. Of these, molar conductivity is a transport property of the system, while the others are thermodynamic properties.

MIAC, denoted as $\gamma_{\pm}^m$, and the osmotic coefficient, denoted as ϕ, are associated with the fugacity of the ions and the solvent, respectively. The fugacity coefficient of the component i in the mixture, represented as $\hat{\varphi}_i$, is determined using Eq. 9.53:

$$RT \ln \hat{\varphi}_i(T, P, \mathbf{n}) = \left[\frac{\partial A^r}{\partial n_i}\right]_{T,V} - RT \ln Z \tag{9.53}$$

In Eq. 9.53, $Z = \frac{PV}{Nk_BT}$ represents the compressibility factor, and $R = k_BN_A$ denotes the ideal gas constant. The asymmetrical rational activity coefficient of ions (γ_i^*) is defined as shown in Eq. 9.54:

$$\gamma_i^* = \frac{\hat{\varphi}_i(T, P, \mathbf{n})}{\hat{\varphi}_i^\infty(T, P, \mathbf{n}^\infty)} \tag{9.54}$$

In Eq. 9.54, $\hat{\varphi}_i^\infty$ represents the fugacity coefficient of ion i in the infinitely diluted solution. The activity coefficient of the ion i on the molality scale is subsequently determined using Eq. 9.55:

$$\gamma_i^m = x_w\gamma_i^* \tag{9.55}$$

In Eq. 9.55, x_w stands for the mole fraction of water. MIAC in the molality scale is derived from Eq. 9.56:

$$\ln\gamma_\pm^m = \frac{1}{\nu_+ + \nu_-}(\nu_+ \ln\gamma_+^m + \nu_- \ln\gamma_-^m) \tag{9.56}$$

In Eq. 9.56, ν_+ and ν_- are the stoichiometry coefficients of the cation and the anion where the salt is dissolved in the solution. The activity coefficient of neutral compounds, water, in this study is defined as Eq. 9.57:

$$\gamma_w = \frac{\hat{\varphi}_w(T, P, \mathbf{n})}{\varphi_w(T, P)} \tag{9.57}$$

In Eq. 9.57, $\varphi_w(T, P)$ is the fugacity coefficients of pure water. The osmotic coefficient is defined as Eq. 9.58:

$$\phi(T, P, \mathbf{n}) = -\frac{\ln x_w\gamma_w}{(\nu_+ + \nu_-)mM_w} \tag{9.58}$$

In Eq. 9.58, m is the molality of the electrolyte, and M_w is the molecular weight of water. Finally, the molar conductivity is defined as Eq. 9.59:

$$\Lambda = \frac{\chi}{c_E} \tag{9.59}$$

In Eq. 9.59, c_E is the molarity of the electrolyte defined in Eq. 9.1.

9.1.7 Unified Framework

Before exploring the introduction of the unified framework, it is crucial to establish the relationship between a transport property, such as electrical conductivity, and the thermodynamic properties of the system. When the electrolyte is completely dissociated within the solution, the electrical conductivity and thermodynamic properties are entirely independent of one another, at least when viewed from a macroscopic perspective. Conversely, in situations where the ion-ion association plays a significant role and is taken into account, a significant correlation exists between the thermodynamic properties, as illustrated in Figure 9.3.

As shown in Figure 9.3, the equations that govern the concentration-dependent behavior of ion pairing are controlled by thermodynamic models. In this work, we employ an EoS, while in chapters 6 and 8, an implicit solvent model was utilized for this purpose. The extent of ion pairing can be quantified either by calculating the number density of ion pairs or by assessing the fraction of unbound (or free) ions.

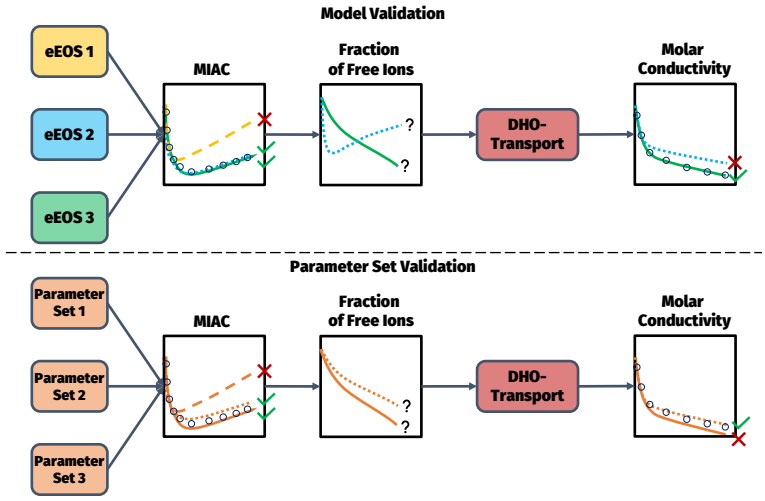

Figure 9.3. The unified framework for investigation of ion-ion association in electrolyte solutions.

It is essential to emphasize that the utilization of the fraction of unbound ions is recommended. This preference arises from the complexity of multi-component systems containing various types of ions, where the number of different ion pairs increases significantly. Consequently, working with the number density of ion pairs may not be a practical approach. In a system comprising M cations and N anions, the total number of type of ions equals $M + N$, while the count of ion pairs is $M \times N$.

Determining the extent of ion pairing at the reference state, quantified by the association constant at infinite dilution, proves challenging when relying solely on thermodynamic approaches. Several physical models have been proposed to address this issue, but they often lack accuracy, except in cases of strong ion pairing, and typically require adjustments based on experimental data [84]. The most precise method for estimating the association constant at infinite dilution, or at the very least fine-tuning these physical models, involves the use of electrical conductivity. Unlike many thermodynamic properties, electrical conductivity can be measured at extremely low salt concentrations with a high degree of precision. Consequently, it can be concluded that the reference state of ion pairing can be determined by electrical conductivity.

In addition to the points mentioned above, thermodynamic models lack crucial information regarding the structural properties of solutions. As elucidated in Chapter 6, all models that we investigated were capable of predicting MIAC in strongly associative aqueous solutions through parameter estimation. However, upon closer examination, it became evident that the predicted fraction of unbound ions exhibited both quantitative and qualitative disparities. This has led us to a standstill, as thermodynamic models and their associated properties do not enable us to offer further insights into the accuracy of these models.

Furthermore, spectroscopic techniques such as UV/vis, NMR, or Raman spectroscopy have been shown to be unreliable in quantifying the extent of ion pairing in electrolyte solutions [313]. Instead, relaxation methods prove to be more suitable tools for this purpose [314]. However, it is worth noting that studies quantifying the extent of ion pairing using relaxation methods are limited in scope and primarily focus on a few electrolytes. Another limitation of relaxation methods is their applicability only to relatively strong associations. Additionally, it appears that the results obtained through relaxation methods are subject to

some degree of uncertainty.

For example, in 2004, Buchner et al. [315] employed dielectric relaxation spectroscopy (DRS) to identify three distinct types of ion pairs: CIP, SSIP, and SIP in $MgSO_4$ aqueous solutions. However, in a more recent investigation, Mamatkulov et al. [316] demonstrated that within the $MgSO_4$-H_2O system, only SIPs and SSIPs could be detected. They meticulously replicated dielectric relaxation spectra using MD simulations based on experimental data. Subsequently, they compared the RDF of magnesium and sulfate ions with that of sulfate ions and water molecules, ultimately concluding that the ion pairs in magnesium sulfate solutions are indeed solvent-separated.

Nevertheless, it is worth noting that the extent of ion pairing initially reported by Buchner et al. [315] has faced recent challenges [265, 317, 318]. Consequently, the reliability of relaxation methods for quantifying the extent of ion pairing has come into question.

Electrical conductivity also plays a vital role in validating the predicted fraction of unbound ions. This is due to the fact that the electrical conductivity of an electrolyte solution exhibits a high sensitivity to both the type and concentration of charged species present in the solution. Any variation in these charged species resulting from the ion-ion association can significantly impact the electrical conductivity. When we combine a reliable model for electrical conductivity with the predicted fraction of unbound ions, as described in Section 9.1.3, we can expect to obtain an accurate prediction of electrical conductivity, provided that the fraction of unbound ions has been accurately predicted.

The comprehensive examination of ion pairing through the integration of both thermodynamic properties and electrical conductivity also serves as a valuable tool in the parameter estimation of electrolyte equations of state. This topic constitutes the focus of our forthcoming studies. In the present investigation, we employ this unified framework, illustrated in Figure 9.3, to validate models or parameter sets.

9.2 Results

In this section, we begin by presenting the parameters employed in our study for both the Binding eSAFT-VR-Mie model and the electrical conductivity model. Subsequently, we present the results of our unified framework, focusing on three binary salt-water systems at 298.15 K. For each binary system, we begin by reviewing the evidence of ion pairing from experimental methods available in the literature. Following this, we assess the accuracy of selected prominent electrolyte equations of state from the literature. Finally, we compare the predictions of our unified framework, pertaining to liquid density, MIAC, osmotic coefficient, and molar conductivity, with the experimental data for the same three binary salt-water systems, all at 298.15 K and 1 bar.

9.2.1 Parameters

In this study, we refrain from performing any parameter estimation. The properties of the systems are solely calculated predictively, accounting for the ion-ion association. The parameters pertaining to the solvent molecules have been adopted from the values reported by Dufal et al. [308]. A summary of these parameters is provided in Table 9.1:

Table 9.1. SAFT-VR-Mie parameters for water [308].

Solvent	m_{seg}	$\epsilon/k_B\ (K)$	$\sigma\ (m)$	λ_r	λ_a	$\epsilon^{AB}/k_B\ (K)$	$K^{AB} \times\ (m^3)$
H_2O	1.0	418.0	3.0555E-10	35.823	6.0	1600.0	496.66E-30

The parameters of the ions used in this study have been sourced from the research carried out by Selam et al. [70]. These ion-specific parameters are detailed in Table 9.2. It should be noted that for both thermodynamic and transport properties, a consistent ionic diameter will be employed throughout this study.

Eq. 9.60 represents the formula for the dispersion energy between ions, both like and unlike, as proposed by Selam et al. [70].

$$\epsilon_{ij} = \frac{3}{8} \frac{\alpha_{0,i}\alpha_{0,j}}{(4\pi\varepsilon_0)^2\sigma_{ij}^6} \frac{I_i I_j}{I_i + I_j} \tag{9.60}$$

In this equation, $\alpha_{0,i}$ represents the electronic polarizability of the species, while I_i denotes the ionization potential of the species.

The ionic conductivity at infinite dilution for the ions used in this study are tabulated in Table 9.3.

In the figures presented in this section, the lines corresponding to the model predictions are labeled as either S1 or S2. The results obtained for the properties of the system without taking into account the effects of ion-ion association are referred to as the S1 label. Specifically, for MAIC, osmotic coefficient, and liquid density, the S1 lines replicate the findings of Selam et al. [70]. However, for molar conductivity, the S1 lines replicate the results reported by Naseri Boroujeni et al. [200].

Adjacent to each curve labeled S2, we provide the corresponding association constant at infinite dilution (K_{+-}°). It is worth noting that, across all systems, the highest association constant at infinite dilution has been sourced from the literature and represents the most reliable value reported in the literature.

All calculations carried out in this study employ composition-independent values for the RSP (ε_r) and viscosity (η) of water. Given that all calculations are performed at 298.15 K, these parameters are set to $\varepsilon_r = 78.34$ and $\eta = 0.890 \times 10^{-3}\ Pa \cdot s$.

9.2.2 NaCl-H_2O

Sodium chloride aqueous solutions are typically categorized as non-associative electrolyte solutions. Nevertheless, it is essential to note that the distinction between non-associative and associative electrolyte solutions has yet to be definitively established.

From DRS studies of aqueous sodium chloride solutions, Buchner et al. [320] did not observe an additional relaxation process associated with ion pairs. Recent research, employing DRS and MD simulations, has similarly reported the absence of detectable ion pairs in sodium chloride aqueous solutions [316, 321, 322]. Conversely, experimental investigations

Table 9.2. Parameters for Ions [70].

Ions	$\alpha_0\ (m^3)$	$I\ (e.V)$	$\sigma\ (m)$	$\sigma^B\ (m)$	λ_r	λ_a	$\epsilon_{iw}/k_B(K)$
Na^+	0.179E-24	47.286	2.1607E-10	3.360E-10	12	6	187.62
Mg^{2+}	0.094E-24	80.144	2.3783E-10	2.910E-10	12	6	1371.65
NO_3^-	4.049E-24	3.9370	4.0346E-10	4.280E-10	12	6	283.32
Cl^-	3.660E-24	3.6130	3.0999E-10	3.874E-10	12	6	594.05
SO_4^{2-}	4.432E-24	2.6000	2.7886E-10	4.665E-10	12	6	761.50

Table 9.3. The ionic conductivity at infinite dilution of ions studied in this work at 298.15 K [319].

Ions	Na^+	Cl^-	Mg^{2+}	$(SO_4)^{2-}$
$\lambda_i^0 \times 10^4\ (S \cdot m^2 \cdot mol^{-1})$	50.08	76.31	53.00	80.00

of electrical conductivity, both at low concentrations [149] and in highly concentrated solutions [148], have demonstrated the presence of ion pairs in the NaCl-H_2O system. However, it is noteworthy that the association constant at infinite dilution appears to depend on the concentration range under investigation and the specific conductivity model employed.

The formation of ion pairs in aqueous sodium chloride solutions has also been extensively explored through MD simulations. Fennell et al. [323] conducted investigations of the association constant at infinite dilution for alkali halide solutions, utilizing various force fields and considering a system comprising 2 ions and 864 water molecules. Their findings indicated an association constant at infinite dilution equal to 0.6 $L \cdot mol^{-1}$ for NaCl-H_2O at 298.15 K. Numerous MD simulations have confirmed the existence of ion pairs in aqueous sodium chloride solutions [324–328]. For instance, Lyubartsev et al. [326] proposed that in NaCl aqueous solutions, the ratio of ion pairs increases from 4% to nearly 50% as the salt concentration increases from 0.5 to 4 mol/L.

Nevertheless, it is important to highlight that, in comparison to other systems investigated within this chapter, the extent of ion pairing in NaCl-H_2O systems is notably lower. Therefore, the inclusion of ion pairing should not be anticipated to miraculously resolve the discrepancies between models and experimental data. Nonetheless, studying the impact of including ion pairing in this system holds significant value for two primary reasons. Firstly, it allows us to assess whether the inclusion of ion pairing in cases where the affinity for ion-ion association is very weak has any adverse effects on already acceptable results. Secondly, it provides an opportunity to evaluate the capability of the unified framework to investigate systems with a very low likelihood of forming ion pairs.

It is worth noting that NaCl-H_2O system represents one of the most extensively studied systems within the realm of electrolyte solutions thermodynamics. This system finds its place in nearly every study dedicated to electrolyte equations of state. A wide array of equations of state, utilizing various parameter estimation methodologies and a diverse selection of RSP models, have been employed to predict or estimate the thermodynamic properties of this system. In Table 9.4, we present the average absolute relative deviation (AARD%) which is defined in Eq. 9.61 for the estimation of several electrolyte equations of state concerning MIAC, osmotic coefficient, and liquid density, as reported in the literature.

$$AARD\% = \frac{1}{N_d} \sum_{i=1}^{N_d} \left| \frac{X_i^{calc} - X_i^{data}}{X_i^{data}} \right| \tag{9.61}$$

Upon comparing the AARD% values of the models presented in Table 9.4 with those found in the respective references, it becomes evident that the accuracy of the models can be significantly influenced by simple variations in parameter estimation strategies or by examining the impact of employing different RSP models. For example, the eCPA used by Schlaikjer et al. [53] and Olsen et al. [51] are the same as those developed by Maribo-Mogensen et al. [42]. The difference between the studies stems primarily from the variation of parameter estimation strategy or the choice of RSP. This holds true when one compares the works of Selam et al. [70] with Novak et al. [72, 73] or the works of Ahmed et al. [77] and Yang et al. [329].

Figure 9.5 illustrates the behavior of the liquid density, MIAC, osmotic coefficient, and molar conductivity in aqueous sodium chloride solutions at 298.15 K. In this figure and in all subsequent figures throughout this chapter, the lines represent model predictions, as indicated by the legend, while the symbols denote experimental data obtained from the literature.

These properties were calculated using the Binding eSAFT-VR-Mie and eSAFT-VR-Mie models in conjunction with the electrical conductivity model for single-salt systems. S1 curves correspond to the work of Selam et al. [70], where the ion-ion association is not considered. S2 curves represent the results obtained using the Binding eSAFT-VR-Mie

Table 9.4. Summary of the AARD% of the equations of state reported in the literature for NaCl-H_2O solution.

		AARD%		
eEoS	Ref.	$\gamma_{\pm}^{m}$	ϕ	ρ
eCPA	Maribo-Mogensen et al. [42]	2.37	1.48	0.73
	Schlaikjer et al. [53]	6.96	9.37	0.75
	Olsen et al. [53]	1.95	1.62	0.581
ePC-SAFT	Held et al. [56]	3.43	-	0.74
	Held et al. [59]	-	2.95	0.69
ePPC-SAFT	Rozmus et al. [76]	2.47	-	3.48
	Ahmed et al. [77]	6.2	-	-
	Yang et al. [329]	0.76-2.2	-	0.38-0.79
SAFT-VRE	Schreckenberg et al. [67]	5.51	1.55	1.74
eSAFT-VR-Mie	Eriksen et al. [69]	20.43	3.04	5.07
	Selam et al. [70]	2.55	2.07	0.99
	Novak et al. [72]	3.1	-	-
	Novak et al. [73]	3.7-6.1	-	0.5-6.9

model introduced in this study, with association constants at infinite dilution (K_{+-}°) set to 0.5, 0.3, and 0.1 $mol \cdot L^{-1}$. The selection of the association constant at infinite dilution will be extensively discussed in Section 9.3.2.

The details of calculations of thermodynamic properties including but not limited to the volume solver algorithm, site fraction solver, derivative calculations can be found in the existing literature [8, 330–332] and will not be explained here.

Figure 9.4a demonstrates that the liquid density of the solution exhibits insensitivity, or very slight sensitivity, to the inclusion of ion-ion association in the EoS. As is evident in this figure, all the curves closely overlap with each other. A minor deviation can be observed at extremely high salt molalities.

In contrast to the liquid density, MIAC, the osmotic coefficient, and the molar conductivity of the solution exhibit a high degree of sensitivity to inclusion of ion-ion association, as well as the specific value chosen for the association constant at infinite dilution.

From Figure 9.4b, it can be seen that the results of eSAFT-VR-Mie (S1) from Selam et al. [70] for MIAC of the electrolyte are in better agreement with the experimental data compared to Binding eSAFT-VR-Mie (S2). It is neither surprising nor interesting since the result of a model that has been adjusted to the experimental data is better than a model where no adjusting parameter are used. Furthermore, according to our previous discussion, sodium chloride is slightly associative. As a result, it cannot be expected that the estimated MIAC is modified by including an ion-ion association. However, it can be observed that the green curve is also close to the experimental data.

The results of the osmotic coefficient depicted in Figure 9.4 differ from the MIAC. As observed in this figure, the agreement with the experimental data is better for Binding eSAFT-VR-Mie with $K_{+-}^{\circ} = 0.1\ mol \cdot L^{-1}$ compared to eSAFT-VR-Mie. What makes this observation intriguing is that the osmotic coefficient data were not utilized in the parameter estimation of eSAFT-VR-Mie by Selam et al. [70]. Consequently, although the MIAC (used in parameter estimation) and osmotic coefficient are correlated, this comparison provides a more equitable assessment of eSAFT-VR-Mie and Binding eSAFT-VR-Mie.

It is evident that the predicted molar conductivity, when considering ion-ion association with $K_{+-}^{\circ} = 0.1\ mol \cdot L^{-1}$, exhibits modifications compared to the S1 curve, where ion pairing is neglected. However, a noticeable deviation from the experimental data still persists at higher concentrations. Interestingly, increasing the association constant results in an

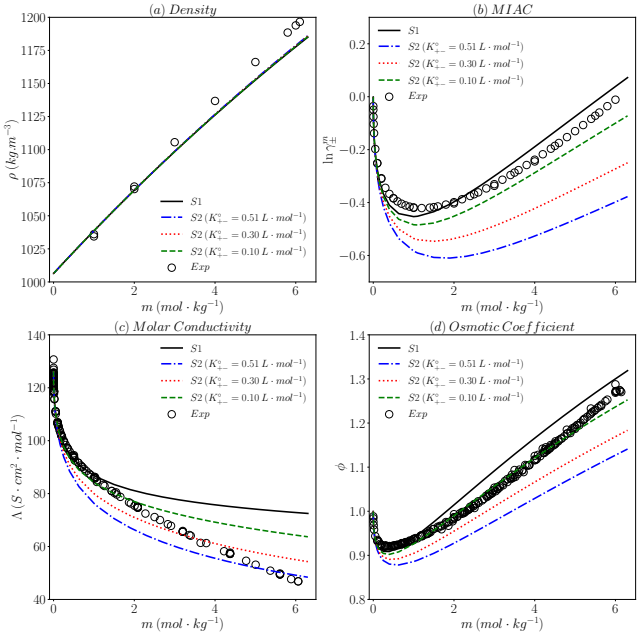

Figure 9.4. This figure compares the predictions with the experimental data of NaCl-H_2O at 298.15 K for (a) liquid density (ρ), (b) MIAC ($\ln \gamma^m_{\pm}$), (c) molar conductivity (Λ), and (d) osmotic coefficient (ϕ). S1 is denoted to the predictions of the EoS or the electrical conductivity model where the ion-ion association is ignored. S2 is the prediction that includes the effect of the ion-ion association corresponding to the association constant written in front of it. The experimental data denoted as points are from ref. [90] for MIAC, from ref. [90] for osmotic coefficient, from ref. [131, 134, 148, 149, 166] for electrical conductivity and from ref. [333] for density.

underestimation of molar conductivity, even at very low molalities, as indicated by the blue and red curves in Figure 9.4c.

Figure 9.5 shows the fraction of unbound ions (free ions) predicted by the Binding eSAFT-VR-Mie model at 298.15 K, with the association constant at infinite dilution ranging from 0.1 to 0.51 mol/L. Notably, for this electrolyte, the fraction of free ions for both cations and anions is equal, denoted as $\alpha_+ = \alpha_-$.

As observed in this figure, an increase in K°_{+-} results in a decrease in the fraction of free ions. Additionally, the variation of the fraction of free ions with salt molality follows either a linear trend or closely approximates linearity. In cases where the predictions of MIAC, the osmotic coefficient, and the molar conductivity are in better agreement, as indicated by the green dashed lines, the variation of the fraction of free ions is linear, ranging from 1 at infinite dilution to nearly 0.9 at $m = 6\, mol \cdot kg^{-1}$.

Figure 9.6 provides an overview of the contributions to the activity coefficient of both cations and anions, originating from the terms PHYS, ASSOC, DH and MAL. The definitions of these terms can be found in Table 9.5. These contributions to the Helmholtz free energy

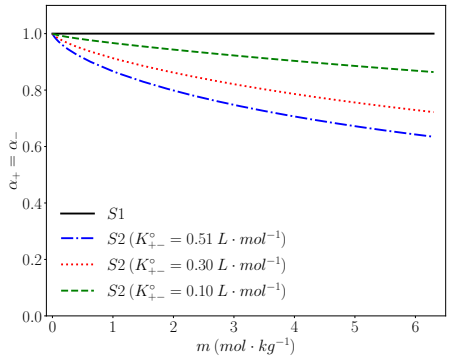

Figure 9.5. This figure presents the fraction of free ions ($\alpha_+ = \alpha_-$) for NaCl-H_2O at 298.15 K. S1 corresponds to the eSAFT-VR-Mie that consider full dissociation. S2 curves corresponds to Binding eSAFT-VR-Mie with the associations constant at infinite dilution (K°_{+-}) equals to 0.51, 0.30, and 0.10 $L \cdot mol^{-1}$ for blue, red, and green curves, respectively.

are obtained from Eq. 9.62.

$$\ln \gamma_i^{CONT} = \frac{1}{RT}\left[\left(\frac{\partial A^{CONT}}{\partial n_i}\right)_{T,V,n_j} - \left(\frac{\partial A^{CONT}}{\partial n_i}\right)_{T,V,\infty}\right] \tag{9.62}$$

The colored lines in Figure 9.6 correspond to the colored lines in Figures 9.4 and 9.5, where the Binding eSAFT-VR-Mie is utilized for the calculations. On the contrary, the black lines represent the contributions to the activity coefficient when ion pairing is not considered (eSAFT-VR-Mie). It should be noted that the PHYS, ASSOC, and DH contributions of the Binding eSAFT-VR-Mie EoS are identical to those of eSAFT-VR-Mie. Consequently, in Figure 9.6, these contributions are displayed in black for eSAFT-VR-Mie. The differentiating factor between Binding eSAFT-VR-Mie and eSAFT-VR-Mie lies in the contributions from the MAL term. In the case of eSAFT-VR-Mie, this contribution remains zero (black dashed dotted lines in Figure 9.6). However, for the Binding eSAFT-VR-Mie, the MAL contribution is nonzero and varies with salt molality.

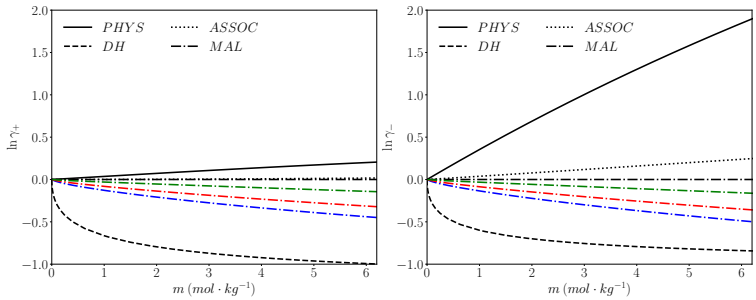

Figure 9.6. This figure presents the contributions to the activity coefficients of cation ($\ln \gamma_+$) and anion ($\ln \gamma_-$) for NaCl-H_2O at 298.15 K. Colored lines corresponds to colored ones in figures 9.4 and 9.5. Black lines are contributions to the activity coefficient from the eSAFT-VR-Mie.

Table 9.5. The Contributions to the activity coefficient.

Term	Description
PHYS	$\ln \gamma_i^{MONO} + \ln \gamma_i^{CHAIN} - \ln Z$
ASSOC	$\ln \gamma_i^{ASSOC}$
DH	$\ln \gamma_i^{DH}$
MAL	$\ln \gamma_i^{MAL}$

The primary takeaway from Figure 9.6 is that the inclusion of ion-ion association introduces an additional negative contribution to the activity coefficient of both cations and anions. This explains why the incorporation of the ion-ion association leads to a downward shift in the predicted MIAC. Furthermore, it should be noted that the variation of the MAL contribution with salt molality exhibits an almost linear behavior.

Upon assessing the predictions made by the Binding eSAFT-VR-Mie for sodium chloride aqueous solutions, several observations come to light. Notably, the inclusion of the ion-ion association does not compromise the already commendable results yielded by the eSAFT-VR-Mie. In fact, the opposite is evident: introducing the ion-ion association has subtly refined predictions related to molar conductivity and the osmotic coefficient.

Moreover, it is evident that even in the absence of ion-ion association considerations, the model can produce reasonably accurate results. This outcome aligns with expectations, given that the NaCl-H_2O system exhibits only mild associative behavior. Consequently, any effects arising from neglecting ion-ion associations can be counterbalanced by fine-tuning model parameters during the parameter estimation process.

9.2.3 Na_2SO_4-H_2O

Sodium sulfate aqueous solutions constitute the second system under investigation to assess the impact of ion-ion association. In comparison to sodium chloride, sodium sulfate is more associative because of the propensity of sulfate ions to form ion pairs. However, it remains less associative compared to the $MgSO_4$ aqueous solution, which will be examined in the subsequent section.

The association of ions in this electrolyte follows the following reaction equilibrium:

$$Na^+ + (SO_4)^{2-} \rightleftharpoons (NaSO_4)^- \tag{9.63}$$

As depicted in Eq. 9.63, ion pairs in the case of this electrolyte also carry charge and play a role in the electrical conductance process. This underscores the significance of studying this system, particularly in light of Marcus's observation [80] that the primary limitation of utilizing electrical conductivity to investigate ion pairing lies in its applicability to asymmetrical electrolytes. With the development of a multi-salt extension for the DHO-based electrical conductivity model (as outlined in Chapter 5), we now possess a robust theoretical framework for examining ion pairing in asymmetrical electrolyte solutions. Consequently, it can be asserted that the investigation of ion pairing in such systems through electrical conductivity is no longer constrained by the previously mentioned disadvantage.

Investigations into the presence of ion pairs in aqueous sodium sulfate solutions have extended beyond electrical conductivity and encompassed various other methodologies. These include studies based on the activity coefficient [334], the potentiometric analysis [335–337], the DRS [338], the MD simulations [316,339,340], and the spectroscopic techniques [341–343].

For this electrolyte, Gilligan and Atkinson proposed a two-step mechanism based on ultrasonic relaxation data [344]. Spectroscopic methods [341–343] have indicated that the formation of CIP is unlikely. DRS [338] has also shown that the formation of SSIP and SIP leads to a more consistent association constant at infinite dilution with potentiometric

studies. In contrast, a recent study that combined MD simulations and DRS [316] has suggested that the dominant ion pairs in this system are CIP.

Without additional structural investigations, it remains challenging to definitively determine which of the statements regarding the type of ion pairs in sodium sulfate solutions is more closely aligned with the actual behavior of the system. Nevertheless, it can be confidently asserted that this system exhibits ion association tendencies. Unlike sodium chloride aqueous solutions, where the evidence regarding ion pairing is mixed, both simulation and experimental investigations consistently provide evidence of ion pair formation in sodium sulfate solutions.

From the macroscopic examination of ion pairing, it can be asserted that classical approaches that utilize thermodynamic and electrical conductivity properties continue to hold value. Hence, as detailed in Section 9.1.7, a concurrent investigation of both thermodynamic properties and electrical conductivity proves to be an advantageous approach, offering a comprehensive understanding of the dynamics of ions within the solution.

In the domain of thermodynamic modeling, sodium sulfate electrolyte solutions have been subject to investigation by several electrolyte equations of state, including but not limited to eCPA [42,52], ePC-SAFT [56,57,59], and eSAFT-VR-Mie [69,70]. Table 9.6 provides the AARD% of the predicted MIAC, osmotic coefficient, and liquid density by the respective equations of state.

All the studies listed in Table 9.6, apart from Held et al.'s [57], have assumed that sodium sulfate aqueous solutions completely dissociate. Notably, the table reveals that the predictive errors of the models consistently exhibit higher magnitudes when compared to the sodium chloride system.

Furthermore, Held et al. [57] approached sodium sulfate aqueous solutions as if they were weak electrolytes, adjusting the association constant on a molality scale. This treatment of ion pairing aligns with chemical approaches. However, it can be gleaned from the AARD% values in Table 9.6 that the inclusion of the ion-ion association has led to improved estimates of MIAC. In a subsequent study, Held et al. [59] adopted a different parameter estimation strategy, and despite the improved predictive performance when considering the ion-ion association, they chose to disregard this effect. They were able to identify a set of parameters that resulted in a reduced deviation from the experimental data.

AARD% values for other electrolyte equations of state have revealed substantial deviations from the experimental data. Eriksen [345] postulated that this deviation may be attributed to the omission of effects of ion-ion association.

Figure 9.7 illustrates the impact of incorporating ion pairing on liquid density, MIAC, molar conductivity, and osmotic coefficient. In a manner similar to Figure 9.4, the black lines depict the predicted properties employing eSAFT-VR-Mie [70] for thermodynamic properties. For molar conductivity, this line represents the prediction under the assumption of

Table 9.6. Summary of the AARD% of the equations of state reported in the literature for Na_2SO_4-H_2O solution.

		AARD%		
eEoS	Ref.	$\gamma^m_\pm$	ϕ	ρ
eCPA	Maribo-Mogensen et al. [42]	3.71	2.06	4.59
	Schlaikjer et al. [53]	6.96	9.37	0.75
ePC-SAFT	Held et al. [56]	32.63	-	0.41
	Held et al. [57]	6.43	-	0.41
	Held et al. [59]	-	2.41	0.87
eSAFT-VR-Mie	Eriksen [345]	-	39.21	1.34
	Selam et al. [70]	17.49	16.47	0.74

complete dissociation, employing equations for the single-salt case (equations 9.35, 9.41, and 9.39). The colored lines correspond to the Binding eSAFT-VR-Mie model elucidated in Section 9.1.1, and the molar conductivity is determined using the multi-salt model (equations 9.35, 9.44, and 9.39).

Figure 9.7a reveals that the inclusion of the ion-ion association has an exceedingly minimal impact, almost negligible, on the prediction of liquid density. This observation aligns with the findings in Figure 9.4. Similar to the sodium chloride system, the incorporation of the ion-ion association results in a downward shift in the predictions of MIAC, molar conductivity and osmotic coefficient compared to the S1 curve, where ion pairing is disregarded. This shift becomes more pronounced as the association constant at infinite dilution increases. Notably, the association constants at infinite dilution for this system are one order of magnitude greater than those for the sodium chloride system, as evidenced by Figure 9.7.

Unlike the sodium chloride system, as depicted in Figure 9.7, the S1 curves representing the predictions for MIAC, molar conductivity and osmotic coefficient under the assumption of complete dissociation deviate from the experimental data. The incorporation of the ion-ion association leads to improved predictions for both the osmotic coefficient and the MIAC compared to the predictions of eSAFT-VR-Mie [70] (S1 curve). However, when utilizing an association constant at infinite dilution from the literature (blue curves), it is evident that both the MIAC and osmotic coefficient are underestimated. For MIAC, the green curve (where $K^{\circ}_{+-} = 1.7\,L \cdot mol^{-1}$) shows a closer alignment with the experimental data, while for the osmotic coefficient, the red curve (with $K^{\circ}_{+-} = 4.4\,L \cdot mol^{-1}$) shows a better fit to the experimental data.

Figure 9.7c, which presents the predictions of molar conductivity, highlights that neglecting the ion-ion association leads to overestimations of molar conductivity, while incorporating the ion-ion association results in underestimations. Furthermore, the degree of underestimation increases with greater association constants at infinite dilution.

Figure 9.8 illustrates the fraction of unbound ions for the Na_2SO_4-H_2O system. In this figure, the fraction of unbound cations and anions is indicated by α_+ and α_-, respectively. Initially, it is evident that the fraction of free ions for cations and anions differs by a factor of two, as dictated by mass balance considerations. Furthermore, the figure reveals that the fraction of free ions exhibits a steep decline when the salt molality is below $0.5\,mol \cdot kg^{-1}$. At higher concentrations, the fraction of free ions decreases almost linearly with the salt concentration.

Figure 9.9 illustrates the contributions to the activity coefficient derived from the terms PHYS, ASSOC, DH and MAL, as defined in Table 9.5. In this figure, similar to Figure 9.6, the colored curves represent the MAL contributions, corresponding to the colored curves in Figures 9.7 and 9.8. Meanwhile, the black curves denote contributions shared between eSAFT-VR-Mie and Binding eSAFT-VR-Mie.

Figure 9.9 illustrates that the inclusion of the ion-ion association leads to an additional negative contribution to the activity coefficient of the ions. The negative contribution of the sulfate ion, as shown in Figure 9.9, exceeds that of the sodium ion. Furthermore, it is observed that the contribution from the MAL increases with larger association constants at infinite dilution.

9.2.4 $MgSO_4$-H_2O

Aqueous solutions of $MgSO_4$ have received significant attention in both theoretical and experimental studies, owing to their relevance in fields such as biochemistry, physiology and their prevalence as a major component of seawater. The exploration of the thermodynamics, structural properties, and dynamic behavior of ion-ion and ion-solvent interactions in these solutions have been the focus of research. Of particular interest has been the investigation of ion pairing, or more broadly, ion-ion association in aqueous $MgSO_4$ solutions. This interest

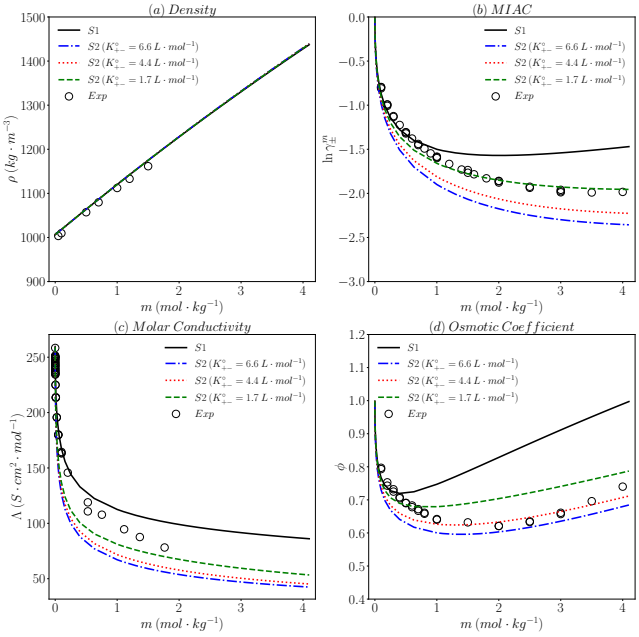

Figure 9.7. This figure compares the predictions with the experimental data of Na_2SO_4-H_2O at 298.15 K for (a) the liquid density (ρ), (b) the MIAC ($\ln \gamma^{m}_{\pm}$), (c) the molar conductivity (Λ), and (d) the osmotic coefficient (ϕ). S1 is denoted to the predictions of the EoS or the electrical conductivity model where the ion-ion association is ignored. S2 is the estimations including the effect of ion-ion association corresponding to the association constant written in front of it. Experimental data denoted as points are from ref. [90,219,346] for the MIAC, from ref. [90,263] for the osmotic coefficient, from ref. [129, 134, 141, 160] for the electrical conductivity, and from ref. [141] for the liquid density

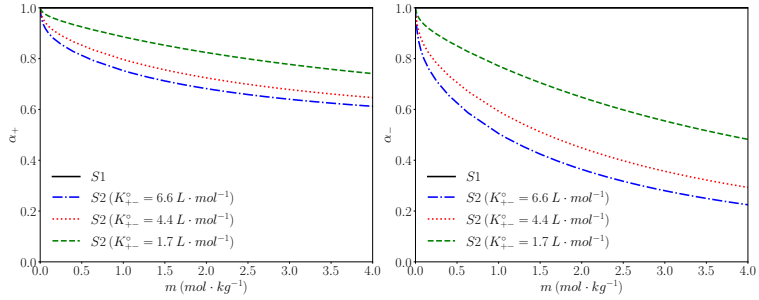

Figure 9.8. This figure presents the fraction of free ions (α_+ and α_-) for Na_2SO_4-H_2O at 298.15 K. S1 corresponds to the eSAFT-VR-Mie that consider full dissociation. S2 curves corresponds to Binding eSAFT-VR-Mie with the associations constant at infinite dilution (K°_{+-}) equals to 6.6, 4.4, and 1.7 $L \cdot mol^{-1}$ for blue, red, and green curves, respectively.

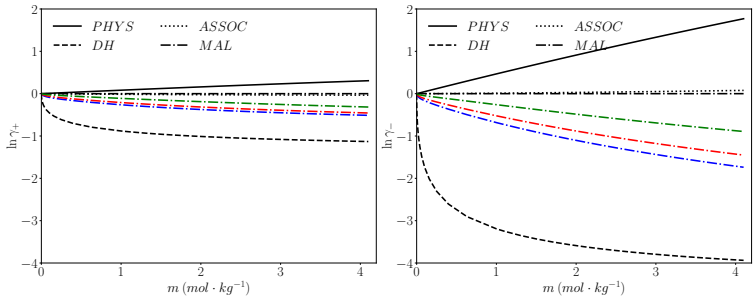

Figure 9.9. This figure presents the contributions to the activity coefficients of cation ($\ln \gamma_+$) and anion ($\ln \gamma_-$) for Na_2SO_4-H_2O at 298.15 K.

dates back to the seminal work by Eigen and Tamm [347, 348], who introduced the concept of multi-step ion pairing based on sound absorption relaxation processes.

Various methods have been employed to investigate the dynamics and structure of ion pairing in aqueous $MgSO_4$ solutions since then. These methods include Raman spectroscopy [189,191,343,349–352], DRS [264,314–316], terahertz and femtosecond infrared spectroscopy [266], and sum frequency spectroscopy [353], among others.

While these methods offer insight into the structure and dynamics of ion-ion and ion-solvent interactions, achieving a consistent and comprehensive understanding of these dynamics in $MgSO_4$ aqueous solutions still requires further research efforts. In the meantime, it remains crucial to investigate the thermodynamics of the ion-ion association using more advanced macroscopic approaches, as proposed in this study.

The association of ions in $MgSO_4$-H_2O solutions has been methodically examined through different avenues. One approach focuses on the investigation of thermodynamic properties, utilizing implicit solvent models, as discussed in the works by Tikanen et al. [354] and Simonin et al. [163]. A separate line of inquiry has been the interpretation of electrical conductivity data, as shown by studies by Tomsic et al. [130], Turq et al. [112] and Chhih et la. [113]. For both methodologies, model parameters are meticulously tuned to align with the target experimental data, be it MIAC or molar conductivity, resulting in the formulation of a semi-empirical model.

In Chapter 6, we delved into the phenomenon of ion pairing within $MgSO_4$-H_2O solutions, contrasting the predictions of four implicit solvent models: FLGG [233, 234, 236], EG [220–222], ZYS [242], and BiMSA [20]. Remarkably, all of these models adhered to the RPM, assuming uniform size for both cations and anions. Our findings indicated that, despite their inherent differences, each model could be effectively tuned to match the MIAC experimental data. However, the proportions of unbound ions predicted by each differed both qualitatively and quantitatively. It has been proposed that molar conductivity might serve as a validation tool for these estimates, given the profound impact the species distribution exerts on the molar conductivity of a solution.

Within the realm of electrolyte equations of state, the phenomenon of ion pairing in aqueous $MgSO_4$ solutions is often overlooked. A summary of the discrepancies observed in the electrolyte equations of state for the $MgSO_4$-H_2O system can be found in Table 9.7.

From Table 9.7, it is evident that the AARD% for the $MgSO_4$ system is consistently higher compared to the sodium chloride system. Furthermore, the $MgSO_4$ system has been notably less explored in numerous electrolyte equations of state.

Figure 9.10 presents various properties of the aqueous magnesium sulfate solution at 298.15 K, including liquid density, MIAC, molar conductivity, and osmotic coefficient. The S1 labeled curves are predictions from the eSAFT-VR-Mie model [70], which covers liquid

Table 9.7. Summary of the AARD% of the equations of state reported in the literature for $MgSO_4$-H_2O solution.

		AARD%		
eEoS	Ref.	$\gamma_{\pm}^{m}$	ϕ	ρ
eCPA	Maribo-Mogensen et al. [42]	7.94	7.81	0.79
	Schlaikjer et al. [53]	3.64	4.86	0.84
ePC-SAFT	Held et al. [56]	19.36	-	0.54
eSAFT-VR-Mie	Eriksen [345]	-	12.61	0.849
	Selam et al. [70]	13.92	11.28	0.67

density, MIAC, and osmotic coefficient. The molar conductivity under S1 is based on the predictions of the single-salt model, which assumes full dissociation. In contrast, the S2 curves highlight predictions from the Binding eSAFT-VR-Mie, with the association constants explicitly noted. For molar conductivity, the S2 curves use predictions that factor in the fraction of unbound ions from the Binding eSAFT-VR-Mie EoS. This representation offers a detailed comparison between experimental data and model predictions for the $MgSO_4$ solution at the given temperature.

Just as with aqueous solutions of sodium chloride and sodium sulfate, the liquid density predictions for the $MgSO_4$ system seem to be largely unaffected by the incorporation of ion-ion association factors. This is evident from Figure 9.10a, where all plotted curves closely converge. The fidelity of these density predictions stems from the refinements implemented by Selam et al. [70] in the eSAFT-VR-Mie model.

Regarding this system, Figure 9.10b reveals a deviation in the predicted MIAC by eSAFT-VR-Mie from the experimental data when concentrations approach 1 $mol \cdot kg^{-1}$. However, the Binding eSAFT-VR-Mie predictions are found to be reliable when $K_{+-}^{\circ} = 80.7\, L \cdot mol^{-1}$, a value which is nearly half of what has been previously cited in the literature. The use of prior values for the association constant at infinite dilution led to an underestimation of the MIAC.

The influence of incorporating ion-ion associations in model predictions becomes even clearer when contrasting the S1 curve with the S2 curves in Figure 9.10d. This comparison illustrates that, independent of the precise value of the association constant at infinite dilution, the S2 curves are more aligned with the experimental data than the S1 curve. A similar trend can be discerned from graph c of Figure 9.10. Here, while the S2 curves align remarkably well with the experimental data, the S1 curve tends to overestimate the molar conductivity.

For the osmotic coefficient, even more pronounced modifications relative to eSAFT-VR-Mie predictions are evident. At elevated salt concentrations, the predictions of eSAFT-VR-Mie (represented by the S1 curve) overshoot the experimental data. On the other hand, the Binding eSAFT-VR-Mie predictions lie much closer to the experimental data. At diluted concentrations, where a minimum is observed in the osmotic coefficient experimental data, neither the predictions from eSAFT-VR-Mie nor those from Binding eSAFT-VR-Mie closely match the observed values.

To encapsulate, the inclusion of the ion-ion association provides improved accuracy in predicting MIAC, molar conductivity, and osmotic coefficient for the $MgSO_4$ system.

Figure 9.11 shows the fraction of unbound ions in aqueous magnesium sulfate solutions at 298.15 K. An examination of this figure reveals that the trends exhibited by the curves representing the fraction of free ions (as represented by the red, blue, and green curves) differ markedly from those observed for sodium chloride and sodium sulfate systems. Specifically, in Figure 9.11, there is a swift decline in the fraction of unbound ions as salt concentrations increase. Following this initial sharp decline, the rate at which the fraction of unbound ions

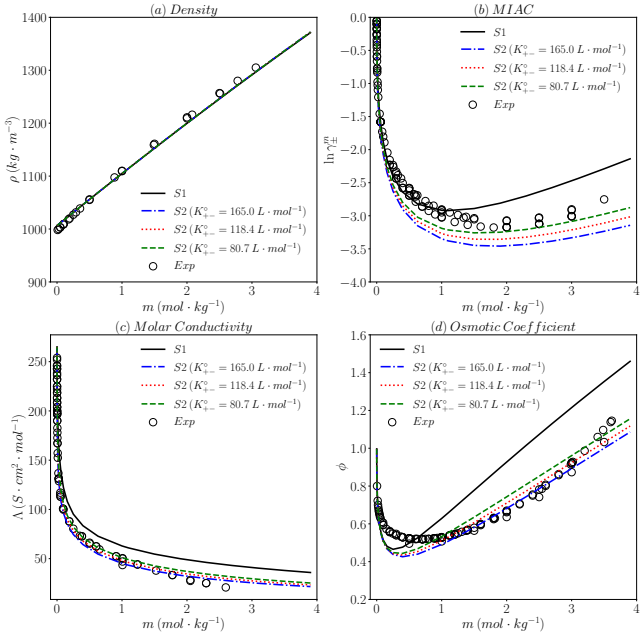

Figure 9.10. This figure compares the predictions with the experimental data of $MgSO_4$-H_2O at 298.15 K for (a) the liquid density (ρ), (b) the MIAC ($\ln \gamma^m_\pm$), (c) the molar conductivity (Λ), and (d) the osmotic coefficient (ϕ). S1 is denoted to the predictions of the EoS or the electrical conductivity model where the ion-ion association is ignored. S2 is the estimations that include the effect of the ion-ion association corresponding to the association constant written in from it. Experimental data denoted as points are from ref. [7,90,219,263,355–357] for the MIAC, from ref. [90,263,355,357–362] for the osmotic coefficient, from ref. [129,130] for the electrical conductivity, and from ref. [363,364] for the liquid density

changes in relation to salt concentration becomes more gradual. At elevated salt concentrations, a nearly linear drop in both α_+ and α_- is discernible as a function of m.

Figure 9.12 displays the various contributions to the activity coefficient for the $MgSO_4$-H_2O system, in alignment with the definitions provided in Table 9.5. Mirroring figures 9.6 and 9.9, the contributions that stem from the PHYS, ASSOC, and DH terms, which are common to both the eSAFT-VR-Mie and Binding eSAFT-VR-Mie, are illustrated using black lines. Meanwhile, the contributions of the MAL term, which correlates with the association constant at infinite dilution as shown in figures 9.11 and 9.10, are also delineated.

From Figure 9.12, it is evident that the primary positive contribution to the activity coefficient arises from the PHYS term. Conversely, the DH and MAL terms contribute negatively. In particular, the DH term stands out as the most significant contributor, overshadowing the impact of the MAL term. That said, the contribution from the MAL term, although smaller relative to the DH, is far from insignificant. Furthermore, when compared with other systems, as depicted in Figures 9.6 and 9.9, the contribution of MAL in the $MgSO_4$

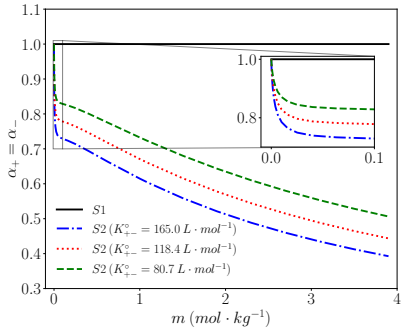

Figure 9.11. This figure presents the fraction of free ions (α_+ and α_-) for $MgSO_4$-H_2O at 298.15 K is depicted against the salt molality (m). S1 corresponds to the eSAFT-VR-Mie that consider full dissociation. S2 curves corresponds to Binding eSAFT-VR-Mie with the associations constant at infinite dilution (K°_{+-}) equals to 165.0, 118.4, and 80.7 $L \cdot mol^{-1}$ for blue, red, and green curves, respectively.

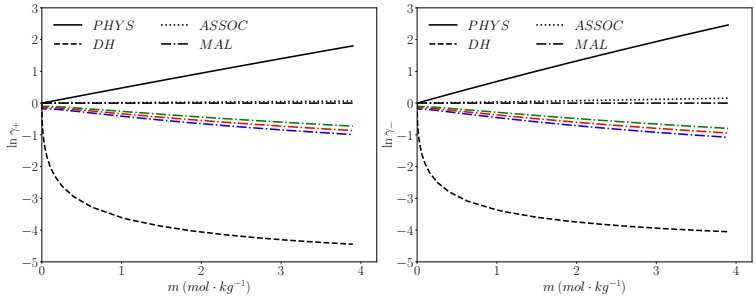

Figure 9.12. This figure presents the contributions to the activity coefficients of cation ($\ln \gamma_+$) and anion ($\ln \gamma_-$) for $MgSO_4$-H_2O at 298.15 K. Black curves corresponds to the the terms shared with the SAFT-VR-Mie and Binding eSAFT-VR-Mie. blue, red, and green curves corresponds to the MAL term with the associations constant at infinite dilution (K°_{+-}) equals to 165.0, 118.4, and 80.7 $L \cdot mol^{-1}$, respectively.

system appears more pronounced. At extremely low salt concentrations, the contribution from the MAL term displays rapid variations as the salt concentration changes. In contrast, at moderate to high concentrations, its change is more linear in relation to the salt concentration.

9.3 Discussion

In Section 9.2, we compared the predicted properties - liquid density, MIAC, molar conductivity, and osmotic coefficient - of three aqueous electrolyte solutions at 298.15 K with experimental data. Moreover, the fraction of free ions and contributions to the activity coefficient were illustrated for each system.

The analysis underscored that the inclusion of the ion-ion association has a negligible

impact on the liquid density predictions. Factoring in the ion-ion association yielded more accurate predictions for sodium and magnesium sulfate solutions. However, for the sodium chloride aqueous solution, slight improvements were observed in contrast to the eSAFT-VR-Mie predictions.

In this section, the effect of considering the ion-ion association on the macroscopic properties of the system will be further discussed. Onsager's bookkeeping rule will be introduced, and the importance of the association constant at infinite dilution will be investigated. The argument around the importance of ion pairing will be addressed, and what is ignored in this study will be explained.

9.3.1 How ion-ion association affects the predictions of $\gamma_{\pm}^{m}$, ϕ, ρ, and Λ?

In the literature, a frequently cited reason for the divergence between model predictions and experimental data is the assumption of full dissociation. The inclusion of ion-ion association is commonly suggested as a remedy to bridge the gap between theoretical and experimental findings. In this section, we delve into the circumstances under which ion-ion association impacts the predictions of the electrolyte equations of state, and when it remains inconsequential.

The influence of accounting for ion-ion associations, particularly in our approach, is rather direct. As evidenced by figures 9.4, 9.7, and 9.10, the inclusion of the ion-ion association has a negligible impact on the prediction of liquid density. This observation is crucial, given that estimating liquid density presents a significant challenge within the framework of electrolyte equations of state. In general, it has been observed that the primary determinant for liquid density estimation is the ionic diameter.

Figures 9.4, 9.7 and 9.10 illustrate that the inclusion of the ion-ion association causes a downward shift in the curves from eSAFT-VR-Mie to Binding eSAFT-VR-Mie for MIAC, molar conductivity, and osmotic coefficient.

For the prediction of MIAC, the contributions to the activity coefficient are shown in figures 9.6, 9.9, and 9.12. As observed in these figures, the contribution of MAL is consistently negative and exhibits an almost linear variation at high salt concentrations. Consequently, accounting for the ion-ion association invariably introduces an additional negative contribution to the activity coefficient, leading to a downward shift of the MIAC curve.

For molar conductivity, the impact of incorporating ion-ion association is more nuanced than that of MIAC. When this property is considered, the inclusion of ion-ion association either decreases the number of charged species contributing to electrical conductance (in symmetrical electrolytes) or decreases the charge of the species involved in the conductance process. In either scenario, the predicted specific conductivity is reduced when ion-ion association is taken into account. In the systems we examined, the predicted molar conductivity consistently shifts downward relative to the predictions based on full dissociation.

A similar trend observed for MIAC can also be seen for osmotic coefficient. Taking ion pairing into account leads to a downward shift in the curves. This outcome is anticipated, given that the osmotic coefficient is related to the MIAC of the electrolyte through the Gibbs-Duhem equation (Eq. 9.64).

$$\ln \gamma_{\pm}^{m} = \phi - 1 + \int_{0}^{m} \frac{\phi - 1}{m} dm \tag{9.64}$$

In summary, the incorporation of the ion-ion association has a negligible impact on the prediction of liquid density. However, for MIAC, molar conductivity, and osmotic coefficient, factoring in ion-ion association leads to a downward shift in the curves. Conclusively, it is not reasonable to expect that simply including ion-ion association (without re-evaluating the parameter estimation) would adjust the predictions of these properties when the model, which assumes full dissociation, underestimates the property.

9.3.2 Importance of standard state association constant; Onsager's Bookkeeping rule

Bjerrum [216] introduced a model for the association constant at infinite dilution concerning ion pairing. He posited that the upper limit of the integral, as indicated in Eq. 9.24, could be set at q_{ij}, where the likelihood of encountering the counter ion j near the central ion i reaches a minimum.

Onsager [91] regarding the Bjerrum's choice of this cut-off distance pointed out that:

> *"Bjerrum's choice is good but we could vary it within reason. In a complete theory this would not matter; what we remove from one side of the ledger would be entered elsewhere with the same effect."*

This is commonly referred to as Onsager's bookkeeping rule [365]. This aligns with Bjerrum's beliefs regarding this selection. He remarked:

> *"Let us tentatively affirm that ion pairs, with an internal distance of less than that corresponding to the minimum, are to he denoted as associated and all other ion pairs as free. Naturally this distinction between free and associated ions is rather arbitrary."*

These two quotes from two of the most prominent scientists in the context of electrolyte solutions could be used as a guideline for further investigation of ion pairing in electrolyte solutions. From these statements, it can be understood that an exact choice for the association constant does not exist. As a result, the focus should be on theory-experiment agreement rather than on fixing the reference state. With this guideline in mind, we investigated the effect of considering the ion-ion association in electrolyte solutions by adopting three association constant. One of them is the value reported in the literature, the other two are reduced values since the experimental values resulted in under prediction of the properties (see figures 9.4, 9.7, and 9.10).

In this section, we delve into the selection of the reference state association constant by examining the values reported in the literature and the models devised for it.

Figure 9.13 illustrates the predicted association constant at infinite dilution using the Bjerrum model (as represented by Eq. 9.24). Here, the upper limit of the integral spans from σ_{+-} to $5\sigma_{+-}$. In this figure, individual points represent the K°_{+-} where Bjerrum's specified choice is employed as the upper limit.

Table 9.8 lists the association constants at infinite dilution as reported in the literature. These values have been determined using various methods, including electrical conductivity, DRS, Raman spectroscopy, ultrasonic absorption, MIAC, and MD simulations.

When comparing the values reported in the literature with the points depicted in Figure 9.13, it becomes evident that using the Bjerrum's choice typically leads to an overestimation of the association constant at infinite dilution. However, the model does account for the

Table 9.8. The association constant at infinite dilution of the systems studied in this work reported in the literature from electrical conductivity (EC) [130, 148, 149, 159], DRS [264, 315], Raman Spectroscopy (RS) [349, 351], Ultrasonic Absorption (UA) [347, 366], MIAC [354], and MD Simulations (MD) [323, 367].

Salt	Lit. (EC)	Lit. (DRS)	Lit. (MIAC)	Lit (RS)	Lit. (UA)	Lit. (MD)
NaCl	0.37, 2.5	-	-	-	-	0.60, 0.76
Na_2SO_4	12.6	6.7, 24.0	6.6	-	-	-
$MgSO_4$	100-240	162, 167	164	165, 167	165, 197	-

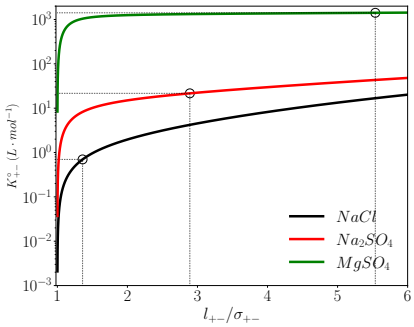

Figure 9.13. The association constant at infinite dilution (K°_{+-} predicted by the Bjerrum model where the upper limit of integral (l_{+-}) varies from σ_{+-} to $5\sigma_{+-}$. Points show the Bjerrum choice for the upper limit and the corresponding association constant.

effect of ion valences. In particular, as the valence type of the ions increases, Bjerrum's model predicts a greater K°_{+-}.

Apart from the discrepancies between the Bjerrum's model (using his specified choice for the upper limit) and the values reported by the literature, Table 9.8 reveals that the association constant at infinite dilution spans a broad range. For example, the association constant at infinite dilution for $MgSO_4$ aqueous solutions can fluctuate between 100 and 240, as highlighted by Apelblat [159], relying solely on the electrical conductivity data. For Na_2SO_4 aqueous solutions, it is observed that selecting SSIP and SIP leads to an association constant of 6.4, in stark contrast to 24.0 when SSIP and CIP are identified as ion pairs [338]. From MD simulations, Fennel et al. [323] emphasized the significance of force field selection. They demonstrated that the association constant for lithium halide solutions can vary by orders of magnitude depending on the chosen force fields.

In summary, there is significant uncertainty surrounding the association constant at infinite dilution. The values reported in the literature are shown to be influenced by the model employed to interpret the data, the range of salt concentration, the selection of ion pair types and the choice of force fields. From this analysis, there is no alternative but to adjust the association constant at infinite dilution, and consequently the upper limit of the integral. Thus, adhering to Onsager's bookkeeping rule is not merely an option; it is imperative.

In light of our investigation, as shown in figures 9.4, 9.7 and 9.10, it is often the case that a smaller value for the association constant than what is reported in the literature (as shown in Table 9.8) leads to satisfactory accuracy. The root of this observation can be attributed to a couple of factors.

First and foremost, this study utilizes parameters presented by Selam et al. [70] for the computations. These parameters (σ_i and ϵ_{iw}) have been fine-tuned to align with experimental data of liquid density and MIAC. This suggests that during the optimization process, there is an underlying effort to make eSAFT-VR-Mie predictions closely resemble the experimental data. Consequently, any oversight of ion pairing within the model might have been counterbalanced during the parameter estimation phase. The osmotic coefficient graphs, data for which was not incorporated in Selam et al.'s [70] parameter estimation, specifically figures 9.4d, 9.7d and 9.10d, bolster this hypothesis. In these visual representations, the modifications in the predicted osmotic coefficient by Binding eSAFT-VR-Mie appear to be more pronounced compared to MIAC.

Thus, it can be inferred that aspects of the ion pairing's contribution might have been

inherently accounted for during the parameter estimation. This inclusion potentially explains why less pronounced ion pairing leads to a harmonious alignment with the experimental data.

Onsager's bookkeeping rule suggests that the selection of the cut-off distance and, subsequently, the value of the association constant at infinite dilution is not of primary importance as long as the model can effectively predict properties that have been measured devoid of specific assumptions or data manipulation. In other words, if a model adeptly predicts macroscopic properties such as MIAC, electrical conductivity, and osmotic coefficient, the concurrence of the association constant at infinite dilution with other methodologies is not paramount.

However, it is worth noting that the assessment of the association constant should be integrated into the parameter estimation process. Opting for the upper limit of the integral, as advocated by Naseri Boroujeni [286], represents a rational choice. Another viable avenue involves incorporating short-range solvation effects empirically within the Bjerrum model, as delineated by Barthel [254] and subsequently adopted by others [213,252,253,368]. Adjusting the association constant at infinite dilution directly based on experimental data is yet another approach, although it is advised to exercise caution with this method. Doing so might reduce the model's ability to extrapolate to varied temperatures or solvents other than water, limiting its broader applicability.

9.3.3 What If Ion-Ion Association Is Ignored?

Most electrolyte equations of state often omit the influence of ion-ion association, as only a limited number of studies take this effect into account. Based on data from Tables 9.4, 9.6, and 9.7, these models can still produce results that meet engineering requirements. However, when it comes to strongly associative electrolyte solutions, the accuracy of these equations of state diminishes. Some might argue that these approximations suffice for engineering needs. They may further contend that, given the computational demands of electrolyte equations of state, incorporating ion-ion association would intensify the computational costs, potentially rendering these models less practical for engineers.

Foremost, numerous studies have repeatedly underscored the occurrence of ion-ion associations in electrolyte solutions [193, 315]. This phenomenon becomes especially significant in multivalent electrolyte solutions, under elevated temperatures, and in solvents with low permittivity. Hence, the debate should transition from whether ion-ion associations occur to whether their effects can be feasibly overlooked.

Furthermore, it is essential to recognize that bypassing ion-ion associations essentially disregards one of the primary factors governing long-range interactions. Relying on modifications to short-range interactions, like adjusting the k_{ij} in mixing rules, cannot be seen as genuine remedies for this omission. Incorporating association sites, akin to those for hydrogen bonding, still represents a short-range solution to a fundamentally long-range problem.

Moreover, when a crucial physical aspect of a system is sidestepped, compensatory adjustments in parameters are often made during parameter estimation to fit certain macroscopic properties. Such compensations might be misleading and can obstruct the accurate extrapolation of data for systems not previously considered during parameter estimation.

In conclusion, the significance of the ion-ion association varies with the system. It is imperative to understand the particular system under study before passing judgment on the relevance of ion-ion association. For example, while ion pairing might be inconsequential for sodium chloride aqueous solutions, falling within an acceptable error margin, it becomes indispensable for systems like magnesium sulfate.

The computational demands of the Binding eSAFT-VR-Mie are undeniably higher than those of the eSAFT-VR-Mie. However, during the development of the BiDH theory, we ensured that the influence of the ion-ion association is captured without significantly increasing computational costs. In particular, when a solution contains only one type of cation and

anion, the theory offers an analytical solution for determining the fraction of free ions. This is crucial, especially given that parameter estimation, which is computationally intensive, is primarily carried out for binary salt-water systems. Having an analytical solution greatly reduces the computational time required to determine the fraction of free ions.

For more complex situations, as detailed in ref. [286], the strength of association is not influenced by the degree of association, differentiating it from its MSA counterparts [20]. This means that efficient methods similar to those used in hydrogen bonding calculations can be applied to determine the fraction of free ions.

In conclusion, while factoring in the ion-ion association does elevate the computational demands of the equations of state, the increase is not substantial enough to deter their practical application in engineering contexts.

9.3.4 Higher Aggregates

Another point of contention regarding the inclusion of ion-ion association centers on the aspects that have been overlooked within this model. Like all models, while this one might be more physically attuned to the system's reality, it still operates under certain assumptions.

Primarily, within the BiDH theory and consequently in this context, ion-ion association is confined to the formation of ion pairs. This implies that the model disregards the potential formation of larger aggregates. In the scope of the systems examined in this research, this simplification is defendable. To our current understanding, there is either no compelling evidence pointing to the formation of larger aggregates in these systems, or the emergence of triplet ions is so limited that it can be effectively neglected. However, there are certain electrolyte solutions, different from those explored here, where ion complexes might indeed form. In these instances, bypassing the potential development of larger aggregates is an indefensible assumption. As a consequence, there is a need to refine and expand the BiDH model to accommodate the formation of these higher-order aggregates.

9.4 Summary and Conclusions

In this study, we developed a new EoS for electrolyte solutions. The non-electrostatic component was derived from the SAFT-VR-Mie framework, while the electrostatic component was based on the BiDH theory, which effectively captures ion-ion interactions and associations. We proposed a unified approach to the study of electrolyte solutions, emphasizing the role of ion-ion associations. Within this model, we analyzed various thermodynamic properties of the solutions, including liquid density, MIAC, osmotic coefficient, and electrical conductivity.

Using our EoS and the unified approach, we predicted the properties of three different binary salt-water systems at 298.15 K. Notably, throughout our calculations of thermodynamic properties and electrical conductivity, we did not adjust any parameters to match experimental data. When comparing our model's predictions with the experimental data, we observed interesting differences. Specifically, the prediction of liquid density was relatively unchanged by the ion-ion associations. However, incorporation of these associations noticeably influenced the values of the MIAC, molar conductivity, and osmotic coefficient, pushing them downward compared to models that ignore ion-ion associations.

After reviewing experimental data related to sodium chloride, sodium sulfate, and magnesium sulfate, we found clear evidence of ion pairing. Interestingly, the degree of association was seen to be in the sequence $NaCl < Na_2SO_4 < MgSO_4$. Our findings highlighted that while the effect of considering ion-ion associations on modifying the predicted properties for sodium chloride aqueous solutions is subtle, the implications for sodium and magnesium sulfate aqueous solutions are significantly more pronounced.

Chapter Message

Incorporation of ion-ion association in the property prediction of electrolyte solutions is important, and indeed, result in better agreement with the experimental data. However, one might be cautious, since it does not solve all the problems.

CHAPTER 10
Conclusions and Future Works

10.1 Summary of Findings

Predicting the thermodynamic, transport, and physical properties of electrolyte solutions, which are crucial in various industrial and natural processes, continues to pose a formidable task for engineers and scientists. Despite considerable recent efforts to address these challenges, the current state of modeling tools remains unsatisfactory.

This Ph.D. thesis, stemming from the ERC-funded project titled "New Paradigm in Electrolyte Thermodynamics," endeavors to advance the comprehension of ion-ion association in electrolyte solutions. Two concurrent lines of research were pursued and subsequently integrated into a cohesive framework. The thesis, structured in four parts, aligns with this research design. The initial part addresses the identification of a knowledge gap. Part II delves into the investigation of electrical conductivity, a transport property of electrolyte solutions. Part III focuses on the thermodynamic modeling of the ion-ion association. In the concluding part, insights gained from preceding parts, along with the developed models, were combined to present a unified framework for predicting the properties of electrolyte solutions, with a specific emphasis on the ion-ion association.

Part II of the thesis involved a comprehensive review of existing research on the electrical conductivity of electrolyte solutions. Prominent models for predicting electrical conductivity in such solutions were identified and systematically and impartially assessed. To account for ion-solvent interactions, an effort was made to incorporate them by employing composition-dependent relative static permittivity and viscosity.

It has been shown that there is a clear need to evolve new models grounded in the DHO theory that accurately account for the size-asymmetry of ions and are versatile enough to be expanded to multi-salt systems. In addition, it has been concluded that the MSA, MSA-Simple, and DHO3 models stand out.

Ultimately, two novel models for the electrical conductivity of electrolyte solutions, assuming complete dissociation, were formulated based on the Ebeling hierarchy of Smoluchowski dynamics and DHO theory. These models were meticulously validated through extensive comparison with the experimental data. The precision of the developed models was thoroughly evaluated, revealing that, when the ion-ion association can be disregarded, these models exhibit predictive accuracy. Furthermore, the prevailing notion in the literature suggesting that electrical conductivity models based on the DHO theory are solely applicable to low-concentration solutions was challenged. It was demonstrated that these models are as accurate as the MSA-based counterparts, essentially resembling twins of the MSA-transport models.

In the third part of the thesis, the thermodynamic perspective on the ion-ion association, particularly ion pairing, was explored. A comprehensive review of the literature on the thermodynamic modeling of ion pairing was conducted. Various equations of state for charged hard sphere fluids were identified and systematically compared.

In this comparative study, different models for associative electrolyte solutions were evaluated and compared with numerical solutions of the PB equation, MC simulations, and experimental data. Notably, despite differences in theoretical foundations, all models demonstrated the capability to estimate the MIAC of electrolyte solutions when certain parameters were adjusted to align with the experimental data. The fraction of unbound ions exhibited

a significant variation, even though the predicted MIAC curves overlapped. The validation of the fraction of free ions, crucially emphasizing electrical conductivity, revealed that the FLGG model provided a more accurate depiction of the system's physics than the others.

Additionally, a novel EoS for these systems, named BiDH, was developed on the basis of the DH, Kirkwood, Wertheim, and RCA theories. This EoS was thoroughly validated for future application by comparing its predictions for the MIAC, the osmotic coefficient, and the IIAC with MC simulations documented in the literature.

Conclusively, the developed EoS exhibited promising predictive capabilities for charged hard sphere fluids with ion-ion association. Comparisons with MC simulations not only validated the model but also showcased its accuracy and applicability across diverse electrolyte systems.

In the concluding section of the thesis, Part IV, an in-depth examination of ion-ion association was conducted within a unified framework. Initially, the solvent was treated as a continuum medium, and a combination of the BiDH EoS and electrical conductivity models was employed to estimate the electrical conductivity of associative electrolyte solutions.

Successful incorporation of ion pairing into the prediction of electrical conductivity was demonstrated across three crucial systems: 2:2 aqueous sulfates, NaCl-water-1,4-dioxane, and ionic liquid-co-solvent systems. Consistently, the integration of the BiDH EoS and the electrical conductivity model resulted in notable adjustments to the predicted electrical conductivity across these diverse systems.

The model's capacity to accurately predict the electrical conductivity of electrolytes forming ion complexes was rigorously assessed. Results indicated a close alignment between model predictions, accounting for ion complex formation, and experimental data for such systems, highlighting the reliability and robustness of the model, even in more intricate scenarios.

Subsequently, a new electrolyte EoS was formulated, leveraging the SAFT-VR-Mie EoS for the non-electrostatic component and the BiDH EoS for the electrostatic part. A unified framework was introduced for the validation and development of models when considering ion pairing. The method was applied to predict various thermodynamic properties of associative aqueous electrolyte solutions, including the liquid density, MIAC, osmotic coefficient, and electrical conductivity.

The analysis revealed that the prediction of the liquid density remained relatively unaffected by ion-ion associations. However, the inclusion of these associations notably influenced the values of the MIAC, molar conductivity, and osmotic coefficient, causing them to decrease in comparison to models neglecting the ion-ion associations.

On investigation of experimental data related to sodium chloride, sodium sulfate, and magnesium sulfate, clear evidence of ion pairing emerged. Interestingly, the degree of association followed the sequence $NaCl < Na_2SO_4 < MgSO_4$. This observation underscored that, while the impact of considering ion-ion associations on modifying predicted properties for sodium chloride aqueous solutions is subtle, the implications for sodium and magnesium sulfate aqueous solutions are markedly more pronounced.

10.2 Impact of the Research

In this Ph.D. thesis, I, along with other colleagues in the ERC project, have endeavored to expand the boundaries of knowledge concerning the thermodynamics of electrolyte solutions. Specifically, I conducted various types of research to shed light on the concept of ion-ion association. Although I cannot assess the impact and quality of the research, I can list the impacts we attempted to make on the scientific community.

We have devoted a considerable amount of time to a subject that we deemed important, but which the community considered a dead end. Initially, electrical conductivity was not a popular topic, yet it has been demonstrated to be significant due to its various applications

in batteries and energy storage, as well as its role in thermodynamic modeling of electrolyte solutions. After three years of research, I can confidently say that our published works have made a positive contribution to the understanding of the chemical engineering community regarding electrical conductivity. Furthermore, we have developed two new models for electrical conductivity that the community can benefit from. Notably, the mixed electrolyte model eliminates the need for engineering averaging to predict the electrical conductivity of multi-component electrolyte solutions.

In the area of thermodynamic modeling of ion-ion association, which has been studied for more than a hundred years, we looked back at "old works" that are familiar to physicists but not so much to chemical engineers. Our investigation included a comparative study of these theories, identifying and addressing gaps in knowledge concerning equations of state based on the DH theory. This led to the development of the BiDH model, which, in my opinion, fills the void and ensures that the chemical engineering community will no longer encounter the challenge of lacking robust theories for ion-ion association.

The primary contribution of this Ph.D. thesis to the scientific community lies in the introduction of a unified framework for studying ion-ion association. With the development of this framework, we provide the community with a valuable guide for model development when considering the ion-ion association in the physics of the system.

10.3 Future Works

Similar to the approach adopted in various engineering disciplines, our research delved into theory and model development, necessitating the formulation of simplifying assumptions. As is customary in the intricate landscape of scientific inquiry, these assumptions served as a pragmatic framework to facilitate exploration and analysis.

Taking into account the theories we have discussed, I will now outline the possible extensions of them, providing a guide for further investigation within the scope of our discoveries. Additionally, I will point out potential areas of focus for future studies, recognizing the ever-changing nature of scientific exploration and the ongoing pursuit of more profound understanding and comprehensive information.

Theory Development:

- Generalizing the model developed for the electrical conductivity of electrolyte solutions to other transport properties through Onsager transport coefficients.
- Developing robust and reliable models for the prediction of the ionic conductivity at infinite dilution.
- Extension of the BiDH model to account for formation of ion aggregates.
- Integration of ion-ion and ion-solvent associations in the theory development.
- Prediction of the relative static permittivity of associative electrolyte solutions.

Model Development:

- Performing a parameter estimation for the Binding eSAFT-VR-Mie.
- Implementing the unified framework in other equations of state.
- Using the developed framework in non-aqueous and mixed solvent electrolyte solutions.
- Using the developed framework in ionic liquid and ionic liquid-co-solvent systems.
- Investigating the impact of the ion-ion association on liquid-liquid equilibrium.

Bibliography

[1] J.-C. De Hemptinne, G. M. Kontogeorgis, R. Dohrn, I. G. Economou, A. Ten Kate, S. Kuitunen, L. Fele Zilnik, M. G. De Angelis, and V. Vesovic, "A view on the future of applied thermodynamics," *Industrial & Engineering Chemistry Research*, vol. 61, no. 39, pp. 14664–14680, 2022.

[2] S. Gupta, J. R. Elliott, A. Anderko, J. Crosthwaite, W. G. Chapman, and C. T. Lira, "Current Practices and Continuing Needs in Thermophysical Properties for the Chemical Industry," *Industrial & Engineering Chemistry Research*, vol. 62, no. 8, pp. 3394–3427, 2023.

[3] G. M. Kontogeorgis, R. Dohrn, I. G. Economou, J.-C. de Hemptinne, A. Ten Kate, S. Kuitunen, M. Mooijer, L. F. Zilnik, and V. Vesovic, "Industrial requirements for thermodynamic and transport properties: 2020," *Industrial & engineering chemistry research*, vol. 60, no. 13, pp. 4987–5013, 2021.

[4] P. Debye and E. Hückel, "Zur Theorie Der Elektrolyte. I. Gefrierpunktserniedrigung Und Verwandte Erscheinungen. Phys," *Physikalische Zeitschrift*, vol. 24, pp. 185–206, 1923.

[5] L. Blum, "Mean spherical model for asymmetric electrolytes I. Method of solution," *Molecular Physics*, vol. 30, no. 5, pp. 1529–1535, 1975.

[6] L. Blum and J. S. Høye, "Mean spherical model for asymmetric electrolytes. 2. Thermodynamic properties and the pair correlation function," *Journal of Physical Chemistry*, vol. 81, no. 13, pp. 1311–1316, 1977.

[7] K. S. Pitzer and G. Mayorga, "Thermodynamics of electrolytes. II. Activity and osmotic coefficients for strong electrolytes with one or both ions univalent," *The Journal of Physical Chemistry*, vol. 77, no. 19, pp. 2300–2308, 1973.

[8] J. Mollerup and M. L. Michelsen, *Thermodynamic Models: Fundamentals & Computational Aspects*. Tie-Line Publications, 2004.

[9] G. M. Kontogeorgis, B. Maribo-Mogensen, and K. Thomsen, "The Debye-Hückel theory and its importance in modeling electrolyte solutions," *Fluid Phase Equilibria*, vol. 462, pp. 130–152, 2018.

[10] A. H. Harvey, T. W. Copeman, and J. M. Prausnitz, "Explicit approximations to the mean spherical approximation for electrolyte systems with unequal ion sizes," *The Journal of Physical Chemistry*, vol. 92, no. 22, pp. 6432–6436, 1988.

[11] L. Blum and d. Wei, "Analytical solution of the mean spherical approximation for an arbitrary mixture of ions in a dipolar solvent," *The Journal of chemical physics*, vol. 87, no. 1, pp. 555–565, 1987.

[12] D. Wei and L. Blum, "The mean spherical approximation for an arbitrary mixture of ions in a dipolar solvent: Approximate solution, pair correlation functions, and thermodynamics," *The Journal of chemical physics*, vol. 87, no. 5, pp. 2999–3007, 1987.

[13] J.-P. Simonin, "On the solution of the mean-spherical approximation (MSA) for ions in a dipolar solvent in the general case," *AIP Advances*, vol. 10, no. 9, 2020.

[14] L. Blum, "Solution of the mean spherical approximation for hard ions and dipoles of arbitrary size," *Journal of Statistical Physics*, vol. 18, no. 5, pp. 451–474, 1978.

[15] L. Blum, "Solution of a model for the solventelectrolyte interactions in the mean spherical approximation," *The Journal of Chemical Physics*, vol. 61, no. 5, pp. 2129–2133, 1974.

[16] L. Blum, F. Vericat, and W. R. Fawcett, "On the mean spherical approximation for hard ions and dipoles," *The Journal of chemical physics*, vol. 96, no. 4, pp. 3039–3044, 1992.

[17] Z.-P. Liu, Y.-G. Li, and J.-F. Lu, "Low-Density Expansion of the Solution of Mean Spherical Approximation for Ion Dipole Mixtures," *The Journal of Physical Chemistry B*, vol. 106, no. 20, pp. 5266–5274, 2002.

[18] S. Herzog, J. Gross, and W. Arlt, "Equation of state for aqueous electrolyte systems based on the semirestricted non-primitive mean spherical approximation," *Fluid phase equilibria*, vol. 297, no. 1, pp. 23–33, 2010.

[19] L. Blum and O. Bernard, "The general solution of the binding mean spherical approximation for pairing ions," *Journal of Statistical Physics*, vol. 79, no. 3-4, pp. 569–583, 1995.

[20] O. Bernard and L. Blum, "Binding mean spherical approximation for pairing ions: An exponential approximation and thermodynamics," *Journal of Chemical Physics*, vol. 104, no. 12, pp. 4746–4754, 1996.

[21] Y. V. Kalyuzhnyi and M. F. Holovko, "An analytical study of the effects of association in a 2-2 electrolyte solution I. Associative mean spherical approximation," *Molecular Physics*, vol. 80, no. 5, pp. 1165–1176, 1993.

[22] Y. V. Kalyuzhnyi, I. A. Protsykevytch, and M. F. Holovko, "Solution of the associative Percus-Yevick approximation for the n-component mixture of dimerizing hard spheres," *Chemical Physics Letters*, vol. 215, no. 1-3, pp. 1–4, 1993.

[23] Y. V. Kalyuzhnyi, V. Vlachy, and P. T. Cummings, "Modeling solution of flexible polyelectrolyte in explicit solvent," *Chemical Physics Letters*, vol. 438, no. 4-6, pp. 238–243, 2007.

[24] M. F. Holovko and Y. V. Kalyuzhnyi, "On the effects of association in the statistical theory of ionic systems. Analytic solution of the PY-MSA version of the wertheim theory," *Molecular Physics*, vol. 73, no. 5, pp. 1145–1157, 1991.

[25] Y. V. Kalyuzhnyi, M. F. Holovko, and V. Vlachy, "Highly asymmetric electrolytes in the associative mean-spherical approximation," *Journal of Statistical Physics*, vol. 100, no. 1-2, pp. 243–265, 2000.

[26] Y. V. Kalyuzhnyi, M. F. Holovko, and A. D. Haymet, "Integral equation theory for associating liquids: Weakly associating 2-2 electrolytes," *The Journal of Chemical Physics*, vol. 95, no. 12, pp. 9151–9164, 1991.

[27] Y. V. Kalyuzhnyi, G. Stell, M. L. Llano-Restrepo, W. G. Chapman, and M. F. Holovko, "Primitive models of chemical association. I. Theory and simulation for dimerization," *The Journal of Chemical Physics*, vol. 101, no. 9, pp. 7939–7952, 1994.

[28] Y. V. Kalyuzhnyi and M. F. Holovko, "Thermodynamics of the associative mean spherical approximation for the fluid of dimerizing particles," *Journal of Chemical Physics*, vol. 108, no. 9, pp. 3709–3715, 1998.

[29] Y. V. Kalyuzhnyi, V. Vlachy, M. F. Holovko, and G. Stell, "Multidensity integral equation theory for highly asymmetric electrolyte solutions," *The Journal of Chemical Physics*, vol. 102, no. 14, pp. 5770–5780, 1995.

[30] C. Chen and Y. Song, "Generalized electrolyteNRTL model for mixedsolvent electrolyte systems," *AIChE Journal*, vol. 50, no. 8, pp. 1928–1941, 2004.

[31] B. Mock, L. B. Evans, and C. Chen, "Thermodynamic representation of phase equilibria of mixedsolvent electrolyte systems," *AIChE journal*, vol. 32, no. 10, pp. 1655–1664, 1986.

[32] G. H. van Bochove, G. J. P. Krooshof, and T. W. de Loos, "Modelling of liquidliquid equilibria of mixed solvent electrolyte systems using the extended electrolyte NRTL," *Fluid Phase Equilibria*, vol. 171, no. 1-2, pp. 45–58, 2000.

[33] K. Thomsen, "Modeling electrolyte solutions with the extended universal quasichemical (UNIQUAC) model," *Pure and applied chemistry*, vol. 77, no. 3, pp. 531–542, 2005.

[34] M. C. Iliuta, K. Thomsen, and P. Rasmussen, "Extended UNIQUAC model for correlation and prediction of vapourliquidsolid equilibria in aqueous salt systems containing non-electrolytes. Part A. Methanolwatersalt systems," *Chemical Engineering Science*, vol. 55, no. 14, pp. 2673–2686, 2000.

[35] E. Djamali, A. T. Kan, and M. B. Tomson, "A priori prediction of thermodynamic properties of electrolytes in mixed aqueousorganic solvents to extreme temperatures," *The Journal of Physical Chemistry B*, vol. 116, no. 30, pp. 9033–9042, 2012.

[36] K. Thomsen, M. C. Iliuta, and P. Rasmussen, "Extended UNIQUAC model for correlation and prediction of vaporliquidliquidsolid equilibria in aqueous salt systems containing non-electrolytes. Part B. Alcohol (ethanol, propanols, butanols)watersalt systems," *Chemical engineering science*, vol. 59, no. 17, pp. 3631–3647, 2004.

[37] T. Gerlach, S. Müller, and I. Smirnova, "Development of a COSMORS based model for the calculation of phase equilibria in electrolyte systems," *AIChE Journal*, vol. 64, no. 1, pp. 272–285, 2018.

[38] L. C. Kroger, S. Muller, I. Smirnova, and K. Leonhard, "Prediction of solvation free energies of ionic solutes in neutral solvents," *The Journal of Physical Chemistry A*, vol. 124, no. 20, pp. 4171–4181, 2020.

[39] G. M. Kontogeorgis, A. Schlaikjer, M. D. Olsen, B. Maribo-Mogensen, K. Thomsen, N. von Solms, and X. Liang, "A review of electrolyte equations of state with emphasis on those based on cubic and cubic-plus-association (CPA) models," *International Journal of Thermophysics*, vol. 43, no. 4, p. 54, 2022.

[40] G. M. Kontogeorgis, E. C. Voutsas, I. V. Yakoumis, and D. P. Tassios, "An equation of state for associating fluids," *Industrial and Engineering Chemistry Research*, vol. 35, no. 11, pp. 4310–4318, 1996.

[41] B. Maribo-Mogensen, *Development of an Electrolyte CPA Equation of state for Applications in the Petroleum and Chemical Industries*. PhD thesis, Technical University of Denmark, Kgs. Lyngby, 2014.

[42] B. Maribo-Mogensen, K. Thomsen, and G. M. Kontogeorgis, "An electrolyte CPA equation of state for mixed solvent electrolytes," *AIChE Journal*, vol. 61, no. 9, pp. 2933–2950, 2015.

[43] J. Wu and J. M. Prausnitz, "Phase equilibria for systems containing hydrocarbons, water, and salt: An extended Peng Robinson equation of state," *Industrial & Engineering Chemistry Research*, vol. 37, no. 5, pp. 1634–1643, 1998.

[44] R. Inchekel, J.-C. de Hemptinne, and W. Fürst, "The simultaneous representation of dielectric constant, volume and activity coefficients using an electrolyte equation of state," *Fluid Phase Equilibria*, vol. 271, no. 1-2, pp. 19–27, 2008.

[45] X. Courtial, N. Ferrando, J.-C. de Hemptinne, and P. Mougin, "Electrolyte CPA equation of state for very high temperature and pressure reservoir and basin applications," *Geochimica et Cosmochimica Acta*, vol. 142, pp. 1–14, 2014.

[46] S. Chabab, P. Théveneau, J. Corvisier, C. Coquelet, P. Paricaud, C. Houriez, and E. El Ahmar, "Thermodynamic study of the CO2H2ONaCl system: Measurements of CO2 solubility and modeling of phase equilibria using Soreide and Whitson, electrolyte CPA and SIT models," *International Journal of Greenhouse Gas Control*, vol. 91, p. 102825, 2019.

[47] L. Sun, G. M. Kontogeorgis, N. von Solms, and X. Liang, "Modeling of gas solubility using the electrolyte cubic plus association equation of state," *Industrial & Engineering Chemistry Research*, vol. 58, no. 37, pp. 17555–17567, 2019.

[48] L. Sun, X. Liang, N. Von Solms, and G. M. Kontogeorgis, "Modeling Tetra-n-butyl ammonium halides aqueous solutions with the electrolyte cubic plus association equation of state," *Fluid Phase Equilibria*, vol. 486, pp. 37–47, 2019.

[49] L. Sun, X. Liang, N. von Solms, and G. M. Kontogeorgis, "Solubility modeling of air in aqueous electrolyte solutions with the e-CPA equation of state," *Industrial & Engineering Chemistry Research*, vol. 59, no. 41, pp. 18693–18704, 2020.

[50] M. D. Olsen, G. M. Kontogeorgis, J.-C. de Hemptinne, X. Liang, and N. von Solms, "Comparisons of equation of state models for electrolytes: e-CPA and e-PPC-SAFT," *Fluid Phase Equilibria*, vol. 571, p. 113804, 2023.

[51] M. D. Olsen, G. M. Kontogeorgis, X. Liang, and N. von Solms, "Investigation of the performance of e-CPA for a wide range of properties for aqueous NaCl solutions," *Fluid Phase Equilibria*, vol. 548, p. 113167, 2021.

[52] A. Schlaikjer, K. Thomsen, and G. M. Kontogeorgis, "Simultaneous description of activity coefficients and solubility with eCPA," *Industrial & Engineering Chemistry Research*, vol. 56, no. 4, pp. 1074–1089, 2017.

[53] A. Schlaikjer, K. Thomsen, and G. M. Kontogeorgis, "eCPA: An ion-specific approach to parametrization," *Fluid Phase Equilibria*, vol. 470, pp. 176–187, 2018.

[54] J. Gross and G. Sadowski, "Perturbed-chain SAFT: An equation of state based on a perturbation theory for chain molecules," *Industrial and Engineering Chemistry Research*, vol. 40, no. 4, pp. 1244–1260, 2001.

[55] J. Gross and G. Sadowski, "Application of the perturbed-chain SAFT equation of state to associating systems," *Industrial & engineering chemistry research*, vol. 41, no. 22, pp. 5510–5515, 2002.

[56] C. Held, L. F. Cameretti, and G. Sadowski, "Modeling aqueous electrolyte solutions: Part 1. Fully dissociated electrolytes," *Fluid Phase Equilibria*, vol. 270, no. 1-2, pp. 87–96, 2008.

[57] C. Held and G. Sadowski, "Modeling aqueous electrolyte solutions. Part 2. Weak electrolytes," *Fluid Phase Equilibria*, vol. 279, no. 2, pp. 141–148, 2009.

[58] L. F. Cameretti, G. Sadowski, and J. M. Mollerup, "Modeling of aqueous electrolyte solutions with perturbed-chain statistical associated fluid theory," *Industrial & engineering chemistry research*, vol. 44, no. 9, pp. 3355–3362, 2005.

[59] C. Held, T. Reschke, S. Mohammad, A. Luza, and G. Sadowski, "ePC-SAFT revised," *Chemical Engineering Research and Design*, vol. 92, no. 12, pp. 2884–2897, 2014.

[60] M. Bülow, X. Ji, and C. Held, "Incorporating a concentration-dependent dielectric constant into ePC-SAFT. An application to binary mixtures containing ionic liquids," *Fluid Phase Equilibria*, vol. 492, pp. 26–33, 2019.

[61] M. Bülow, M. Ascani, and C. Held, "ePC-SAFT advanced-Part I: Physical meaning of including a concentration-dependent dielectric constant in the born term and in the Debye-Hückel theory," *Fluid Phase Equilibria*, vol. 535, p. 112967, 2021.

[62] M. Bülow, M. Ascani, and C. Held, "ePC-SAFT advancedPart II: Application to salt solubility in ionic and organic solvents and the impact of ion pairing," *Fluid Phase Equilibria*, vol. 537, p. 112989, 2021.

[63] M. Ascani and C. Held, "Prediction of saltingout in liquidliquid twophase systems with ePCSAFT: Effect of the Born term and of a concentrationdependent dielectric constant," *Zeitschrift für anorganische und allgemeine Chemie*, vol. 647, no. 12, pp. 1305–1314, 2021.

[64] A. Gil-Villegas, A. Galindo, P. J. Whitehead, S. J. Mills, G. Jackson, and A. N. Burgess, "Statistical associating fluid theory for chain molecules with attractive potentials of variable range," *The Journal of chemical physics*, vol. 106, no. 10, pp. 4168–4186, 1997.

[65] A. G. L. A. D. Alejandro and G.-V. G. JACKSON, "The thermodynamics of mixtures and the corresponding mixing rules in the SAFT-VR approach for potentials of variable range," *Molecular Physics*, vol. 93, no. 2, pp. 241–252, 1998.

[66] A. Galindo, A. Gil-Villegas, G. Jackson, and A. N. Burgess, "SAFT-VRE: phase behavior of electrolyte solutions with the statistical associating fluid theory for potentials of variable range," *The Journal of Physical Chemistry B*, vol. 103, no. 46, pp. 10272–10281, 1999.

[67] J. M. A. Schreckenberg, S. Dufal, A. J. Haslam, C. S. Adjiman, G. Jackson, and A. Galindo, "Modelling of the thermodynamic and solvation properties of electrolyte solutions with the statistical associating fluid theory for potentials of variable range," *Molecular Physics*, vol. 112, no. 17, pp. 2339–2364, 2014.

[68] T. Lafitte, A. Apostolakou, C. Avendaño, A. Galindo, C. S. Adjiman, E. A. Müller, and G. Jackson, "Accurate statistical associating fluid theory for chain molecules formed from Mie segments," *Journal of Chemical Physics*, vol. 139, no. 15, p. 154504, 2013.

[69] D. K. Eriksen, G. Lazarou, A. Galindo, G. Jackson, C. S. Adjiman, and A. J. Haslam, "Development of intermolecular potential models for electrolyte solutions using an electrolyte SAFT-VR Mie equation of state," *Molecular Physics*, vol. 114, pp. 2724–2749, 9 2016.

[70] M. A. Selam, I. G. Economou, and M. Castier, "A thermodynamic model for strong aqueous electrolytes based on the eSAFT-VR Mie equation of state," *Fluid Phase Equilibria*, vol. 464, pp. 47–63, 2018.

[71] N. Novak, G. M. Kontogeorgis, M. Castier, and I. G. Economou, "Mixed Solvent Electrolyte Solutions: A Review and Calculations with the eSAFT-VR Mie Equation of State," *Industrial & Engineering Chemistry Research*, vol. 62, no. 34, pp. 13646–13665, 2023.

[72] N. Novak, G. M. Kontogeorgis, M. Castier, and I. G. Economou, "Modeling of gas solubility in aqueous electrolyte solutions with the eSAFT-VR Mie equation of state," *Industrial & Engineering Chemistry Research*, vol. 60, no. 42, pp. 15327–15342, 2021.

[73] N. Novak, G. M. Kontogeorgis, M. Castier, and I. G. Economou, "Extension of the eSAFT-VR Mie equation of state from aqueous to non-aqueous electrolyte solutions," *Fluid Phase Equilibria*, vol. 565, 2023.

[74] N. Novak, G. M. Kontogeorgis, M. Castier, and I. G. Economou, "Theoretical considerations on single and mixed solvent electrolyte solutions," *Fluid Phase Equilibria*, p. 113924, 2023.

[75] P. J. Walker, X. Liang, and G. M. Kontogeorgis, "Importance of the Relative Static Permittivity in electrolyte SAFT-VR Mie Equations of State," *Fluid Phase Equilibria*, vol. 551, p. 113256, 2022.

[76] J. Rozmus, J.-C. de Hemptinne, A. Galindo, S. Dufal, and P. Mougin, "Modeling of strong electrolytes with ePPC-SAFT up to high temperatures," *Industrial & Engineering Chemistry Research*, vol. 52, no. 29, pp. 9979–9994, 2013.

[77] S. Ahmed, N. Ferrando, J.-C. De Hemptinne, J.-P. Simonin, O. Bernard, and O. Baudouin, "Modeling of mixed-solvent electrolyte systems," *Fluid Phase Equilibria*, vol. 459, pp. 138–157, 2018.

[78] M. D. Olsen, *Capabilities and Limitations of the Classical Primitive Electrolyte Equation of State Approach.* PhD thesis, Technical University of Denmark, Kgs. Lyngby, 2022.

[79] B. Maribo-Mogensen, G. M. Kontogeorgis, and K. Thomsen, "Comparison of the DebyeHückel and the Mean Spherical Approximation Theories for Electrolyte Solutions," *Industrial & Engineering Chemistry Research*, vol. 51, pp. 5353–5363, 4 2012.

[80] Y. Marcus and G. Hefter, "Ion pairing," *Chemical Reviews*, vol. 106, no. 11, pp. 4585–4621, 2006.

[81] N. F. Van Der Vegt, K. Haldrup, S. Roke, J. Zheng, M. Lund, and H. J. Bakker, "Water-Mediated Ion Pairing: Occurrence and Relevance," 2016.

[82] M. Kohns, G. Lazarou, S. Kournopoulos, E. Forte, F. A. Perdomo, G. Jackson, C. S. Adjiman, and A. Galindo, "Predictive models for the phase behaviour and solution properties of weak electrolytes: nitric, sulphuric, and carbonic acids," *Physical Chemistry Chemical Physics*, vol. 22, no. 27, pp. 15248–15269, 2020.

[83] L. Onsager and R. M. Fuoss, "Irreversible processes in electrolytes. Diffusion, conductance, and viscous flow in arbitrary mixtures of strong electrolytes," *Journal of Physical Chemistry*, vol. 36, no. 11, pp. 2689–2778, 1932.

[84] J. M. G. Barthel, H. Krienke, and W. Kunz, *Physical chemistry of electrolyte solutions: modern aspects*, vol. 5. Springer Science & Business Media, 1998.

[85] K. J. Laidler and J. H. Meiser, *Physical chemistry*. Boston, MA: Houghton Mifflin (Academic), 3 ed., 1999.

[86] P. Debye and E. Hückel, "Zur Theorie der Elektrolyte. II. Das Grenzgesetz für die elektrische Leitfähigkeit," *Physikalische Zeitschrift*, vol. 24, pp. 305–325, 1923.

[87] L. Onsager, "Zur Theorie der Elektrolyte. I," *Physikalische Zeitschrift*, vol. 27, p. 388, 1926.

[88] L. Onsager, "Zur Theorie der Elektrolyte. II," *Physikalische Zeitschrift*, vol. 28, p. 277, 1927.

[89] J. O. Bockris and A. K. N. Reddy, *Modern Electrochemistry: An Introduction to an Interdisciplinary Area*, vol. 1. New York: Springer, 1973.

[90] R. A. Robinson and R. H. Stokes, *Electrolyte solutions*. Courier Corporation, 2002.

[91] H. Hemmer, H. Holden, and K. S., *The collected works of lars Onsegar*, vol. 17. World Scientific, 1996.

[92] E. Pitts, "An extension of the theory of the conductivity and viscosity of electrolyte solutions," *Proceedings of the Royal Society of London. Series A. Mathematical and Physical Sciences*, vol. 217, no. 1128, pp. 43–70, 1953.

[93] H. Falkenhagen and E. L. Vernon, "LXII. The viscosity of strong electrolyte solutions according to electrostatic theory," *The London, Edinburgh, and Dublin Philosophical Magazine and Journal of Science*, vol. 14, pp. 537–565, 10 1932.

[94] R. M. Fuoss and L. Onsager, "Conductance of unassociated electrolytes," *Journal of Physical Chemistry*, vol. 61, no. 5, pp. 668–682, 1957.

[95] R. M. Fuoss and L. Onsager, "The conductance of symmetrical ELECTROLYTES. I. Potential of total force," *Journal of Physical Chemistry*, vol. 66, no. 9, pp. 1722–1726, 1962.

[96] R. M. Fuoss and L. Onsager, "The conductance of symmetrical electrolytes. II. The relaxation field," *Journal of Physical Chemistry*, vol. 67, no. 3, pp. 621–628, 1963.

[97] R. M. Fuoss and L. Onsager, "The conductance of symmetrical electrolytes.1a IV. Hydrodynamic and osmotic terms in the relaxation field," *Journal of Physical Chemistry*, vol. 68, no. 1, pp. 1–8, 1964.

[98] R. M. Fuoss, L. Onsager, and J. F. Skinner, "The conductance of symmetrical electrolytes. V. The conductance equation," *Journal of Physical Chemistry*, vol. 69, no. 8, pp. 2581–2594, 1965.

[99] R. M. Fuoss and L. Onsager, "The conductance of symmetrical electrolytes. III. Electrophoresis," *Journal of Physical Chemistry*, vol. 67, no. 3, pp. 628–632, 1963.

[100] R. M. Fuoss, "Review of the theory of electrolytic conductance," 1978.

[101] H. Falkenhagen, M. Leist, and G. Kelbg, "Zur Theorie der Leitfähigkeit starker nicht assoziierender Elektrolyte bei höheren Konzentrationen," *Annalen der Physik*, vol. 446, no. 1, pp. 51–59, 1952.

[102] H. Falkenhagen and G. Kelbg, "Zur quantitativen Theorie des WienEffektes in konzentrierteren elektrolytischen Lösungen," *Zeitschrift für Elektrochemie, Berichte der Bunsengesellschaft für physikalische Chemie*, vol. 58, no. 9, pp. 653–655, 1954.

[103] J. Quint and A. Viallard, "The electrophoretic effect for the case of electrolyte mixtures," *Journal of Solution Chemistry*, vol. 7, no. 7, pp. 525–531, 1978.

[104] J. Quint and A. Viallard, "The electrophoretic effect for the case of electrolyte mixtures," *Journal of Solution Chemistry*, vol. 7, no. 7, pp. 525–531, 1978.

[105] J. Quint and A. Viallard, "Electrical conductance of electrolyte mixtures of any type," *Journal of Solution Chemistry*, vol. 7, no. 7, pp. 533–548, 1978.

[106] W. H. Lee and R. J. Wheaton, "Conductance of symmetrical, unsymmetrical and mixed electrolytes. Part 1. - Relaxation terms," *Journal of the Chemical Society, Faraday Transactions 2: Molecular and Chemical Physics*, vol. 74, pp. 743–766, 1978.

[107] W. H. Lee and R. J. Wheaton, "Conductance of symmetrical, unsymmetrical and mixed electrolytes. Part 2. - Hydrodynamic terms and complete conductance equation," *Journal of the Chemical Society, Faraday Transactions 2: Molecular and Chemical Physics*, vol. 74, pp. 1456–1482, 1978.

[108] W. H. Lee and R. J. Wheaton, "Conductance of symmetrical, unsymmetrical and mixed electrolytes. Part 3. - Examination of new model and analysis of data for symmetrical electrolytes," *Journal of the Chemical Society, Faraday Transactions 2: Molecular and Chemical Physics*, vol. 75, pp. 1128–1145, 1979.

[109] L. Onsager and S. K. Kim, "The Relaxation Effects in Mixed Strong Electrolytes," *The Journal of Physical Chemistry*, vol. 61, pp. 215–229, 2 1957.

[110] W. Ebeling, R. Feistel, G. Kelbg, and R. Sandig, "Generalizations of Onsagers Semiphenomenological Theory of Electrolytic Conductance," *Journal of Non-Equilibrium Thermodynamics*, vol. 3, no. 1, pp. 11–28, 1978.

[111] O. Bernard, W. Kunz, P. Turq, and L. Blum, "Conductance in electrolyte solutions using the mean spherical approximation," *Journal of Physical Chemistry*, vol. 96, no. 9, pp. 3833–3840, 1992.

[112] P. Turq, L. Blum, O. Bernard, and W. Kunz, "Conductance in associated electrolytes using the mean spherical approximation," *Journal of Physical Chemistry*, vol. 99, no. 2, pp. 822–827, 1995.

[113] A. Chhih, P. Turq, O. Bernard, J. M. G. Barthel, and L. Blum, "Transport coefficients and apparent charges of concentrated electrolyte solutions - Equations for practical use," *Berichte der Bunsengesellschaft für physikalische Chemie*, vol. 98, no. 12, pp. 1516–1525, 1994.

[114] J.-F. Dufrêche, O. Bernard, and P. Turq, "Transport equations for concentrated electrolyte solutions: Reference frame, mutual diffusion," *The Journal of Chemical Physics*, vol. 116, pp. 2085–2097, 2 2002.

[115] J. F. Dufrêche, O. Bernard, S. Durand-Vidal, and P. Turq, "Analytical theories of transport in concentrated electrolyte solutions from the MSA," *Journal of Physical Chemistry B*, vol. 109, no. 20, pp. 9873–9884, 2005.

[116] S. Van Damme and J. Deconinck, "Relaxation Effect on the Onsager Coefficients of Mixed Strong Electrolytes in the Mean Spherical Approximation," *The Journal of Physical Chemistry B*, vol. 111, no. 19, pp. 5308–5315, 2007.

[117] G. M. Roger, S. Durand-Vidal, O. Bernard, and P. Turq, "Electrical conductivity of mixed electrolytes: Modeling within the mean spherical approximation," *Journal of Physical Chemistry B*, vol. 113, no. 25, pp. 8670–8674, 2009.

[118] D. Fraenkel, "An improved theory of the electric conductance of ionic solutions based on the concept of the ion-atmosphere's smaller-ion shell," *Physical Chemistry Chemical Physics*, vol. 20, no. 47, pp. 29896–29909, 2018.

[119] Y. Avni, D. Andelman, and H. Orland, "Conductance of concentrated electrolytes: Multivalency and the Wien effect," *The Journal of Chemical Physics*, vol. 157, p. 154502, 10 2022.

[120] S. Naseri Boroujeni, X. Liang, B. Maribo-Mogensen, and G. M. Kontogeorgis, "Comparison of Models for the Prediction of the Electrical Conductivity of Electrolyte Solutions," *Industrial & Engineering Chemistry Research*, vol. 61, pp. 3168–3185, 2 2022.

[121] O. Bernard, M. Jardat, B. Rotenberg, and P. Illien, "On analytical theories for conductivity and self-diffusion in concentrated electrolytes," *arXiv preprint arXiv:2306.16737*, 2023.

[122] J. Keizer, *Statistical thermodynamics of nonequilibrium processes*. New York: Springer Science & Business Media, 2012.

[123] A. Cabada, "Greens Functions in the Theory of Ordinary Differential Equations," in *Greens Functions in the Theory of Ordinary Differential Equations*, pp. 1–139, New York Heidelberg Dordrecht London: Springer, 2014.

[124] S. Naseri Boroujeni, B. Maribo-Mogensen, X. Liang, and G. M. Kontogeorgis, "On the estimation of equivalent conductivity of electrolyte solutions: The effect of relative static permittivity and viscosity," *Fluid Phase Equilibria*, vol. 567, p. 113698, 4 2023.

[125] L. Onsager, "Report on a revision of the conductivity theory," *Transactions of the Faraday Society*, vol. 23, pp. 341–349, 1927.

[126] L. Blum, "Simple method for the computation of thermodynamic properties of electrolytes in the mean spherical approximation," *Journal of Physical Chemistry*, vol. 92, no. 10, pp. 2969–2970, 1988.

[127] A. Anderko and M. M. Lencka, "Computation of Electrical Conductivity of Multicomponent Aqueous Systems in Wide Concentration and Temperature Ranges," *Industrial and Engineering Chemistry Research*, vol. 36, no. 5, pp. 1932–1943, 1997.

[128] R. M. Fuoss, "Conductance-concentration function for associated symmetrical electrolytes," *The Journal of Physical Chemistry*, vol. 79, no. 5, pp. 525–540, 1975.

[129] R. Holze, *Physical Chemistry 9B2 (Electrochemistry) : Electrical Conductivities and Equilibria of Electrochemical Systems - Part 2: Deep Eutectic Solvents and Electrolyte Solutions*. Berlin, Heidelberg: Springer Berlin Heidelberg, 1 ed., 2016.

[130] M. Tomšič, M. Bešter-Rogač, A. Jamnik, R. Neueder, and J. Barthel, "Conductivity of magnesium sulfate in water from 5 to 35°c and from infinite dilution to saturation," *Journal of Solution Chemistry*, vol. 31, no. 1, pp. 19–31, 2002.

[131] M. Postler, "Conductance of concentrated aqueous solutions of electrolytes. I. Strong uni-univalent electrolytes," *Collection of Czechoslovak Chemical Communications*, vol. 35, no. 2, pp. 535–544, 1970.

[132] M. Postler, "Conductance of concentrated aqueous solutions of electrolytes. I. Strong uni-univalent electrolytes," *Collection of Czechoslovak Chemical Communications*, vol. 35, no. 2, pp. 535–544, 1970.

[133] J. Lange, "Zur Leitfähigkeit starker Elektrolyte," *Zeitschrift für Physikalische Chemie*, vol. 188, no. 1, pp. 284–315, 1941.

[134] R. B. McCleskey, "Electrical conductivity of electrolytes found in natural waters from (5 to 90) °c," *Journal of Chemical and Engineering Data*, vol. 56, no. 2, pp. 317–327, 2011.

[135] H. Piekarski, M. Tkaczyk, A. Bald, and A. Szejgis, "Conductivity study of NaCl and NaI solutions in water - 2-butoxyethanol mixtures at 298.15k. The effect of ion pairing on the standard dissolution enthalpies of NaCl and NaI," *Journal of Molecular Liquids*, vol. 73-74, 1997.

[136] A. Borun, A. Florczak, and A. Bald, "Conductance studies of NaCl, KCl, NaBr, NaI, NaBPh4, Bu4NI, and NaClO4 in water+ 2-butoxyethanol mixtures at T= 298.15 K," *Journal of Chemical & Engineering Data*, vol. 55, no. 9, pp. 3725–3730, 2010.

[137] Y. P. Jimenez, M. E. Taboada, E. K. Flores, and H. R. Galleguillos, "Density, viscosity, and electrical conductivity in the potassium sulfate + water + 1-propanol system at different temperatures," *Journal of Chemical and Engineering Data*, vol. 54, no. 6, 2009.

[138] A. Wypych-Stasiewicz, A. Boruń, J. Benko, and A. Bald, "Conductance studies of KI, LiBr, LiNO3, AgNO3, Et4NI and the limiting ionic conductance in water + propan-1-ol mixtures at 298.15 K," *Journal of Molecular Liquids*, vol. 178, 2013.

[139] A. Wypych-Stasiewicz, J. Benko, O. Vollrov, and A. Bald, "Conductance studies of Et4NIO4, Et 4NClO4, Bu4NI, Et4NI and the limiting ionic conductance in water + acetonitrile mixtures at 298.15 K," *Journal of Molecular Liquids*, vol. 190, 2014.

[140] A. Wahab, S. Mahiuddin, G. Hefter, W. Kunz, B. Minofar, and P. Jungwirth, "Ultrasonic velocities, densities, viscosities, electrical conductivities, raman spectra, and molecular dynamics simulations of aqueous solutions of Mg(OAc)2 and Mg(NO3)2: Hofmeister effects and ion pair formation," *Journal of Physical Chemistry B*, vol. 109, no. 50, 2005.

[141] T. Isono, "Density, Viscosity, and Electrolytic Conductivity of Concentrated Aqueous Electrolyte Solutions at Several Temperatures. Alkaline-Earth Chlorides, LaCI3, Na2SC4, NaNC3, NaBr, KNC3, KBr, and Cd(NO3)2," *Journal of Chemical and Engineering Data*, vol. 29, no. 1, pp. 45–52, 1984.

[142] D. Ghosh and B. Das, "Electrical conductances of tetrabutylammonium bromide, sodium tetraphenylborate, and sodium bromide in acetonitrile (1) + water (2) mixtures at (308.15, 313.15, and 318.15)K," *Journal of Chemical and Engineering Data*, vol. 49, no. 6, 2004.

[143] K. Maeda, K. Maeno, K. Fukui, M. Moritoki, and H. Kuramochi, "Electrical conductivity of aqueous ethanol solutions containing ammonium salts under high pressure at 298 K," *Journal of Chemical and Engineering Data*, vol. 58, no. 2, 2013.

[144] A. Cartón, F. Sobrón, M. De La Fuente, and E. De Blas, "Composition, density, viscosity, electrical conductivity, and refractive index of saturated solutions of lithium formate + water + ethanol," *Journal of Chemical and Engineering Data*, vol. 41, no. 1, 1996.

[145] Hafiz-ur-Rehman and M. S. Ansari, "Density, viscosity, and electrical conductivity measurements on the ternary system H2O + C2H5OH + LiCl over the entire ranges of solvent composition and LiCl solubility from (-5 to +50)°C," *Journal of Chemical and Engineering Data*, vol. 53, no. 9, 2008.

[146] A. Chatterjee and B. Das, "Electrical conductances of tetrabutylammonium bromide, sodium tetraphenylborate, and sodium bromide in methanol (1) + water (2) mixtures at (298.15, 308.15, and 318.15) K," *Journal of Chemical and Engineering Data*, vol. 51, no. 4, 2006.

[147] X. Wu, Y. Gong, S. Xu, Z. Yan, X. Zhang, and S. Yang, "Electrical Conductivity of Lithium Chloride, Lithium Bromide, and Lithium Iodide Electrolytes in Methanol, Water, and Their Binary Mixtures," *Journal of Chemical and Engineering Data*, vol. 64, no. 10, 2019.

[148] M. Bešter-Rogač, R. Neueder, and J. Barthel, "Conductivity of sodium chloride in water + 1,4-dioxane mixtures from 5 to 35°C. II. Concentrated solutions," *Journal of Solution Chemistry*, vol. 29, no. 1, pp. 51–60, 2000.

[149] M. Bešter-Rogač, R. Neueder, and J. Barthel, "Conductivity of sodium chloride in water + 1,4-dioxane mixtures at temperature from 5 to 35°C I. Dilute solution," *Journal of Solution Chemistry*, vol. 28, no. 9, pp. 1071–1086, 1999.

[150] M. Bešter-Rogač, "Electrical conductivity of concentrated aqueous solutions of divalent metal sulfates," *Journal of Chemical and Engineering Data*, vol. 53, no. 6, 2008.

[151] D. Fraenkel, "Theoretical interpretation of the limiting electric conductivity in ionic solution," *Molecular Physics*, vol. 115, no. 23, pp. 2944–2950, 2017.

[152] D. Fraenkel, "A new theoretical development of the limiting electric conductivity of ions in solution," *Molecular Physics*, vol. 116, no. 18, pp. 2271–2293, 2018.

[153] R. M. Fuoss and L. Onsager, "Conductance of unassociated electrolytes," *Journal of Physical Chemistry*, vol. 61, no. 5, pp. 668–682, 1957.

[154] P. Wang, A. Anderko, and R. D. Young, "Modeling electrical conductivity in concentrated and mixed-solvent electrolyte solutions," *Industrial and Engineering Chemistry Research*, vol. 43, no. 25, pp. 8083–8092, 2004.

[155] Y. Marcus, "Ionic Radii in Aqueous Solutions," *Chemical Reviews*, vol. 88, no. 8, pp. 1475–1498, 1988.

[156] W. M. Haynes, D. R. Lide, and T. J. Bruno, eds., *CRC Handbook of Chemistry and Physics*. CRC Press, 97 ed., 6 2016.

[157] J. M. G. Barthel, R. Buchner, and M. A. Münsterer, *CDS Volume XII, Part 2: Dielectric Properties of Water and Aqueous Electrolyte Solutions*. Frankfurt: DECHEMA, 1995.

[158] A. Apelblat, "Representation of electrical conductances for polyvalent electrolytes by the quint-viallard conductivity equation. Part 4. symmetrical 2:2, 3:3 and unsymmetrical 2:1, 3:1 and 1:3 type electrolytes in pure organic solvents," *Journal of Solution Chemistry*, vol. 40, no. 7, pp. 1234–1257, 2011.

[159] A. Apelblat, "Representation of electrical conductances for polyvalent electrolytes by the quint-viallard conductivity equation. Part 1. symmetrical 2:2 type electrolytes. Dilute aqueous solutions of alkaline earth metal sulfates and transition metal sulfates," *Journal of Solution Chemistry*, vol. 40, no. 7, pp. 1209–1233, 2011.

[160] T. L. Broadwater and D. F. Evans, "The conductance of divalent Ions in H2O at 10 and 25°C and in D2O," *Journal of Solution Chemistry*, vol. 3, no. 10, pp. 757–769, 1974.

[161] J. P. Simonin, L. Blum, and P. Turq, "Real ionic solutions in the mean spherical approximation. 1. Simple salts in the primitive model," *Journal of Physical Chemistry*, vol. 100, no. 18, pp. 7704–7709, 1996.

[162] J. P. Simonin, "Real ionic solutions in the mean spherical approximation. 2. Pure strong electrolytes up to very high concentrations, and mixtures, in the primitive model," *Journal of Physical Chemistry B*, vol. 101, no. 21, pp. 4313–4320, 1997.

[163] J. P. Simonin, O. Bernard, and L. Blum, "Real ionic solutions in the mean spherical approximation. 3. Osmotic and activity coefficients for associating electrolytes in the primitive model," *Journal of Physical Chemistry B*, vol. 102, no. 22, pp. 4411–4417, 1998.

[164] J. M. Barthel, Roland M. Neueneder, and Roland Meier, *Dechema Chemistry Data Series / Electolyte data collection / Viscosity of Aqueous Solutions: CoO4S-O6SU*. Frankfurt am Main, Germany: DECHEMA, 1998.

[165] J. M. Barthel, Roland M. Neueneder, and Roland Meier, *Dechema Chemistry Data Series / Electolyte data collection / Viscosity of Aqueous Solutions: AgC104-C14016Th*. Frankfurt am Main, Germany: DECHEMA, 1998.

[166] G. J. Janz, B. G. Oliver, G. R. Lakshminarayanan, and G. E. Mayer, "Electrical conductance, diffusion, viscosity, and density of sodium nitrate, sodium perchlorate, and sodium thiocyanate in concentrated aqueous solutions," *Journal of Physical Chemistry*, vol. 74, no. 6, pp. 1285–1289, 1970.

[167] J. Barthel, H. Krienke, R. Neueder, and M. F. Holovko, "The role of ion-aggregate formation in the calculation of physical properties of electrolyte solutions," in *Fluid Phase Equilibria*, vol. 194-197, pp. 107–122, 2002.

[168] J. Barthel, H.-J. Gores, G. Schmeer, and R. Wachter, "Non-aqueous electrolyte solutions in chemistry and modern technology," in *Physical and inorganic chemistry*, pp. 33–144, Springer, 1983.

[169] M. Bešter-Rogač, N. Hauptman, and J. Barthel, "Conductometric study of ion association of divalent symmetric electrolytes: II. MgSO4 in water + 1,4-dioxane mixtures," *Journal of Molecular Liquids*, vol. 131-132, no. SPEC. ISS., 2007.

[170] E. Grüneisen, "Abhandl. d. physikal.-techn," *Reichsanstalt*, vol. 4, p. 239, 1905.

[171] H. Falkenhagen and M. Dole, "Die innere reibung von elektrolytischen losungen und ihre deutung nach der Debyeschen theorie," *Phys. Z*, vol. 30, pp. 611–622, 1929.

[172] G. Jones and M. Dole, "The viscosity of aqueous solutions of strong electrolytes with special reference to barium chloride," *Journal of the American Chemical Society*, vol. 51, no. 10, pp. 2950–2964, 1929.

[173] K. Ibuki and M. Nakahara, "Dielectric friction theory of the viscosity of electrolyte solutions," *The Journal of Chemical Physics*, vol. 85, no. 12, pp. 7312–7317, 1986.

[174] J. Hubbard and L. Onsager, "Dielectric dispersion and dielectric friction in electrolyte solutions. I," *The Journal of Chemical Physics*, vol. 67, no. 11, pp. 4850–4857, 1977.

[175] J. B. Hubbard, "Dielectric dispersion and dielectric friction in electrolyte solutions. II," *The Journal of Chemical Physics*, vol. 68, no. 4, pp. 1649–1664, 1977.

[176] J. B. Hubbard, P. Colonomos, and P. G. Wolynes, "Molecular theory of solvated ion dynamics. III. the kinetic dielectric decrement," *The Journal of Chemical Physics*, vol. 71, no. 6, pp. 2652–2661, 1979.

[177] B. F. Wishaw and R. H. Stokes, "The Diffusion Coefficients and Conductances of Some Concentrated Electrolyte Solutions at 25°," *Journal of the American Chemical Society*, vol. 76, no. 8, pp. 2065–2071, 1954.

[178] A. N. Campbell and E. M. Kartzmark, "The Electrical Conductance Of Strong Electrolytes: A Test Of Stokes Equation," *Canadian Journal of Chemistry*, vol. 33, no. 5, pp. 887–894, 1955.

[179] M. Della Monica, A. Ceglie, and A. Agostiano, "A conductivity equation for concentrated aqueous solutions," *Electrochimica Acta*, vol. 29, no. 7, pp. 933–937, 1984.

[180] M. Della Monica, A. Ceglie, and A. Agostiano, "Extension of the Falkenhagen equation to the conductivity of concentrated electrolyte solutions," *Journal of Physical Chemistry*, vol. 88, no. 10, pp. 2124–2127, 1984.

[181] M. Della Monica, "Conductance equation for concentrated electrolyte solution," *Electrochimica Acta*, vol. 29, no. 2, 1984.

[182] S. S. Islam, R. L. Gupta, and K. Ismail, "Extension of the Falkenhagen-LeistKelbg Equation to the Electrical Conductance of Concentrated Aqueous Electrolytes," *Journal of Chemical and Engineering Data*, vol. 36, no. 1, pp. 102–104, 1991.

[183] C. W. Outhwaite, "Numerical solution of a Poisson-Boltzmann theory for a primitive model electrolyte with size and charge asymmetric ions," *Journal of the Chemical Society, Faraday Transactions 2: Molecular and Chemical Physics*, vol. 83, no. 6, pp. 949–959, 1987.

[184] S. Naseri Boroujeni, B. Maribo-Mogensen, X. Liang, and G. M. Kontogeorgis, "New Electrical Conductivity Model for Electrolyte Solutions Based on the DebyeHückelOnsager Theory," *The Journal of Physical Chemistry B*, vol. 127, pp. 9954–9975, 11 2023.

[185] M. C. Abramo, C. Caccamo, G. Malescio, G. Pizzimenti, and S. A. Rogde, "Equilibrium properties of charged hard spheres of different diameters in the electrolyte solution regime: Monte Carlo and integral equation results," *The Journal of Chemical Physics*, vol. 80, no. 9, pp. 4396–4402, 1984.

[186] S. Katayama, "Conductometric Determination of Ion-association Constants for Magnesium and Nickel Sulfates in Aqueous Solutions at Various Temperatures between 0°C and 45°C," *Bulletin of the Chemical Society of Japan*, vol. 46, no. 1, pp. 106–109, 1973.

[187] W. J. Xie, Z. Zhang, and Y. Q. Gao, "Ion Pairing in Alkali Nitrate Electrolyte Solutions," *Journal of Physical Chemistry B*, vol. 120, no. 9, pp. 2343–2351, 2016.

[188] J. P. Simonin, "Determination of Thermodynamic Complexity Constants and Speciation for Multicomplexing Electrolytes within the Mean Spherical Approximation Model," *Industrial and Engineering Chemistry Research*, vol. 58, no. 1, 2019.

[189] W. W. Rudolph, G. Irmer, and G. T. Hefter, "Raman spectroscopic investigation of speciation in MgSO4(aq)," *Physical Chemistry Chemical Physics*, vol. 5, no. 23, pp. 5253–5261, 2003.

[190] W. W. Rudolph and G. Irmer, "Raman spectroscopic investigation of speciation in MnSO4(aq)," *Journal of Solution Chemistry*, vol. 43, no. 3, pp. 465–485, 2014.

[191] Y. Wan, X. Wang, W. Hu, and I. M. Chou, "Raman Spectroscopic Observations of the Ion Association between Mg(2+) and SO4(2-) in MgSO4-Saturated Droplets at Temperatures of U+2264 380 °C," *The journal of physical chemistry. A*, vol. 119, no. 34, pp. 9027–9036, 2015.

[192] R. Buchner, T. Chen, and G. Hefter, "Complexity in "simple" electrolyte solutions: Ion pairing in MgSO4(aq)," *Journal of Physical Chemistry B*, vol. 108, no. 7, pp. 2365–2375, 2004.

[193] C. Akilan, G. Hefter, N. Rohman, and R. Buchner, "Ion association and hydration in aqueous solutions of copper(II) Sulfate from 5 to 65 °C by dielectric spectroscopy," *Journal of Physical Chemistry B*, vol. 110, no. 30, pp. 14961–14970, 2006.

[194] T. Chen, G. Hefter, and R. Buchner, "Ion association and hydration in aqueous solutions of nickel(II) and cobalt(II) sulfate," *Journal of Solution Chemistry*, vol. 34, no. 9, pp. 1045–1066, 2005.

[195] B. Bagchi, "Microscopic derivation of the Hubbard-Onsager-Zwanzig expression of limiting ionic conductivity," *Journal of Chemical Physics*, vol. 109, no. 10, pp. 3989–3993, 1998.

[196] M. Della Monica, G. Petrella, A. Sacco, and S. Bufo, "Transference numbers in concentrated sodium chloride solutions," *Electrochimica Acta*, vol. 24, no. 9, pp. 1013–1017, 1979.

[197] D. G. Miller, "Application of irreversible thermodynamics to electrolyte solutions. I. Determination of ionic transport coefficients lij for isothermal vector transport processes in binary electrolyte systems," *Journal of Physical Chemistry*, vol. 70, no. 8, pp. 2639–2659, 1966.

[198] S. Phang and R. H. Stokes, "Density, viscosity, conductance, and transference number of concentrated aqueous magnesium chloride at 25°C," *Journal of Solution Chemistry*, vol. 9, no. 7, pp. 497–505, 1980.

[199] H. Weingärtner, B. M. Braun, and J. M. Schmoll, "Isothermal transport coefficients in concentrated aqueous solutions of unsymmetrical electrolytes: LaCl3 at 25 °C," *Journal of Physical Chemistry*, vol. 91, no. 4, pp. 979–985, 1987.

[200] S. Naseri Boroujeni, B. Maribo-Mogensen, X. Liang, and G. M. Kontogeorgis, "A Novel Model for Predicting the Electrical Conductivity of Multi-salt Electrolyte Solutions," *Journal of Physical Chemistry B (submitted)*, 2023.

[201] S. Durand-Vidal, P. Turq, O. Bernard, C. Treiner, and L. Blum, "New perspectives in transport phenomena in electrolytes," *Physica A: Statistical Mechanics and its Applications*, vol. 231, no. 1-3, 1996.

[202] R. P. Brent, *Algorithms for minimization without derivatives*. Courier Corporation, 2013.

[203] A. E. Stearn, "Ionic equilibria of strong electrolytes," *Journal of the American Chemical Society*, vol. 44, pp. 670–678, 4 1922.

[204] R. Suhrmann and I. Wiedersich, "Über die Beeinflussung der H+-Ionenleitfähigkeit durch Fremdionen in wäßriger Lösung," *Zeitschrift für anorganische und allgemeine Chemie*, vol. 272, pp. 167–181, 2 1953.

[205] R. E. Hamm and T. G. Thompson, "Specific Gravities and Electrical Conductances of Some Calcium Sulfate Solutions and Mixtures of Sodium Chloride and Calcium Sulfate," *Journal of the American Chemical Society*, vol. 63, no. 5, pp. 1418–1422, 1941.

[206] R. W. Bremner, T. G. Thompson, and C. L. Utterback, "Electrical Conductances of Pure and Mixed Salt Solutions in the Temperature Range 0 to 25°," *Journal of the American Chemical Society*, vol. 61, no. 5, pp. 1219–1223, 1939.

[207] H. Bianchi, H. R. Corti, and R. Fernández-Prini, "The conductivity of dilute solutions of mixed electrolytes. Part 1. - The system NaCl-BaCl2-H2O at 298.2 K," *Journal of the Chemical Society, Faraday Transactions 1: Physical Chemistry in Condensed Phases*, vol. 83, no. 9, pp. 3027–3037, 1987.

[208] H. Bianchi, H. R. Corti, and R. Fernandez-Prini, "The conductivity of dilute solutions of mixed electrolytes. Part 2: The system NaCl-MgCl2 at 25°C," *Journal of Solution Chemistry*, vol. 21, no. 11, pp. 1107–1114, 1992.

[209] P. Van Rysselberghe and L. Nutting, "Conductivities of One-Molal Mixtures of Alkali Halides and Nitrates," *Journal of the American Chemical Society*, vol. 59, no. 2, pp. 333–336, 1937.

[210] H. Bianchi, H. R. Corti, and R. Fernández-Prini, "The conductivity of concentrated aqueous mixtures of NaCl and MgCl2 at 25°C," *Journal of Solution Chemistry*, vol. 18, no. 5, pp. 485–491, 1989.

[211] P. Van Rysselberghe, S. W. Grinnell, and J. M. Carlson, "Conductivities of Concentrated Binary Mixtures of Electrolytes with a Common Anion and at Least One Ion of Charge Two," *Journal of the American Chemical Society*, vol. 59, no. 2, pp. 336–339, 1937.

[212] P. Van Rysselberghe and G. Lee, "Conductivities of Concentrated Mixtures of the Nitrates of Some Uni-, Di-, and Trivalent Cations in Aqueous Solution," *Journal of the American Chemical Society*, vol. 60, no. 11, pp. 2776–2779, 1938.

[213] M. Bester Rogac, V. Babic, T. M. Perger, R. Neueder, and J. Barthel, "Conductometric study of ion association of divalent symmetric electrolytes: I. CoSO4, NiSO4, CuSO4 and ZnSO4 in water," *Journal of molecular liquids*, vol. 118, no. 1-3, pp. 111–118, 2005.

[214] S. Naseri Boroujeni, B. Maribo-Mogensen, X. Liang, and G. M. Kontogeorgis, "Mean ionic activity coefficient of associative electrolyte solutions: A comparison study," *Journal of Molecular Liquids*, vol. 386, p. 122509, 2023.

[215] A. Apelblat, "The Representation of Electrical Conductances for Polyvalent Electrolytes by the QuintViallard Conductivity Equation: Part 7. Unsymmetrical 1:2 Type Electrolytes. Alkali Metal (Li, Na, K, Rb and Cs) Sulfates and Ammonium Sulfate," *Journal of Solution Chemistry*, vol. 46, no. 1, pp. 103–123, 2017.

[216] N. Bjerrum, "Investigations on Association of Ions. I. The Influence of Association of Ions on the Activity of the Ions at Intermediate Degrees of Association," *Kgl. Danske Videnskab. Selskab*, vol. 7, pp. 1–48, 1926.

[217] C. A. Kraus, "The ion-pair concept, its evolution and some applications.," *The Journal of Physical Chemistry*, vol. 60, no. 2, pp. 129–141, 1956.

[218] M. Szwarc, "Ions and ion pairs," *Accounts of Chemical Research*, vol. 2, no. 3, pp. 87–96, 1969.

[219] H. S. Harned and B. B. Owen, *The Physical Chemistry of Electrolytic Solutions*. New York: Reinhold Publishing Corporation, 1950.

[220] W. Ebeling and M. Grigo, "An Analytical Calculation of the Equation of State and the Critical Point in a Dense Classical Fluid of Charged Hard Spheres," *Annalen der Physik*, vol. 492, no. 1, pp. 21–30, 1980.

[221] W. Ebeling and M. Grigo, "Mean spherical approximation-mass action law theory of equilibrium and conductance in ionic solutions," *Journal of Solution Chemistry*, vol. 11, no. 3, pp. 151–167, 1982.

[222] W. Ebeling and M. Grigo, "Radial Distribution Function in a Modified Bjerrum Model for Associating Electrolytes," *Zeitschrift für Physikalische Chemie*, vol. 265O, no. 1, pp. 1072–1078, 1984.

[223] M. Grigo and W. Ebeling, "Remarks on the correlation function implied by the Bjerrum theory of ion pairing," *Journal of solution chemistry*, vol. 13, pp. 321–333, 1984.

[224] N. F. Carnahan and K. E. Starling, "Equation of state for nonattracting rigid spheres," *The Journal of Chemical Physics*, vol. 51, no. 2, 1969.

[225] S. Yeh, "Phase separation of ionic fluids: an extended ebeling-grigo approach," *Journal of Physical Chemistry*, vol. 100, no. 4, pp. 1415–1419, 1996.

[226] A. C. Tikanen and W. Ronald Fawcett, "The Role of Solvent Permittivity in Estimation of Electrolyte Activity Coefficients for Systems with Ion Pairing on the Basis of the Mean Spherical Approximationof," *Berichte der Bunsengesellschaft/Physical Chemistry Chemical Physics*, vol. 100, no. 5, pp. 634–640, 1996.

[227] A. C. Tikanen and W. R. Fawcett, "Application of the mean spherical approximation and ion association to describe the activity coefficients of aqueous 1:1 electrolytes," *Journal of Electroanalytical Chemistry*, vol. 439, no. 1, pp. 107–113, 1997.

[228] W. R. Fawcett and A. C. Tikanen, "Role of solvent permittivity in estimation of electrolyte activity coefficients on the basis of the mean spherical approximation," *Journal of Physical Chemistry*, vol. 100, no. 10, pp. 4251–4255, 1996.

[229] W. R. Fawcett and A. C. Tikanen, "Application of the mean spherical approximation to the estimation of electrolyte activity coefficients in methanol solutions," *Journal of Molecular Liquids*, vol. 73-74, pp. 373–384, 1997.

[230] G. A. Mansoori, N. F. Carnahan, K. E. Starling, and T. W. Leland, "Equilibrium thermodynamic properties of the mixture of hard spheres," *The Journal of Chemical Physics*, vol. 54, no. 4, pp. 1523–1525, 1971.

[231] W. Ebeling and K. Scherwinski, "On the estimation of theoretical individual activity coefficients of electrolytes: I. Hard sphere model," *Zeitschrift für Physikalische Chemie*, vol. 264, no. 1, pp. 1–14, 1983.

[232] M. E. Fisher and Y. Levin, "Criticality in ionic fluids: Debye-Hückel theory, Bjerrum, and beyond," *Physical Review Letters*, vol. 71, no. 23, p. 3826, 1993.

[233] Y. Levin and M. E. Fisher, "Criticality in the hard-sphere ionic fluid," *Physica A: Statistical Mechanics and its Applications*, vol. 225, no. 2, pp. 164–220, 1996.

[234] Y. Levin, X. J. Li, and M. E. Fisher, "Coulombic criticality in general dimensions," *Physical Review Letters*, vol. 73, no. 20, pp. 2716–2719, 1994.

[235] J. G. Kirkwood, "Theory of solutions of molecules containing widely separated charges with special application to zwitterions," *The Journal of Chemical Physics*, vol. 2, no. 7, pp. 351–361, 1934.

[236] B. Guillot and Y. Guissani, "Towards a theory of coexistence and criticality in real molten salts," *Molecular Physics*, vol. 87, no. 1, pp. 37–86, 1996.

[237] V. C. Weiss and W. Schroer, "Macroscopic theory for equilibrium Properties of ionic-dipolar mixtures and application to an ionic model fluid," *Journal of Chemical Physics*, vol. 108, no. 18, pp. 7747–7757, 1998.

[238] H. Weingärtner and W. Schröer, "Criticality of ionic fluids," *Advances in Chemical Physics*, pp. 1–66, 2001.

[239] W. Schröer, "A short history of phase transitions in ionic fluids," *Contributions to Plasma Physics*, vol. 52, no. 1, pp. 78–88, 2012.

[240] G. Stell and Y. Zhou, "Chemical association in simple models of molecular and ionic fluids," *The Journal of Chemical Physics*, vol. 91, no. 6, pp. 1507–1515, 1989.

[241] G. Stell and Y. Zhou, "Microscopic modelling of association," *Fluid Phase Equilibria*, vol. 79, no. C, pp. 1–20, 1992.

[242] Y. Zhou and G. Stell, "Criticality of charged systems. II. The binary mixture of hard spheres and ions," *The Journal of Chemical Physics*, vol. 102, no. 14, pp. 5796–5802, 1995.

[243] Y. Zhou and G. Stell, "Chemical association in simple models of molecular and ionic fluids. III. The cavity function," *The Journal of Chemical Physics*, vol. 96, no. 2, 1992.

[244] Y. Zhou, S. Yeh, and G. Stell, "Criticality of charged systems. I. The restricted primitive model," *The Journal of Chemical Physics*, vol. 102, no. 14, pp. 5785–5795, 1995.

[245] Y. Zhou and G. Stell, "Chemical association in simple models of molecular and ionic fluids. II. Thermodynamic properties," *The Journal of Chemical Physics*, vol. 96, no. 2, 1992.

[246] M. S. Wertheim, "Fluids with highly directional attractive forces. III. Multiple attraction sites," *Journal of Statistical Physics*, vol. 42, no. 3-4, pp. 459–476, 1986.

[247] M. S. Wertheim, "Fluids with highly directional attractive forces. II. Thermodynamic perturbation theory and integral equations," *Journal of Statistical Physics*, vol. 35, no. 1-2, pp. 35–47, 1984.

[248] M. S. Wertheim, "Fluids of dimerizing hard spheres, and fluid mixtures of hard spheres and dispheres," *The Journal of Chemical Physics*, vol. 85, no. 5, pp. 2929–2936, 1986.

[249] M. S. Wertheim, "Fluids with highly directional attractive forces. I. Statistical thermodynamics," *Journal of Statistical Physics*, vol. 35, no. 1-2, pp. 19–34, 1984.

[250] M. S. Wertheim, "Fluids with highly directional attractive forces. IV. Equilibrium polymerization," *Journal of Statistical Physics*, vol. 42, no. 3-4, pp. 477–492, 1986.

[251] M. S. Wertheim, "Thermodynamic perturbation theory of polymerization," *The Journal of Chemical Physics*, vol. 87, no. 12, pp. 7323–7331, 1987.

[252] H. Krienke and J. Barthel, "MSA models of ion association in electrolyte solutions," *Zeitschrift fur Physikalische Chemie*, vol. 204, no. 1-2, pp. 71–83, 1998.

[253] H. Krienke and J. Barthel, "Association concepts in electrolyte solutions," *Journal of Molecular Liquids*, vol. 78, no. 1-2, pp. 123–138, 1998.

[254] J. Barthel, "The Temperature Dependence of the Properties of Electrolyte Solutions. I. A SemiPhenomenological Approach to an Electrolyte Theory Including Short Range Forces," *Berichte der Bunsengesellschaft für physikalische Chemie*, vol. 83, no. 3, pp. 252–257, 1979.

[255] W. Ebeling, "Zur theorie der bjerrumschen ionenassoziation in elektrolyten," *Zeitschrift für Physikalische Chemie*, vol. 238, no. 1, pp. 400–402, 1968.

[256] F. Malatesta, "The Activity Coefficients of High-Charge Electrolytes in Aqueous Dilute Solutions," *Journal of Solution Chemistry*, vol. 49, no. 12, pp. 1536–1551, 2020.

[257] G. M. Silva, X. Liang, and G. M. Kontogeorgis, "Investigation of the Limits of the Linearized PoissonBoltzmann Equation," *The Journal of Physical Chemistry B*, vol. 126, pp. 4112–4131, 5 2022.

[258] S. Lamperski, "The individual and mean activity coefficients of an electrolyte from the inverse GCMC simulation," *Molecular Simulation*, vol. 33, no. 15, pp. 1193–1198, 2007.

[259] J. P. Valleau and L. K. Cohen, "Primitive model electrolytes. I. Grand canonical Monte Carlo computations," *The Journal of Chemical Physics*, vol. 72, no. 11, pp. 5935–5941, 1979.

[260] E. Gutiérrez-Valladares, M. Lukšič, B. Millán-Malo, B. Hribar-Lee, and V. Vlachy, "Primitive model electrolytes. A comparison of the HNC approximation for the activity coefficient with Monte Carlo data," *Condensed Matter Physics*, vol. 14, no. 3, pp. 1–15, 2011.

[261] F. Malatesta, L. Carbonaro, N. Fanelli, S. Ferrini, and A. Giacomelli, "Activity and osmotic coefficients from the emf of liquid-membrane cells. VII: Co(ClO4)2, Ni(ClO4)2, K2SO4, CdSO4, CoSO4, and NiSO4," *Journal of Solution Chemistry*, vol. 28, no. 5, 1999.

[262] F. Malatesta and R. Zamboni, "Activity and osmotic coefficients from the EMF of liquid membrane cells. VI-ZnSO4, MgSO4, CaSO4, and SrSO4 in water at 25°C," *Journal of Solution Chemistry*, vol. 26, no. 8, 1997.

[263] M. E. Guendouzi, A. Mounir, and A. Dinane, "Water activity, osmotic and activity coefficients of aqueous solutions of Li2SO4, Na2SO4, K2SO4, (NH4)2SO4, MgSO4, MnSO4, NiSO4, CuSO4, and ZnSO4 at T = 298.15 K," *Journal of Chemical Thermodynamics*, vol. 35, no. 2, 2003.

[264] C. Akilan, N. Rohman, G. Hefter, and R. Buchner, "Temperature effects on ion association and hydration in MgSO4 by dielectric spectroscopy," *ChemPhysChem*, vol. 7, no. 11, pp. 2319–2330, 2006.

[265] F. Sebastiani, A. V. Verde, M. Heyden, G. Schwaab, and M. Havenith, "Cooperativity and ion pairing in magnesium sulfate aqueous solutions from the dilute regime to the solubility limit," *Physical Chemistry Chemical Physics*, vol. 22, no. 21, 2020.

[266] K. J. Tielrooij, N. Garcia-Araez, M. Bonn, and H. J. Bakker, "Cooperativity in ion hydration," *Science*, vol. 328, no. 5981, 2010.

[267] A. Vila Verde, M. Santer, and R. Lipowsky, "Solvent-shared pairs of densely charged ions induce intense but short-range supra-additive slowdown of water rotation," *Physical Chemistry Chemical Physics*, vol. 18, no. 3, 2016.

[268] Y. Marcus, "On the activity coefficients of charge-symmetrical ion pairs," *Journal of Molecular Liquids*, vol. 123, no. 1, 2006.

[269] "CERE, DTU, DTU Electrolyte Database," 2022.

[270] H. Weingärtner, V. C. Weiss, and W. Schröer, "Ion association and electrical conductance minimum in Debye-Hueckel-based theories of the hard sphere ionic fluid," *Journal of Chemical Physics*, vol. 113, no. 2, pp. 762–770, 2000.

[271] J. P. Simonin, O. Bernard, and L. Blum, "Ionic solutions in the binding mean spherical approximation: Thermodynamic properties of mixtures of associating electrolytes," *Journal of Physical Chemistry B*, vol. 103, no. 4, pp. 699–704, 1999.

[272] J. P. Simonin and O. Bernard, "Organic electrolyte solutions: Modeling of deviations from ideality within the binding mean spherical approximation," *Fluid Phase Equilibria*, vol. 468, pp. 58–69, 2018.

[273] A. Ruas, P. Pochon, J. P. Simonin, and P. Moisy, "Nitric acid: Modeling osmotic coefficients and acid-base dissociation using the BIMSA theory," *Dalton Transactions*, vol. 39, no. 42, pp. 10148–10153, 2010.

[274] A. Ruas, P. Pochon, S. Hlushak, J.-P. Simonin, O. Bernard, and P. Moisy, "Speciation in Aqueous Solutions of Nitric Acid Estimated Within the Binding mean Spherical Approximation (BiMSA)," *Procedia Chemistry*, vol. 7, 2012.

[275] A. Ruas, P. Moisy, J. P. Simonin, O. Bernard, J. F. Dufrêche, and P. Turq, "Lanthanide salts solutions: Representation of osmotic coefficients within the binding mean spherical approximation," *Journal of Physical Chemistry B*, vol. 109, no. 11, pp. 5243–5248, 2005.

[276] N. Papaiconomou, J. P. Simonin, and O. Bernard, "Aqueous solutions of ionic liquids. Description of osmotic coefficients within the Binding Mean Spherical Approximation," *Journal of Chemical Thermodynamics*, vol. 91, pp. 445–451, 2015.

[277] N. Papaiconomou, J. P. Simonin, and O. Bernard, "Solutions of alkylammonium and bulky anions: Description of osmotic coefficients within the binding mean spherical approximation," *Industrial and Engineering Chemistry Research*, vol. 51, no. 28, pp. 9661–9668, 2012.

[278] J. Torres-Arenas, J. P. Simonin, O. Bernard, A. Ruas, and P. Moisy, "Thermodynamics of binary and ternary solutions of multivalent electrolytes with formation of 1:1 And 1:2 complexes, within the mean spherical approximation," *Industrial and Engineering Chemistry Research*, vol. 49, no. 4, pp. 1937–1946, 2010.

[279] T. Vilariño, O. Bernard, and J. P. Simonin, "Ionic solutions in the binding mean spherical approximation. Thermodynamics of associating electrolytes up to very high concentrations," *Journal of Physical Chemistry B*, vol. 108, no. 18, pp. 5763–5770, 2004.

[280] N. Von Solms and Y. C. Chiew, "Analytical integral equation theory for a restricted primitive model of polyelectrolytes and counterions within the mean spherical approximation. I. Thermodynamic properties," *Journal of Chemical Physics*, vol. 111, no. 10, pp. 4839–4850, 1999.

[281] N. Von Solms and Y. C. Chiew, "Analytical integral equation theory for a restricted primitive model of polyelectrolytes and counterions within the mean spherical approximation. II. Radial distribution functions," *Journal of Chemical Physics*, vol. 118, no. 9, pp. 4321–4330, 2003.

[282] B. E. Vakarin, Y. DUDA, and M. F. HOLOVKO, "Integral equation theory for the four bonding sites model of I. Structure factor and compressibility associating fluids," *Molecular Physics*, vol. 90, no. 4, 1997.

[283] O. Bernard and J. P. Simonin, "Thermodynamic properties of ring polyelectrolytes in the binding mean spherical approximation," *Journal of Molecular Liquids*, vol. 228, pp. 121–125, 2017.

[284] O. Bernard and J. P. Simonin, "Association of counterions on polyelectrolytes: Thermodynamic properties in the binding mean spherical approximation," *Journal of Molecular Liquids*, vol. 270, pp. 14–24, 2018.

[285] W. G. Chapman, K. E. Gubbins, G. Jackson, and M. Radosz, "New reference equation of state for associating liquids," *Industrial & engineering chemistry research*, vol. 29, no. 8, pp. 1709–1721, 1990.

[286] S. Naseri Boroujeni, B. Maribo-Mogensen, X. Liang, and G. M. Kontogeorgis, "Binding DebyeHückel theory for associative electrolyte solutions," *The Journal of Chemical Physics*, vol. 159, no. 15, 2023.

[287] T. Boublík, "HardSphere Equation of State," *The Journal of Chemical Physics*, vol. 53, pp. 471–472, 9 1970.

[288] M. Born, "Volumen und hydratationswärme der ionen," *Zeitschrift für physik*, vol. 1, no. 1, pp. 45–48, 1920.

[289] Z. Abbas, E. Ahlberg, and S. Nordholm, "Monte Carlo simulations of salt solutions: Exploring the validity of primitive models," *Journal of Physical Chemistry B*, vol. 113, no. 17, pp. 5905–5916, 2009.

[290] D. Gillespie, M. Valiskó, and D. Boda, "Electrostatic correlations in electrolytes: Contribution of screening ion interactions to the excess chemical potential," *Journal of Chemical Physics*, vol. 155, no. 22, p. 221102, 2021.

[291] B. R. Svensson and C. E. Woodward, "Widom's method for uniform and non-uniform electrolyte solutions," *Molecular Physics*, vol. 64, no. 2, pp. 247–259, 1988.

[292] B. Widom, "Some topics in the theory of fluids," *The Journal of Chemical Physics*, vol. 39, no. 11, pp. 2808–2812, 1963.

[293] A. Malasics and D. Boda, "An efficient iterative grand canonical Monte Carlo algorithm to determine individual ionic chemical potentials in electrolytes," *The Journal of chemical physics*, vol. 132, no. 24, 2010.

[294] J. S. Høye and D. Gillespie, "Individual ion species chemical potentials in the Mean Spherical Approximation," *The Journal of Chemical Physics*, vol. 156, no. 24, 2022.

[295] M. Valiskó and D. Boda, "Resurrection of Hückels idea: Decoupling ionion and ion-water terms in activity coefficients via the state-dependent dielectric constant," *Fluid Phase Equilibria*, vol. 572, p. 113826, 2023.

[296] L. Sun, Q. Lei, B. Peng, G. M. Kontogeorgis, and X. Liang, "An analysis of the parameters in the Debye-Hückel theory," *Fluid Phase Equilibria*, vol. 556, p. 113398, 2022.

[297] R. M. Fuoss and C. A. Kraus, "Properties of Electrolytic Solutions. II. The Evaluations of $\Delta 0$ and of K for Incompletely Dissociated Electrolytes," *Journal of the American Chemical Society*, vol. 55, no. 2, pp. 476–488, 1933.

[298] W. Beichel, P. Eiden, and I. Krossing, "Establishing consistent van der waals volumes of polyatomic ions from crystal structures," *ChemPhysChem*, vol. 14, no. 14, 2013.

[299] H. Wang, Z. Zuo, L. Lu, A. Laaksonen, Y. Wang, X. Lu, and X. Ji, "Experimental and theoretical study on ion association in [Hmim][halide]+water/isopropanol mixtures," *Fluid Phase Equilibria*, vol. 566, p. 113680, 2023.

[300] A. Stoppa, J. Hunger, and R. Buchner, "Conductivities of binary mixtures of ionic liquids with polar solvents," *Journal of Chemical and Engineering Data*, vol. 54, no. 2, pp. 472–479, 2009.

[301] M. Bešter-Rogač, A. Stoppa, and R. Buchner, "Ion association of imidazolium ionic liquids in acetonitrile," *Journal of Physical Chemistry B*, vol. 118, no. 5, pp. 1426–1435, 2014.

[302] J.-P. Simonin, "Thermodynamic consistency in the modeling of speciation in self-complexing electrolytes," *Industrial & Engineering Chemistry Research*, vol. 56, no. 34, pp. 9721–9733, 2017.

[303] J.-P. Simonin and W. Verweij, "A Simplified Mean Spherical Approximation Model for the Description of Activity Coefficients in Electrolyte Mixtures," *Industrial & Engineering Chemistry Research*, vol. 61, no. 35, pp. 13265–13274, 2022.

[304] W. Verweij and J.-P. Simonin, "Implementing the Mean Spherical Approximation model in the speciation code CHEAQS Next at high salt concentrations," *Journal of Solution Chemistry*, vol. 49, no. 11, pp. 1319–1327, 2020.

[305] J.-P. Simonin, "Determination of Thermodynamic Complexity Constants and Speciation for Multicomplexing Electrolytes within the Mean Spherical Approximation Model," *Industrial & Engineering Chemistry Research*, vol. 58, no. 1, pp. 448–460, 2018.

[306] R. M. Smith, A. E. Martell, and R. J. Motekaitis, "NIST Critically Selected Stability Constants of Metal Complexes: Version 8.0," 2004.

[307] A. J. Rabinowitsch, "Über die anomale Dissoziation in wässerigen Lösungen: I. Abhandlung," *Zeitschrift für Physikalische Chemie*, vol. 99, no. 1, pp. 338–360, 1921.

[308] S. Dufal, T. Lafitte, A. J. Haslam, A. Galindo, G. N. I. Clark, C. Vega, and G. Jackson, "The A in SAFT: developing the contribution of association to the Helmholtz free energy within a Wertheim TPT1 treatment of generic Mie fluids," *Molecular Physics*, vol. 113, no. 9-10, pp. 948–984, 2015.

[309] J. A. Barker and D. Henderson, "What is" liquid"? Understanding the states of matter," *Reviews of Modern Physics*, vol. 48, no. 4, p. 587, 1976.

[310] J. A. Barker and D. Henderson, "Perturbation theory and equation of state for fluids. II. A successful theory of liquids," *The Journal of chemical physics*, vol. 47, no. 11, pp. 4714–4721, 1967.

[311] G. Jackson, W. G. Chapman, and K. E. Gubbins, "Phase equilibria of associating fluids of spherical and chain molecules," *International Journal of Thermophysics*, vol. 9, pp. 769–779, 1988.

[312] W. G. Chapman, G. Jackson, and K. E. Gubbins, "Phase equilibria of associating fluids: chain molecules with multiple bonding sites," *Molecular Physics*, vol. 65, no. 5, pp. 1057–1079, 1988.

[313] G. Hefter, "When spectroscopy fails: the measurement of ion pairing," *Pure and applied chemistry*, vol. 78, no. 8, pp. 1571–1586, 2006.

[314] R. Buchner, "What can be learnt from dielectric relaxation spectroscopy about ion solvation and association?," *Pure and Applied Chemistry*, vol. 80, no. 6, pp. 1239–1252, 2008.

[315] R. Buchner, T. Chen, and G. Hefter, "Complexity in simple electrolyte solutions: ion pairing in MgSO4 (aq)," *The Journal of Physical Chemistry B*, vol. 108, no. 7, pp. 2365–2375, 2004.

[316] S. I. Mamatkulov, K. F. Rinne, R. Buchner, R. R. Netz, and D. J. Bonthuis, "Water-separated ion pairs cause the slow dielectric mode of magnesium sulfate solutions," *The Journal of Chemical Physics*, vol. 148, no. 22, 2018.

[317] A. Vila Verde and R. Lipowsky, "Cooperative slowdown of water rotation near densely charged ions is intense but short-ranged," *The Journal of Physical Chemistry B*, vol. 117, no. 36, pp. 10556–10566, 2013.

[318] A. V. Verde, M. Santer, and R. Lipowsky, "Solvent-shared pairs of densely charged ions induce intense but short-range supra-additive slowdown of water rotation," *Physical Chemistry Chemical Physics*, vol. 18, no. 3, pp. 1918–1930, 2016.

[319] W. M. Haynes, *CRC Handbook of Chemistry and Physics*. Boca Raton: CRC Press, 97 ed., 2016.

[320] R. Buchner, G. T. Hefter, and P. M. May, "Dielectric relaxation of aqueous NaCl solutions," *The Journal of Physical Chemistry A*, vol. 103, no. 1, pp. 1–9, 1999.

[321] K. F. Rinne, S. Gekle, and R. R. Netz, "Ion-specific solvation water dynamics: single water versus collective water effects," *The Journal of Physical Chemistry A*, vol. 118, no. 50, pp. 11667–11677, 2014.

[322] K. F. Rinne, S. Gekle, and R. R. Netz, "Dissecting ion-specific dielectric spectra of sodium-halide solutions into solvation water and ionic contributions," *The Journal of Chemical Physics*, vol. 141, no. 21, 2014.

[323] C. J. Fennell, A. Bizjak, V. Vlachy, and K. A. Dill, "Ion pairing in molecular simulations of aqueous alkali halide solutions," *The Journal of Physical Chemistry B*, vol. 113, no. 19, pp. 6782–6791, 2009.

[324] K. Yui, M. Sakuma, and T. Funazukuri, "Molecular dynamics simulation on ion-pair association of NaCl from ambient to supercritical water," *Fluid phase equilibria*, vol. 297, no. 2, pp. 227–235, 2010.

[325] M. Kelley, A. Donley, S. Clark, and A. Clark, "Structure and dynamics of NaCl ion pairing in solutions of water and methanol," *The Journal of Physical Chemistry B*, vol. 119, no. 51, pp. 15652–15661, 2015.

[326] A. P. Lyubartsev and A. Laaksonen, "Concentration effects in aqueous NaCl solutions. A molecular dynamics simulation," *The Journal of Physical Chemistry*, vol. 100, no. 40, pp. 16410–16418, 1996.

[327] J. Tong, B. Peng, G. M. Kontogeorgis, and X. Liang, "Behavior of the aqueous sodium chloride solutions from molecular simulations and theories," *Journal of Molecular Liquids*, vol. 371, p. 121086, 2023.

[328] S. Blazquez, M. M. Conde, and C. Vega, "Scaled charges for ions: An improvement but not the final word for modeling electrolytes in water," *The Journal of Chemical Physics*, vol. 158, no. 5, 2023.

[329] F. Yang, T. D. Ngo, J. S. R. Pinto, G. M. Kontogeorgis, and J.-C. de Hemptinne, "Systematic evaluation of parameterization approaches for the ePPC-SAFT model for aqueous alkali halide solutions," *Fluid Phase Equilibria*, vol. 570, p. 113778, 2023.

[330] G. M. Kontogeorgis and G. K. Folas, *Thermodynamic models for industrial applications: from classical and advanced mixing rules to association theories*. John Wiley & Sons, 2009.

[331] M. L. Michelsen and E. M. Hendriks, "Physical properties from association models," *Fluid phase equilibria*, vol. 180, no. 1-2, pp. 165–174, 2001.

[332] M. L. Michelsen, "Robust and efficient solution procedures for association models," *Industrial & engineering chemistry research*, vol. 45, no. 25, pp. 8449–8453, 2006.

[333] L. A. Romankiw and I. M. Chou, "Densities of aqueous sodium chloride, potassium chloride, magnesium chloride, and calcium chloride binary solutions in the concentration range 0.5-6.1 m at 25, 30, 35, 40, and 45. degree. C," *Journal of Chemical and Engineering Data*, vol. 28, no. 3, pp. 300–305, 1983.

[334] E. J. Reardon, "Dissociation constants of some monovalent sulfate ion pairs at 25. deg. from stoichiometric activity coefficients," *The Journal of Physical Chemistry*, vol. 79, no. 5, pp. 422–425, 1975.

[335] S. G. Capewell, G. Hefter, and P. M. May, "Potentiometric investigation of the weak association of sodium and carbonate ions at 25 C," *Journal of solution chemistry*, vol. 27, pp. 865–877, 1998.

[336] S. G. Capewell, G. T. Hefter, P. Sipos, and P. M. May, "Protonation and sodium ion-pairing of the sulfite ion in concentrated aqueous electrolyte solutions," *Journal of solution chemistry*, vol. 26, pp. 957–972, 1997.

[337] G. S. Pokrovski, J. Schott, and A. S. Sergeyev, "Experimental determination of the stability constants of NaSO4 and NaB (OH) 40 in hydrothermal solutions using a new high-temperature sodium-selective glass electrodeImplications for boron isotopic fractionation," *Chemical Geology*, vol. 124, no. 3-4, pp. 253–265, 1995.

[338] R. Buchner, S. G. Capewell, G. Hefter, and P. M. May, "Ion-pair and solvent relaxation processes in aqueous Na2SO4 solutions," *The Journal of Physical Chemistry B*, vol. 103, no. 7, pp. 1185–1192, 1999.

[339] J. Reimer, M. Steele-MacInnis, J. M. Wambach, and F. Vogel, "Ion association in hydrothermal sodium sulfate solutions studied by modulated FT-IR-Raman spectroscopy and molecular dynamics," *The Journal of Physical Chemistry B*, vol. 119, no. 30, pp. 9847–9857, 2015.

[340] E. Wernersson and P. Jungwirth, "Effect of water polarizability on the properties of solutions of polyvalent ions: Simulations of aqueous sodium sulfate with different force fields," *Journal of Chemical Theory and Computation*, vol. 6, no. 10, pp. 3233–3240, 2010.

[341] K. Fujita and M. Kimura, "The Raman band shape and vibrational relaxation of the ν1 mode of SO42 in Na2SO4 and (NH4) 2SO4 aqueous solutions," *Journal of Raman Spectroscopy*, vol. 11, no. 2, pp. 108–111, 1981.

[342] R. E. Hester and R. A. Plane, "A Raman spectrophotometric comparison of interionic association in aqueous solutions of metal nitrates, sulfates, and perchlorates," *Inorganic Chemistry*, vol. 3, no. 5, pp. 769–770, 1964.

[343] F. P. Daly, C. W. Brown, and D. R. Kester, "Sodium and magnesium sulfate ion pairing. Evidence from Raman spectroscopy," *The Journal of physical chemistry*, vol. 76, no. 24, pp. 3664–3668, 1972.

[344] T. J. Gilligan III and G. Atkinson, "Ultrasonic absorption in aqueous alkali metal sulfate solutions," *The Journal of Physical Chemistry*, vol. 84, no. 2, pp. 208–213, 1980.

[345] D. Eriksen, *Molecular-based approaches to modelling carbonate-reservoir fluids: Electrolyte phase equilibria, and the description of the fluid-fluid interface*. PhD thesis, Imperial College London, London, 2017.

[346] J. A. Rard, S. L. Clegg, and D. A. Palmer, "Isopiestic determination of the osmotic coefficients of Na2SO4 (aq) at 25 and 50 C, and representation with ion-interaction (Pitzer) and mole fraction thermodynamic models," *Journal of solution chemistry*, vol. 29, pp. 1–49, 2000.

[347] M. Eigen and U. K. Tamm, "Schallabsorption in Elektrolytlösungen als Folge chemischer Relaxation II. Meßergebnisse und Relaxationsmechanismen für 22-wertige Elektrolyte," *Zeitschrift für Elektrochemie, Berichte der Bunsengesellschaft für physikalische Chemie*, vol. 66, pp. 107–121, 3 1962.

[348] M. Eigen and K. Tamm, "Schallabsorption in elektrolytlösungen als folge chemischer relaxation I. Relaxationstheorie der mehrstufigen dissoziation," *Zeitschrift für Elektrochemie, Berichte der Bunsengesellschaft für physikalische Chemie*, vol. 66, no. 2, pp. 93–107, 1962.

[349] V. Tomišić and V. Simeon, "Raman spectra of aqueous solutions of strong electrolytes: evolving-factor analysis," *Physical Chemistry Chemical Physics*, vol. 2, no. 9, pp. 1943–1949, 2000.

[350] S. Jahn and C. Schmidt, "Speciation in aqueous MgSO4 fluids at high pressures and high temperatures from ab initio molecular dynamics and Raman spectroscopy," *The Journal of Physical Chemistry B*, vol. 114, no. 47, pp. 15565–15572, 2010.

[351] F. Rull, C. Balarew, J. L. Alvarez, F. Sobron, and A. Rodriguez, "Raman spectroscopic study of ion association in aqueous magnesium sulphate solutions," *Journal of Raman Spectroscopy*, vol. 25, no. 12, pp. 933–941, 1994.

[352] A. R. Davis and B. G. Oliver, "Raman spectroscopic evidence for contact ion pairing in aqueous magnesium sulfate solutions," *The Journal of Physical Chemistry*, vol. 77, no. 10, pp. 1315–1316, 1973.

[353] L. Gotte, K. M. Parry, W. Hua, D. Verreault, H. C. Allen, and D. J. Tobias, "Solvent-shared ion pairs at the airsolution interface of magnesium chloride and sulfate solutions revealed by sum frequency spectroscopy and molecular dynamics simulations," *The Journal of Physical Chemistry A*, vol. 121, no. 34, pp. 6450–6459, 2017.

[354] A. C. Tikanen and W. R. Fawcett, "The role of solvent permittivity in estimation of electrolyte activity coefficients for systems with ion pairing on the basis of the mean spherical approximation," *Berichte der Bunsengesellschaft für physikalische Chemie*, vol. 100, no. 5, pp. 634–640, 1996.

[355] D. G. Archer and J. A. Rard, "Isopiestic Investigation of the Osmotic and Activity Coefficients of Aqueous MgSO4 and the Solubility of MgSO4 7H2O (cr) at 298.15 K: Thermodynamic Properties of the MgSO4+ H2O System to 440 K," *Journal of Chemical & Engineering Data*, vol. 43, no. 5, pp. 791–806, 1998.

[356] F. Malatesta and R. Zamboni, "Activity and osmotic coefficients from the EMF of liquid membrane cells. VI-ZnSO 4, MgSO 4, CaSO 4, and SrSO 4 in water at 25 C," *Journal of solution chemistry*, vol. 26, pp. 791–815, 1997.

[357] J. Miladinović, R. Ninković, M. Todorović, and J. A. Rard, "Isopiestic Investigation of the Osmotic and Activity Coefficients of {y MgCl 2+(1 y) MgSO 4}(aq) and the Osmotic Coefficients of Na 2 SO 4 MgSO 4 (aq) at 298.15 K," *Journal of solution chemistry*, vol. 37, pp. 307–329, 2008.

[358] C. W. Childs and R. F. Platford, "Excess free energies of mixing at temperatures below 25°. Isopiestic measurements on the systems H2O-NaCl-Na2SO4 and H2O-NaCl-MgSO4," *Australian Journal of Chemistry*, vol. 24, no. 12, pp. 2487–2491, 1971.

[359] J. Zhang, D. Li, Y. Yao, B. Sun, D. Zeng, and P.-S. Song, "Thermodynamic properties of LiCl+ MgSO4+ H2O at temperatures from 273.15 K to 373.15 K and representation with Pitzer ion-interaction model," *Journal of Chemical & Engineering Data*, vol. 61, no. 7, pp. 2277–2291, 2016.

[360] W. Kangro and A. Groeneveld, "Konzentrierte wäßrige Lösungen, I," *Zeitschrift für Physikalische Chemie*, vol. 32, no. 1_2, pp. 110–126, 1962.

[361] R. F. Platford, "Osmotic coefficients of aqueous solutions of seven compounds at 0. deg.," *Journal of Chemical and Engineering Data*, vol. 18, no. 2, pp. 215–217, 1973.

[362] J. A. Rard and D. G. Miller, "Isopiestic determination of the Osmotic coefficients of aqueous sodium sulfate, magnesium sulfate, and sodium sulfate-magnesium sulfate at 25. degree. C," *Journal of Chemical and Engineering Data*, vol. 26, no. 1, pp. 33–38, 1981.

[363] B. M. Fabuss, A. Korosi, and A. K. M. S. Hug, "Densities of Binary and Ternary Aqueous Solutions of NaCl, Na2SO4 and MgSO4 of Sea Waters, and Sea Water Concentrates.," *Journal of Chemical and Engineering Data*, vol. 11, no. 3, pp. 325–331, 1966.

[364] A. Korosi and B. M. Fabuss, "Viscosities of binary aqueous solutions of sodium chloride, potassium chloride, sodium sulfate, and magnesium sulfate at concentrations and temperatures of interest in desalination processes," *Journal of Chemical & Engineering Data*, vol. 13, no. 4, pp. 548–552, 1968.

[365] W. Ebeling, S. Hilbert, and H. Krienke, "On Bjerrum's mass action law for electrolytes and Onsager's bookkeeping rule," *Journal of molecular liquids*, vol. 96, pp. 409–423, 2002.

[366] G. Atkinson and S. Petrucci, "Ion association of magnesium sulfate in water at 25," *The Journal of Physical Chemistry*, vol. 70, no. 10, pp. 3122–3128, 1966.

[367] A. A. Chen and R. V. Pappu, "Quantitative characterization of ion pairing and cluster formation in strong 1: 1 electrolytes," *The Journal of Physical Chemistry B*, vol. 111, no. 23, pp. 6469–6478, 2007.

[368] H. Krienke, J. Barthel, M. Holovko, I. Protsykevich, and Y. Kalyushnyi, "Osmotic and activity coefficients of strongly associated electrolytes over large concentration ranges from chemical model calculations," *Journal of Molecular Liquids*, vol. 87, no. 2-3, pp. 191–216, 2000.

[369] R. Buchner, G. T. Hefter, and P. M. May, "Dielectric relaxation of aqueous NaCl solutions," *Journal of Physical Chemistry A*, vol. 103, no. 1, pp. 1–9, 1999.

Appendices

APPENDIX A

PhD Activities

A.1 List of Publications

1. S. Naseri Boroujeni, X. Liang, B. Maribo-Mogensen, and G. M. Kontogeorgis, 2022. Comparison of Models for the Prediction of the Electrical Conductivity of Electrolyte Solutions. Industrial & Engineering Chemistry Research, 61(8), pp. 3168-3185.

2. S. Naseri Boroujeni, B. Maribo-Mogensen, X. Liang, and G. M. Kontogeorgis, 2023. On the Estimation of Equivalent conductivity of Electrolyte Solutions: The Effect of Relative Static Permittivity and Viscosity. Fluid Phase Equilibria, 567, p. 113698.

3. S. Naseri Boroujeni, B. Maribo-Mogensen, X. Liang, and G. M. Kontogeorgis, 2023. Mean Ionic Activity Coefficient of Associative Electrolyte Solutions: A Comparison Study. Journal of Molecular Liquids, 386, p. 122509.

4. S. Naseri Boroujeni, B. Maribo-Mogensen, X. Liang, and G. M. Kontogeorgis, 2023. New Electrical Conductivity Model for Electrolyte Solutions Based on the Debye-Hückel-Onsager Theory. Journal of Physical Chemistry B, 127(11), pp. 9954-9975.

5. S. Naseri Boroujeni, B. Maribo-Mogensen, X. Liang, and G. M. Kontogeorgis, 2023. Binding Debye-Hückel Theory for Associative Electrolyte Solutions. Journal of Chemical Physics, 159 (15), p. 154503.

6. S. Naseri Boroujeni, B. Maribo-Mogensen, X. Liang, and G. M. Kontogeorgis, 2023. A Novel Model for Predicting the Electrical Conductivity of Multi-salt Electrolyte Solutions. Journal of Physical Chemistry B (submitted).

7. S. Naseri Boroujeni, B. Maribo-Mogensen, X. Liang, and G. M. Kontogeorgis, 2024. A Theoretical and Practical Investigation of Ion-ion Association in Electrolyte Solutions (in preparation).

A.2 Attended Conferences

A.2.1 International Conferences

1. 32nd ESAT, Graz, Austria, 2022. Oral: Electrical Conductivity of Associative Electrolyte Solutions. S. Naseri Boroujeni, B. Maribo-Mogensen, X. Liang, and G. M. Kontogeorgis.

2. 32nd ESAT, Graz, Austria, 2022. Poster: A Predictive Analysis of Electrical Conductivity Models for Electrolyte Solutions. S. Naseri Boroujeni, B. Maribo-Mogensen, X. Liang, and G. M. Kontogeorgis.

3. 27th Thermodynamics Conference, Bath, UK, 2022. Poster: A Predictive Analysis of Implicit Solvent Models for Associative Electrolyte Solutions. S. Naseri Boroujeni, B. Maribo-Mogensen, X. Liang, and G. M. Kontogeorgis.

4. 27th Thermodynamics Conference, Bath, UK, 2022. Poster: Thermodynamic Properties of Associative Electrolyte Solutions; An Implicit Solvent Model. S. Naseri Boroujeni, B. Maribo-Mogensen, X. Liang, and G. M. Kontogeorgis.
5. PPEPPD, Tarragona, Spain, 2023. Poster: A New Model for the Electrical Conductivity of Electrolyte Solutions from the Debye-Hückel-Onsager Theory. S. Naseri Boroujeni, B. Maribo-Mogensen, X. Liang, and G. M. Kontogeorgis.
6. AIChE Annual Meeting, Orlando, USA, 2023. Oral: A Unified Model for the Thermodynamic, Transport, and Physical Properties of Associative Electrolyte Solutions. S. Naseri Boroujeni, B. Maribo-Mogensen, X. Liang, and G. M. Kontogeorgis.
7. AIChE Annual Meeting, Orlando, USA, 2023. Oral: Binding Debye-Hückel Equation of State for Charged Hard Sphere Fluids. S. Naseri Boroujeni, B. Maribo-Mogensen, X. Liang, and G. M. Kontogeorgis.

A.2.2 Internal Meetings

1. CERE and KT Consortium Annual Discussion Meeting, online, 2021. Oral: An Evaluation Study of the Reliability and Applicability of Current Electric Conductance Models in Electrolyte Solutions. S. Naseri Boroujeni, X. Liang, B. Maribo-Mogensen, and G. M. Kontogeorgis.
2. CERE and KT Consortium Annual Discussion Meeting, Snekkersten, Denmark, 2022. Oral: Ion-ion Association Insight from Electrical Conductivity and Mean Ionic Activity Coefficient. S. Naseri Boroujeni, B. Maribo-Mogensen, X. Liang, and G. M. Kontogeorgis.
3. CERE and KT Consortium Annual Discussion Meeting, Snekkersten, Denmark, 2022. Poster: Thermodynamic Properties of Associative Electrolyte Solutions; A Chemical Approach. S. Naseri Boroujeni, B. Maribo-Mogensen, X. Liang, and G. M. Kontogeorgis.
4. ERC Project Internal Meeting, Online, 2023. Oral: Ion-ion Association in Electrolyte Solutions. S. Naseri Boroujeni, B. Maribo-Mogensen, X. Liang, and G. M. Kontogeorgis.
5. CERE and KT Consortium Annual Discussion Meeting, Hesingør, Denmark, 2023. Oral: Ion-ion Association in Electrolyte Solutions; A Theoretical Study of Mean Ionic Activity Coefficient, Electrical Conductivity, and Relative Static Permittivity. S. Naseri Boroujeni, B. Maribo-Mogensen, X. Liang, and G. M. Kontogeorgis.
6. CERE and KT Consortium Annual Discussion Meeting, Hesingør, Denmark, 2023. Poster: Debye-Hückel Based Theories for Thermodynamic and Transport Properties of Charged Hard Sphere Fluids. S. Naseri Boroujeni, B. Maribo-Mogensen, X. Liang, and G. M. Kontogeorgis.

A.3 Attended Courses

1. Thermodynamic Models Fundamentals and Computational Aspects
2. Electrolyte Solutions: Thermodynamics, Crystallization, Separation methods
3. Summer School on Uncertainty and Sensitivity Analysis of Model Output in Engineering Applications

4. How to write a Scientific Paper
5. Sustainability Evaluation and Communication
6. Advances in Chemical and Biochemical Engineering

A.4 Teaching

1. Teacher Assistant in Thermodynamic Models Fundamentals and Computational Aspects
2. Teacher Assistant in Chemical Engineering Model Analysis

APPENDIX B
Electrical Conductivity Models

B.1 MSA Model

$$\frac{\delta k_1^{Rel}}{k} = -\frac{\kappa_q^2}{3} \mathrm{F}_{1,ij} \mathrm{F}_{2,ij} \tag{B.1}$$

$$\mathrm{F}_{1,ij} = \left[\mathrm{i}_0 \left(\kappa_q \sigma_{ij} \right) - \frac{4\pi\varepsilon_0\varepsilon_r k_B T}{e^2 Z_i Z_j} \kappa_q \sigma_{ij}^2 \mathrm{i}_1 \left(\kappa_q \sigma_{ij} \right) \right] \tag{B.2}$$

$$i_0 \left(\kappa_q \sigma_{ij} \right) = \frac{\sinh \left(\kappa_q \sigma_{ij} \right)}{\kappa_q \sigma_{ij}} \tag{B.3}$$

$$i_1 \left(\kappa_q \sigma_{ij} \right) = \frac{\cosh \left(\kappa_q \sigma_{ij} \right)}{\kappa_q \sigma_{ij}} - \frac{\sinh \left(\kappa_q \sigma_{ij} \right)}{\kappa_q^2 \sigma_{ij}^2} \tag{B.4}$$

$$\mathrm{F}_{2,ij} = \left[\frac{-\kappa_q \mathrm{A}_{ij} \exp \left(-\kappa_q \sigma_{ij} \right)}{\kappa_q^2 + 2\Gamma\kappa_q + 2\Gamma^2 - \frac{2\Gamma^2}{\alpha^2} \sum_k \rho_k a_k^2 \exp \left(-\kappa_q \sigma_k \right)} \right] \tag{B.5}$$

$$\mathrm{A}_{ij} = \frac{e^2 Z_i Z_j}{4\pi\varepsilon_0\varepsilon_r k_B T \left(1 + \Gamma\sigma_i \right) \left(1 + \Gamma\sigma_j \right)} \tag{B.6}$$

$$4\Gamma^2 = \frac{e^2}{\varepsilon_0\varepsilon_r k_B T} \sum_k \rho_k \left(\frac{Z_k - \frac{\pi}{2\Delta} P_n \sigma_k^2}{\left(1 + \Gamma\sigma_k \right)} \right)^2 \tag{B.7}$$

$$P_n = \frac{1}{\Omega} \sum_k \frac{\rho_k \sigma_k Z_k}{1 + \Gamma\sigma_k} \tag{B.8}$$

$$\Omega = 1 + \frac{\pi}{2\Delta} \sum_k \frac{\rho_k \sigma_k^3}{1 + \Gamma\sigma_k} \tag{B.9}$$

$$\Delta = 1 - \frac{\pi}{6} \sum_k \rho_k \sigma_k^3 \tag{B.10}$$

$$a_k \approx \frac{\alpha^2}{2\Gamma} \frac{Z_k}{1 + \Gamma\sigma_k} \tag{B.11}$$

$$\alpha^2 = \frac{e^2}{\varepsilon_0\varepsilon_r k_B T} \tag{B.12}$$

$$\frac{\delta k_2^{Rel}}{k} = -\frac{\kappa_q^2}{3} \mathrm{B}_{ij}^2 \mathrm{F}_{1,ij} \left[\left(\frac{x^2 + \kappa_q^2}{x^2 - \kappa_q^2} \right) \mathrm{F}_{3,ij} + \frac{\kappa_q \mathrm{C}_{ij}}{x - \kappa_q} \mathrm{F}_{4,ij} + \left(1 + x\sigma_{ij} \right) \mathrm{F}_{5,ij} \right] \tag{B.13}$$

$$\mathrm{F}_{3,ij} = \frac{\kappa_q^2}{4x^2}\exp\left(2x\sigma_{ij}\right)\mathrm{E}_1\left(\left(2x+\kappa_q\right)\sigma_{ij}\right) + \frac{\exp\left(-\kappa_q\sigma_{ij}\right)}{4x^2\sigma_{ij}^2}\left[1+\left(2x-\kappa_q\right)\sigma_{ij}\right] \tag{B.14}$$

$$\begin{aligned}\mathrm{F}_{4,ij} = \quad & \frac{x^2-2\kappa_q^2}{2\kappa_q\left(x+\kappa_q\right)}\exp\left(x\sigma_{ij}\right)\mathrm{E}_1\left(\left(x+2\kappa_q\right)\sigma_{ij}\right) \\ & -\frac{\exp\left(-2\kappa_q\sigma_{ij}\right)}{2\kappa_q\left(x+\kappa_q\right)\sigma_{ij}^2}\left(1+x\sigma_{ij}\right) + \frac{\kappa_q \mathrm{C}_{ij}}{x-\kappa_q}\mathrm{F}_{ij}^4\end{aligned} \tag{B.15}$$

$$\begin{aligned}\mathrm{F}_{5,ij} = \quad & \frac{\left(x^2-\kappa_q^2\right)^2}{4x^2\kappa_q^2}\exp\left(x\sigma_{ij}\right)\mathrm{E}_1\left(\left(x+\kappa_q\right)\sigma_{ij}\right) \\ & -\frac{x^2}{4\kappa_q^2}\exp\left(\left(x-\kappa_q\right)\sigma_{ij}\right)\mathrm{E}_1\left(x\sigma_{ij}\right)\left(1+\kappa_q\sigma_{ij}\right) \\ & +\frac{\exp\left(-\kappa_q\sigma_{ij}\right)}{4x^2\kappa_q^2}\left(1+\left(x-\kappa_q\right)\sigma_{ij}+\frac{x^3\sigma_{ij}^2}{\kappa_q}\right)\end{aligned} \tag{B.16}$$

$$\mathrm{B}_{ij} = \frac{e^2 Z_i Z_j}{4\pi\varepsilon_0\varepsilon_r k_B T\left(1+\Gamma\sigma_i\right)\left(1+\Gamma\sigma_j\right)\left(1+\Gamma^2\bar{\sigma^2}\right)} \tag{B.17}$$

$$\mathrm{C}_{ij} = \cosh\left(\kappa_q\sigma_{ij}\right) + \frac{x}{\kappa_q}\sinh\left(\kappa_q\sigma_{ij}\right) \tag{B.18}$$

$$\mathrm{E}_1\left(r\right) = \int_r^\infty \frac{\exp\left(-\kappa_q r\right)}{r}dr \tag{B.19}$$

$$x = \frac{2\Gamma\left(1+\Gamma\bar{\sigma}\right)}{1-\Gamma^2\bar{d\sigma}^2} \tag{B.20}$$

$$\bar{\sigma}^n = \frac{1}{\alpha^2}\sum_k \rho_k a_k^2 \sigma_k^n \tag{B.21}$$

$$\frac{\delta k_1^{Hyd}}{k} = \frac{-4\Gamma^2\mathrm{B}_{ij}k_B T}{48\pi\eta\left(D_i^0+D_j^0\right)}\mathrm{F}_{1,ij}\left[\left(1+x\sigma_{ij}+\frac{x^2\sigma_{ij}^2}{3}\right)\mathrm{F}_{6,ij}+\mathrm{F}_{7,ij}\right] \tag{B.22}$$

$$\begin{aligned}\mathrm{F}_{6,ij} = \quad & \frac{x^2}{\kappa_q^2}\exp\left(\left(x-\kappa_q\right)\sigma_{ij}\right)\mathrm{E}_1\left(x\sigma_{ij}\right)\left(1+\kappa_q\sigma_{ij}\right) \\ & -\frac{x^2\exp\left(-\kappa_q\sigma_{ij}\right)}{\kappa_q\left(x+\kappa_q\right)} - \frac{x^2}{\kappa_q^2}\mathrm{E}_1\left(\left(x+\kappa_q\right)\sigma_{ij}\right) \\ & +\left(\frac{\left(2x^2-\kappa_q^2\right)}{x^2}\right)\exp\left(x\sigma_{ij}\right)\mathrm{E}_1\left(\left(x+\kappa_q\right)\sigma_{ij}\right) \\ & -\frac{\exp\left(-\kappa_q\sigma_{ij}\right)}{x^2\sigma_{ij}^2}\left(1+\left(x-\kappa_q\right)\sigma_{ij}\right) - \frac{x\exp\left(-\kappa_q\sigma_{ij}\right)}{x+\kappa_q}\end{aligned} \tag{B.23}$$

$$\begin{aligned} \mathrm{F}_{7,ij} = \quad & \frac{\exp\left(-\kappa_q \sigma_{ij}\right)}{x^2 \sigma_{ij}^2} \left(1 + \left(2x - \kappa_q\right) \sigma_{ij}\right) \\ & - \frac{\left(4x^2 - \kappa_q^2\right)}{x^2} \exp\left(2x\sigma_{ij}\right) \mathrm{E}_1\left(\left(2x + \kappa_q\right) \sigma_{ij}\right) \end{aligned} \tag{B.24}$$

$$\frac{\delta\ v^{el\ 1}}{v_i^0} = -\frac{k_B T}{3\pi\eta D_i^0} \left[\frac{\Gamma}{1 + \Gamma\sigma_i} + \frac{\pi}{2\Delta} \frac{P_n \sigma_i}{Z_i \left(1 + \Gamma\sigma_i\right)} + \frac{\pi}{Z_i} \sum_k \rho_k \sigma_k \sigma_{ik}^2 \right] \tag{B.25}$$

$$\frac{\delta\ v^{el\ 2}}{v_i^0} = \mathrm{F}_{8,ij} + \mathrm{F}_{9,ij} \tag{B.26}$$

$$\begin{aligned} \mathrm{F}_{8,ij} = \quad & \frac{k_B T \kappa_q^2 \mathrm{B}_{ij}}{24\pi\eta D_i^0 \left(x^2 - \kappa_q^2\right) \sigma_{ij}^2 \left(1 + \Gamma\sigma_i\right) \left(1 + \Gamma\sigma_j\right)} \\ & \Bigg[\left(1 + 2x\sigma_{ij}\right) - \mathrm{C}_{ij} \exp\left(-x\sigma_{ij}\right) \left(1 + \left(x - \kappa_q\right) \sigma_{ij}\right) \\ & - 2x^2 \sigma_{ij}^2 \exp\left(2x\sigma_{ij}\right) \mathrm{E}_1\left(2x\sigma_{ij}\right) \\ & + \mathrm{C}_{ij} \left(x^2 + \kappa_q^2\right) \sigma_{ij}^2 \exp\left(x\sigma_{ij}\right) \mathrm{E}_1\left(\left(x + \kappa_q\right) \sigma_{ij}\right) \Bigg] \end{aligned} \tag{B.27}$$

$$\begin{aligned} \mathrm{F}_{9,ij} = \quad & \frac{k_B T}{12\pi\eta D_i^0 \left(1 + \Gamma\sigma_i\right) \left(1 + \Gamma_j\right)} \left[\cosh\left(\kappa_q \sigma_{ij}\right) - \frac{\sinh\left(\kappa_q \sigma_{ij}\right)}{\kappa_q \sigma_{ij}} \right] \\ & \left[\frac{\kappa_q^3 \exp\left(-\kappa_q \sigma_{ij}\right)}{\kappa_q^2 + 2\Gamma\kappa_q + 2\Gamma^2 - \frac{2\Gamma^2}{\alpha^2} \sum_k \rho_k a_k^2 \exp\left(-\kappa_q \sigma_k\right)} \right] \end{aligned} \tag{B.28}$$

B.2 QV Model

$$
\begin{aligned}
\frac{\delta k_{1,2}}{k} \quad &= -\frac{\kappa a b}{3}\frac{q}{1+\sqrt{q}}\frac{1+\left(1+\sqrt{q}\right)\left(\frac{\kappa a}{2}\right)}{(1+\kappa a)\left[1+\kappa a\sqrt{q}+q\left(\frac{\kappa^2 a^2}{3}\right)\right]} \\
&+\frac{\kappa^2 a^2}{6}\frac{q}{\left[1+\kappa a\sqrt{q}+q\left(\frac{\kappa^2 a^2}{3}\right)\right]}+\frac{\kappa^2 a^2 b^2}{6}q\frac{\mathrm{P}_1(\kappa a,\ q)}{(1+\kappa a)^2\left[1+\kappa a\sqrt{q}+q\left(\frac{\kappa^2 a^2}{3}\right)\right]} \\
&+\frac{\kappa^2 a^2 b}{6}q\frac{\mathrm{P}_2(\kappa a,\ q)}{(1+\kappa a)^2\left[1+\kappa a\sqrt{q}+q\left(\frac{\kappa^2 a^2}{3}\right)\right]} \\
&-\frac{\kappa^2 a^2 b^2}{6}\frac{q}{1-q}\frac{\mathrm{P}_3(\kappa a,\ q)}{(1+\kappa a)^2\left[1+\kappa a\sqrt{q}+q\left(\frac{\kappa^2 a^2}{3}\right)\right]^2} \\
&-\frac{\kappa^4 a^4 b}{12}q\frac{\mathrm{P}_4(\kappa a,\ q)}{(1+\kappa a)^2\left[1+\kappa a\sqrt{q}+q\left(\frac{\kappa^2 a^2}{3}\right)\right]} \\
&+Fe\frac{\kappa^2 a b}{48\pi\eta}q\frac{(|Z_+|+|Z_-|)}{\lambda_+^0+\lambda_-^0}\frac{\mathrm{P}_5(\kappa a,\ q)}{(1+\kappa a)^2\left[1+\kappa a\sqrt{q}+q\left(\frac{\kappa^2 a^2}{3}\right)\right]} \\
&+Fe\frac{\kappa^2 a}{36\pi\eta}q\frac{(|Z_+|+|Z_-|)}{\lambda_+^0+\lambda_-^0}\frac{1}{(1+\kappa a)^2\left[1+\kappa a\sqrt{q}+q\left(\frac{\kappa^2 a^2}{3}\right)\right]} \\
&-\frac{\kappa^2 a^2 b^2}{9}\left(\frac{q}{1+\sqrt{q}}\right)^2\left[\frac{1+\left(1+\sqrt{q}\right)\left(\frac{\kappa a}{2}\right)}{(1+\kappa a)\left[1+\kappa a\sqrt{q}+q\left(\frac{\kappa^2 a^2}{3}\right)\right]}\right]^2 \\
&+\frac{\kappa^4 a^4}{36}\frac{q^2}{\left[1+\kappa a\sqrt{q}+q\left(\frac{\kappa^2 a^2}{3}\right)\right]^2}
\end{aligned}
\tag{B.29}
$$

$$
\begin{aligned}
\frac{\Delta k_2^P}{k} \quad &= -\frac{\kappa^2 a^2}{6}\left(\frac{q}{b}-\frac{q}{1+\kappa a}\right) \\
&-\frac{\kappa^3 a^3}{9}\frac{q^2}{1+\sqrt{q}}\frac{1+\left(1+\sqrt{q}\right)\left(\frac{\kappa a}{2}\right)}{(1+\kappa a)\left[1+\kappa a\sqrt{q}+q\left(\frac{\kappa^2 a^2}{3}\right)\right]} \\
&-\frac{\kappa^4 a^4}{18 b}\frac{q^2}{1+\sqrt{q}}\frac{1}{\left[1+\kappa a\sqrt{q}+q\left(\frac{\kappa^2 a^2}{3}\right)\right]}
\end{aligned}
\tag{B.30}
$$

$$
\begin{aligned}
\frac{\delta v_i}{v_i^0} \quad &= \frac{Fe\,|Z_i|}{\lambda_i^0}\Bigg[-\frac{\kappa}{6\pi\eta\,(1+\kappa a)}-\frac{\kappa^2 abZ_i}{12\pi\eta}\frac{(Z_+ + Z_-)}{|Z_+|\,|Z_-|}\frac{\mathrm{Tr}\,(2\kappa a)}{1+\kappa a} \\
&+\frac{\kappa^3 a^2}{36\pi\eta}\frac{q^2}{1+\sqrt{q}}\frac{1+\left(1+\sqrt{q}\right)\left(\frac{\kappa a}{2}\right)}{(1+\kappa a)\left[1+\kappa a\sqrt{q}+q\left(\frac{\kappa^2 a^2}{3}\right)\right]} \\
&-\frac{\kappa^2 a}{48\pi\eta}q\frac{(1+\kappa a)+\kappa^2 a^2\mathrm{Tr}\,(\kappa a)}{(1+\kappa a)} \\
&-\frac{\kappa^2 ab}{48\pi\eta}q\frac{\mathrm{Tr}\,(2\kappa a)-0.5\left[1+\kappa a+\frac{\kappa^2 a^2}{2}\right]\mathrm{Tr}\,(\kappa a)-\frac{(3+\kappa a)}{4}}{(1+\kappa a)^2}+\frac{\kappa^2 a}{24\pi\eta}\frac{q}{b} \\
&+\frac{\kappa^4 a^3}{72\pi\eta}\frac{q^2}{1-q}\frac{1}{\left[1+\kappa a\sqrt{q}+q\left(\frac{\kappa^2 a^2}{3}\right)\right]}\frac{1}{b}-\frac{\kappa^2 a}{24\pi\eta}\frac{q}{1+\kappa a} \\
&-\frac{\kappa^2 ab}{24\pi\eta}\frac{q}{1-q}\frac{\mathrm{Q}_1\,(\kappa a,\ q)}{(1+\kappa a)^2\left[1+\kappa a\sqrt{q}+q\left(\frac{\kappa^2 a^2}{3}\right)\right]} \\
&-\frac{\kappa^4 a^3}{48\pi\eta}\frac{q}{1-q}\frac{\mathrm{Q}_2\,(\kappa a,\ q)}{(1+\kappa a)^2\left[1+\kappa a\sqrt{q}+q\left(\frac{\kappa^2 a^2}{3}\right)\right]}\Bigg]
\end{aligned}
\tag{B.31}
$$

$$
\mathrm{Tr}\,(\gamma\kappa a)=\exp(\gamma\kappa a)\int_\infty^a\frac{\exp(-\gamma\kappa r)}{r}dr \tag{B.32}
$$

For the formulation of $\mathrm{Q}_{1,2}\,(\kappa a,\ q)$ and $P_{1,2,\ldots,5}\,(\kappa a,\ q)$, the reader can refer to the original papers [103–105].

APPENDIX C

Implicit Solvent Models

C.1 Ebeling and Grigo (EG) Approach

$$\frac{\beta}{N}A^r = \frac{\beta}{N}\left(A^{HS} + A^{MSA}\right) \tag{C.1}$$

$$\beta P = \beta\left(P^{id} + P^{HS} + P^{MSA}\right) \tag{C.2}$$

$$\ln \gamma_i'^c = \left(\ln \gamma_i^{HS} + \ln {\gamma_i}^{MSA}\right) \tag{C.3}$$

$$\gamma_{\pm}^c = \alpha \gamma_{\pm}'^c \tag{C.4}$$

$$\frac{\beta A^{HS}}{N} = \frac{\eta\left(4-3\eta\right)}{\left(1-\eta\right)^2} \tag{C.5}$$

$$\beta P^{HS} = \rho_0 \frac{2\eta\left(2-\eta\right)}{\left(1-\eta\right)^3} \tag{C.6}$$

$$\ln {\gamma_i}^{HS} = \frac{3\eta^3 - 9\eta^2 + 8\eta}{\left(1-\eta\right)^3} \tag{C.7}$$

$$\eta = \frac{\pi\rho_0\sigma^3}{6} \tag{C.8}$$

$$\frac{\beta A^{MSA}}{N} = -\frac{1}{12\pi\rho_0\sigma^3}\left[2 + 6x' - 3x'^2 - 2\left(1+2x'\right)^{3/2}\right] \tag{C.9}$$

$$\beta P^{MSA} = \frac{1}{12\pi\sigma^3}\left[2 + 3x' - 3x'\left(1+2x'\right)^{1/2} - 2\left(1+2x'\right)^{3/2}\right] \tag{C.10}$$

$$\ln {\gamma_i}^{MSA} = -b\left(\frac{x'\left(1+x'-\sqrt{1+2x'}\right)}{\sqrt{1+2x'}}\right) \tag{C.11}$$

$$x' = \kappa'\sigma = \sqrt{\frac{\alpha\rho_0\left(Ze\right)^2}{k_B T \varepsilon_0 \varepsilon_r}}\sigma \tag{C.12}$$

$$\frac{2\left(1-\alpha\right)}{\rho_0\alpha^2} = K_{+-}^{\circ}\left[\gamma_{\pm}'^{MSA}\right]^2 \tag{C.13}$$

C.2 Fisher-Levin-Guillot-Guissani (FLGG) Approach

$$\beta P = \beta \left(P^{id} + P^{HS} + P^{DH} + P^{DI} \right) \tag{C.14}$$

$$\ln \gamma_i'^{c} = \left(\ln {\gamma_i}^{HS} + \ln {\gamma_i}^{DH} + \ln {\gamma_i}^{DI} \right) \tag{C.15}$$

$$\frac{2\left(1-\alpha\right)}{\rho_0 \alpha^2} = K_A^0 \ \frac{\gamma_+ \gamma_-}{\gamma_{ip}} \tag{C.16}$$

$$\frac{\beta A^{HS}}{N} = \left(1+\alpha\right) \rho_0 \frac{\eta_m \left(4 - \ 3\eta_m\right)}{2\left(1 - \ \eta_m\right)^2} \tag{C.17}$$

$$\eta_m = \frac{1}{12} \pi \left(1+\alpha\right) \rho_0 \sigma_m^3 \tag{C.18}$$

$$\sigma_m = \left(\frac{2\alpha}{1+\alpha} \right)^2 \sigma^3 + \frac{4\alpha\left(1-\alpha\right)}{\left(1+\alpha\right)^2} \left(\frac{\sigma + \sigma_{eff}}{2} \right)^3 + \left(\frac{1-\alpha}{1+\alpha} \right)^2 \sigma_{eff}^3 \tag{C.19}$$

$$\beta P^{HS} = \left(1+\alpha\right) \frac{\rho_0}{2} \frac{2\eta_m \left(2 - \eta_m\right)}{\left(1-\eta_m\right)^3} \tag{C.20}$$

$$\ln {\gamma_i}^{HS} = \eta_m \frac{3{\eta_m}^2 - 9\eta_m + 8}{\left(1-\eta_m\right)^3} + 2\eta_m \frac{2-\eta_m}{\left(1-\eta_m\right)^3} f\left(\alpha\right) \tag{C.21}$$

$$f\left(\alpha\right) = \frac{4\alpha\left(1-\alpha\right)}{\left(1+\alpha\right)^2} \left(\frac{\sigma}{\sigma_m} \right)^3 + \left(\frac{\left(1-\alpha\right)^2 - 2\alpha\left(1-\alpha\right)}{\left(1+\alpha\right)^2} \right) \left(\frac{\sigma + \sigma_{eff}}{2\sigma_m} \right)^3 - 2 \left(\frac{1-\alpha}{1+\alpha} \right)^2 \left(\frac{\sigma_{eff}}{\sigma_m} \right)^3 \tag{C.22}$$

$$\frac{\beta A^{DH}}{N} = -\frac{1}{4\pi\rho_0\sigma^3} \left[\ln\left(1+x'\right) - x' + \frac{x'^2}{2} \right] \tag{C.23}$$

$$\beta P^{DH} = -\frac{1}{8\pi\sigma^3} \left[\left(1+x'\right) - \frac{1}{1+x'} - 2\ln\left(1+x'\right) \right] \tag{C.24}$$

$$\ln {\gamma_i}^{DH} = -\frac{\lambda Z^2}{2\sigma} \frac{x'}{1+x'} \tag{C.25}$$

$$\frac{\beta A^{DI}}{N} = -\frac{e^2 Z^2}{8\pi\varepsilon_0\varepsilon_r k_B T \sigma} \left(1-\alpha\right) \left(\frac{\sigma}{\sigma_{eff}} \right)^3 x_{eff}^2 \omega\left(x_{eff}\right) \tag{C.26}$$

$$\omega\left(x_{eff}\right) = \frac{3}{x_{eff}^4} \left[\ln\left(1 + x_{eff} + \frac{1}{3}x_{eff}^2\right) - x_{eff} + \frac{1}{6}x_{eff}^2 \right] \tag{C.27}$$

$$P^{DI} = \frac{e^2 Z^2}{16\pi\varepsilon_0\varepsilon_r k_B T \sigma} \left(1-\alpha\right) \rho_0 \left(\frac{\sigma}{\sigma_{eff}} \right)^3 \Omega\left(x_{eff}\right) \tag{C.28}$$

$$\Omega\left(x_{eff}\right) = \frac{3}{x_{eff}} \left[\frac{\ln\left(1 + x_{eff} + \frac{1}{3}x_{eff}^2\right)}{x_{eff}} - \frac{1 + \frac{5}{6}x_{eff} + \frac{1}{6}x_{eff}^2}{1 + x_{eff} + \frac{1}{3}x_{eff}^2} \right] \tag{C.29}$$

$$\ln {\gamma_i}^{DI} = -\frac{\lambda Z^2}{\sigma} \frac{1-\alpha}{\alpha} \left(\frac{\sigma_{eff}}{\sigma} \right)^3 \Omega\left(x_{eff}\right) \tag{C.30}$$

C.3 Zhou-Yeh-Stell (ZYS) Approach

$$\beta P = \beta \left(P^{id} + P^{HS} + P^{MSA} + P^{MAL} \right) \tag{C.31}$$

$$\beta P^{MSA} = \frac{1}{12\pi\sigma^3} \left[2 + 3x - 3x \left(1 + 2x \right)^{1/2} - 2 \left(1 + 2x \right)^{3/2} \right] \tag{C.32}$$

$$\beta P^{MAL} = - \left(1 - \alpha \right) \frac{\rho_0}{2} \left[\frac{1 + \eta - 0.5\eta^2}{\left(1 - 0.5\eta \right) \left(1 - \eta \right)} - \frac{1}{4\pi\rho_0\sigma^3} \left[\frac{\left(x + 2 \right) \sqrt{1 + 2x} - 3x - 2}{\sqrt{1 + 2x}} \right] \right] \tag{C.33}$$

$$\ln \gamma_i = \left(\ln {\gamma_i}^{HS} + \ln {\gamma_i}^{MSA} + \ln {\gamma_i}^{MAL} \right) \tag{C.34}$$

$$\ln {\gamma_i}^{MSA} = -b \left(\frac{x \left(1 + x - \sqrt{1 + 2x} \right)}{\sqrt{1 + 2x}} \right) \tag{C.35}$$

$$\ln {\gamma_i}^{MAL} = \ln \left(\alpha \right) - \frac{1 - \alpha}{2} \frac{5\eta - 2\eta^2}{\left(2 - \eta \right) \left(1 - \eta \right)} + \frac{1 - \alpha}{8\pi\rho_0\sigma^3} \left[\frac{\left(x + 2 \right) \sqrt{1 + 2x} - 3x - 2}{\sqrt{1 + 2x}} \right] \tag{C.36}$$

C.4 Binding Mean Spherical Approximation (BiMSA) Approach

$$\beta P = \beta \left(P^{id} + P^{CS} + P^{BiMSA} + P^{MAL} \right) \tag{C.37}$$

$$\beta P^{BiMSA} = - \frac{\left[\Gamma^B \right]^3}{3\pi} \tag{C.38}$$

$$\beta P^{MAL} = - \left(1 - \alpha \right) \frac{\rho_0}{2} \left[\frac{1 + \eta - 0.5\eta^2}{\left(1 - 0.5\eta \right) \left(1 - \eta \right)} \right] \tag{C.39}$$

$$\ln \gamma_i = \left(\ln {\gamma_i}^{CS} + \ln {\gamma_i}^{BiMSA} + \ln {\gamma_i}^{MAL} \right) \tag{C.40}$$

$$\ln {\gamma_i}^{BiMSA} = - \frac{\lambda Z^2}{\sigma} \frac{\Gamma^B \sigma}{1 + \Gamma^B \sigma} \tag{C.41}$$

$$\ln {\gamma_i}^{MAL} = \ln \left(\alpha \right) - \frac{1 - \alpha}{4} \frac{5\eta - 2\eta^2}{\left(1 - \eta \right) \left(1 - 0.5\eta \right)} \tag{C.42}$$

APPENDIX D

Supporting Figures

D.1 Chapter 4

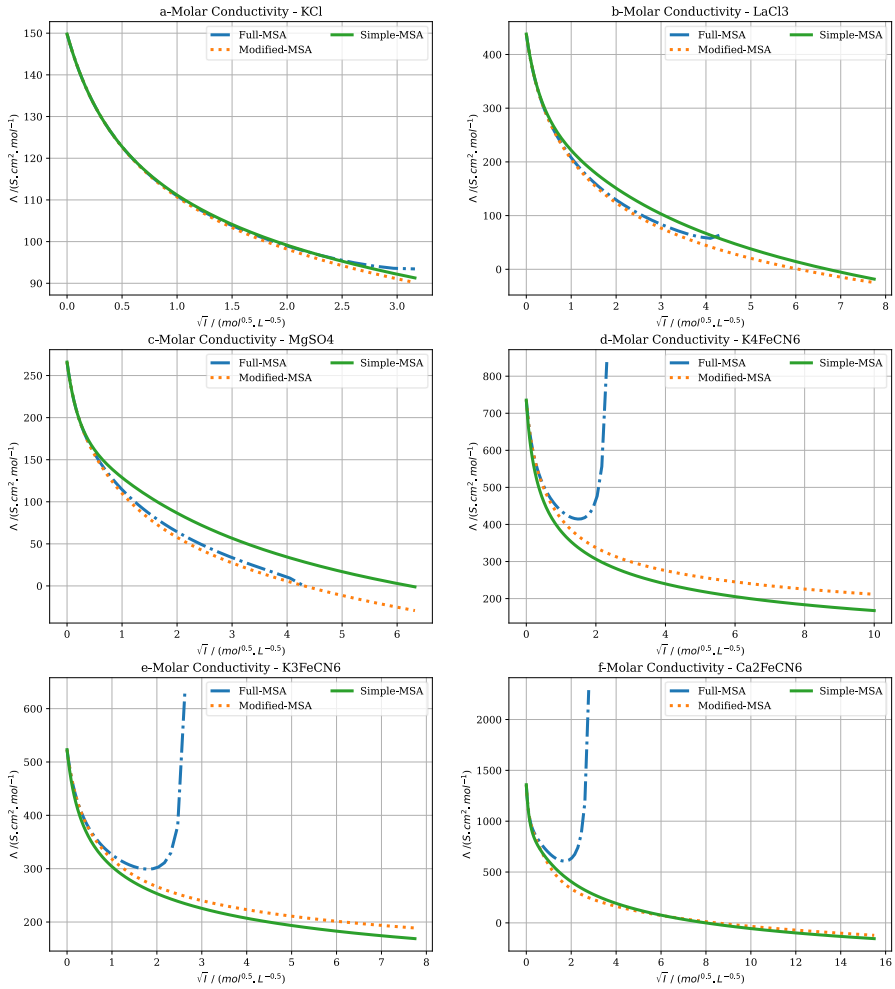

Figure D.1. The comparison of three formulations of MSA models (Simple, Full, and Modified) for (a) KCl, (b) $LaCl_3$, (c) $MgSO_4$, (d) $K_4Fe(CN)_6$, (e) $K_3Fe(CN)_6$, (f) $Ca_2Fe(CN)_6$ at 298.15 K in water. Reprinted with permission from ref. [120]. Copyright 2022 American Chemical Society.

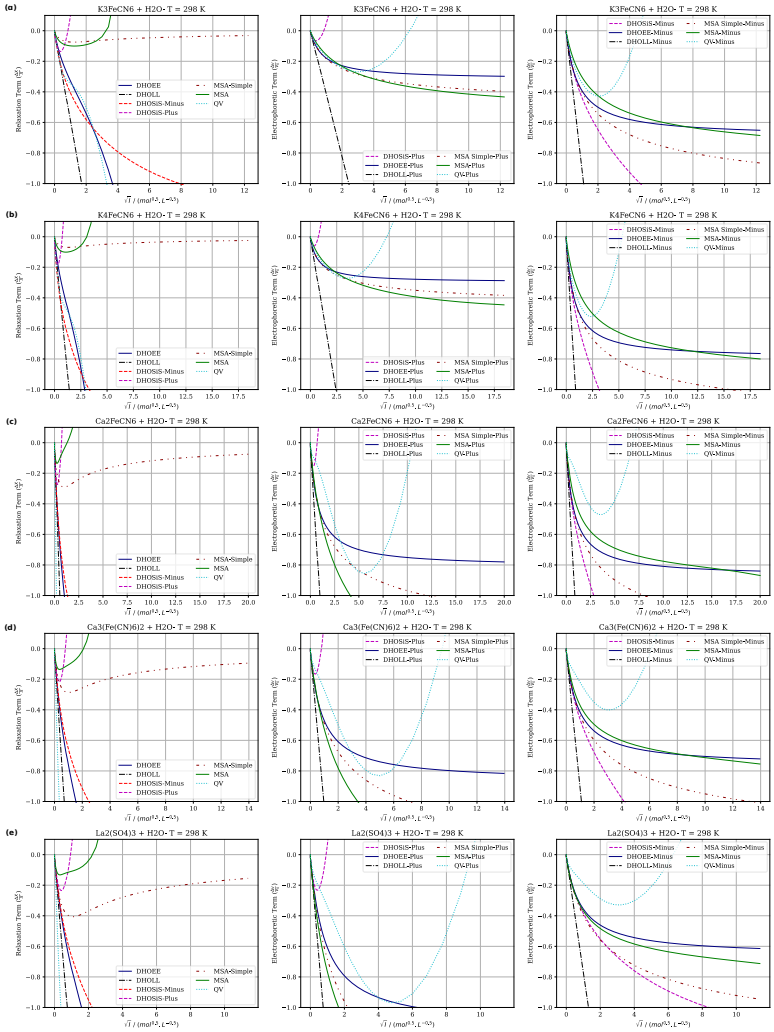

Figure D.2. The relaxation term and electrophoretic term of (a) $K_3Fe(CN)_6$ (1:3), (b) $Ca_3(Fe(CN)_6)_2$ (2:3), (c) $La_2(SO_4)_3$ (3:2), (d) $Ca_2Fe(CN)_6$ (2:4), (e) $K_4Fe(CN)_6$ (1:4) predicted by DHOLL, DHOEE, DHOSiS, MSA, MSA Simple and QV models versus the square root of ionic strength at 298.15 K. Reprinted with permission from ref. [120]. Copyright 2022 American Chemical Society.

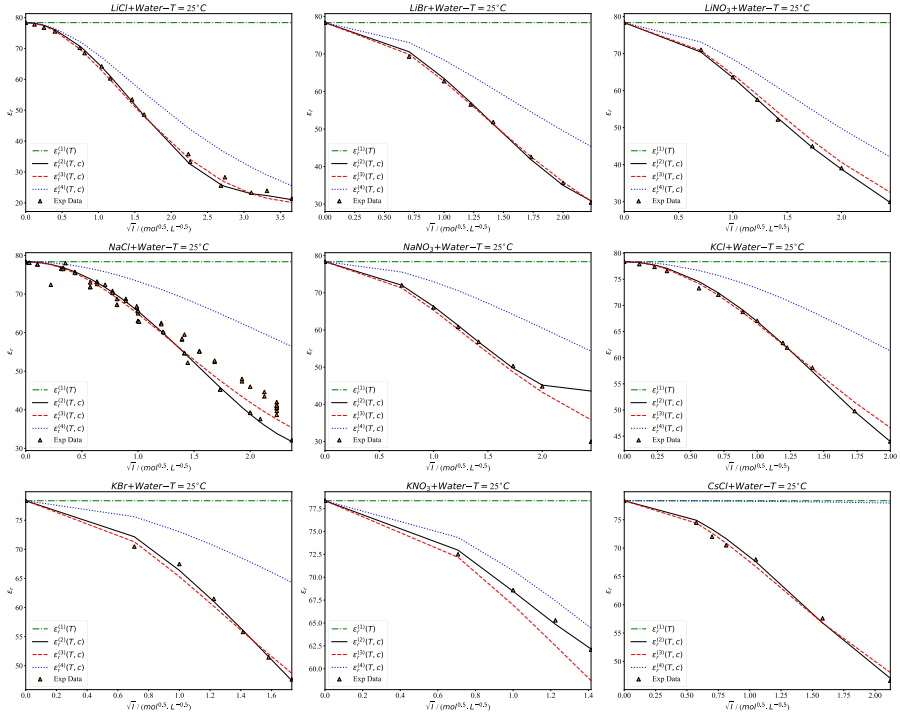

Figure D.3. The RSP of a) LiCl, b) $LiNO_3$, c) NaCl, d) $NaNO_3$, e) KCl, and f) KNO_3 at 298.15 k estimated by RSP models (exp. data are from references [157, 369]). Reprinted from ref. [124], Copyright 2023, with permission from Elsevier.

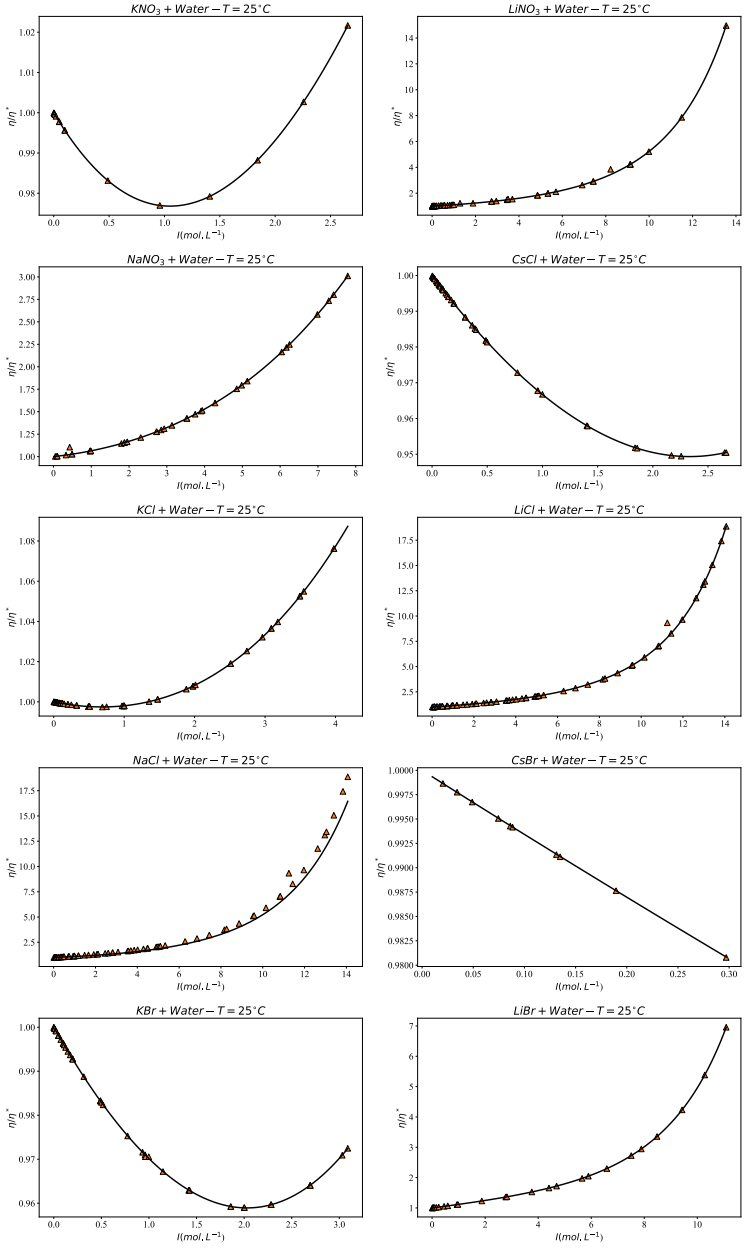

Figure D.4. The viscosity of NaCl-water system at 298.15 K estimated by Eq. 3.42 (experimental data are from references [164,165]). Reprinted from ref. [124], Copyright 2023, with permission from Elsevier.

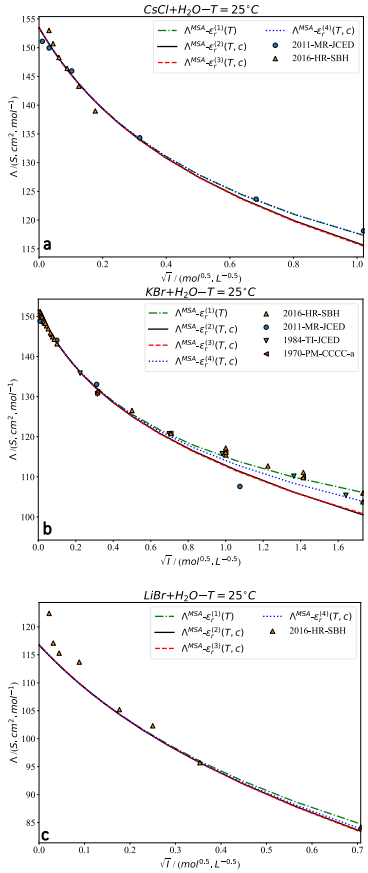

Figure D.5. The effect of a concentration dependent RSP on the prediction of MSA model for a) CsCl, b) KBr, and c) LiBr at 298.15 (acronyms 2016-HR-SBH [129], 2011-MR-JCED [134] , 1984-TI-JCED [141], and 1970-PM-CCCC-a [131] show the references for the collected data points). Reprinted from ref. [124], Copyright 2023, with permission from Elsevier.

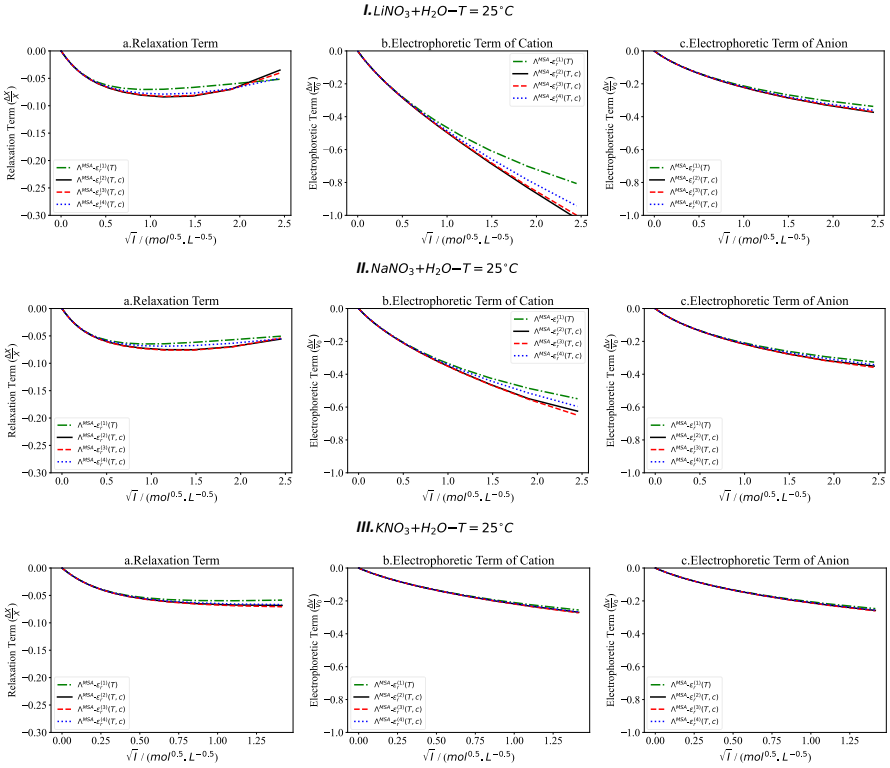

Figure D.6. The effect of a concentration-dependent RSP on contributions to the relaxation and electrophoretic terms predicted by the MSA model for (I) $LiNO_3$, (II) $NaNO_3$, and (III) KNO_3-water systems at 298.15 K. Reprinted from ref. [124], Copyright 2023, with permission from Elsevier.

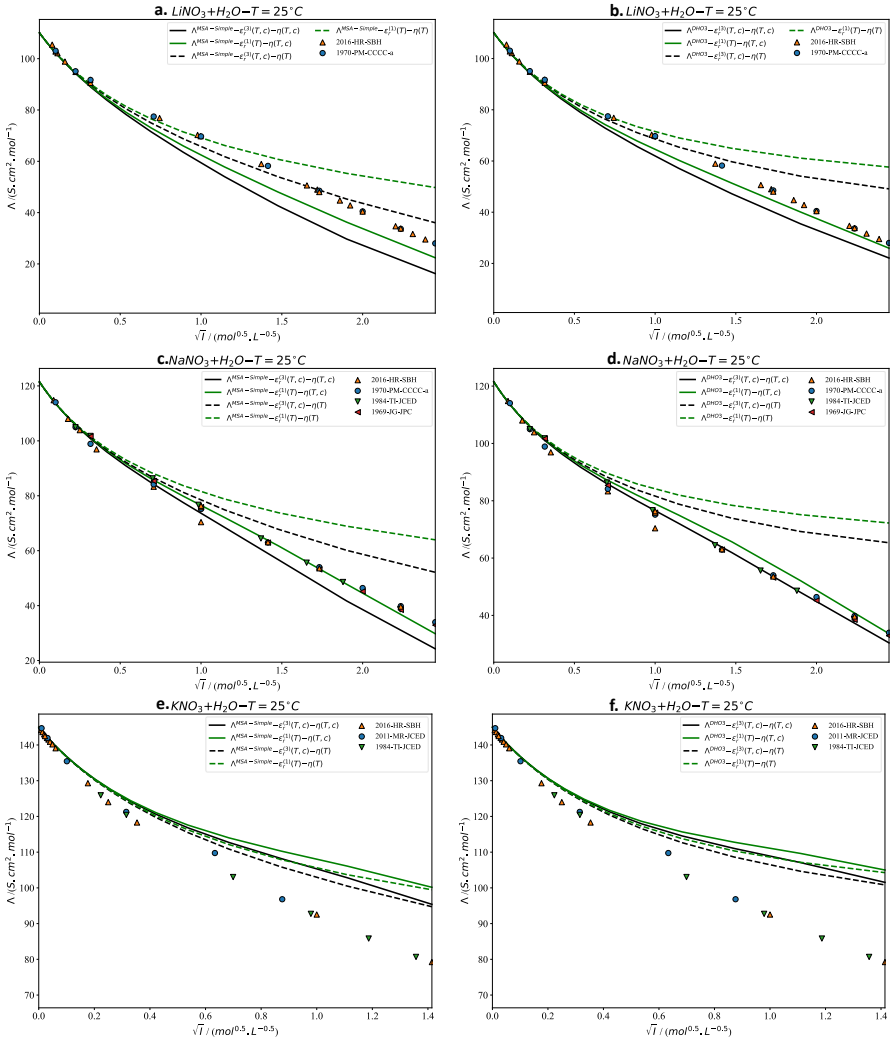

Figure D.7. The effect of a concentration-dependent viscosity and RSP on the MSA-Simple and DHO3 predictions for $LiNO_3$, $NaNO_3$, and KNO_3-water systems at 298.15 K (Acronyms are the same as in Figure 3.10). Reprinted from ref. [124], Copyright 2023, with permission from Elsevier.

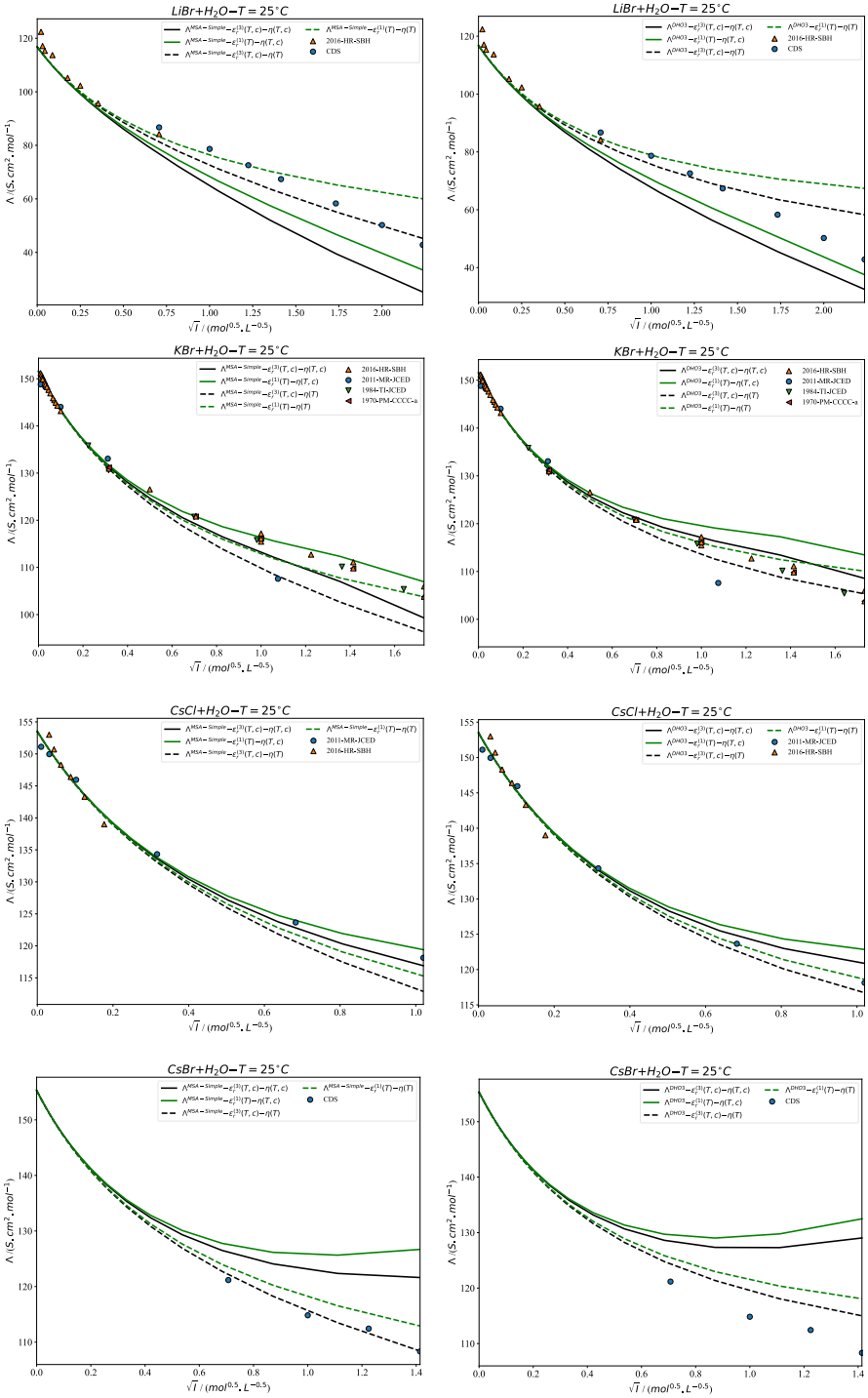

Figure D.8. The effect of a concentration-dependent viscosity and RSP on the MSA-Simple and DHO3 predictions for LiBr, KBr, CsCl, CsBr-water solutions at 298.15 K (Acronyms are the same as in Figure 3.10). Reprinted from ref. [124], Copyright 2023, with permission from Elsevier.

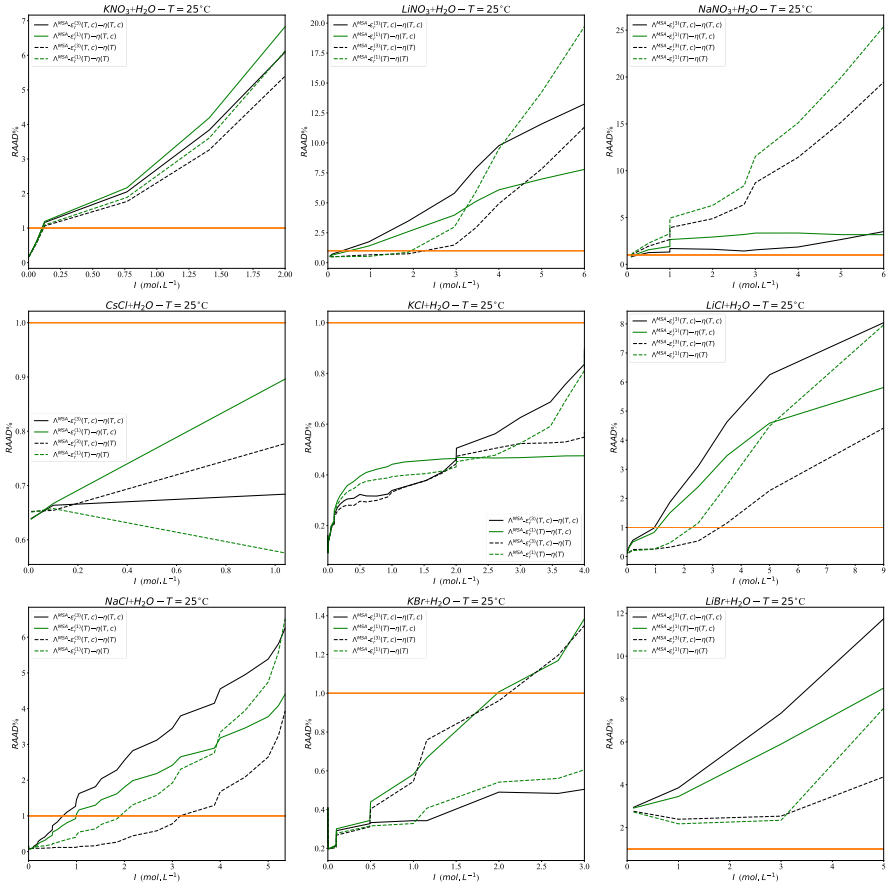

Figure D.9. The relative average absolute deviation in percent (RAAD%) of MSA model predictions when the solvents and solutions RSP and viscosity are used for LiCl, $LiNO_3$, NaCl, $NaNO_3$, KCl, KNO_3, LiBr, KBr, and CsCl aqueous solutions at 298.15 K. Reprinted from ref. [124], Copyright 2023, with permission from Elsevier.

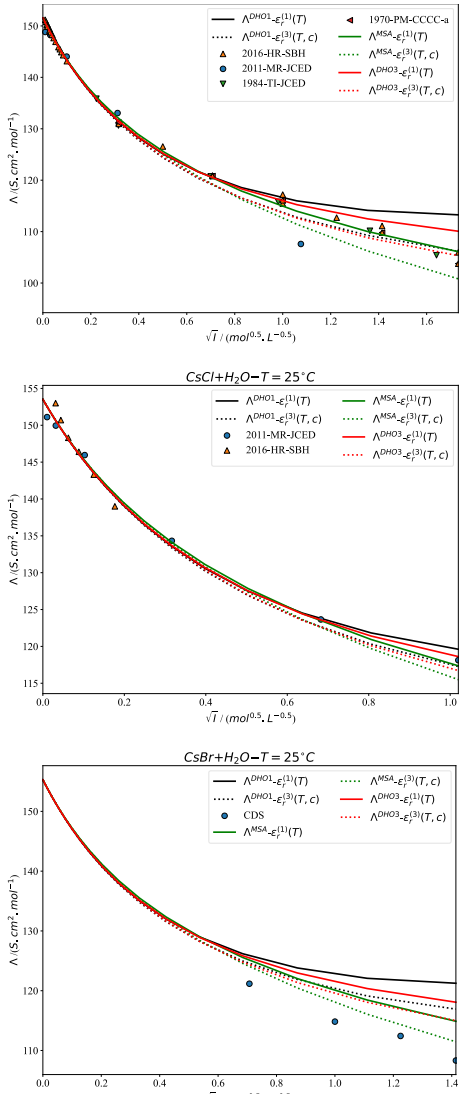

Figure D.10. The Comparison of DHO1, DHO3, and MSA predictions when the RSP model 1 and 3 are used for KBr, CsCl, and CsBr aqueous solutions at 298.15 K. Reprinted from ref. [124], Copyright 2023, with permission from Elsevier.

D.2 Chapter 5

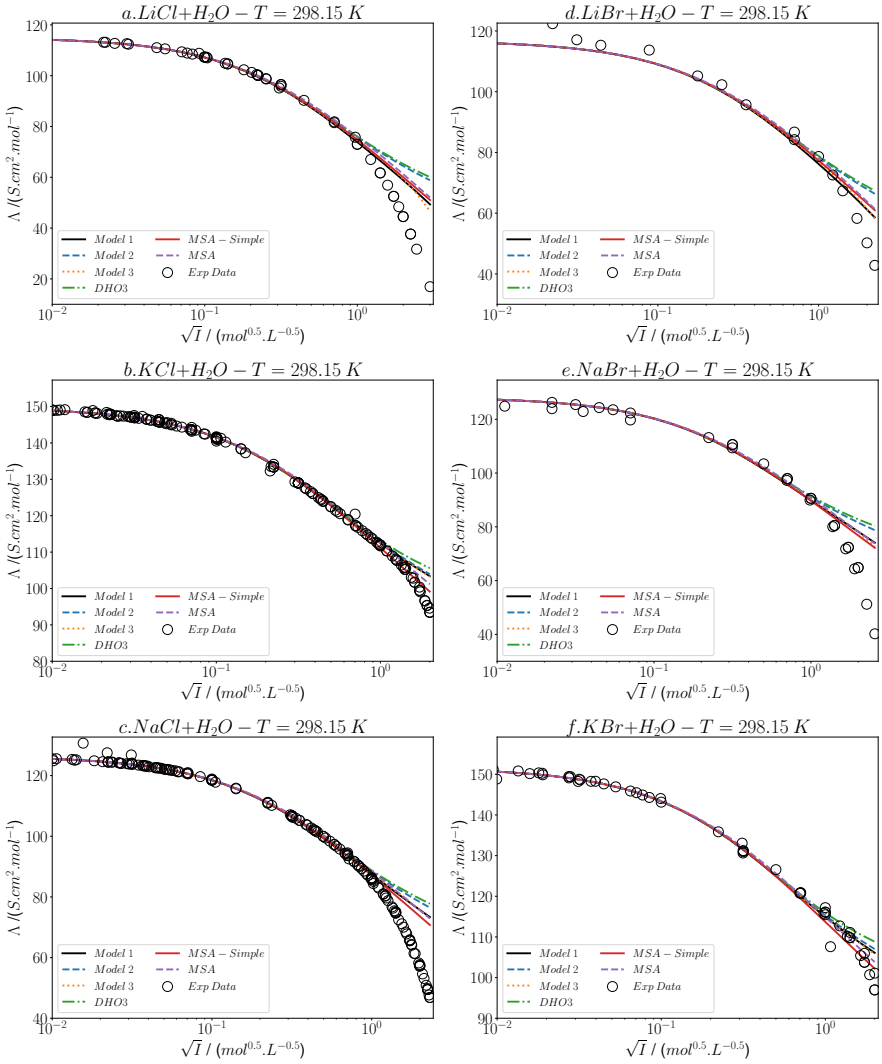

Figure D.11. The molar conductivity predicted by Models 1-3, MSA, MSA-simple, and DHO3 models and compared with experimental measurements for (a) LiCl, (b) LiBr, (c) KCl, (d) NaBr, (e) NaCl, and (f) KBr aqueous solutions at 298.15 K. Reprinted with permission from ref. [184]. Copyright 2023 American Chemical Society.

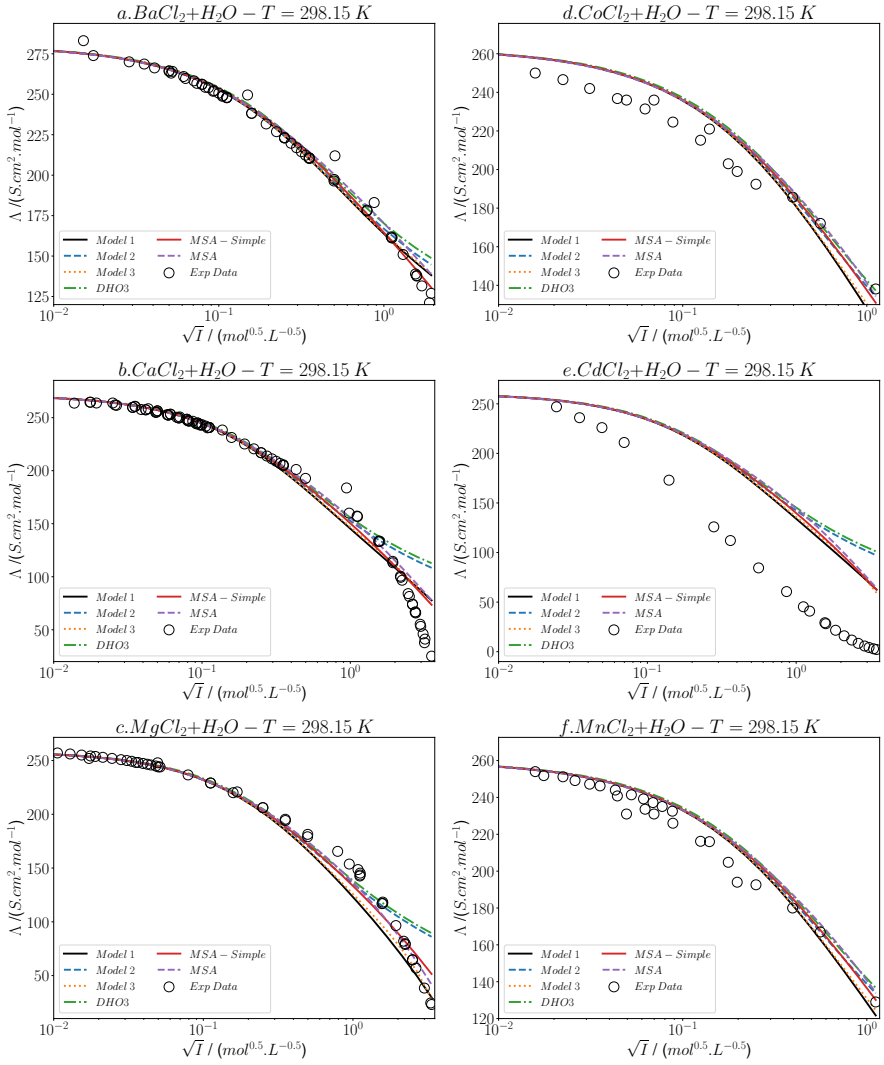

Figure D.12. The same as D.11, but for (a) $BaCl_2$, (b) $CoCl_2$, (c) $CaCl_2$, (d) $CdCl_2$, (e) $MgCl_2$, and (f) $MnCl_2$ aqueous solutions at 298.15 K. Reprinted with permission from ref. [184]. Copyright 2023 American Chemical Society.

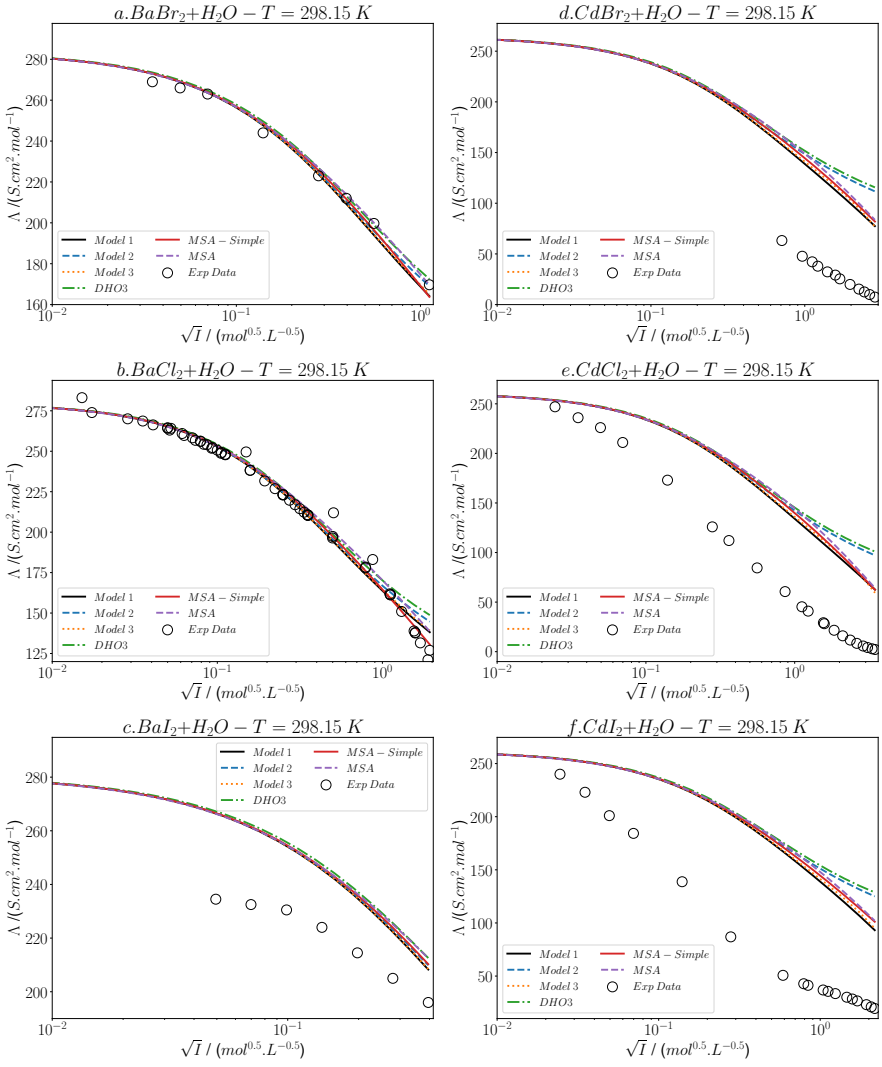

Figure D.13. The same as D.11, but for (a) $BaBr_2$, (b) $CoBr_2$, (c) $CaBr_2$, (d) $CdBr_2$, (e) $MgBr_2$, and (f) $MnBr_2$ aqueous solutions at 298.15 K. Reprinted with permission from ref. [184]. Copyright 2023 American Chemical Society.

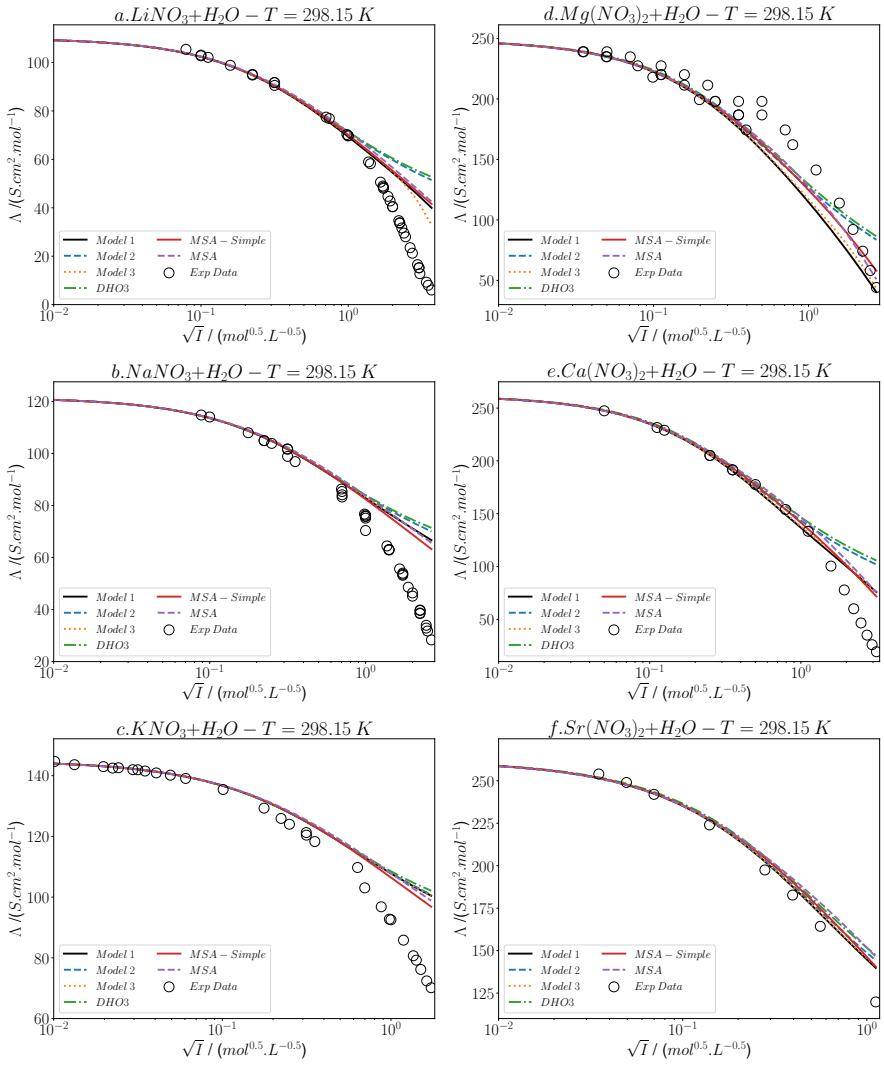

Figure D.14. The same as D.11, but for (a) $LiNO_3$, (b) $Mg(NO_3)_2$, (c) $NaNO_3$, (d) $Ca(NO_3)_2$, (e) KNO_3, and (f) $Sr(NO_3)_2$ aqueous solutions at 298.15 K. Reprinted with permission from ref. [184]. Copyright 2023 American Chemical Society.

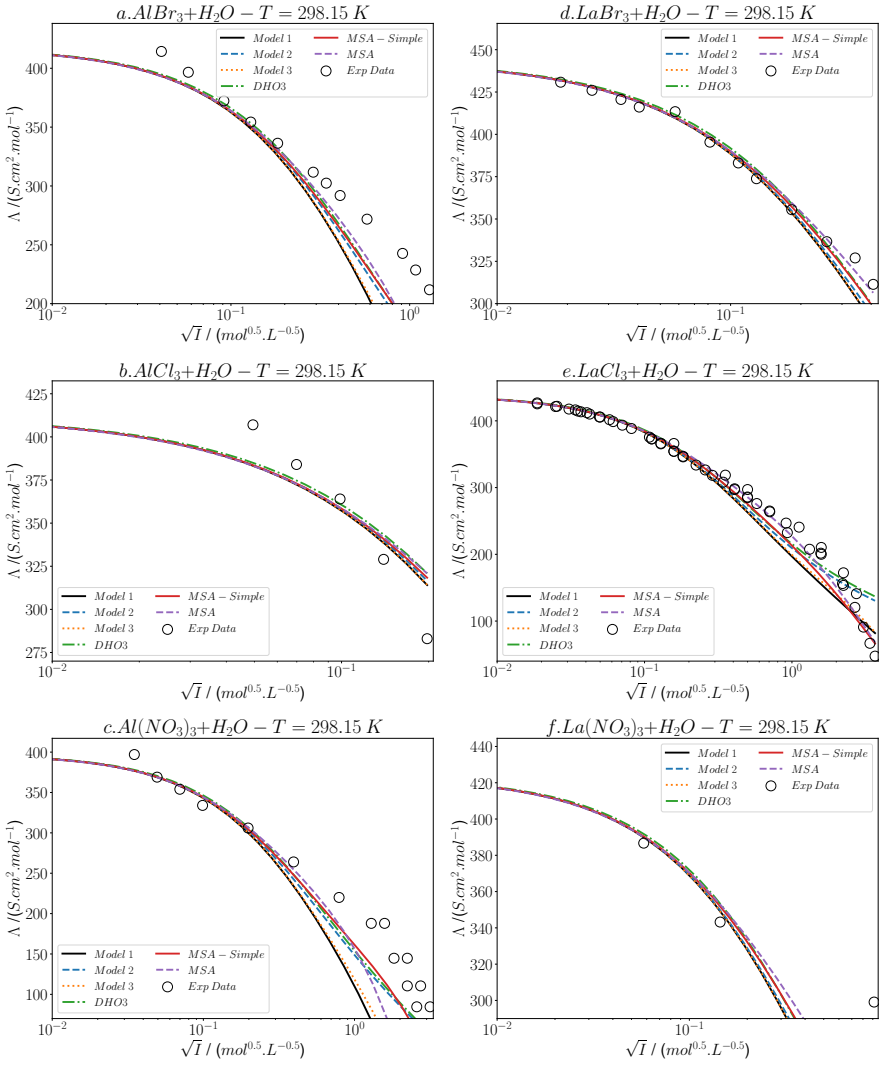

Figure D.15. The same as D.11, but for (a) $AlBr_3$, (b) $AlCl_3$, (c) $Al(NO_3)_3$, (d) $LaBr_3$, (e) $LaCl_3$, and (f) $La(NO_3)_3$ aqueous solutions at 298.15 K. Reprinted with permission from ref. [184]. Copyright 2023 American Chemical Society.

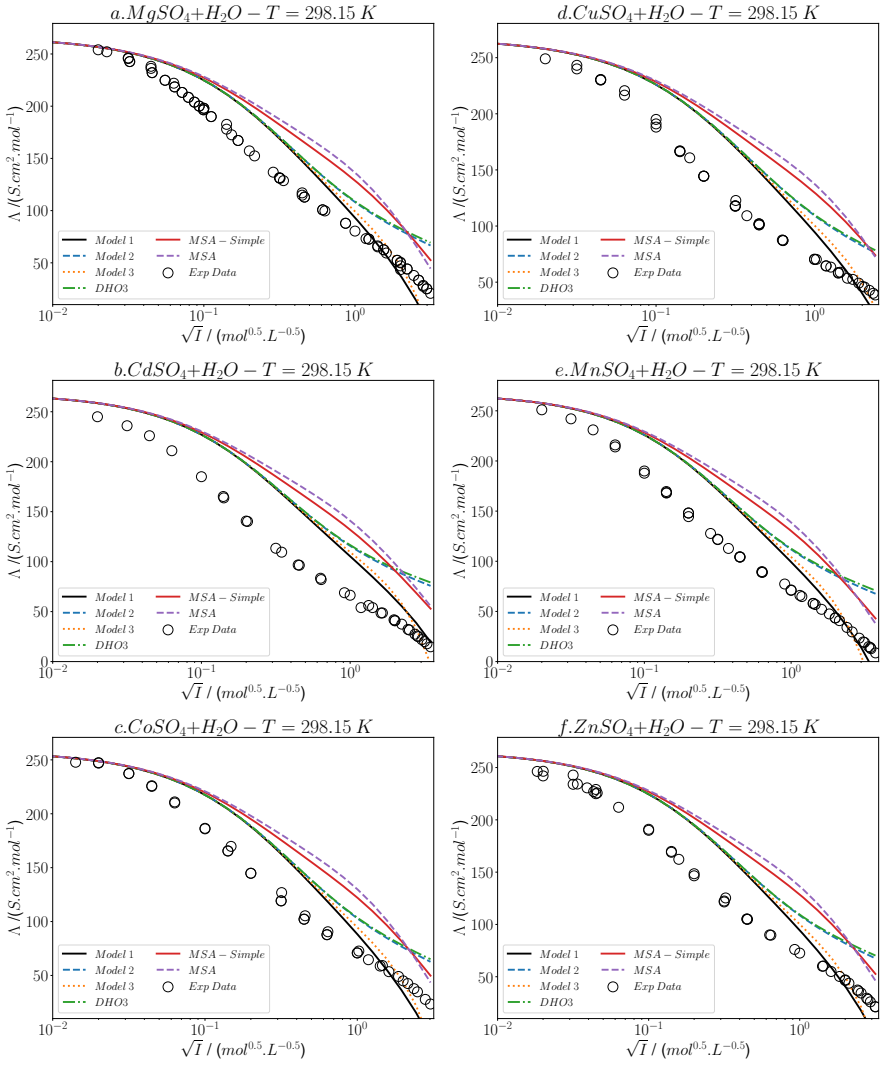

Figure D.16. The same as D.11, but for (a) $MgSO_4$, (b) $CdSO_4$, (c) $CoSO_4$, (d) $CuSO_4$, (e) $MnSO_4$, and (f) $ZnSO_4$ aqueous solutions at 298.15 K. Reprinted with permission from ref. [184]. Copyright 2023 American Chemical Society.

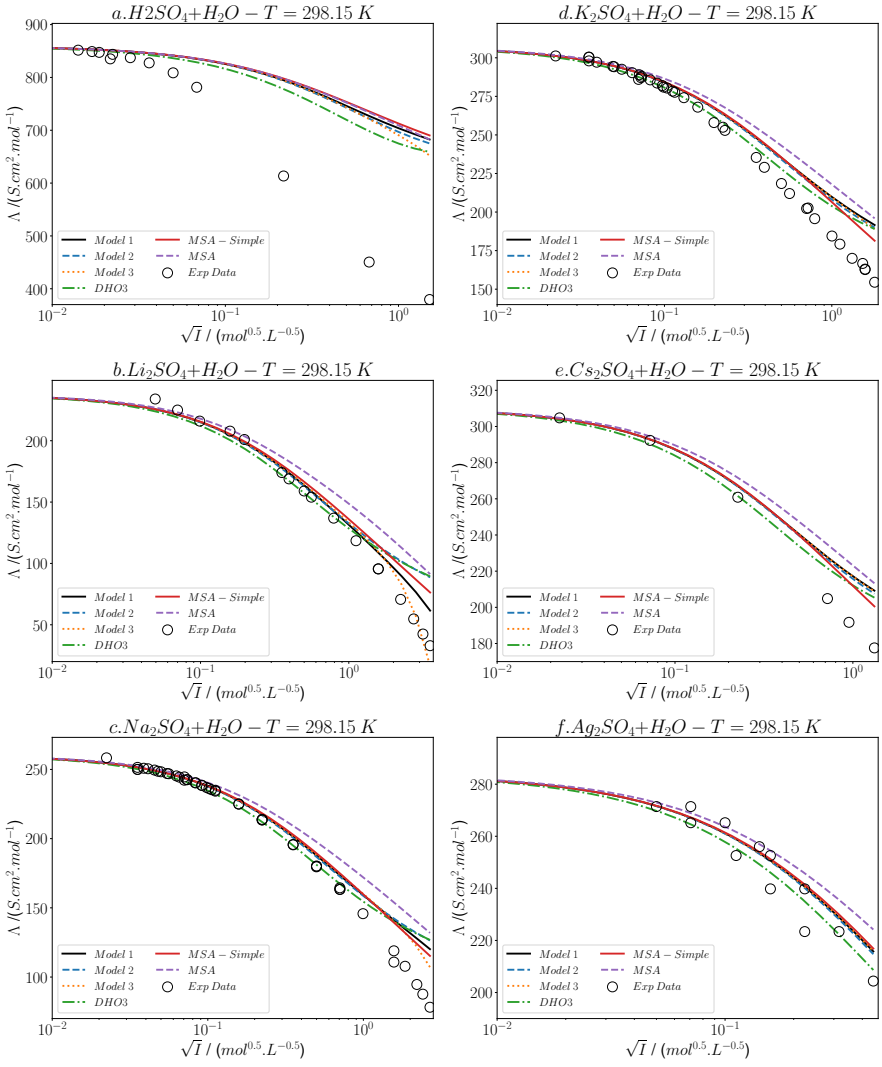

Figure D.17. The same as D.11, but for (a) H_2SO_4, (b) Li_2SO_4, (c) Na_2SO_4, (d) K_2SO_4, (e) Cs_2SO_4, and (f) Ag_2SO_4 aqueous solutions at 298.15 K. Reprinted with permission from ref. [184]. Copyright 2023 American Chemical Society.

D.3 Chapter 7

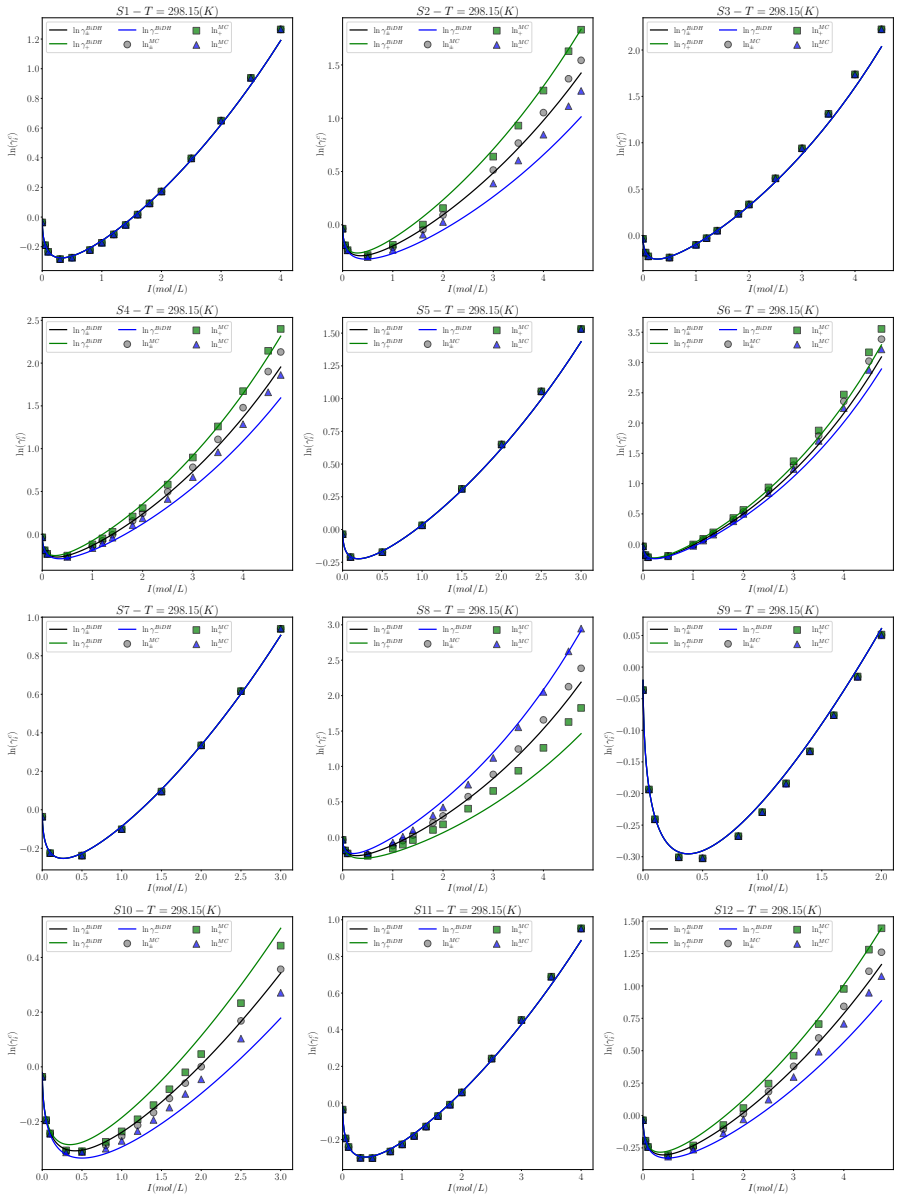

Figure D.18. Comparison of the BiDH predictions with the MC simulations for systems S1-S12 [289].

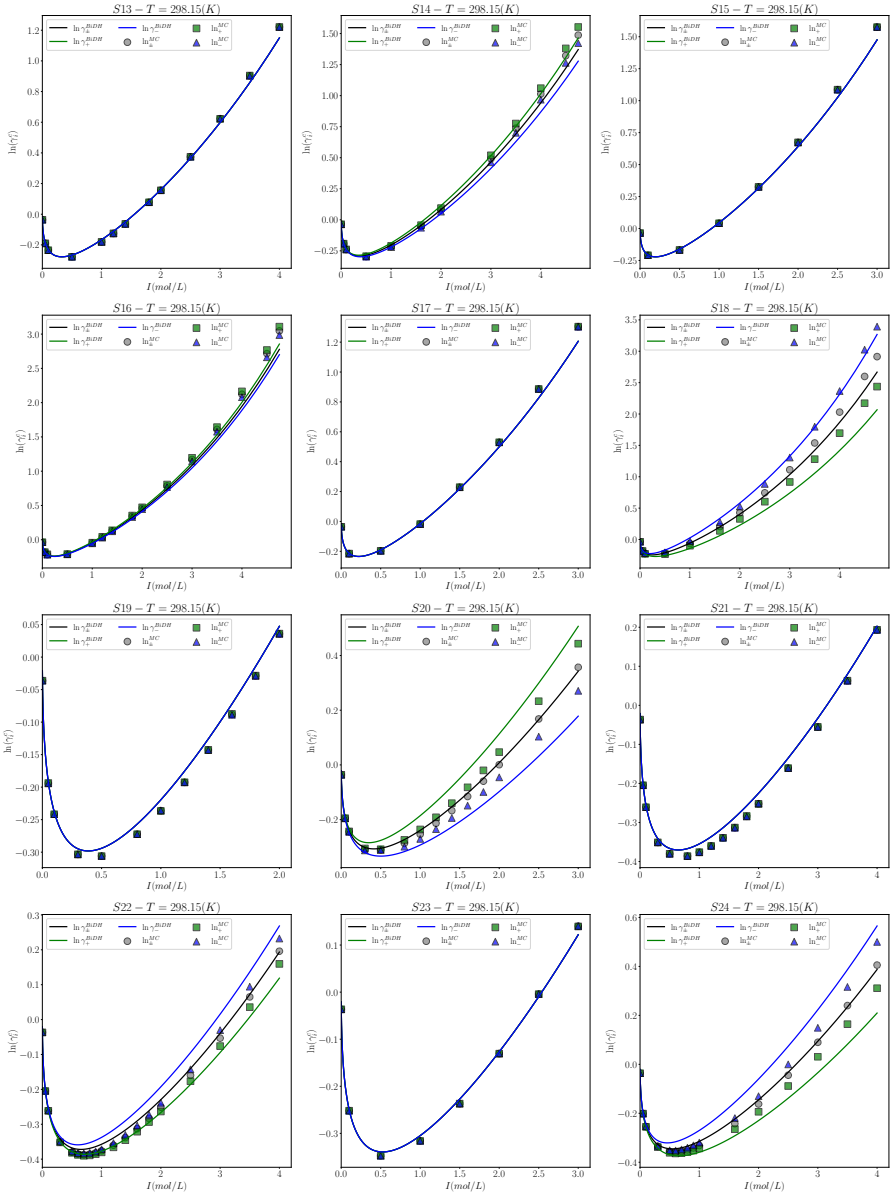

Figure D.19. Comparison of the BiDH predictions with the MC simulations for systems S13-S24 [289].

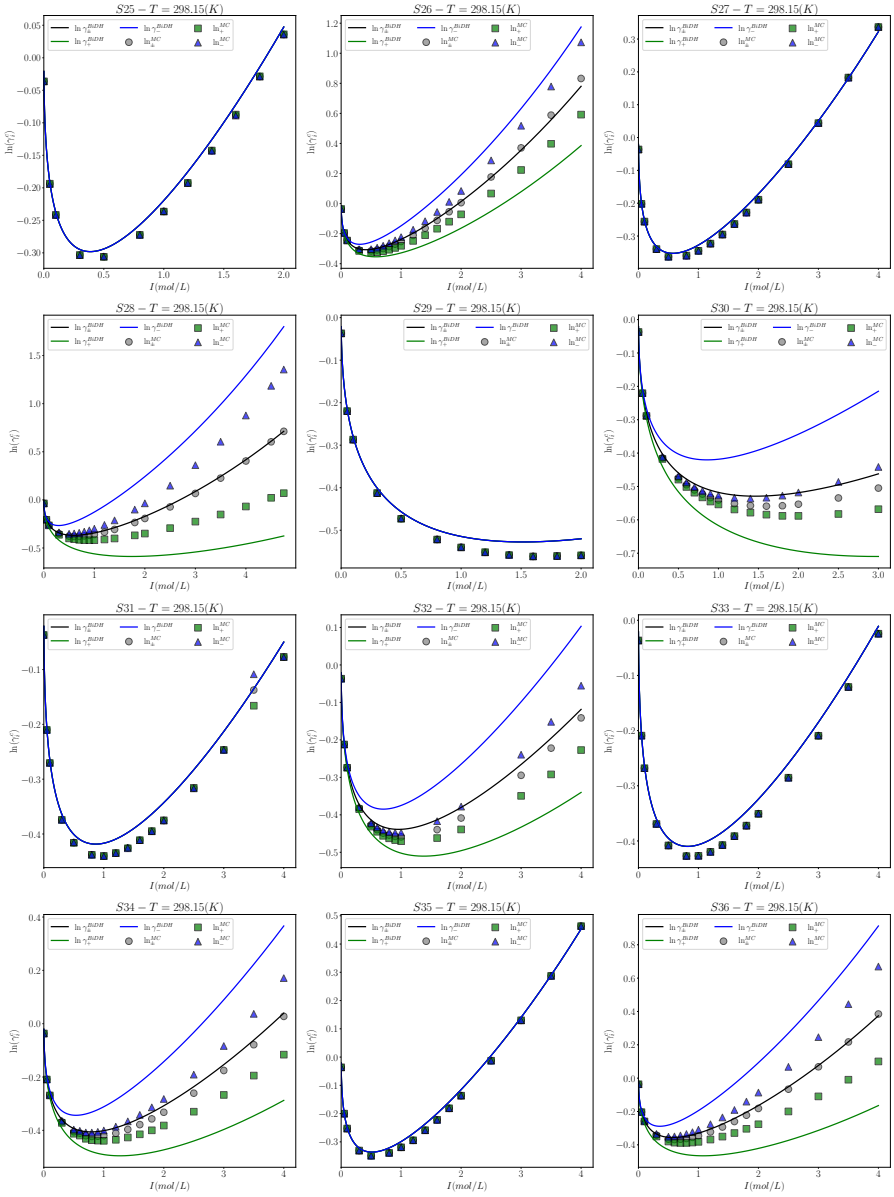

Figure D.20. Comparison of the BiDH predictions with the MC simulations for systems S25-S36 [289].

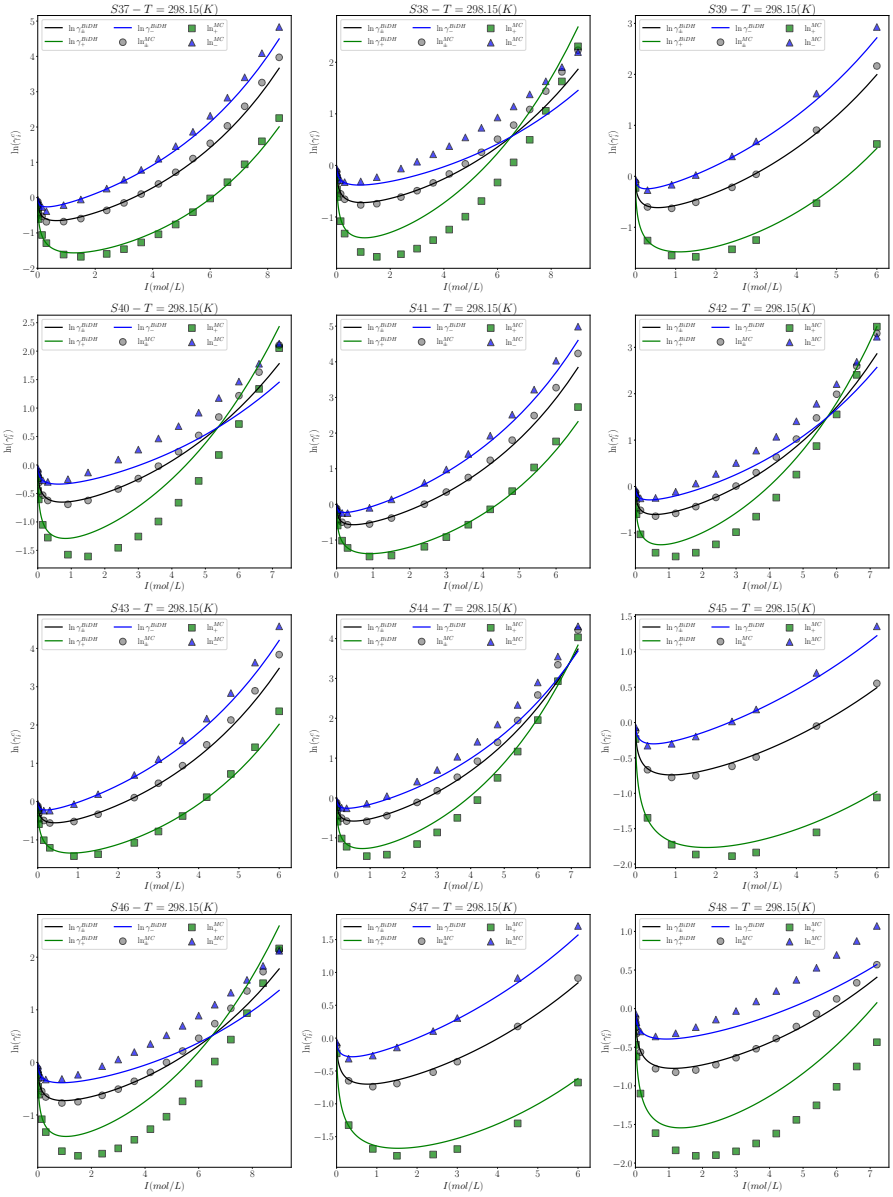

Figure D.21. Comparison of the BiDH predictions with the MC simulations for systems S37-S48 [289].

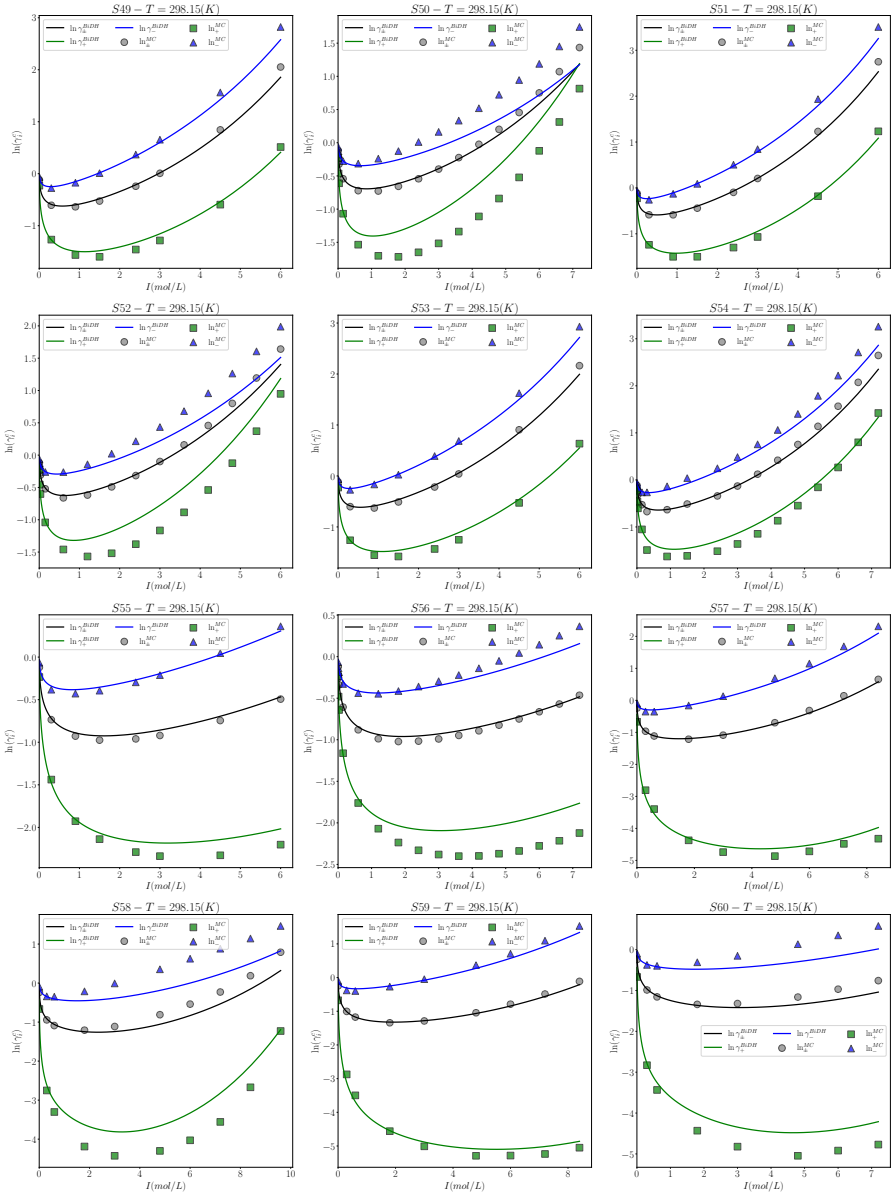

Figure D.22. Comparison of the BiDH predictions with the MC simulations for systems S49-S60 [289].

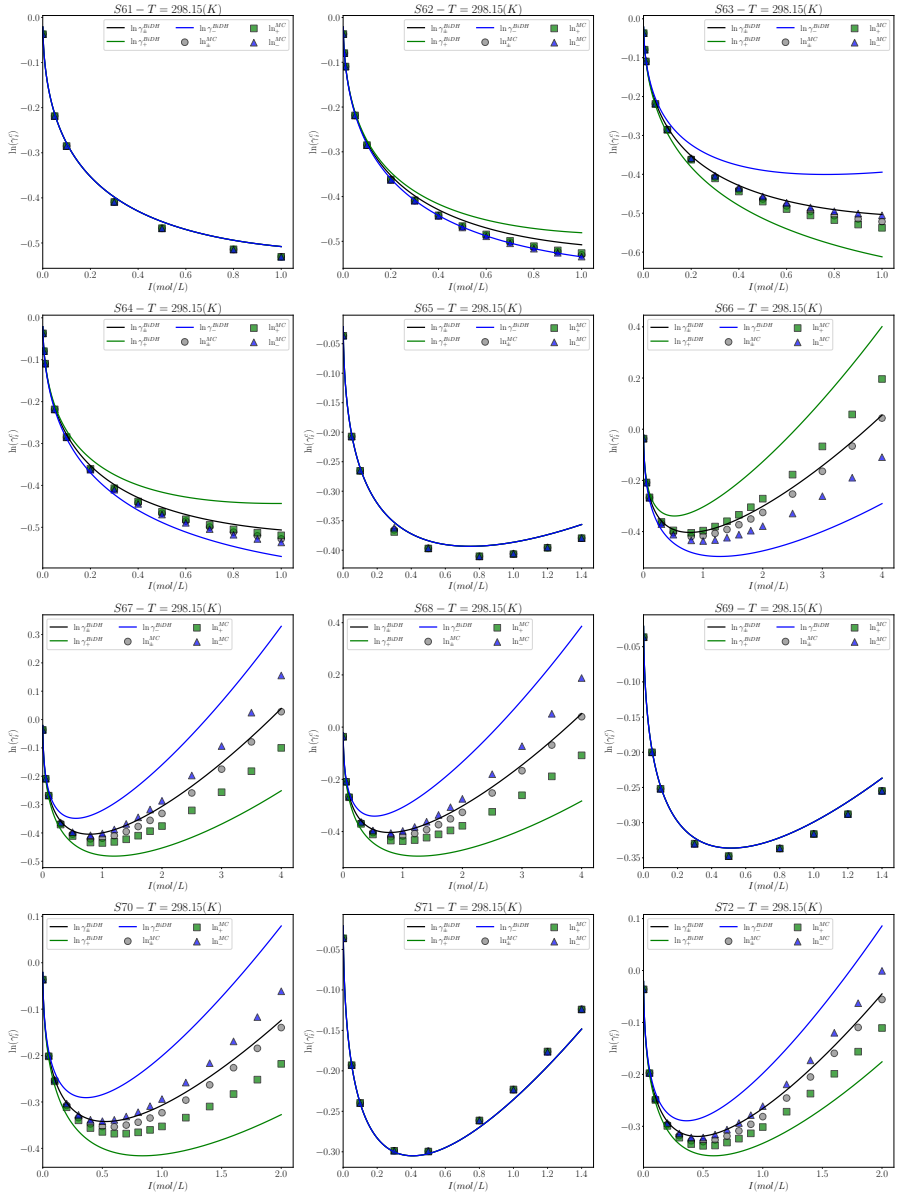

Figure D.23. Comparison of the BiDH predictions with the MC simulations for systems S61-S72 [289].

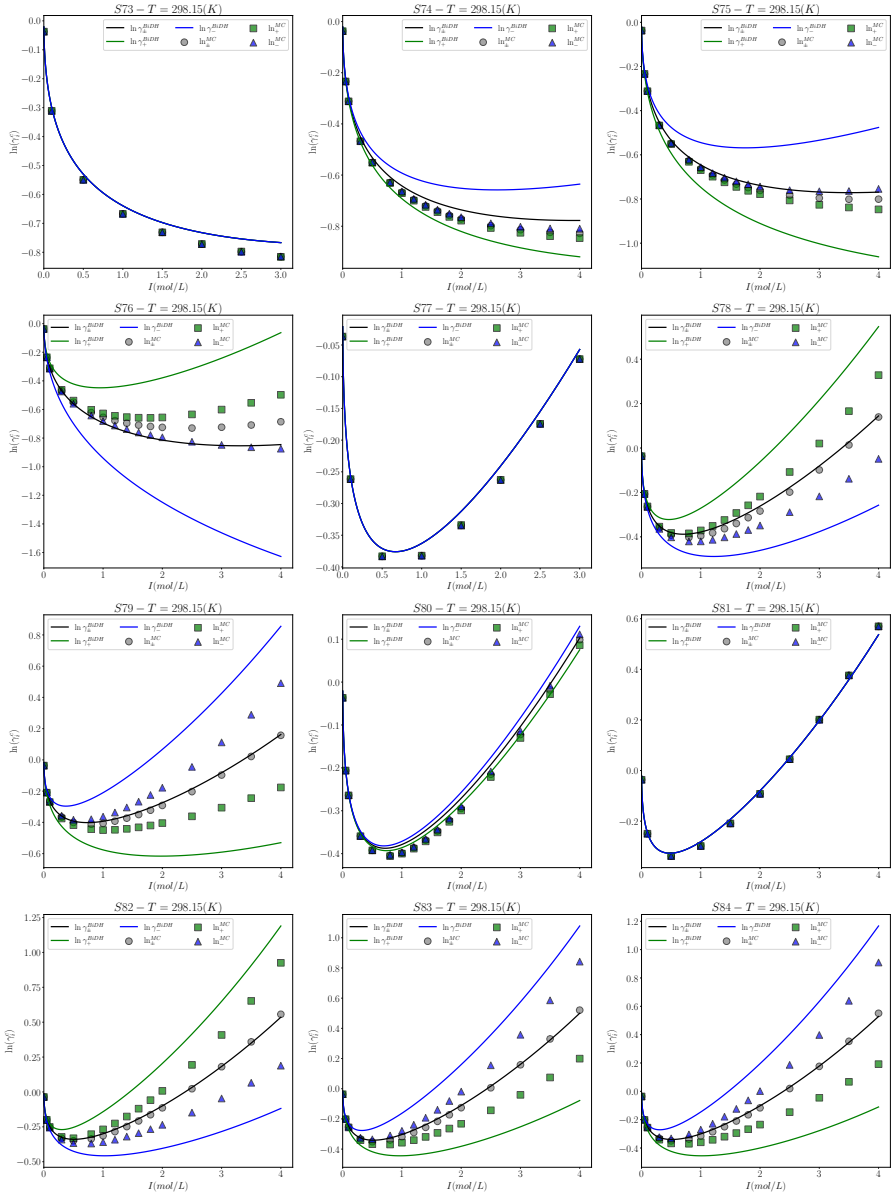

Figure D.24. Comparison of the BiDH predictions with the MC simulations for systems S73-S84 [289].

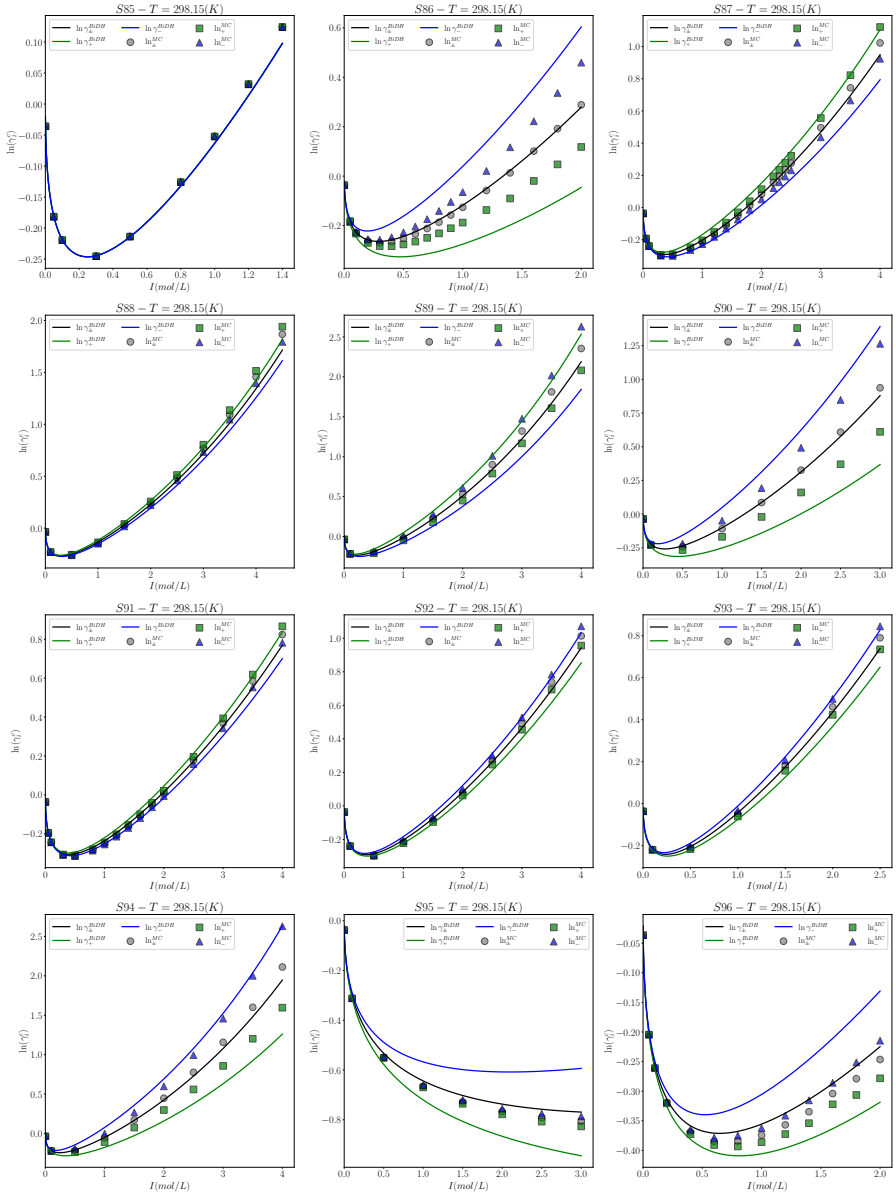

Figure D.25. Comparison of the BiDH predictions with the MC simulations for systems S85-S96 [289].

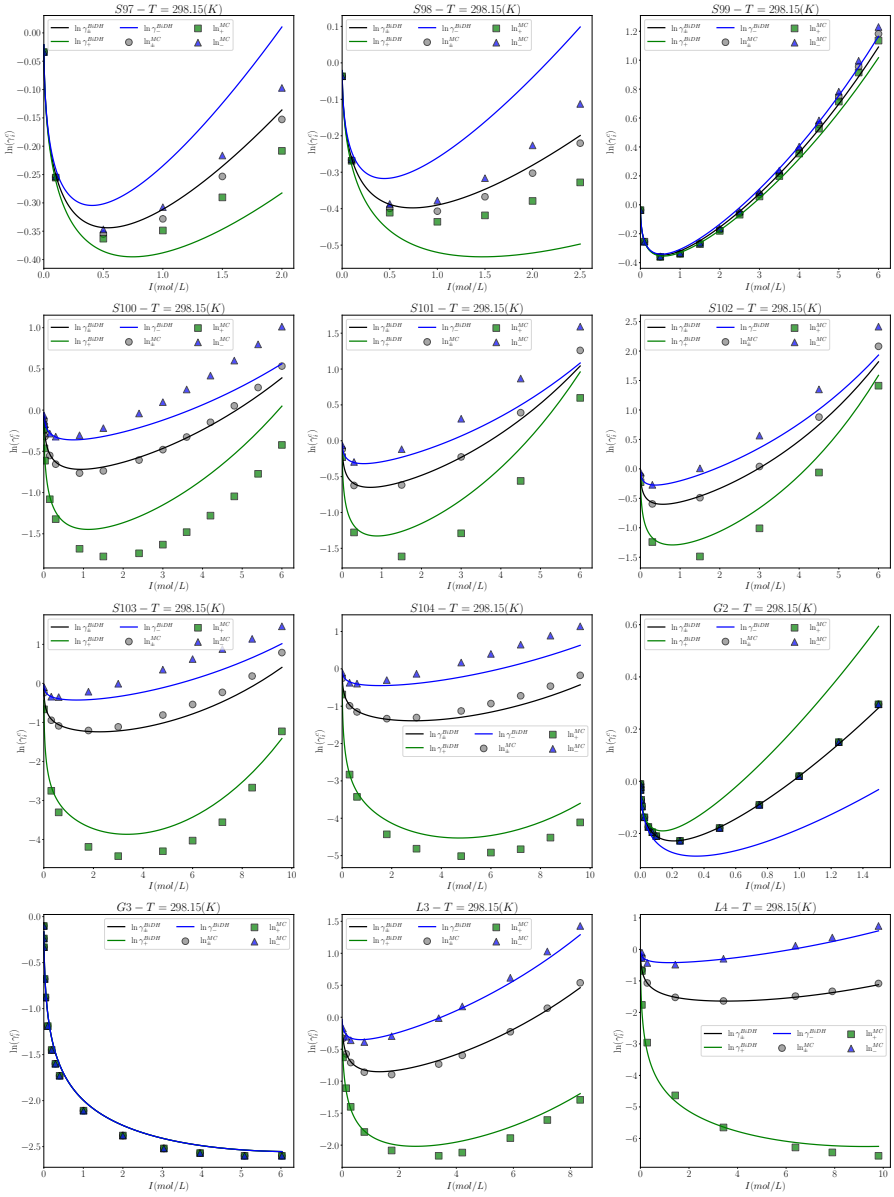

Figure D.26. Comparison of the BiDH predictions with the MC simulations for systems S97-L4 [64, 258, 289].

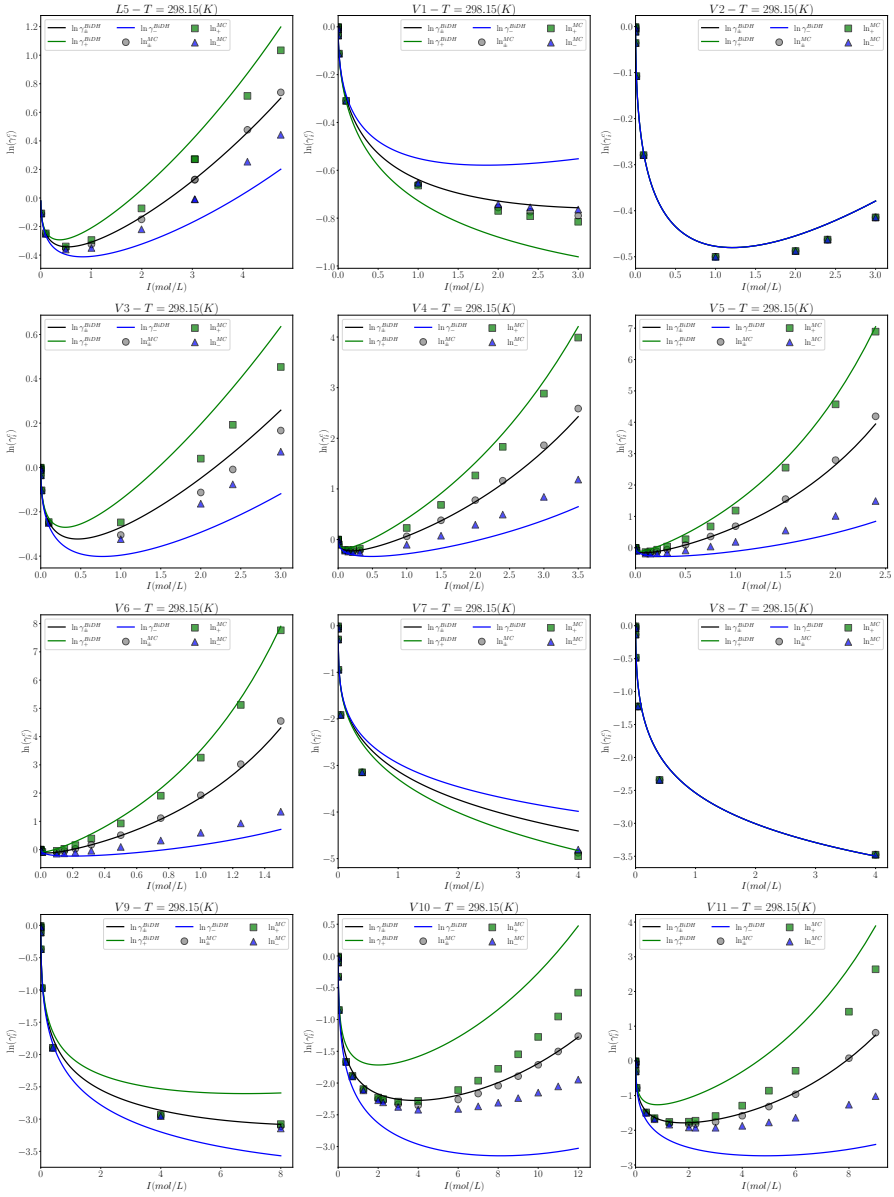

Figure D.27. Comparison of the BiDH predictions with the MC simulations for systems L5-V11 [258, 290].

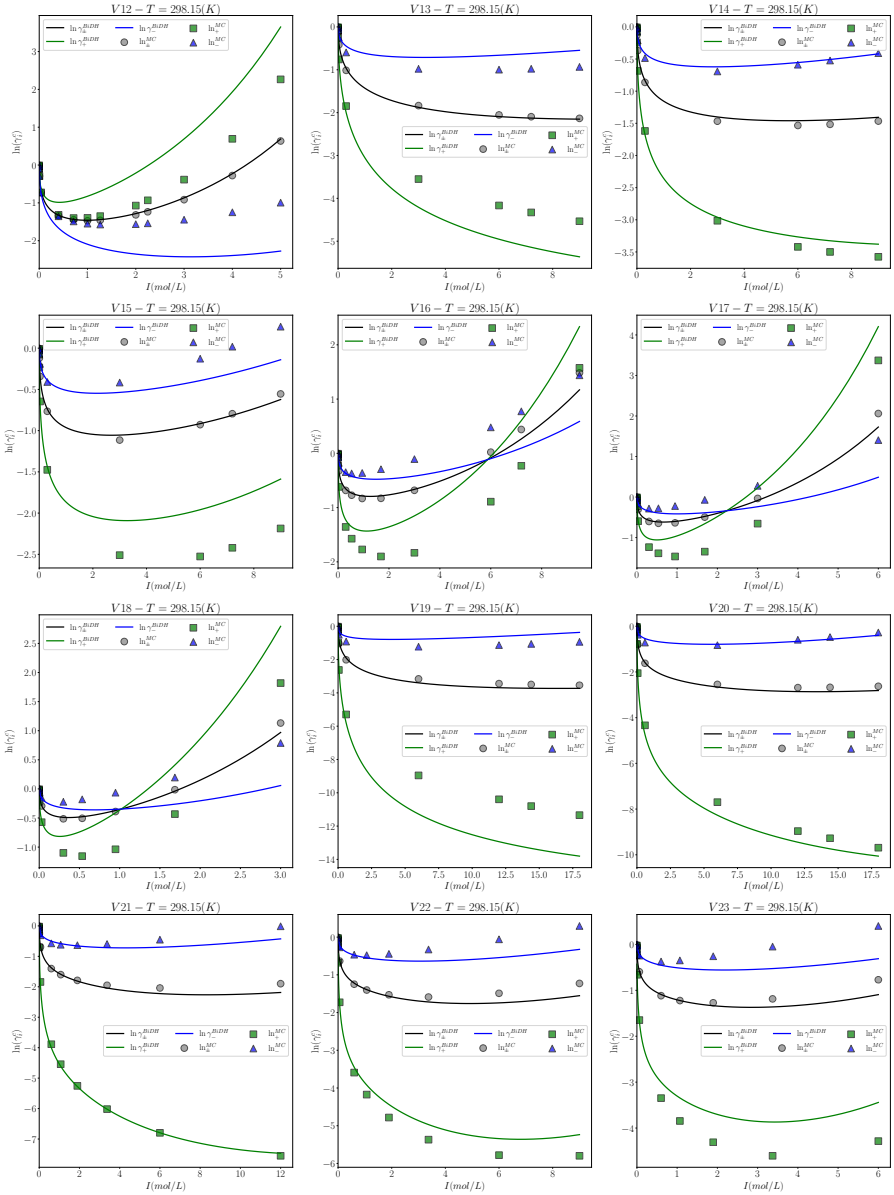

Figure D.28. Comparison of the BiDH predictions with the MC simulations for systems V12-V23 [290].

D.4 Chapter 8

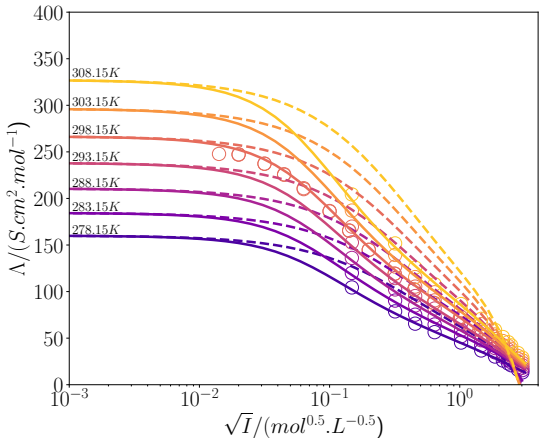

Figure D.29. The molar conductivity of $CoSO_4$ aqueous solutions predicted by the Model 3 where ion pairing is (solid lines) and is not (dashed lines) considered (symbols are experimental measurements from ref. [130]). Reprinted with permission from ref. [184]. Copyright 2023 American Chemical Society.

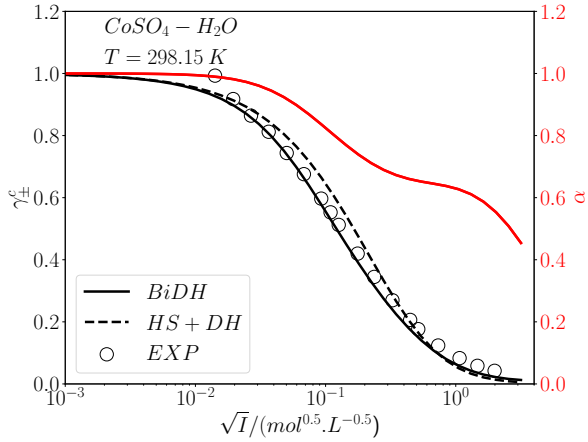

Figure D.30. The molar conductivity of $CoSO_4$ aqueous solutions predicted by the Model 3 where ion pairing is (solid lines) and is not (dashed lines) considered (symbols are experimental measurements from ref. [130]).

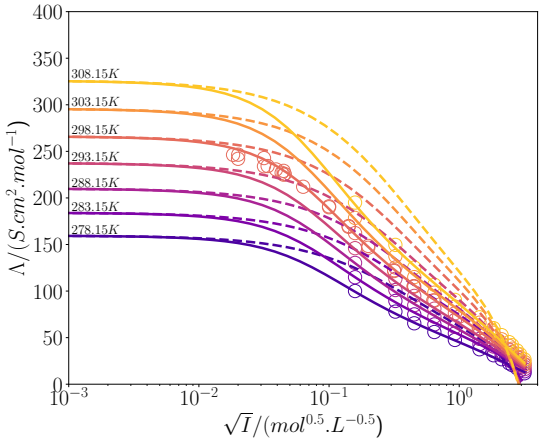

Figure D.31. The molar conductivity of $ZnSO_4$ aqueous solutions predicted by the Model 3 where ion pairing is (solid lines) and is not (dashed lines) considered (symbols are experimental measurements from ref. [130]). Reprinted with permission from ref. [184]. Copyright 2023 American Chemical Society.

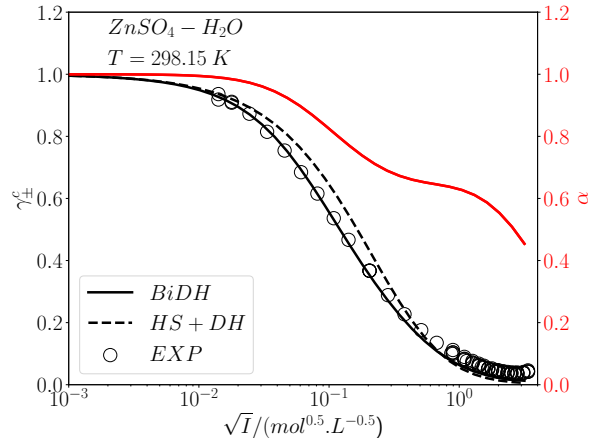

Figure D.32. The molar conductivity of $ZnSO_4$ aqueous solutions predicted by the Model 3 where ion pairing is (solid lines) and is not (dashed lines) considered (symbols are experimental measurements from ref. [130]).

{2.7182818284}ϑφερτυθιοπσδφγηξκλ